

020024

AD-A143 290

*Preliminary Reports, Memoranda
and Technical Notes of the
Materials Research Council
Summer Conference*

La Jolla, California

July 1982

Sponsored by
Defense Advanced Research Projects Agency
ARPA Order No. 4000

DTIC
ELECTE
JUL 20 1984
S D

APPROVED FOR PUBLIC RELEASE,
DISTRIBUTION IS UNLIMITED (A)

Department of Materials and Metallurgical Engineering

DTIC FILE COPY



84 07 16 09T

Accession For	
NTIS	<input checked="" type="checkbox"/>
DTIC	<input type="checkbox"/>
Unprocessed	<input type="checkbox"/>
Justification	
By <u>Per Ltr. on file</u>	
Distribution/	
Availability Codes	
Dist	Avail and/or Special
<u>A/1</u>	



PRELIMINARY REPORTS, MEMORANDA AND TECHNICAL NOTES
of the
MATERIALS RESEARCH COUNCIL SUMMER CONFERENCE
La Jolla, California
July 1982

DARPA Order No.: 4000
Program Code No.: P2D10
Contractor: The Regents of The University of Michigan
Effective Date of Contract: 10 June 82
Amount of Contract: \$406,663
Contract No.: MDA903-82-G-0428
Principal Investigator: Professor Maurice J. Sinnott
Department of Chemical Engineering
The University of Michigan
Ann Arbor, Michigan 48109
(313) 764-4314

The views and conclusions contained in this document are those of the authors and should not be interpreted as necessarily representing the official policies, either expressed or implied, of the Defense Advanced Research Projects Agency of the U.S. Government.

TABLE OF CONTENTS

- I. Foreword
- II. Steering Committee
- III. Participants
- VI. Preliminary Reports, Memoranda and Technical Notes

The following papers fall into two categories; (1) papers in a state ready for publication, and (2) reports and memoranda for limited distribution representing work in progress. The former category is available for general distribution and in some cases are in the process of publication in the appropriate technical journals. The limited distribution reports and memoranda represent initial ideas, problem suggestions, position papers, and status reports and are aimed primarily to stimulate discussion with the Council. However, they are available subject to the author's release by request to the Project Director.

<u>TITLE</u>	PART A	<u>PAGE</u>
SECTION I. Introduction and Objectives.....		1
SECTION II. Key Issues.....		2
SECTION III. Summary of Presentations.....		9
SECTION IV. Presentations.....		17
DARPA Materials Science Division Interest in Nondestructive Microstructure Characterization		
R. E. Green.....		17
Acoustic Emission - Microstructure Relationships		
H.N.G. Wadley and R. Mehrabian.....		20
Ultrasonic Attenuation in Ceramics		
A. G. Evans.....		68
Measurement of Material Properties by Acoustic Methods		
G. S. Kino.....		70
Acoustic Microscopy For Materials Studies		
G.A.D. Briggs.....		73

<u>TITLE</u>	<u>PAGE</u>
Ultrasonic Scattering as a Method of Grain Structure Characterization E. P. Papadakis.....	89
Ultrasonic Nondestructive Characterization of Metallurgical Microstructures and Transformations M. Rosen and R. Mehrabian.....	103
The Measurement of Residual Stress by X-ray Diffraction M. R. James.....	127
New Applications of Electromagnetic-Acoustic Transducers: Determination of Residual Stress in Plates and Nondestructive Evaluation of Butt Weldments C. M. Fortunko, R. B. King and R. E. Schramm.....	141
Application of Synchrotron Radiation to Materials Science M. Kuriyama and W. J. Boettinger.....	164
Photothermal Imaging Applied to Microstructural Analysis J. C. Murphy and L. C. Aamodt.....	186
Nondestructive Characterization (NDC) by Means of Eddy Current Conductivity Testing M. Rosen, H. T. Yolken and R. Mehrabian.....	204
New Destructive Evaluation of Defects Using Long Wavelength Neutrons B. B. Rath.....	213
Nondestructive Microstructure Characterization - Comments M. Cohen.....	218
Nondestructive Microstructure Characterization - Comments J. P. Hirth.....	221
Comprehensive Requirements for Nondestructive Microstructure Characterization J. C. Williams.....	222
Optical Techniques for ND Materials Characterization J. W. Wagner.....	226
SECTION V. Agenda.....	230
Attendees.....	232

PART B		
<u>TITLE</u>		<u>PAGE</u>
SECTION I.	Introduction.....	1
SECTION II.	Key Issues.....	2
SECTION III.	Summaries of Sessions	
	A. Session I.....	11
	B. Session II.....	14
	C. Session III.....	15
	D. Discussion Session - L. A. Jacobson.....	19
SECTION IV.	Summaries of Presentations	
	Introductory Remarks	
	L. A. Jacobson.....	24
	Studies of Some Microstructure - Property Relationships	
	J. C. Williams.....	26
	Ideal Microstructures for Resistance to Hydrogen Assisted and Stress Corrosion Fracture	
	A. W. Thompson.....	29
	Ideal Microstructures in Precipitation Hardening	
	A. J. Ardell.....	31
	Ideal Microstructures	
	J. D. Embury.....	35
	Applications of RSP	
	J. D. Embury.....	37
	Some Ideal Microstructures from the Standpoint of RSP	
	M. Cohen.....	38
	Optimum Microstructure	
	B. B Rath.....	40
	Toughening Mechanisms in Brittle Solids	
	A. G. Evans.....	42
	Hydrogen Effects on Ductile Fracture and Plastic Instability	
	J. P. Hirth.....	44
	Strain Rate Effects	
	R. Stevenson.....	46

<u>TITLE</u>	<u>PAGE</u>
Microstructure, Continuum Mechanics and Material Instabilities B. Budiansky and J. W. Hutchinson.....	48
Ideal Microstructures via RSP R. Mehrabian.....	50
SECTION V. Program and List of Attendees.....	52
SECTION VI. Contributions Developed at the MRC Summer Meeting	
Overview of Fracture B. Budiansky, A. G. Evans, J. P. Hirth and J. W. Hutchinson.....	54
On Mechanical Connections Between Strength and Toughness B. Budiansky, A. G. Evans and J. W. Hutchinson.....	59
Ductility Variations with Volume Fraction and Strength of Inclusions J. W. Hutchinson, B. Budiansky and A. G. Evans.....	67
Crystal Slip Factors in Brittle Fracture Initiation J. P. Hirth.....	75
Cleavage Fracture in Mild Steels A. G. Evans and J.W. Hutchinson.....	88

PART C

<u>TITLE</u>	<u>PAGE</u>
Considerations on the Supercomputer Chip D. K. Ferry, T. C. McGill, R. S. Bauer, H. Ehrenreich, G. H. Vineyard, P. A. Wolff, and M. S. Wrighton.....	1
Very Small and High Speed Semiconductor Devices T. C. McGill, D. K. Ferry, H. Ehrenreich and R. S. Bauer.....	7
Diagnostics for VLSI Semiconductor Devices R. S. Bauer and T. C. McGill.....	26
Device Scaling Limitations of VLSI Diagnostics R. S. Bauer.....	47
Schottky Barrier Infrared Charge Coupled Device Arrays T. C. McGill and D. K. Ferry.....	52

<u>TITLE</u>	<u>PAGE</u>
Possible Improvements in Schottky Barrier Infrared Charge Coupled Device Arrays T. C. McGill.....	63
Magnetic Semiconductors: Report of Meeting H. Ehrenreich.....	72
Dislocations, Jogs, and Vacancies in (HgCd)Te H. Ehrenreich and J. P. Hirth.....	81
Speculations Concerning Applications of Semimagnetic Semiconductors P. A. Wolff.....	90
The Semiconductor Space-Charge Triode D. K. Ferry and T. C. McGill.....	100
Opportunities for Research in Conducting Polymers and Monolayer Techniques M. S. Wrighton.....	110

PART D

<u>TITLE</u>	<u>PAGE</u>
DARPA Perspective on Polymer Opportunities R. E. Green.....	1
Opportunities in Polymers J. L. Margrave.....	3
Solid State Properties of Polymer Blends F. E. Karasz.....	14
Mechanical Properties of Polymers L. K. DeVries.....	27
Durability of Polymers R. K. Eby.....	48
Engineering Aspects of Composite Materials K. L. Reifsnider.....	53
Nondestructive Evaluation of Composites E. G. Henneke.....	58
Nondestructive Evaluation of Polymers G. S. Kino.....	72
Materials With Controlled Damping Properties P. H. Lindenmeyer.....	80

PART E

<u>TITLE</u>	<u>PAGE</u>
Acoustic Microscopy R. Mehrabian.....	1
Quantitative Applications of Acoustic Microscopy to Microstructural Evaluation G. S. Kino.....	3
Acoustic Attenuation and Velocity Measurement as a Probe for Measurement of Microstructure and Residual Stress in Metals G. S. Kino.....	16
The Effects of Dislocations on Acoustic Attenuation in Metals G. S. Kino.....	29
Measurement of Attenuation Due to Dislocations G. S. Kino.....	32
Acoustic Attenuation and Velocity Change in Two Phase Materials G. S. Kino and A. G. Evans.....	44
Effects of Precipitates on Acoustic Attenuation A. G. Evans and J. C. Williams.....	47
Prospects for Acoustic Emission Determination of Microstructure and the Control of Metals Processing Hayden Wadley.....	50
Comments on the Workshop on Nondestructive Microstructure Characterization G. H. Vineyard.....	51

PART F

<u>TITLE</u>	<u>PAGE</u>
Nonlinear Optical Materials for Laser Protection A. Macleod and L. E. Cross.....	1
A Proposed Breakdown Switch for Laser Protection G. H. Vineyard.....	15
The Fundamental Limits on the Spectral Purity of Laser Fields A. Yariv.....	24
Photorefractive Materials and Optical Processing A. Yariv, C. M. Stickley, E. Cross and A. Macleod.....	40

PART G

<u>TITLE</u>	<u>PAGE</u>
Carbon/Carbon Turbine Engines E. E. Hucke.....	1
Comments on Carbon/Carbon Composites Development J. C. Williams.....	5
Carbon-Carbon Engine A. Macleod.....	8
Energetic Materials J. L. Margrave.....	10
A High Energy Shaped Microcomposite Explosive System E. E. Hucke.....	21
Some Comments on the Relationship Between Fracture Modes in Stress Corrosion Cracking J. C. Williams.....	22
Stress Intensity Factors of Delaminated Surface Coatings J. W. Hutchinson, B. Budiansky and A. G. Evans.....	25
On Size Effects in Void Nucleation A. G. Evans, J. W. Hutchinson and B. Budiansky.....	32
Some Comments on the Directionality of Hot Rolled Titanium Plate J. C. Williams.....	37
Synchrotron Radiation J. W. Wagner.....	39
Comments on "Doping a Plastic Scintillator" by Dr. B. D. Geelhood, Naval Ocean Systems Center M. Wrighton and T. C. McGill.....	41
Kinetics and Energetics of Sublimation of C_n and/or M_xC_y Species from Graphite and from Metal Carbides J. L. Margrave.....	44
Infrared Matrix Isolation Spectrum of the Si_2C Molecule Z. Ismail, R. H. Hauge, L. Fredin, J. L. Margrave.....	48

Forword

This collection of papers does not constitute a formal reporting of the activities of the DARPA Materials Research Council Summer Conference. Each report, memoranda or technical note is a draft of the author or authors and is their work alone. The Steering Committee, in conjunction with the authors, will decide how this material can best be presented as a formal report to DARPA.

STEERING COMMITTEE

Dr. George H. Vineyard
Division of Applied Sciences
Harvard University
Pierce Hall
Cambridge, MA 02138

Professor Henry Ehrenreich
Pierce Hall
Harvard University
Cambridge, MA 02138

Professor John P. Hirth
Metallurgical Engineering Dept.
Ohio State University
Columbus, OH 43201

Professor Thomas C. McGill
Applied Physics Dept.
M.S. 128-95
California Institute of Technology
Pasadena, CA 91125

Dr. Robert Mehrabian
National Bureau of Standards
Washington, DC 20234

PROJECT DIRECTOR

Professor Maurice J. Sinnott
Project Director
Chemical Engineering Dept.
2094 H. H. Dow Building
The University of Michigan
Ann Arbor, MI 48109

PARTICIPANTS

Dr. Robert S. Bauer
4538 Alpine Road
Portola Valley, CA 94025

Professor Bernard Budiansky
Division of Applied Sciences
Pierce Hall
Harvard University
Cambridge, MA 02138

Professor Brice Carnahan
Computer Consultant
Chemical Engineering Dept.
3146 H. H. Dow Building
The University of Michigan
Ann Arbor, MI 48109

Professor Leslie E. Cross
Electrical Engineering
Pennsylvania State University
251A Materials Research Labs.
University Park, PA 16801

Professor Anthony G. Evans
University of California
Lawrence Berkeley Labs.
1 Cyclotron Road
Berkeley, CA 94720

Professor David K. Ferry
Dept. Electrical Engineering
Colorado State University
Fort Collins, CO 80523

Professor Edward E. Hucke
Assoc. Project Director
Dept. Mat. & Met. Engineering
2090 H. H. Dow Building
The University of Michigan
Ann Arbor, MI 48109

Professor John W. Hutchinson
Div. of Applied Sciences
316 Pierce Hall
Harvard University
Cambridge, MA 02138

Professor Gordon S. Kino
Ginzton Laboratory
Stanford University
Stanford, CA 94305

Professor Angus Macleod
Optical Science Center
University of Arizona
Tucson, Arizona 85721

John L. Margrave, Vice President
Rice University
316 Lovett Hall
Houston, TX 77001

Professor J. C. Williams
Metallurgy & Materials Science
Carnegie-Mellon University
Pittsburgh, PA 15213

Professor P. A. Wolff, Director
Bitter National Magnet Laboratory
Massachusetts Inst. of Technology
Cambridge, MA 02139

Professor Mark S. Wrighton
Department of Chemistry
Room 6-335
Massachusetts Inst. of Technology
Cambridge, MA 02139

Professor Amnon Yariv
Electrical Engineering Dept.
California Institute of Technology
Pasadena, CA 91125

SECTION I
REPORT ON THE DARPA-MRC MEETING
ON
NONDESTRUCTIVE MICROSTRUCTURE CHARACTERIZATION

R. Mehrabian and A. G. Evans

INTRODUCTION AND OBJECTIVES

A two day workshop on Nondestructive Microstructure Characterization was held on July 6-7 as a portion of the 1982 MRC meeting. The program and list of attendees are appended (Section V. of this report). The objectives of the workshop were:

- To review the present status of specific nondestructive microstructure characterization techniques, and to identify future scientific and technological goals.
- To discuss the strengths and limitations of those techniques that may be used for in-situ monitoring and control of microstructural changes and residual stresses during processing. Emphasis is also placed on techniques that may be used on components at intermittent steps during fabrication, as well as in the finished products.
- To examine the potential of new techniques such as acoustic microscopy and synchrotron radiation for studying microstructural features of materials, as corollary tools to established techniques such as analytical electron microscopy.

The results of the workshop are presented in three sections of the following report. Section II presents key issues regarding the present status and future directions that emerged from the workshop. Section III contains a summary of the different sessions, and Section IV is a series of individual contributions. The latter contributions include summaries of presentations, prepared discussions and comments.

SECTION II

KEY ISSUES

At the workshop, a number of presentations were made by invited specialists in different areas of nondestructive microstructure characterization and residual strain determination.

These included:

Microstructure Characterization	• Acoustic Emission
	• Ultrasonic Scattering
	• Acoustic Microscopy
	• X-ray and Synchrotron Imaging
	• Photothermal Imaging
Residual Strain Analysis	• Acoustic Velocity and Phase Changes
	• X-ray Analysis of Residual Strain

These presentations, together with spontaneous discussion, led to the elucidation of some key issues representing the present status, research needs, technological applications, and potential of specific techniques for in-situ monitoring of microstructural and residual strain changes during processing. An outline of these key issues now follows. References are provided to the summary and the detailed presentations in Sections III and IV, where appropriate.

FUNDAMENTALS

Acoustic Emission

1. General formalisms now exist for prediction of acoustic emission (AE) waveforms associated with the formation of infinitesimal microcracks, gliding dislocations and phase transitions in linear elastic isotropic bodies of simple geometry

(such as the infinite half-space and the infinite plate). Further work is required to predict signals from finite sized sources in elastic bodies with anisotropy and attenuation (Wadley and Mehrabian).

2. The inverse problem (determination of the AE source function from a set of measured signals) still lacks a general solution. New deconvolution methods need to be developed and applied to the problem of source characterization. In addition, critical experiments are required, wherein the acoustic emission from real microstructural changes can be controlled and its properties independently deduced. For example, an ideal source may be the fracture of selective grain boundaries in a unidirectionally solidified specimen subject to a high intensity pulsed laser (or electron beam heat flux). Alternatively, the martensitic transformation of discrete small precipitates may constitute a predictable source. The transformation may be thermally generated (during cooling) or stress induced. Systems with the requisite microstructural control include Fe particles in Cu and tetragonal ZrO_2 particles in partially stabilized ZrO_2 .

Ultrasonic Scattering

1. A generalized theory of scattering in a single phase polycrystal containing a size distribution of equiaxed grains, has not yet been developed. Such a theory is needed if the inverse problem of uniquely characterizing the grain size distribution from acoustic attenuation or backscattering is to be realized. The essential theoretical basis for the problem is

available. However, the analysis is unwieldy and continued effort is needed to provide the requisite solutions.

2. Important textural effects on scattering require further theoretical and experimental study. Again, the essential theoretical principles are available, but substantial effort is needed to generate useful solutions of general applicability. Two major effects need to be distinguished in this context: preferred grain orientation and grain distortion. Preferred orientation effects without distortion can be directly incorporated into theoretical scattering descriptions for equiaxed grains; Fe-3% Si steel would provide a good model for experimental validation (Cohen). Grain distortion effects provide an additional element of difficulty; but regarding the grains as an array of cylinders with preferred orientation may be analytically tractable and should be pursued.

3. Effects of precipitation on scattering are known to exist, but fundamental descriptions of the scattering process are not available. Precipitates at peak hardness are invariably too small to be regarded as individual scatterers. Hence, their influence on scattering resides in their effect on the impedance of the grain (primarily through the elastic anisotropy). Fundamental descriptions of this problem are clearly feasible, based on composite theory. Experimental measurements of local changes in impedance during precipitation, using the acoustic microscope, are an important adjunct to studies of precipitation effects.

4. Most available studies of ultrasonic scattering have been confined to attenuation measurements, which provide an assessment of the microstructural entities averaged over the path length of the acoustic wave. Additional spatial information can be obtained using backscattering measurements. This possibility can be readily exploited with available measurement techniques.

5. The presence of dislocations can also contribute to ultrasonic attenuation by internal friction mechanisms. However, significant levels of attenuation (relative to grain scattering), in the MHz range, only obtain when the product of the loop lengths and densities of the mobile dislocations is relatively large. Consequently, modest levels of work hardening are known to contribute significantly to attenuation (attenuation $\propto f^2$), in some cases. It has also been conjectured (Rosen) that matrix dislocations created around precipitates following the transition to incoherence may induce significant attenuation. This suggestion requires further study, with emphasis on the mobile dislocations generated by precipitation, coupled with the frequency dependence of the attenuation.

Acoustic Microscopy

Advanced acoustic microscopes, such as those at Stanford (Quate) and Oxford (Briggs), offer unique opportunities for probing certain near surface microstructural features on polished test specimens. It is clearly evident that the technique (by virtue of its sensitivity to local differences in acoustic impedance), is capable of detecting cracks, delaminations or

voids of lateral extent $> 10 \mu\text{m}$, subject to residual opening. This unique advantage requires further exploitation. Grains can also be distinguished (this is not, of course, a unique capability). The other microstructural features capable of identification in the acoustic microscope are not yet evident. Theoretical scattering analysis, coupled with systematic observations, are needed to permit the full potential of the acoustic microscope to be realized.

Synchrotron Radiation

The unique characteristics of synchrotron radiation (high photon flux and tunability) permit its application to the study of important materials science problems ranging from oxidation to phase transformation. For example, the high photon flux of the synchrotron should permit reduced data acquisition times, and hence, dynamic real-time studies of metallic glass crystallization, grain boundary migration, precipitation and ordering phenomena.

PROCESS CONTROL

Acoustic Emission

1. Acoustic emission has been highly successful for in-process monitoring of spot welding and heavy section welding (Wadley and Mehrabian). The technique is used to detect certain crack and void formation processes. The primary limitation of this technique (that requires further study) is concerned with the present inability to assess defect severity, on-line, and hence, to provide a unique repair criterion.

2. There is a clear potential to further develop acoustic emission, both for in-process control of microstructure and detection of crack formation. For example, it is quite probable that correlations may be deduced between acoustic emission and microstructure during directed high energy surface melting and resolidification. Control of heat flux distributions and scanning speeds could be coupled to a feedback system that senses spiking (deep penetration) during melting or hot tearing (cracking) during resolidification. Exploratory studies to search for such correlations are clearly required.

3. Critical experiments are also required to indentify the ranges of fault conditions that may be reliably detected for various materials processing procedures. For example, can fish-tail cracking be detected during rolling? The early detection of such fault conditions would produce improved process efficiency and product quality.

Ultrasonic Scattering

1. New experimental techniques are being developed for acoustic nondestructive characterization of metallurgical microstructures using state of the art laser and optical technologies. Examples include real-time monitoring of certain precipitation processes, grain growth, and post-transformation characterization in processes such as rapid solidification (e.g., determination of the extent of solute supersaturation). Both basic work to enhance our understanding of the phenomena

involved, and applied work to exploit these new techniques in metallurgical processing are needed (Rosen and Mehrabian).

2. Progress has recently been made in our understanding of the various structural changes (e.g., martensitic transformations, coherent and incoherent precipitation, decomposition of retained austenite, etc.) that occur during aging and tempering of Fe-Ni-C martensitic alloys. The development of acoustic methods and measurements that relate to these well-documented microstructural features may have direct practical application to many aspects of steel technology (Cohen).

X-Ray Analysis of Residual Strain

Improvements in x-ray generation and detection are bringing measurement times down to the order of minutes. While this may not be sufficiently fast for real-time monitoring of surface residual stresses during processing, it is very useful for intermittent sampling of components to test for consistency in process control. Examples of applications include carburizing, nitriding, grinding and surface heat treatments, all of which produce residual stress fields that can be optimized.

SECTION III

SUMMARY OF PRESENTATIONS

Wadley reviewed the current understanding of the relationships between source events and acoustic emission signals. These relationships were used to account for experimental observations of the microstructural sensitivity of plasticity and fracture generated acoustic emission in several aluminum alloys and a model ferritic steel. The strengths and weaknesses of the acoustic emission technique for in-process monitoring and microstructural control were also noted. It was pointed out that the intensity of acoustic emission from deformation, fracture and phase transitions is very dependent upon microstructure. Using existing instrumentation, it should now be possible to search for empirical correlations (at least for specific materials systems) between properties of acoustic emission and critical metallurgical variables, such as grain size, precipitate type and distribution, inclusion content. etc., and to explore the feasibility of using such relations for in-process monitoring and control of microstructures. More fundamentally based correlations between microstructure and acoustic emission await further theoretical development and improved transducers/signal processing capabilities.

Welding was used as an example of a very promising ongoing application of acoustic emission for in-process monitoring. The major weakness of acoustic emission in this application is an inability to uniquely identify the source from the detected

signals. New measurement methods (recently developed at NBS) have introduced the potential for measuring the source properties of martensitic phase transformation, as well as, cracks formed during rapid solidification of metallic substrates (subjected to high intensity laser and electron beam sources). Further development of these techniques, coupled with improved understanding of the dynamic properties of the sources involved, would serve as good laboratory examples of acoustic emission in-process monitoring.

Acoustic scattering measurements were described by Evans, Papadakis and Kino. These clearly provide a basis for measuring the size distribution, at the large extreme, of the largest microstructural features (grains, pores, inclusions) in predominantly single phase random polycrystals. This can be achieved using one of two available theoretical approximations (Papadakis, Evans), which appear to exhibit adequate predictability (albeit that the development of a more comprehensive theory should be encouraged). The measurement technique requires both the determination of the attenuation over an appreciable range of frequency (e.g., about an order of magnitude) and a matching of the attenuation with curves predicted for a range of scale and shape parameters (descriptive of grain and pore size distributions). Short pulses contain a sufficient frequency range to permit such measurements to be accomplished quickly (given the appropriate signal analysis capability). However, it should be recognized that few measurements of this

type have been conducted at this juncture; hence, the precision and reproducibility of the technique requires careful assessment before proceeding.

The utility of scattering techniques for assessing the microstructure of multiphase materials is less evident, especially when these microstructures are not well characterized by other techniques. Existing data (Papadakis, Kino, Rosen) clearly indicate effects of precipitates on attenuation, suggestive of the potential for gaining microstructural information from scattering data (at least on specific systems). The influences of precipitates on scattering are presumably predicated through their influence on the elastic constants of the grains. However, measurements of changes in these constants with precipitation (e.g., using acoustic microscopy), or the use of available modulus predictions, to rationalize measured scattering trends have not been attempted. Such studies can clearly be conducted with available measurement techniques and theoretical descriptions. The product of systematic studies of this type would permit rational judgements concerning the potential of scattering measurements for microstructural characterization.

New ultrasonic generation, detection and analysis techniques employing state of the art laser and optical technologies for real-time monitoring of solid state transformations are becoming available (Rosen). Examples were given of precipitation processes in aluminum alloys and crystallization of metallic glasses. Careful measurements were made on specific alloy

systems coupled with other microstructural characterization techniques (e.g., electron microscopy) to correlate changes in ultrasonic velocity and attenuation to crystallization and loss of coherency during precipitation, respectively. These preliminary experiments show applicability of ultrasonic characterization, for both property determination and metallurgical process control. However, the full long range potential of these techniques can only be realized through a better coupling of emerging scattering and internal friction theories, with specific experiments in which microstructures are carefully controlled and characterized.

Ultrasonic determinations of residual stress, described by Kino and Fortunko, are predicated upon measurements of local changes in acoustic velocity or phase. The changes that require measurement are small relative to absolute values, and hence, effects of microstructural variability on the absolute quantities require systematic elimination. Internal, local calibration of the absolute velocity and phase are thus needed to obtain reasonable estimates of the residual stress. This requirement has, thus far, restricted the general utility of acoustic techniques. Some success has been achieved by applying known loads to a component, in order to obtain the local calibration coefficients from the consequent changes in velocity or phase. However, further research is needed to develop an acoustic technique for unambiguous residual stress determination.

The acoustic techniques, given the eventual capability for internal calibration, offer several important advantages (relative to x-ray methods). Focused transducers, in principle, allow element-by-element residual strain analysis, and hence, are not restricted to the near surface. Alternatively, surface waves permit the surface stresses to be probed over a depth similar to the wavelength of the induced Rayleigh wave. Equally important, electromagnetic transducers permit such measurements to be made in a noncontact mode. However, the necessity for element-by-element velocity and phase calibration, as a prerequisite for effective stress determination, is re-emphasized.

X-ray methods of residual stress analysis, summarized by James, have now reached a sufficient level of sophistication that very accurate determinations, averaged over the depth of x-ray penetration, are now feasible. The instrumentation required for this purpose has not yet been incorporated into portable x-ray machines, but this development involves tractable technological problems. The principal limitation of the x-ray method for nondestructive, in situ, stress determination resides in its limited penetration depth ($\sim 20\mu\text{m}$) at the required wavelengths. This limitation is unlikely to be circumvented. Nevertheless, the extensive application of the x-ray method clearly provides invaluable information about the order and spatial variation of the residual stress in the near surface.

The best application of x-ray surface analysis can be in the optimization of specific manufacturing processes. These in-

clude case carburizing and nitriding, grinding procedures, and heat treatments with laser and induction heating, all of which produce residual stress fields that can be optimized.

The acoustic microscope, by imaging the interaction between longitudinal and Rayleigh waves, provides an acoustic image of the near surface, as described by Briggs and Kino. This image is associated with microstructural entities that exhibit deviations in acoustic impedance, as well as, lateral dimensions exceeding the wavelength of the acoustic wave ($\sim 10 \mu\text{m}$ for most microscopes). Deviations from surface planarity are also imaged by the longitudinal, Rayleigh wave interaction. Near surface microcracks, voids and delaminations, subject to residual openings, can thus be uniquely probed using the acoustic microscope. Inclusions with an acoustic impedance that differs significantly from the matrix impedance, can also be directly imaged. Additionally, certain internal interfaces are amenable to detection. For example, the change in acoustic impedance across grain boundaries permits the detections of such boundaries in materials containing suitably coarse grains. Domains and twin interfaces with the appropriate acoustic characteristics are also capable of detection.

The presence of small ($\sim 100\text{\AA}$) precipitates at grain boundaries, by modifying the acoustic impedance of the boundary, may induce detectable contrast changes that imply their presence. However, direct imaging of the precipitates is not possible at reasonable operating frequencies ($\sim 40 \text{ GHz}$). Simi-

larly, intragranular precipitates modify the impedance of the grains and change the grain contrast. These changes should be amenable to analysis, by using the microscope as an impedance (elastic) microprobe, at the grain size level. Specific determinations of grain impedance, using the acoustic microscope, are thus of direct utility for interpreting effects of microstructure on acoustic attenuation and backscattering. The acoustic microscope can thus provide microstructural information that complements information available from conventional (optical, electron, x-ray) techniques. However, it should be recognized that the method in its present form, has limited utility as a nondestructive technique, because polished, planar surfaces are required and only the near surface grains can be probed.

The unique characteristics of synchrotron radiation (high photon flux and tunability) permit its application to a range of problems in materials science (Kuriyama and Boettinger). Specific examples include application of EXAFS to obtain partial radial distribution functions in multicomponent metallic glasses and complex crystal structures, and determination of oxidation mechanisms under environmental conditions. X-ray topographic techniques, using both white and monochromatic beams, are also being developed for microstructural characterization, including mapping of strains or other lattice parameter variations within a material. The high photon flux of the synchrotron should also permit decreased data acquisition time,

hence, dynamic real-time studies of crack tip plastic zone development, in situ metallic glass characterization, and observation of precipitation and ordering phenomena.

Recent advances in photothermal imaging techniques (e.g., scanning photoacoustic detection and photothermal deflection imaging) and their possible application to surface microstructural analysis, were described by Murphy. Emphasis was placed on photothermal deflection imaging which in principle, should permit local measurement of thermal conductivity and heat capacity and their variations with microstructure across a sample surface. The technique utilizes an external laser (pump) heating source and a second laser beam (probe), which passes near and parallel to the heated surface and is deflected by the adjacent modulated gas temperature. Variations in thermal conductivity can then be deduced in principle by coupling these measurements to three dimensional heat flow calculations.

SECTION IV

DARPA MATERIALS SCIENCE DIVISION INTEREST IN NONDESTRUCTIVE MICROSTRUCTURE CHARACTERIZATION

R. E. Green

Currently, the Materials Sciences Division of DARPA is supporting efforts in several areas which can benefit from research in nondestructive microstructure characterization. In this regard, microstructure is to be taken in a broad, generic sense as any material alteration which plays a major role in influencing the physical properties. It is not the intent of non-destructive microstructure characterization to compete with optical or electron microscopic techniques, but rather to complement them by optimizing existing and developing new techniques for rapid determination of the physical properties of materials in bulk without the necessity of cutting out test specimens and preparing them for microscopic examination. There are several motivations for DARPA's interest in such efforts.

First of all we desire to improve our materials synthesis and processing methods by developing sensors and techniques for control of materials manufacturing processes. Such techniques would be capable of assessing the desired properties of the material being processed and, if the values of the properties measured deviated from those desired, feed-back to the processing system would change the parameters necessary to bring the material back into specification.

Secondly, we desire to be able to nondestructively assess the material characteristics of a variety of materials after manufacture to make certain that the materials meet specifications. If reliable nondestructive techniques could be established to do this a considerable saving in time and money would be the result.

The third main reason for desiring to develop techniques for nondestructively characterizing unflawed materials is that DARPA and other service agencies have supported a large amount of research over the past ten years in the area of nondestructive evaluation of materials emphasizing detection and sizing of cracks. One of the major reasons that these efforts have only met with partial success is that the response of the various measurement systems to the unflawed material was not determined prior to probing for cracks. Often the large grain size, multiple phases, or texture present in the base material either precludes detection of the flaws present or modifies the received signal so markedly that misjudgements are made as to the location and severity of the flaw. A prime example of this is the Air Force Retirement-for-Cause Program in which F-100 engine disks are to be nondestructively inspected for cracks, the severity of the crack assessed using fracture mechanics analysis, and a decision made as to whether or not to place the disk back in an aircraft engine or discard it. At the present time, no attention to any residual stress (strain) existing in the disk is considered in the analysis because there is no reliable

nondestructive technique which can measure the residual stresses (strains) in bulk specimens. Since very large residual stresses (strains) can be developed in these disks by a variety of means, the neglect of residual stresses (strains) clearly presents a serious hazard to the successful implementation of the Retirement-for-Cause Program.

In addition to DARPA support of the Retirement-for-Cause Program, other presently supported programs which will benefit from reliable nondestructive microstructure characterization techniques are laser aided machining, high speed machining, perfect welding, chemical ceramics processing, solid lubricated bearings, rapid solidification technology materials, failure of polymers, acoustic emission monitoring of crack growth, and a number of programs directed at the use of ultrasonics and eddy currents for the quantitative nondestructive evaluation of flaws.

ACOUSTIC EMISSION - MICROSTRUCTURE RELATIONSHIPS

H. N. G. Wadley and R. Mehrabian

ABSTRACT

Acoustic emission signals are the elastic waves emitted by sudden localized changes of stress; events that may occur during metals processing due to plastic deformations, cracking and phase transitions. In this review, the basic physical relationships between the source event and the temporal behavior of acoustic emission signals are presented and used to account for experimental observations of the microstructure sensitivity of plasticity and fracture generated acoustic emission in representative aluminum alloys and a model ferritic steel. These studies indicate acoustic emission provides complimentary dynamic information about the energetic deformation and fracture processes of solids. The contribution this information could make to both laboratory studies of metal processing and in process monitoring for feedback control on the production line are reviewed.

INTRODUCTION

Acoustic emission is the term we use for the elastic waves generated by abrupt localized changes of stress in a solid¹. The waves are detected with transducers which measure transient (ms-time scale) surface displacements of the body². The acoustic emission signal is thus the transient response of a body to deformation while a stress-strain curve would be the analogous static response to the same deformation.

Acoustic emission has received widespread study as a nondestructive evaluation (NDE) technique for monitoring structural integrity^{3,4} and as a laboratory tool to aid the study of deformation and fracture processes^{5,6,7,8}. More recently, it is beginning to be considered as a candidate technique for in-process monitoring.

The driving force for this latter application is recognition of the need to measure the changes that occur in materials during processing for quality control and feedback into the processing procedures to improve productivity. Because acoustic emission signals may be emitted by the very mechanisms by which a material responds to processing, it has great potential as an in-process NDE technique.

The purpose of this paper is to review the current understanding of the relationships between source events and acoustic emission signals and to use this to assess the strengths and weaknesses of the acoustic emission technique for in-process monitoring and microstructure control. It will be

shown that whilst the technique is not perfect for all aspects of metal processing control, it has much to offer for certain processing procedures, particularly the detection of cracking and monitoring of rapid phase transitions.

SOURCE-SIGNAL RELATIONSHIPS

Acoustic emission signals are generated by changes of stress in a body¹. Such stress changes are brought about by:

- Plasticity
- Cracking
- Phase transitions
- Thermal expansions, etc.

The elastic waves propagate from the source region and cause transient displacements of the body that can be detected with transducers and recorded electronically, Fig. 1¹⁰. We should like to measure these signals and use them to monitor metals processing.

Elastodynamic techniques have been applied with success to the prediction of acoustic emission from stress change sources^{5,9,11}. The basic approach consists of:

- Decomposition of the source into a combination of force dipoles (and higher order multipoles, if necessary) acting at a point, Fig. 2.
- Evaluation of the surface displacement waveform for each dipole component assuming step function time dependence (evaluate the body's dynamic elastic Green's tensor).

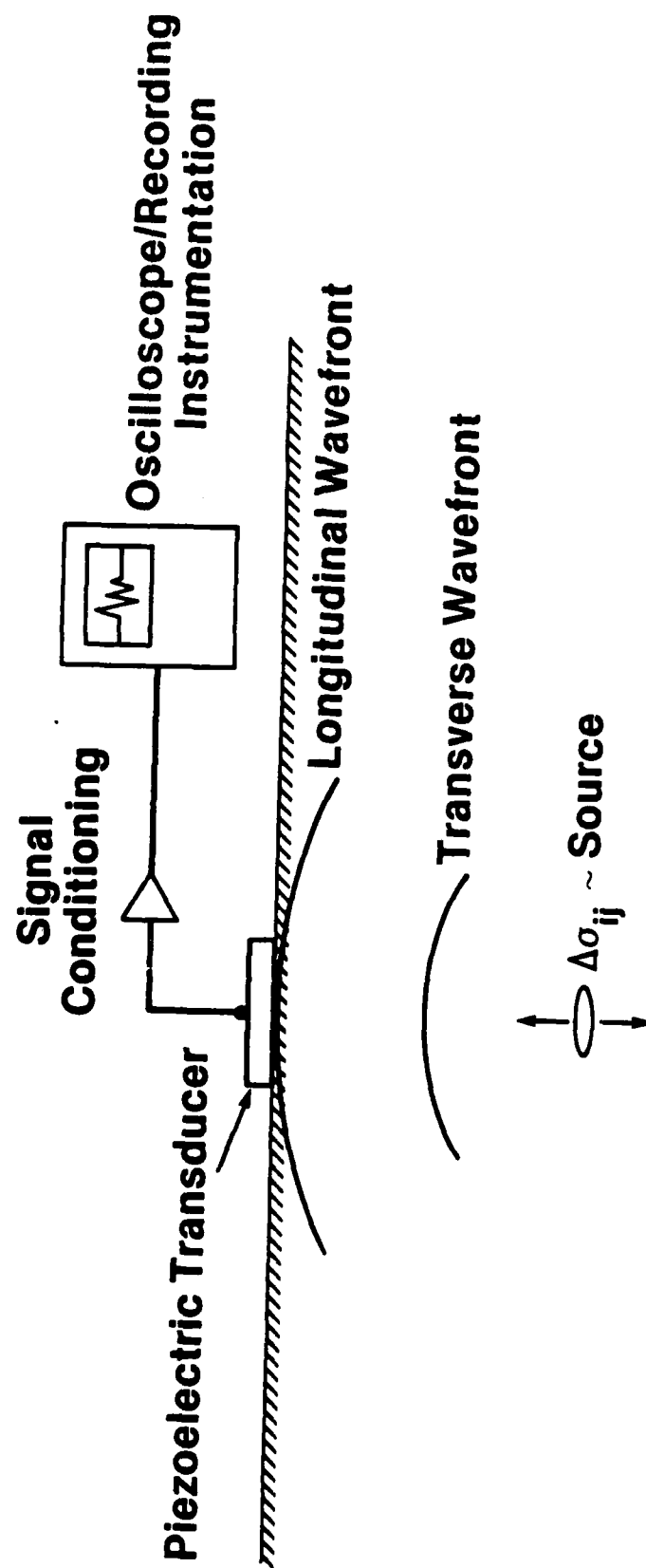


Fig. 1. The longitudinal and transverse elastic waves radiated by a stress change source propagate to the surface of a body causing transient surface displacements. These are converted, by a piezoelectric crystal, to a voltage-time waveform that can be recorded or observed on an oscilloscope.

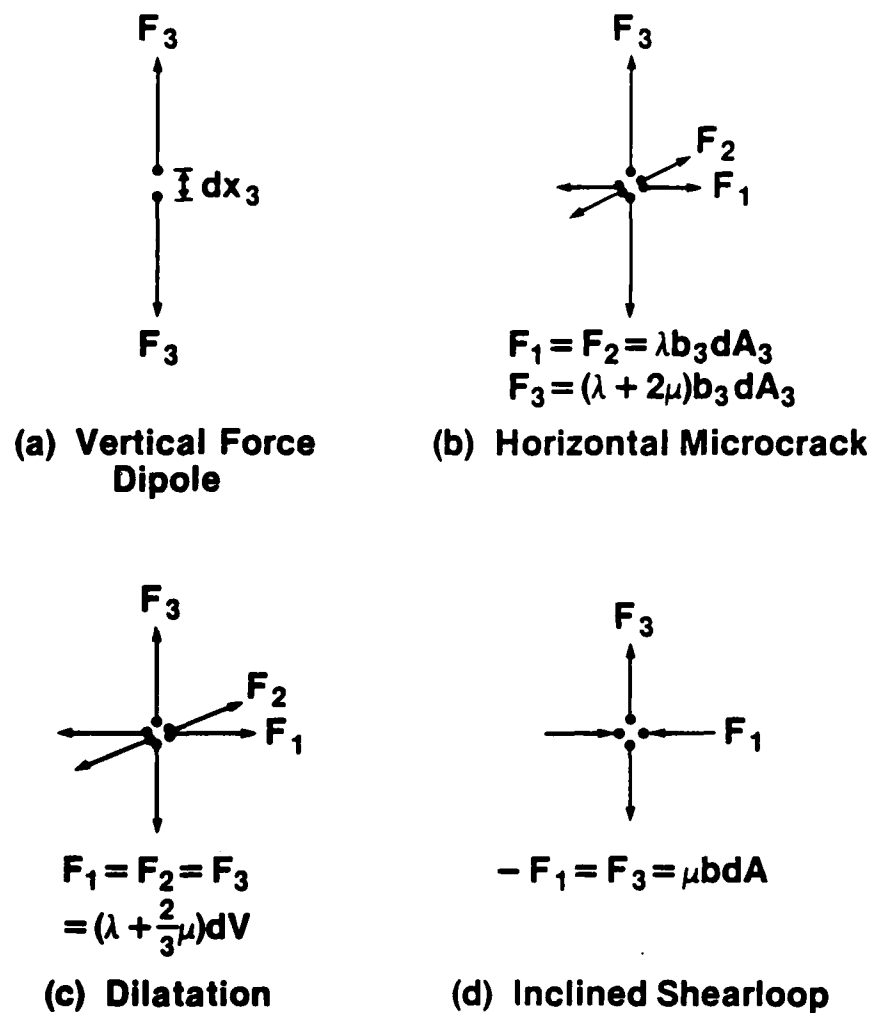


Figure 2. Force dipole representations of three acoustic emission source types; (b) the mode I crack, (c) the hydrostatic dilatation (thermal expansion/phase change) and (d) plastic flow. λ and μ are Lamé's constants for an isotropic elastic solid, b_3 the crack face opening, b the Burger's vector and dA the defect area.

- Addition of the waveforms of the dipoles representing the source and convolution with the source time function, Fig. 3.

The simplest, physically realistic, geometry to study is the elastic half-space. From Fig. 3, we see that acoustic emission signals at the epicentre of such a half-space¹¹ are dominated by a delta function at the longitudinal wave arrival time ($\sim 4\mu\text{s}$) and a step (tending to restore displacement towards zero) at the transverse arrival time ($\sim 8\mu\text{s}$). The dilation source generates no shear components reflecting the absence of shear deformations in the source.

The amplitude of the acoustic emission waveform is controlled by four factors:

- The strength of the source. That is the magnitude (units of Nm) of the individual dipole components.
- The orientation of the source with respect to the surface (and in the case of the microcrack, the principal stress axes).
- The duration, τ , of the source, Fig. 4, because the pulse area (amplitude-time product) is proportional to source strength. Increasing the width of the pulse, therefore decreases peak amplitude when source strength remains constant.
- The source-epicenter distance, Fig. 5, because of energy conservation in the spherically expanding wavefront.

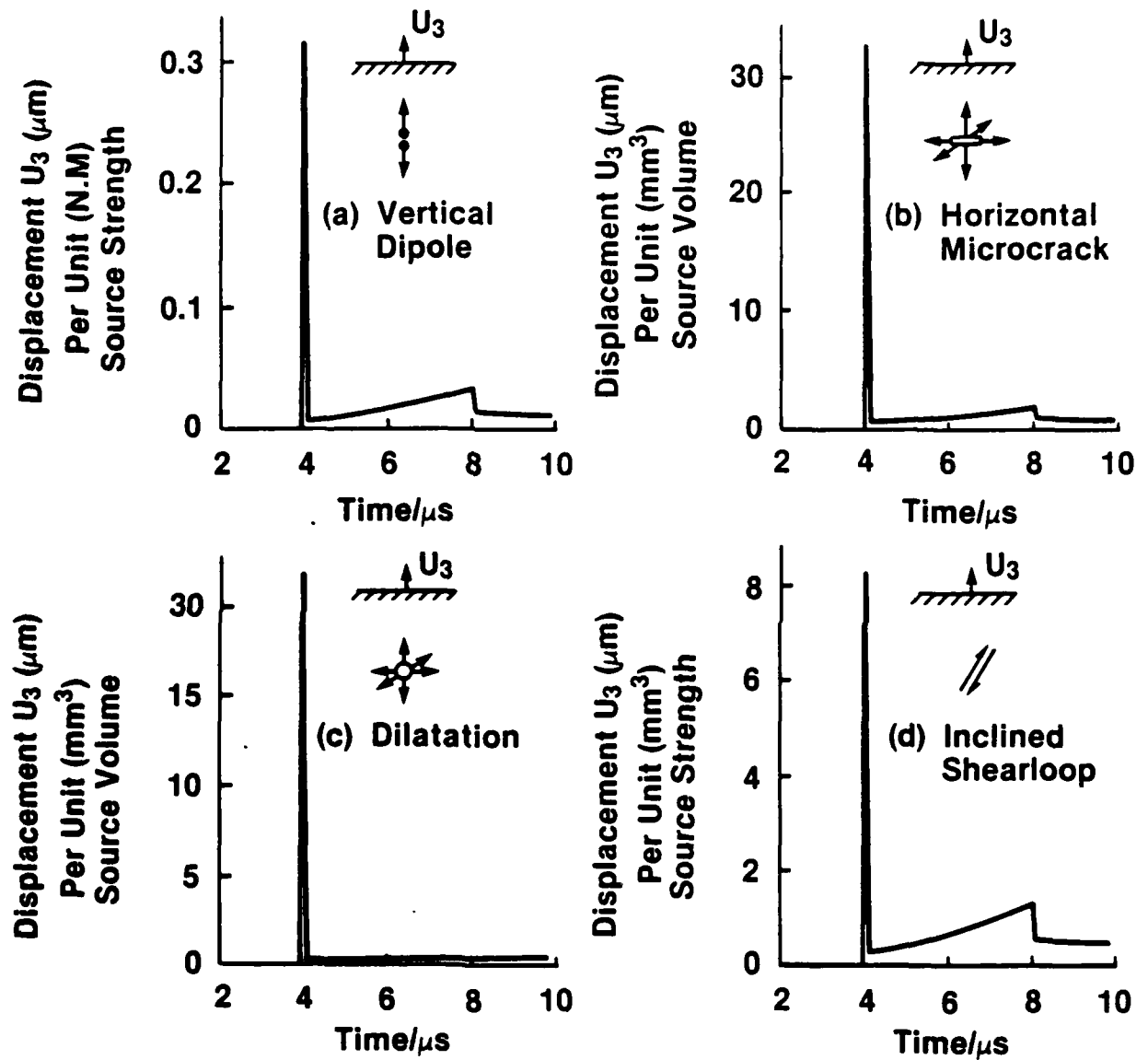


Figure 3. Vertical component of surface displacement waveforms evaluated at epicentre of a half-space for the acoustic emission sources of Fig. 2. The source-epicentre distance was 25 mm, the time dependence of the source assumed Gaussian (30ns half width), $C_1 = 6250 \text{ ms}^{-1}$ and $C_2 = 3125 \text{ ms}^{-1}$.

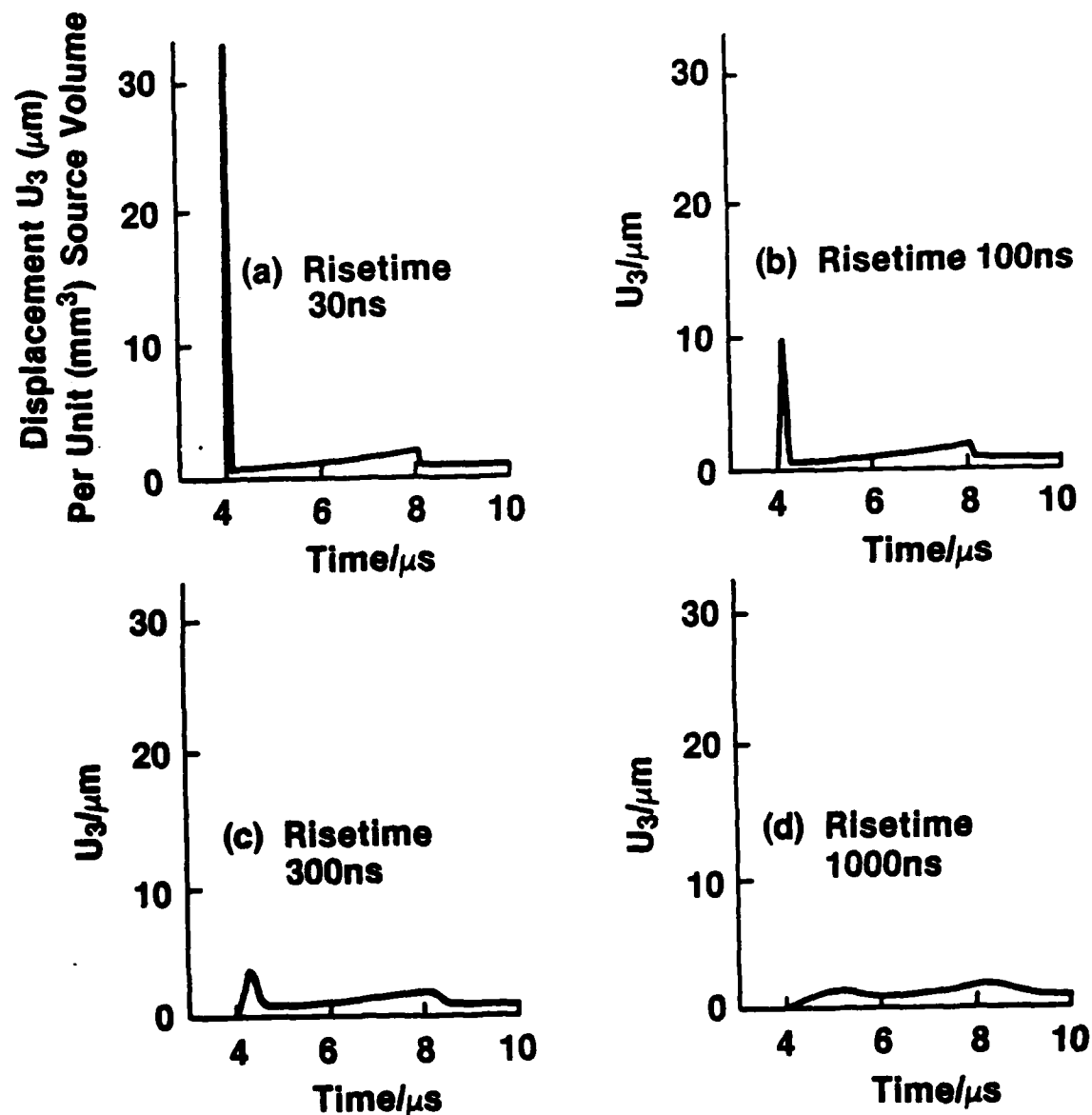


Figure 4. Showing the effect of increasing source duration for a mode I microcrack upon the surface displacement waveform. The area under the L arrival (at 4 μs) is proportional to source strength and so increasing the source duration reduces, proportionately, the peak amplitude.

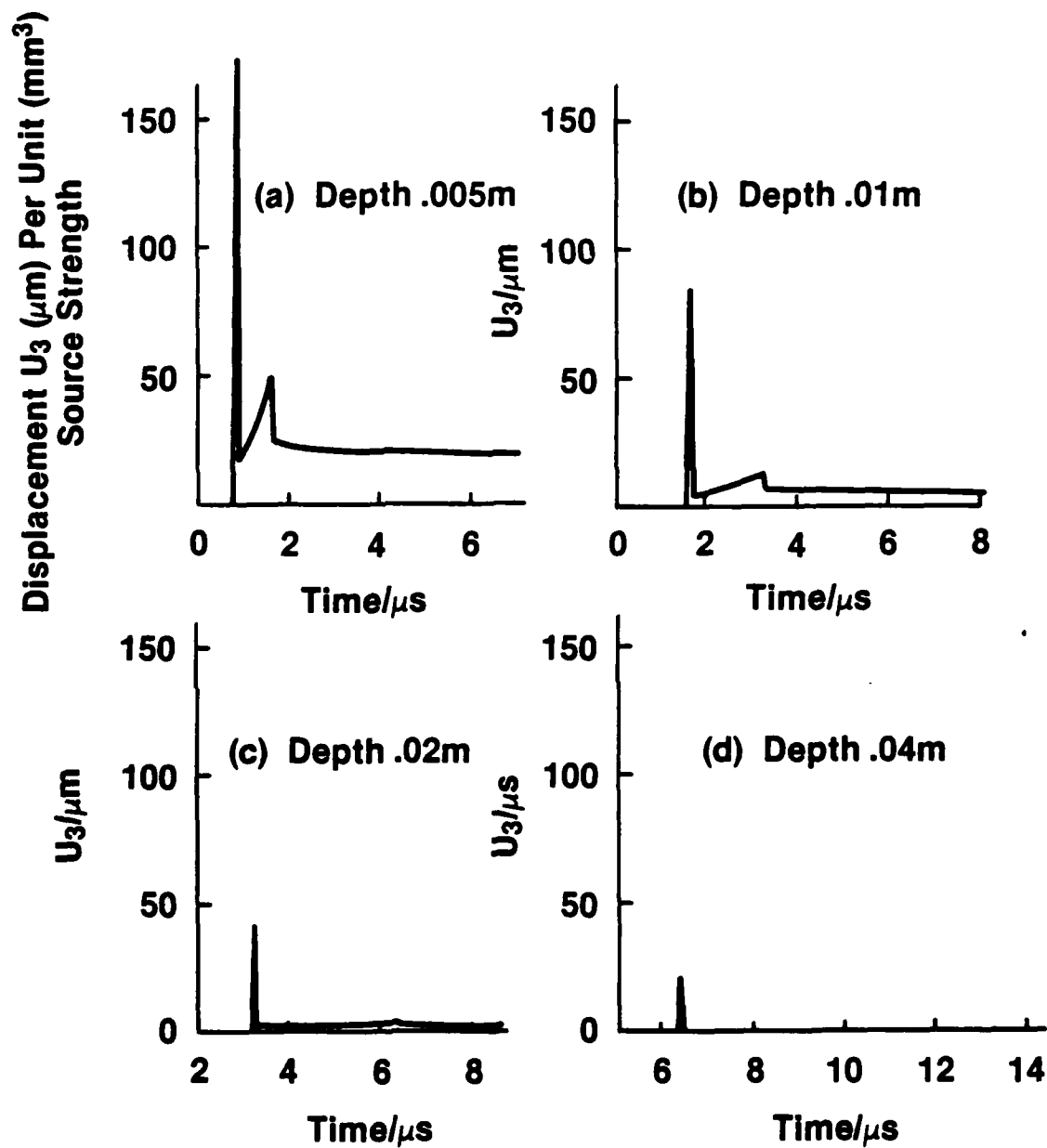


Figure 5. The effect of source-epicentre distance for the mode I microcrack source with a 30 ns duration.

These relationships are summarized in expressions for the delta function strengths and epicenter displacements of three source types in Table I.

TABLE I. Acoustic Emission Source Strength and Epicentre Displacement Relations

	Dislocation Source	Microcrack Source	Dilation Source
Source Strength	$C_2^2 b \delta A \sin^2 \theta$	$b_c \delta A \cos^2 \theta + \lambda \sin^2 \theta$	$(\lambda - \frac{2}{3} \mu) \delta v$
	$2\pi r c_1^3$	$2\pi r c_1 (\lambda + 2\mu)$	$2\pi r$
Epicentre Displacement	$b a v c_2^2$	$8(1 - \gamma^2) \sigma a^2 v$	$(\lambda + \frac{2}{3} \mu) \delta v$
	$r c_1^3$	$3 E c_1 r$	$2\pi r \tau$

where:

c_1 = Longitudinal wavespeed (ms^{-1})

c_2 = Transverse wavespeed (ms^{-1})

b = Burgers vector of dislocation (m)

δA = Area of source (m^2)

r = Source-epicenter distance (m)

θ = Angle of source to vertical

b_c = Crack opening displacement (m)

λ, μ = Lamé constants (Nm^{-2})

δv = volume expansion of source (m^3)

τ = Duration of source (s)
 a = Source radius (m)
 E = Young's Modulus (Nm^{-2})
 σ = Tensile stress (Nm^{-2})
 ν = Poison's ratio

The acoustic emission from metals is thus dependent upon the elastic properties (λ, μ) of the metal and also upon dynamic properties of the source. The dynamic properties in turn, are controlled by microstructure and test conditions. To give an illustration of this, we shall review a series of experiments where microstructure was the only variable and the relative acoustic emission response was measured during uniaxial tensile deformation.

MICROSTRUCTURE EFFECTS ON ACOUSTIC EMISSION FROM PLASTIC DEFORMATION

Single Crystal Aluminum

A typical result for the acoustic emission intensity (power) variation as a function of strain is shown in Fig. 6⁵. In the experiment, the sample was deformed at a constant slow strain rate and acoustic emission in the frequency range 0.1 to 1.0 MHz measured. We observe that the emission quickly reaches a maximum close to the initiation of plastic flow and that less emission is detected as the strain increases even though the strain rate (total amount of slip per unit time) remained constant.

0.1-1.0 MHz

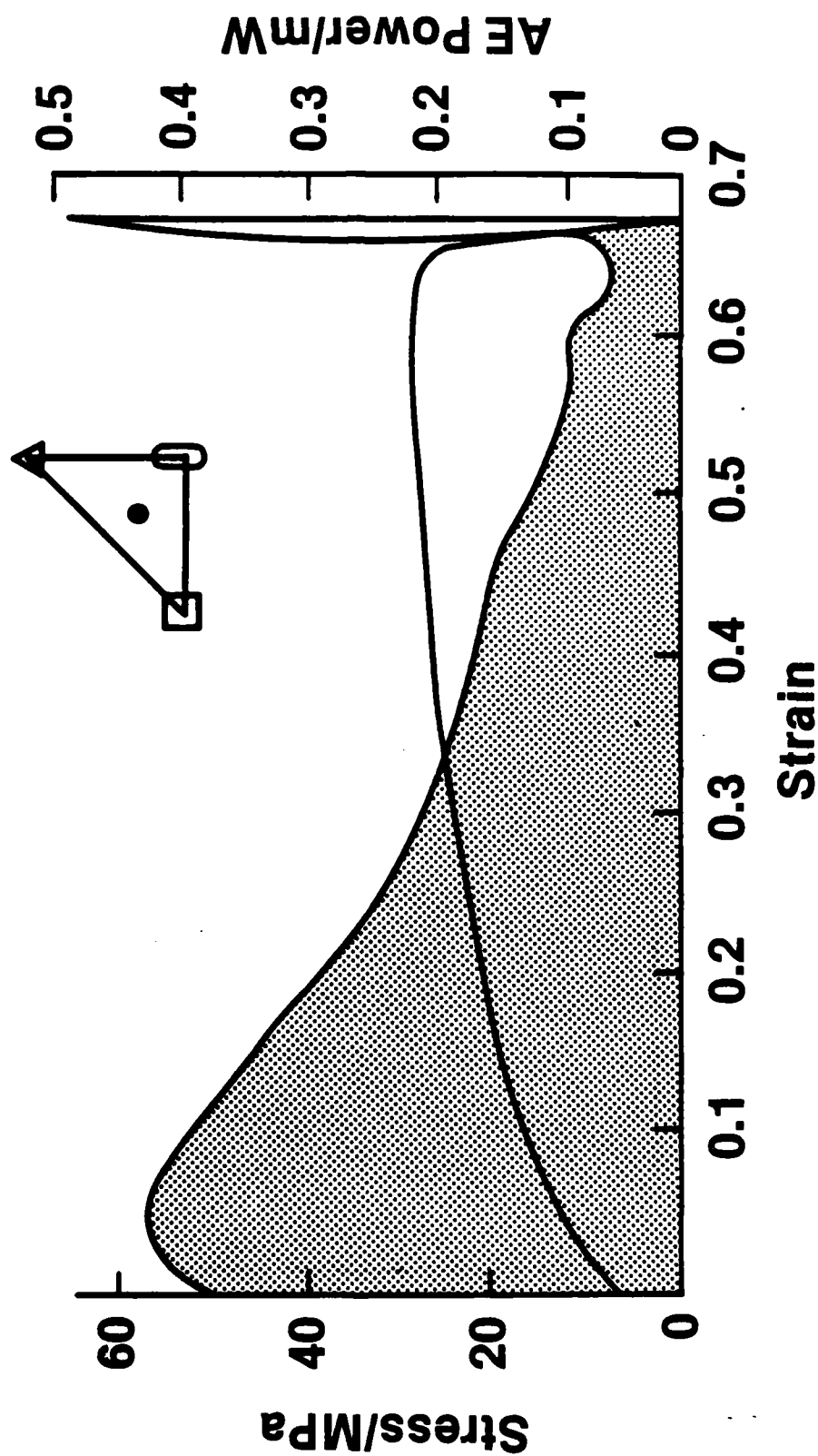


Fig. 6. The acoustic emission intensity (power) during the deformation of pure aluminum decreases with increasing plastic strain once the metal has yielded.

From Table I, we note the maximum displacement from an expanding dislocation loop with velocity v ,

$$U_3 = \frac{c_2^2 b a v}{r c_1^3}$$

Using the values of aluminum of $c_1 = 6400 \text{ ms}^{-1}$, $c_2 = 3200 \text{ ms}^{-1}$ and $b = 2.9 \times 10^{-10} \text{ m}$ and $r = 40 \text{ mm}$, we find

$$U_3 = a v \times (2.8 \times 10^{-13} \text{ sm}^{-1})$$

Now, the smallest displacement detectable with modern acoustic emission transducers is around 10^{-14} m . Using this for U_3 as the detectability threshold, leads to the following condition for a plastic deformation to give a detectable signal:

$$(n) \ a v > 0.035 \text{ m}^2 \text{ s}^{-1}$$

where n is the number of dislocations moving at any instant:

a = the distance of propagation

v = the dislocation velocity.

The a and v parameters of slip events are statistically distributed, Fig. 7, and only those events whose av products are at the extreme of the distribution can generate detectable signals.

At the start of deformation, a considerable fraction of slip events have a large enough value that even quite slow dislocations groups could give detectable signals. As work-

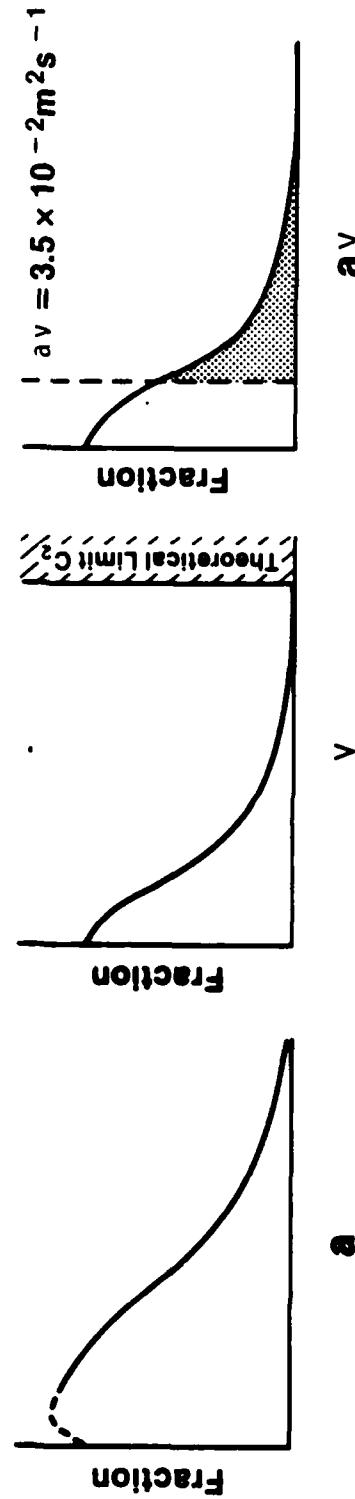


Figure 7. Schematic diagrams of the slip distance and velocity distributions and the distribution of the av product. Only events for which av exceeds a critical value are detectable.

hardening sets in, the dislocation propagation distance is lessened considerably and far fewer events are able to give emissions that can be detected leading to a decrease in detectable acoustic emission intensity.

Grain Size Effects

The introduction of grain boundaries should limit a to distances of the order of the grain size from the very start of deformation. Then, as a becomes less than some critical value determined by dislocation velocity, we would expect a decrease in detectable acoustic emission. This is what experiments have indicated in pure aluminum polycrystalline specimens, Figure 8^{5,10}. The grain size below which acoustic emission rapidly decreases is around 1 mm for which $a < 500\mu\text{m}$ and so $v > 70\text{ms}^{-1}$.

In alloys of aluminum, substitutional impurity segregation to dislocations can occur, even when the alloy element concentration is below the solid solubility. This can drastically alter dislocation velocity and lead to effects such as yield points and dynamic strain aging during deformation. The occurrence of these phenomena is accompanied by intense acoustic emission signals, Fig. 9. The occurrence of the phenomena and their associated emission vary greatly with grain size, Figure 10⁵.

The peak in acoustic emission at a grain size of 0.1mm arises from a competition between two effects:

- As the grain size increases a increases.
- As the grain size increases v decreases.

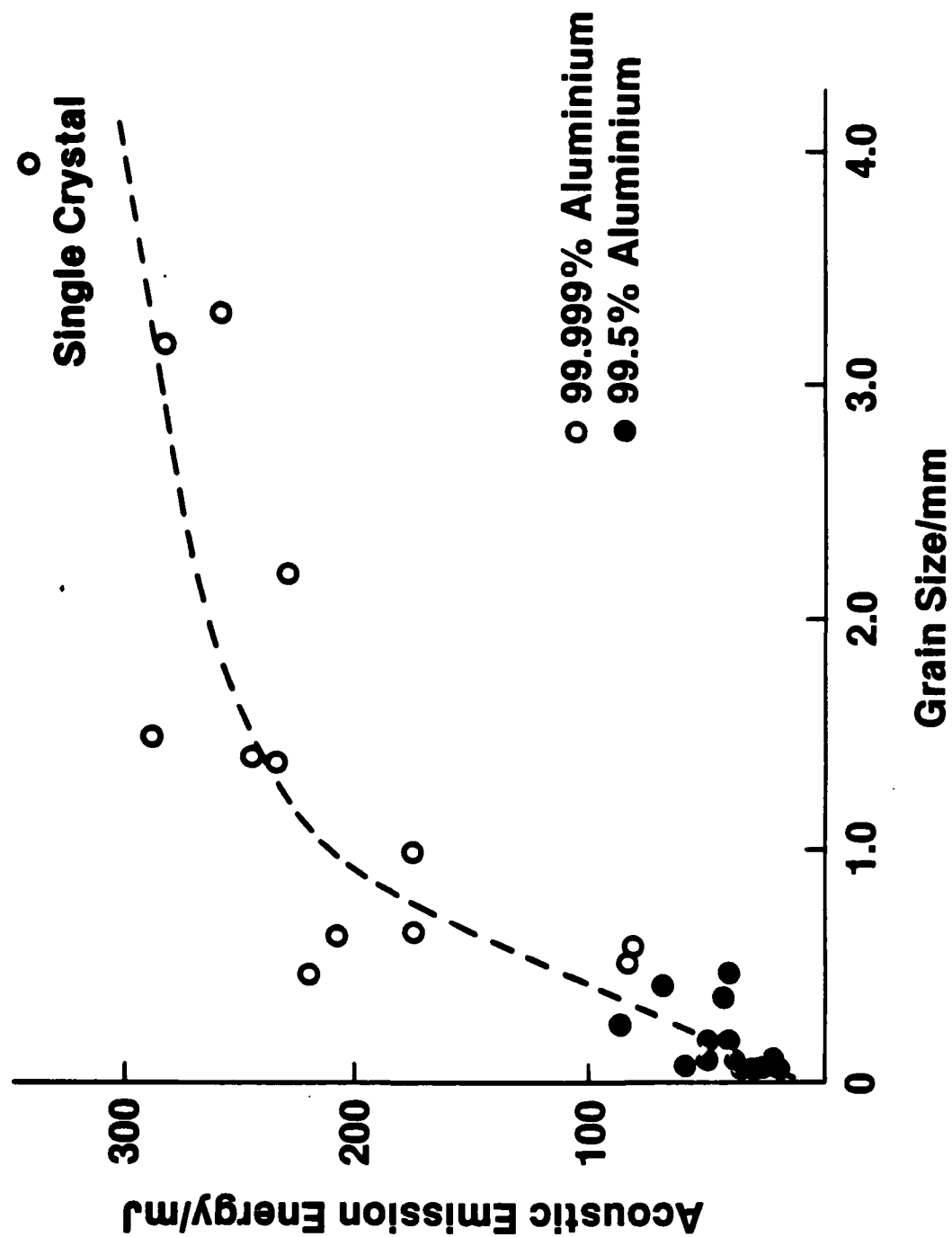


Fig. 8. The integrated acoustic emission power (Energy) of Aluminium single crystals is around 300 mJ. The effect of grain boundaries is to reduce the acoustic emission as the grain size decreases.

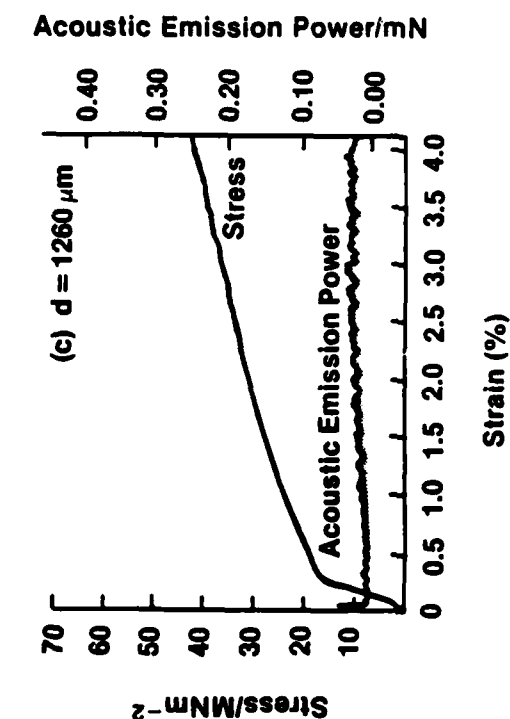
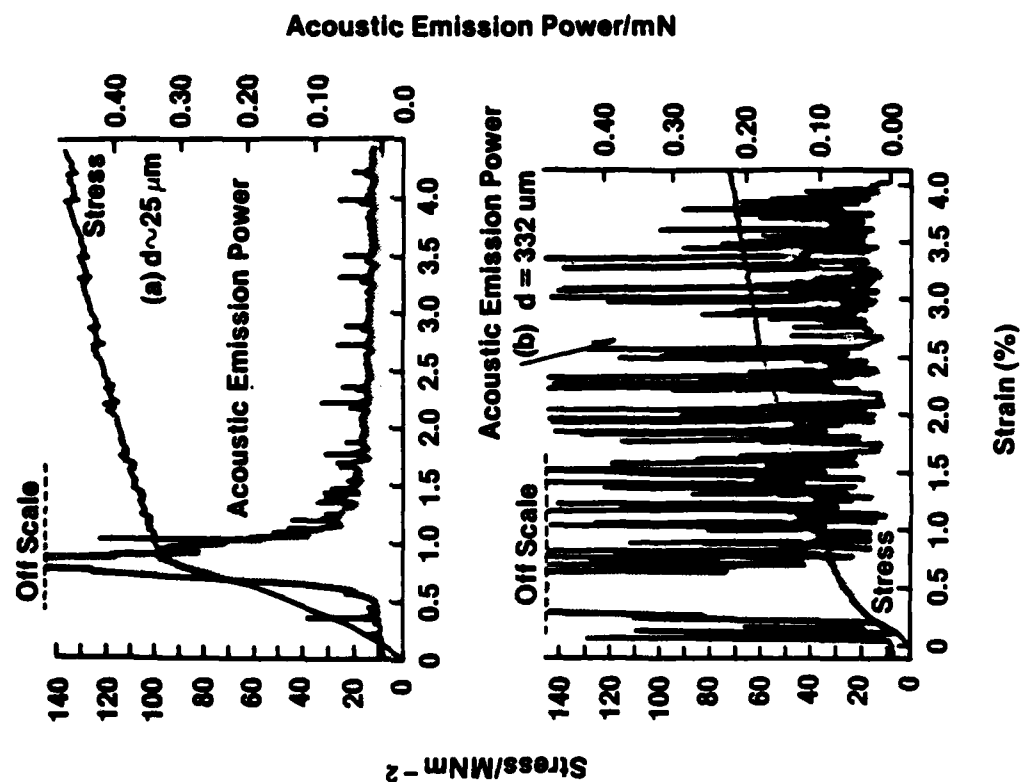


Fig. 9. Acoustic emission is generated during yield drops and dynamic strain aging in Al 1.3 wt % Mg solid solutions, the intensity varying greatly with grain size.



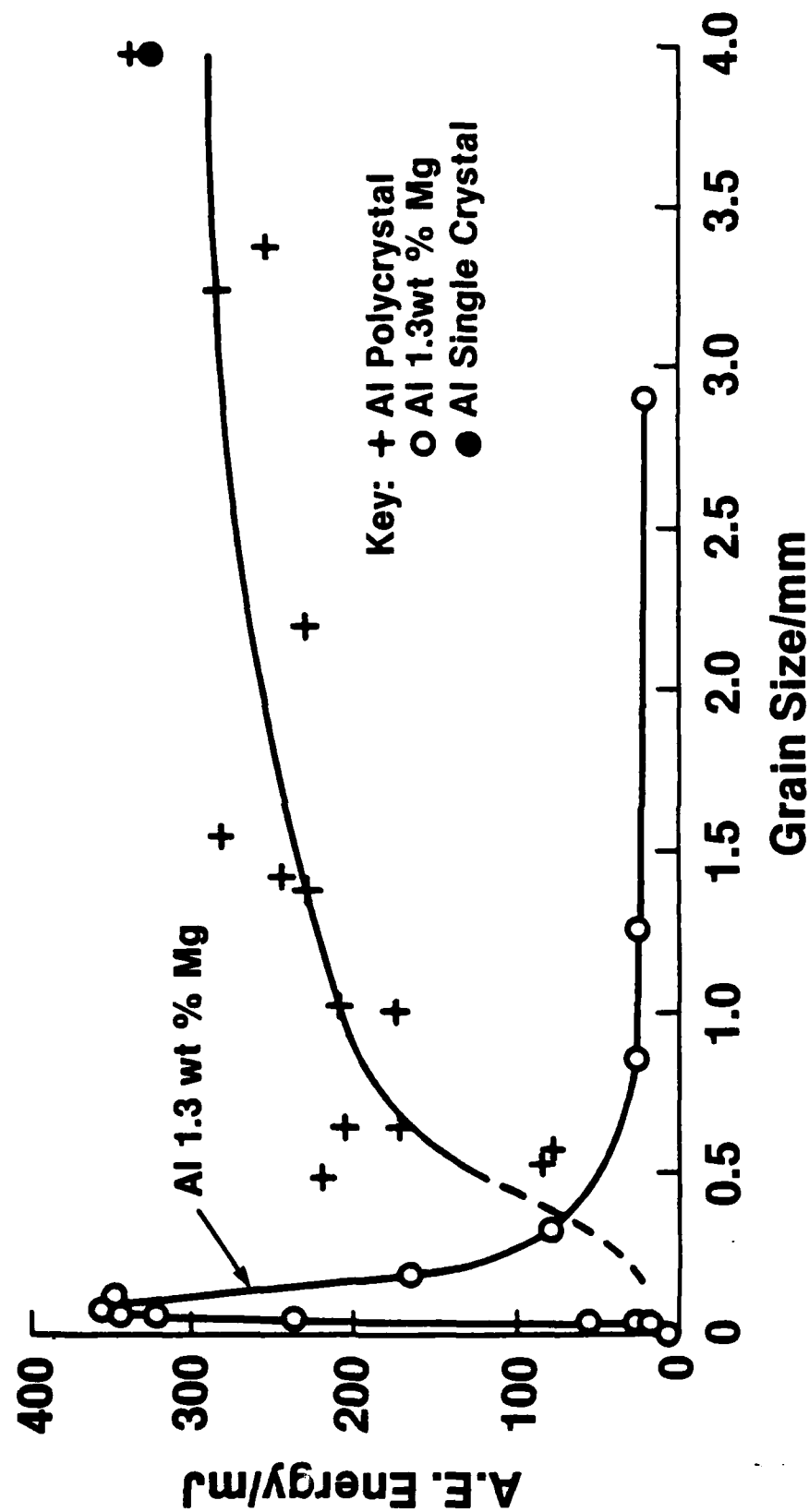


Fig. 10. A comparison of the grain size dependence of acoustic emission from pure aluminium and an aluminium-magnesium solid solution alloy.

The velocity decrease arises because the flow stress decreases with grain size and for grain sizes greater than about 500 μ m, the yield stress is insufficient to separate mobile dislocations from the cloud of Mg atoms segregated to their core. This results in drift controlled motion of dislocations at velocities too low to give acoustic emission, even though propagation distances would be more than adequate for generation of detectable signals.

Precipitation Effects

There are two extreme classes of dislocation-precipitate interaction:

- When the precipitates are strong, widely spaced and incoherent with the matrix, dislocations bow between particles leaving a dislocation loop around the precipitate.

- When the precipitates are weak, closely spaced and coherent with the matrix, dislocations may penetrate the precipitates and shear them.

The former process encourages uniformly distributed slip while the latter leads to the formation of intense slip bands. These bands form because the successive passage of dislocations through shearable precipitates reduces their strength and causes a local strain instability.

Studies in which the precipitate strength, distribution and coherency have been systematically varied^{12,13,14,15}, indicate the uniform slip process of dispersion hardened alloys (strong, relatively widely spaced incoherent precipitates) give

only little detectable acoustic emission because a is limited to the interparticle spacing. On the other hand, when precipitate shear occurs, for example, in lightly aged Al-4wt% Cu, Figs. 11 and 12¹², peak aged Al-5.5 wt% Zn-2.5 wt% Mg, Figs. 13 and 14^{13,14}, or lightly tempered Fe-3.25% Ni-0.21 wt% C steel, Figs. 15 and 16¹⁵, intense acoustic emission signals are observed.

These studies serve to illustrate well the complimentary role acoustic emission plays in the monitoring of plastic flow. In contrast to stress-strain measurements and hardness testing where the integrated static response of the material is measured, acoustic emission measures that part of the slip distribution that exceeds the criterion that $av > 0.035 \text{ m}^2\text{s}^{-1}$ (the high speed events) and this is very sensitive to metallurgical variables, often more so than the stress-strain curve.

From a processing viewpoint, the passive nature of the acoustic emission monitoring instrument together with the sensitivity of the emission to microstructure would indicate a potential nondestructive method for monitoring and feedback control on the production line, subject to background noise levels.

ACOUSTIC EMISSION FROM FRACTURE

Following the procedure used for plasticity, it can be shown that for the formation of a crack of length a at average velocity v to give detectable acoustic emission:

$$a^2v > 5 \times 10^{14} rT \text{ (Watts)}$$

where T is the detection threshold.

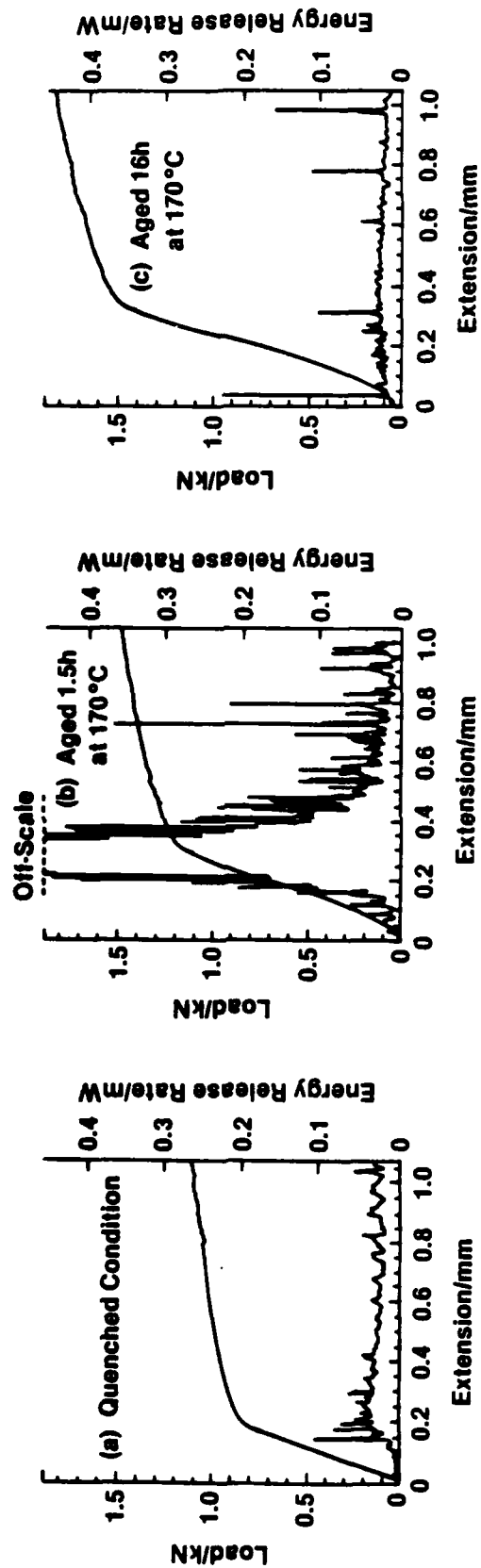


Fig. 11. The initial part of the load-extension curves of three samples of Al 4 wt % Cu aged at 170°C for various times showing the rise in strength with aging. Peak strength occurred after ~100 hs in this alloy. The acoustic emission activity was most intense around yield in samples aged for about 0.5-2 hs at 170°C.



a) 0.5h



b) 2h



c) 50h

Fig. 12. The microstructures of Al₄Cu aged various lengths of time at 170°C.

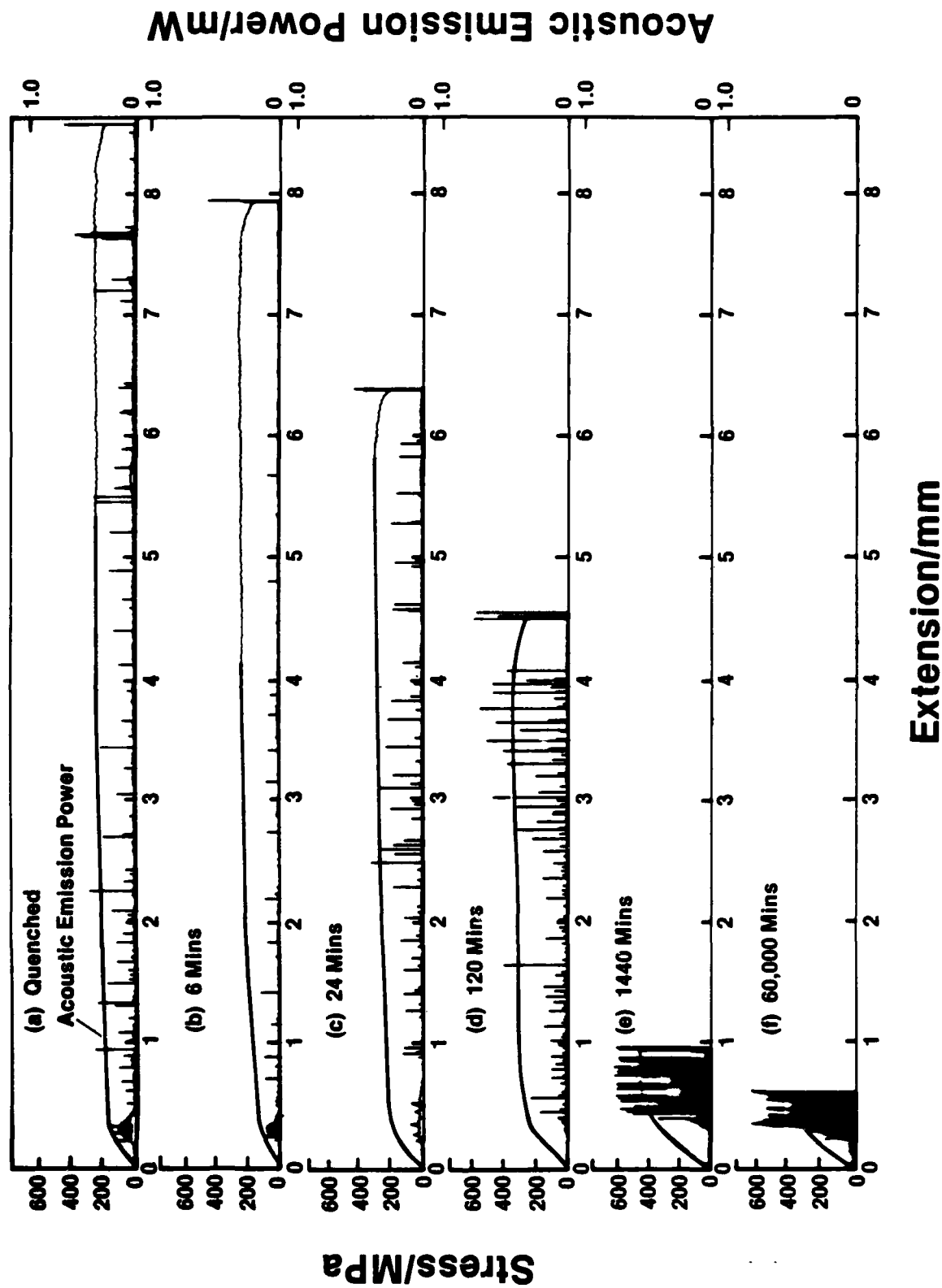


Fig. 13. The stress-extension curves for samples of Al 5.5 wt % Zn 2.5 wt % Mg aged at 120°C for various times. Peak strength occurs after 10,000 minutes of aging at this temperature. The acoustic emission intensity is greatest for material near the peak aged state.

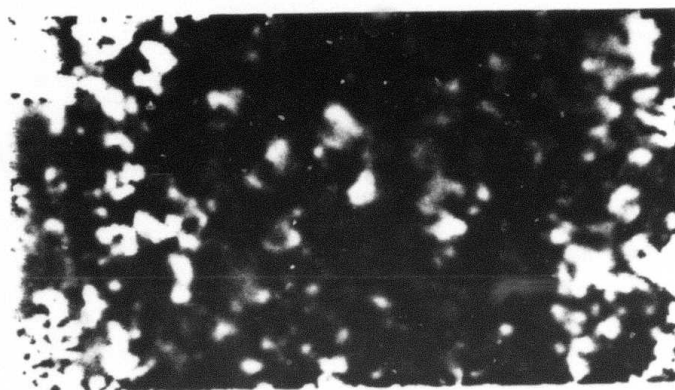
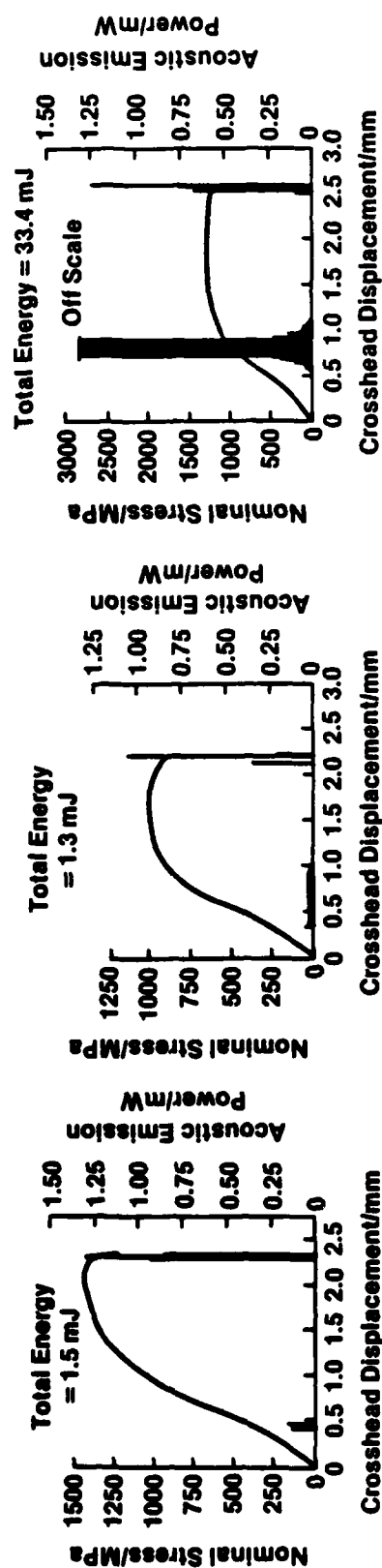


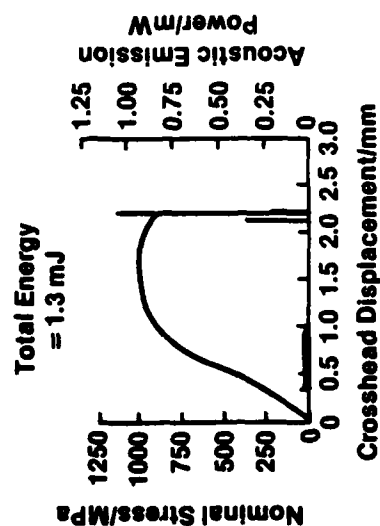
Figure 14. (a) Transmission electron micrograph of cell-like dislocation structure in Al 5.5 wt% Zn 2.5% as quenched.



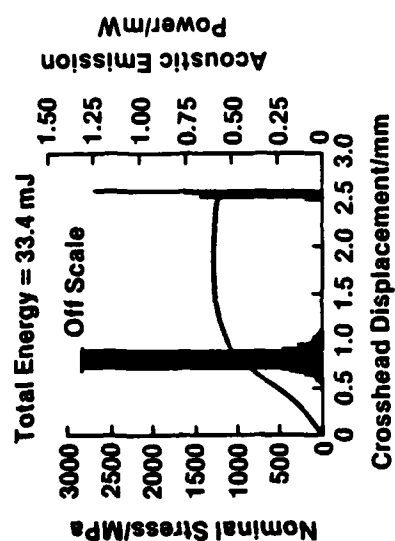
Figure 14. (b) Transmission electron micrograph of intense deformation bands in alloy aged at 120°C for 24 h.



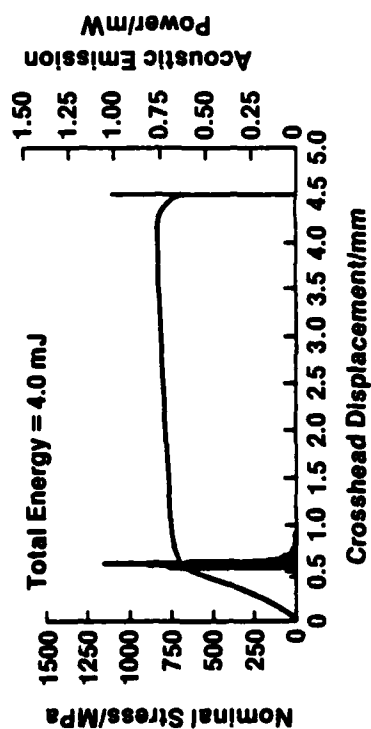
(a) Quenched



(b) 95°C



(c) 283°C



(d) 502°C

Fig. 15. Showing stress-extension curves for samples of Fe 3.5 Ni 0.21 C steel quenched and tempered for 100 minutes at various temperatures. The strength only decreases above ~250°C and the most intense acoustic emission occurs in the highest strength tempers.

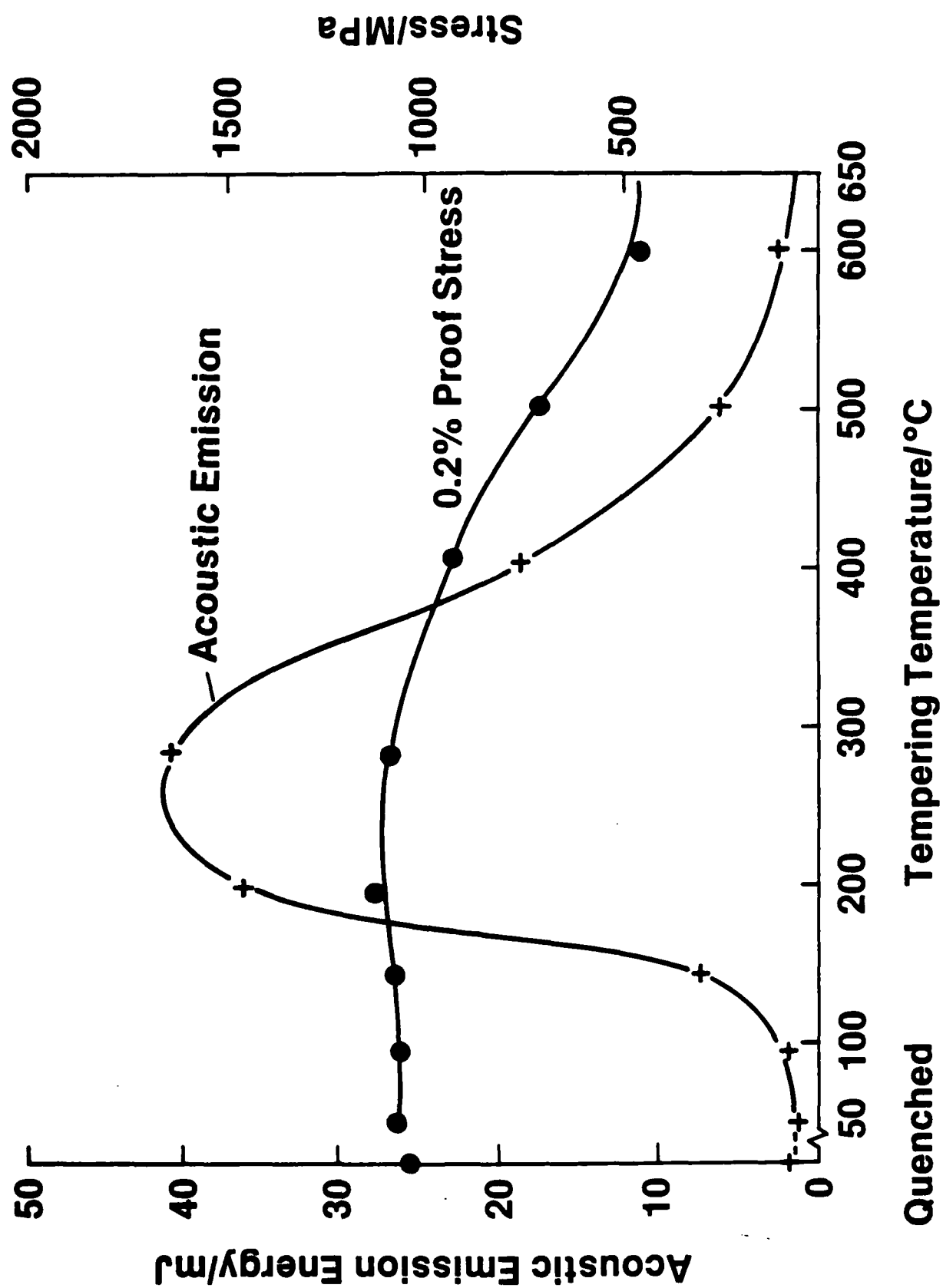


Fig. 16. Showing that the 0.2% proof stress increases slightly upon tempering a 0.21%C steel below 250°C and decreases sharply after higher temperature tempering treatments. The

Using metallographic observations to deduce crack length, and supporting acoustic emission observations to infer v , we can construct a detectability diagram for the various possible modes of fracture in a given material. Such a diagram for steel is shown in Fig. 17, assuming $r = 0.1\text{m}$ and $T = 10^{-13}\text{m}$ (a rather lower value than that used for plasticity to allow for background noise in an operating environment).

Because of the distributed nature of a and v for each fracture process, we have a field of detectability whose boundaries are poorly defined. Only those events occurring to the right of the shaded area give detectable signals. We see that brittle intergranular and cleavage fracture are easily detected while microvoid coalescence will be undetectable.

Interestingly, it is likely that a fraction, at least, of the inclusion distribution generates detectable signals and during processing the monitoring of acoustic emission might provide a basis not only for the detection of cracking, but also of the location of segregates. The reliability of the technique for in-process detection of such defects would be a promising area for further exploration.

ACOUSTIC EMISSION FROM PHASE TRANSITIONS

Many of the thermomechanical treatments materials are subjected to during processing are designed to induce phase transitions to produce optimal microstructure. A need exists for methods to monitor dynamically these processes for feedback control to improve quality and productivity.

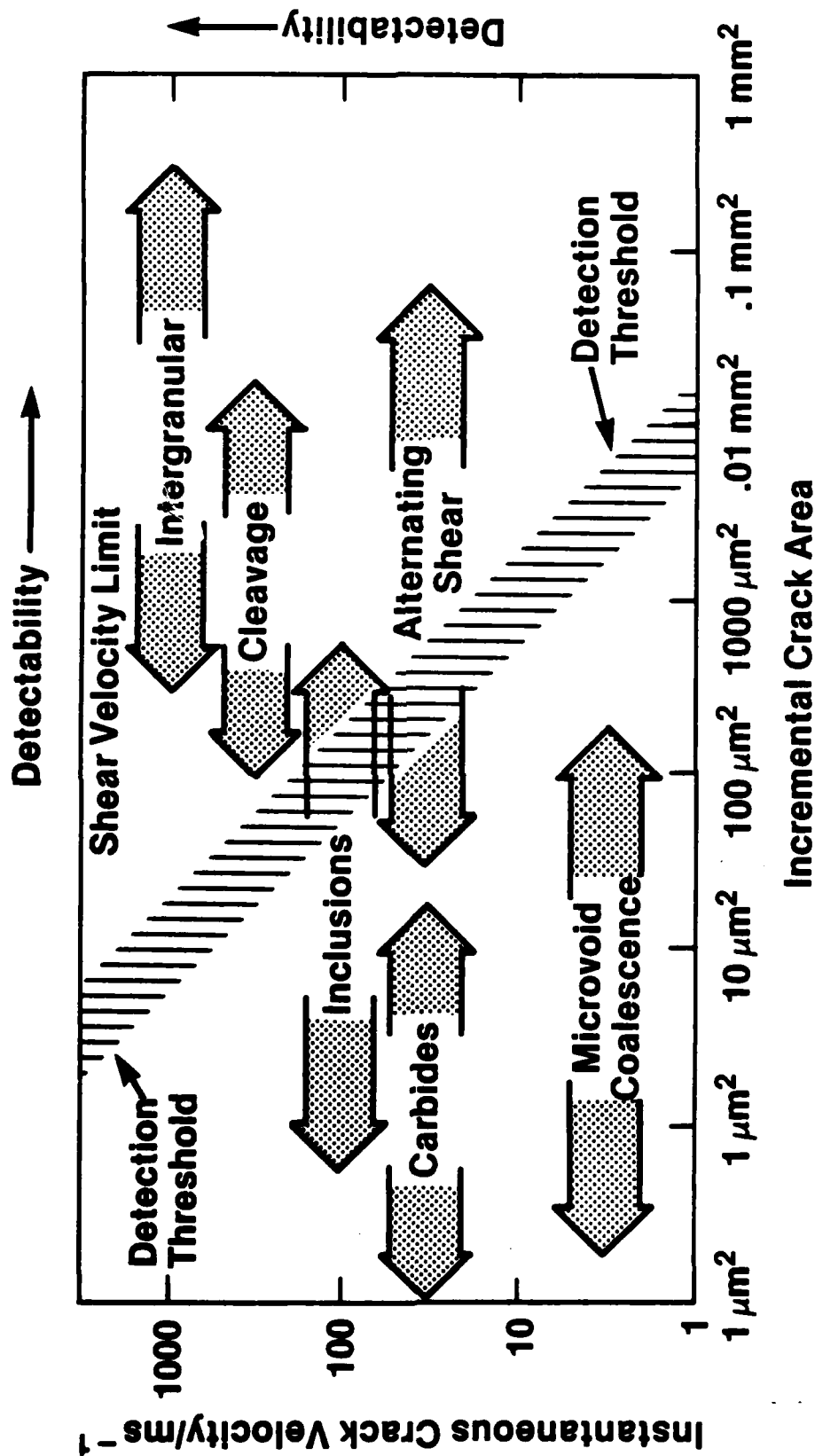


Fig. 17. Detectability of fracture events in steels. Detection threshold assumes transducer P wave sensitivity of 10^{-13} m, source-transducer distance 0.1m, stress 500MNm^{-2} .

Solid State Transformations

Our understanding of acoustic emission sources during plastic deformation and fracture suggests that only certain abrupt phase transitions, such as the martensitic transformation^{16,17} are likely to give detectable acoustic emission signals. Speich and Schwoeble¹⁸ have monitored the acoustic emission emitted by steels undergoing phase transformations. They find:

- The austenite-ferrite transformation and the precipitation of cementite generates no detectable signals.
- The austenite-bainite transformation involving formation of austenite to lath ferrite and carbide precipitation generates no detectable signals.
- The austenite-martensite transformation generates extremely energetic acoustic emission.

The acoustic emission during cooling of a high carbon steel is shown in Fig. 18. It can be seen that as the austenite is cooled towards the M_s temperature ($\sim 200^\circ\text{C}$), acoustic emission signals are emitted as laths of martensite form. Speich and Schwoeble found the acoustic emission to be very sensitive to carbon concentration, Fig. 19, increasing the carbon level.

It would be useful to determine the physical relationships between the source and the emission signal. There are three physical processes that may radiate elastic waves during the martensitic transformation⁹:

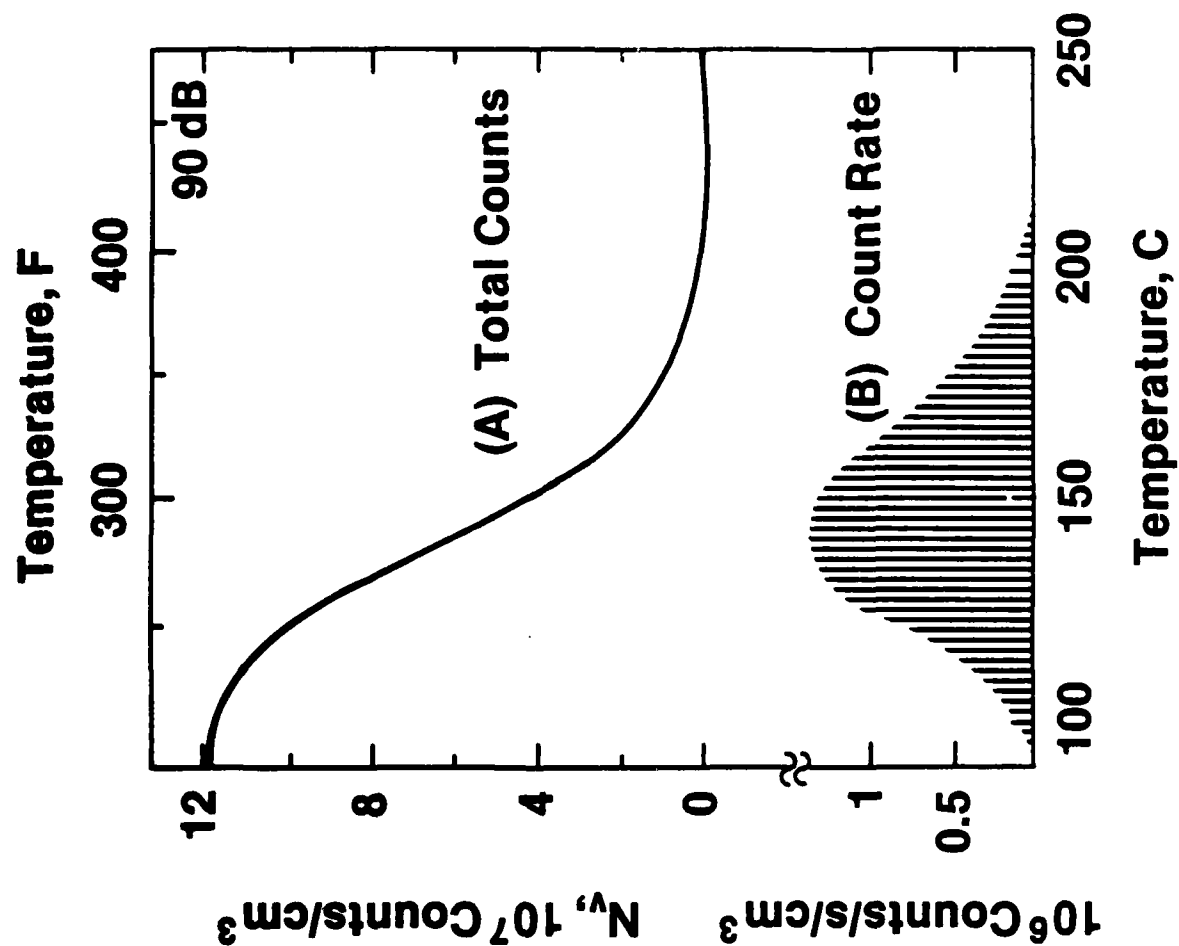


Fig. 18. Upon cooling a high carbon steel ($M_s \sim 200^\circ\text{C}$) acoustic emission signals are detected near the M_s temperature. The acoustic emission rate goes through a maximum and then decreases about 100°C below M_s .

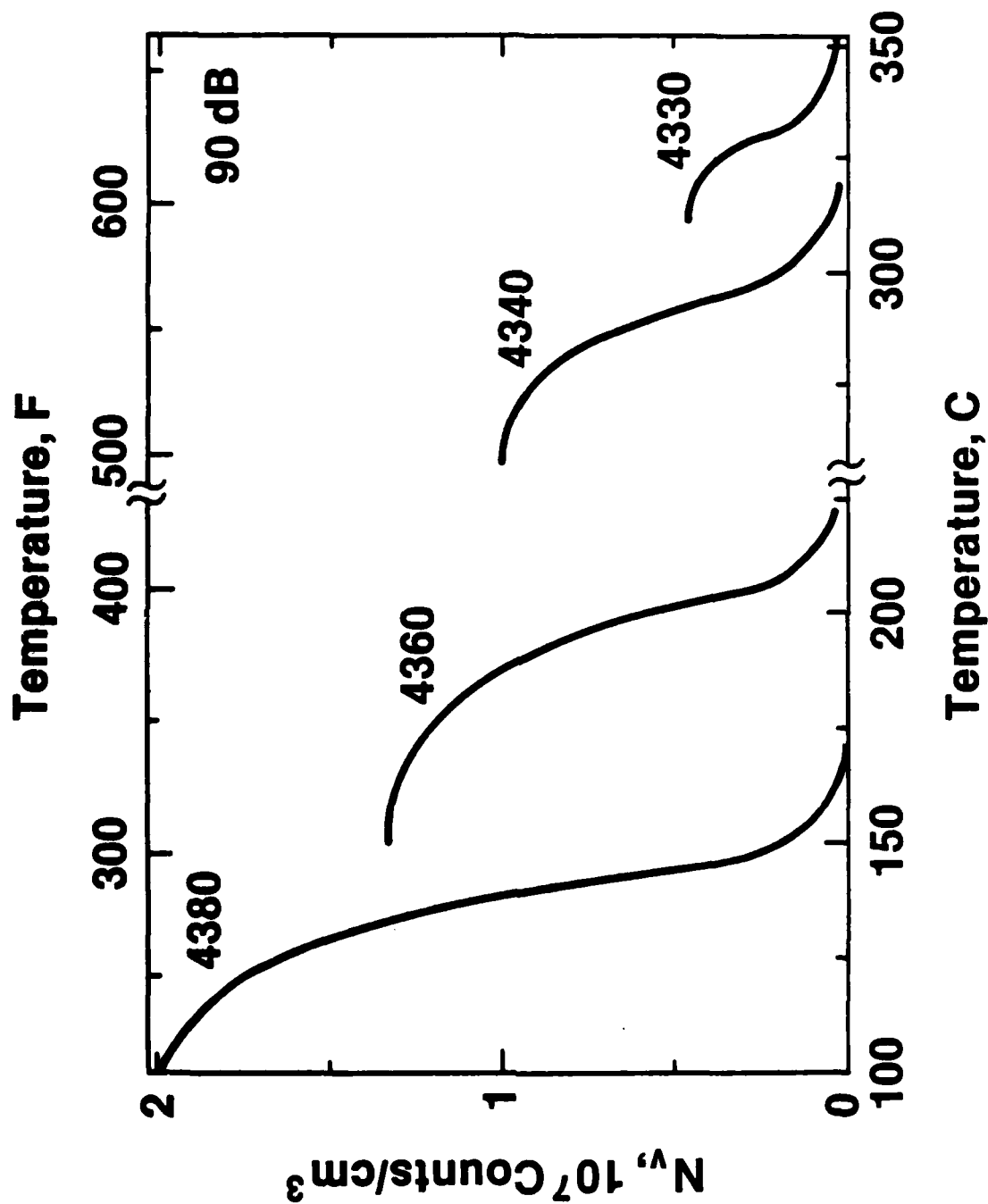


Fig. 19. The acoustic emission activity during the austenite-martensite transformation in steel increases with increasing carbon concentration. The temperature shift of the curves is due to the lowering of the M_s with increasing carbon concentration.

- Changes of elastic constants
- Dynamic momentum changes
- Shape changes

For small applied stresses and laths that propagate at $< 10\%$ the shear wave velocity, the first two terms may be small. It is therefore, a reasonable approximation to assume the acoustic emission is controlled in the main by the shape change. We can estimate the amplitude of the emission from this as follows:

Consider a region of austenite $\sim 25\text{mm}$ below the surface of an isotropic half-space. It transforms to martensite. The shape distortion can be resolved into two components: volume expansion and shear, both of which generate AE.

The emission from the volume expansion can be estimated as follows. For a 1% carbon concentration, the austenite lattice parameter is 3.59\AA , whilst those of martensite 2.848 and 2.977\AA giving a volume dilation of 4.3% . Assuming that a $30\text{ }\mu\text{m}$ radius penny shaped region $2\text{ }\mu\text{m}$ thick transformed, the volume change would be $240\text{ }\mu\text{m}^3$. If the transformation occurs at say 10^3ms^{-1} (30% shear wavespeed), the duration of the source is 30ns and an acoustic emission signal with the temporal form of Fig. 3(c) is radiated. Its peak amplitude will be $30\text{ }\mu\text{m mm}^{-3} \times 240 \times 10^{-9}\text{mm}^3 = 8 \times 10^{-12}\text{m}$, a very large signal, about 800 times greater than the detection threshold of laboratory instrumentation.

Typically, shears of about 20% also occur. These contribute no displacement if they are aligned parallel or perpendicular to the vertical axis. The maximum displacement occurs at 45° when the temporal waveform of Fig. 3(d) must be added to the dilatation signal. To estimate the amplitude, we note the shear is roughly equivalent to about 10^4 dislocations gliding across the disc. Therefore, the peak displacement, from Fig. 3(d), is $(8\mu\text{m per mm}^3) \times b\pi a^2 \times 10^4 = 8 \times 10^{-11}\text{m}$, an order of magnitude greater than that of the dilation.

Therefore, we see that very energetic signals are predicted for martensitic transformations and the monitoring of these ought to be relatively straightforward. The signal strength will depend upon microstructure. The model above would suggest a great sensitivity to grain size, martensite morphology (lath vs. plate martensite), which control the volume that transforms and carbon concentration which controls the distortion.

While precipitation of carbides in steels generates no acoustic emission of detectable amplitude, we speculate that prismatic punching of dislocations and the loss of coherency during precipitation may give detectable signals, but as far as we are aware, there have been no reported studies of this. Interestingly, however, Cannelli and Cantelli¹⁹ have observed acoustic emission during the precipitation of Nb, Ta and V hydrides which they attribute to fracture of hydride precipitates, Fig. 20.

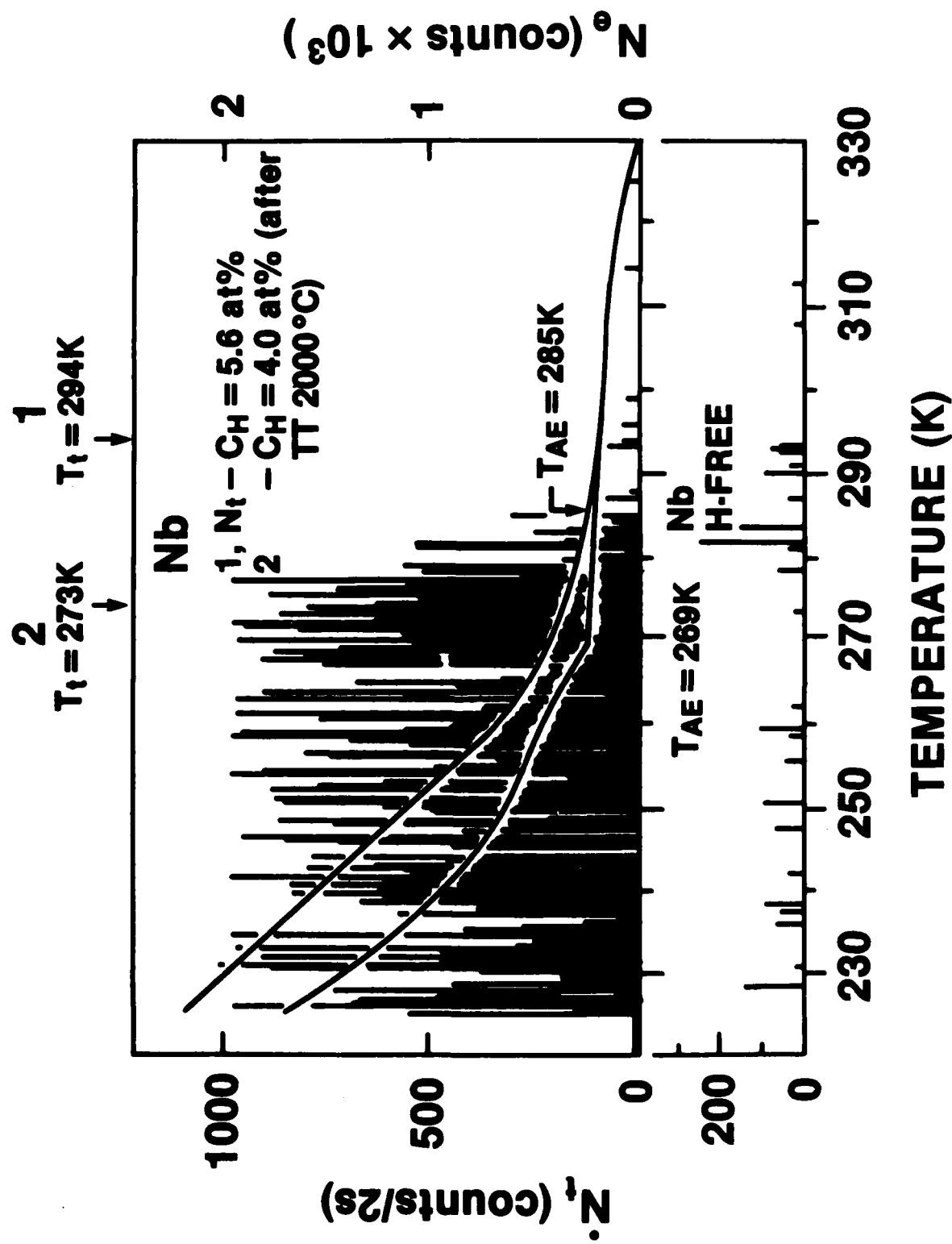


Fig. 20. Showing the generation of acoustic emission during precipitation of Nb-H upon cooling.

Liquid-Solid Transformations

There have been very few studies of acoustic emission during solidification. Work on Pb-Sn and Sn-Bi²⁰ indicated the generation of acoustic emission signals when solidification conditions were such that interdendritic porosity (solidification shrinkage of the final interdendrite liquid) occurs. The emission associated with this process was very intense, though the precise physical mechanism is unclear. This work also indicated the plastic deformation of primary dendrites could also generate low intensity acoustic emissions.

Fuerer and Wunderlin²¹ also measured the acoustic emission during solidification of an Al-4.5%Cu-0.2%Ti alloy and observed acoustic emission generated, they believed, by the formation of porosity. They varied the volume fraction of porosity by adjustment of hydrogen content of the melt and found the solidification acoustic emission was proportional to the volume fraction of porosity, Table II.

TABLE II. Summary of results for solidification emission of Al-4.5Cu-0.2Ti.

H ₂ content/cm ³ at STP/100g	Total A.E. Count	Pore Fraction %
0.05	1.05 x 10 ⁴	0.19
0.17	2.75 x 10 ⁴	0.46
0.23	6.35 x 10 ⁴	0.63

They considered the emission to be generated by the unstable formation of hydrogen "bubbles" in the melt close to the liquid-solid interface. The lower hydrogen solubility of solid aluminum results in a hydrogen supersaturation in the melt close to the liquid-solid interface. The relief of this supersaturation acts as the driving force for H₂ bubble formation in an analogous role to that of strain energy reduction in the formation of cracks. This dilatation source then radiates longitudinal elastic waves that are transmitted through the liquid-solid interface and ultimately detected by a transducer as acoustic emission.

A study of the acoustic emission generated during rapid solidification has recently been initiated by DARPA at NBS. The study is directed toward development of acoustic emission source characterization methodologies and their application to in-process control of rapid solidification processing. Exploratory studies have initially concentrated upon deducing the origin of the acoustic emission generated during electron beam surface melting and resolidification of 2219 and 1100 aluminum alloys.

It has been found that acoustic emission signals are emitted during solid state heating (due to thermoelastic effects similar to those utilized for laser generation of elastic waves²²), melting and resolidification. The acoustic emission emitted during resolidification after attainment of a steady state of temperature field increases with the electron flux due to the increased volume of resolidifying material. For a given

melt depth, the acoustic emission from 2219 aluminum alloy is up to 100 times more energetic than that from 1100 aluminum alloy, Fig. 21.

Metallographic studies have revealed the occurrence of solidification cracking in 2219 aluminum alloy , Fig. 22, whilst no cracking has been observed in 1100 aluminum alloy, Fig. 23. Whilst these results are of a preliminary nature, they do provide encouragement for possible acoustic emission monitoring techniques.

PROCESS MONITORING

Up to this point, we have considered basic aspects of acoustic emission in order to understand the possible contribution it may offer for monitoring metals processing and microstructure characterization. Acoustic emission techniques are already finding application in industry to monitor some processing procedures. One of the most successful is in the weld process monitoring.

The repair of welds is a major cost item in the production of components manufactured from heavy section steel. Heavy section repair can even leave a weld with worse problems than that of the original flaw, because of damage to weld microstructure and additional residual stresses. The removal of flaws through in-process repair can both improve the quality of repair and, provided only one or two weld passes are removed and replaced using automatic welding procedures, result in major cost savings over conventional heavy section post weld repair.

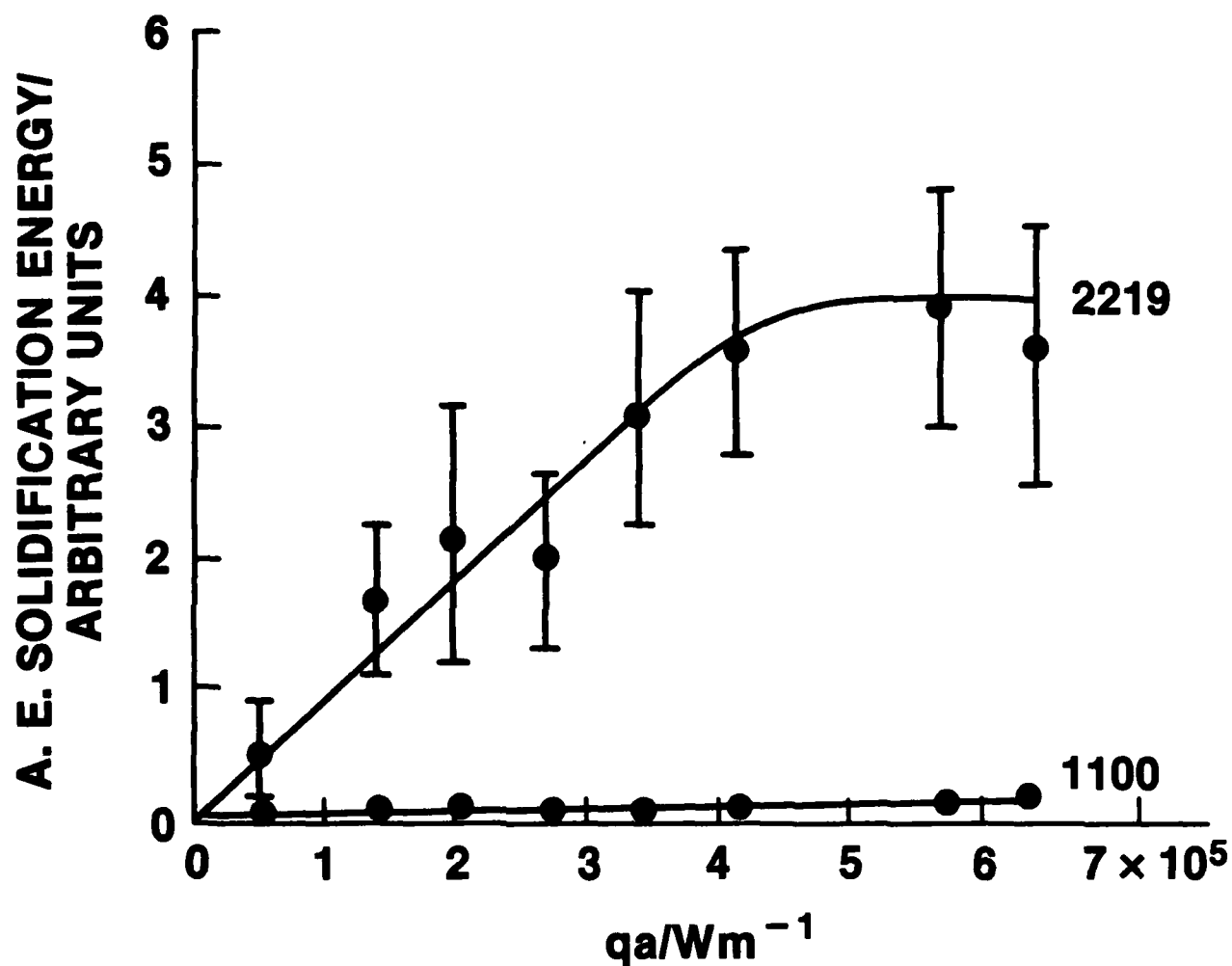


Figure 21. Acoustic emission energy emitted during cooling of electron beam heated 2219 and 1100 aluminum as a function of qa , where q is the absorbed heat flux (Wm^{-2}) and a the radius of the beam (m).

The obstacle to application of in-process weld repair has been lack of an effective in-process sensor to detect flaws dynamically as they form. In-process monitoring using acoustic emission shows great promise in providing the much needed tool.

The primary problem is that both flaw formation and the welding process generate acoustic emission. However, simple spatial and temporal filtering (clustering) has been very successful at discriminating defect signals from noise²³.

As an example, work by Bentley, Dawson and Prine²⁴ monitored automatic and manual submerged arc welding of plates of pressure vessel and 316 stainless steel into which 20 defects were deliberately introduced: Table III. Two sets of instrumentation were used to monitor the welding -the primary difference being positioning of the transducers on opposite plate surfaces. Conventional NDE methods were used to establish that the intended defects were produced, and these methods also detected some natural defects.

It was found that one or another of the sets of instrumentation detected 15 of the independently established 20 major defects, and that each separately detected 10 of them: Table IV. Cracks and slag inclusions were more readily detectable than other defect types.

TABLE III
Welding Details and Summary of Deliberate Defects

Plate	Welding Method	Number of Weld Passes	Total Length of Weld Pass	Type
Mild steel	Manual metal arc	19	20	Hot crack Hot crack Slag inclusion Porosity Lack of fusion
Mild steel	Automatic submerged arc	18	23	Hot crack Slag inclusion Porosity Porosity Lack of fusion
Stain-less steel	Automated submerged arc	14	15	Hot crack Hot crack Slag inclusion Porosity Lack of fusion

TABLE IV

Summary of Defects Which Were Detected by AE

Plate	AE Source	Type of Defect	Intended (I) or Natural (N)
Mild Steel	*	Lack of fusion/slag	N
MMA	4+, 1Δ	Lack of fusion/crack	I
	1+, 2Δ	Crack	I
	5Δ	Porosity	I
	5+, 6Δ	Crack	I
	3+, 7Δ	Slag inclusion	I
Mild steel submerged arc	2Δ	Slag inclusion	I
	2+, 3Δ	Cracks	I
	4Δ	Porosity	I
	1+	Crack and slag/slag	N
	5+	Lack of fusion/slag	I
Stainless submerged arc	3+	Lack of fusion/slag	I
	1+, 3Δ	Crack	I
	6Δ	Crack	I
	4+	Lack of fusion/crack	I

Key: + GARD The number preceeding the symbol is the identifier
 Δ RNL used in Figs. 5-7 of reference (24).

Further RNL processing GARD data

Studies such as this clearly demonstrate the potential of in-process weld monitoring by acoustic emission. The major obstacle is need for reliable techniques of signal analysis to:

- Separate defect signals from noise (to both improve reliability and avoid overcalls)
- Characterize flaws so that only deleterious flaws are repaired.

Other supporting studies of the role of metallurgical and welding variable ought also be initiated to ensure the "quiet" flaw growth does not occur.

While the majority of studies have concentrated upon the monitoring of the welding process itself, it is interesting to note that cracking during post weld heat treatments have been successfully detected in the heat affected zones of austenitic clad A533B pressure vessel steel²⁵.

SUMMARY

Acoustic emission may be considered a candidate technique for in-process monitoring and microstructure characterization for the following reasons:

- The natural material responses to processing (e.g., phase transformations and plasticity) emit acoustic emission enabling possible feedback control of processing procedures.
- Abnormal material responses (e.g., cracking) may emit highly energetic emission signaling poor quality.

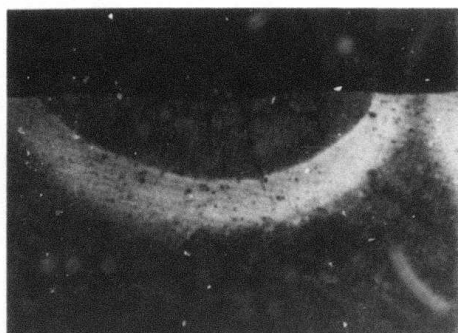
- The passive nature of the technique (it requires no artificial energy sources), its 100% volume coverage (possibly with noncontacting sensors) and the short response time (a few ms) suggests it would be a viable production line monitoring technique.

The problems that must be addressed are:

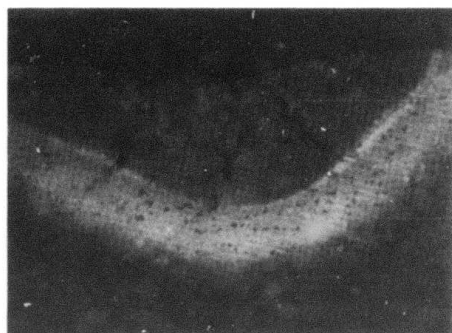
- Noise: The material related emission has to be detected in the presence of noise and some materials/processing procedures may not emit signals with sufficient S:N ratio, Fig. 24.
- Characterization: In practice, many acoustic emissions are detected but only a few may be deleterious defects that must be removed during processing. Signal analysis methods are required which will allow rapid, on-line defect assessment.

ACKNOWLEDGEMENT

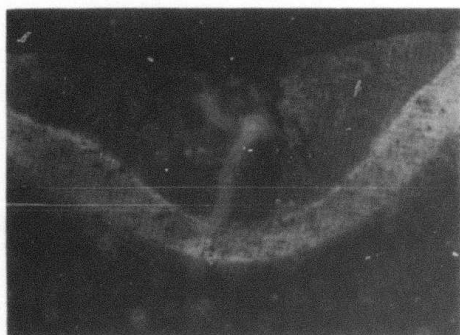
This paper was written under the auspices of the DARPA Materials Research Council, Contract #MDA903-82-C-0428 with The University of Michigan.



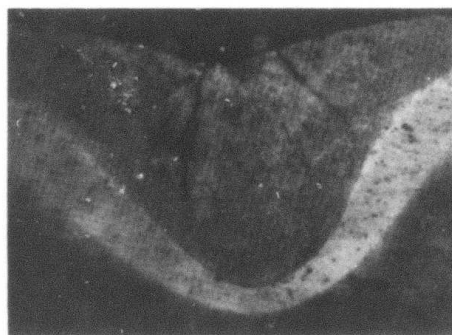
(a) $1.9 \times 10^5 \text{ Wm}^{-1}$



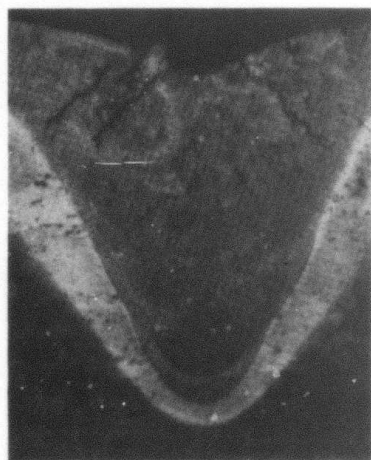
(b) $2.7 \times 10^5 \text{ ms}^{-1}$



(c) $3.3 \times 10^5 \text{ Wm}^{-1}$



(d) $4.1 \times 10^5 \text{ Wm}^{-1}$



(e) $5.7 \times 10^5 \text{ Wm}^{-1}$



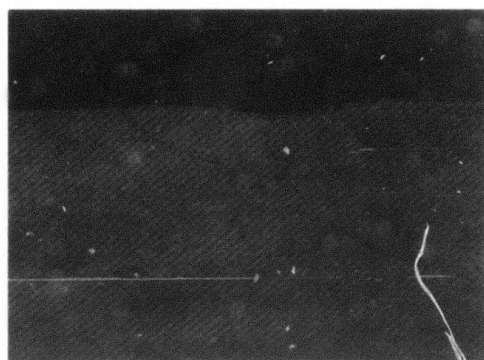
(f) $6.4 \times 10^5 \text{ Wm}^{-1}$

0.5 mm

Fig. 22. The effect of q_a upon melt profile and solidification microstructure of 2219 aluminum.



(a) $1.9 \times 10^5 \text{ Wm}^{-1}$



(b) $2.7 \times 10^5 \text{ ms}^{-1}$



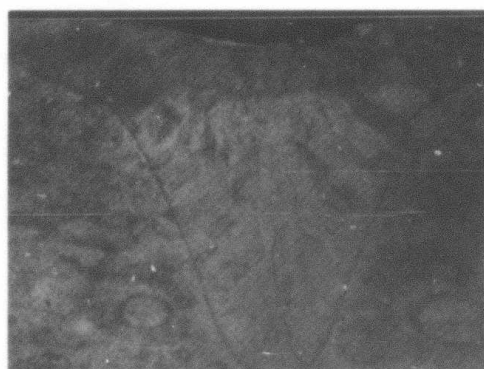
(c) $3.3 \times 10^5 \text{ Wm}^{-1}$



(d) $4.1 \times 10^5 \text{ Wm}^{-1}$



(e) $5.7 \times 10^5 \text{ Wm}^{-1}$



(f) $6.3 \times 10^5 \text{ Wm}^{-1}$

Fig. 23. The effect of q_a upon melt profile and solidification microstructure of 1100 aluminum.

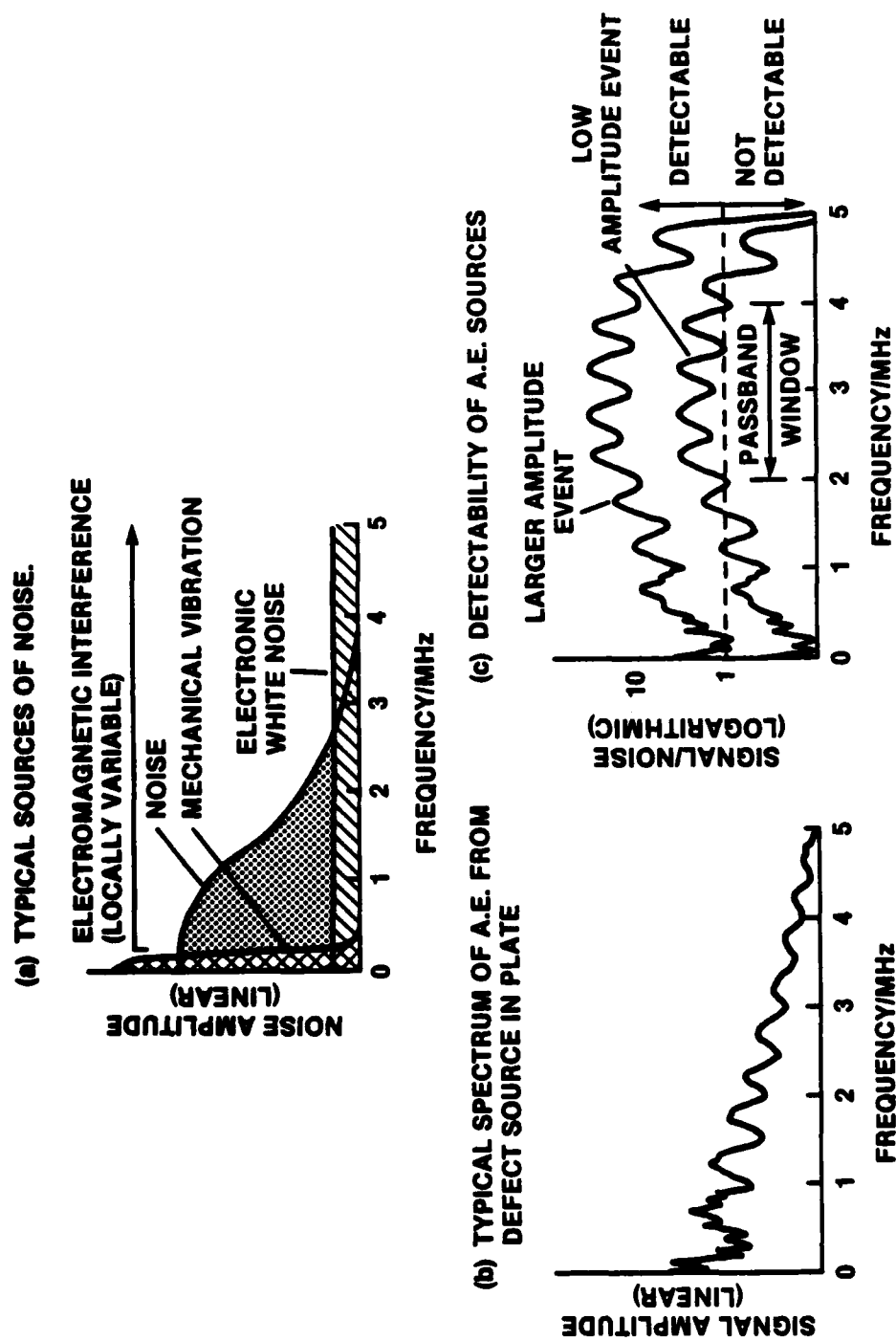


Fig. 24. Schematic to show (a) typical noise sources encountered in AE monitoring; (b) typical AE spectrum (transducer response ignored); (c) detectability of AE source event, ie S/N as a function of frequency. The low amplitude event requires a band-pass window to improve de-

REFERENCES

1. H.N.G. Wadley, C.B. Scruby and J. Speake, Int. Met. Rev. 25(2), 41(1980).
2. W. Sachse and N. Hsu, Physical Acoustics XIV (1980).
3. J.C. Spanner, "Advances in Acoustic Emission", Proc. Int. Conf. Acoustic Emission, Anaheim, CA (1979), H.L. Dunegan and W.F.. Hartman, Eds., Dunhart (1981).
4. J.M. Carlyle, J. Acoustic Soc. Am., Suppl. 1 68, S104 (1980).
5. C. Scruby, H. Wadley and J. Sinclair, Phil Mag A, 44(2), 249(1981).
6. N. Hsu, J.A. Simmons and S.C. Hardy, Mat. Eval. 35, 100 (1977).
7. H.N.G. Wadley, C.B. Scruby and G. Shrimpton, Acta Met 29, 399(1980).
8. H.N.G. Wadley and C.B. Scruby, AERE-R10351, "Elastic Wave Radiation From Cleavage Crack Extension" (1982).
9. J.A. Simmons and R.B. Clough, "Dislocation Modelling of Physical Systems", Proc. Int. Conf., Gainesville, FL, June 1980, Pergamon Press (1981).
10. C.B. Scruby, J.C. Collingwood and H.N.G. Wadley, J. Phys. D. 11, 2359(1978).
11. H.N.G. Wadley and C.B. Scruby, AERE-R10534, "Dynamic Elastic Displacements at the Surface of an Elastic Half-Space due to Defect Sources" (1982).
12. H.N.G. Wadley and C.B Scruby, Metal Science 12, 285(1978).
13. K. Rusbridge, C.B. Scruby and H.N.G. Wadley, AERE-R10363, "Origin of Acoustic Emission in Aged Al-An-Mg Alloys; Part I: The Base Ternary Alloy" (1982).
14. C.B. Scruby, H.N.G. Wadley and K. Rusbridge, AERE-R10364, "Origin of Acoustic Emission in Al-Zn-Mg Alloys; Part II Copper Containing Quarternary Alloys" (1982).
15. H.N.G. Wadley, C.B. Scruby, P. Lane and J.A. Hudson, Metal Science 15, 514, Nov-Dec., 1981.
16. J. Baram and M. Rosen, Scripta Met 13, 565(1979).

17. J. Baram and M. Rosen, Acta Met 30, 655(1982).
18. G.R. Speich and A.J. Schwoeble, ASTM STP-571 40(1975).
19. G. Cannelli and R. Cantelli, "Advances in Acoustic Emission", Proc. Int. Conf. Acoustic Emission, Anaheim, CA, 1979, H.L. Dunegan and W.F. Hartman, Eds., Dunhart (1981).
20. H.M. Tensi and W. Radtke, Metall. 32(7), 681(1978).
21. J. Fuerer and R. Wunderlin, Int. Conf. Solidification and Casting, Metals Society, London, 2, 18(1977).
22. H.N.G. Wadley, J. Simmons, C.K. Stockton, M. Rosen and R. Mehrabian, DARPA/AF Review of Quantitative NDE, Aug. 2-7, 1981, Boulder, CO.
23. D.W. Prine, Fifth International Acoustic Emission Symposium, Tokyo (1980).
24. P.G. Bentley, D.G. Dawson and D. Prine, RNPDE Report ND-R-767 (R) (1982).
25. P. Jax, Proc. 2nd Int. Conf. on Structural Mechanisms in Reactor Technology (Berlin) G614-EUR4820 (1973).

ULTRASONIC ATTENUATION IN CERAMICS

A. G. Evans

Attenuation data for a variety of single phase ceramic polycrystals revealed a strong influence of grain size and an additional influence of large pores. The data indicated a non-unique frequency exponent, f^n (n ranging between 1 and 3). Interpretation of the data (in terms of the influence of the grain and pore size distribution) recognized violation of the long wave length requirement ($n=4$), and that the scattering was dominated by the large extreme of microstructural entities (scattering power $\propto a^6$, where a is the grain size). Consequently, the polycrystalline aggregate was regarded as a dilute solution of intense homogeneous scatterers (the large grains or pores) in an isotropic matrix. The scattering cross section of each scatterer (computed over the complete range of wavelengths), was thus used as the basis for predicting the total scattering by regarding the intense scatterers as non-interacting entities.

The size distribution of large microstructural features was obtained using extreme value principles, by selecting the largest grain (a pore) in an area containing a fixed number of grains (~ 10) and deriving the extreme value distribution of grain volumes. An extreme value distribution of the second type was found to describe the measurements. Direct coupling of the extreme value distribution of grain volumes with the scattering

cross section provided prediction of both the total attenuation and the attenuation attributed to each grain size range. The total attenuation predicted in this manner was within a factor, 2, of the measured attenuation for each material, over the entire frequency range (1-100 MHz). Additionally, the predictions revealed that the attenuation derives almost exclusively from that proportion of the grain volume distribution just below the large extreme, (the very large grains are too sparse to contribute significantly, while the small grains - although large in number - are weak scatterers).

Predicted plots of attenuation as a function of frequency (for selected values of the scale and shape parameters of the grain size distribution) provide a basis for estimating the large extreme of the microstructure from attenuation measurements (obtained over a range of frequencies using short pulses). Additionally, the large microstructural extreme deduced from attenuation measurements provides direct information, in certain materials, pertinent to the prediction of mechanical properties. Specifically, for materials that fail by the fracture of large grains or large pores, the failure probability can be related directly to the attenuation. This prospect merits further attention.

ACKNOWLEDGEMENT

This paper was written under the auspices of the DARPA Materials Research Council, Contract #MDA903-82-C-0428 with The University of Michigan.

MEASUREMENT OF MATERIAL PROPERTIES BY ACOUSTIC METHODS

G. S. Kino

We give here examples of material measurements which can be carried out using acoustic techniques.

These include:

Microstructure Measurements

Hardness, grain size and distribution, texture.

Stress Measurements

2D and 3D inhomogeneous stress states, residual and applied stresses, effect of texture, and calibration problems.

A closely related measurement based on the same techniques is to determine internal temperature distributions in a material. Surface wave techniques also provide important information on near surface parameters such as case hardness, surface microstructure adhesion and bond strength, and near surface stresses due to machining.

Techniques Employed

The basic experimental techniques used depend on extremely accurate measurements of acoustic velocity or phase. Phase is measured to accuracies of .01 to .1°. Attenuation as a function of frequency can also be measured by pulse echo techniques and use of fast Fourier transform methods. Diffraction is taken into account and the results interpreted on the computer. For measurement of microstructure, theoretical tech-

niques of interpreting the attenuation - frequency, velocity - frequency curves to measure grain size and texture are being developed.

Shear waves, Longitudinal waves, Rayleigh waves and to a very limited extent Lamb waves are employed in the measurement. Good scanned dry contact shear waves have been developed, EMAT transducers are used for surface waves. Measurements are carried out from 2 - 300MHz.

Acoustic microscopy gives excellent images of surface structure and is a powerful technique for measuring adhesion. The contrast obtained is due to the fact that both Rayleigh waves and directly reflected waves at normal incidence are obtained. Interference between the two types of waves gives rise to the contrast mechanism. Recent developments involve phase measurement accuracies to determine the Rayleigh wave velocity to 0.1° accuracy (velocity accuracy of better than 1 part in 10⁴). This, makes it possible to scan thickness and adhesion of thin films etc. on a surface.

Future Possibilities

The highly precise acoustic techniques available should make it possible to determine acoustic microstructure properties in some detail. More theory is needed. With this available adaptations of acoustic microscopy to low frequencies will give information on adhesion, texture, case hardness etc. High frequency techniques make it possible to measure the properties of individual crystallites.

Residual stress profiles measurements should yield to these measurement techniques. In particular it looks as if the problem of measuring stress near a weld may be soluble. The problems of texture and calibration are being tackled and good progress is being made. Acoustic Emission needs some understanding of efficiency of emission as function of frequency.

Other Techniques

We have not discussed acousto-optic techniques here. Fiber-optic probes for detecting acoustic waves, effects of surface roughness are being developed and may become very important. Photo-acoustic methods are becoming important for detecting adhesion, stress and surface microstructure. Further development in that direction is expected.

ACKNOWLEDGEMENT

This paper was written under the auspices of the DARPA Materials Research Council, Contract #MDA903-82-C-0428 with The University of Michigan.

ACOUSTIC MICROSCOPY FOR MATERIALS STUDIES

G. A. D. Briggs

INTRODUCTION

Over the past two years transmission and reflection scanning acoustic microscopes have been built at Oxford in collaboration with AERE Harwell. The purpose of our work is to discover applications in materials studies for which acoustic microscopy is suitable, and then to exploit the technique in tackling problems in those areas. The microscopes have been operating for a little under one year now, and this report summarizes our progress in that time.

Transmission Microscopy

Our transmission microscope works at 45 and 140MHz. It is designed for imaging within the bulk of a material, and can accept specimens up to 2mm thick. In passing from crystalline solids to water the refractive index is high, usually greater than four, and this ensures that spherical aberrations due to the lens are negligible. Sadly, however, the same fact causes aberrations, when trying to focus inside a solid with a plane surface, to be very large. The resolution is optimized by using lenses of small numerical aperture, giving us at 140 MHz a resolution of 50 μ m, though features smaller than this can be detected.

When specimens of metals or alloys are imaged in the transmission microscope at these frequencies the most prominent effect is a dappled appearance which is attributed to multiple

scattering at grain boundaries. This has almost 100% contrast. This pattern may contain useful information about the microstructure of the specimen, but for the purpose of imaging other features it is a nuisance. It can be almost eliminated by working at a lower frequency (e.g. 45 MHz), but at the expense of resolution. Nevertheless, despite this result of grain boundary scattering we have had some success in imaging in transmission.

One problem of interest has been the development and growth of diffusion bonds. These are made by grinding the two surfaces to be joined, and then pressing the surfaces together with the grinding directions parallel at a temperature of 0.5-0.8 T_m (the absolute melting point) and at a pressure below that which would cause gross deformation. After small local plastic deformation the bond develops by diffusional processes over a period of up to an hour or so. In order to test a theoretical model of their development, bonds which had been allowed to grow for different times were imaged in transmission. Because the surfaces have been brought together with their grinding directions parallel, long narrow voids are expected to appear corresponding to troughs in the ground surfaces. These might typically be 20 μm wide, and would appear dark in transmission. An image of a deliberately poor bond (bonded for only 3 minutes) in En8 steel is shown in Fig. 1. The dappled appearance is due to the multiple grain boundary scattering. Also visible are dark regions running diagonally across the picture (slight curvature is due to distortions in the temporary imaging electronics). It



|-----|
100 μ m

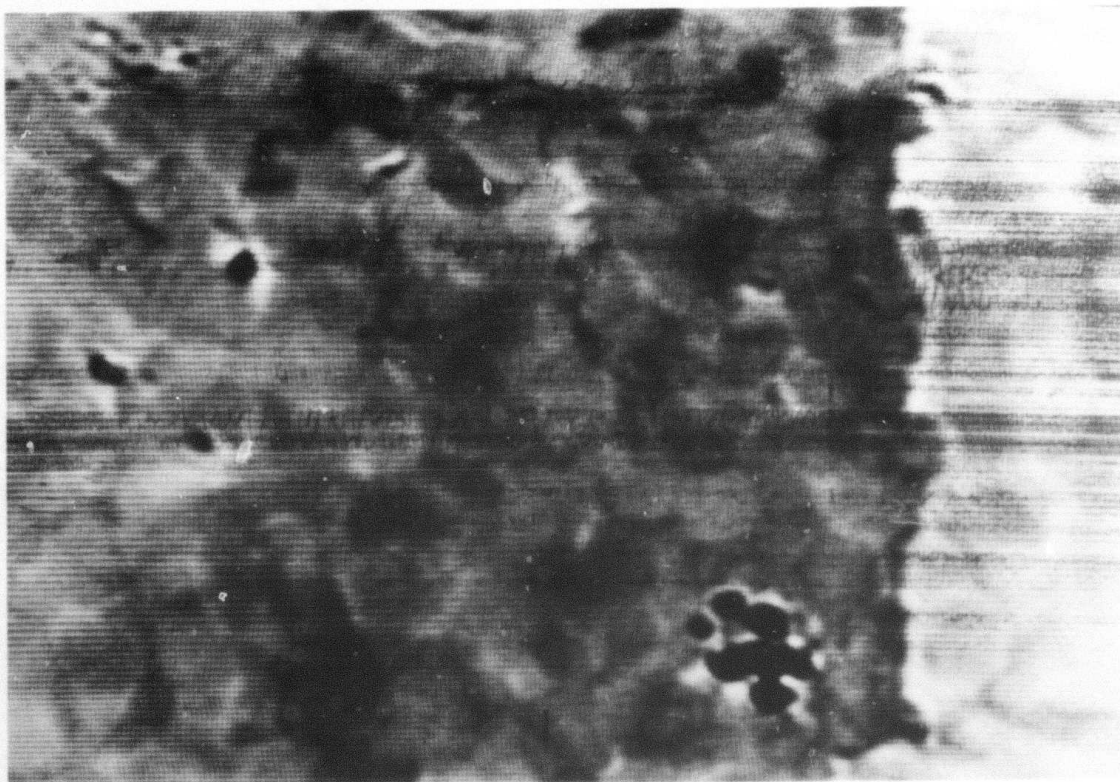
Figure 1. Transmission acoustic micrograph at 140 MHz of a three minute diffusion bond in En8 steel.

is believed that these correspond to features of the bond itself.

Reflection Microscopy

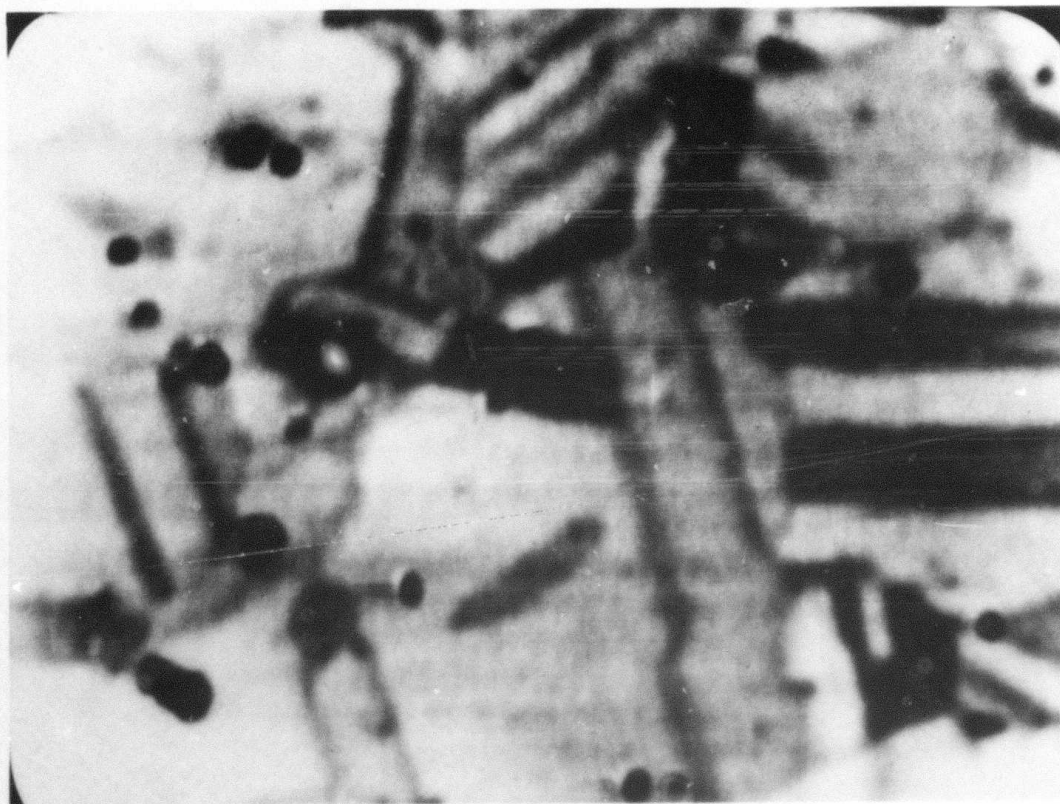
Our reflection microscope currently operates at 730 MHz, giving a surface resolution of 2μ and sampling a comparable depth of the specimen. Contrast is often enhanced by defocusing the specimen 5μ towards the lens. This should not be thought of as focussing under the surface; rather it is a result of interference between waves reflected at different angles to the normal (the $V(z)$ effect).

The easiest material feature to image in reflection from a polished but unetched surface is the grain structure. This is shown in Fig. 2 for PLZT, a transparent ferroelectric ceramic. The contrast arises because of the elastic crystal anisotropy, so that grains at different orientations present different elastic properties to the incident beam. The slightly brighter region to the right of the picture corresponds to a gold film $0.1\mu\text{m}$ thick on the surface. Grains are still acoustically visible through this film. An image of a stainless steel specimen is shown in Fig. 3. Once again the grains are visible, but in addition to contrast between one grain and another there is contrast at the grain boundaries themselves. This contrast undergoes reversals as the lens-object spacing is varied. A theory is being developed to account for this phenomenon and to clarify what information can be determined from it.



|-----|
10 μm

Figure 2. Reflection acoustic micrograph at 730 MHz of a PLZT ceramic.

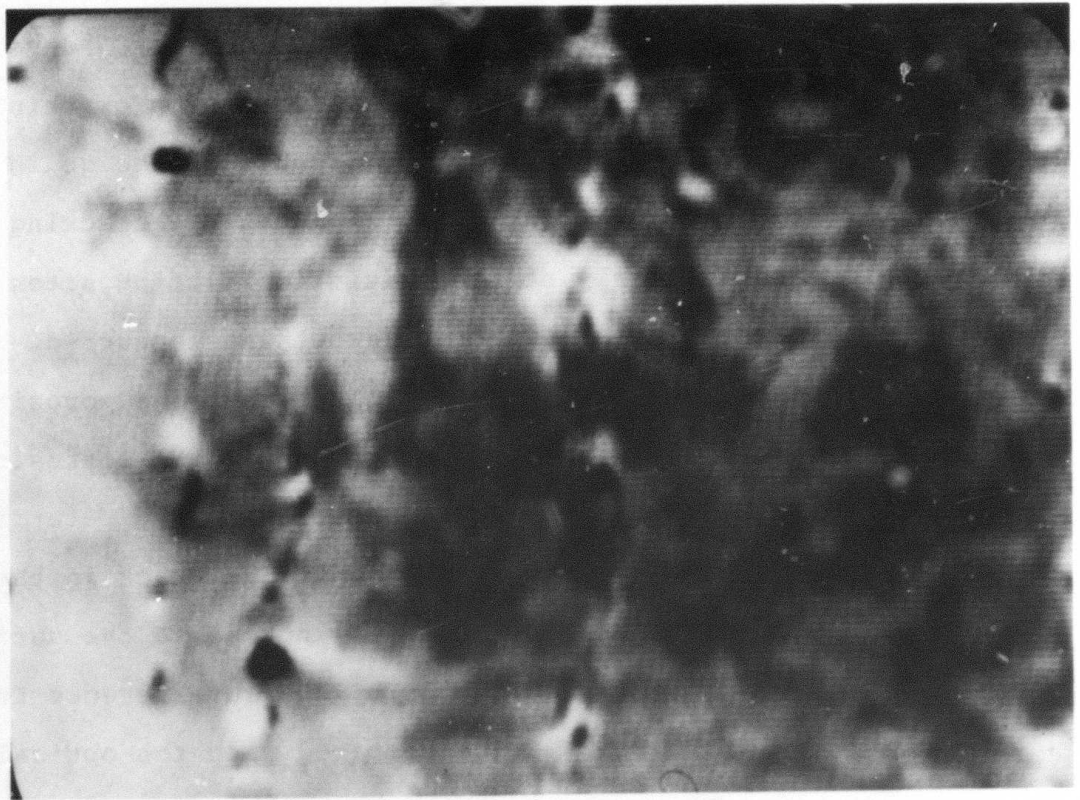


|-----|
20 μm

Figure 3. Acoustic micrograph of stainless steel, polished but not etched. The contrast can be reversed by further defocussing.

There is considerable interest in the study of cracks using the acoustic microscope. Fig. 4 shows a specimen of pipeline steel which has been cyclically loaded for 7 days in a corrosive environment to produce stress corrosion cracking. Stress corrosion cracks can be seen, and because of the grain contrast it is possible to see that in some places the cracking is intergranular, particularly at the initiation pitting sites, while in other places transgranular crack growth has occurred. Fig. 5a is an acoustic image of granite. This contains porosity in the form of cracks which are important because the diffusion of radionucleides into these cracks contributes to retarding their transport in the pathway back to man. The crack in the center of Fig. 5a, which runs approximately normal to the surface, is rendered particularly noticeable by the interference fringes each side of it. This may be compared with the optical image of the same area, Fig. 5b, in which the crack is scarcely visible.

Because the reflection acoustic microscope samples a thickness of about a wavelength, the technique has potential for examining thin films which are bonded to a substrate. Fig. 6a. is an optical micrograph of the surface of a tool. The hard metal substrate is coated with a layer of TiN a few microns thick. During cooling in manufacture the coatings crack in order to allow stress relief. These cracks are so fine that they are scarcely visible optically, although lines of defects caused during metallographic polishing can be seen in Fig. 6a. The same defects are seen in the acoustic image of the same area in



|-----|
20 μm

Figure 4. Acoustic micrograph of stress corrosion cracks in pipeline steel.



|-----|
20 μm

Figure 5a. Acoustic image of granite containing cracks.

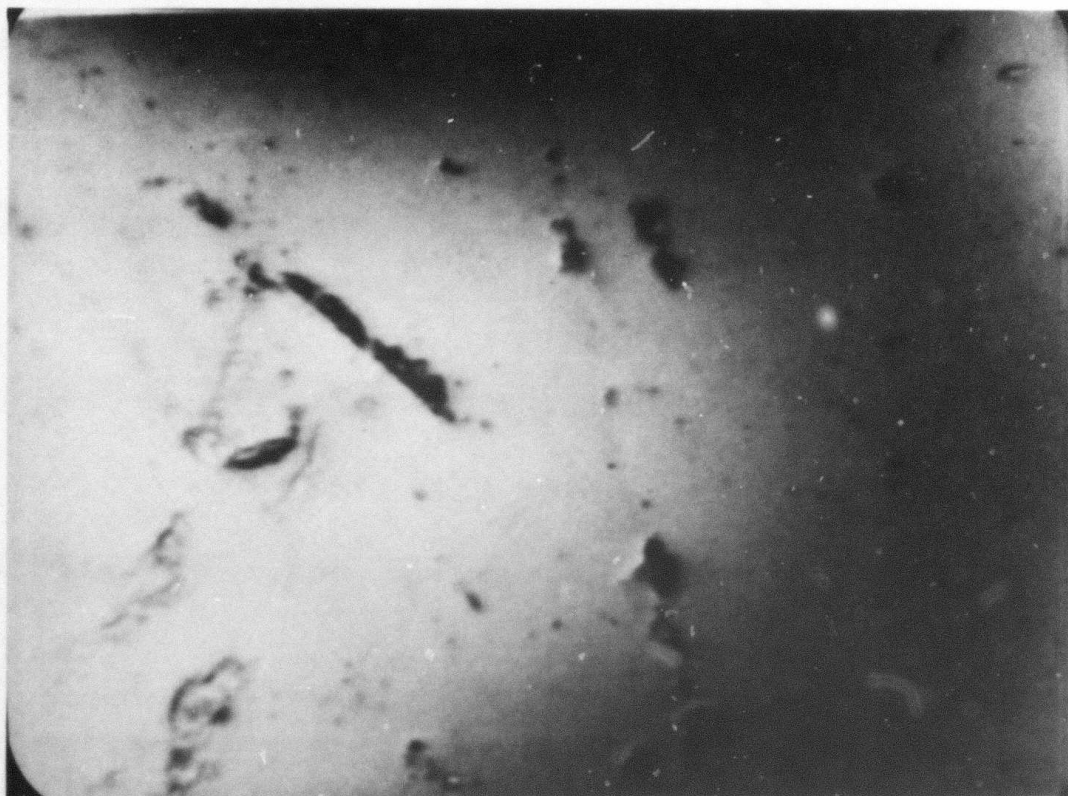
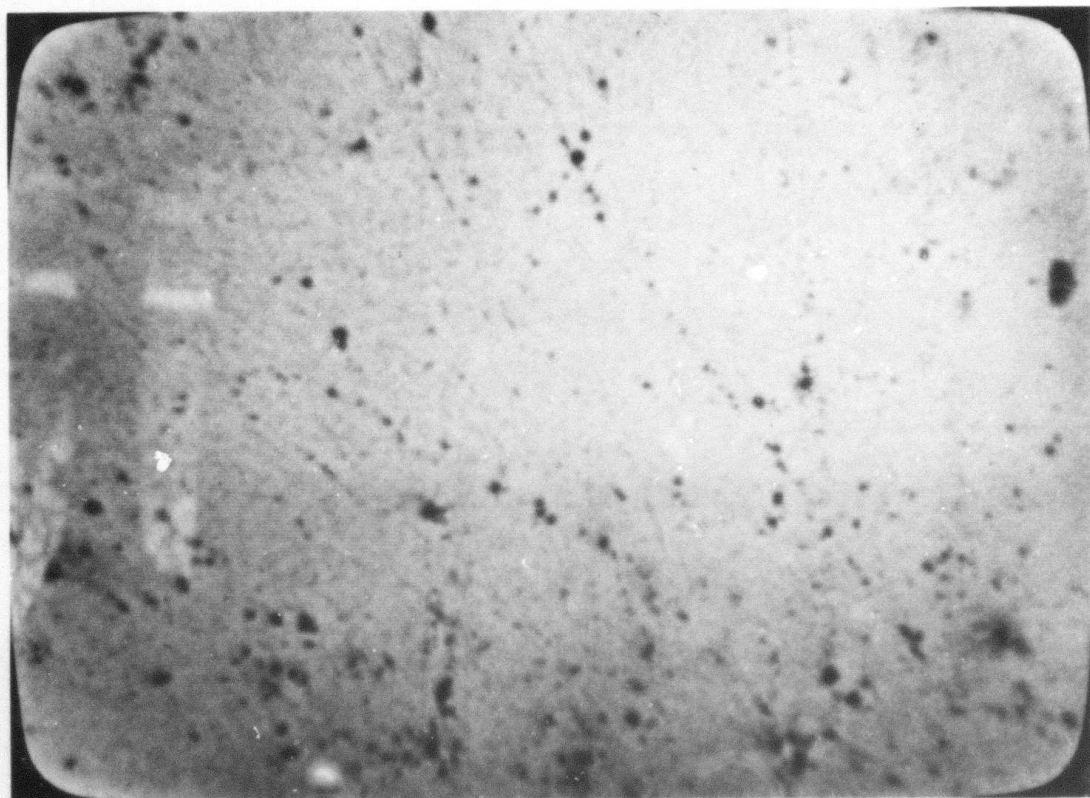


Figure 5b. Optical image of the same area as 5a.



|-----|
20 μm

Figure 6a. Optical image of a hardmetal cutting tool.

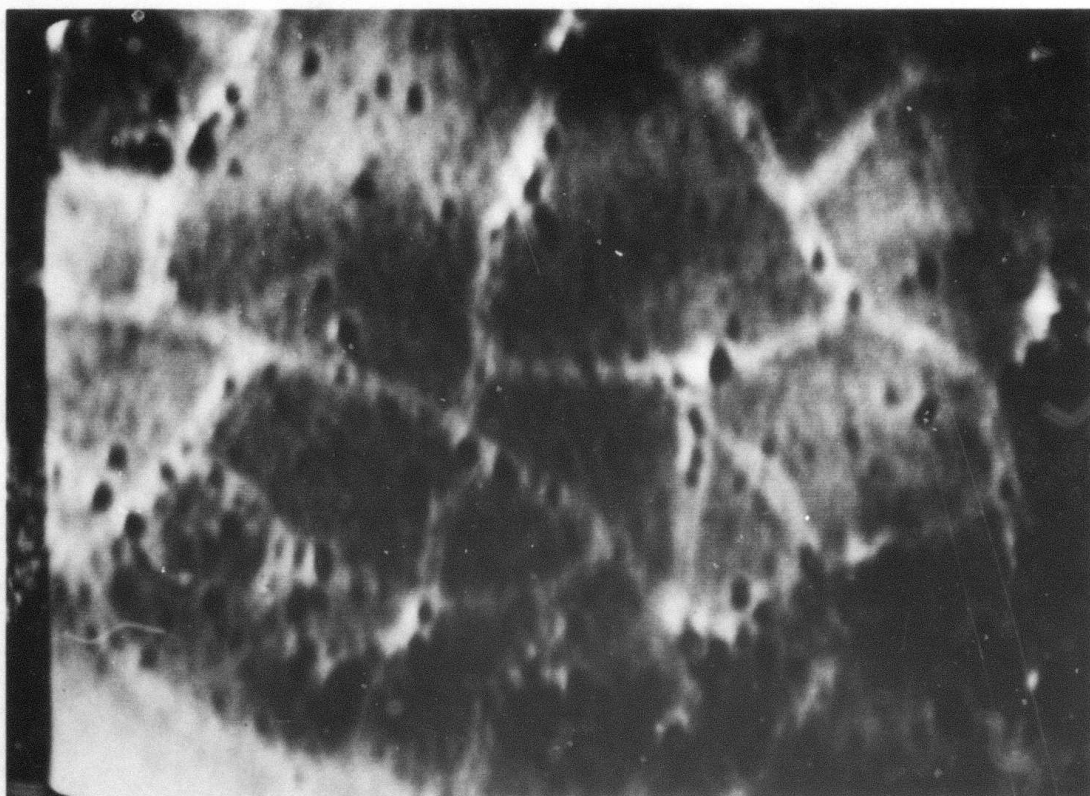
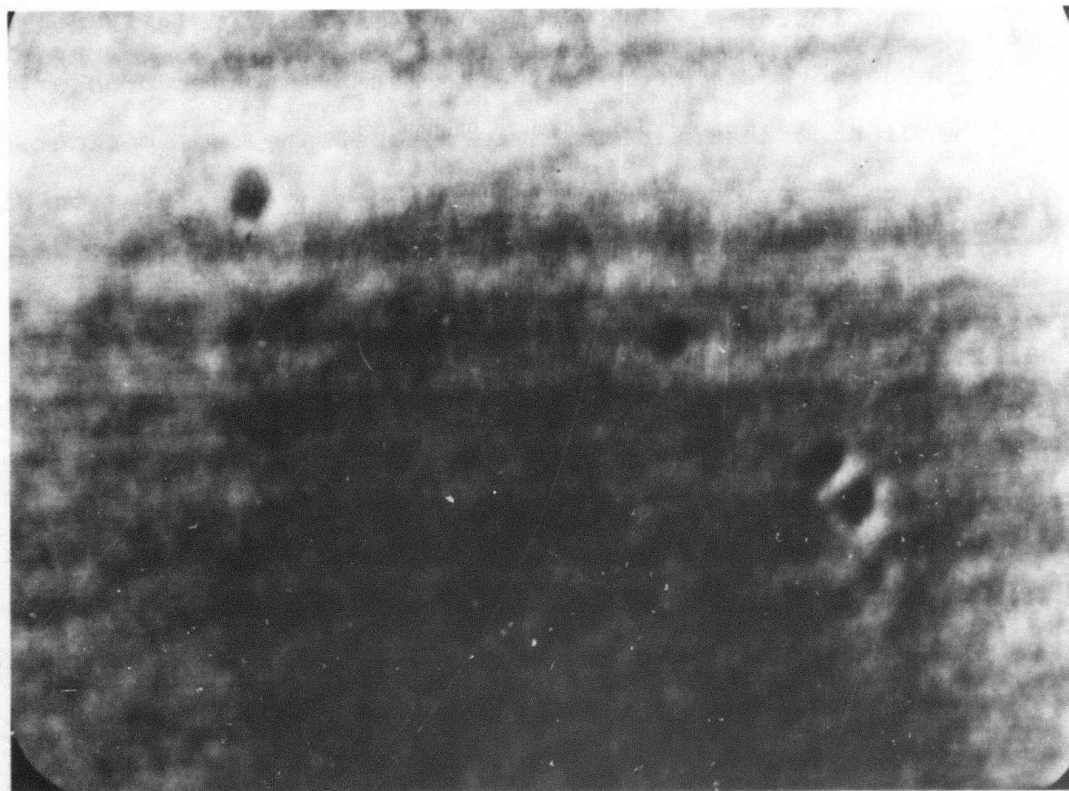


Figure 6b. Acoustic image of the same area as 6a.

Fig. 6b. However in addition there is another network which appears brighter and broader acoustically, and which does not always coincide with the polishing damage. This is believed to be the network of stress relief cracks. Another problem, where the bonding of a surface film to a substrate is important, is in the growth of oxide films. In studies of oxide films on NiCrAl alloys it has been found that the adhesion of the film may be increased if small quantities of yttrium are added. The gross structures of the oxide film on samples with and without yttrium at grain boundaries renders them visible in that alloy, but it is difficult to see any difference optically in the microstructure of the films. Differences can, however, be seen acoustically. This is illustrated in Figs. 7a and b, which are acoustic images of oxide films grown on samples with and without yttrium respectively, by exposing to moist air at 850°C for several hours. The differences between these, and also between similar pairs of images, is now being investigated more quantitatively.

Quantitative Elastic Microprobe

It is well established that the variation in signal as the lens is scanned along its axis in reflection is determined by the elastic properties of the surface being studied. The inversion problem has now been solved, permitting deduction of elastic properties directly from $V(z)$. Further, this can be extended to measurement in the reflection mode of attenuation



20 μm

Figure 7a. Acoustic image of an oxide film grown on a NiCrAl alloy exposed to moist air for several hours at 850°C.

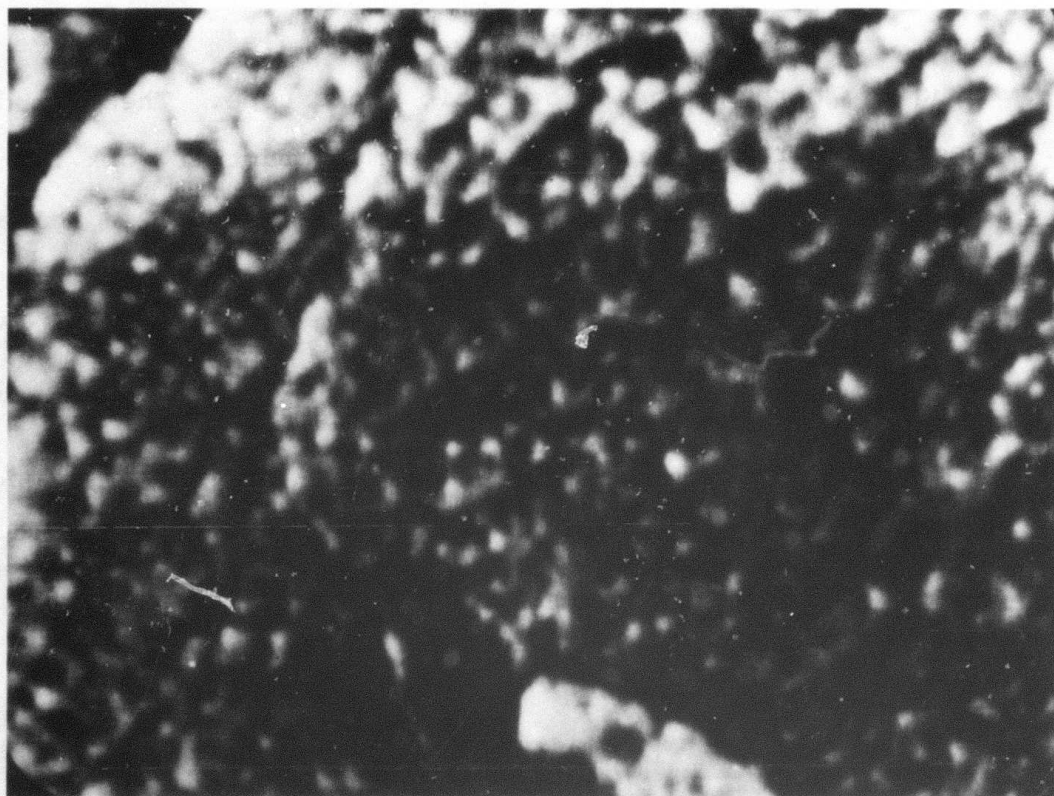


Figure 7b. As 7a, but with yttrium added to the alloy.

and also to the determination of orientation of anisotropic grains etc., both with spacial resolution of a few microns.

CONCLUSION

A variety of problems in materials science have been studied in the scanning acoustic microscope. These studies have been of a preliminary nature, and much further work is needed in each case. Nevertheless, it is hoped that they indicate the kind of areas in which the acoustic microscope may prove useful.

ACKNOWLEDGEMENT

This paper was written under the auspices of the DARPA Materials Research Council, Contract #MDA903-82-C-0428 with The University of Michigan.

ULTRASONIC SCATTERING AS A METHOD OF GRAIN STRUCTURE CHARACTERIZATION

E. P. Papadakis

ABSTRACT

The grains of metals (and ceramics) scatter ultrasonic waves and give rise to, (1) scattered pressure waves as a function of angle, and (2) attenuation of the impinging beam. Various schemes have been devised to measure these two types of disturbances. As in all scattering phenomena, the results are functions of the ratio of wavelength to grain diameter. For ultrasound, the results are also functions of the elastic moduli of the grains. The effective moduli are unknown unless the grains are single crystals. Considerable experimental work has been done to show the effects of transformation products within grain boundaries. The scattering shape factors have been expressed to date only for approximately spherical grains (equiaxed). The results are unambiguous only if it is known that extraneous energy-dissipating mechanisms are negligible. Experimental methods must compensate for other frequency-dependent phenomena such as beam-spreading.

ULTRASONIC SCATTERING AS A METHOD OF GRAIN STRUCTURE CHARACTERIZATION

E. P. Papadakis

INTRODUCTION

The "Inspector" would like to be able to walk up to a manufactured object, interrogate it with a "probe" (read "wand" if you like), and read out unambiguously the valuable engineering parameters of its constituent materials. To approach this Utopia, science and engineering have armed the Inspector with a vast number of probes based upon many physical principles; yet the array is incomplete and the object may still be unknowable unless dissected and made useless.

One of the physical principles available, but unused and only partially studied, is ultrasonic grain scattering; it holds a great potential for further utility. This study summarizes the present state of knowledge and points out the directions for further research. It is the intent of the paper to direct future investigation into research which will be useful, as well as interesting.

WHAT IS KNOWN RIGOROUSLY

Ultrasonic Attenuation

The problem of grain scattering of ultrasonic waves in polycrystalline materials continues to be of interest from both an academic and a practical point of view. Grain scattering is one problem area in which mathematical formulations¹ of wave propagation can be tested rigorously by experiments, namely the

measurement of ultrasonic attenuation.² Grain scattering impedes the inspection of weldments by ultrasonic flaw detectors,³ a deleterious effect, and holds the potential for nondestructive prediction of metal toughness,⁴ an advantageous possibility. Attenuation due to grain scattering is already utilized in a nondestructive inspection method for spot weld nugget size.⁵

Since the early work by Huntington,⁶ Roth,⁷ and Mason and McSkimin^{8,9} who expanded upon Lord Rayleigh's theoretical work¹⁰ on scattering, several authors¹¹⁻¹⁶ have worked out the theory of ultrasonic scattering in polycrystalline materials. Lifshits and Parkhomovskii,¹¹ Bhatia,¹² and Bhatia and Moore¹³ contributed exact formulas for ultrasonic attenuation due to grain scattering. The Russian work found its way into English through papers by Merkulov¹⁴ which were published in translation. The author^{15,16} worked out the method for finding the proper grain size as an average over the grain size distribution. With this grain size (grain volume, diameter, etc.), the theoretical formulas¹¹⁻¹⁴ were found to predict the ultrasonic attenuation in polycrystalline metals quantitatively². The work to date in which the theory is available and agrees with experiments quantitatively is limited to the following cases:

- (1) Homogeneous bulk specimens,
- (2) no preferred orientation,
- (3) equiaxed grains,
- (4) grains which do not exhibit any perturbation to their single-crystal character (no twins, intragranular transformation products, or precipitates).

In general, the attenuation is a function of frequency. The functional dependence falls into three regions depending on the ratio of wavelength λ to average grain diameter \bar{D} as in Table I.

TABLE I. Functional Dependence of Ultrasonic Attenuation Due to Grain Scattering

<u>Region</u>	<u>Range</u>	<u>Dependence</u>
Rayleigh	$\lambda/\bar{D} < 2\pi$	$AT\mu^2 f^4$
Stochastic	$\lambda/\bar{D} \sim 1$	$B\bar{D}\mu^2 f^4$
Diffuse	$\lambda/\bar{D} \gg 1$	$C \mu /\bar{D}$

The other terms in the attenuation are as follows:

A,B,C. Coefficients dependent on sound speed and other parameters.

μ Anisotropy factor. For cubic crystalline grains it is simply $C_{11}-C_{12}-2C_{44}$.

T Average grain volume computed over the grain size distribution as $(\pi/6)([D^6]_{AV} / [D^3]_{AV})$ to account for the scattering power of a single scatterer varying as v^2 while the average number of scatterers per unit volume varies as $1/V$.

\bar{D} Average grain diameter computed over the grain size distribution.

Further explanation of these formulas, including expressions for the coefficients and other expressions for μ for other crystallographic symmetries, are given in Refs. 1,5, 11-16, and 17.

It must be emphasized that the experimental work must be performed properly in order to make experiment agree quantitatively with theory. Subjects, such as beam spreading,^{18,19} absorption of energy by the transducer,²⁰ coupling to the specimen, and so on, must be handled correctly and compensated for exactly. One must also be assured that energy-absorption mechanisms with their own dependence on frequency are negligible. The grain size distribution comes from exacting metallographic analysis which has no shortcut to date.

Ultrasonic Backscattering and Side-scattering

This endeavor has not been pursued as vigorously as attenuation but has a high degree of potential for use in practical situations. Backscattering and side-scattering utilize only one side of the material, study the grain size distribution statistically, and incorporate attenuation indirectly. Beecham²¹ and DiGiacomo²² have worked on these methods. The main characteristic is that the scattered intensity goes through a maximum as a function of frequency at constant geometry because the scattering per grain increases with frequency, but the attenuation does also.

WHAT IS KNOWN EMPIRICALLY

Quantitative comparison between theory and experiment cannot be made in the following cases because the scattering theory has not been worked out:

- (a) inhomogeneous specimens,
- (b) wires and thin sheets,
- (c) specimens with preferred orientation,
- (d) specimens with elongated grains,
- (e) specimens with complex intragranular structure.

Two special cases of the inability to compare theory experiment are also listed here for completeness:

- (f) shear waves [scattering theory for points (1) through (4) in Section II above is complete; theory of ultrasonic beam spreading¹⁸ to correct the attenuation measurements is incomplete],
- (g) longitudinal waves in anisotropic specimens (i.e., with preferred orientation) along symmetry axes other than 3-fold, 4-fold, and 6-fold (theory of beam spreading again incomplete).

A considerable body of experimental work, summarized in Ref. 17, has been performed in the empirical region defined by points (a) through (g). Point (e) has received much attention, particularly with reference to steel. From the above lists, it can be seen that agreement between theory and experiment for ultrasonic grain scattering is good only for a limited number of simple situations.

The list above can be analyzed as follows:

Obviously, inhomogeneous specimens are intractable unless some knowledge of the spatial distribution of properties were to be adduced. The backscattering and side-scattering techniques should be helpful in mapping properties.

Wires and thin sheets are not tractable directly because the "radiation conditions at infinity" are not present for the derivation of ultrasonic scattering cross-sections.

Specimens with preferred orientation would exhibit velocity anisotropy which could indicate the configuration of the orientation. Foreknowledge of the fabrication techniques could help, also. Scattering cross-sections will be changed and will exhibit anisotropy because of the introduction of weighted probabilities (non-random) of crystallographic directions being contiguous from grain to grain. Extruded zinc was found to be anisotropic in scattering,²³ being lowest along the bar axis along which a-axes were aligned.

Specimens with elongated grains should scatter as if they contained cylinders, and the Rayleigh scattering should vary as f^3 for propagation normal to the cylinder axes.

Specimens with complex intragranular structure have received the most attention to date.¹⁷ Empirical results show the following:

(1) If prior grain boundaries can be defined, then the scattering varies with the prior grain volume characterized by T and D as in Table I.

(2) The elastic anisotropy of the intragranular material is reduced below the single-crystal value in proportion to the fineness of the resulting product and the number of directions in which its crystallographic axes can orient with respect to the crystallographic axes of the material originally contained within the prior grain volume.

(3) Each individual particle of intragranular material may form a scattering center, but the effect of the array of them seems to be less than the effect of the original grain volume, despite its reduced (averaged-out) anisotropy.

Examples to substantiate these effects are in the literature¹⁷ and are summarized here:

(1) Two low-alloy hardenable steels showed attenuation varying with their prior austenite (fcc) grain size when austenitized to different temperatures to promote grain growth and then quenched to produce very fine martensite (bct) within the prior austenite grain volumes.

(2) One Fe-30Ni alloy with fcc grains had attenuation agreeing with theory exactly. Upon step-wise quenching at cryogenic temperatures to form bcc platelets in each grain, the attenuation decreased as the martensite platelets became finer and more pervasive (0%, 40%, 90% bcc in steps). One steel showed extraordinary differences in attenuation when 3 pieces all austenitized at the same temperature were cooled at different rates to form different transformation products with different degrees of coarseness. One solution-treated beta-titanium alloy showed a

decrease in scattering attenuation upon being aged. The latter process produced a beta-prime precipitate as an intragranular product, which broke up the prior grains and lowered their anisotropy.

(3) It has been reported that ferrite (bcc iron) in steel acts as independent scattering centers independent of the prior austenite grain volume. The author is currently working on some ASE 1006 steel to attempt to verify this assertion. The prior austenite grains are not visible, so a direct computation of the attenuation on the basis of the ferrite grain size distribution will be required.

WHAT REMAINS TO BE DONE

The remaining work can be subsumed under two categories:

(1) Further theoretical and experimental work to make rigorous the empirical knowledge gained so far. This includes the sheet and rod geometry problem, the question of inhomogeneous specimens, the condition of preferred orientation, and the situations involving intragranular structure.

Concerning intragranular transformation products, one has two problems: (a) the degree of decrease of the original grain anisotropy, and (b) the amount of scattering from the intragranular products themselves.

(2) The second category is the inverse problem. What set of measurements is necessary to characterize the material? Grain

scattering contributes to ultrasonic attenuation, but absorption mechanisms do, also. Grain scattering is proportional to the average grain volume, so it can be an indicator of grain size. Grain scattering, however, as influenced by phase transformation, grain shape, preferred orientation, and certain geometrical and measurement factors. Probably attenuation and side-scattering together will yield much more information than either alone.

In manufacturing, the inverse problem is frequently attacked with the aid of Failure Mode and Effects Analyses (FMEA's). The FMEA is supposed to force the engineer to think up all the things that could go wrong. Each error which could cause a material defect is pinpointed, and an inspection method is prescribed. It is hoped that various deleterious causes do not have opposite effects upon any one inspection method. That is, one wants a monotonic relationship between the desired engineering property and the inspection method output. An example is ultrasonic velocity as a test for nodularity in ductile cast iron. One hundred percent nodularity indicates that all the graphite in the cast iron exhibits spherical morphology. Degradation of the graphite spheres lowers the strength and the ultrasonic velocity. The relationship is monotonic with 100% nodular iron having the highest velocity. Some slightly lower cutoff point for the velocity is chosen to designate acceptable product. Carbides are the only fly in the ointment; they also

raise the velocity, although they are deleterious. A separate test must be devised for them, e.g., eddy currents.

Another example, this time using grain scattering, is a check for fine-grained steel transformed 100% to martensite and tempered. The grain scattering and the absorption would both be minimum, so one would be looking for very low attenuation as the optimum condition. This situation is relatively fail-safe since the errors of all known types, both metallurgical and experimental, tend to increase the attenuation.

Still, the general inverse problem awaits solution. Grain scattering will play an important part.

RECOMMENDATIONS

A. Work out the theory for the cases listed in Section III, where only empirical knowledge and approximations exist. Also, work out the two cases of ultrasonic diffraction theory (f) and (g) in Section III, which are pure physical acoustics and not metallurgy. Then, confirm the new theories by careful experiments.

B. Work out the inverse problem in as great generality as possible, noting that a family of measurements will be needed for any one material at any one stage of fabrication. Note that most of the measurements are not state functions, but are path-dependent, so sequential measurements which follow the production processes may be the most advantageous.

ACKNOWLEDGEMENT

This paper was written under the auspices of the DARPA Materials Research Council, Contract #MDA903-82-C-0428 with The University of Michigan.

REFERENCES

1. E. P. Papadakis, "Revised Grain Scattering Formulas and Tables," J. Acoust. Soc. Am. 37, 703-710(1965).
2. E. P. Papadakis, "Ultrasonic Attenuation Caused by Scattering in Polycrystalline Metals," J. Acoust. Soc. Am. 37, 711-717(1965).
3. S. Serabian, "Influence of Attenuation Upon the Weld Interrogation Distance Amplitude Curve," Mater. Eval. 34 (12), 265-274 (December 1976).
4. A. Vary, "Correlations Among Ultrasonic Propagation Factors and Fracture Toughness Properties of Metallic Materials," Mater. Eval. 36(7), 55-64(June 1978).
5. E. P. Papadakis, "Ultrasonic Velocity and Attenuation: Measurement Methods With Scientific and Industrial Applications," in Physical Acoustics: Principles and Methods, Vol. 12, edited by W.P. Mason and R.N. Thurston (Academic, New York, 1976), pp. 277-374 (esp. pp.343-348).
6. H. B. Huntington, "On Ultrasonic Scattering by Polycrystals," J. Acoust. Soc. Am. 22, 362-364(1950).
7. W. Roth, "Scattering of Ultrasonic Radiation in Polycrystalline Metals," J. Appl. Phys. 19, 901-910(1948).
8. W. P. Mason and H.J. McSkimin, "Attenuation and Scattering of High Frequency Sound Waves in Metals and Glasses," J. Acoust. Soc. Am. 19, 464-473(1947).
9. W. P. Mason and H.J. McSkimin, "Energy Losses of Sound Waves in Metals Due to Scattering and Diffusion," J. Appl. Phys. 19, 940-946(1948).
10. Lord Rayleigh, The Theory of Sound (MacMillan, New York, 1894) 2nd ed., and (Dover, New York, 1945), pp. 149-152.
11. E.M. Lifshits and G.D. Parkhomovskii, Zh. Eksp. Teoret. Fiz. 20, 175-182(1950), (in Russian).
12. A.B. Bhatia, "Scattering of High-Frequency Sound Waves in Polycrystalline Materials," J. Acoust. Soc. Am. 31, 16-23 (1959).
13. A.B. Bhatia and R.A. Moore, "Scattering of High-Frequency Sound Waves in Polycrystalline Materials II," J. Acoust. Soc. Am. 31, 1140-1142 (1959).

14. L. G. Merkulov, "Investigation of Ultrasonic Scattering in Metals," Sov. Phys.-Techn. Phys. 1, 59-69(1965), from J. Tech. Phys. (USSR) 26, 64-73(1956).
15. E. P. Papadakis, "Grain Size Distribution in Metals and Its Influence on Ultrasonic Attenuation Measurements," J. Acoust. Soc. Am. 33, 1616-1621(1961).
16. E. P. Papadakis, "From Micrograph to Grain Size Distribution with Ultrasonic Applications," J. Acoust. Soc. Am. 35, 1586-1594(1964).
17. E. P. Papadakis, "Ultrasonic Attenuation Caused by Scattering in Polycrystalline Media," in Physical Acoustics: Principles and Methods, Vol. 4B, edited by W. P. Mason (Academic, New York 1968), pp. 269-328.
18. E. P. Papadakis, "Ultrasonic Diffraction Loss and Phase Change in Anisotropic Materials," J. Acoust. Soc. Am. 40, 863-876(1966).
19. H. Seki, A. Granato, and R. Truett, "Diffraction Effects in the Ultrasonic Field of a Piston Source and Their Importance in the Accurate Measurement of Attenuation," J. Acoust. Soc. Am. 28, 230-238(1956).
20. E. P. Papadakis, K. A. Fowler, and L. C. Lynnworth, "Ultrasonic Attenuation by Spectrum Analysis of Pulses in Buffer Rods: Method and Diffraction Corrections," J. Acoust. Soc. Am. 53, 1336-1343(1973).
21. D. Beecham,...
22. J. DiGiacomo,...
23. E. P. Papadakis,...

ULTRASONIC NONDESTRUCTIVE CHARACTERIZATION OF METALLURGICAL MICROSTRUCTURES AND TRANSFORMATIONS

M. Rosen and R. Mehrabian

INTRODUCTION

Ultrasonic nondestructive evaluation has traditionally been concerned with the search and location of flaws in materials structures, determination of their distribution and orientation. A considerable body of knowledge has also been accumulated from ultrasonic scattering studies in assessing grain size and orientation effects in materials.

Recently, it has become widely recognized that ultrasonic measurements can be used to characterize materials performance such as strength, toughness, effect of residual stresses so as to supplement, or even replace, the conventional destructive techniques employed in metallurgy. Ultrasonics offers distinct advantages in that materials properties can be verified on actual components of engineering structures.

The scientific literature is extremely scarce in dynamic nondestructive characterization (NDC) whereby, ultrasonic techniques are applied to on-line, real-time, monitoring of microstructures for the control of metallurgical processes. Inherent difficulties related with this type of measurement methodologies include operation at elevated temperatures and in hostile environments. Furthermore, there is little basic data available on the relationships between the metallurgical microstructures and measured ultrasonic responses. Therefore, the full

potential of ultrasonic techniques in this field has yet to be realized.

Recent studies at the National Bureau of Standards (NBS), supported by DARPA, have addressed the specific area of dynamic, real-time nondestructive characterization of metallurgical microstructures, e.g., precipitation hardening of aluminum alloys and crystallization of amorphous alloys¹⁻⁵. Conventional bulk ultrasonic techniques had to be adapted for application to dynamic changes of the microstructure. However, in attempting to dynamically characterize metallurgical processes in amorphous ribbons or structurally modified thin surface layers, the conventional ultrasonic techniques were found to be inadequate. Thus, a new approach for contactless generation and detection of acoustic waves, using a laser generation and laser interferometric detection system was adapted.

The objective of this presentation is to review recent developments in this program in NDC of materials processes. The presentation will be divided into three parts. First, a description will be given of the laser interferometric technique for the detection and analysis of propagating acoustic waves in thin ribbons and microstructurally modified surface layers. The development of the laser interferometer was a joint project, between NBS and Johns Hopkins University (JHU). The second part of the presentation will deal with the dynamic NDC of precipitation hardening phenomena in aluminum alloys. Here, bulk ultrasonic techniques were used for continuous and simultaneous

monitoring of the variations in sound velocity and ultrasonic attenuation during the precipitation process. In the last part, a description will be given of: (a) the application of laser generation -piezoelectric detection of acoustic waves during crystallization of amorphous alloys, and (b) the use of surface Rayleigh waves for metallurgical characterization of microstructurally modified surface layers of bulk crystalline substrates.

LASER GENERATION AND OPTICAL INTERFEROMETRIC DETECTION OF ULTRASONIC WAVES IN SOLIDS

The noncontact feature of both generation and detection of ultrasonic waves can be very advantageous in situations requiring physical separation between the measuring system and the material under investigation, e.g., when high temperatures or hostile atmospheres are involved. Furthermore, the contactless generation and detection precludes interaction with, and modification of, the wave propagation pattern under study. In addition, laser generation of acoustic waves yields a wide variety of propagation modes (longitudinal, transverse and plane modes, Rayleigh waves) over a wide frequency range, thus enhancing the amount of information obtained from a single measurement.

Compressive stress waves that propagate in a material can be generated by transient loads applied by rapid energy transfer from a single-pulse Q-switched high-energy Nd:YAG laser. Propagation of ultrasonic waves in a medium causes surface displacements on the material that can be measured optically by exploiting the phase shift of an optical beam reflected from the

surface of the material. When the reflected beam is combined with a reference optical beam, from a helium-neon laser, optical phase changes are converted into amplitude phase changes that are detectable by a sensitive photodiode. These variations in amplitude are proportional to the surface displacements on the specimen. Potential problems arising from the fact that phase changes also result from relative motion among optical components of the system and from temperature and pressure fluctuations of the ambient air, are prevented by appropriate design of the interferometer. An optical scheme due to Fizeau is particularly suitable for our specific purpose.

The dual probe laser interferometer shown in Fig. 1 was designed and constructed for detection of ultrasonic waves using a combination of two Fizeau interferometers⁶. The two optical probes are separated to allow accurate measurements of travel time of an ultrasonic wave in the material over a well-defined distance. Furthermore, the variation in magnitude of the surface displacements detected by the two interferometers determines the ultrasonic attenuation in the material. Thus, both velocity and attenuation can be measured simultaneously.

Compared with other sensors, optical interferometers offer several advantages. The sensitive area can be made very small, a few micrometers in diameter, for highly localized measurements. Consequently, the surface of the specimen does not necessarily have to be flat optically. The highly focused optical beams permit utilization of specimens with conventionally

Overall Optical System

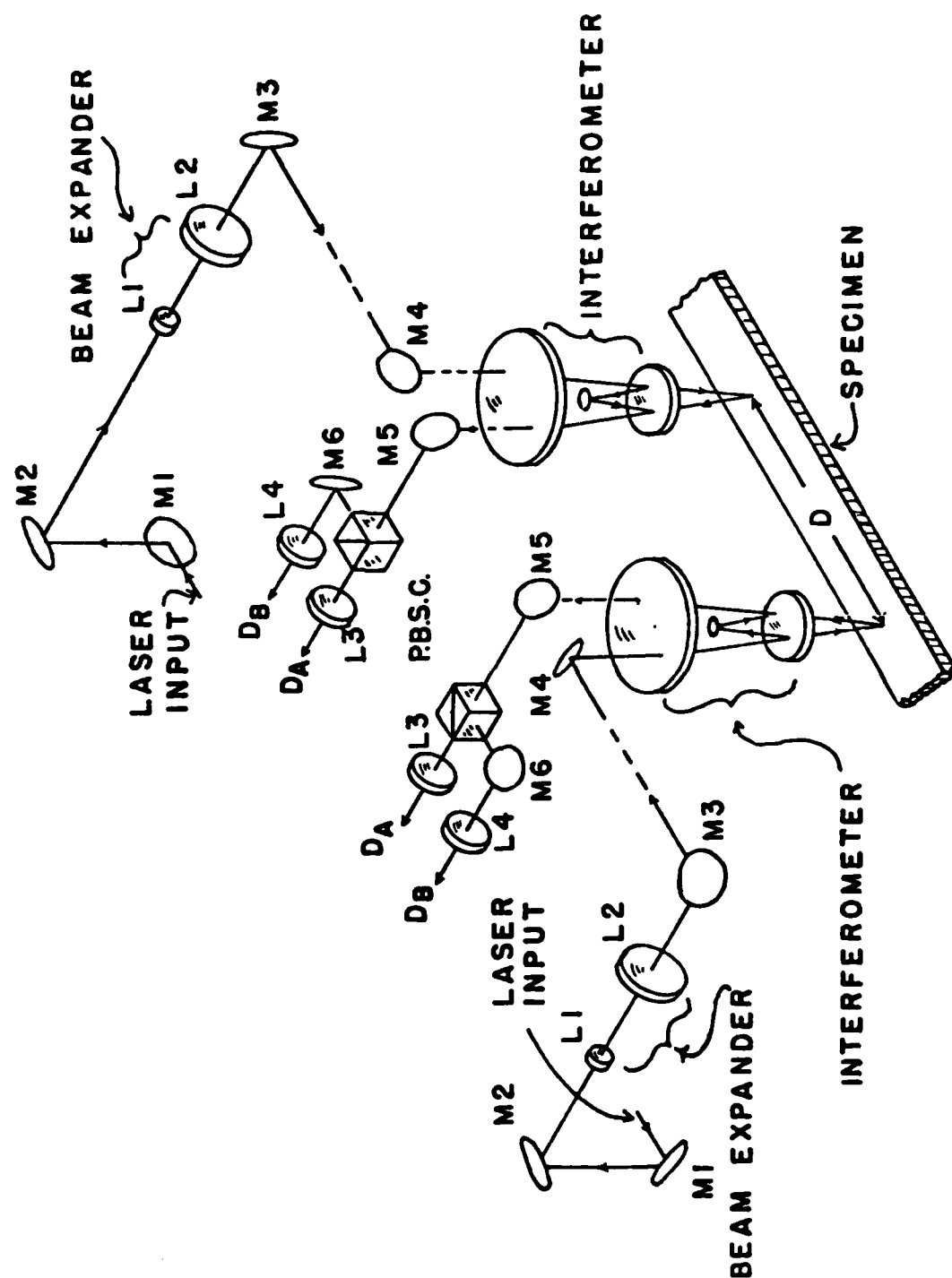


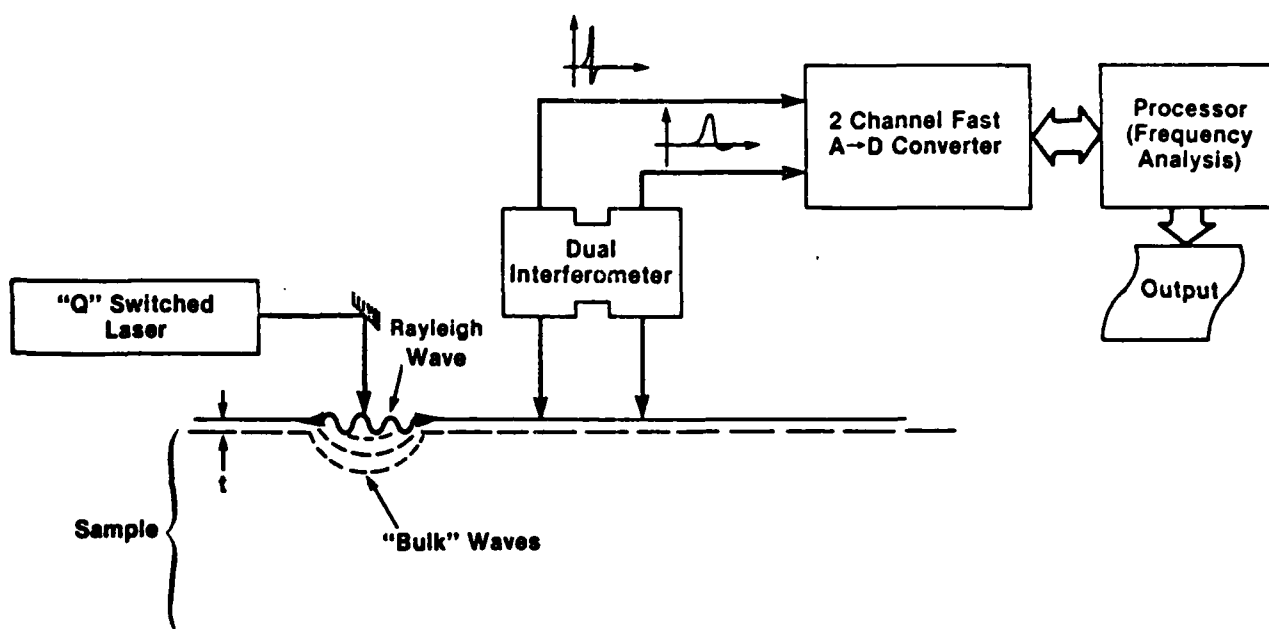
Figure 1. Dual Laser interferometer.

machined surfaces. The measured quantity is displacement. Independent methods of absolute calibration are applicable. Bandwidth, determining the fidelity of reproduction of signal waveforms, is not limited by the character of the transduction process, but by the electronics of the interferometer detectors. Therefore, performance can largely exceed that of conventional piezoelectric transducers. Small signal resolution and bandwidth are related, thus displacements of a few angstroms are detectable at 7 MHz bandwidth.

Laser pulse irradiation produces a stress pulse of short duration (15ns) and relatively high amplitude (up to 200mJ power), making the investigation of very thin (about 20 μ m) and highly attenuating specimens possible. Since a multitude of acoustic wave propagation modes is generated, the dual interferometer provides important information concerning the elastic and anelastic properties of the material under static or dynamic conditions.

Fig. 2 shows a schematic diagram of the generating Q-switched laser and the dual interferometer detection assembly for the investigation of propagation of Rayleigh surface waves in microstructurally modified surface layers. The vertical displacement of the surface due to the propagation of the Rayleigh wave is being detected by the two probes of the wide band optical detectors. Subsequent frequency analysis of the detected displacement pulses yields the frequency dependence of the measured velocities and attenuations. Since the Rayleigh

Rayleigh Waves in Microstructurally Modified Layers



- Wideband Ultrasonic Pulse Generated by Laser Pulse.
- Vertical Displacement v.s. Time Is Measured at Two Different Points by Two Wide Band Optical Detectors (Interferometers).
- Frequency Analysis of the Two Pulses Gives Attenuation v.s. Frequency and Velocity v.s. Frequency Curves.
- Penetration of Rayleigh Waves is Frequency Dependent, the Thickness t of the Microstructurally Modified Layer can be Evaluated From These Curves.

Figure 2. Rayleigh wave measurement in microstructurally modified layers using the dual laser interferometer.

velocity is frequency independent, but the Rayleigh wave penetration into the specimen bulk is not, the thickness of the structurally modified layer can be nondestructively determined. This is in addition to the nondestructive characterization of the elastic and anelastic properties of the modified layer.

The laser generated ultrasonic wave can also be piezoelectrically detected, Fig. 3, by an NBS conical PZT transducer having a flat response between dc and 2 MHz. A silicon photodiode triggers a Nicolet Explorer III digital oscilloscope so that the arrival of the elastic wave can be recorded, and transit time read directly from the oscilloscope screen. This technique was found to be particularly suitable, and highly accurate, for the determination of extensional wave velocities in thin (about 20 μm) and narrow (about 1mm) ribbons.

NDC OF PRECIPITATION HARDENING PHENOMENA IN ALUMINUM ALLOYS

Precipitation hardening, or aging, is an important metallurgical process whereby the material's strength and hardness can be augmented, in several instances, by an order of magnitude. Precipitation hardening is a thermally-activated, diffusion-controlled, process of particular importance in copper, iron, and aluminum-base alloys. The improved mechanical and physical properties of these alloys depend, largely, on the microstructure, spacing, size, shape and distribution of the precipitated particles, as well as on the degree of structural and crystallographic coherency of the particles with the matrix. For example, the precipitation hardening process in aluminum

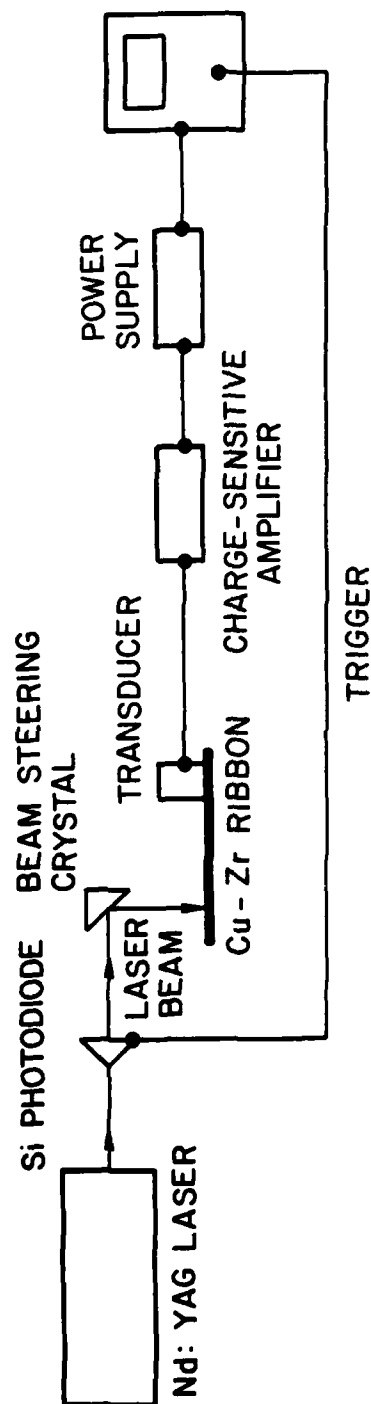


Figure 3. Laser generation - piezoelectric detection of ultrasonic waves in thin ribbons.

alloys involves formation of Guinier-Preston (G.P.) zones, θ'' and θ' particles that are generally coherent or semi-coherent with the matrix and contribute to the strengthening of the alloy. At higher temperatures incoherent θ particles form that reduce dramatically the strength and hardening of the alloy. Of particular importance in aluminum-base alloys are the θ' particles, initially semi-coherent with the matrix, that grow in size as the precipitation process progresses. At a certain critical size, when the stress fields surrounding these precipitates are maximal, dislocation rings (Orowan loops) form around them, thus causing the coherency to be lost. At this point, overaging, or softening, begins.

Of great technological importance is the development of a nondestructive probe that will permit: (a) determination of the extent of matrix supersaturation in alloys prepared by new processes such as rapid solidification, and (b) real-time monitoring of the precipitation hardening process to determine particular events such as the instant when particles lose coherency with the matrix and overaging begins. Of course, solution of the latter problem implicitly addresses the former. The NBS program was specifically designed to explore the potential of ultrasonic NDC for dynamic characterization of the precipitation hardening process.

For dynamic measurements at elevated temperature up to 250°C, ultrasonic evaluation was performed using bulk wave ultrasonics by means of quartz disc transducers held in direct

ultrasonic attenuation were continuously recorded. A pulse-echo overlap technique was employed. Ultrasonic measurements were corroborated with optical and electron microscopy, hardness, strength and eddy current conductivity data.

Figure 4 shows the time dependence of these changes in the sound wave velocity of 2219 aluminum alloy during isothermal aging at three temperatures. The nondestructive characterization of the aging process, as manifested in Fig. 4, shows a series of dips that correspond to the maximal rate of formation of θ'' and θ' particles. Thus, from ultrasonic NDC kinetic parameters can be deduced along with a positive indication about the kind of precipitates prevailing after a given aging time during isothermal heat treatment.

Figure 5 exhibits the variation in hardness of the 2219 aluminum alloy as a function of aging time. The peak hardness depends on the aging temperature. No corresponding feature related with peak hardness is observed on the sound velocity curves, Fig. 4. The reason for this behavior is that the peak hardness is indicative of the loss of coherency of θ' precipitates. Sound wave velocity is thus unaffected by the state of coherency of the particles. Sound velocity, in this particular case, is solely dependent on volume fraction of the precipitates. However, ultrasonic attenuation, Fig. 6, shows large peaks at aging times corresponding with peaks in the hardness curves.

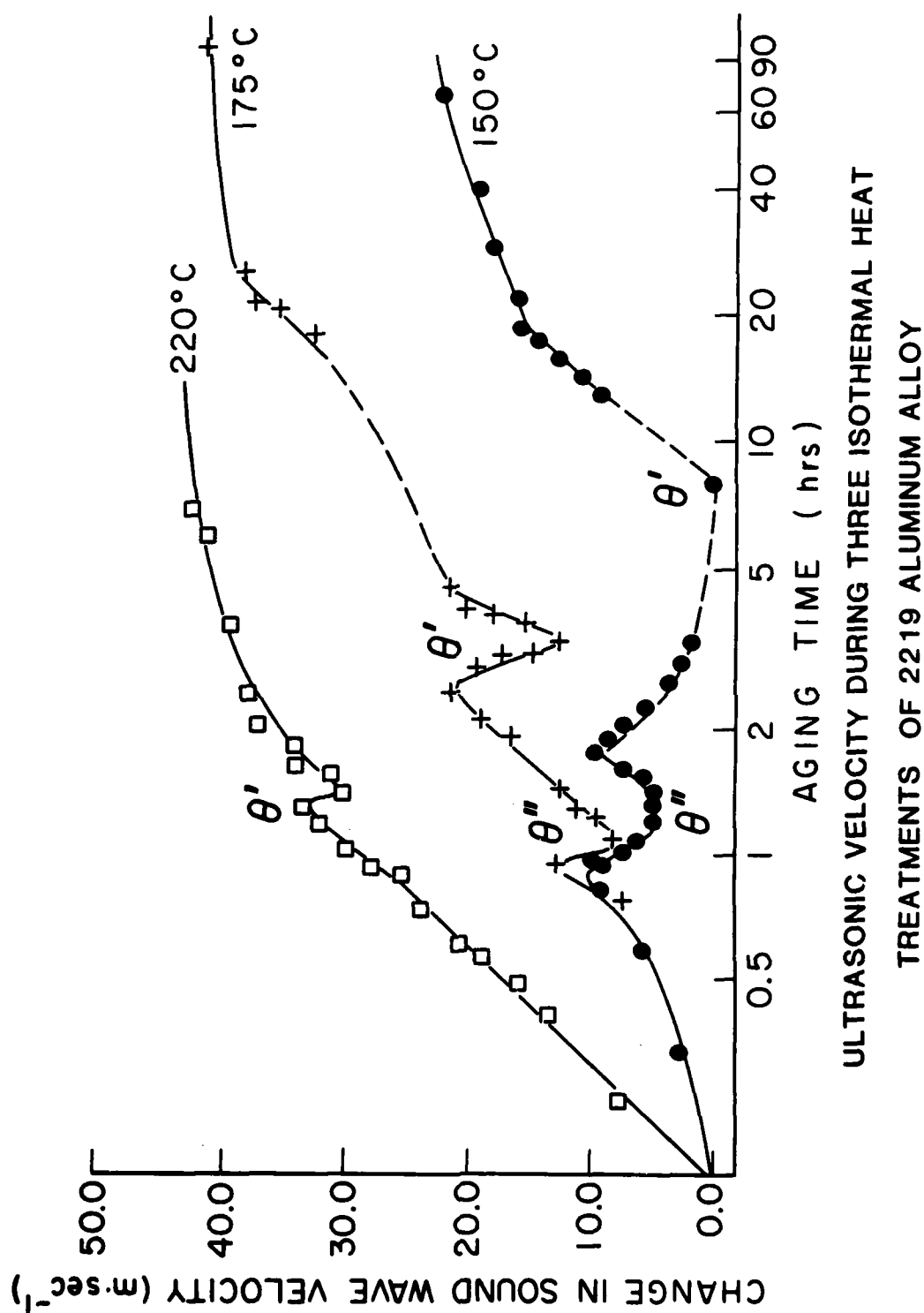


Figure 4. Variation of sound velocity with aging time at three isothermal holding temperatures in 2219 aluminum alloy.

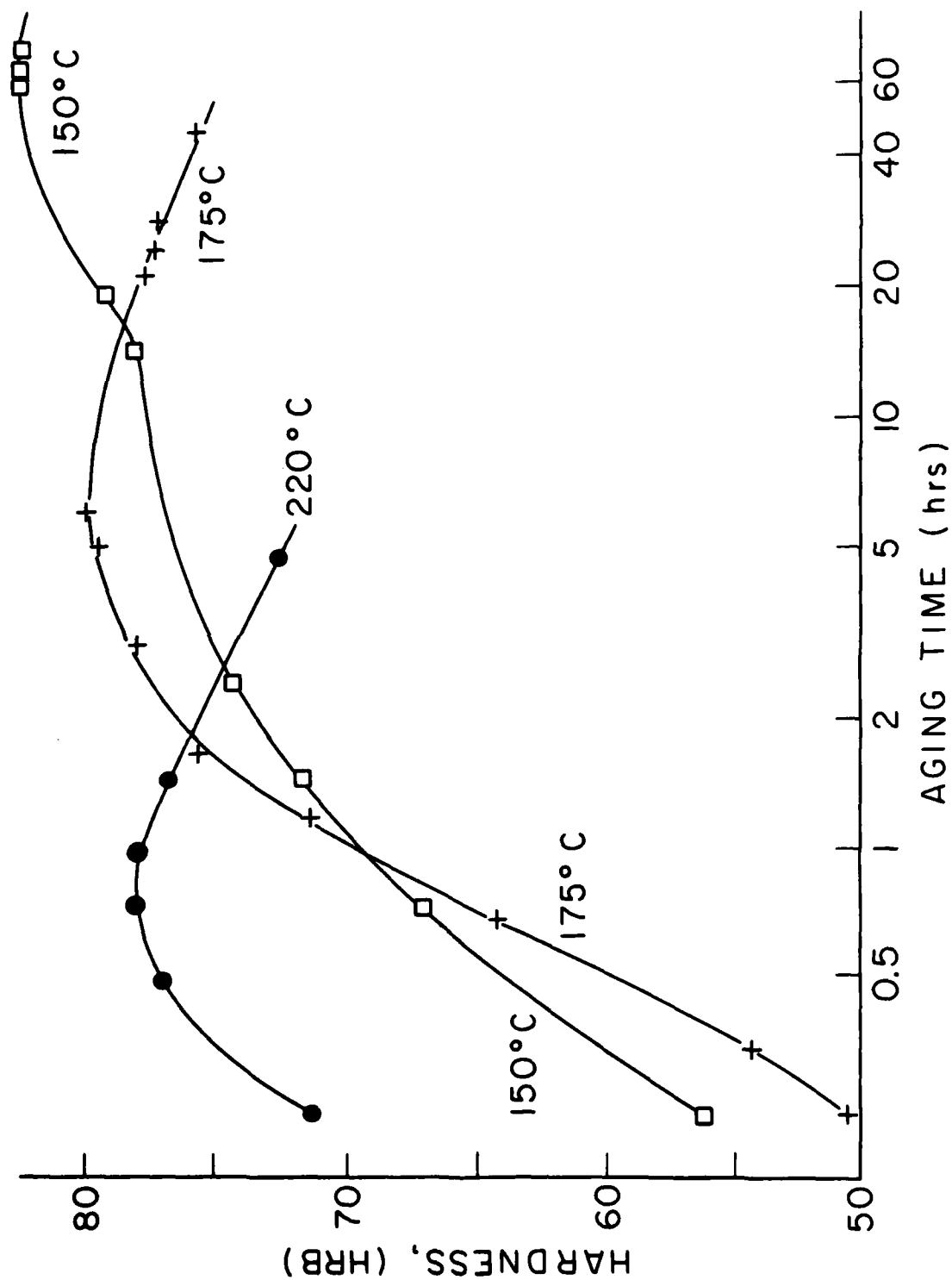


Figure 5. Hardness during three isothermal heat treatments of 2219 aluminum.

The prominent peaks in ultrasonic attenuation, Fig. 6, correspond to the hardness peaks in Fig. 5 and represent the loss of coherency of θ' particles with the matrix and beginning of the softening process. The peaks in ultrasonic attenuation may arise from an interaction between the acoustic vibrations of the ultrasonic waves propagating through the material and the interface dislocations surrounding the θ' particles. The strength of the interaction will depend on the total volume of the θ' particles, their size, shape and distribution. The peak value of attenuation can be qualitatively related with the total volume of semi-coherent precipitates that lost complete coherency with the matrix. The temperature dependence indicated by the shift in the attenuation peaks, Fig. 6, permits the determination of an activation energy that is found to be very close to that obtained from the shift of the hardness peaks. Corroborative evidence was obtained by means of electron microscopy and substantiates the proposed mechanism of coherency loss in this alloy.

In summary, ultrasonic NDC of the precipitation hardening process yields important information with respect to formation of the different precipitates, the extent of the process (from sound velocity data), and indication on the beginning of the softening process of the alloy (peaks in ultrasonic attenuation). Moreover, ultrasonic NDC provides important kinetic parameters, namely, the activation energy of the diffusional processes and growth parameters related to the developing

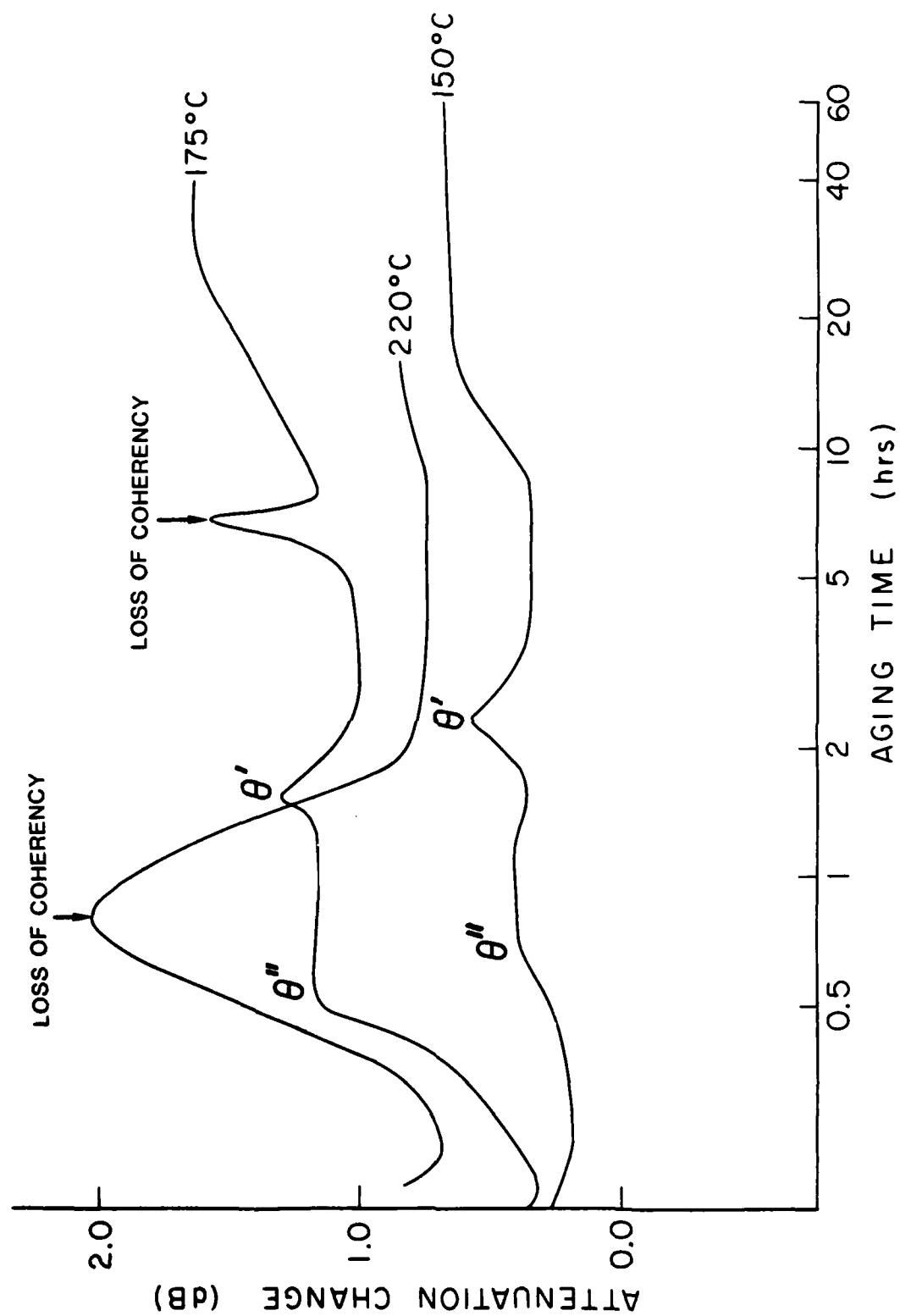


Figure 6. Ultrasonic attenuation during three isothermal heat treatments of 2219 aluminum alloy.

morphology. This investigation demonstrates the feasibility of ultrasonic NDC for on-line, real-time, monitoring and process control of precipitation hardening. Furthermore, the results show that this method of NDC may have applications in determining the extent of solute supersaturation in alloys subjected to rapid solidification processing.

NDC OF CRYSTALLIZATION PROCESSES IN AMORPHOUS MATERIALS AND IN MICROSTRUCTURALLY MODIFIED SURFACE LAYERS

Amorphous alloys, or glassy metals, are solids with frozen-in liquid structures. The absence of translational periodicity in the amorphous state along with the macroscopic compositional homogeneity are the main reasons for their improved properties, e.g., high strength, good corrosion resistance and excellent magnetic behavior.

These unusual mechanical, physical and chemical properties have stimulated extensive scientific and technological interest. One serious problem in the processing and utilization of amorphous alloys, that may limit their future technological applications, is their low thermal stability. When thermomechanical conditions are appropriate, metallic glasses relax structurally and ultimately crystallize into more stable structures resulting in drastic variations in properties. The factors governing the thermal stability of these alloys and their effect on properties are not well understood. For example, upon crystallization, amorphous alloys undergo very large changes in the elastic (40%) and anelastic properties with accompanying re-

duction in plastic properties (embrittlement). For this reason, availability of a nondestructive ultrasonic characterization technique for both property determination and metallurgical process control can be useful. Preliminary results of work in this area are presented here.

There is ample evidence that microstructural modifications of near-surface layers, with concurrent improvements in properties, can be achieved by laser and electron beam irradiation of bulk metallic materials. Rapid melting and resolidification of a surface layer can produce refined structures and more homogeneous materials, or in some instances, new microstructures and phases. Examples of the latter include extended solid solubility and formation of metallic glasses.

Ultrasonic NDC, in particular the contactless generation and detection of Rayleigh surface waves by laser interferometry, can be useful for determination of the properties and geometrical dimensions of structurally modified layers while in the formative or post-solidification stage. Some of the work, performed at NBS and supported by DARPA, will be reviewed here.

Figure 7 exhibits a view from the thin edge of a metallic glass ribbon (PdCuSi) heat treated for different times at a constant temperature, above the glass transition temperature, in order to induce the crystallization process. Fig. 7 shows that the crystallization process in the ribbons is not homogeneous in the bulk. Two coexisting transformation processes are apparent. One begins with a rapid nucleation at the free surfaces,

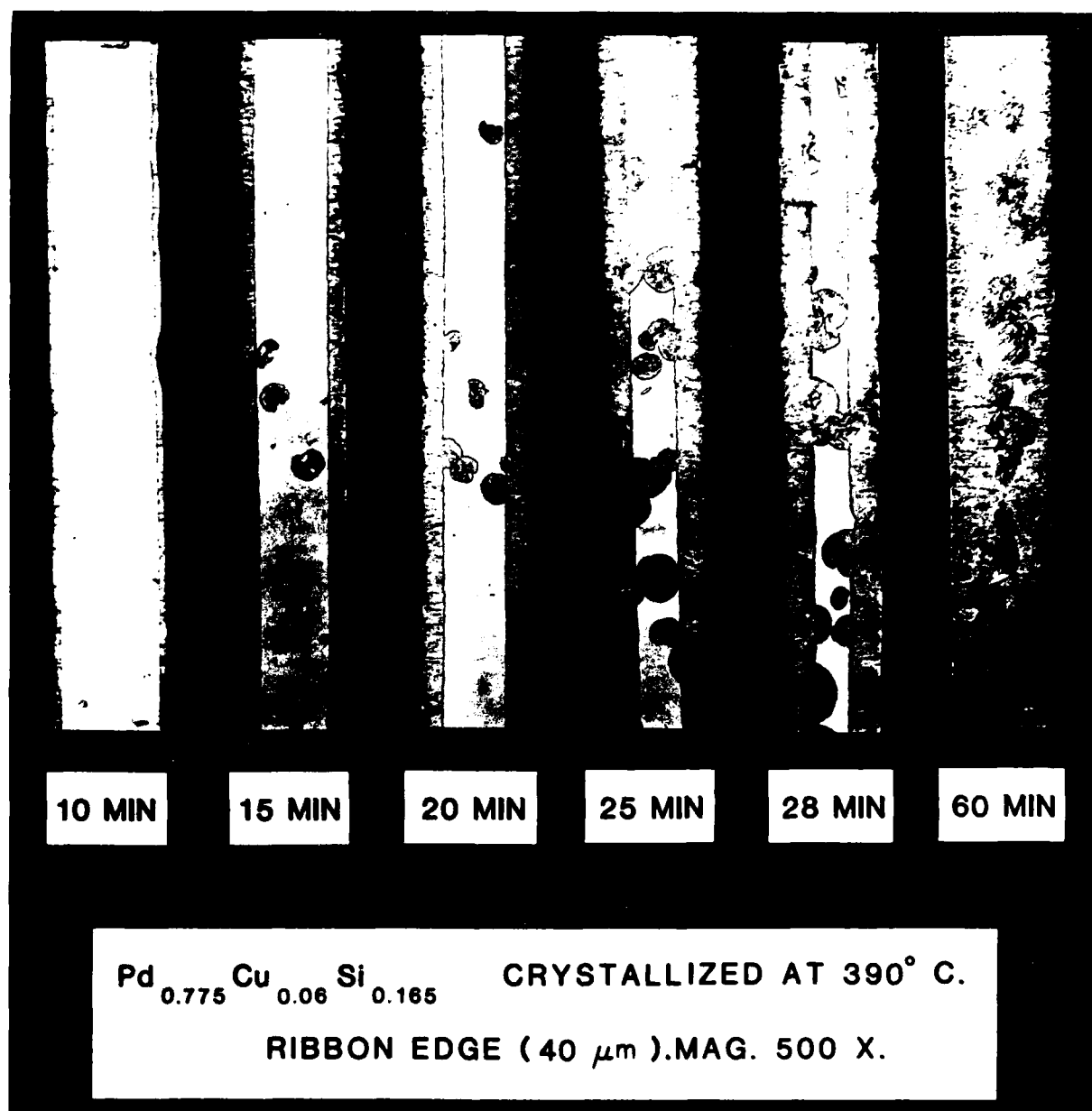


Figure 7. Crystallization sequence of amorphous PdCuSi as a function of time at a constant temperature, by optical metallography.

followed by a frontal growth towards the interior. The other involves homogeneous nucleation of crystallized regions in the bulk followed by spherical growth. The growth rate was determined by means of optical metallography.

Figure 8 shows the ultrasonic NDC of the crystallization process in this metallic glass. The variation of the extensional wave velocity with crystallization time manifests the dramatic changes in the elastic properties with an increase of about 40% in Young's modulus. The sigmoid curves represent the crystallization kinetics which is a thermally activated process. Thus, the kinetic parameters, i.e., activation energy and the growth regime parameter can be determined from the NDC data. Furthermore, the relatively large change in sound velocity before crystallization ensues, i.e., while the material is still in the amorphous state, points toward relaxational processes that are expected to occur. Microhardness measurements, Fig. 9, on the ribbon edge, perpendicular to the length vector of the ribbon, revealed that while in the amorphous, precrystallization state, the material undergoes some important mechanical changes. In the pre-crystallization state microhardness increases drastically. The embrittlement mechanism can be related to the removal of the initially quenched-in free volumes (vacancy clusters). The reduced coordination of the atom complexes in the amorphous state permits shear transformations to be sustained. Consequently, the material is ductile. Heat treatment redistributes the free volumes by short range shuffling of atoms

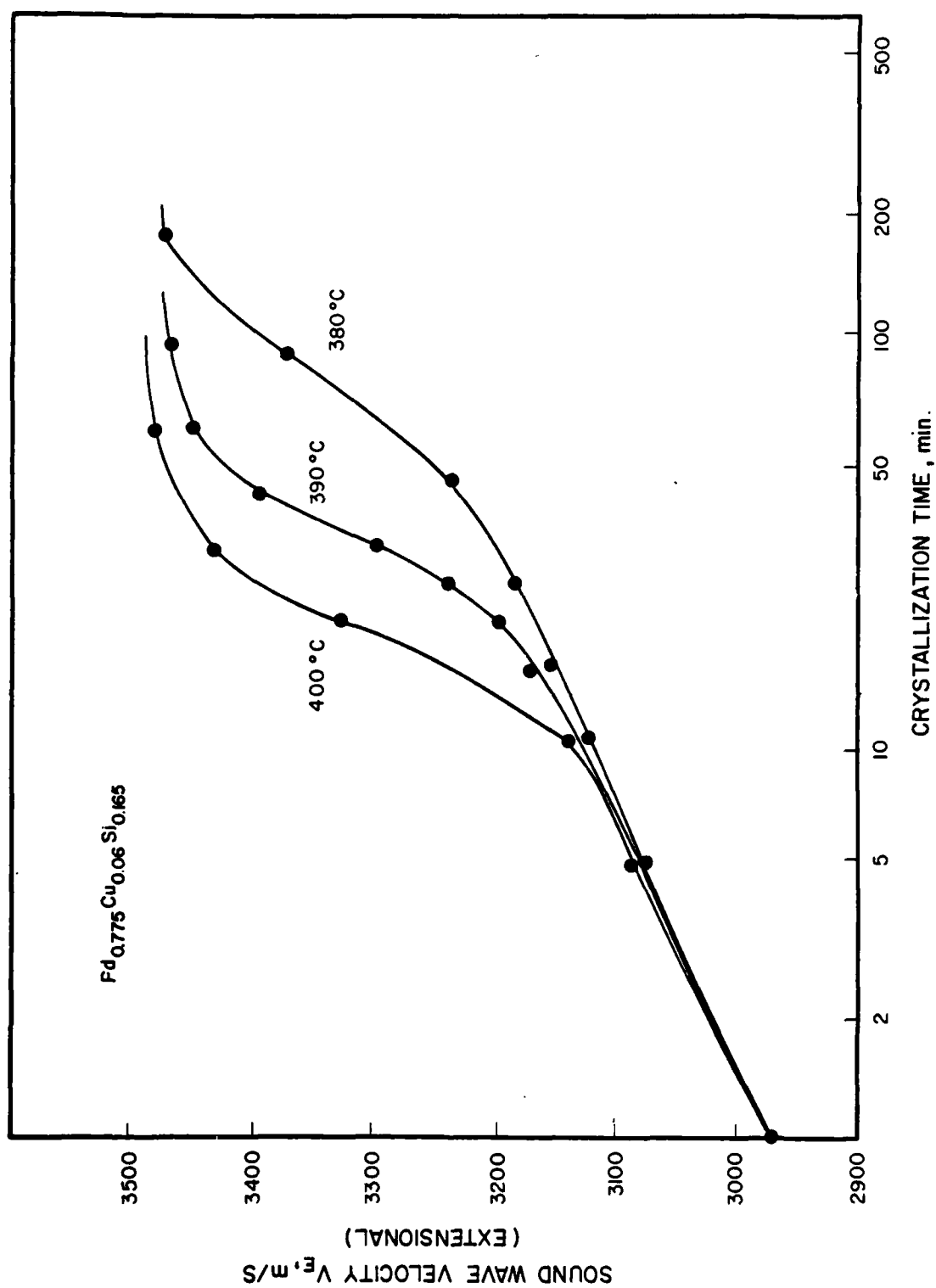


Figure 8. Variation of the extensional wave velocity in PdCuSi during transition from amorphous to crystalline state at three isothermal holding temperatures.

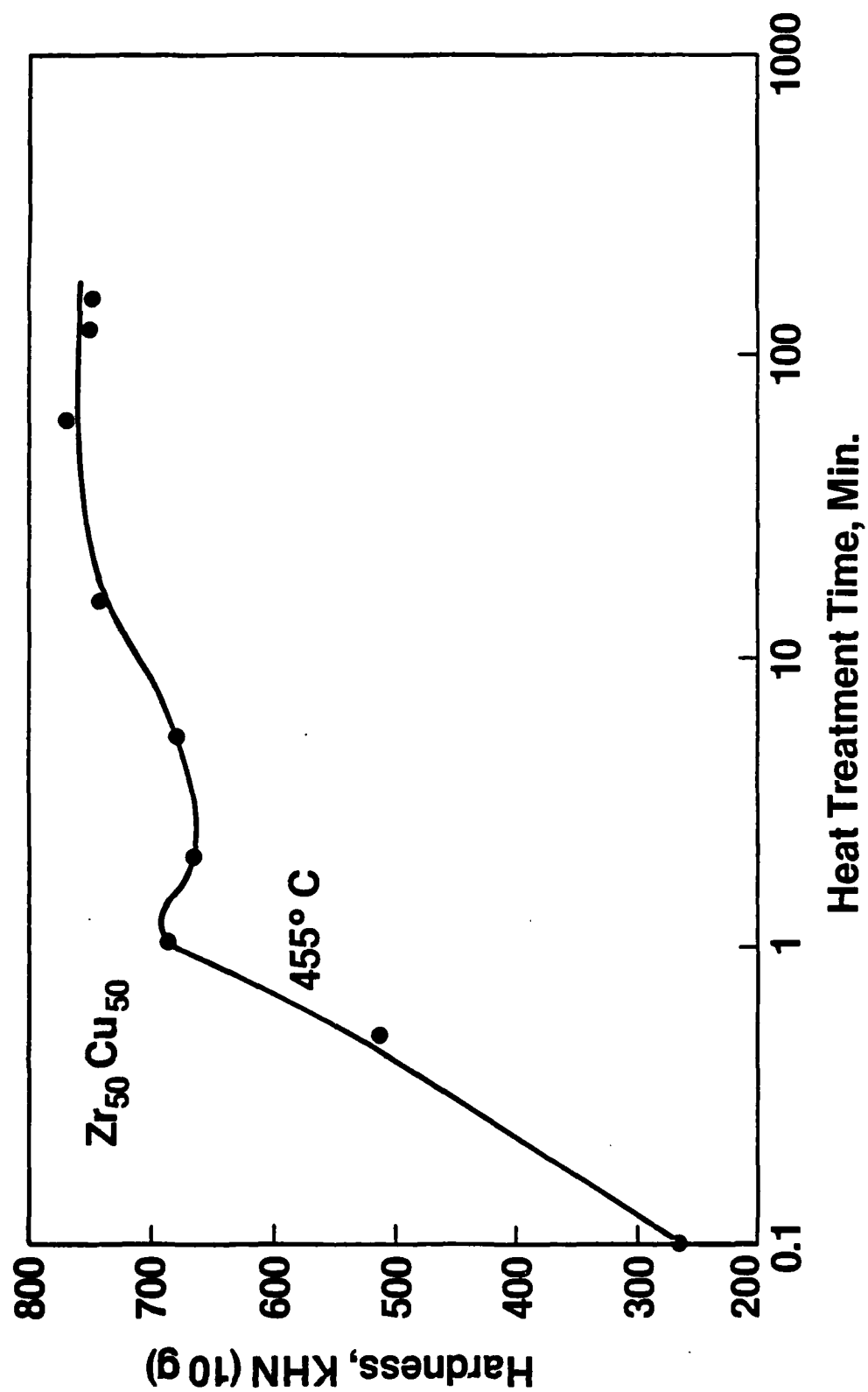


Figure 9. Variation of microhardness during crystallization of an amorphous $CuZr$ alloy at a constant temperature.

and a more rigid close-packed atomic distribution is achieved thereby embrittling the material.

Figure 10 shows an amorphous layer of 1mm average depth produced by electron beam melting and rapid solidification at a crystalline substrate. The bulk dendritic microstructures and the heat affected zone are apparent.

Ultrasonic NDC of the thermally modified peripheral layer was investigated by means of Rayleigh surface waves.

Rayleigh wave velocity is frequency independent. However, the extent of penetration of Rayleigh waves normal to the surface of the material is frequency dependent. Frequency analysis of the virtual Rayleigh wave velocities enables determination of the elastic properties of the layer and gauging its average thickness. Preliminary results from this work indicate that laser generation and laser interferometric detection of both velocity and attenuation should permit a totally contactless characterization of both amorphous and crystalline types of surface modified microstructures.

SUMMARY

New experimental techniques are being developed for nondestructive characterization of metallurgical microstructures using state of the art laser and optical technologies. Examples include real-time monitoring of solid state transformations such as precipitation processes. On the other hand, applications are also envisioned for post-transformation microstructure characterization in processes such as rapid solidification. Both

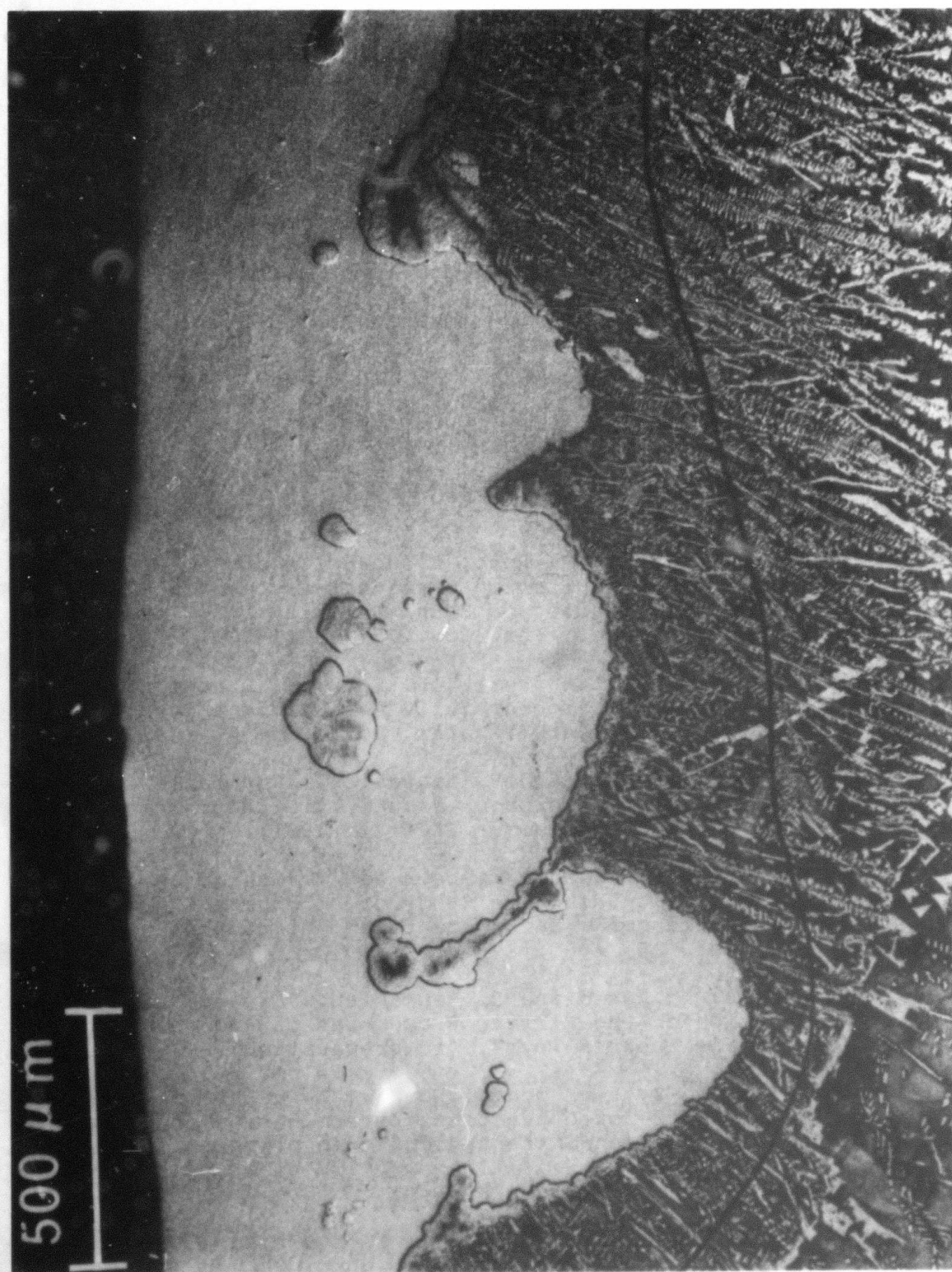


Figure 10. Microstructurally modified layer of PdCuSi by means of electron beam irradiation.

basic work to enhance our understanding of the phenomena involved, and applied work to exploit these new techniques in metallurgical processing are needed.

ACKNOWLEDGEMENT

This paper was written under the auspices of the DARPA Materials Research Council, Contract #MDA903-82-C-0428 with The University of Michigan.

REFERENCES

1. M. Rosen, S. Fick, R. Reno, E. Horowitz and R. Mehrabian, "Kinetics of Precipitation Hardening Process in 2219 Aluminum Alloy Studied by Sound Velocity and Ultrasonic Attenuation", Mater. Sci. Eng. 53, 163(1982).
2. M. Rosen, L. Swartzendruber, S. Fick, E. Horowitz and R. Mehrabian, "Aging Process in 2024 Aluminum Alloy Studied by Means of Eddy Currents", Mater. Sci. Eng. 53, 191(1982).
3. M. Rosen, H. Wadley and R. Mehrabian, "Crystallization Kinetics Study of Amorphous PdCuSi by Ultrasonic Measurements", Scripta Met 15, 1231(1981).
4. J.C. Chang, F. Nadeau, M. Rosen and R. Mehrabian, "Crystallization Kinetics Study of Amorphous Zr₅₀Cu₅₀ by Means of Ultrasonic Measurements and Microhardness", Scripta Met. 16, 1073 (1982).
5. F. Nadeau, M. Rosen and R. Mehrabian, "Effect of Composition on the Elastic Properties of Amorphous and Crystalline Cu-Zr Alloys", (in preparation).
6. C.H. Palmer, S. Fick and M. Rosen, "A Dual-Probe Laser Interferometer for Contactless Determination of Ultrasonic Wave Velocities and Attenuation", (in preparation).

THE MEASUREMENT OF RESIDUAL STRESS BY X-RAY DIFFRACTION

M. R. James

The X-ray diffraction method of residual stress measurement has been known for about 50 years. In spite of its great advantage of being nondestructive, it has only been extensively employed during the last 15 years. Improvements in instrumentation enabling portable equipment and faster measurement time combined with a better understanding of the X-ray technique has contributed to its increased use.

At the present time, the X-ray technique is the only one out of several nondestructive approaches (see Ref. 1 for a review) that is widely used.

After explaining the fundamentals of the method, this paper will examine the improvements made in recent years in both technological (equipment) and theoretical aspects that have led to a greater understanding of just what the X-ray technique is sensing, and when and why X-ray measurements may differ from those of other stress measuring techniques.

A polycrystalline material is shown in Fig. 1 having a fully random orientation of the grain structure. In each of these grains, I have drawn a specific hkl plane. Note that these planes are oriented differently with respect to the surface in each grain. Some of these grains will be aligned so that, when an incident X-ray beam falls on them, the Laue conditions for diffraction will be fulfilled and a diffracted X-ray beam will

be produced. It is described by Bragg's Law, which relates the angle of diffraction, given in Fig. 1 as θ (the angle between the incident radiation and the diffracted radiation), and the interplanar spacing " d " (the lattice spacing between the crystallographic planes). Bragg's Law is simply: $\lambda = 2d \sin\theta$.

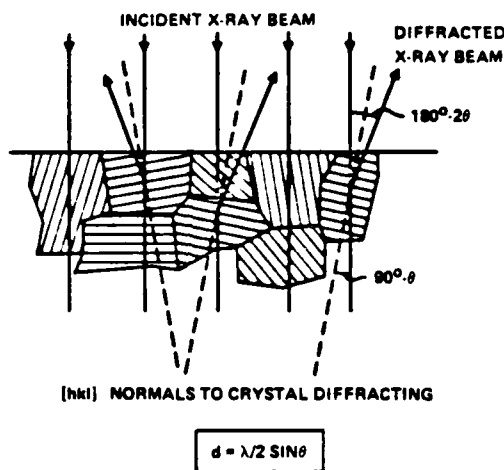


Fig. 1. Principles of X-ray diffraction.

It is evident that not only is there diffraction from the grain shown but, in the three-dimensional case, there are many grains oriented to fill diffraction conditions and in real space a cone of radiation is produced. It is important to note that some grains do not contribute at all to the diffracted radiation. Fig. 2 depicts the same phenomena. Because the material is polycrystalline, the sample may be rotated to bring the same hkl planes in different grains to fulfill the diffraction condition and obtain a diffracted X-ray beam. If the surface of the material is under stress, as shown in Fig. 2, there

will be a resolved component of that stress acting on the lattice planes. When one tilts the sample and looks at the same hkl planes in different grains, the resolved component of the stress on those hkl planes is going to vary, and the a change in the interplanar spacing between these two conditions can be measured. Thus, the interatomic spacing of a family of lattice planes is used as the gauge length for measuring strain.

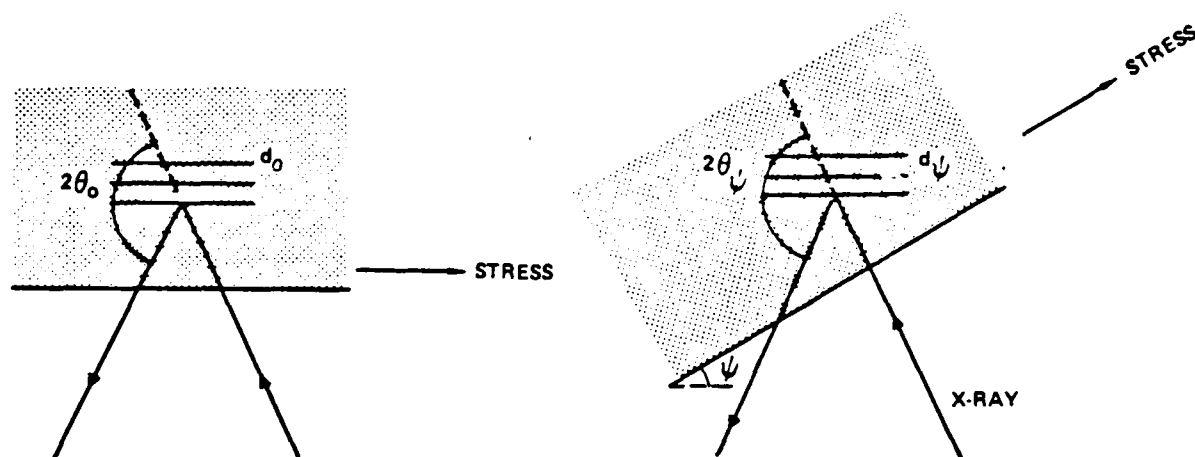


Fig. 2 Principles of X-ray stress measurement.

It is very simple. We have not had to look at a stress-free sample. We have not had to contact the surface of the sample at all. We simply rotate the sample with respect to the incident X-ray beam and we can measure a strain in the material.

One of the important things to recognize immediately is that the X-rays penetrate the surface of the material only to a very shallow depth. For steels, this is normally on the order of 25 μm or so; for ceramics, the penetration depth may be only $\sim 5 \mu\text{m}$. We are obtaining a weighted average of the interplanar spacings over that depth of penetration.

How do we obtain the needed information, 2θ ? In this case, we orient the sample with respect to the X-ray beam, scan the detector along the 2θ axis, and obtain a diffraction peak, as shown in Fig. 3. Using curve fitting procedures and certain correction procedures,² one may define a relative position on the diffraction peak; usually the peak of the profile is used. We then rotate the sample, sweep across 2θ , and measure the diffraction peak again. Because of the change in interplanar spacing, we have a peak shift, $2\Delta\theta$, which is related to the strain.

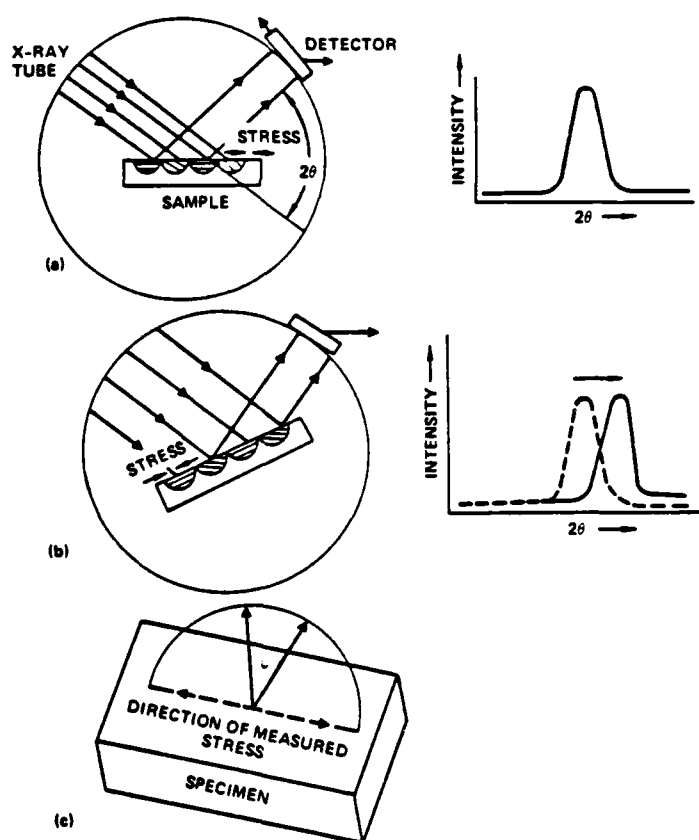


Fig. 3 Obtaining the diffraction angle 2θ .

The strain, of course, is related to the stress, and stress is a tensor property having a direction. The direction that we are measuring the stress in is defined as the intersection of the circle of rotation and the surface of the sample, as illustrated in Fig. 3. The angle Ψ constitutes a measurement of the angle of inclination of the sample as it is tilted. It is actually the angle between the normal to the specimen surface and the normal to the hkl planes that are diffracting, but may simply be thought of as the angle of sample tilt. We also define an arbitrary direction, ϕ , as the direction of the measured stress axis, the longitudinal axis, or whatever else one wishes to select. Of course, one can measure the stress in any direction on the surface of the material.

An illustration of the typical instrumentation that is normally used in a laboratory, the powder diffractometer, is given in Fig. 4. A diverging primary beam of radiation is made to illuminate an area on the sample surface of between 1 square millimeter and, say, 10 square millimeters, so we are averaging the stress over an area 10 millimeters square and about 25 μm deep. The diffracted radiation comes back in a converging beam almost to a point because of the focusing geometry of the powder diffractometer, and it passes through a receiving slit. The receiving slit is used to define the angle, 2θ , which is also dependent upon the position of the sample in this geometry. It is important to carefully position the sample so as not to introduce an experimental error. In terms of stress measurements on

steels, the sample should be positioned to the order of $100\text{ }\mu\text{m}$ or so to get errors on the order of 10-20 MPa.

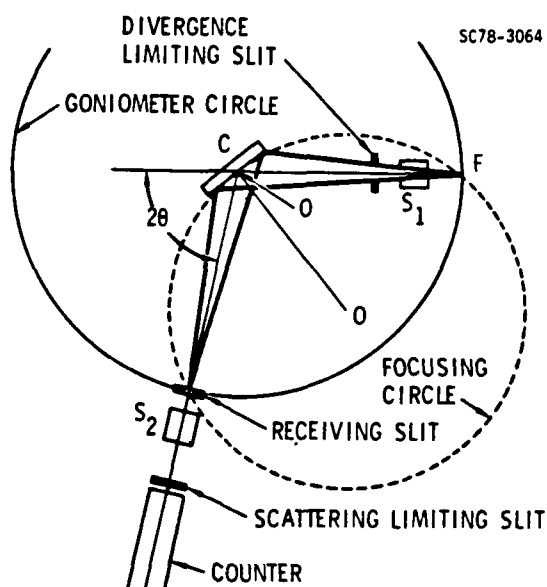


Fig. 4 Schematic of a powder diffractometer.

The instrumental error, then, is in determining the angle 2θ . In defining the peak of the diffraction profile, in positioning the sample and so forth, the instrumental errors usually run on the order of 20 MPa. This is really the precision of the measurement. One can do better than that, but I am quoting a conservative value; it depends on a lot of requirements -- counting statistics, breadth of the diffraction profile, instrumental alignment, etc. A review of the precision and experimental errors can be found in Ref. 2.

In the laboratory how long does the measurement actually take on instrumentation like this? Doing it by hand and assuming a fairly sharp diffraction profile, I would estimate that it

could be done in 20 minutes or so; for broad diffraction profiles, though, the time would be about an hour to two hours. With automated diffractometers and using counting statistics to optimize the time of data collection, one can get that time down to around between 15 to 30 minutes, depending on the breadth of the diffraction profile. For some samples such as ceramics where the intensity is low and the diffraction profiles are very broad, the measurement time is still about 3 hours attesting to the need for automated systems to eliminate the experimental tedium.

Of course, a diffractometer is a large heavy instrument that cannot be moved easily and one cannot put large samples on it. To alleviate this problem, mobile diffractometers have been designed³ and recently, the diffractometer has been completely replaced by a position sensitive detector (PSD).⁴ These instruments are designed to rotate about the sample to measure the interatomic spacing of the different tilts so that large samples can be investigated. With the PSD system, it is now possible to measure surface residual stresses in the field on large structures in operating times of less than 60 sec. A few such instruments will be described during the talk.

Once the strain is determined, we want to relate it to the stress in the surface. I do not want to go into any detailed mathematics of how to derive this relationship between the measured stress and strain. However, I will mention a few assumptions. First, a biaxial stress state is assumed on the

surface of the sample; this is not too bad because we are looking only at a very shallow depth. Second, it is assumed that isotropic elasticity theory is applicable. This creates a few problems here and there but, on the whole, for most materials it is not a bad assumption. Of course, where isotropic elasticity is not valid, the relationship between strain in the lattice planes and surface stress can be derived using anisotropic elasticity. In fact, much work has recently been done without assuming a biaxial stress state. The equations are complicated, but with automated equipment, the full 3-dimensional stress tensor can be obtained.^{5,6} In the simple case, assuming a biaxial stress state and isotropic elasticity, the relation of stress σ_ϕ , in the ϕ direction to the strain $\epsilon_{\phi, \Psi}$ at any tilt Ψ is given by

$$\epsilon_{\phi, \Psi} = \frac{d_{\phi, \Psi} - d_\phi}{d_\phi} = \frac{S_2}{2} \sigma_\phi \sin^2 \Psi + s_1(\sigma_1 + \sigma_2). \quad (1)$$

$S_2/2$ is a proportionality constant between the change in the interplanar spacing, the strain, and the stress. The stress is then related to the strain by a linear function of the angle of tilt, Ψ . The slope of $\epsilon_{\phi, \Psi}$ vs $\sin^2 \Psi$ gives

$$m^* = \frac{\partial \epsilon_{\phi, \Psi}}{\partial \sin^2 \Psi} = \left(\frac{1}{d_\phi} \right) \frac{\partial d_{\phi, \Psi}}{\partial \sin^2 \Psi} \quad (2)$$

so that

$$\sigma_\phi = m^* / \frac{S_2}{2}. \quad (3)$$

According to isotropic elasticity theory, the proportionality constant, $S_2/2$, is a function of the bulk elastic constants

($\frac{S_2}{2} = \frac{1 + \nu}{E}$ and $S_1 = \frac{-\nu}{E}$). The relationship is not always applicable, however, because of elastic anisotropy and the selective nature of the x-ray technique, so normally we term $S_2/2$ and S_1 the x-ray elastic constants and they are experimentally measured in the laboratory. If one looks at all the experimental values in the literature for a given alloy, one finds that they are consistent to within 10 percent. Proper values can thus be obtained from the literature.⁷

If we plot the interplanar spacing versus $\sin^2\psi$, we find that the stress is proportional to the slope divided by the x-ray elastic constant (Eq. 3). All we have to do is determine the slope by measuring the lattice spacing at a number of tilts. Although this is a linear relationship, many people use four or six measurements of the interplanar spacing at various cycles. This is termed the " $\sin^2\psi$ technique." Quite often the "two-tilt method" is used because of the linear proportionality. The lattice spacing is measured only at two ψ values. By using Bragg's Law, one can derive another equation, in which the stress is directly related to the change in a peak position through a term, K , the x-ray stress constant,

$$\sigma_\phi = \left(\frac{E}{1 + \nu} \right) \frac{1}{\sin^2\psi} \frac{\cot\theta}{2} (2\theta_0 - 2\theta_\psi) = K\Delta\theta \quad (4)$$

where

$$K = \frac{E}{1 + \nu} \frac{1}{\sin^2\psi} \frac{\cot\theta}{2}.$$

Again, K is measured experimentally, and many values are tabulated in the literature.

In Fig. 5a. the lattice spacing is plotted versus $\sin^2\psi$, and a good straight line is established. In a majority of cases one finds this kind of relationship. In the literature, however, some other cases are reported. In a few cases, a curvature as shown in Fig. 5b, has been reported. This is due to a very, very steep stress gradient in the surface of the material.^{8,9}

In Fig. 5d, splitting of d versus $\sin^2\psi$ is shown when the sample is inclined in the negative and the positive ψ direction. This is due to a nonbiaxial nature of the surface stress tensor. This has generally been seen during friction wear situations and methods have been developed to obtain the three dimensional stress tensor in this situation.¹⁰

Another anomalous pattern shows up as oscillations in d versus $\sin^2\psi$ (Fig. 5c). There is interesting controversy as to what they are attributable--whether it is elastic anisotropy, plastic anisotropy, or the development of textural microstresses during the deformation process, and there are various ways to treat this problem.^{2,5} What is most important I think, is that we know fairly well when such oscillations are expected to occur. It is always important in any new situation to verify that d vs $\sin^2\psi$ is linear before proceeding with the traditional X-ray measurement.

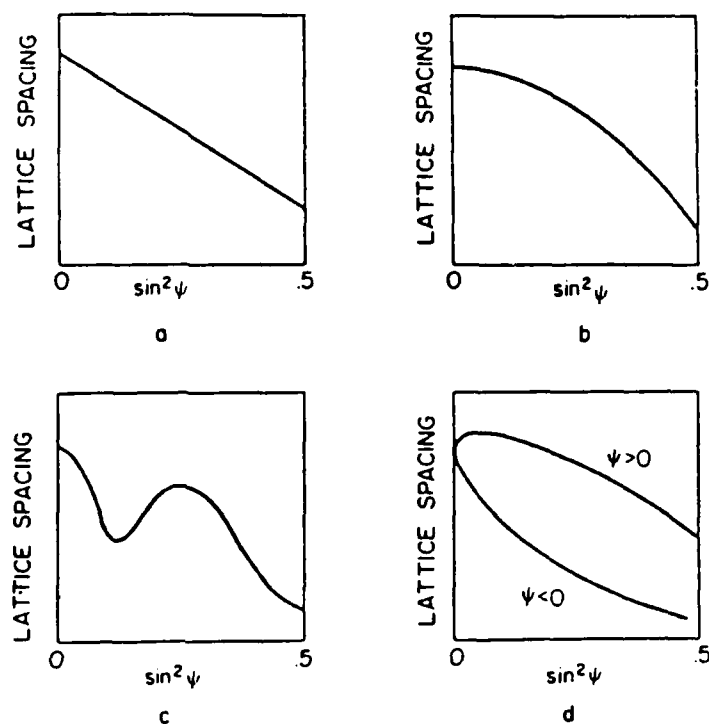


Fig. 5. Possible dependencies between d versus $\sin^2 \psi$.

Because the X-ray technique is so widely used, control of instrumental factors and well-defined experimental procedures have been repeatedly published, so that one may quickly become familiar with the technique.¹¹ There are certain well-known fundamental limitations, such as excessively large grain size (in aluminum alloys or weldments, for example) and the effects of plastic deformation, that detract from universal acceptance of the technique, but investigations are continuing into proper interpretation of the results in these circumstances. In a majority of manufacturing processes (grinding, machining, shot peening, heat treating, case carburizing), the X-ray technique is accurate.

One quite common complaint of the X-ray diffraction technique is that it is only surface sensitive, sampling a layer of less than 25 μm . The validity of accepting the residual stresses in this thin layer as representative of the bulk may be suspect from a design engineer's viewpoint; however, this unique advantage of the X-ray method is often used to determine the distribution of stress with depth by systematically removing thin surface layers electrochemically and then remeasuring the stress. Correction procedures for relaxation during layer removal and effective beam penetration have been developed. The fact that the X-ray technique is noncontacting makes this procedure very easy. (In fact, not having physical contact with the specimen allows for remote measurements, such as at high temperatures or in specific, even aggressive environments.) Since surface initiated failures are of primary importance in dynamically loaded components, surface stresses and their distribution with depth are often very important.

The selective nature of the X-ray technique makes possible the investigation of stresses in individual phases that may be compensating each other. The ability to precisely select the area of illumination by collimating the X-ray beam provides the ability to map the stress distribution on a fine scale. This technique has been used to show that large variations in surface stress may occur in abusively ground samples due to local heating. Restricting the areas of sampling on a surface is also useful in determining stresses on curved surfaces with

radii down to about 1 millimeter. A number of applications and examples will be presented during the talk to point out the versatility of the measurement.

It should be remembered that the results of X-ray investigations have often been used in the interpretation of the role of residual stresses in the deformation and fatigue resistance of engineering material. It is in fact, the only technique used to study the stability of residual stresses during dynamic loading. The recent advances in instrumentation should help instigate a movement of the X-ray diffraction stress measurement technique from the laboratory to a general-purpose testing tool. The development of new instrumentation and specific packaging arrangements will allow the X-ray technique to be used in many areas where equipment limitations have prohibited its application in the past.

ACKNOWLEDGEMENT

This paper was written under the auspices of the DARPA Materials Research Council, Contract #MDA903-82-C-0428 with The University of Michigan.

REFERENCES

1. M. R. James and O. Buck, CRC Critical Reviews in Solid State and Materials Sciences, 9, Issue 1, pp. 61-105 (1980).
2. M. R. James and J. B. Cohen, "The Measurement of Residual Stresses by X-Ray Diffraction Techniques," in Treatise on Materials Science and Technology, 19A, ed. H. Hermon, Academic Press, NY, pp. 1-62 (1980).
3. B. Jaensson, Materials Sci. and Eng., 43, pp. 169-176 (1980).
4. M. R. James and J. B. Cohen, J. Testing and Eval., 6, pp. 91-97 (1978).
5. H. Dolle, J. Appl. Cryst., 12, pp. 489-501 (1979).
6. J. B. Cohen, H. Dolle and M. R. James, National Bureau of Standards Special Publication, 567, pp. 453-477 (1980).
7. P. S. Prevey, Adv. in X-Ray Analysis, 20, pp. 345-354 (1977).
8. T. Shiraiwa and Y. Sakamoto, Sumito Search, 7, pp. 159-169 (1972).
9. I. C. Noyan, "Effect of Gradients in Multi-Axial Stress States on Residual Stress Measurements with X-Rays," ONR Tech. Report 6, Contract N00014-80-C-0116, 1982.
10. J. Dolle and J. B. Cohen, Metall. Trans., 11A, pp. 159-169 (1980).
11. M. E. Hilley, J. A. Larson, C.F. Jatzak and R.E. Ricklets (eds.), Residual Stress Measurements by X-ray Diffraction, SAE Information Report J784a, SAE, Warrendale, Pennsylvania.

NEW APPLICATIONS OF ELECTROMAGNETIC-ACOUSTIC TRANSDUCERS:
DETERMINATION OF RESIDUAL STRESS STATES IN PLATES AND
NONDESTRUCTIVE EVALUATION OF BUTT WELDMENTS

C. M. Fortunko, R. B. King and R. E. Schramm

In this summary, emphasis is placed on new applications of certain types of electromagnetic-acoustic transducers (EMATs) that can generate and detect special ultrasonic probing signals: the horizontally polarized shear waves (SH waves). Specifically, attention is focused on the special properties of SH waves that make it feasible to evaluate weldments using ultrasonic signals whose wavelength is long compared to flaw dimensions, and a new experimental procedure that permits the direct measurement of in-plane residual stresses in a textured engineering alloy.

The principle of operation of an electromagnetic-acoustic transducer is illustrated in Fig. 1, which shows a primitive electromagnetic-acoustic transducer element. The EMAT element in Fig. 1 is composed of a wire conductor and a source of strong magnetic field. The wire conductor carries a dynamic current I_ω which induces dynamic eddy currents J_ω at the surface of a metal part. The presence of the strong magnetic bias field H_0 causes Lorentz forces, which can generate elastic waves that propagate radially away from the wire conductor. The polarization of the elastic waves depends on the direction of the magnetic field H_0 . Detection is accomplished by reciprocal pro-

cesses. In certain ferromagnetics, magnetostrictive generation and detection is also possible.

Many practical EMAT types can be constructed by assembling different arrangements of wires and magnets. In particular, it is possible to construct very efficient transducers of shear waves that are polarized parallel to the free surface (SH waves). An example of an SH wave EMAT is shown in Fig. 2.

The EMATs shown in Fig. 2 have been used in an experimental system designed to evaluate the girth welds of large, cross-country pipelines. A block diagram of this system is shown in Fig. 3.

The configuration of Fig. 3 uses two SH wave EMATs that are aimed colinearly along the normal to the weld. The transmitter EMAT, positioned between the weld and the receiver EMAT, generates two SH wave signals of equal amplitudes that travel in opposite directions. The ultrasonic signal 1 signifies the weld region while the ultrasonic signal 2 travels directly to the receiver EMAT. Signal 2 is used as a reference to calibrate the efficiency of the transmitter EMAT. If a flaw is present in the weld, then a reflected signal 3 is also detected by the receiver EMAT.

The system shown in Fig. 3 can be very sensitive to planar flaws in the weld because SH waves are not very sensitive to the weld crown. Physically, this is related to the fact that the SH waves are much more uniformly distributed through the thickness of a plate than vertically polarized ultrasonic

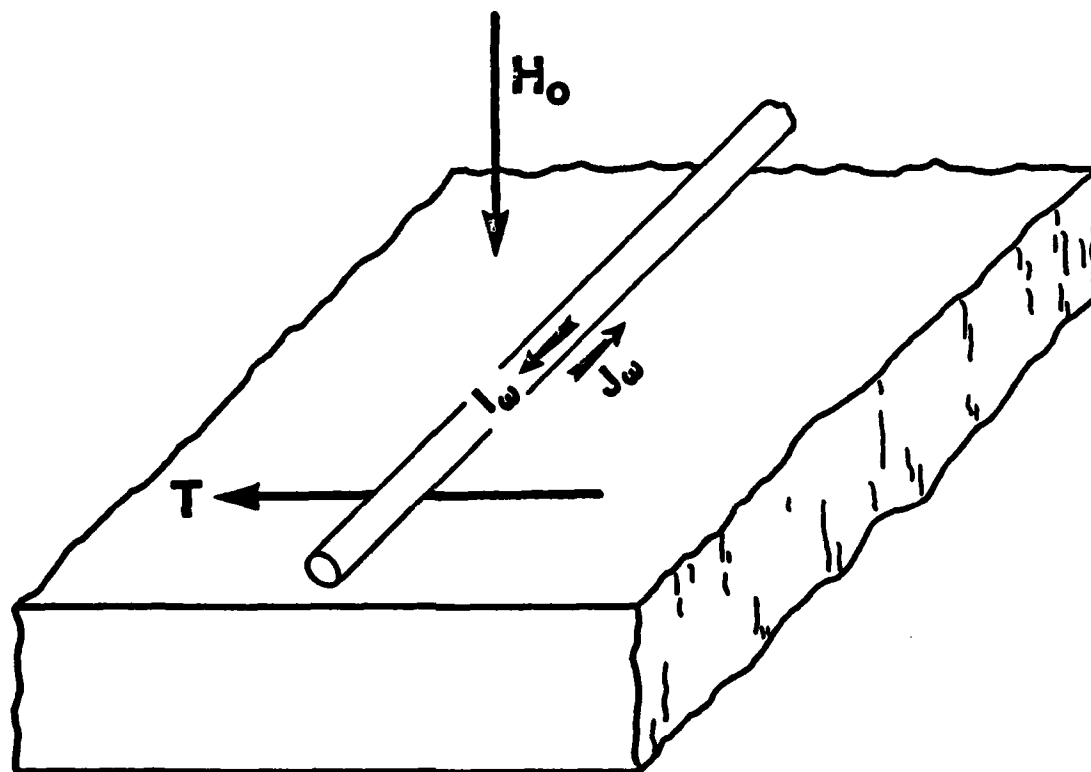


Figure 1. A primitive SH wave EMAT.

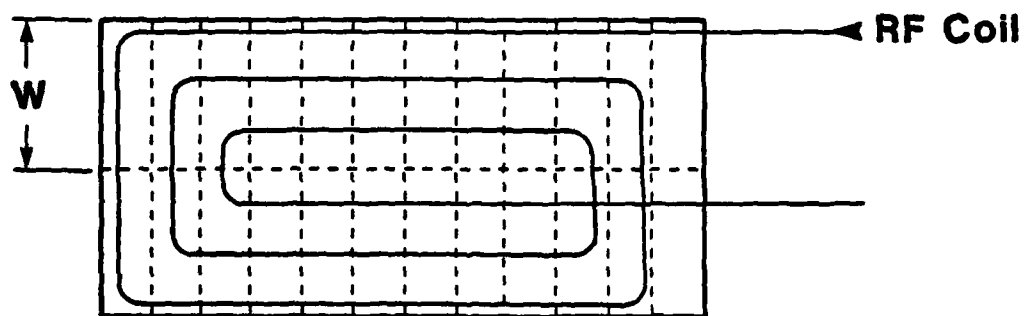
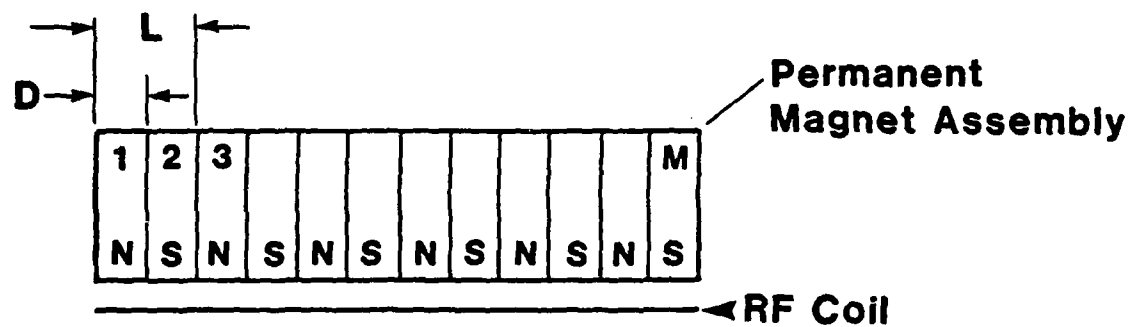


Figure 2. An efficient SH wave EMAT for weld inspection.

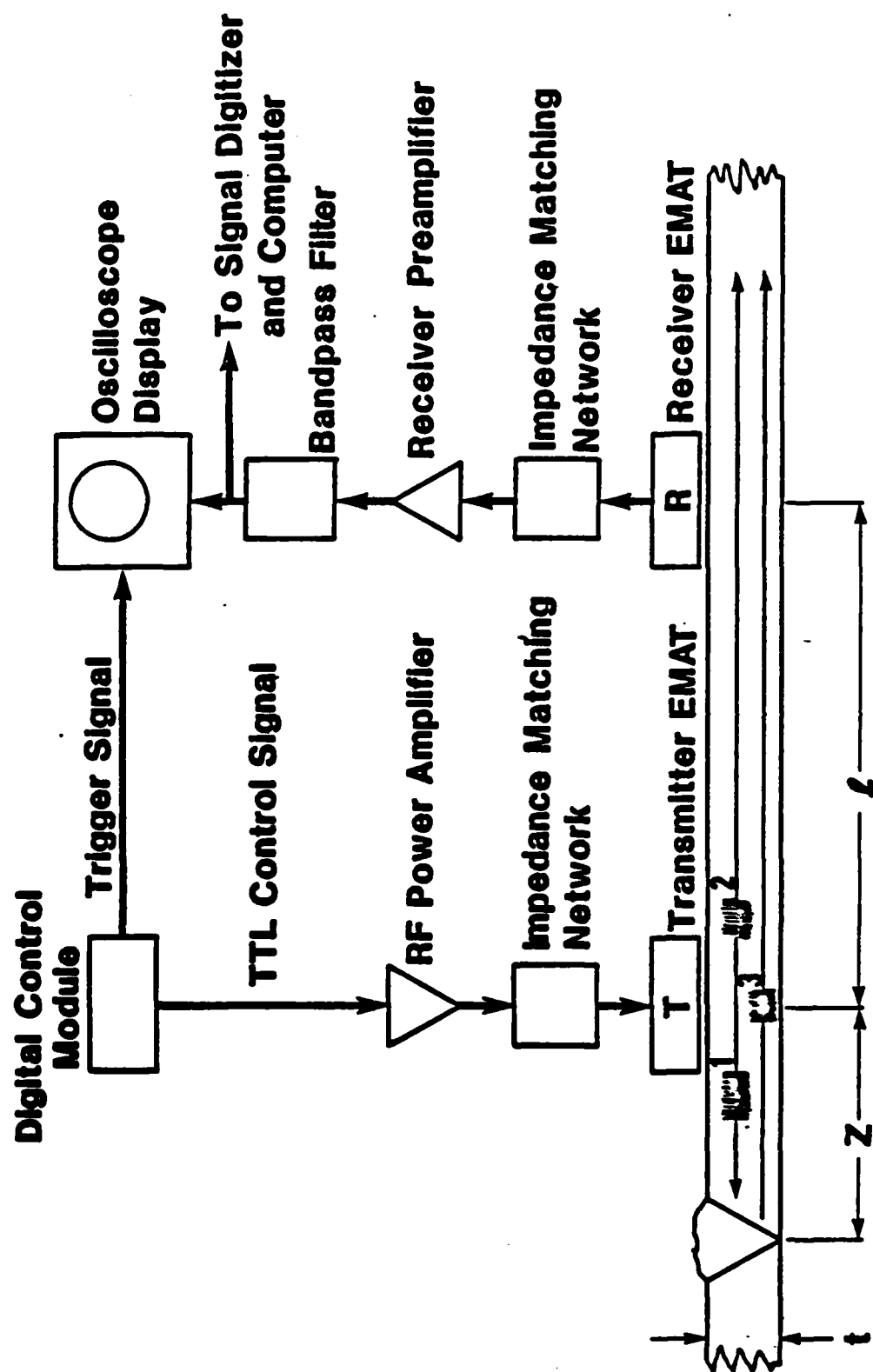


Figure 3. An SH wave EMAT system for ultrasonic evaluation of pipeline girth welds.

signals (Lamb waves). Also, SH waves can propagate at grazing incidence, in contrast to SV and L waves.

Another advantage of the system depicted in Fig. 3 is that it operates in the long-wavelength region. As a result, the scattered SH wave amplitude increases monotonically with flaw through-wall depth. This is very desirable for flaw sizing on the basis of amplitude and phase information. An example of a flaw-sizing curve is shown in Fig. 4.

In Fig. 4, the normalized reflection amplitude ratio (ratio of signals 2 and 3) is plotted as a fraction of flaw depth, for a buried, planar located near the mid-plane of the plate. Also shown in Fig. 4 is the variation of the reflected amplitude ratio as a function of the distance between the EMAT and the weld. The background ultrasonic signals, carried by reflections from the weld crown and the weld root, are shown in Fig. 4 using a broken horizontal line. Similar curves are available for surface flaws and procedures exist for classifying flaws in terms of position within the weld and orientation.

The ultimate sensitivity limits of the system in Fig. 3 are outlined in Figs. 5 and 6, for surface and buried, planar flaws. Also shown in Figs. 5 and 6 are flaw size limits defined by the industry-wide workmanship standard (API-1104) and an accept-reject curve derived using a conservative fitness-for-purpose analysis.

The technical approach outlined above exemplifies a non-destructive testing procedure that was evolved as a result of a

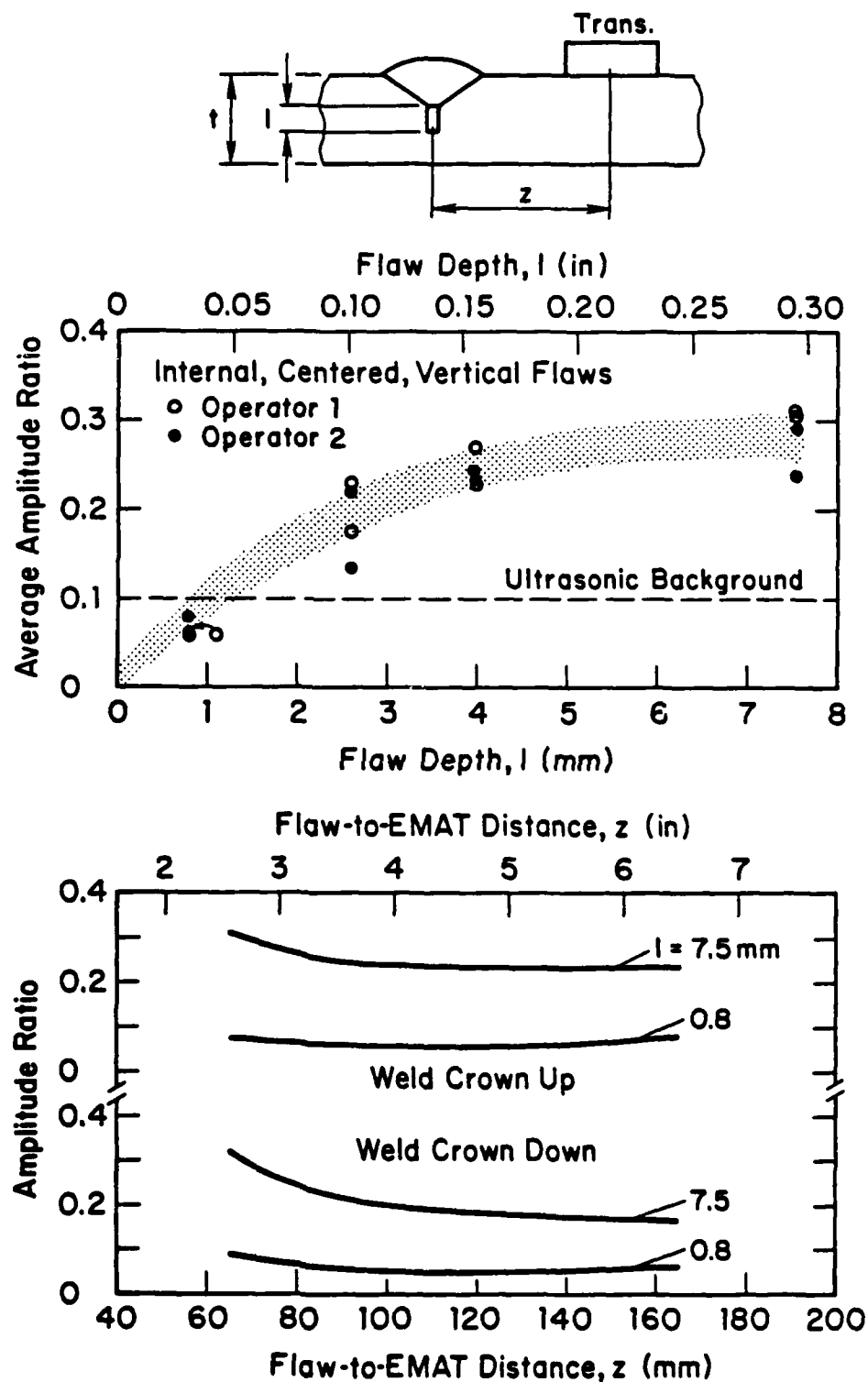


Figure 4. An experimental curve for sizing buried, planar flaws in butt welds.

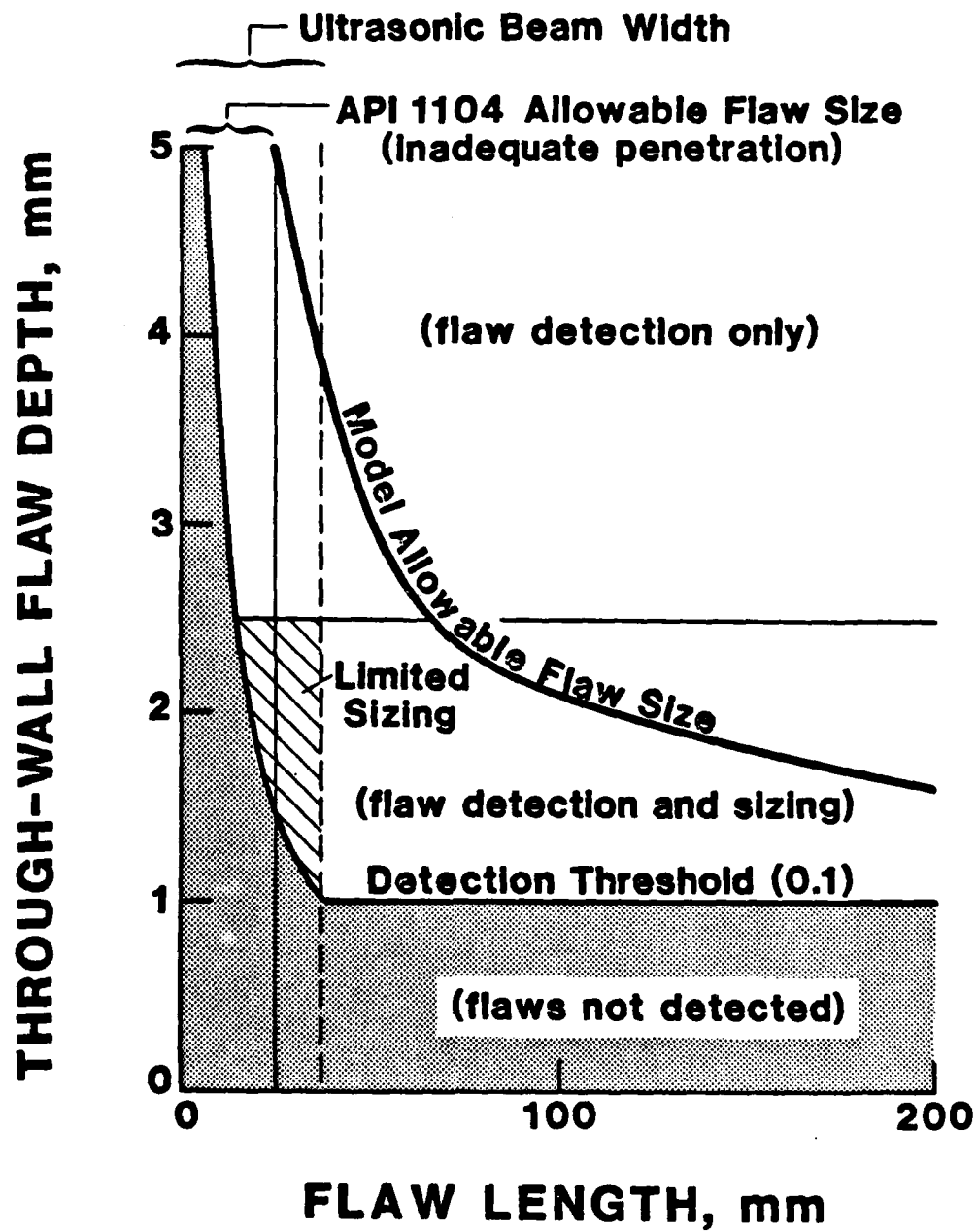


Figure 5. Sensitivity limits for vertically-oriented surface flaws.

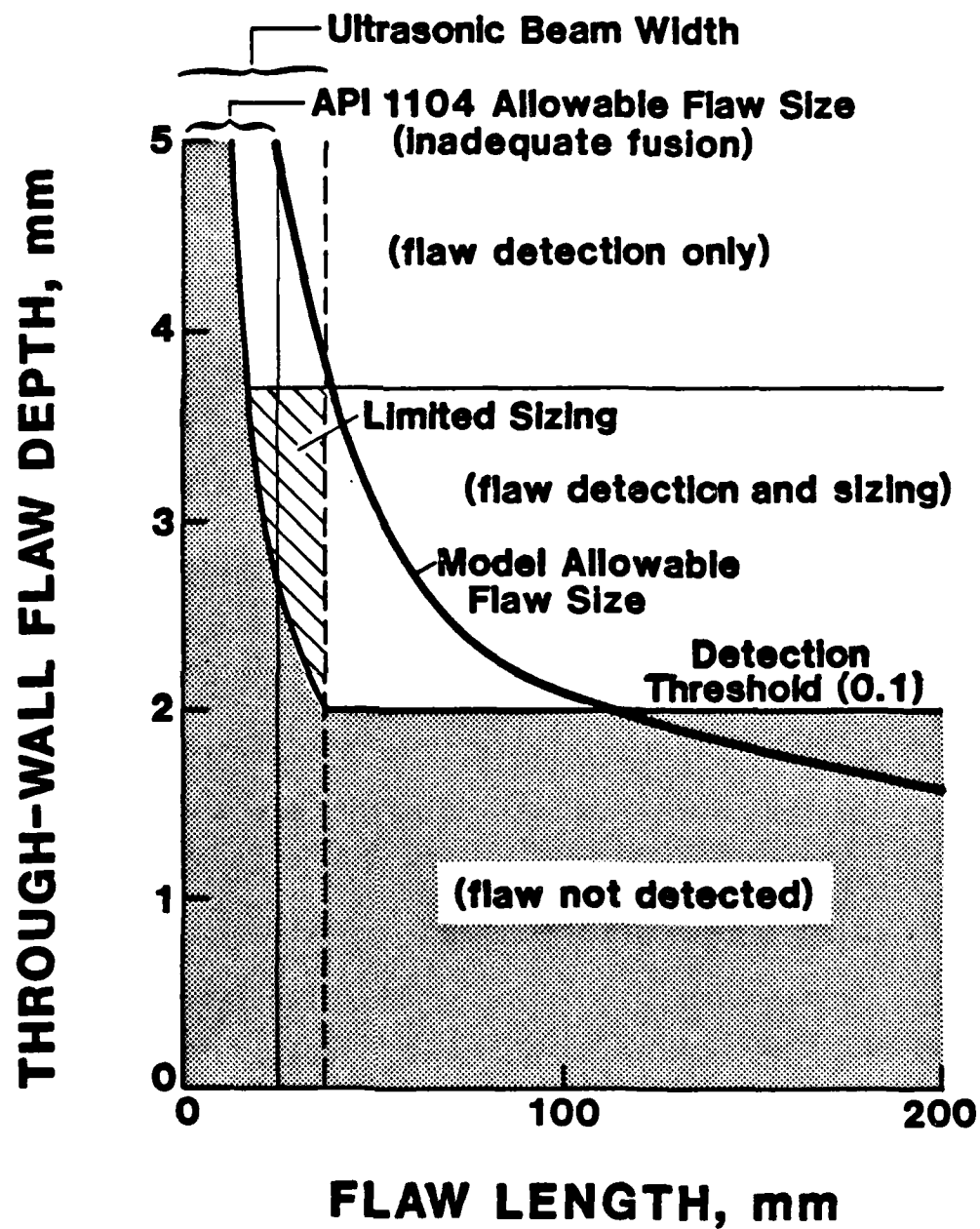


Figure 6. Sensitivity limits for vertically-oriented buried flaws.

close collaboration of specialists in the fields of fracture mechanics, nondestructive testing and materials science.

Recently, a new type of electromagnetic-acoustic transducer has been developed. In contrast to the relatively narrow-band SH wave EMAT of Fig. 2, the new EMAT can generate and receive broadband SH wave signals that propagate in the plane normal to a plate. Two possible configurations of the new EMAT are shown in Fig. 7.

In contrast to the "end-fire" EMAT of Fig. 2, the compact EMATs of Fig. 7 can generate and receive SH wave type signals from a very wide range of angles in the plane bisecting the EMAT and normal to the plate. The radiation patterns of the two EMATs are shown in Fig. 8 and 9.

The broad angular radiation patterns are useful for two important applications: measurement of in-plane residual stress states in plates and construction of very long synthetic and dynamically-focused arrays, which are needed to improve the spatial resolution of weld inspection systems.

A major problem that hinders the application of ultrasonic velocity measurements to characterization of residual stresses, is the necessity of separating the effect of stress on elastic wave velocities from material effects. Specifically, the presence of material texture can cause serious errors in the values of stress inferred from acoustical birefringence measurements, which is the most commonly used technique.

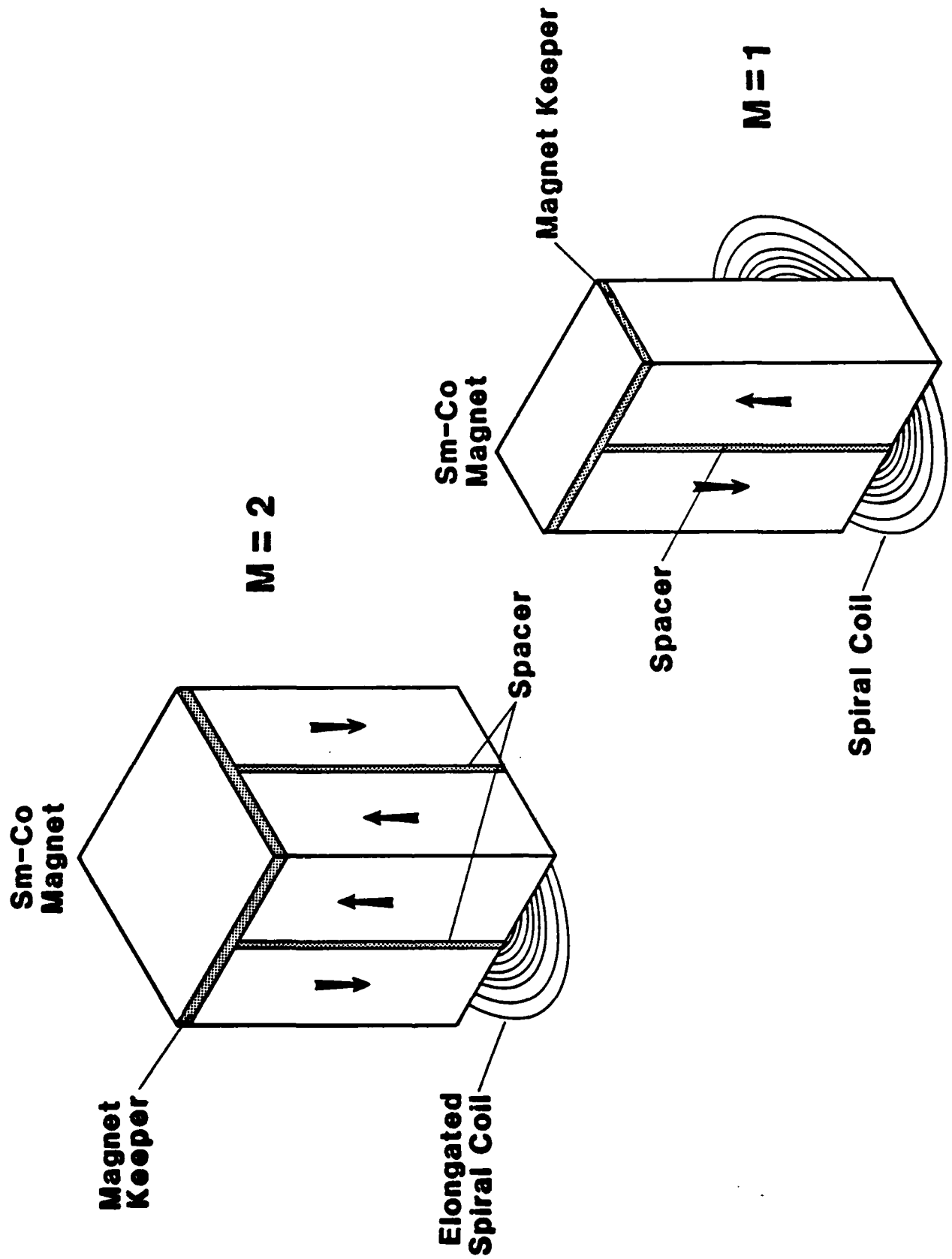


Figure 7. Broadband SII wave EMATs.

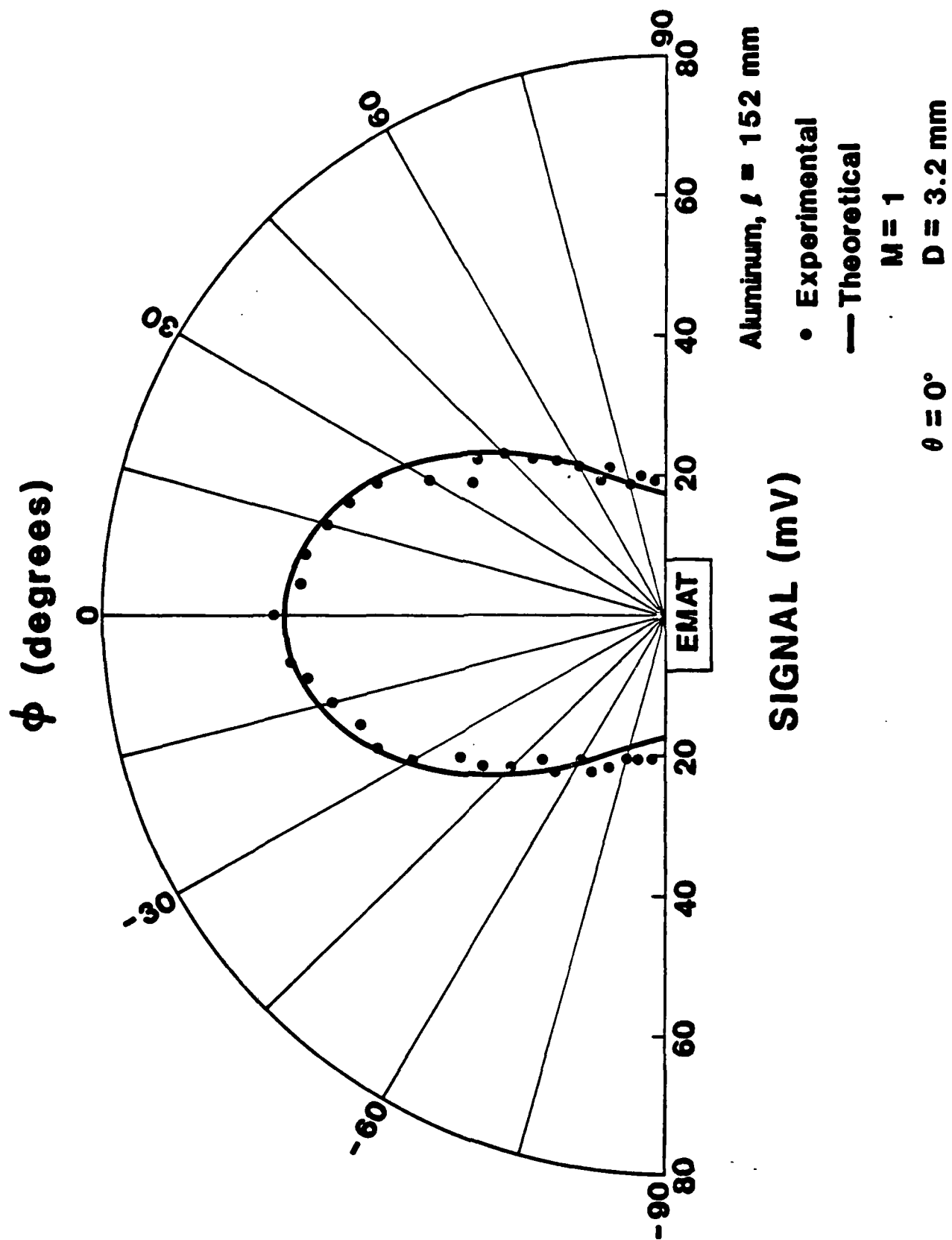


Figure 8. Radiation pattern of the $M=1$ EMAT.

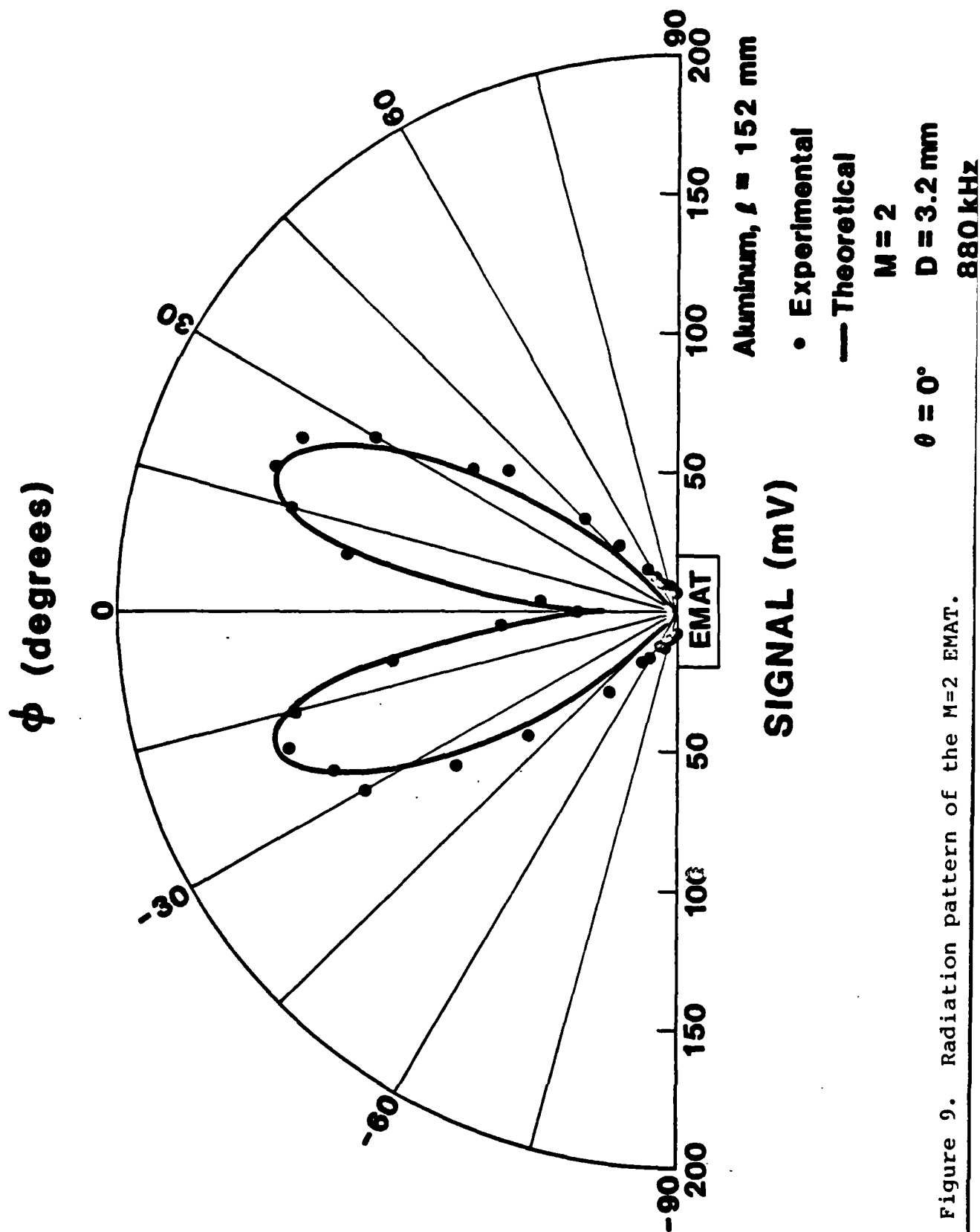


Figure 9. Radiation pattern of the $M=2$ EMAT.

Here, we describe a new experimental procedure for separating the effects of stress and texture on the basis of shear wave velocity measurements. The new procedure is based on recent theoretical findings. Specifically, the new procedure is based on the fact that measurements with SH waves can provide sufficient information to determine both stress and texture using the birefringence of SH waves that propagate at oblique angles with respect to the free surface.

A practical experimental system, using two EMATs of Fig. 7, for determining the in-plane stress states in a plate is shown in Fig. 10.

In Fig. 10, two SH wave EMATs are used to measure the transmission phases of SH wave signals that are reflected between the free surface of a plate. It is assumed here that the principal stress directions lie in the planes of symmetry of material texture. Measurements are then made in the two orthogonal planes of symmetry that are normal to the plate. The procedure is based on the fact that the propagation of the SH wave signals at different oblique angles provides independent, new information. Clearly, the configuration of Fig. 10 is very flexible.

Figure 11 shows a rolled aluminum plate test specimen that was used to evaluate the new procedure. The test specimen contains an over-sized stainless steel (304) cylindrical plug that causes a known distribution of stress in the plate. (The plug was inserted after precooling to 78°K.) Also shown in

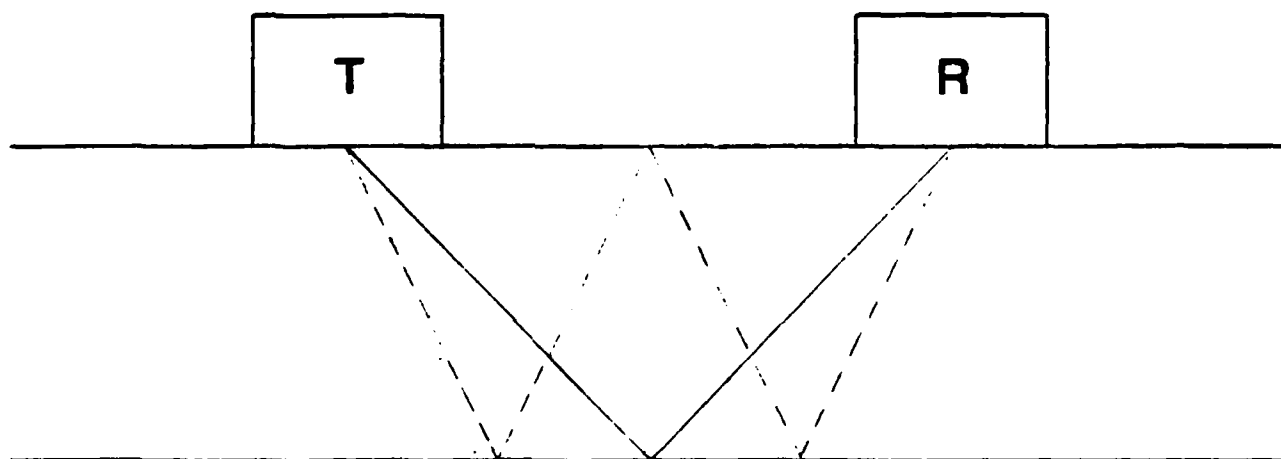


Figure 10. An experimental configuration for measuring in-plane stresses in plates.

Fig. 10 is the rolling direction and the scan line used to map the in-plane residual stresses as a function of distance from the plug boundary. The experimental results are shown in Fig. 12.

In Fig. 12, the difference in the two in-plane residual stress components (σ_1 and σ_2) is plotted as a function of the distance from the plug boundary. Also shown, using a solid line, is the calculated stress state, which has been verified independently using strain gages attached to the surface of the plate. The experimental and theoretical results adhere very clearly, showing the efficacy of the new experimental procedure. Also shown, for contrast, are experimental results which were obtained using a conventional birefringence theory to invert the experimental data. Clearly, the conventional results lead to an unconservative estimate of residual stress states in this specimen.

Another important new application of the new SH wave EMATs shown in Fig. 7 involves the construction of very long synthetic aperture and dynamically focused arrays for nondestructive evaluation of thick weldments.

Figure 13 shows the focusing performance of a 50mm long, focusing array that is driven using a 550-kHz signal with a 30% fractional bandwidth. A contour map presentation (linear scale) is used to represent the amplitude of the ultrasonic field near the focal point of the array when all pulses are correlated. The following cases are studied here: 1) the focal point

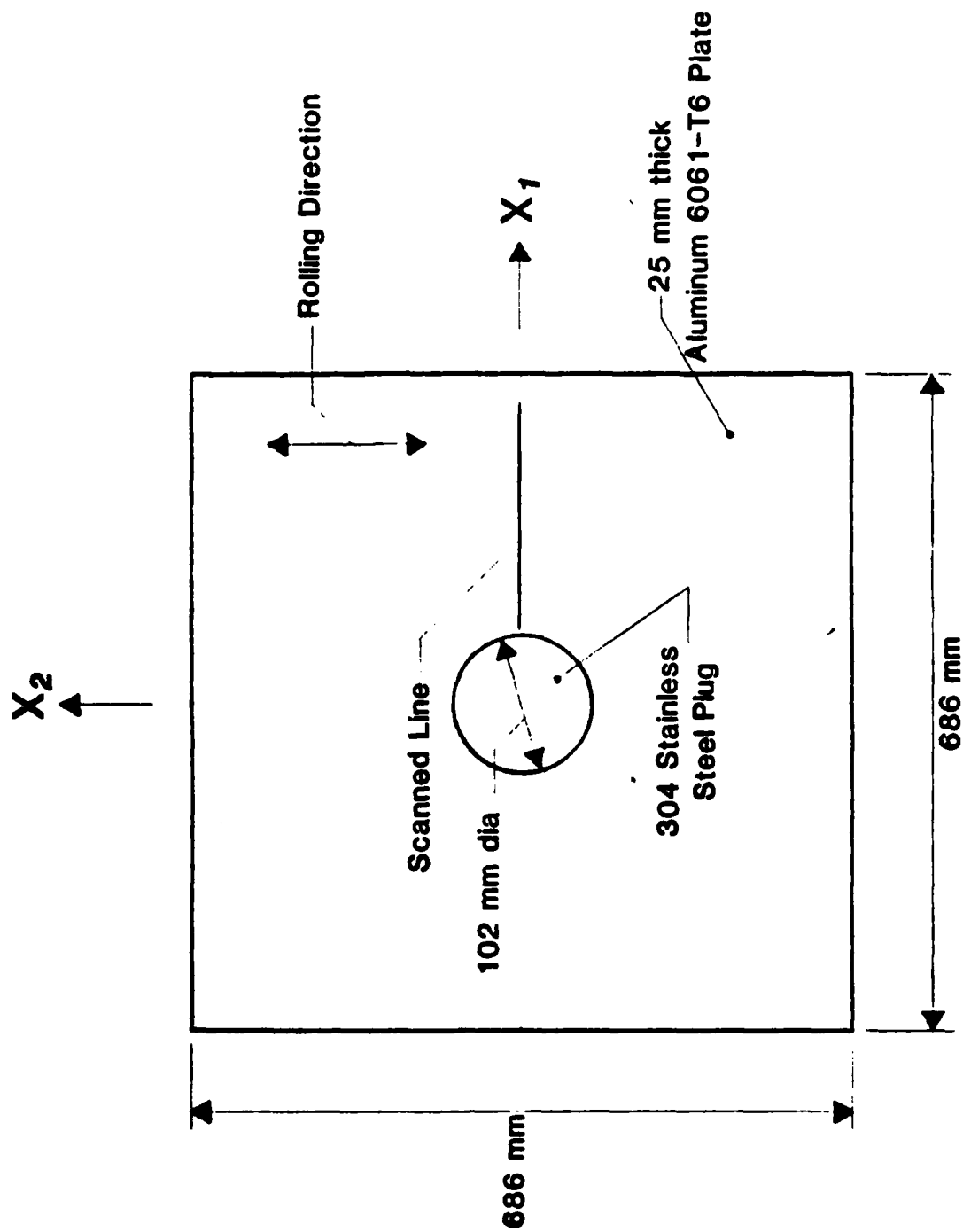


Figure 11. A test specimen with a known residual stress state.

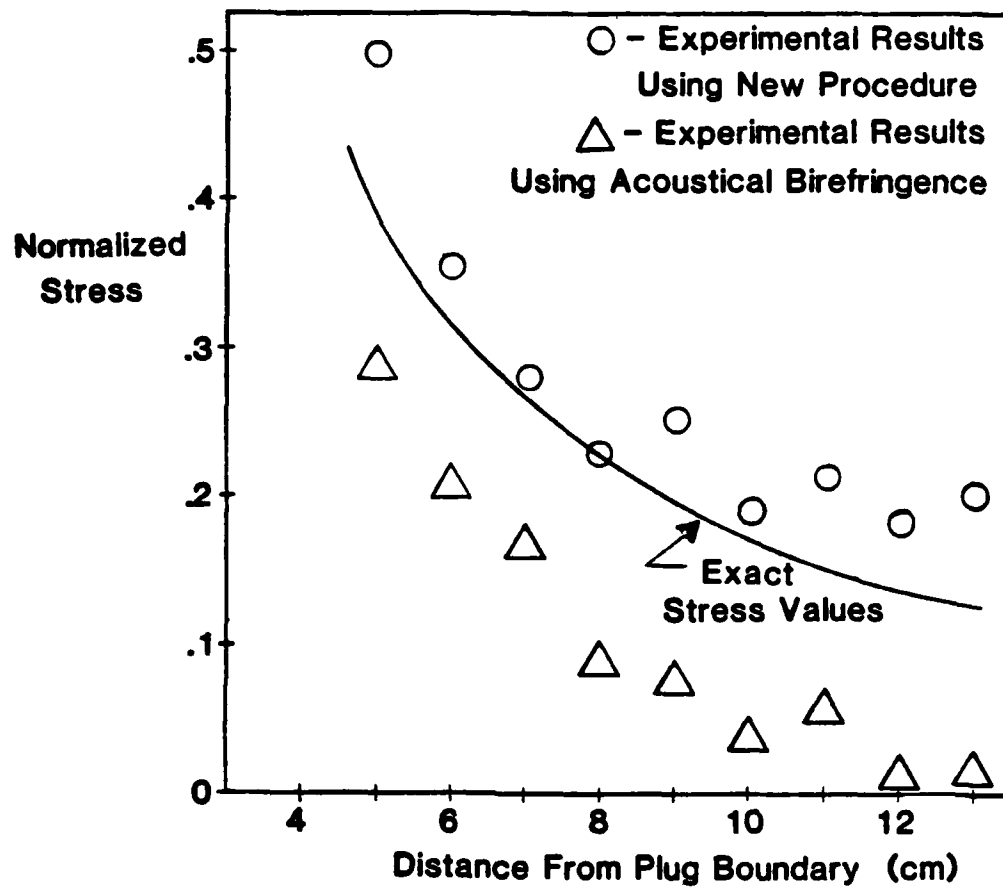


Figure 12. Residual stress states measured using the new experimental procedure.

located directly below the center of the array, 2) the focal point located directly below the edge of the array, and 3) the focal point located 50mm in front of the array.

In all cases, the focal points are located 25mm below the free surface. The relative amplitudes of the correlated signals are indicated above the respective contours, and the contour lines are spaced at 0.1 intervals in relation to the peak amplitude. To illustrate the improved range resolution performance obtainable with pulsed EMAT arrays, Fig. 14 shows the ultrasonic fields of the same physical array driven by monochromatic (continuous) signals. Again, the same contour map presentation convention is used. The focusing performance of a sparse (undersampled) array is shown in Fig. 15.

It is clear from the above, that efficient ultrasonic arrays capable of oblique focusing can be constructed using SH wave EMATs. The efficacy of such arrays is assured by the uniform coupling efficiency of the EMATs, which do not require fluid coupling to the surface. (Indirectly, the reliability of the coupling was demonstrated in the experiment designed to determine the in-plane stress states in a plate.)

The above results demonstrate the advantage of using SH wave EMATs in practical applications. However, the practicality of such systems is limited at the present time by the inadequate proliferation of EMAT systems in the scientific community and misconceptions in regard to the difficulties of obtaining usable signal levels. In many applications, EMATs offer greater sensi-

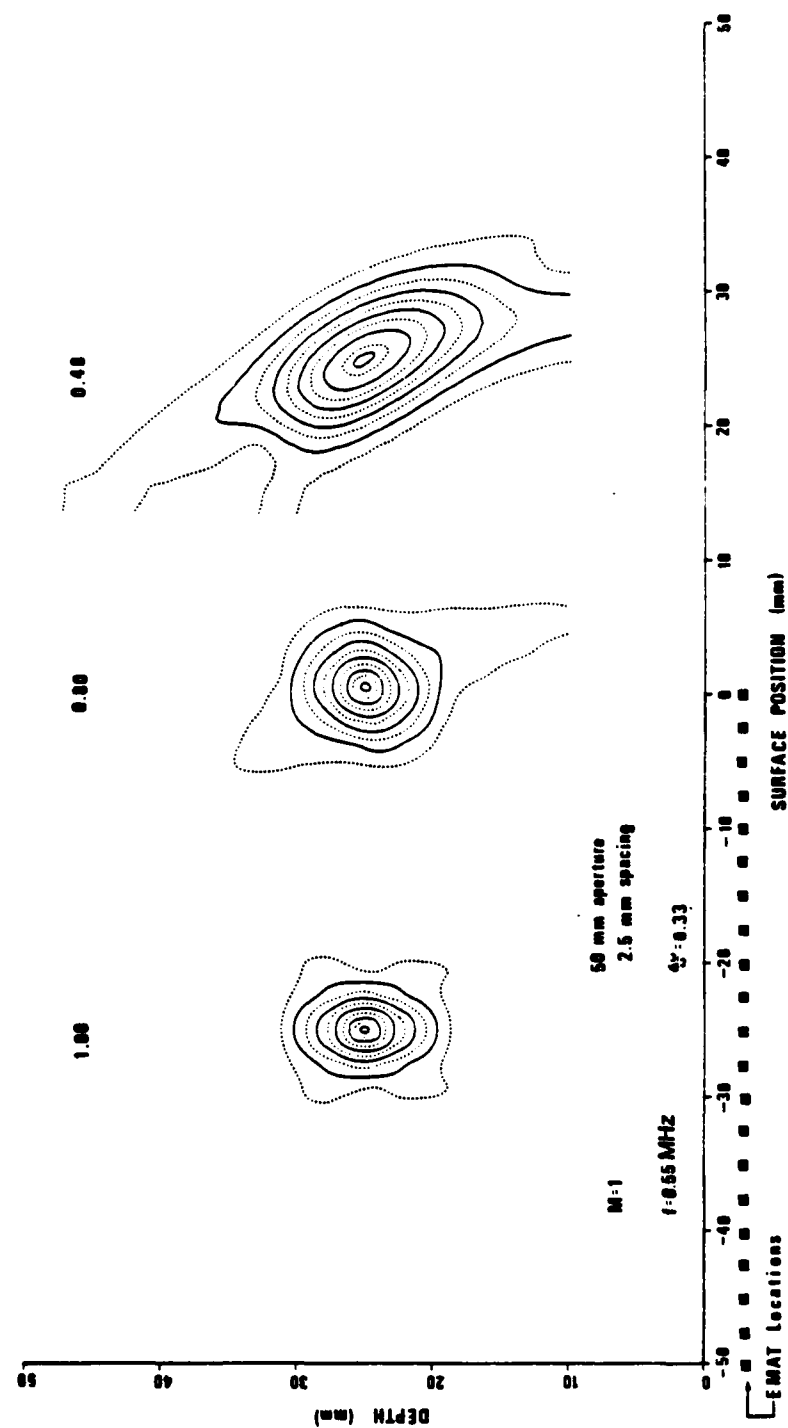


Figure 13. Focusing performance of a pulsed SH wave EMAT array.

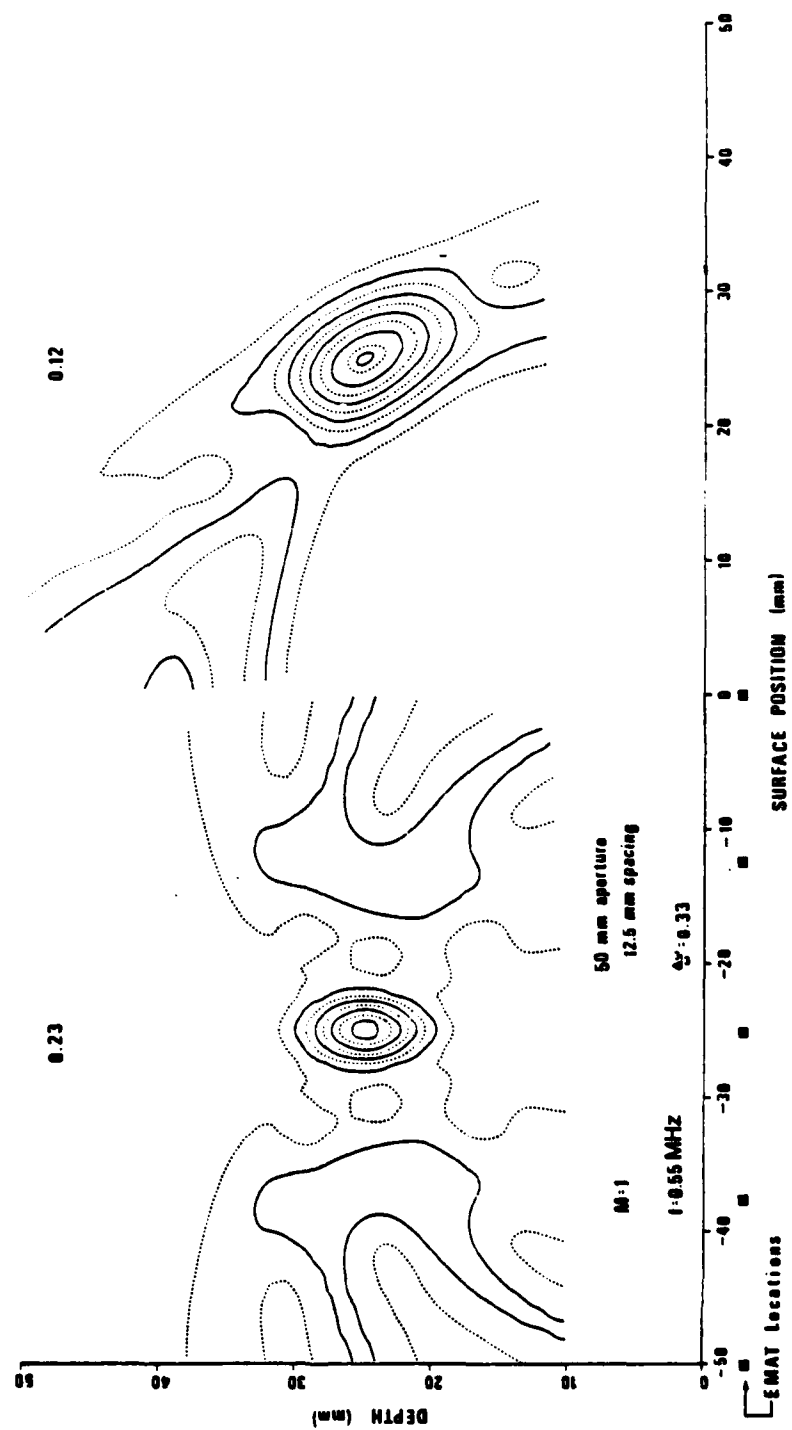


Figure 15. Focusing performance of a pulsed, undersampled array.

tivity and accuracy than other ultrasonic transducer types. This is particularly true when an ultrasonic background level exists that is higher than the electronic (Johnson) noise level.

ACKNOWLEDGEMENTS

This work was supported by the Welding Research Council, the U.S. Navy -Navy Sea Systems Command, the Defense Advanced Research Projects Agency, the National Bureau of Standards -Office of Nondestructive Evaluation, and the Department of Transportation -Office of Pipeline Safety Regulations.

This paper was written under the auspices of the DARPA Materials Research Council, Contract #MDA903-82-C-0428 with The University of Michigan.

APPLICATION OF SYNCHROTRON RADIATION TO MATERIALS SCIENCE

M. Kuriyama and W. J. Boettinger

INTRODUCTION

Electrons constrained to move in a curved path experience a centripetal acceleration, and thus emit radiation over a wide solid angle, as predicted by Maxwell's equations. As the velocity of electrons approaches the speed of light, the pattern of radiation, called the Larmor pattern, is distorted by relativistic effects, and exhibits a sharp directionality of its propagation with extremely high fluxes. Normally, the electron's speed is maintained constant in a storage ring, after being accelerated to near light speed in a synchronous fashion. The radiation is confined to within an extremely thin and flat horizontal plane, which contains the electron orbit in the storage ring. The vertical divergence of the radiation (orthogonal to the storage ring) is given by a relation $1/\gamma = 105/E(\text{Gev})$ arc second, where E is the electron energy.

The tail of the continuous radiation spectrum moves up to the x-ray energy region as the electron energy increases in the Gev range, thus providing applications in materials science. The unique features of synchrotron radiation thus include a continuous spectrum with high flux, brightness and intensity, and extreme collimation in the vertical direction. In addition, synchrotron radiation has a pulsed time structure (pulses of a less than nanosecond width with a microsecond interval), and

well defined polarization states. At most synchrotron facilities operated at the GeV range, the spectrum ranging from 3 keV ($\sim 4\text{\AA}$) to 30 keV ($\sim 0.4\text{\AA}$) can readily be made available for x-ray experiments. The flux is of the order of 10^{13} photons $\text{s}^{-1} \text{mr}^{-1} \text{mA}^{-1}$ in a 1% energy bandpass. The vertical divergence, $1/\gamma$, of the beam is between 20 and 50 arc seconds for 2~5 GeV electron energies. The divergence in the orbital plane is limited by apertures in the beam transport, and is typically several to tens of mr. The radiation is linearly polarized in the orbital plane of electrons.

X-RAY EXPERIMENTAL STATIONS AT SYNCHROTRON FACILITIES IN THE UNITED STATES

Three facilities, SPEAR at SLAC (Stanford), CHESS at CESR (Cornell) and NSLS at Brookhaven National Laboratory, can be used as a hard x-ray source in the United States. The first two are electron-positron storage rings, already in operation. The last one, an electron storage ring, serves exclusively as an x-ray (light) source and is under construction. In all of these three facilities, similar individual beam lines have been developed for various experiments in solid state physics, physical chemistry and materials science, by utilizing the unique features of synchrotron radiation, particularly high flux and wavelength tunability.

We describe here, as an example, the NBS/NRL beam lines for Materials Science, which are being assembled at NSLS. The beam lines include facilities for real time topography, small

angle scattering, inelastic scattering spectroscopy and crystallography. Scientific problems are aimed at advancing materials science by utilizing techniques previously impractical. For example, the high flux in the synchrotron beam greatly improves the possible observation of fine scale ($\sim 1-10\mu\text{m}$) phenomena in materials in real time. The energy and momentum resolution can be made extremely good so as to increase the precision in the determination of the atomic coordination and arrangement. Furthermore, the wavelength tunability of the radiation with the desired energy band pass enables us to focus on a particular atomic species (elemental tunability) for the precise determination of behavior under the influence of neighboring atoms in different local volumes.

We will discuss some of the results obtained by using synchrotron radiation (mainly at CHESS and SPEAR) in Materials Science to indicate great promise in the application of synchrotron radiation to materials science. Although unaccustomed, we will divide topics in two areas; research concerning phenomena statistically averaged in space (in other words, traditional solid state physics), and research concerning phenomena occurring differently in spatially separated regions (in other words, materials science). When possible, both types of measurement can be made as a function of time.

STATISTICALLY AVERAGED EFFECTS

The first example is in the area of crystallography. The high flux and continuous energy spectrum of synchrotron

radiation enables the quick acquisition of data, such as lattice parameters, using energy dispersive diffractometry, from samples, in-situ, under various environmental conditions. For example, to advance the synthesis technique of new materials of superior physical properties, such as solid lubricants for cruise missile engines, Skelton et.al.¹ at NRL have exploited the energy dispersive diffractometry technique under extreme high pressure of tens of GPa (using a diamond anvil pressure cell) and a wide range of temperatures (0.03 K to 3000°C). Since such a high pressure can be achieved only by reducing the size of the pressure chamber to microscopic dimensions, (10^{-3} mm³), it is impossible to obtain data within a realistic time frame, using conventional x-ray sources. Use of synchrotron radiation not only makes it possible to obtain such data in rapid succession, but also permits the study of phenomena heretofore immeasurable, e.g., structural measurements of phase transformation reaction rates in the time frame of seconds to minutes. As specific examples, they observed the first order phase transition in potassium iodide from the NaCl structure to the CsCl structure, as a function of pressure and temperature. At room temperature (23°C), this transition is induced at a pressure of 1.8 GPa, while at a pressure of 1.5 GPa, the transition can be thermally induced at about 100°C. For these observations, each diffraction energy spectrum was recorded in 100 sec.

In small angle scattering, the high flux and extreme collimation of synchrotron radiation permit the further improvement of x-ray angular resolution within a limited space. (For ordinary x-ray sources, a distance of the order of 10 meters is required to obtain adequate resolution.) At NBS, a double crystal system was employed, using asymmetric diffraction, to prepare a nearly parallel beam (~ 1 arc second divergence) and detect the scattered beams to within a second of arc of the direct beam². An intensity profile of small angle scattering from a block copolymer, polyethelene polystyrene, showed a well-resolved isolated peak corresponding to 750Å chain length. Normally, the existing "pinhole" small angle scattering instruments barely detect this peak. From the observed profile, this technique demonstrated the capability of detecting 4000 Å or larger particle sizes or chain lengths.

An absorption spectrum near the x-ray absorption edge of an element has a fine structure variation as the incident x-ray energy changes. This is called Extended X-Ray Absorption Fine Structure (EXAFS). Such a fine structure is closely related to the chemical state and the nearest neighbor interaction of an atom of this element in a condensed matter. These fine structures normally appear within a several hundred electron volts range above the edge. A high energy resolution is, therefore, required to obtain these fine structures. The elemental tunability and high flux of synchrotron radiation provides a significant advantage in this area of research. Here we describe

two examples of EXAFS experiments at NBS, which constitute prototypes for future synchrotron inelastic scattering experiments.

When amorphous alloys are annealed far below the crystallization temperature, structural changes (i.e., "relaxation") and concomitant reduction in density are often seen. Partial radial distribution functions around the nickel atoms in glassy NiP, obtained from EXAFS, have indicated that, in the NiP case, at least two metastable states exist for a single composition. EXAFS spectra have been obtained for glassy Ni₇₅P₂₅ samples d.c. plated and pulse plated, as well as, polycrystalline Ni₃P powder and pure Ni foils. The results indicate that the measured spectra are dominated by the Ni to P distances, and these distances in the pulse plated sample are stretched by $\sim 0.1\text{\AA}$, as compared to the crystalline Ni₃P and the d.c. plated samples. These results are in agreement with recent Mossbauer measurements on similar samples and with published density results. However, none of the earlier methods could probe the radial distribution directly.

To obtain structural information on thin (less than 30 \AA) or interfacial layers on materials, a more advanced method is required. This is called Surface EXAFS or SEXAFS, which permits measurements from samples in-situ under environmental conditions. As an example, a structural study of passive films on iron is described here. The samples were 50 \AA thick vapor deposited Fe films on glass, which were passivated by either a

chromate or a nitrite passivating solution. Near edge and extended x-ray absorption fine structure spectra were measured on these films, as well as on bulk Fe and on an air-exposed film. The energy position of the K-edge discontinuity of a material is a function of the effective charge and the electronic configuration of the absorbing atom. The edge shift of the chromate-formed film was 5.0 ± 2 eV lower than either the nitrite-formed film or the air-formed film (which were within 2 eV of each other). This indicates a significantly lower coordination charge for the chromate-formed film and a likely greater covalency is the bonding of the iron in this film.

The EXAFS data was Fourier transformed to obtain the radial distribution function (RDF) about the Fe site. A comparison of the first neighbor and the second neighbor coordination shells in the RDF can be used as a measure of "the relative disorder in a material." It was found that the air-formed film exhibited the most order (crystallinity) and the chromate-formed film the most disorder, while the nitrite-formed film was intermediate between the two. This suggests that the passive layers in the chromate-formed film are arranged in a glass-like structure about the Fe atoms.

MICROSTRUCTURAL EFFECTS

When a white beam of x-rays is incident on a crystal, an array of diffracted beams (a Laue pattern) is created, where each spot of the Laue pattern is of roughly the same size as the beam on the sample. Within each spot can be observed a fine

structure related to the microstructure in the sample. This fine structure is the basis of the method of x-ray topography. Depending on the wavelength of the radiation, the diffraction geometry, and/or the perfection of the crystalline samples, the depth (or thickness) of material observed can range between 1 μm (Bragg geometry) and 1 mm (Laue geometry). Topographs are obtained for the detailed interpretation of images produced by x-ray diffraction by real crystals.

Broadly speaking, synchrotron topography can be categorized into two basic classes: white beam topography and monochromatic beam topography. The ultimate objective of monochromatic radiation topography is the quantitative microstructure characterization leading to detailed structural modelling or the mapping of strains or other lattice parameter variations within a sample. As demonstrated later, this requires a careful, detailed interpretation of a sequence of topographs taken at slightly different orientations. There are many situations, however, where such a detailed study is neither required nor possible. Because of the wide variety of materials and microstructures of interest in materials science, a simple and rapid method for data collection is desirable. White radiation (Laue) topography is particularly suited to this end, for example, in the early detection of a crystal grain newly formed from the melt. The direction and magnitude of dislocation Burger's vectors, or the determination of active slip systems can readily be obtained from a Laue pattern containing different diffracting

planes simultaneously. Particularly exciting is the ability to apply x-ray topographic techniques to polycrystalline materials and "single crystals" of poor perfection.

White beam synchrotron topography requires only three optical elements: the source, the sample and the detector. The method is the same as the Laue reflection or transmission methods commonly used for crystal orientation. The sample is placed in the white synchrotron beam and a Laue pattern is recorded either on film or on a phosphor (for real time observation) viewed by a TV camera. Each Laue spot contains the fine structure of a topograph as shown in Fig. 1. Grains of arbitrary orientation are imaged because the sample itself selects the appropriate wavelength to locally satisfy the Bragg condition. Accurate positioning and orientation alignment are not required, and data can be obtained from several Laue spots simultaneously. Of course, there are serious shortcomings in this technique, involving the variation of wavelength within Laue spots. However, depending upon microstructures of interest, this is the easiest technique to implement. (In terms of defect analysis, however, it is probably the most complex).

A typical synchrotron radiation white beam Laue photograph (a set of topographs) is shown in Fig. 1, which was taken from a Czochralski grown Ni crystal in the transmission geometry. This crystal contains several subgrains with misorientations of $\sim 1^\circ$. At a quick glance, it is easily recognized that the position of the oval shaped subgrain shifts as the position

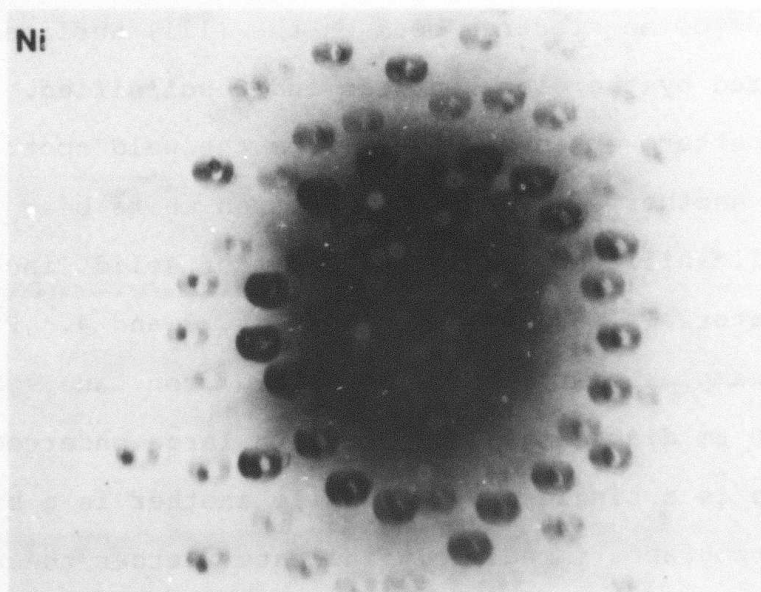


Figure 1. Synchrotron white beam transmission topograph of Czochralski grown Ni crystal containing subgrains. Note the changing shifted position of the oval shaped sub-grain in various Laue spots around the central spot.

of the Laue spot changes around the central spot, indicating the orientation (rotation) of this subgrain relative to the major grain. This demonstrates a typical merit of white beam topography for a quick and overall assessment of microstructures. Even residual stress effects can easily be detected as shown in Fig. 2. This is a Laue set of synchrotron white beam transmission topographs of a Si crystal, which contains a spot created by the incidence of an electron beam on the (111) surface. This spot was melted by the electron beam and resolidified. The residual stress pattern extends outward from the weld spot.

Another benefit of synchrotron white beam topography is the applicability to almost any sort of solid, including industrial materials, as evidenced in Figs. 3 and 4. Figure 3 shows a few examples of topographs obtained from Laue spots of Al powder, 100 μm diameter solidified with large undercooling. One particle is a single crystal, while another is a bicrystal. These topographs immediately indicate whether these particles are solidified from a single nucleus or multiple nucleation sites. Also, information is obtained as to whether these grains are deformed by strains, as seen in Fig. 3.c. Figure 4 demonstrates microstructures in a monocrystal turbine blade superalloy. Actually, these topographs were obtained by monochromatic topography. A topograph in the top right is essentially equivalent to a Laue spot in white radiation topography. When the beam is optically tight, the mosaic structure in this sample is clearly evident as shown by the missing regions in the top

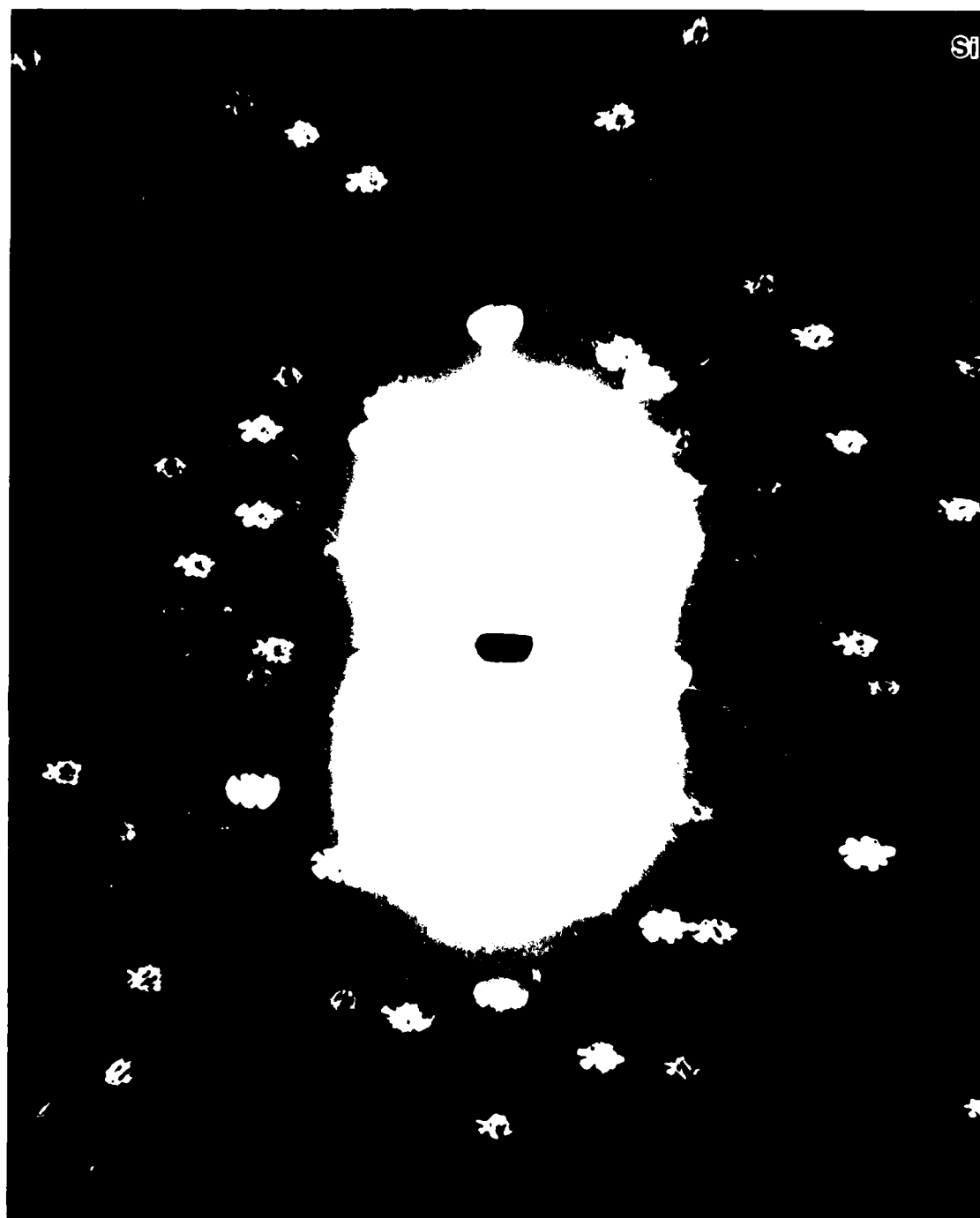


Figure 2. Synchrotron white beam transmission topographs of an electron beam melted and resolidified spot on a 111 surface of Si. Notice the residual stress pattern which extends outward from the weld spot.

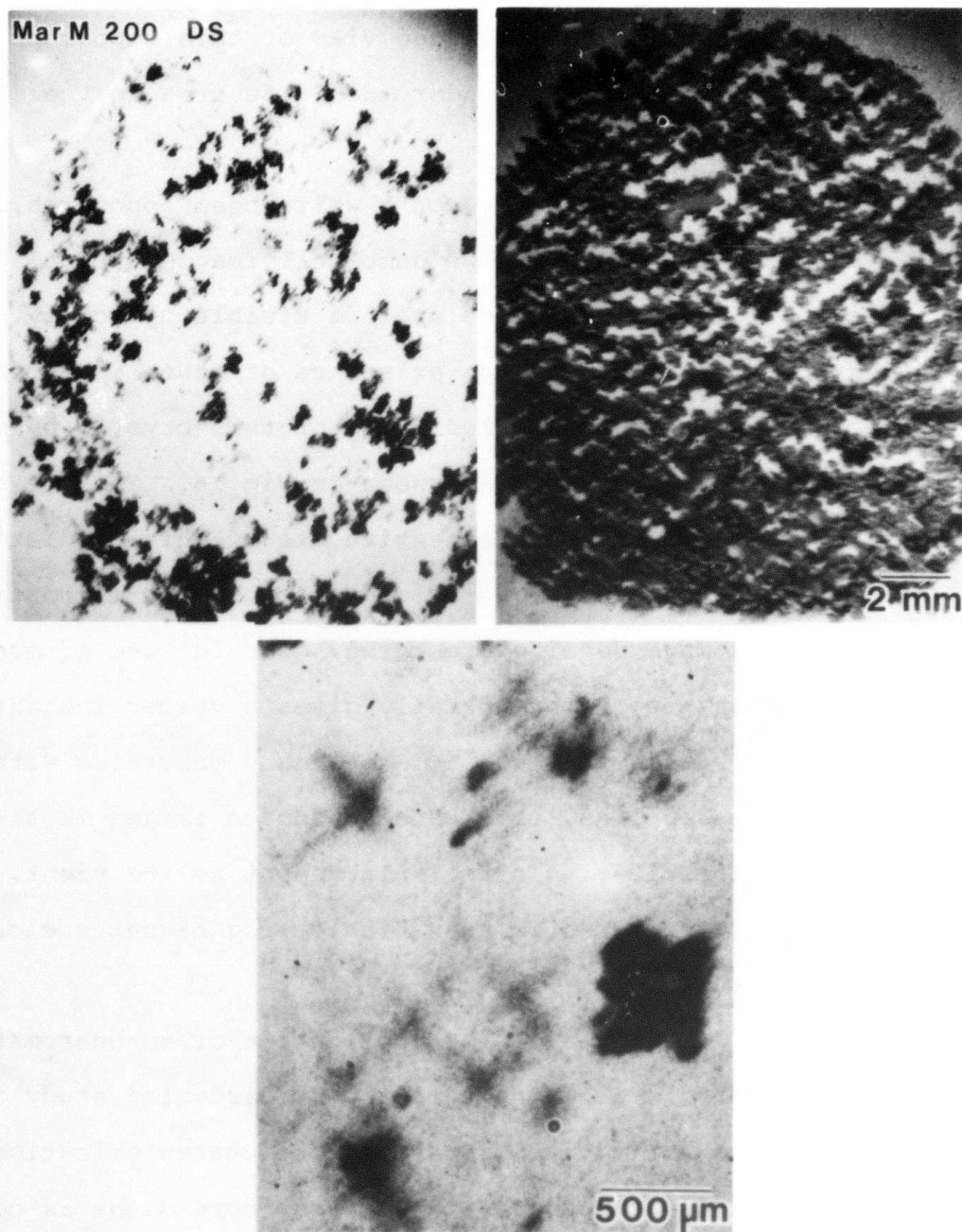


Figure 4. ACT topographs taken of a directionally solidified $[(001)]$ Mar M 200 monocrystal. The mosaic structure is evident in the top left and full diffraction is obtained by rocking the crystal a 1° during exposure. The bottom picture is an enlargement showing a grain composed of a single dendrite.

left of Fig. 4. An enlarged view of this topograph indicates the development of secondary dendrite arms in the [100] and [010] directions.

An enlarged view of a white beam topograph, Fig. 5, of a Fe 24 at % Al alloy shows dumb-bell images typical of inclusions. These inclusions are not visible optically. This topograph also indicates the existence of other imperfections, prompting a more detailed study of this crystal by monochromatic radiation topography, as shown in Fig. 6. This is a typical representation of the effective use of white radiation topography, that is, a rapid assessment of crystal microstructure leading to a more detailed research. Careful use of monochromatic radiation topography normally gives a deeper insight about microstructures. Figure 6 shows many subgrains within the large grain, as well as, the magnetic domain images in the [001] and [010] directions. In the enlargement at the right, a fine fringe pattern can be seen, indicating magnetic closure domains at the surface.

An example of the application of monochromatic radiation topography is shown next in a work hardening study as one step towards quantitative microstructure characterization. The work hardening which occurs at hardness impressions is considered to be a major factor in determining the microhardness properties of single crystals or of individual grains within polycrystalline materials. For example, the orientation dependence of the crystal work hardening determines the level of microhardness

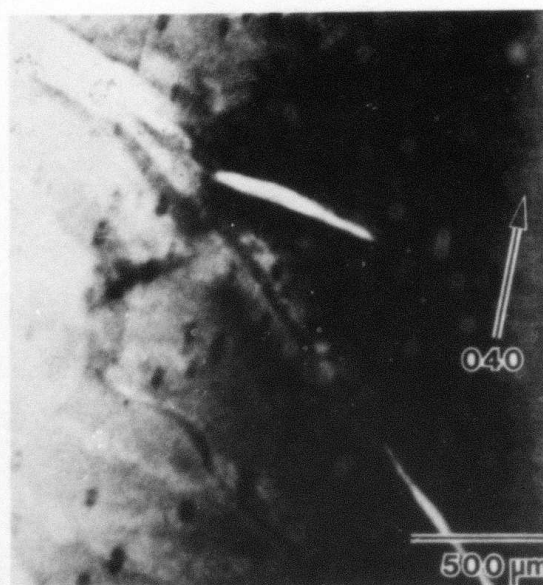


Figure 5. Enlarged view of 040 white beam topograph of Fe-24 at% Al grain showing dumbbell image contrast of inclusions.

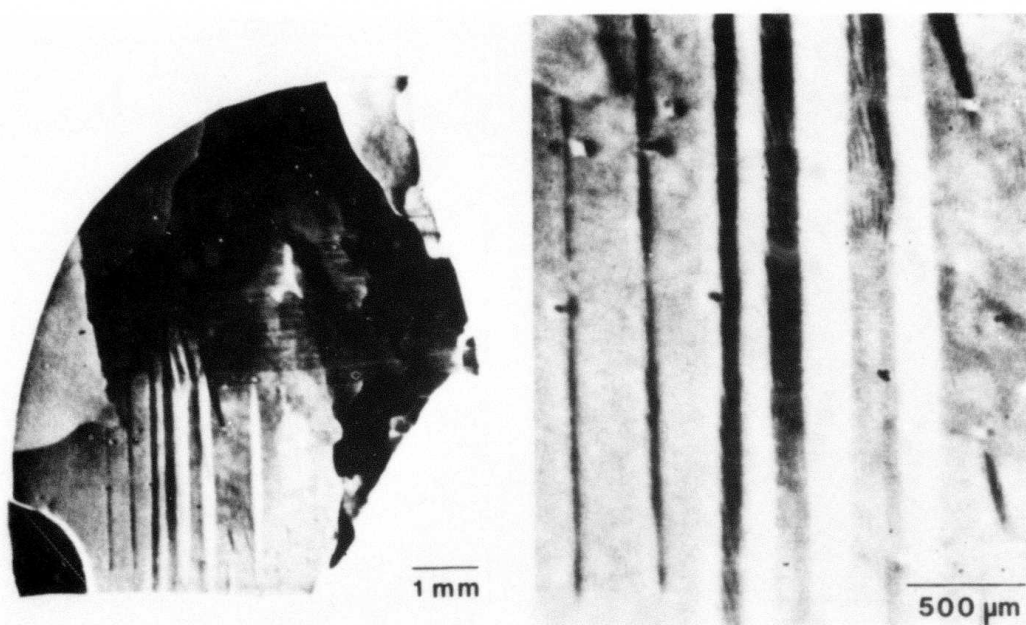


Figure 6. ACT surface reflection topographs of grain in Fe-24 at% Al alloy. Note the subgrains within the large grain as well as the magnetic domain images.

pressure and hardness anisotropy which is measured for different direction of the indenter axes of Knoop or diamond pyramid impressions. The pressure and anisotropy are critically dependent on how a particular set of slip systems is activated by micro-hardness indentations. As an initial attempt to develop a quantitative method of analyzing local strains within a crystal by x-ray topography, we employed a real time topographic system previously developed³ with a second generation image intensifier to the characterization of hardness indentations in a NaCl crystal and a copper crystal, using synchrotron radiation at CHESS.

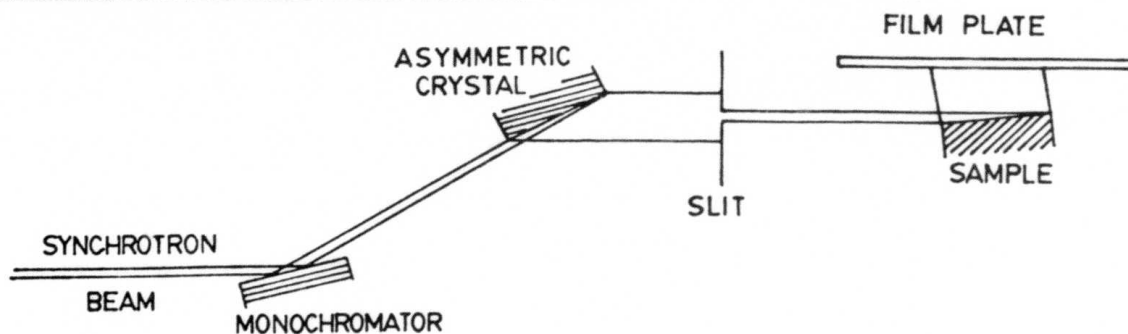
We obtained a series of topographs as a function of x-ray glancing angle, while the whole sequence was recorded on a video tape, to confirm the prediction of image contrast inversion⁽⁴⁾. This kind of experiment has been impractical or impossible with laboratory x-ray sources. Figure 7 shows x-ray optical arrangement for changing glancing angle θ_{in} as well as a 044 topograph of NaCl at θ_{in} = Bragg angle. Images around indentation impressions were analyzed in a similar fashion to a previous work on Cu⁵ for the determination of active slip systems and slip directions. We also obtained a series of topographs from a Cu crystal with Knoop indentations as a function of θ_{in} as well as θ_{out} (observation angle), as shown in Fig. 8. This set of topographs is required for the detailed (quantitative) information on strains associated with indentation impressions. Without synchrotron radiation, it is impossible to



$\bar{1}00$
010

$\vec{H}(0\bar{4}4)_{NP}$

.3mm



SYNCHROTRON RADIATION TOPOGRAPHY OF SODIUM CHLORIDE

8 KeV Synchrotron Radiation Operated at 5.25 GeV 16 mA

Exposure Time : 5 minutes on Ilford L-4 50 μ m Nuclear Emulsion Plate

Figure 7. An $0\bar{4}4$ topograph of an indented NaCl crystal taken at the exact Bragg angle. The inset illustrates an x-ray optical arrangement for changing the glancing angle θ_{in} .

SYNCHROTRON RADIATION TOPOGRAPHY OF COPPER CRYSTAL IN THE BRAGG GEOMETRY

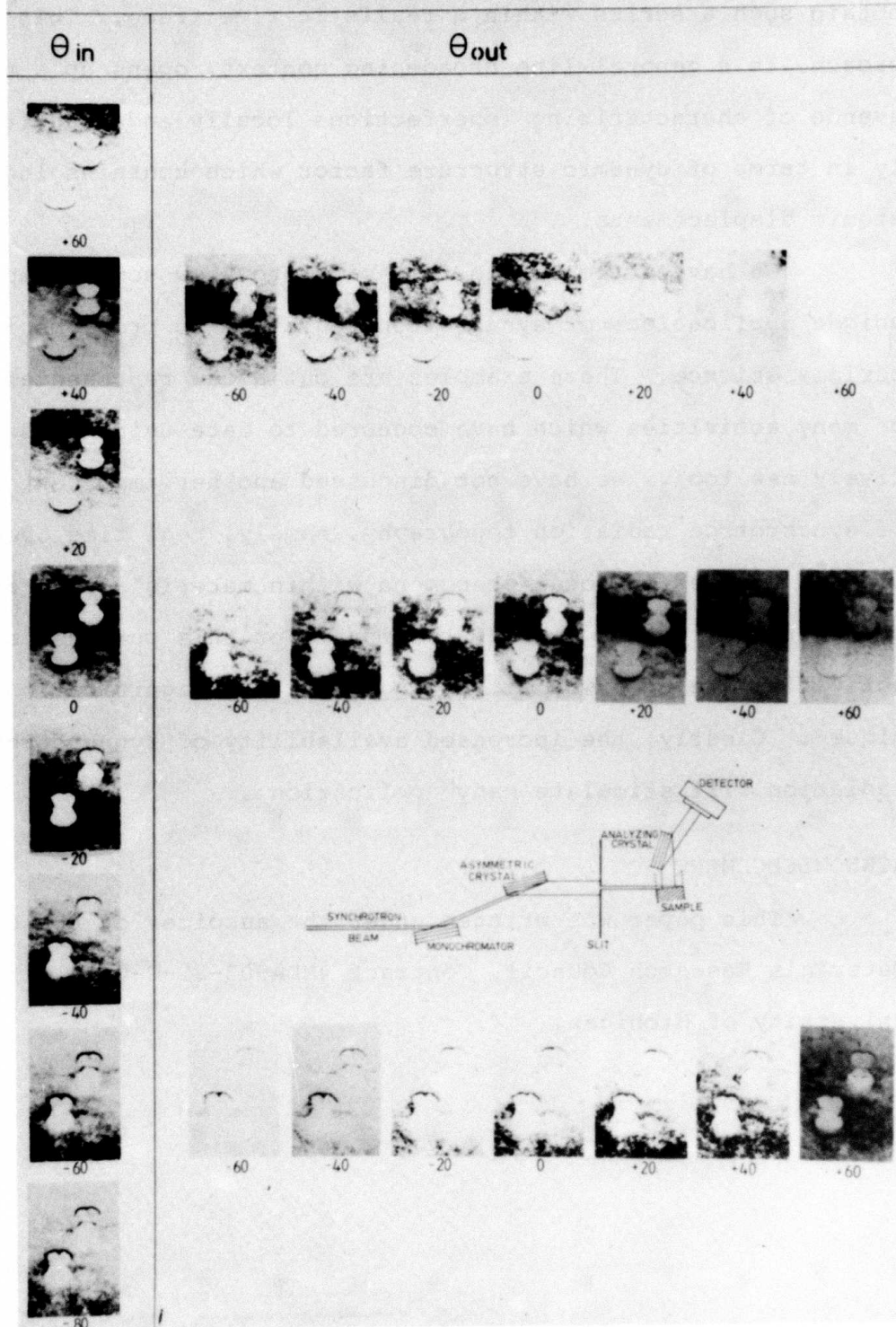


Figure 8. A series of topographs from a Cu crystal with Knoop indentations. Each topograph was taken at a different glancing angle θ_{in} and a different observation angle. This set of topographs opens up a new avenue for quantitative characterization.

obtain such a series within a realistic time frame. This approach, in a general line broadening context, opens up a new avenue of characterizing imperfections locally and quantitatively in terms of dynamic structure factor which contains local atomic displacements.

We have attempted in this paper to show some examples of unique applications of synchrotron radiation to problems in materials science. These examples are but a few representations of many activities which have occurred to date using this relatively new tool. We have not discussed another important aspect of synchrotron radiation topography, namely, real time observation of changes of local phenomena within materials such as phase transitions or tensile testing. For this purpose, several activities are underway, including the x-ray magnification technique³. Clearly, the increased availability of synchrotron radiation will stimulate many applications.

ACKNOWLEDGEMENT

This paper was written under the auspices of the DARPA Materials Research Council, Contract #MDA903-82-C-0428 with The University of Michigan.

REFERENCES

1. E. F. Skelton, J. Kirkland and S. B. Qadri, J. Appl. Cryst. 15, 82(1982).
2. H. Chen and M. Kuriyama, J. Appl. Cryst. 14, 280(1981).
3. W. J. Boettinger, R. C. Dobbyn, H. E. Burdette and M. Kuriyama, Nuclear Instruments and Methods 195, 355(1982).
4. M. Kuriyama and G. G. Cohen, Z. Naturforsch (1982) 379, in press.
5. K. C. Yoo, B. Roessler, R. W. Armstrong and M. Kuriyama, Script Metallurgica 15, 1245(1981).

PHOTOTHERMAL IMAGING APPLIED TO MICROSTRUCTURAL ANALYSIS

J. C. Murphy and L. C. Aamodt

PHOTOTHERMAL IMAGING

The bulk and surface temperatures of an externally heated sample are determined by the balance between the rate of heat input, the rate of conversion of the input to stored energy and the net rate of heat loss by heat conduction or radiation. This relationship is summarized in Fig. 1. When the optical, thermal, structural and photochemical properties of the sample vary from point to point, the induced temperature change produced by heating also varies spatially. Under certain conditions if the sample temperature can be measured then the sample parameters can be determined. Recently, there have been a number of papers describing methods of determining spatially resolved, time varying excess temperatures produced by amplitude modulated laser and electron beam sources^{1,2,3,4,5,6}. We use the term dynamic thermal imaging to represent this class of experiments. In most of the experiments reported to date a focused source was used to heat a small spot on the sample. The thermal image of the sample was constructed by scanning the source. In principle measurement of the entire temperature field of the sample without scanning is possible if a detector array is used. However, there has apparently been no work in this area for the case of ac induced temperatures. Successful

SAMPLE TEMPERATURE CHANGE	OPTICAL ABSORPTION	PHOTOTHERMAL CONVERSION
$\overbrace{\Delta T_s(x, y)} = \underbrace{I_o(\lambda, x, y)}_{\text{INCIDENT LIGHT}} * \overbrace{\beta(\lambda, x, y)} * \underbrace{H(\lambda, x, y) * PC(\lambda, x, y)}_{\text{EFFECTIVE THERMAL PARAMETERS}}$		

Figure 1.

measurements of dc temperatures have of course been known for many years under the name thermography.

If dynamic thermal imaging is to be developed as a quantitative tool for microstructural analysis, it is essential that methods be developed which allow the optical, thermal and photochemical parameters to be determined individually. In this case the term, thermal parameters, includes physical parameters such as thermal conductivity and heat capacity and structural features of the sample such as voids, cracks and regions of internal strain which change the rate of heat conduction in the sample. Up to this point much of the work in the dynamic thermal imaging area has concentrated on detecting the effect of different sample properties on the surface and bulk temperatures of the sample. Temperature images have been obtained which represent changes in structural or physical properties. However, the interpretation of the images has generally assumed that some properties were constant. For example, in work on imaging structural defects in metals, the images that are obtained are interpreted assuming that the optical absorption, thermal conductivity and heat capacity are constant throughout the sample and that the only origin for surface temperature changes in the sample is presence of structural defects such as voids or cracks^{3,4}.

In this report we present an analysis of localized heating of a homogeneous solid which includes solution of the three dimensional heat equation^{7,8}. A three dimensional

treatment is clearly required in principle when a focused laser or electron source is used for excitation purposes. It has been possible to use a one dimensional treatment whenever scanning photoacoustic detection is used because of the specific nature of the detection process^{9,7}. The same simplification applies to piezoelectric detection which does not use very high frequency sound and acoustic focusing^{10,11}. However, both of these imaging methods are unable to achieve separation of heat capacity and thermal conductivity. This point will be discussed in greater detail below and in the presentation. In addition, we discuss a new method of dynamic thermal imaging which uses laser beams both for heat generation and for detection^{12,13,14}. This method provides a number of operational advantages since it is sensitive, non-contacting and requires no cell for detection (hence adaptable to large specimens). It also has certain fundamental advantages over photoacoustic imaging since the detection process is localized in a certain sense. This makes it possible to determine the temperature profile of the region heated by the laser source. One consequence is that in principle this new method, which we call photothermal deflection imaging, can determine thermal conductivity separately from heat capacity.

PHOTOTHERMAL DEFLECTION IMAGING

This method relies on thermal transfer to a gas or liquid in thermal contact with the sample surface in a way similar to the scanning photoacoustic imaging method^{1,2}. In this

case, however, detection involves the use of a second laser beam which passes near the heated surface and is deflected by the dynamic thermal lens formed by the time modulated temperature in the gas^{15,16}. Fig. 2 shows the thermal lens produced and the relative positions of the pump and probe laser beams. Note that the two beams do not in general intersect. Also note that two orthogonal deflection signals are present respectively parallel and perpendicular to the plane of the sample. One of the components (normal component) has been shown⁷ to depend on the local surface temperature averaged along the ray path of the probe beam while the second depends on the component of the local temperature gradient orthogonal to the probe ray direction also averaged along the ray path. Because of this dependence on the temperature gradient, the photothermal deflection method can measure transport properties such as the thermal conductivity under appropriate circumstances. In imaging applications an image can be generated by scanning both pump and probe beams across the sample in a coordinated motion. No enclosed cell is needed for the measurement, unlike the photoacoustic case, hence application of the method to large samples is possible. Also, since the signal is an average along the probe ray path, there is a partial localization of the detection process. This opens other alternative methods of scanning the sample which may be important in special cases. Finally, the method is more sensitive in the sense of minimum detectable temperature change than the photoacoustic method in ideal cases. Whether this advantage

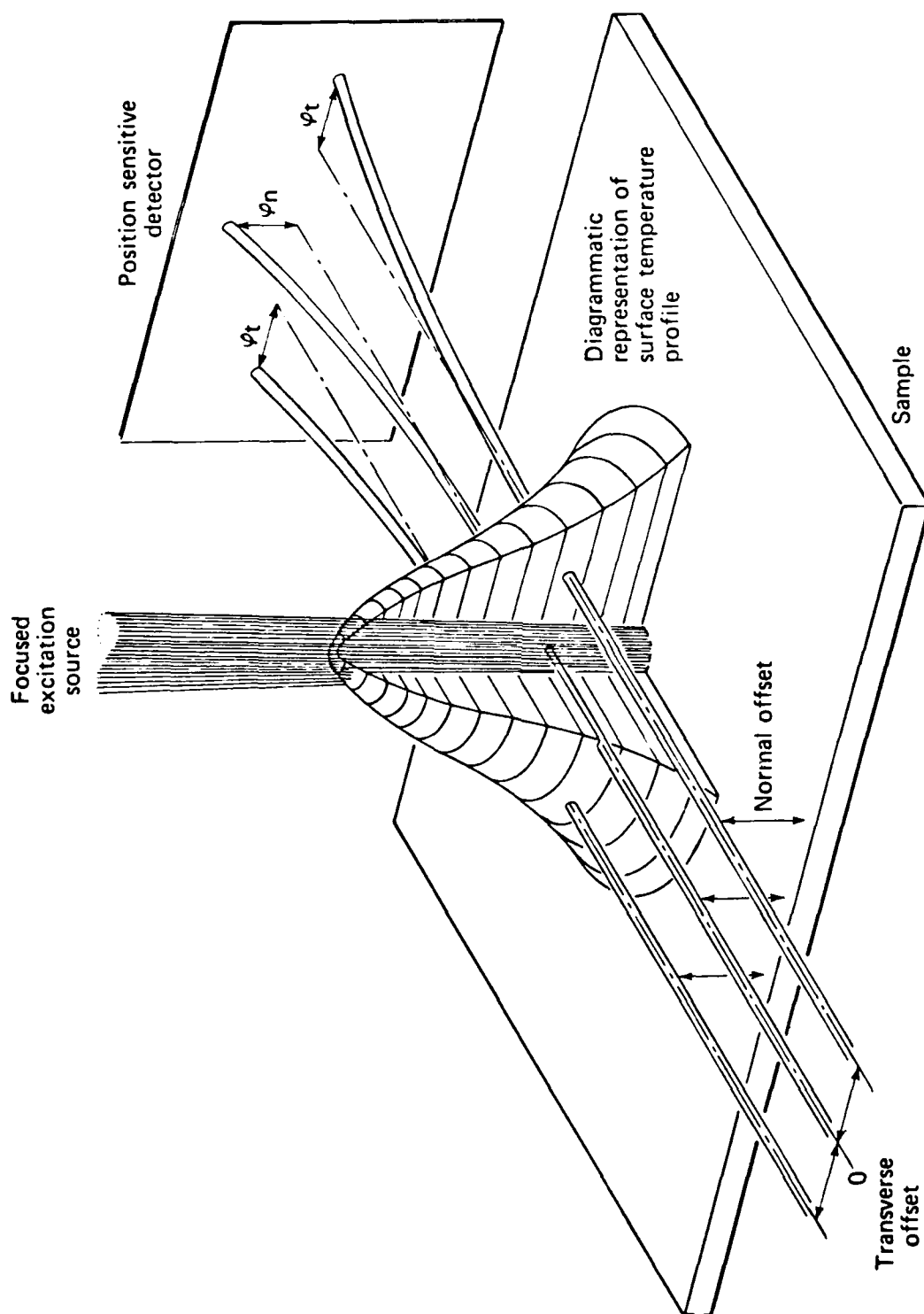


Figure 2.

could be realized in practical experimental situations is unclear. Very recently, a variant of the deflection imaging method has been developed which involves reflection of the probe beam from the sample. In this case two orthogonal deflection components are present, however, the response of each component can be shown to depend on orthogonal components of the sample surface temperature gradient in the plane of the sample.

Fig. 3 shows the measured dependence of the two orthogonal components (normal and transverse) on the separation distance between pump and probe beam. Note that the transverse component vanishes for intersecting beams. This feature also can be seen by inspection of Fig. 2. However, the disappearance of the transverse deflection amplitude under these conditions depends on equal contributions to the deflection from induced temperature gradients on either side of the plane determined by the probe ray direction and the sample normal passing through the center of the thermal lens shown in Fig. 2. This compensation exists only for a symmetric thermal lens. If the lens is not symmetric possibly because of spatial changes in optical or thermal properties, then cancellation does not occur. This feature is potentially important in applications both to study of defects in materials and to determination of the material properties of heterogeneous materials where grain boundaries and other spatial variations exist. Fig. 4 shows an application to a partially sintered transition metal oxide ceramic where a small crack and several inclusions are present.

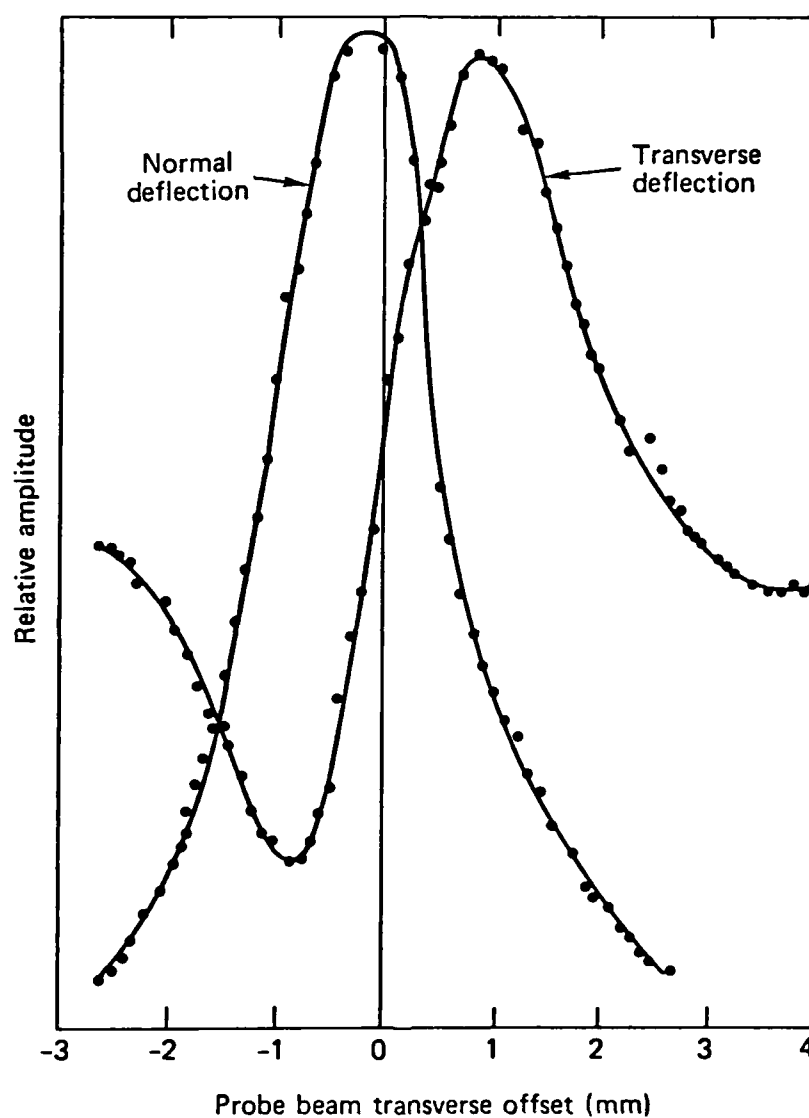


Figure 3.

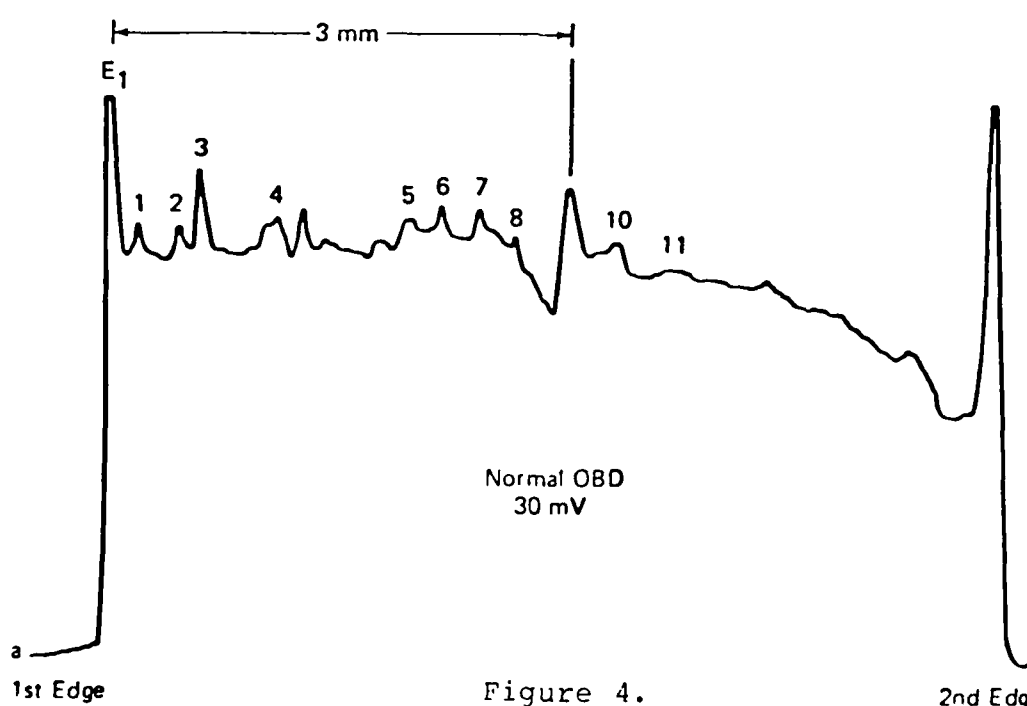
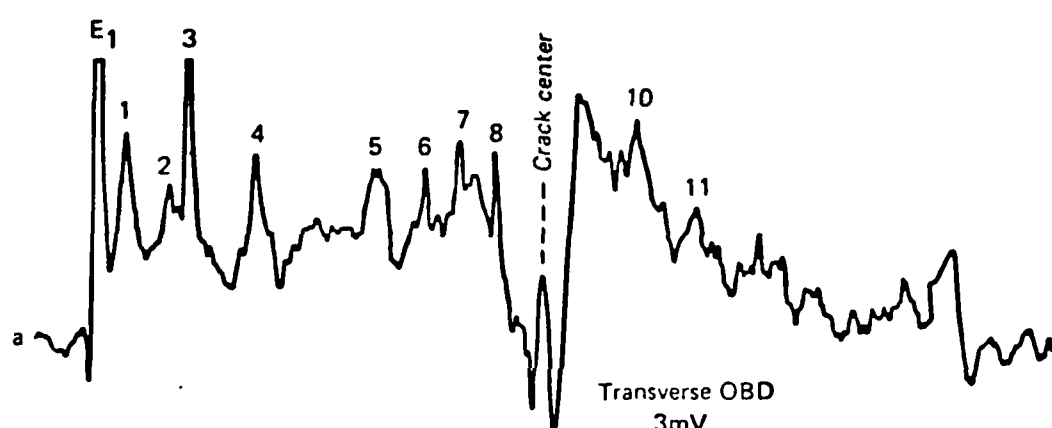
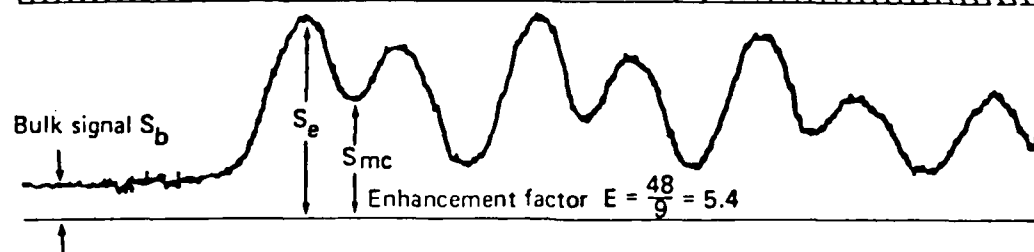
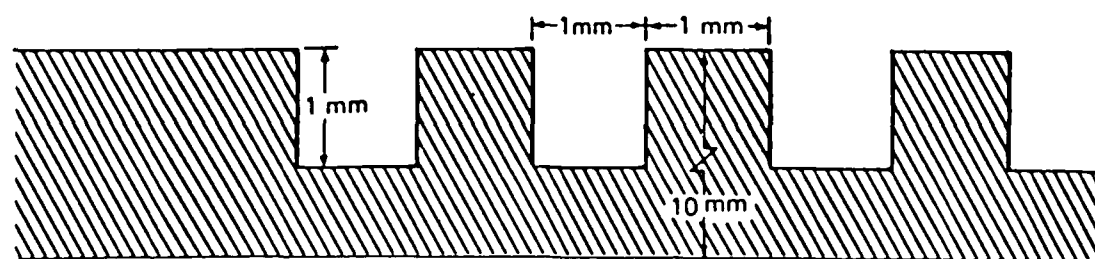


Figure 4.

The upper/lower traces are normal/transverse scans respectively. The transverse scan amplitude is small everywhere but near the crack or inclusions because of the compensation effect noted above. The signals at the sample edges and at the crack are three dimensional thermal diffusion effects which have been treated analytically¹⁵.

ANALYSIS OF SAMPLE TEMPERATURE UNDER LOCAL HEATING

Most present dynamic thermal imaging methods involve use of a scanning laser or electron beam. In this section the time varying surface temperature produced by an amplitude modulated laser beam is considered. The initial analysis applies only to homogeneous samples with spatially uniform thermal and optical properties. If the spatial changes in sample properties are slow enough that both optical and thermal events can be considered to be in an effectively homogeneous sample, this analysis can be extended to those samples as well. The other limiting case of discontinuous thermal and optical properties has also been considered analytically and experimentally. A brief description of this work will be given. This latter development may be applicable to sintered materials and metals with discrete grain structure. In this analysis the laser source is assumed to have a gaussian profile. A schematic diagram of the pertinent sample and beam geometry is shown in Fig. 5. The probe beam propagates in a gas in thermal contact with the surface. The intensity of the laser source is assumed to be low enough that the temperature dependent material parameters of the

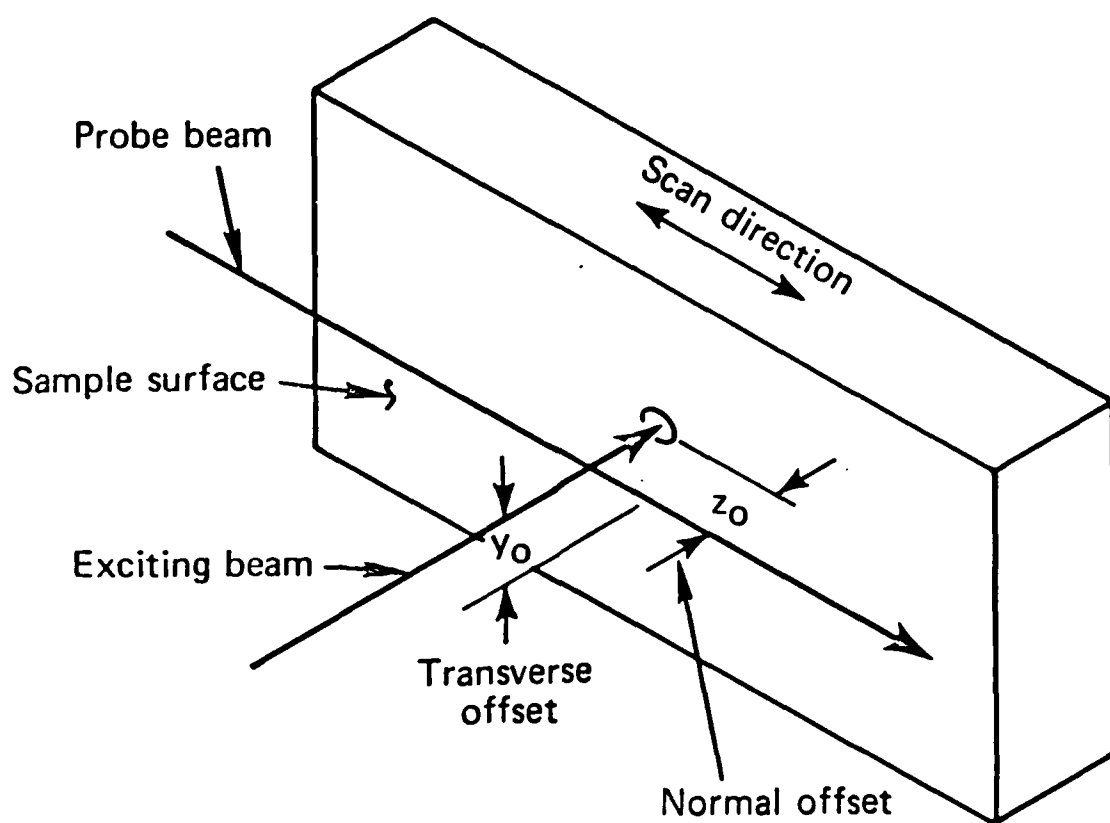


Figure 5.

sample can be considered to be constants with respect to the excess temperature generated by laser heating. This restrictive assumption is inappropriate for laser annealing and other high power applications.

For thermally isotropic samples, the sample and gas temperatures obtained from solution of the three dimensional heat equation are,

$$T_g(r,z) = \int_0^\alpha \tau(\lambda) \lambda h(\lambda) J_0(\lambda r) \exp(-b_g z) d\lambda \quad (1)$$

$$T_s(r) = \int_0^\alpha t(\lambda) \lambda h(\lambda) J_0(\lambda r) d\lambda \quad (2)$$

In deriving Eqs. 1, 2 an harmonic time response was assumed, $h(\lambda) = I_0 R^2 \exp(-\lambda^2 R^2/4)/2$, $b_i = (\lambda^2 + a_i^2)^{1/2}$ with $a_i = (2j)^{1/2}/\delta_i$ where δ is the thermal diffusion length and

$$t(\lambda) = \beta / [(k_s b_s + k_g b_g) (\beta + b_s)] \quad (3)$$

represents the sample response for a thermally thick sample. The one dimensional result

$$t(0) = \beta / [(k_s a_s + k_g a_g) (\beta + a_s)] \quad (4)$$

is obtained if $\lambda = 0$. Special cases of both the one dimensional and three dimensional versions of these expressions correspond directly with those found in the theory of signal generation in photoacoustic spectroscopy i.e. thermally thick and optically thick etc. For example, Eq. 2 shows a linear dependence on the optical absorption coefficient when $\beta \delta < 1$ and saturation behavior when $\beta \delta > 1$. In a medium with fixed β , k and C these

two regions are reached experimentally by varying w since $\delta = (2\alpha/w)^{1/2}$. For this case the explicit expressions for the saturated and unsaturated cases are,

$$t(o) = 1/\sqrt{2k_s C_s w} \quad \text{saturated} \quad (5)$$

$$t(o) = \beta/jwC_s \quad \text{unsaturated} \quad (6)$$

Note that the unsaturated case allows the thermal capacity to be determined experimentally if the optical absorption is known. For the saturated case the optical absorption coefficient drops out, however, the signal is determined by the product of both thermal parameters. In scanning a sample with spatially varying β , k and C it is not possible to determine the individual parameter values uniquely using a one dimensional analysis. It is significant that photoacoustic detection is equivalent to a one dimensional solution even when the three dimensional gas and sample temperatures are used since the photoacoustic signal is determined by the excess temperature averaged over the entire sample⁷. When the three dimensional solution represented by Eq. 3 is considered, the results are qualitatively similar to the one dimensional results in that the special cases (thermally thick etc.) are still present and saturation occurs for large B . However, the conditions for saturation change and require conditions both on $\beta\delta$ and on βR where R is the radius of the pump beam.

The temperature field in the gas given by Eq. 2 causes a gradient in the index of refraction of the gas which deflects

the probe beam. For the geometry of Fig. 5 the two deflection components correspond to the two components of the index gradient are

$$\phi_n = - \frac{2dn}{ndT} \int_0^\alpha t(\lambda)h(\lambda)b_g \exp(-b_g z) \cos(\lambda y) d\lambda \quad (7)$$

$$\phi_t = - \frac{2dn}{ndT} \int_0^\alpha t(\lambda)h(\lambda)\lambda \exp(-b_g z) \sin(\lambda y) d\lambda \quad (8)$$

The subscripts n and t refer to the normal and transverse deflections respectively. For surface skimming probe beams where $z=0$ in equations and, the gas temperature evaluated at the sample surface equals the sample temperature and the normal and transverse deflections are respectively,

$$\begin{aligned} \phi_n(y) &= - \frac{Rdn}{ndT} b_g T(y) \\ \phi_t(y) &= - \frac{Rdn}{ndT} \delta T(y) / \delta y \end{aligned} \quad (9)$$

Consider the slope of the transverse deflection evaluated at $y=0$ (intersecting beams). This is given by the expression

$$S = (\delta \phi_t / \delta y)_{y=0} = - \frac{2dn}{ndT} \int_0^\alpha t(\lambda)h(\lambda)\lambda^2 d\lambda \quad (10)$$

This integral may be approximately determined analytically to be

$$S \approx I_0 \frac{\sqrt{\pi} \operatorname{erf}(R/\sqrt{2}\delta)}{RY} + j \frac{\exp(-R^2/2\delta^2)}{k_s} \quad (11)$$

for a saturated thermally thick sample. Other cases may also be evaluated. Note that for large δ/R the photothermal signal depends exclusively on k the thermal conductivity, while for small

δ/R it depends on the thermal admittance $Y = (j\omega kC)^{1/2}$. The last result is essentially the photoacoustic signal result. This integral may also be evaluated numerically. Fig. 6 gives the calculated result defined in terms of a quantity we term the thermal character. Note that the photoacoustic result always involves a product of two sample parameters, while the deflection signal depends on these parameters individually in appropriate regions of β , k , C and .

CONCLUSION

Dynamic thermal imaging is potentially important for studying spatially varying properties of materials on a very wide scale. Present applications of photoacoustic spectroscopy give some indication of the potential range. Studies have included measurement of optical absorption properties, thermal properties with reference to phase transitions, amorphous to crystalline transitions in semiconductors, structural defects such as voids and cracks and measurement of temperature dependent thermal parameters themselves and photochemical properties including measurement of quantum efficiency of phosphors and semiconductors, photosynthesis and photocatalytic reactions and electrochemical processes. In specific materials many of these processes are spatially distinct and may be proper objects for study using thermal imaging methods. While this field is still in early stages of development, progress is rapid and it appears that in a number of cases local properties of materials in the classes noted may be measureable by these methods.

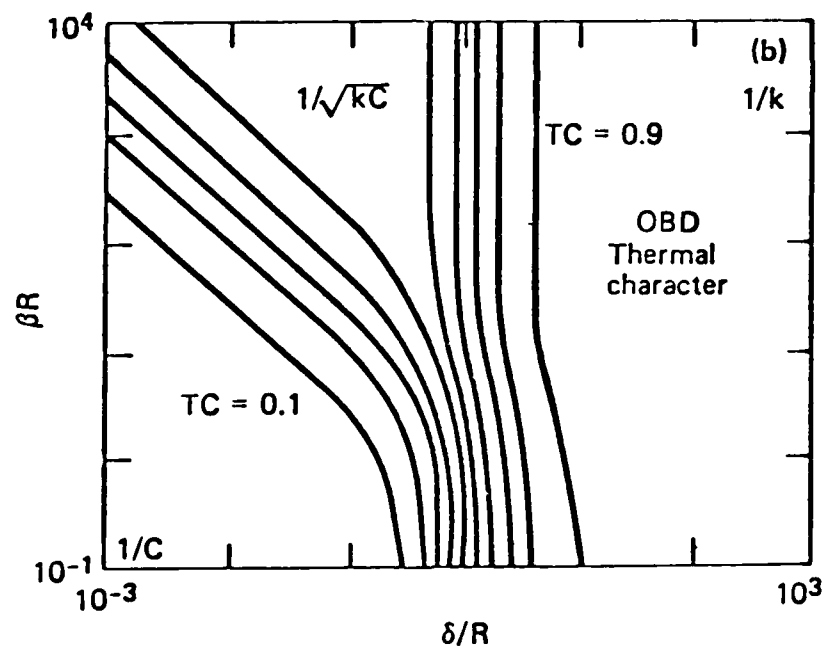
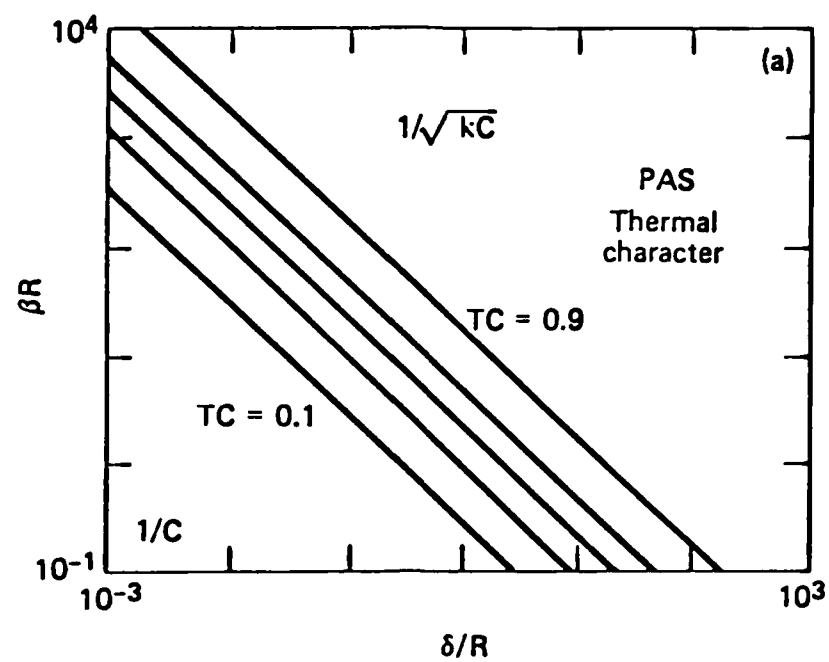


Figure 6.

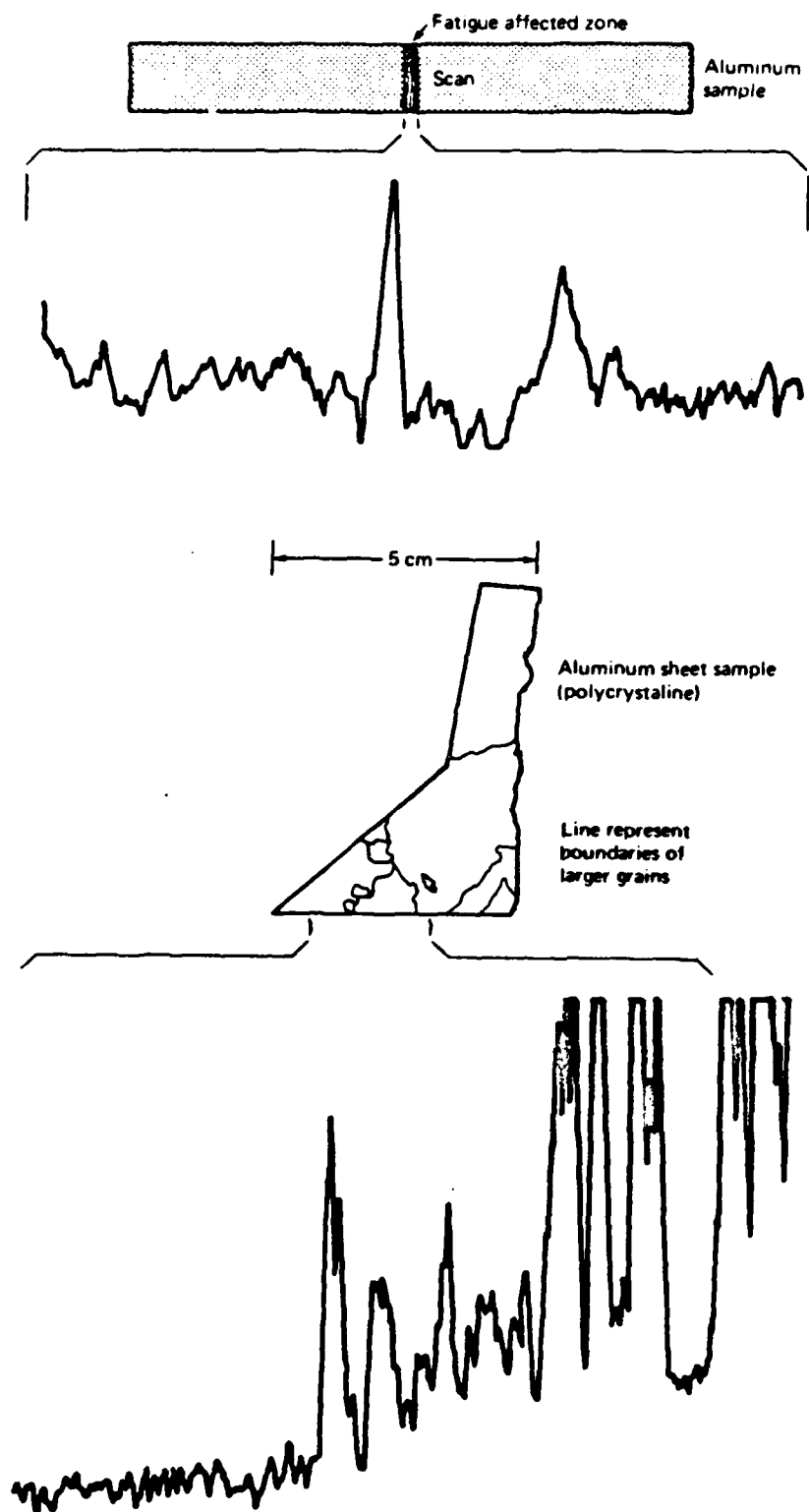


Figure 7.

ACKNOWLEDGEMENT

This paper was written under the auspices of the DARPA Materials Research Council, Contract #MDA903-82-C-0428 with The University of Michigan.

REFERENCES

1. Y. H. Wong, R. L. Thomas, G. F. Hawkins, Appl. Phys. Lettr. 32, 138(1978).
2. J. J. Pouch, R. L. Thomas, Y. H. Wong, J. Schuldies, J. Srinivasan J. Opt. Soc. Am. 70, 562 (1980).
3. G. Busse. Appl. Phys. Lettr. 35, 759(1979).
4. G. Busse, A. Ograbeck, J. Appl. Phys. 51, 3576(1980).
5. G. S. Cargill, A. Rosencwaig, Nature 286(1980).
6. M. Luukhala, S. G. Askerov, Electronics Lettr. 16, 84 (1980).
7. L. C. Aamodt, J. C. Murphy, J. Appl. Phys. 52, 4903(1981).
8. L. C. Aamodt, J. C. Murphy, "Thermal Effects in Photothermal Spectroscopy and Photothermal Imaging", submitted.
9. F. A. McDonald, Appl. Phys. Lettr. 36, 123(1980).
10. G. Busse, A. Rosencwaig, Appl. Phys. Lettr. 36, 815(1980).
11. J. Opsal, A. Rosencwaig, J. Appl. Phys. 53, 4240(1982).
12. J. C. Murphy, L. C. Aamodt, Appl. Phys. Lettr. 38, 196 (1981).
13. J. C. Murphy, L. C. Aamodt, Appl. Phys. Lettr. 39, 519 (1981).
14. J. C. Murphy, L. C. Aamodt, Second International Conference On Photoacoustic Spectroscopy, Berkeley, CA, June 22-25(1981).
15. L. C. Aamodt, J. C. Murphy, Appl. Optics 21, 111(1982).

NONDESTRUCTIVE CHARACTERIZATION (NDC)
BY MEANS OF EDDY CURRENT CONDUCTIVITY TESTING

M. Rosen, H. T. Yolken and R. Mehrabian

INTRODUCTION

Eddy current techniques have been used extensively for nondestructive inspection of electrically conducting specimens for structural defects and irregularities.^{1,2} Applications include detection of cracks, voids, and inclusions, and determination of the thickness of nonconductive coatings on electrically conductive base materials. In general, eddy current conductivity measurements have been extremely effective for locating structural flaws near the specimen surface.

The principle of operation of eddy current techniques is based on electromagnetic induction of eddy currents when a coil carrying alternating current is brought near a metallic specimen. The magnitude of the induced eddy currents depends on the magnitude and frequency of the alternating current, and on the electrical and magnetic properties of the material to be inspected. Structural discontinuities or compositional inhomogeneities may affect the electrical conductivity of the material. The presence of such defects changes the apparent impedance of the pickup coil, thus giving an indication of changes in the physical, chemical and metallurgical structure of the material.

The induced eddy currents decay exponentially with depth and are concentrated near the surface of the sample, resulting in a "skin effect." The depth of penetration can be expressed

in terms of the frequency of the alternating current, as well as the magnetic permeability and electrical conductivity of the material to be characterized. In addition, the reduction in current with depth is also governed by the eddy current coil geometry. The greater the exciting frequency, conductivity and permeability, the smaller the depth at which eddy currents can be induced in the metal. In ferrous alloys, with a high value of magnetic permeability, the penetration is rather shallow even at low frequencies.

Eddy currents have been used as a nondestructive evaluation tool for diverse applications, e.g., contactless measurements of electrical conductivity at elevated temperatures, detection of voids in bonding layers, wall thickness determination in tubes and plates, changes in material properties while fatigue is in progress, and variations in the state of stress of metallic surfaces. Recently, eddy current conductivity has been used to detect the variations in mechanical properties (strength and hardness) of age-hardenable aluminum alloys.

The ease of operation and application of the eddy current technique makes it particularly attractive as an NDE tool for field inspection. However, eddy current conductivity is a result of several contributions that depend on the intrinsic physical and chemical properties of the material. Interpretation and analysis of experimental data may be difficult indeed as they depend on a profound understanding of metallurgical phenomena that are responsible for the measured values of the

eddy current conductivity and their relationship with the mechanical properties of the material.

In addition, the concepts and theory that relate these intrinsic properties and the geometry of the material to eddy current conductivity have not been well formulated to date. However, an effort is underway³ to develop this needed base of theoretical understanding. The development of adequate theory should be given priority in the development of eddy current testing.

Another current weakness in the method is the lack of adequate measurement methods to properly characterize eddy current coils. Lack of coil characterization has resulted in non-compatible non-quantitative results between users. Coil characterization should also be given priority in eddy current testing development.

A case in point, illustrating the lack of knowledge concerning the correlation between eddy current conductivity and metallurgical properties based on a recent investigation at NBS that reflects the intrinsic complexity, will be discussed in the following section. It deals with the age-hardening process in a precipitation-hardening aluminum alloy and the relationship between variations in eddy current conductivity and mechanical properties of the alloy. It was found that a useful characterization of the process and logical conclusions can be derived from eddy current measurements only if the metallurgical phenomena responsible for the observed changes in eddy current

conductivity are well understood.

Eddy Current Conductivity in 2024 Aluminum Alloy

Electrical conductivity measurements, employing AC, DC and eddy current techniques are often used in order to determine the progress and the kinetics of precipitation-hardening processes.^{4,5}

The variation of the electrical conductivity with aging results from two main contributions that may have opposing effects and thus cause ambiguities in the interpretation of observed behavior. First, a decrease in eddy current conductivity is noted with the appearance of very fine precipitates (GP zones) that are evenly distributed in the supersaturated aluminum matrix. These particles have nearly critical dimensions for efficient scattering of electrons and contribute substantially to increased strength and hardness of the material. Additional contributions for reduced electrical conductivity of the alloy are due to the frozen-in vacancies in the aluminum matrix (during rapid cooling from the solutionizing temperature of about 500°C), and presence of a relatively large concentration of dissolved elements (e.g., Cu and Mg) that are efficient electron scatters.

As the age hardening process continues, with accompanying increase in strength and hardness of the alloy, the eddy current conductivity begins to increase. This opposite trend is due to the change in morphology of the particles and the "purification" of the matrix when large amounts of copper and mag-

nesium atoms leave the matrix in the form of solute-rich precipitates.

Fig. 1 shows the variation of the electrical conductivity as a function of aging time of 2024 aluminum alloy at different isothermal holding temperatures. The initial conductivity value, before aging, was 31.5% IACS (International Annealed Copper Standard). The salient features in Fig. 1 are as follows:

- a. Initial decrease in conductivity at each isothermal aging temperature in the range between 21 and 190°C; the rate of decrease being enhanced with increasing aging temperature.
- b. Conductivity decreases with aging time at temperatures between 21 and 50°C, and although at different rates, attains an identical ultimate value of 29.5% IACS for the fully aged alloy.
- c. The eddy current conductivity above 150°C increases with isothermal aging temperature after the initial decrease. The variation of the conductivity with aging time at 150°C is extremely sluggish. It remains nearly constant for about 30 hours of aging.
- d. The ultimate value of the electrical conductivity for fully aged specimens, at temperatures above 170°C, is 41% IACS (not shown in Fig. 1). This value is attained after 50 h at 190°C, and after somewhat longer times at lower isothermal aging temperatures.

Fig. 2 shows the variation of hardness as a function of isothermal aging. During the first 10 hours of aging at temperatures between 150 and 190°C the hardness invariably increases. In contrast, as shown on Fig. 1, the electrical conductivity

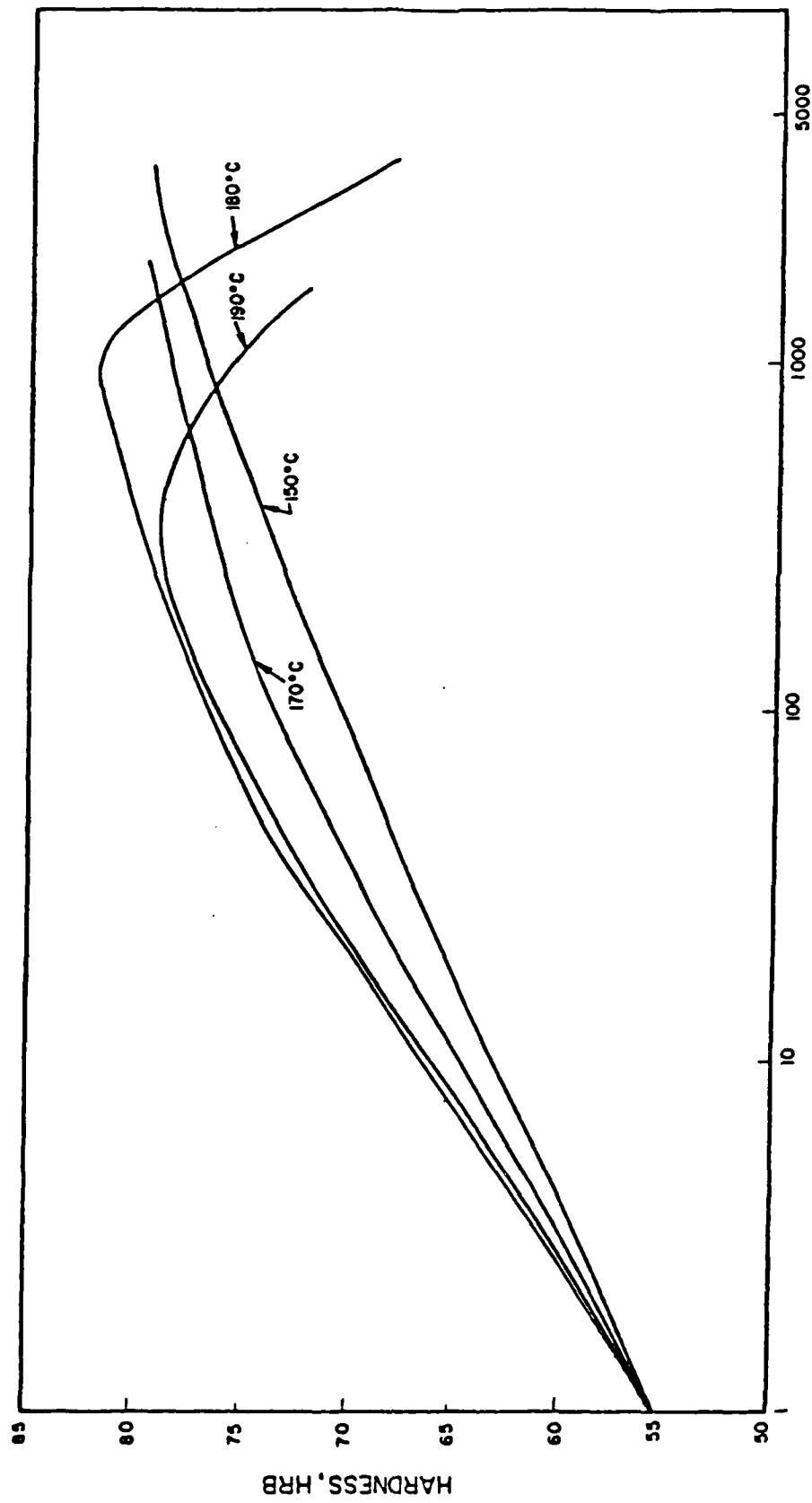


Figure 1. Hardness as a function of aging time, at different aging temperatures, of 2024 aluminum alloy.

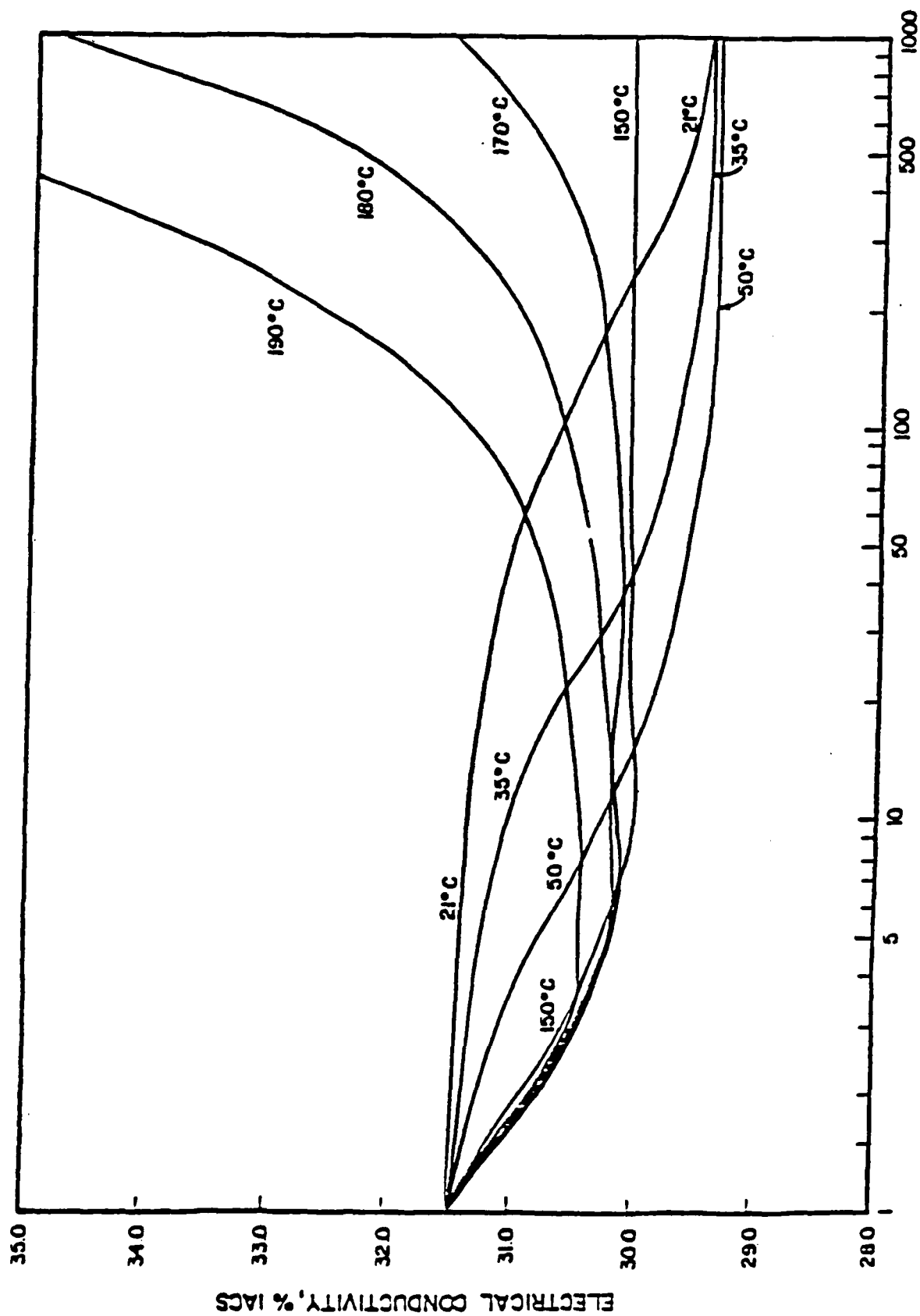


Figure 2. Eddy current conductivity as a function of aging time, at different aging temperatures, of 2024 aluminum alloy.

can either increase or decrease depending on the type and distribution of the precipitates involved.

The results of this research illustrate that in age-hardened 2024 aluminum alloy a given mechanical property, such as hardness, can be associated with a wide range of eddy current conductivities between 29.5 and 41% IACS. These widely differing conductivities are a manifestation of differences in the microstructure of the material. Therefore, a straightforward correlation between the mechanical properties and the non-destructive eddy current data was not possible unless the metallurgical processes that produced the specific microstructure sequence were considered⁴.

SUMMARY

Eddy current conductivity testing is currently a useful NDE tool for flaw detection. However, it is extremely sensitive to specific microstructural features of an alloy. Its use as a nondestructive characterization technique should be limited to alloy compositions and processing sequences for which correlations between microstructure and electrical conductivity have been well established. If microstructure/property relationships are also available, then the eddy current technique can be of considerable value.

There is lack of methodology to characterize eddy current coils. In addition, theoretical work relating eddy currents to materials properties should be expanded.

The ease of operation and application of the eddy current technique and its high sensitivity justify further research that will lead to improved correlations between eddy current data and relevant metallurgical processes/compositions/microstructures and properties.

ACKNOWLEDGEMENT

This paper was written under the auspices of the DARPA Materials Research Council, Contract #MDA903-82-C-0428 with The University of Michigan.

REFERENCES

1. "Eddy Current Inspection" Metals Handbook Vol. 11, "Nondestructive Inspection and Quality Control, 8th edition, pp. 75-92, American Society for Metals, Metals Park, Ohio (1976).
2. "Eddy-Current Characterization of Materials Structures," George Birnbaum and George Free, editors, ASTM Special Technical Publication 722, (1981).
3. "A Boundary Integral Equation Method for Calculating the Eddy-Current Distribution in a Long Cylindrical Bar with a Crack," A. H. Kahn and R. Spal in Eddy Current Characterization of Materials and Structures, ASTM Tech. Pub. 722, G. Birnbaum and G. Free, Eds., pp. 298, (1981).
4. M. Rosen, E. Horowitz, L. Swartzendruber, S. Fick and R. Mehrabian, Matl. Sci. Eng. 53, 191 (1982).
5. D. Turnbull, M. S. Rosenblum, and H. N. Treafin, Acta. Met. 8, 277 (1960).

ON DESTRUCTIVE EVALUATION OF DEFECTS USING
LONG WAVELENGTH NEUTRONS

B. B. Rath

Microstructural flaws and defects in crystalline, as well as noncrystalline solids, can be effectively evaluated using long wavelength neutrons. Size and distribution of flaws, such as microcracks, pores precipitates, inclusions and dispersoids, can be determined from the measurements of small angle scattered intensities as a function of scattering angle. Although, in principle, the method is analogous to x-ray scattering, it has a number of advantages which makes it unique for nondestructively evaluating flaws in solids. For example; 1) neutrons penetrate to large depths in solids, 2) using an appropriate velocity selector, monochromatic waves ranging anywhere between 4 Å to 12 Å can be used for investigation. Selection of wavelengths which are greater than twice the largest interplanar spacing of the crystalline lattice eliminates scattering due to multiple Bragg reflection, and, 3) since neutrons have distinctly different scattering cross sections for neighboring elements in the periodic table, alloys containing such elements can be easily identified. The method is particularly sensitive to defect sizes in the range of 50 to 1000 Å. Small angle neutron scattering (SANS) studies have several applications to metallurgical problems, such as void formation and growth during creep and superplastic forming, precipitation and early stages of other solid state transformations, monotonic stress or

fatigue induced microcracks and residual porosities in powder consolidates. Kinetics of many metallurgical processes can be evaluated by this method in a nondestructive manner.

The intensity of a scattered neutron from a particle or a void, I_{avg} , has been described by Guinier as:

$$I_{avg} = A_e^2 f_k \exp\left\{-\frac{q^2 R_g^2}{3}\right\} \quad (1)$$

where A_e and f_k are the scattering amplitude and scattering factor, respectively, q is the wave vector and R_g is the radius of gyration. q is given by the relation

$$q = \frac{4\pi \sin\theta}{\lambda}$$

where θ is the scattering angle and λ is the neutron wavelength. When the solid contains a large number of defects corresponding to a distribution in R_g , the intensity can be described as:

$$I = I_0 \int N(R_g) \exp\left\{-\frac{q^2 R_g^2}{3}\right\} dR_g \quad (2)$$

where the experimentally measured quantities are I and q . The equation is numerically solved using one of several algorithms, which yields a size distribution of defects. Of course, if all defects are of nearly the same size, it can be simply evaluated from the slope of the $\ln I$ vs q^2 plots.

A position sensitive area detector usually containing a 64x64 element matrix is used to measure scattering profiles. This approach provides detailed information on defect anisotropy. A two dimensional intensity contour of scattered neutrons resulting from voids in a superplastically deformed Cu-alloy is illustrated in Fig. 1.

Several studies are underway at the Naval Research Laboratory, Oak Ridge National Laboratory and the National Bureau of Standards to characterize defect nucleation and growth in various alloy systems. One example is shown here to illustrate the potentials of SANS as an NDE method. The experiment consisted of a stainless steel powder isostatically consolidated at temperatures ranging between 800 and 1200°C. The residual porosities were measured by SANS. The systematically increasing scattered intensities at all size ranges with decreasing consolidation temperatures is shown in Fig. 2. Since the intensity profile for the 1200°C samples (A5-A6) were nearly identical to that of a wrought alloy, it was assumed that alloys A5 and A6 were free of defects. The relative void volume, evaluated from the integrated SANS intensities were found to increase by a factor of 8, due to decreasing consolidation temperature.

ACKNOWLEDGEMENT

This paper was written under the auspices of the DARPA Materials Research Council, Contract #MDA903-82-C-0428 with The University of Michigan.

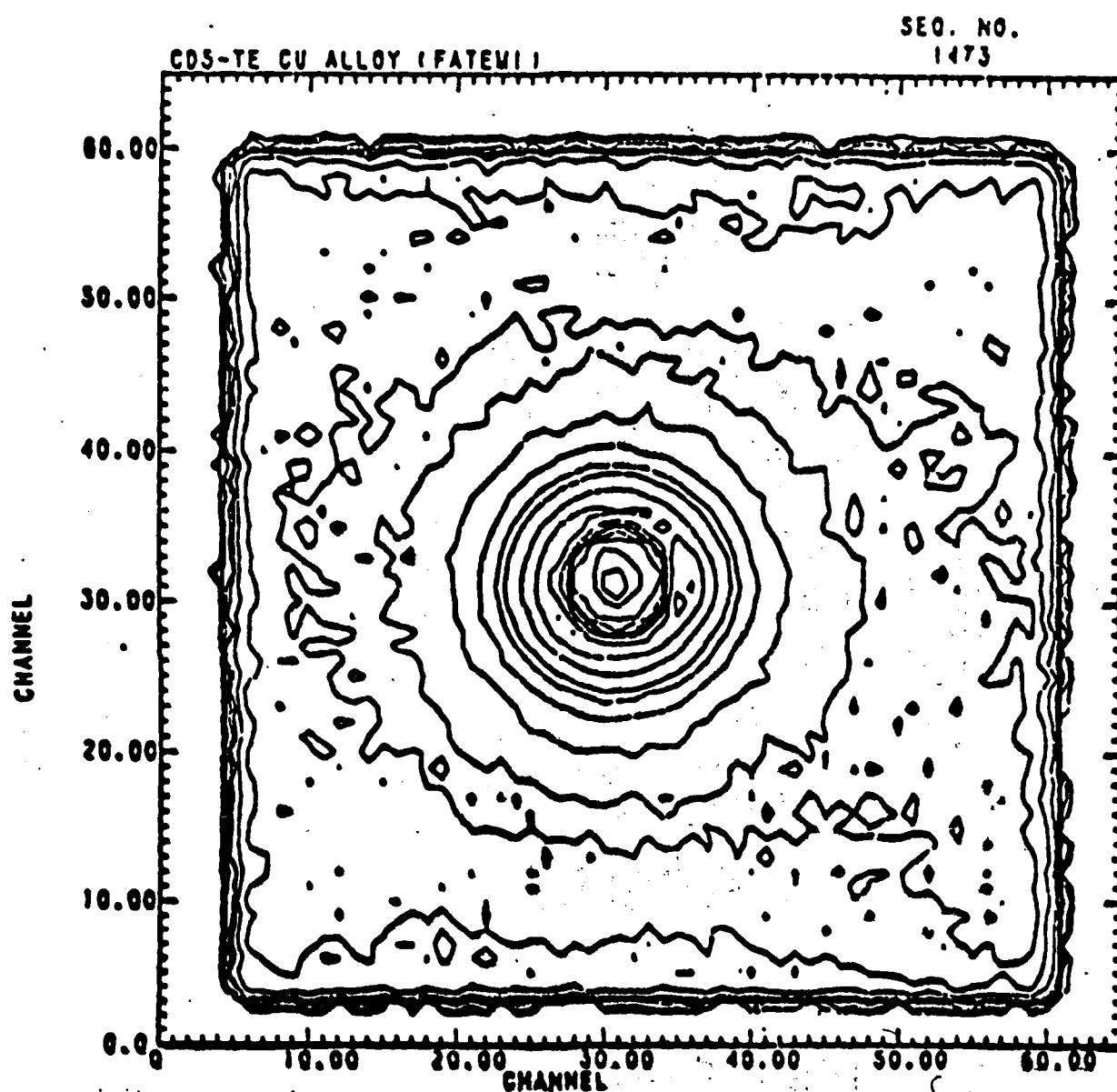


Figure 1. Two dimensional intensity contour of scattered neutrons from superlastically deformed Cu-alloy (at 14.36 m).

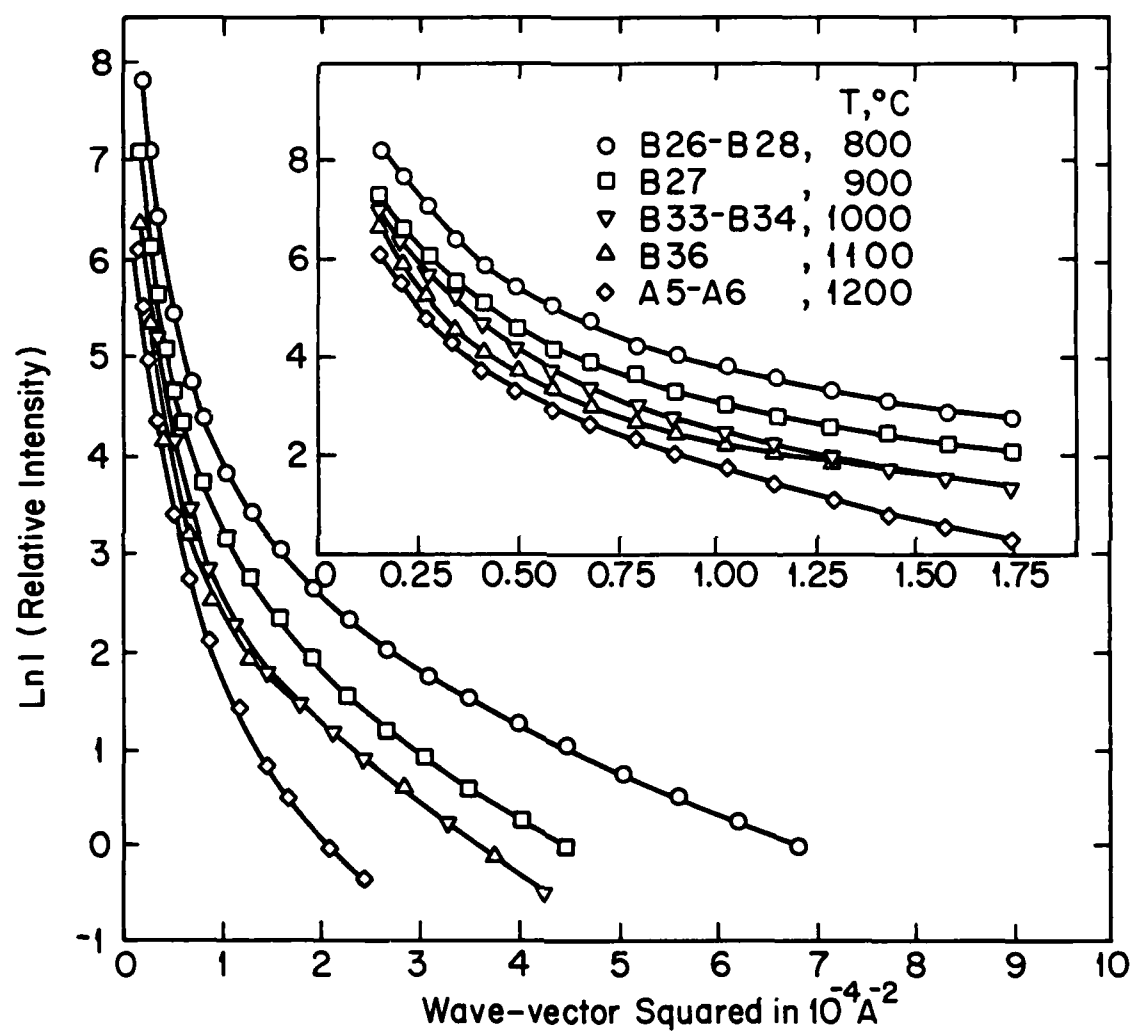


Figure 2. Guinier profiles of powder-compacted stainless steel Fe-21Cr-6Ni-9Mn-0.02C-0.25N(wt%).

NONDESTRUCTIVE MICROSTRUCTURE CHARACTERIZATION - COMMENTS

M. Cohen

At the present time, detailed studies are underway on the aging and tempering of Fe-Ni-C martensitic alloys with the aid of several techniques, including TEM, STEM, Mossbauer spectroscopy, atom-probe analysis, etc. The structural changes run the gamut of martensitic transformations, clusterings of carbon atoms, coherent and incoherent precipitation sequences, Ostwald ripening of dispersed carbide particles, relaxation phenomena, changes in dislocation density, and decomposition of retained austenite. The corresponding changes in mechanical properties are large and illuminating.

A great deal of progress has been made already in identifying and interpreting the above structural changes. Accordingly, it may prove quite useful to include acoustic measurements in this program as a systematic way of relating such observations back to a wide variety of well-documented microstructural features and associated mechanical behavior. Furthermore, even if the correlations cannot be generalized, or understood theoretically yet, they may have direct practical application to many aspects of steel technology.

The theory of heterogeneous martensitic nucleation predicts that there are some very potent pre-existing sites in the parent phase, which nucleate on cooling before the martensite-start temperature (M_s) is reached, but are so few in number that

such events are not detected by the usual methods for determining the M_s temperature. Acoustic emission would seem like an ideal technique for detecting these occasional events, in view of the displacive nature and fast growth rate of martensitic transformations when the nucleating conditions are achieved. In fact, audible clicks are sometimes heard when martensitic plates happen to form in a burst due to autocatalysis.

With very slow cooling of the parent phase, it should be possible to pick up acoustic signals from the propagation of single martensitic units. In principle, this could give important information about the dynamics of martensitic growth, as well as the elastic-wave characteristics generated by the process.

There is now some question as to whether the correlation between ultrasonic attenuation and grain size includes twin interfaces and faults which partition the grains and contribute to a refinement of the grain size from the standpoint of mechanical properties and phase transformations. The point will have to be settled before one can say what kind of grain size is being evaluated by the ultrasonic findings. Also, if the ultrasonic scattering by grain boundaries is really different from that of twin boundaries, this distinction may provide some insight into the physics of the scattering process.

Crystalline textures in polycrystalline specimens can be produced, with minimal distortion of grain shapes, by recrystallization and grain growth processes. This is commercial

practice with the Fe-3%Si steels used for transformer-core laminations. Various preferred orientations can be obtained in this way for ultrasonic testing, without having to contend with the elongated or pancaked grains that result from rolling operations.

ACKNOWLEDGEMENT

This paper was written under the auspices of the DARPA Materials Research Council, Contract #MDA903-82-C-0428 with The University of Michigan.

NONDESTRUCTIVE MICROSTRUCTURE CHARACTERIZATION - COMMENTS

J. P. Hirth

A topic not mentioned at the meeting was that of Stoneley waves. These are the internal equivalent, at grain boundaries and other interfaces, of the surface Rayleigh waves. The excitation of such waves would provide a true grain boundary mechanism for the attenuation of bulk sonic waves.

The excitation would be relatively large when the wave length is equal to or smaller than the grain diameter or size of the other interfacial features compared to the case when it was larger than the grain diameter. In particular, such excitation could account for the otherwise puzzling observations by Briggs of twin boundaries in stainless steel in the acoustic microscope. He was dealing with a short wave length situation where the effect would be relatively more important as just mentioned.

The formalism for treating Stoneley waves in the anisotropic elastic case has been developed by D. M. Barnett and J. Lothe, J. Phys. F: Metal Phys. 4, 1613(1974).

ACKNOWLEDGEMENT

This paper was written under the auspices of the DARPA Materials Research Council, Contract #MDA903-82-C-0428 with The University of Michigan.

COMPREHENSIVE REQUIREMENTS FOR NONDESTRUCTIVE MICROSTRUCTURE CHARACTERIZATION

J. C. Williams

There is increasing evidence that correlations between microstructure and specific mechanical properties can be made with reasonable certainty, provided a complete enough set of microstructural features/characteristics are known. Such correlations become particularly useful when the pertinent microstructural details can be deduced by nondestructive methods. Accordingly, it becomes important to decide which microstructural features must be measured nondestructively. To this end, it is appropriate to separate the materials of interest into two groups; those which have simple microstructures consisting of a single phase and possibly some pores or inclusions, and those which have complex microstructures consisting of two or more constituents, distributed either as discrete phases or as precipitates in a continuous matrix. The following examples outline some of the correlations between microstructure and properties which seem to be generally applicable.

Yield Strength - The yield strength of simple microstructures depends on grain size, solute content, texture (in this context, texture is used to represent preferred crystallographic orientation), substructure and/or dislocation density and impurity content and distribution. In complex microstructures, the volume fractions and sizes of constituents also affect the yield stress in addition to the features mentioned above.

Fracture Strength - In simple microstructures, the fracture strength depends on the inclusion size and spacing, the grain size, texture, and in the case of ductile fracture, on the work hardening rate, and possibly, the deformation mode. In complex microstructures, all of the above mentioned factors are important, but in addition, the size and morphology of the constituents and the strength of the interfaces which bound these are also important.

There are many other fracture-related properties which are of general interest, but for which the correlation with microstructure has not been qualitatively developed. These properties include fracture toughness, J_{IC} , tearing modulus, fatigue strength, fatigue crack propagation, and stress corrosion susceptibility. Although there are specific materials for which there are empirical correlations between microstructure, and say, fracture toughness, no generally applicable correlations currently exist. Such correlations are the subject of continuing study and the concurrent development of nondestructive methods for microstructure characterization should be pursued to ensure that the predictive capability for properties using nondestructing methods can be extended to these other properties in a timely fashion. Accordingly, a list of material/microstructures characteristics which could be useful, if they were determined by nondestructive methods, is shown in Table 1.

TABLE 1: USEFUL MICROSTRUCTURAL/MATERIAL FEATURES

SIMPLE MICROSTRUCTURES - Single Phase & Inclusions

- Grain size, grain size distribution
- Grain boundary strength
- Impurity content & distribution
- Grain aspect ratio
- Texture (crystallographic)
- Slip character
- Dislocation - Solute interactions
- Substructure
- Hardness

COMPLEX MICROSTRUCTURES - Multiphase Alloys or Precipitation

Hardening Alloys

- Constitution - types, volume fraction, morphology & size of constituents
- Nature of boundaries - second phase films, composition, character
- Slip character, deformation mode
- Texture of each constituent
- Distribution of constituents

Finally, the size or scale of the various microstructural features of interest has a direct bearing on the techniques which may be useful in nondestructively evaluating them. For most materials, the features of interest vary from 5 to 250 μ m. A list of typical sizes is shown in Table 2. This range is too broad to be measureable by a single technique, therefore, it may be useful to consider the simultaneous employment of complementary techniques so that this entire size range is covered.

TABLE 2

CHARACTERISTIC DIMENSIONS

• grains	1-250 μ m
• inclusions	< 1 μ m
• second phases	1-25 μ m
• precipitates	5-1000 Å
• boundary	5-20 Å
• substructure	1000-10,000 Å

ACKNOWLEDGEMENT

This paper was written under the auspices of the DARPA Materials Research Council, Contract #MDA903-82-C-0428 with The University of Michigan.

OPTICAL TECHNIQUES FOR ND MATERIALS CHARACTERIZATION

J. W. Wagner

While there is undoubtedly considerable research ongoing in noncoherent optical techniques suitable for the investigation of materials characteristics, this discussion will center on coherent optical techniques only. Applications of coherent optical techniques can be separated into two categories. The first category of techniques includes those which are used for the detection and transduction. A prime example of this class of techniques includes the numerous forms of interferometers used in acoustic, photothermal, and mechanical studies. The output of such systems is not a direct function of the interaction of the light with the material being tested. Instead, the signal is a result of heat or sound propagation through the material and detected optically.

In recent years, improvements in the performance of this category of optical systems have been made primarily in the areas of increased sensitivity and bandwidth. In light of the advantages gained by using these non-contacting, low distortion transducers, further efforts to improve bandwidth and sensitivity should be supported. At present, sensitivities as low as 10^{-4} Å have been obtained using very narrow bandwidth systems taking full advantage of coherent averaging in detecting CW acoustic signals¹. A broader band systems, such as the one described by Rosen for his work with amorphous materials, has a sensitivity of about 1Å with 7 MHz bandwidth.

The second category of coherent optical techniques are those which provide insight into materials properties based directly upon the interaction of light with the material. Techniques such as holography, coherent optical processing, speckle metrology, and optical surface interactions, fall into this category. The initial implementation of several of these techniques followed close on the heels of the discovery of the laser in the 1960's. Labeled at that time as solutions looking for problems, development of several of these was soon dropped. However, with recent advances in fiber and electro-optics, these techniques are being rediscovered and show considerable promise for ND materials characterization.

Holography is one such rediscovered technique. Suffering initially from reasonably poor resolution ($\approx 250\mu$) and limited by conventional photographic recording technique applications in materials characterization, were quite limited. New recording media and temporal modulation techniques^{2,3} promise to extend considerably the utility of holographic non destructive testing. In a project underway at FDA's Center for Medical Device Analysis, the wear surface of orthopedic implants is recorded such that holographic fringes form as a function of the surface contours. By frequency modulating the laser and phase detecting the moving fringes in the output plane, surface features as small as 1/1000 of a fringe (2.5\AA) may be detected. Application of this heterodyne holographic interferometry to generating full-field display of traveling surface acoustic

waves is to be investigated at Johns Hopkins in the near future.

Coherent optical processing techniques have been used both for image enhancement and pattern recognition. The latter application would seem to hold considerable promise in the materials characterization area. Optical correlation or matched filtering is one form of pattern recognition filtering. A film plate is exposed using a holographic technique such that it is "matched" to the pattern of light scattered by some reference surface. Light scattered through the filter by any other surface will produce a strong output beam only if the test surface is identical to the reference surface. This technique has been used to detect surface deformation (cracks, slip bands) due to fatigue of Fe-3Si in as few as 200 cycles⁴. Considerable follow-up should be done to assess just what changes are responsible for the observed correlation. Presumably, development of the optical system could provide a means to "recognize" surface grain size, texture, or other surface characteristics during processing.

While all of the techniques discussed above may be applied to either rough or polished surfaces, speckle techniques require a roughened surface with features on the order of 200 to 500 μm . Sensitivity to surface displacement is much better than that, however. Speckle techniques have been used to compute vacancy populations based on changes in crystal dimensions⁵. Surface roughness characterization, rapid Moire-type interfer-

ometry, and surface strain measurements are claimed to be possible from this technique⁵.

Finally, let me conclude (as I should have begun) with the disclaimer that this is far from a comprehensive review of coherent optical test techniques applicable to materials characterization. Instead, it is my intent to show by these few examples that optical techniques are showing considerable promise as non-contact methods, both for research and in process control for detecting and measuring materials surface microstructure. The ultimate speed of operation and the simplicity of implementation of these techniques, coupled with the preliminary results by the identified investigators, provides encouragement for continued support of development of optical techniques for materials characterization.

ACKNOWLEDGEMENT

This paper was written under the auspices of the DARPA Materials Research Council, Contract #MDA903-82-C-0428 with The University of Michigan.

REFERENCES

1. Palmer, Fick, et al, 1979
2. Massie, et al.
3. R. Dandliker Neuchatel, Switz.
4. R. L. Bond, et al, University of Arkansas and S.W. Research Institute.
5. R. K. Erf, "Speckle Metrology".

SECTION V
MRC WORKSHOP
ON
NONDESTRUCTIVE MICROSTRUCTURE CHARACTERIZATION

JULY 6-7, 1982

Scripps Elementary School
La Jolla, California

SESSION I July 6

Chairman: R. Mehrabian

"Review of DARPA Programs in Nondestructive Characterization"
R. E. Green, Jr., Defense Advanced Research Projects Agency,
Arlington, Virginia

"Acoustic Emission - Microstructure Relationships"
H. N. G. Wadley, Atomic Energy Research Establishment,
Harwell, England

"Acoustic Determination of Microstructures in Ceramics"
A. G. Evans, University of California, Berkeley, California

"Measurement of Material Properties by Acoustic Methods"
G. Kino, Stanford University, Stanford, California

"Application of Acoustic Microscopy to Materials Science"
A. Briggs, University of Oxford, Oxford, England

SESSION II

Chairman: A. G. Evans

"Ultrasonic Scattering As a Method of Grain Structure
Characterization"
E. P. Papadakis, Ford Motor Company, Detroit, Michigan

"Ultrasonic Characterization of Metallurgical Microstructures
and Transformations"
M. Rosen, Johns Hopkins University, Baltimore, Maryland

General Discussion

MRC WORKSHOP
ON
NONDESTRUCTIVE MICROSTRUCTURE CHARACTERIZATION
(continued)

SESSION III - July 7

Chairman: R. E. Green, Jr.

"X-Ray Measurements of Residual Stress"

M. R. James, Rockwell International Science Center,
Thousand Oaks, California

"The Use of Electromagnetic Acoustic Transducers in Weld
Inspection and Residual Stress Measurements.

C. M. Fortunko, NBS, Boulder, Co.

"Application of Synchrotron Radiation to Materials Science"

M. Kuriyama and W. J. Boettinger, National Bureau of
Standards, Washington, D.C.

"Photothermal Imaging Applied to Materials Characterization"

J. C. Murphy, Johns Hopkins University, Baltimore, Maryland

SESSION IV

Leaders: R. E. Green, Jr., A. G. Evans and R. Mehrabian

Discussion

The intent of this session will be to summarize the present status of the fields discussed, and to identify future scientific and technological goals. It is anticipated that emphasis will be placed on the use of nondestructive characterization techniques for control of microstructures during processing.

MRC WORKSHOP
ON
NONDESTRUCTIVE MICROSTRUCTURE CHARACTERIZATION

July 6-7, 1982

ATTENDEES

<u>Name</u>	<u>Company or Institution</u>
H. Wadley	Univ. Maryland
Gordon Kino	Stanford U./MRC
Andrew Briggs	Oxford Univ.
Tom Yolken	National Bureau of Standards
Franklin F.Y. Wang	State Univ. of New York - Stony Brook
Loren A. Jacobson	DARPA/MSD
Jim Williams	Carnegie-Mellon Univ./MRC
Tony Evans	U.C. Berkeley/MRC
George Vineyard	Brookhaven National Lab/MRC
John Hirth	Ohio State Univ.
Vincent V. Horvath	Bethlehem Steel - Research
Moshe Rosen	Johns Hopkins Univ. & Nat. Bur. of Stds.
Bill Boettinger	Metallurgy Div., Nat. Bur. of Stds.
Masao Kuriyama	Metallurgy Div., Nat. Bur. of Stds.
Norbert Elsner	General Atomic, LaJolla
Mike James	Rockwell Science Ctr, Ca.
John Murphy	Johns Hopkins Applied Physics Lab
Mike Lauriente	U.S. Dept of Transportation
Jim Wagner	USDHHS/Food & Drug Admin.
Bhakta B. Rath	Naval Research Lab, Wash. D.C.

ATTENDEES
(continued)

Morris Cohen	M.I.T. Cambridge, MA
B. Budiansky	Harvard Univ./MRC
Ed Hucke	Univ. of Mich./MRC
Edward Mueller	FDA Center for Med Dev Analysis
Robert E. Green	DARPA/MSD
Robert Mehrabian	NBS
Chris Fortunko	NBS
Emmanuel P. Papadakis	Ford

INTRODUCTION

A conference on ideal microstructures was held on 8-9 July 1982. The focus of the meeting was alloy design to optimize mechanical properties, particularly strength and toughness, from a microstructural viewpoint. The possibility of alloy preparation by rapid solidification processing was a factor in the presentations as well.

The first part of the following report is a set of Key Issues, suggesting experiments, that emerged from the conference discussions. Next appear summaries of the four sessions and then summaries of the individual contributions.

A set of contributions at the MRC meeting were stimulated by the conference. These appear as a set of five papers immediately following the other parts of the report because of the close connection to the conference itself. The papers all deal with mechanical properties from a dual mechanics - microstructure viewpoint.

KEY ISSUES

1. Effect of dispersion size on properties.
 - a. Yield strength: Orowan theory and experiment verify that yield strength should increase as particle spacing decreases (hence as particle size decreases for a fixed volume fraction) provided the particles are impenetrable by dislocations (Ardell).^{*} The trend is reversed only below a particle size where dislocations can readily cross-slip or climb around particles. Rough estimates indicate that this critical size is ~10nm, but experiment and theory are needed to verify this.
 - b. Ductile fracture: Since ductile fracture (initiation or stable crack growth) occurs by particle decohesion (or, less-often, particle cracking) and finer void spacings enhance mode I (normal) or mixed mode I-II (shear) failure (Hutchinson), it was suggested that increased interface cohesion of particles would help and that a critical size existed, below which decohesion would not occur. Subsequent work at the conference (Evans and Hutchinson) has demonstrated that increased cohesion helps provided that the cohesion exceeds a critical value which depends on volume fraction, but otherwise that changes in cohesion have no effect.

^{*}Names in parentheses refer to the written comments, of participants, included in this report.

Also, the estimate of the critical size for decohesion of ~ 14 nm by Argon is a lower bound if the local plastic strain is uniform but is an overestimate if plastic strain can be concentrated in dislocation pileups. Experiments to follow up on these ideas, some new, are called for.

- c. Brittle fracture: For years, the ductile-brittle transition has been little understood in terms of mechanism. Ritchie, Rice and Knott focussed attention on the possibility of a critical stress being achieved for steel at a grain diameter or so ahead of a crack where a cracked carbide particle could act as a nucleus for cleavage. Yet (Evans et al), K_{IC} -T plots show an abrupt change at the DBTT and not a smooth one as predicted by the model, and estimates of the critical distance vary from 1 or 2 to 10 grain diameters. Possibilities include (Evans, et al), R-curve type crack resistance with microcracks extending over grains but not propagating further; the critical event then being linking of a set of these and dynamic pop in of a crack from a particle to the matrix; or extension of pre-existing cracks at particles into single grains, with the cracks eventually linking up to form an unstable cleavage crack. Unresolved issues are the requirements to propagate a cleavage crack across a boundary where the crack orientation changes (requiring added crack surface area or linking shear zones); the local events needed for particle cracking and whether these, at the dislocation level, determine the ductile

brittle transition temperature; whether microcracks exist in a zone near the crack initiation point as suggested by an R-curve-type model; and whether crack initiation indeed occurs ahead of the precracked region. Also, a statistical distribution of particle sizes and strengths could mean that the critical event occurs from one to ten grain diameters ahead of a crack, (Evans) tying the mechanics of the Ritchie et al model to a perhaps more realistic microstructural mechanism. Some of these new ideas are evidently amenable to experimental test.

2. Effects of grain size.

A decrease in grain size always increases yield strength or flow stress, an effect which is large provided that the size exceeds a critical value of $\sim 1\mu\text{m}$ where substructure becomes a more important strengthening mechanism (Thompson). Empirical correlations for steels also indicate that decreasing grain size is the only strengthening mechanism that also increases toughness. However, this trend is also limited by the decreased work hardening rate and increased tendency for strain localization associated with it. Thus, an optimum grain size exists for a given material.

3. Dispersion hardening.

Dispersion hardening is attractive compared to other hardening mechanisms because: dispersoids pin grain boundaries and aid in achieving fine grain or substructure sizes (item 2); they provide large increases in yield or flow

stress (proportional to the inverse particle spacing) while they are impenetrable and non-bypassable; and they give large values of work-hardening rate which provides resistance to plastic instability. The problems with dispersions are those mentioned in item 1, concerning their role as crack or void sources.

4. Diffuse hardening mechanisms.

Argon classified as "diffuse" hardening mechanisms those which increase yield stress; do not affect slip character or $d\sigma/dT$; have little or no positive effect or a negative effect on work-hardening, and as a consequence decrease the resistance to plastic instability. These include grain-size hardening (item 2), solid solution hardening, and the various forms of precipitation hardening (Ardell). Because of the decreased resistance to plastic instability, these mechanisms are not as attractive as primary strengthening mechanisms as they are as secondary mechanisms in conjunction with dispersion hardening. This holds true in particular for RSP.

5. Work hardening.

Despite the theoretical and experimental activity since the 1950's, we still have little knowledge of the detailed mechanism of work hardening, particularly in polycrystals or multiphase systems and at high strains.

6. J and tearing modulus as a function of yield stress.

Continuum mechanics models predict that if the critical crack opening displacement for crack nucleation and propagation is constant, that the value of J_{IC} should increase with yield strength while the value of the tearing modulus dJ/da should decrease with increasing yield strength (Budiansky). There are data to support the latter effect, but some measurements indicate an inverse relation of J_{IC} and yield strength. Evidently, the experiments also conflict with the mechanics prediction (which has some support in a compilation by Paris) that materials with large J have small dJ/da and vice-versa. This suggests a possible role of microstructure leading to a dependence of the critical crack opening displacement δ_{IC} on yield strength.

7. Additivity of strengthening mechanisms.

In the absence of detailed studies or predictions, most treatments consider that multiple mechanisms contribute linearly to strength. For the special case of point obstacles and simple dislocation line tension, Argon noted that the rule instead should be the square root of the sum of the squares of the individual contributions. Work is clearly needed to provide better guidelines in this important subject area.

8. Dislocation mechanisms.

A major problem in complex structures in relating microstructural mechanism to macroscopic properties such as flow

stress is the statistical averaging problem. To first order, single dislocation models for Orowan hardening, precipitation hardening, etc., are known. However, averaging must be done over $\sim 10^{14}$ segments, each experiencing differing resolved external stresses and, more importantly, different resolved internal stresses arising from interactions with other segments. In the absence of guidelines, simple averaging is assumed, for example in the relation of strain rate to dislocation density and dislocation velocity. Some work on a limited number of segments, but nevertheless distributed realistically in three dimensions, is needed to indicate the accuracy of the simple averaging process. To second order, more refined single dislocation calculations, using anisotropic elasticity, nonlinear inhomogeneity effects for second-phase particles, and dropping the simple line tension model, are needed to better define the force-distance curves necessary in the dislocation rate theories.

9. Limiting volume fraction of dispersoid.

Of importance in RSR alloy design is the issue of the limiting volume fraction of dispersion. Where strength alone is the dominant design criterion or where interface cohesion prevents void formation, properties improve with decreased spacing (or increased volume fraction at constant size). For particles poorly wet by the matrix in the capillarity sense, a limit should be the percolation limit of 18-25 percent, and some work on steels tends to confirm this

limit. On the other hand when the particles are wet by the matrix, as for tungsten carbide in cobalt, the material has useful properties. Wetability increases with decreased surface energy of the particle-matrix interface, or, equivalently with increased interface cohesion. Work is needed to establish alloy design guidelines.

10. Plastic instability.

Some work on the initiation of plastic instability, particularly at surfaces (Hirth) is in quite good agreement with continuum mechanics predictions of critical strains. Yet hydrogen charging has been shown to drastically lower these strains (by about a factor of two). Work is needed to determine whether strong local defects such as sharp micro-notches could produce such changes in the continuum predictions, and to determine whether the role of hydrogen is to produce such defects.

11. Cyclic crack growth.

In cyclic loading, wavy slip alloys appear superior in low cycle fatigue, where crack initiation is important, but poorer in $da/dN - \Delta K$ crack growth compared to planar slip alloys. This is clearly a microstructural effect and deserves further study.

12. Transformation induced plasticity.

In a number of alloys, resistance to plastic instability is provided by martensite transformation as a function of strain. The J resistance curve does not appear to be opti-

mized at the same conditions of strain rate, temperature and composition as the necking resistance in tension (Cohen). An important issue is whether martensite forms continuously during the deformation process and influences necking resistance throughout the uniform strain increment or whether it preferentially forms locally at incipient necks. In other words is the TRIP effect a local or global one? If local, the models for transformation toughening of ceramics by Evans and Hutchinson could apply as well for TRIP materials in the plastic zone at crack tips.

13. Multiaxial stress and strain effects.

As mentioned in more detail (Embury) work on multiaxial stress effects is only beginning. Certainly from both a continuum (Hutchinson) and microstructural (Embury) viewpoint, void formation and the propensity for plastic instability are influenced by hydrostatic tension. Also the strength-differential effect reflects multiaxial stress influences. Similarly, strain path has been shown to be an important factor influencing strain to failure in sheet steel and aluminum. There is little guideline on how microstructural variables relate to these effects.

14. Design needs.

As emphasized (Jacobson), alloy design should not be focussed on a single property. The potential spectrum of property needs for given designs should be considered. In many cases secondary properties such as buckling resistance

or density may be limiting. A systems approach to materials and design seems to be the optimum method for improving overall structural efficiency.

15. Other effects.

While receiving some attention at the meeting, other properties are quite important and could receive equal attention with the yield-toughness properties emphasized in the above enumeration. Environmental interactions (Thompson, Hirth) can lead to severe degradation and could be limiting in RSP structures. Fatigue properties, particularly initiation, relate perhaps more closely to events at the crystal plasticity-microstructure level than the yield-toughness properties. Optimization of yield-toughness behavior almost certainly would not give optimum corrosion or fatigue resistance.

16. Production of precipitation hardening materials by RSP.

It is fairly clear that materials which are precipitation hardened in the absence of dispersoids or very small grains have a tendency for strain localization. They thus do not typically have particularly attractive ductility. Accordingly, if RSP is used to make materials which are precipitation hardening then it appears to be advantageous to take advantage of this technology to introduce either grain refinement or dispersoids in addition to the intrinsic precipitates which form during aging.

SUMMARY OF SESSION I

In introducing the microstructure-property topic, Jacobson noted that there were up to ten important properties that influenced material selection in DOD systems. Often a so-called secondary property such as buckling resistance can be limiting instead of, say, yield strength. For many applications to DOD, density is a primary property and should be emphasized in alloy design. He then gave several examples of variations in properties, not understood but presumably dependant on microstructural differences. These included the presence or absence of stage II in $da/dN-\Delta K$ curves; the role of crack initiation in a damage tolerance criterion for fatigue life; the role of periodic overload in fatigue crack propagation; and the role of processing variables in losing control of idealized microstructures produced, for example, by RST-HIP.

Williams then pinpointed key issues in alloy design and gave several examples. In a RST powder Al-10Mn alloy, much larger strains to initiate voids were achieved compared to oxide dispersion systems. This was achieved by reducing the Al_6Mn precipitate size to 100-250nm, together with substructure refinement on processing abetted by the fine precipitates. Second, he noted that, at the same yield strength, there was a trade-off in elongation versus toughness in α - β Ti alloys depending on the morphologies of the primary α phase. Widmanstatten α plates produced high toughness with low elongation with the opposite trend being produced by spherical α

particles. Finally he discussed the opposite effects on crack initiation versus propagation of slip character in Ti alloys. In low-cycle fatigue, initiation dominated, planar slip alloys are poorer (unlike pure fcc metals), however they are better than wavy slip alloys in sustained crack growth, $da/dN \sim \Delta K$, tests.

Thompson discussed environmental effects. He showed that times to failure could vary by factors of 10^3 among steels of the same yield strength. Also he showed a dramatic variation of "embrittlement index", $\Delta R.A./\%RA$, with yield strength, indicating the fallacy of the old idea that low strength steels were immune to hydrogen embrittlement. As an example of a "red herring" he mentioned the old concern about degradation of properties associated with precipitate free zones at grain boundaries in Al alloys, a factor which was found to be unimportant in influencing toughness after extensive tests. He indicated that a key for improvement in environmental embrittlement resistance is in decreasing grain and substructure size, giving us an example a Ni-base alloy with γ' precipitate with sub-boundary size fixed by yttrium oxide particles.

Precipitation and dispersion hardening were considered by Ardell. He noted that there were five strengthening factors: coherency, ordering, modulus, stacking-fault, and Orowan hardening. The first four of these involve particle cutting, incomplete dislocation bowout and a strengthening increment proportional to the obstacle strength to the $3/2$ power and

particle radius and volume fraction to the one-half power. The latter has a similar strength dependence but varies inversely with particle spacing and hence inversely with particle size. He mentioned that theory and experiment were in good agreement for the ordering and stacking fault cases, where the dislocations were in the interior of the particles, and for the Orowan case, but not in the other cases (the degree of this agreement was considered in the discussion as mentioned later).

Finally, Embury addressed some specific aspects of microstructural variation and strain localization. One factor was whether average or extreme value or positional microstructure variables are important. For example clusters of Al_2O_3 in low S steels degrade toughness, and the surface volume fraction of inclusions may differ from the bulk and may dominate crack initiation. He then discussed several effects of strain localization: internal buckling of oriented plate precipitates giving shear localization; indirect effects of localization during processing such as preferential recrystallization along prior localization bands. He concluded by discussing multiaxial stress effects with superposed hydrostatic pressure influencing void initiation as a function of strain in polycrystals and changing the mode of localization (necking instead of shearing off) of alloy single crystals.

SUMMARY OF SESSION II

Session II of the symposium included short talks by Morris Cohen, Bhakta Rath and Tony Evans. Cohen presented a number of examples of what rapid solidification processing can contribute to the achievement of new microstructures and microstructural controls. A specific case of a controlled dispersion of manganese sulfide particles in steels was discussed. He also presented an example of an unusual microstructure relationship to properties exhibited by iron-nickel alloys that undergo martensitic transformation during deformation.

Rath discussed factors involved in the development of microstructural features through nucleation and growth processes. Other topics that he treated included crack growth rate transitions, amorphous to crystalline transitions in magnetic alloys, alloys with high damping capability, and ways in which microstructure gradients could lead to improved properties and property combinations.

Evans discussed the toughening of ceramics by particles which undergo a phase transformation due to the stress field of a crack. The change in toughness was related to the nature of the particle size and size distribution, a more narrow distribution having a more pronounced effect. Particle morphology also has an effect, those with a higher aspect ratio leading to a greater toughness improvement.

SUMMARY OF SESSION III

The presentations in this session tended to deal more with the mechanics aspects of materials performance than with microstructure development or microstructure -property relations per se.

In the first presentation Hirth described the effects of hydrogen on the flow and plastic instability of spheroidized plain carbon steel. He showed that the stages of ductile fracture in these materials were the following:

- 1) surface roughening
- 2) void initiation
- 3) void profusion
- 4) crack initiation

His results showed that both hydrogen charged and uncharged specimens exhibited the same behavior, but that the strain to initiate each stage of fracture was smaller in the hydrogen charged specimens. A check of the strain for onset of surface roughening was made in the context of theoretical models and good agreement was found. The mechanism by which hydrogen increases the tendency for plastic instability is not yet clear but the effect is nevertheless a very pronounced one. Moreover, since the macroscopic stress-strain curve is unaffected by the introduction of hydrogen some uncertainties arise when establishing criteria for judging material performance.

Stevenson described the strain hardening and strain rate sensitivity of materials in a cup-type forming test. He used

several simple constitutive expressions to fit his data and found that the Voce relation best described his data for 5132-0 Al both at room temperature and at 77K. However for 2036-T4 Voce's relation still held at room temperature but at 77K the behavior changed to where it was better accounted for by the Swift relation. TEM examination and arguments based on analogy to work by Humphries and Hirsch were presented to account for this change in behavior in the 2036-T4 material. The accumulation of large numbers of prismatic loops around the individual particles during low temperature (77K) deformation was suggested. The TEM evidence for this in the case of the Al alloys was complicated by the high dislocation density in the vicinity of the particles. However, the data did show that the strain hardening behavior of the 2036 Alloy could be altered by heat treatment. This permits some control over the formability by deferring fracture until larger total strain.

Argon next addressed the issue of ductile fracture and strength at temperatures where diffusion effects are negligible ($T < 0.4T_m$). He discussed void formation at particles and made the point that there was a minimum particle size below which voids do not form. This size was shown to be $\sim 140\text{\AA}$. He also suggested that the strain required to produce coalescence of the voids is only dependent on the void volume fraction within the context of a material with a fixed strain hardening rate. Moreover, it is advisable to use particles which give rapid particle hardening so that the particle sizes which correspond to peak

strength (or at least high strength) are less than the minimum size for void formation. On the other hand particles which are too small can be by-passed by thermally activated processes; this results in a strong temperature dependence of the yield stress. Finally Argon discussed the role of strain hardening on the fracture resistance and made the point that low strain hardening materials were very prone to plastic instability. Only in materials hardened by diffuse mechanisms is the strain hardening rate independent of strength. Here diffuse strengthening mechanisms are defined as those which increase the level of the stress-strain curve without altering the slip character or reduced the work hardening rate. This is another attractive reason to seek diffuse strengthening particles or mechanisms.

Hutchinson discussed ductile failure by a void growth and coalescence mechanism. He divides ductile failure into a prelocalization stage in which an array of small voids is formed and a localization stage in which these voids coalesce to produce failure. The localization stage can occur in two ways: by an in-plane localization in which the fracture plane tends to be normal to the tensile axis and by void sheet formation in which the fracture plane is inclined to the tensile axis. The former is typical of low strength, high strain hardening materials whereas the latter is more consistent with high strength, low strain hardening materials. Hutchinson related the onset of instability to surface rumpling and shear band formation but high work hardening rates tend to reduce the occurrence of these in-

stabilities. He also predicted strong strain state dependence of instability with plane strain augmenting the onset of the instabilities.

Budiansky discussed the trade-offs between strength and toughness. He separated the onset of crack growth into the case of a static crack and that of a growing crack. He assumed that for static cracks there is a critical crack opening displacement, δ_{IC} , which corresponds to the onset of crack extension and that the product of yield stress and δ_{IC} is equal to J_{IC} . This analysis suggests that as σ_y increases, J_{IC} increases. This clearly does not agree with the bulk of J_{IC} data. For growing cracks he assumed a constant crack tip geometry and has performed an analysis which suggests that the J value at steady state crack growth (J_{SS}), gets larger as yield stress gets smaller. This tends to agree better with existing data on tearing modulus (T). In this connection he also mentioned a collation of data by Paris which showed that as J_{IC} increases T tends to decrease. There was some discussion which left the general validity of this correlation in question.

SYMPOSIUM ON IDEAL MICROSTRUCTURES

DISCUSSION SESSION, 9 JULY 82

L. A. Jacobson

It is difficult, if not impossible, to give an accurate and complete report on a discussion session covering a topic that is so broad as "ideal microstructures". Even if one were to be more specific in defining "ideal microstructures" as being those which lead to optimum combinations of material properties, the discussion could not be fairly treated from this perspective, because few points were raised bearing on the narrowed issue. Further, it must be admitted that a certain measure of bias invariably creeps into even the most well intentioned attempt to give an objective accounting of the proceedings. Let me be very frank about my bias, it is based on my firm belief that there are materials behavior phenomena, or combinations thereof, that continue to fuddle the solid mechanics community, a resolution of which might be found by incorporating the understanding of microstructure-property relationships claimed by the metallurgy or materials science community. I must admit that my belief was very soundly shaken; first, by the continuum assertion that many macroscopic phenomena could be adequately accounted for, given the detailed stress-strain curve of a material, without invoking any microstructural explanations; second, by the many exceptions to general microstructure-property relationships that were cited by metallurgists. There was general

agreement from both camps that work-hardening, a most important feature of a stress-strain curve, is not well understood. The significant reduction due to hydrogen of the critical strain for surface roughening, a phenomenon which can be accurately treated in the absence of hydrogen by a continuum analysis, could not be explained by either a continuum or a microstructure model.

If some conclusion could be drawn relating to the larger problem of structural design, and its concern with the complete materials property spectrum, it was not evident from the discussion, for cyclic phenomena and rate effects were largely ignored. There was posed, however, an interesting challenge to the metallurgical community, in this regard: given that one could construct a table of important properties, and that the best values of such properties were entered (undoubtedly represented by different materials), could one material be identified for which all the properties were within at least 10% of the best values. While there was no attempt to deal with this challenge on the spot, it would appear to be a most useful exercise to undertake, perhaps in some modified form, in which, properties could be normalized, where appropriate, by some microstructure insensitive parameter (elastic modulus?).

Most of the discussion time was spent on the microstructural factors which influence yield strength. It was emphasized that there are still unresolved issues relating to the bowing of dislocations between obstacles, and the statistics of dislocation penetration of an array of obstacles. This circumstance

appears to continue because statistical models are difficult to check by experiment.

Some general rules for maximizing yield strength were proposed: 1) That grain size or subgrain cell size be as small as possible, subject to the caveat that if the size is too small, instability can result from the large number of dislocation sinks; 2) That dispersed particles be as small as possible, so long as they are not penetrable, also with a caveat, that particles not be so small that they can be bypassed by cross-slip. There are obvious interactions between rules 1 and 2, insofar as smaller grain size or cell size will be stabilized by dispersed particles. Factors not connected with the general rules were discussed; it is clear that a strong interface between particle and matrix is beneficial; it is not so clear how the aspect ratio of particles can influence yield strength, but may influence fracture initiation based on the somewhat controversial hypothesis that there is a critical particle dimension below which the particle cannot be cracked due to the accumulated dislocation loop strain. Discussion of the combining of strengthening mechanisms, such as dispersion strengthening with solution strengthening, or order strengthening, did not lead to agreement on a method for treating such combinations.

On the subjects of fracture and fatigue, it was evident that more understanding is needed on the effects of dispersed particle size on fatigue crack or fracture initiation. It was

also suggested that fatigue crack propagation could be insensitive to microstructural variations.

A most important outcome of the discussion session was the identification of several key experiments that could improve our understanding of microstructure-property relations. Greater control over the dispersion of SiO_2 particles in copper might be achieved through internal oxidation of fine alloy powder particles, and an additional variable could be introduced by adding a third element to change stacking fault energy. Other model systems for testing dispersion strengthening models were suggested: Al-Fe, Al-Ti-B, Fe-Ni with manganese sulfide particles and dispersions in austenitic stainless steels. Processing of all systems would be by rapid solidification, but problems arise in performing mechanical property tests on fine powders. Hardness tests could be useful, but would also be difficult to perform. Melt-spun ribbon may provide an alternative rapidly solidified product on which mechanical property tests could be performed. It was noted that tests should be made on as-solidified material because consolidation variables could lead to loss of control over the microstructural variable of interest and/or the introduction of unwanted additional microstructural features. Other experiments that should be performed include a test of the combination of dispersion strengthening and order strengthening, using perhaps a γ' forming nickel base alloy in which compounds such as Ni_xMo form as dispersed particles. Again, rapid solidification would be necessary in order to control microstructure.

In summary, it seems clear that at the present time, we cannot adequately specify an ideal microstructure which will lead to an optimum combination of mechanical properties. Guidelines are needed for microstructural design, and the most useful experimental efforts should be those which address single mechanisms of strengthening or fracture initiation, and the key issue of how to properly treat combinations of microstructural mechanisms. While rapid solidification processing does give a new dimension to control of microstructure, exercise of such control in the development of improved engineering alloys must await better definitions of microstructure design guidelines.

INTRODUCTORY REMARKS

L. A. Jacobson

Higher performance structural materials for future systems are being developed with the overall objective of reducing the weight of the structure. Such weight savings, in the aircraft context, translate into increased range or payload; hence the justification for DoD and DARPA involvement. It is evident from the analysis of potential structural weight savings that both first and second tier material properties must be considered, particularly for those components which are governed by durability and damage tolerance as primary failure criteria. In many components it is necessary to consider a secondary failure mode possibility, in addition to the primary mode, in determining more realistic weight savings achievable with an alternative material. This emphasizes the need to consider combinations of properties in developing new materials.

Evidence of the important role that microstructure plays in governing individual properties and combinations of properties is rapidly accumulating. One might, therefore, hope to define an ideal microstructure as one which either maximizes one property without compromising others, or which leads to simultaneous increases in several properties. Rapid solidification technology promises a new dimension in our ability to control microstructures. It is clear, however, that attention must be paid to all steps in the processing of rapidly solidified

STUDIES OF SOME MICROSTRUCTURE - PROPERTY RELATIONSHIPS

J. C. Williams

Rather than treat ideal microstructures per se, this presentation used three examples of microstructure-property studies which illustrate areas that possibly are worthy of further study or consideration.

The first example was a Al-10Mn alloy made from RSP powder by hot pressing and extruding. The TEM microstructure showed that relatively small sub-grains ($0.25-0.5\mu\text{m}$) and small ($500-1000\text{\AA}$) Al_6Mn particles were present. Increasing hot pressing temperatures tended to coarsen the scale of both of these microstructural features. The strength naturally scales with microstructure but the fracture strains in all cases were large ($\sim 35\%$) compared to many alloys which contain small particles, e.g., ODS Ni or Ni-Cr alloys. Thus the role of small particles in the nucleation of voids was questioned. Further it was shown that TEM observations made in the neck of fractured tensile specimens gave no indication of the formation of voids at the Al_6Mn particles. This left the question of whether the particles were too small to form voids or whether they were especially well-bonded to the matrix.

The second example was that of wrought Ti alloys in which the effect of α morphology, as affected by processing history, was described. It was shown that the fracture toughness of β -forged Ti-6Al-2Sn-4Zr-6Mo was $\sim 55 \text{ ksi}\sqrt{\text{in}}$ whereas in the $\alpha+\beta$

materials, from initial solidified product to final component configuration, lest control of the microstructure be lost during consolidation or forming operations.

We hope that this seminar will provide an opportunity for us to share with one another various perspectives on microstructure/property relationships. A combined metallurgy-mechanics examination of ideal microstructure should help to better define what features ought to be important for control of one or more properties, and should lead to suggestions for key experiments.

forged condition the toughness was $\sim 23 \text{ ksi } \sqrt{\text{in.}}$. These differences in toughness, at constant strength level, were shown to result from large variations in fracture path as a function of microstructure. It was also shown that the local fracture mode was ductile in both cases. It was suggested that increased fracture path roughness at constant unit crack propagation energy leads to greater total energy dissipation during crack extension and hence gives rise to larger toughness values.

The third example related to cyclic properties. It was shown that in Ti-Al alloys, the Al content controls the slip character. During low cycle fatigue tests conducted under full reversed loading ($R = -1$) alloys which exhibit planar, localized slip tend to initiate cracks along slip bands and at fewer cycles than in wavy slip alloys. Thus strain localization has been suggested to be deleterious to crack initiation. On the other hand, the planar, localized slip alloys exhibit higher ΔK_{th} and lower crack growth rates than the wavy slip alloys. These differences were attributed to slip reversibility differences and thus less damage accumulation in the crack tip plastic zone in planar slip alloys where the slip is more reversible. These observations emphasize the differences between crack initiation and crack growth performance of alloys such as these. Moreover, it raises an important question regarding the optimization of alloy performance relative to either crack initiation or crack growth, but casts doubt on the prospect for overall optimization.

ACKNOWLEDGEMENT

This paper was written under the auspices of the DARPA Materials Research Council, Contract #MDA903-82-C-0428 with The University of Michigan.

IDEAL MICROSTRUCTURES FOR RESISTANCE TO HYDROGEN-ASSISTED AND STRESS CORROSION FRACTURE

A. W. Thompson

Considerable information has emerged about desirable microstructures of steels, both of high and low strengths, and austenitic stainless steels. Less complete but suggestive information is also available for titanium, aluminum and nickel alloys. The attached table* is a summary of this information in a reasonable current state; the referenced reviews at the foot of the table are the source for much though not all of the content of the table.

For the most part, there exist no materials which incorporate even the bulk of these recommendations in a particular alloy system. Thus one has only a kind of "piece-wise" confidence in this approach. Certainly one major need is to test extensively (and revise or replace as necessary) these recommendations. The primitive state of theoretical understanding of environmental behavior is also a problem, since it means that in the foreseeable future such recommendations are necessarily highly empirical. However, it appears likely that the broad outlines of ideal microstructures for environmental fracture resistance are now visible.

ACKNOWLEDGEMENT

This paper was written under the auspices of the DARPA Materials Research Council, Contract #MDA903-82-C-0428 with The University of Michigan.

RECOMMENDATIONS FOR IDEAL MICROSTRUCTURES OF ALLOYS
RESISTANT TO HYDROGEN-ASSISTED CRACKING/FRACTURE

Design Variables	Ferritic and Martensitic Steels	Austenitic Stainless Steels	Titanium Alloys	Nickel Alloys*	Aluminum Alloys*
Chemistry	Control or avoid S, P, C, Mn and Cr	Control or avoid N, P, As, Sb, Bi, C and Cr	Control or avoid Al, Sn, and O	Control or avoid S, Sn, Sb, Cr, Fe	Control or avoid Fe, Si, Mn, Zn
Grain Size and Substructure	Refine	Refine	Refine	Refine	Refine
Second-Phase Particles	Duplex distribution for strengthening and trapping	Duplex distribution for trapping and nonplanar slip	Avoid fine α dispersion, esp. at grain boundaries	Duplex distribution for strength and trapping	Duplex distribution for trapping and non-planar slip
Microstructure	High strength: ausformed, tempered bainite or martensite. Low strengths: fine, spheroidal carbides in ferrite	Fine dispersion of δ ferrite; avoid continuous carbides	Acicular $\alpha+\beta$, some all β	Avoid continuous δ or η networks, esp. at grain bds.	Avoid planar slip of long distances
Thermal Treatment	Ensure compatibility of crack path and microstructure	Thermomechanical working	Establish proper distribution of α and β	Thermomechanical working	Thermomechanical working
Texture	Sharp texture for intergranular cracking; random texture for transgranular cracking	-----	Randomize texture of α phase	-----	-----

*Recommendations tentative because information is less complete.

References: A. W. Thompson and I. M. Bernstein, Advances in Corrosion Science and Technology, Vol. 7, pp. 53-175 Plenum, New York, 1980; I. M. Bernstein and A. W. Thompson, Alloy and Microstructural Design, pp. 303-47, Academic, New York, 1976; A. W. Thompson, Environment-sensitive Fracture of Engineering Materials, pp. 379-410, TMS-AIME, Warrendale, 1979.

IDEAL MICROSTRUCTURES IN PRECIPITATION HARDENING

A. J. Ardell

The purpose of this presentation was to demonstrate the extent to which experimental results on precipitation hardening agree with various theories of this process. The precipitation hardening mechanisms discussed were coherency hardening, order strengthening, modulus hardening, stacking-fault strengthening and Orowan hardening (which is really the mechanism of dispersion strengthening). The simplest versions of the four precipitation hardening mechanisms all predict that the increment in the CRSS or yield stress is proportional to $\alpha^{3/2}(\langle r \rangle f)^{1/2}$, where α is a constant characteristic of the mechanism, $\langle r \rangle$ is the average particle radius and f is the precipitate volume fraction. The theories all assume that the precipitates are spherical and coherent, and are hence sheared by dislocations in the underaged condition, to which the simple theories apply. Beyond peak strength, or in dispersion-strengthened alloys in general, the Orowan process (which predicts a $\langle r \rangle^{-1}$ dependence) usually, though not always, obtains.

It turns out that the theories of coherency hardening and modulus hardening (with the possible exception of some data on Al-Zn-Mg) are in very poor quantitative agreement with experimental data. The reasons for this are most likely that the theories themselves are very complicated and require unrealistic assumptions in order to make solutions to the equations tract-

able, and the alloys used to test them are not ideally suited to the task. For instance, Cu-Co alloys aged to contain spherical, metastable f.c.c. Co precipitates, are undoubtedly strengthened to some extent by virtue of the relatively large coherency strains surrounding the particles. However, there is also a large shear modulus difference between the precipitate and matrix phases which should produce a significant modulus hardening contribution that has never been estimated. The ideal microstructure for testing coherency hardening theories would be an alloy containing spherical, coherent, misfitting precipitates which are disordered with no modulus mismatch and possessing the same stacking-fault energy as the matrix. I am aware of no such alloys.

The theories of order hardening and stacking-fault strengthening are in much better shape. They are much simpler theories than the other two for two reasons; there is no dislocation-precipitate interaction until the dislocation has entered the particle; the dislocation can interact only with those precipitates that physically intersect its slip plane (this is, of course, a consequence of the first reason), rendering the statistical problem of dislocation-precipitate encounters much easier to handle. These two theories have been highly successful in predicting quantitatively the strengthening observed experimentally in alloys with nearly ideal microstructures (e.g. Ni-Al strengthened by ordered γ' precipitates in the

case of order hardening and Al-Ag strengthened by spherical Ag-rich G.P. zones in the case of stacking-fault strengthening).

Provided that proper care is taken in the interpretation of experimental results, the Orowan mechanism accurately describes the data. Good examples are provided by Cu-SiO₂, Cu-Al₂O₃, Cu₃Au-SiO₂, etc. alloys prepared by internal oxidation.

If we were to pose the question "How well do existing theories of precipitation hardening predict the strengthening observed in an alloy ideally suited, in a microstructural sense, for testing it?" The answer is clearly sometimes, but not always. Hence, even if we can create the ideal microstructure, we cannot always predict its mechanical behavior.

SUGGESTED EXPERIMENT

Purpose -To produce an "ideal" microstructure consisting of small (30-50 Å dia) spherical impenetrable particles to produce an alloy of high yield strength and work-hardening rate, and to study the interaction of both size and grain size in the fracture behavior.

System -Internally oxidized Cu-0.1% Si powders prepared by RSP. Powder dia. to be in range 30-50 μm. After low temperature (Ca 300-400°C) internal oxidation, powders to be consolidated (e.g. by HIPing) into test specimens.

Advantages - Yield strength predictable by Orowan equation. Incoherent SiO₂ particles are spherical and amorphous (hence impenetrable, except by fracture), resulting in high yield, high

work-hardening rate. Particle size can be varied by varying internal oxidation temperature. Particles highly resistant to coarsening. Grain size perhaps variable.

ACKNOWLEDGEMENT

This paper was written under the auspices of the DARPA Materials Research Council, Contract #MDA903-32-C-0428 with The University of Michigan.

IDEAL MICROSTRUCTURES

J. D. Embury

In order to keep the question of ideal microstructures in perspective in relation to engineering applications, I believe it is necessary to ask the following questions:

1. Which vital properties are determined by average microstructure quantities e.g. dependence of σ_y or $\bar{f}^{1/2}$, $\bar{r}^{1/2}$, etc. and which are determined key extreme values of local volume fraction f or size r of inclusions? It is possible that many aspects of damage tolerance fall into the extreme category. This becomes crucial in considering the use of microstructures with large volume fractions of second phase which RST can produce.

2. For many applications we need to consider the scale of structure relative to the scale of the product for which we wish to apply the material. For these the average inclusion size must be less than $2\mu\text{m}$. One real advantage of RST may be not to refine the scale of strengthening particle but to revive the scale of inclusions as outlined in Cohen's presentation.

3. Cognisance must be taken not only of initial RST processing but subsequent total process path. We know very little of the role of strain path. This can produce conditions of local instability. We can only really utilize RST in a broad sense if we consider subsequent effects such as the role of hydrostatic pressure.

4. The role of strain localization is clearly crucial in considering the use of fine scale structures. This influences other features such as recrystallization, fracture processes and even possibly processes such as wear and erosion.

5. One feature of RST is that there is solute trapping so that in general we have both second phase, fine grain size and solute strengthening. Solute effects are not well understood at large strains and similarly in cyclic hardening may be much more rapid.

ACKNOWLEDGEMENT

This paper was written under the auspices of the DARPA Materials Research Council, Contract #MDA903-82-C-0428 with The University of Michigan.

APPLICATIONS OF R.S.P.

J. D. Embury

We can consider new types of materials but the range is not the molecular engineering approach of Argon; it is still limited by diffusion controlled growth and the detailed nucleation processes. However it may be possible to form oxides, carbides, etc., directly from supersaturation, not by internal oxidation etc. Also attention should be given to the form of unusual precipitates formed in RST materials: can we stabilize larger volume functions of b.c.c. Cu in Fe, etc.?

RST should be considered in the broad sense not only of new homogenous fine scale structure but laminates with different surface structures, etc.: e.g., melt spin plus cladding. An alternative would be RSP plus new forming operations, powder forging, liquid phase sintering, superplastic forming by thermal forming, etc.

On the design side, I feel it is necessary to define windows of objectives such as change in K_{IC} vs σ_y curves, shift of da/dN vs. ΔK , or, in a more general sense, the change in boundaries of deformation or fracture map in RST versus conventional materials.

ACKNOWLEDGEMENT

This paper was written under the auspices of the DARPA Materials Research Council, Contract #MDA903-82-C-0428 with The University of Michigan.

SOME IDEAL MICROSTRUCTURES FROM THE STANDPOINT
OF RAPID SOLIDIFICATION PROCESSING

M. Cohen

Recent research on RSP, using high sulfur stainless steel as a model system, has confirmed an alloy-design guideline, namely, that extremely fine dispersions of very stable second-phase precipitates ($\sim 100\text{\AA}$) can be achieved by rapid cooling from the liquid state under conditions which favor the massive mode of solidification. This finding means that (a) second-phase dispersions can be selected with widely different mechanical properties, including very high strength and stiffness, and (b) such particles will resist Ostwald ripening even at elevated temperatures because of their unusually low solubility in the matrix phase. Clearly, then, relatively unshearable particles can be brought into existence. At the same time, such precipitates may be coherent as well as incoherent, and they appear to be in a size range which can optimize not only dispersion strengthening but also grain-boundary pinning and suppression of void initiation.

On another aspect of ideal microstructures, new attempts are now being made to enhance the strength, ductility and toughness of metastable austenitic steels via mechanically-induced martensitic transformations. Thus far, the ductility has been tripled at strength levels in the range of 175-200 ksi, but the exact role of the transformation in this respect remains to be determined. In sharp-crack tests, however, it has become evi-

dent that fine-tuning of the composition and its uniformity will be necessary in order to obtain the optimal amount of transformation in the plastic zone ahead of a moving crack. RSP alloys should prove beneficial for this purpose. A further contribution to the overall strength level can be derived from the RSP-control of second-phase precipitates. In any case, the deformation-induced transformation along growing cracks in J-value tests offers a graphic display of the plastic conditions at hand, and thus it is able to provide new information about the local response of a material to fracturing processes.

ACKNOWLEDGEMENT

This paper was written under the auspices of the DARPA Materials Research Council, Contract #MDA903-32-C-0428 with The University of Michigan.

OPTIMUM MICROSTRUCTURE

B. B. Rath

Optimization of microstructure for specific property requirements of structural alloys consists of three major efforts. The first is involved in developing a sound theoretical understanding of the evolution of microstructural parameters and their basic relationship with the desired property. Since parameters such as grain size, precipitate size and distribution are important features of microstructure, the nature of the time dependent change of nucleation frequency and growth rate are important to our basic understanding of the processes.

The second deals with a clear development of necessary empiricism relating major properties such as flow stress and crack propagation rates to specific microstructural parameters.

The third, and perhaps the most important is to develop experimental methods to produce engineering materials with an optimization in microstructural gradients. Since in service most materials require wear, corrosion and/or fatigue resistance, the microstructure on and near the surface region has to be designed differently from that of the bulk, which should be consistent with the required strength, toughness and crack tolerant properties. These two microstructural conditions have to be mutually compatible with an appropriate gradient in order to eliminate any sharp discontinuities.

Programs at the Naval Research Laboratory emphasize these research thrusts. Some of the current findings on each one of these three topics are presented.

ACKNOWLEDGEMENT

This paper was written under the auspices of the DARPA Materials Research Council, Contract #MDA903-82-C-0428 with The University of Michigan.

TOUGHENING MECHANISMS IN BRITTLE SOLIDS

A. G. Evans

Microstructural effects on the toughness of brittle materials (being multiplicative vis-a-vis the planar crack), provide a useful basis for assessing certain microstructural influences on the toughness of metallic alloys. Three toughening mechanisms have been analysed: transformation toughening, microcrack toughening and deflection toughening. The transformation toughening derives from the crack shielding associated with the compressive residual stresses induced within the transformation zone. The toughening is consequently dominated by the transformed wake: resulting in R-curve behavior. The R-curve evolves over a crack advance of magnitude $\sim 5h$, where h is the height of the transformation zone. The asymptotic toughening associated with the dilational component e^T of the transformation strain is given explicitly by;

$$\Delta K_{IC} = [0.22/(1-\nu)] E e^T c / h$$

where c is the particle volume concentration, and E is Young's modulus. Microstructural effects are contained in the zone dimension h : which in turn, is dictated by nucleation considerations. Strong particle size and temperature effects thus result. The deviatoric component of the transformation strain may also contribute to the toughness, but the details have not yet been evaluated.

The development of a discrete microcrack zone can also be a source of toughness. Microcracks develop in the presence of residual stress (e.g., due to thermal expansion mismatch). Partial relief of the residual stress by microcracking results in an effective transformation strain and hence, crack shielding comparable in form to martensite transformation shielding; while the increased compliance of the microcrack zone results in additional shielding. However, the shielding is partially counteracted by the reduced local toughness induced by the microcracking. Consequently, the net toughening is relatively smaller than can be achieved by martensite transformations.

The deflection of cracks by microstructural features also contributes to toughness. Analysis of this toughening mechanism indicates a dependence only on particle volume fraction and morphology (size and temperature effects are not important). Specifically, rod-shaped particles, which induce substantial crack twist, provide the major toughening. The toughening develops primarily for volume concentrations up to ~ 0.2 and depends appreciably on aspect ratio. The maximum toughness that can be achieved by this mechanism is ~ 2 to 3 , at aspect ratios of ≤ 10 .

ACKNOWLEDGEMENT

This paper was written under the auspices of the DARPA Materials Research Council, Contract #MDA903-32-C-0423 with The University of Michigan.

HYDROGEN EFFECTS ON DUCTILE FRACTURE AND PLASTIC INSTABILITY

J. P. Hirth

In a series of tests on spherodized plain carbon steels, hydrogen has been shown to degrade ductile fracture resistance by enhancing plastic instability. U-notched plane strain bend bars fail by a mixed-mode I-II crack emanating from the notch root and propagating along a characteristic slip trace (shear band). Microstructural study indicates that shear bands initiate at the surface and propagate into the interior. The localized shear produces incompatibility stresses which cause voids to initiate and grow at carbide particle interfaces. Ultimately, the void formation and localization augment one another and the crack forms.

Based on the deformation theory of Hutchinson and Tvergaard, shear instabilities should be preceded at lower strains by surface instability in the form of roughness. Observations of polished notch roots and polished plane strain tensile specimens confirm that roughening does occur at a strain in good agreement with the theory for an elastic-plastic material with a corner on its yield surface. In agreement also with theory, but not earlier qualitative predictions, the presence of a strain gradient did not influence the results: the critical strain was the same for bend bars and tensile bars. Also in agreement with theory, the tendency for instability was greatly reduced in uniaxial round-bar tensile tests.

The initial strains in the bend bars for surface roughening, void initiation, void profusion and crack initiation in air were 0.24, 0.26, 0.34 and 0.42, respectively. After precharging with hydrogen these values decreased to 0.09, 0.13, 0.19 and 0.21, respectively. Also at even lower strains, well below the strain for void initiation, the early stages of surface relief occur at lower strains in the precharging case. Thus, hydrogen degrades the properties by enhancing the tendency for shear localization in agreement with the indirect deductions based on microstructural observation.

The mechanism is a micromechanism unresolvable at the scale of scanning electron microscopy after testing. It could be related to enhancement of slip step height by absorption of hydrogen on the emergent step, for example. It must be a dramatic effect as a "defect" in the context of plasticity theory, however, since the value of ~ 0.24 is a lower bound prediction from theory for a given stress-strain curve. Yet hydrogen, while markedly influencing the critical strain, has an unresolvable effect on the stress strain curve.

The implication of these results for microstructural design is twofold. First, bulk effects can be markedly affected by surface phenomena (instability initiation) and, second, these can in turn depend sensitively on enviromental effects.

ACKNOWLEDGEMENT

This paper was written under the auspices of the DARPA Materials Research Council, Contract #MDA903-82-C-0428 with The University of Michigan.

STRAIN RATE EFFECTS

R. Stevenson

In sheet metal stamping a significant fraction of the materials related effects can be rationalized by using the total elongation measured in a tensile test as the index of material performance - thus to optimize performance both strain hardening and strain rate hardening should be optimized.

In low carbon steels the most effective way of improving strain rate sensitivity is by lowering the deformation temperature; increasing the interstitial carbon content lowers the strain rate sensitivity.

In the aluminum alloys 5182-0 and 2036-T4, cooling to 77K results in a major increase in uniform elongation - post-uniform elongation (attributable to strain rate hardening, while strain hardening is virtually unaffected). However the character of the strain hardening in these alloys is not the same: at both room temperature and 77K the 5182-0 follows the Voce formalism best while 2036-T4 follows the Voce formalism only at room temperature with the 77K data best described by a Swift formalism. Assuming that this difference in best fit strain hardening formalism is significant and is attributable to microstructural effects, the most likely candidate is the difference in concentration of Mn-rich dispersions in the two materials.

By heat treatment of the 2036 alloy, the strain hardening can be modified and rationalized in terms of enhanced dislocation accumulation at particles.

ACKNOWLEDGEMENT

This paper was written under the auspices of the DARPA Materials Research Council, Contract #MDA903-82-C-0428 with The University of Michigan.

MICROSTRUCTURE, CONTINUUM MECHANICS, AND MATERIAL INSTABILITIES

B. Budiansky and J. W. Hutchinson

Unstable material behavior under load has several well-known manifestations -necking, shear band formation, surface wrinkling. Are the conditions of stress and strain under which these instabilities occur influenced by microstructure? The answer is obviously yes. The point of this short note, however, is to urge the viewpoint that, in general, microstructure is relevant mainly through its effect on the macroscopic constitutive relations governing the material. Thus, regardless of how a particular set of plastic stress-strain-time relations comes to govern the behavior of a given material, such phenomena as necking and Luders band formation should be predictable by a continuum approach based on these relations. To be sure, some of the instabilities may be sensitive to the scale and size of unavoidable geometrical and physical imperfections, and these may, in turn, be driven by microstructural parameters (such as grain size.) But the macroscopic properties remain by far the most powerful constraints on the instabilities. Thus when experimental observations appear to show a relation between microstructure and material instability, the first attempt to rationalize the connection should always look to the intermediate, and probably decisive, role of the concomitant constitutive relations. A note of warning: some of the instability phenomena

are very sensitive to the form of the polyaxial constitutive equations, and to rate effects. Just getting a stress-strain curve in tension, and plugging into one of the easy, standard theories of plasticity may not suffice.

ACKNOWLEDGEMENT

This paper was written under the auspices of the DARPA Materials Research Council, Contract #MDA903-82-C-0428 with The University of Michigan.

IDEAL MICROSTRUCTURES VIA RAPID SOLIDIFICATION PROCESSING

R. Mehrabian

There is a need to carry out fundamental rapid solidification studies to establish the feasibility of producing improved dispersion strengthened microstructures and, hence, improved properties. The interrelationships between "rapid solidification" processing/composition and microstructure can be established on submicron powders produced by the Electrohydrodynamic (EHD) technique¹. Since these powders are electron transparent, it is possible to analyze the evolution of a complete microstructure from nucleation until the end of solidification without recourse to thinning procedures. Microstructural observations can then be coupled with thermodynamic, kinetic and heat flow concepts to elucidate the thermal history and solidification mode of the fine powders and their effects on the second phase dispersoids. The dispersoids can form either during solidification or as a consequence of solid state transformation (either during cooling of the powders to room temperature or subsequent controlled reheating while in the electron microscope).

The advantages of the technique described above include:

- A large number of alloy compositions can be systematically studied in a short time - only a few milligrams of powder are needed and produced in the EHD atomizer.
- Large undercoolings are generally obtained prior to nucleation, thus significantly extending the range of

possible microstructures (e.g., through extended solid solubility), due to extremely high solid/liquid interface velocities during recalescence.

- It is usually possible to distinguish second phase particles produced during solidification from post-solidification precipitates, i.e., intercellular segregation can be readily distinguished from solid state precipitates which have orientation relationships with the primary phase.
- Controlled reheating experiments to precipitate fine dispersions can be carried out in the electron microscope. In the extreme, the powder particle itself can be remelted, undercooled and resolidified in-situ.
- Conceivably, a technique could be devised to deform some of the powders and study dislocation/precipitate interactions in the TEM.

ACKNOWLEDGEMENT

This paper was written under the auspices of the DARPA Materials Research Council, Contract #MDA903-82-C-0428 with The University of Michigan.

REFERENCES

1. C.G. Levi and R. Mehrabian, "Microstructures of Rapidly Solidified Aluminum Alloy Submicron Powders", Met. Trans. A, Vol 13A, p.13, 1982.

IDEAL MICROSTRUCTURES

July 8-9, 1982

Materials Research Council Meeting
Scripps Elementary School
2225 Torrey Pines Road
La Jolla, California

Thursday July 8, 1982

Session I. Chairman - J. Hirth

L. Jacobson
J. Williams
A. Thompson
A. Ardell
D. Embury

Session II. Chairman - L. Jacobson

M. Cohen
B. Rath
A. Evans

Session III. Chairman - J. Williams

J. Hirth
R. Stevenson
A. Argon
J. Hutchinson
B. Budiansky

Friday, July 9, 1982

Session I. Chairman - J. Hirth

Session II. Chairman - J. Williams

Session III. Chairman - L. Jacobson

Summary & Discussion

IDEAL MICROSTRUCTURES

July 8, 1982

Attendees

<u>Name</u>	<u>Company or Institution</u>
A. W. Thompson	Carnegie-Mellon Univ.
J. D. Embury	McMaster Univ.
A. J. Ardell	UCLA
R. Stevenson	G.M. Res.
A. S. Argon	MIT
J. P. Hirth	Ohio State U.
A. G. Evans	U. Cal. Berkeley
G. Kino	Stanford
M. Cohen	MIT
H. Ehrenreich	Harvard
G. Vineyard	Brookhaven
B. Budiansky	Harvard
M. Rosen	Johns Hopkins
E. E. Hucke	U. of Mich.
J. W. Hutchinson	Harvard
J. C. Williams	Carnegie-Mellon U.
B. B. Rath	NRL
J. L. Margrave	Rice U.
R. Mehrabian	NBS
E. C. van Reuth	DARPA
L. A. Jacobson	DARPA

AN OVERVIEW OF THE FRACTURE TOUGHNESS PROBLEM

B. Budiansky, A. G. Evans, J. P. Hirth & J. W. Hutchinson

INTRODUCTION

In the discussion at the Ideal Microstructures conference, it emerged that there were few theoretical guidelines for the role of microstructures in influencing fracture toughness. As a result, various aspects of the problem were addressed at the MRC Summer Meeting and are presented as the following four papers. They have some overlap, so here we give the highlights of the set of papers and a set of suggested critical experiments.

Highlights of the Following Papers:

Effects of microstructure on ductile fracture are critically dependent upon the volume concentrations of the various second phases (precipitates, dispersoids and inclusions), and their adherence to the plastically deforming host. In general, J_{IC} is enhanced (Budiansky, et al) by reducing the volume concentration of the more weakly adherent second phases (which nucleate holes prior to fracture). However, it is essential to identify the second phases that exert the prime influence on fracture. The ductile instability that constitutes crack advance depends exclusively on the volume concentration of holes and hence, is related to the volume concentration of the initiating particles. High volume concentrations of particles that

are also capable of hole nucleation at modest strains are thus of prime importance. The fracture dominating particles are consequently dependent upon the total spectrum of second phases*. Specifically, larger inclusions that decohere at small strains are dominant when they are in a sufficient volume concentration that the associated instability strain is small (Hutchinson, et al). Consequently, as the concentration of the larger inclusion is reduced, the instability strain can exceed the nucleation strain for the next level of second phase particles (e.g., carbides in steels). Nucleation at the smaller particles then results in an appreciable increase in the volume concentration of holes, inducing almost instant instability. When this condition is reached, fracture is dominated by the adherence of the fracture initiating particles (Hutchinson, et al).

The role of the precipitates, or small dispersoids, on J_{IC} depends upon the nature of the fracture dominating particles. For fracture dominated by the growth of voids from weakly bonded inclusions, decreasing the dispersoid spacing to increase the flow stress also increases the toughness (Budiansky, et al). However, when fracture is dictated by the nucleation of voids at more adherent smaller particles, decreasing the dispersoid spac-

*Up to three levels of second phases particles are envisioned: relatively larger inclusions ($\sim 10\mu$), weakly bonded to the matrix that may participate in fracture, but not in yield strengthening; small ($\sim 50-200\text{\AA}$) dispersoids, well bonded to the matrix, that affect yield but are not directly responsible for fracture; intermediate sized particles ($0.1-1\mu$), moderately well bonded, that may influence both yield and fracture. The latter are exemplified by carbides in steels and, perhaps, constituent phases in Al alloys.

ing reduces the void nucleation strain and J_{IC} depends upon the competing influence of an increasing yield strength and a decreasing crack opening displacement; J_{IC} may thus decrease. This competition between yield strength and toughness is clearly most prevalent in high strength materials. Nevertheless, it is feasible to increase both the flow strength and the toughness of high strength materials, if the changes in the dispersoid spacing needed to increase the flow stress are accompanied by a corresponding increase in the adherence of the particles responsible for void nucleation (the dispersoids and particles could be the same phase in special cases).

Systematic attempts to increase adherence, while strengthening with fine dispersoids, are presently impeded by a poor comprehension of the factors that dictate the interface resistance to void nucleation. Theoretical treatments do not predict a size effect on void nucleation at particles (except in very small particles $\lesssim 100\text{\AA}$), and experimental evidence for the size effect is ambiguous. It is not evident, therefore, that particle size reduction would yield the desired increase in adherence. Fundamental studies of adherence are needed to address this important issue. Impurity absorption at interfaces will clearly be important in this context.

For brittle fracture propagation, a model which fits most observations considers that small dispersed particles (e.g., carbides) crack ahead of the major crack tip. Consequently, extension of the major crack will proceed by a coales-

cence process, when the stress ahead of the major crack exceeds the effective cleavage strength in the presence of the cracked particles. Factors favoring the prevention of particle cracking, which would favor high toughness and low DBTT, include (Hirth): small grain size, small particle size, and variations of other parameters which lower yield strength. Enhanced cross-slip also helps, but a decreased slip spacing can either aid or hinder fracture resistance, as discussed in the following treatment (Hirth).

Once particles crack, the probability of their extension into the matrix depends on the statistics of particle size distribution and the intensified stress near the crack tip. The treatment of this problem is given (Evans and Hutchinson) in a following paper. The development indicates that, in accord with intuition, an increase in cleavage strength (associated with a reduction in size of the cracked particles) and a lower flow stress* are the two major factors enhancing toughness. Weak enhancement effects are provided by a decreased grain size, a decreased work hardening rate, and a smaller volume fraction of particles. Note should be made of the partially counteracting influences of particle size. Specifically, a decreased particle size will increase the effective cleavage strength, but may, in some cases (dependent upon alloy content), increase the yield strength, resulting in a reduced K_{IC} .

*More explicitly, a low value of the normal tension in the presence of plastic flow.

Some Critical Experiments:

1. Test for failure strain as a function of particle volume fraction, with a given particle size distribution, to test the predictions of Hutchinson, et al.
2. Probe the region near the crack initiation site in brittle fracture for non-propagating microcracks, perhaps by acoustic microscopy.
3. Study the region near a crack tip, or near the fracture surface, of a ductile fracture proceeding by localization, to determine whether void formation at particles triggers the instability or vice versa.
4. Fine particle size and fine grain size appear to generally aid toughness in the brittle region. A limit may exist, however, when the fine particles increase yield strength more rapidly than the cleavage strength of the matrix. The existence of this limit should be explored experimentally.
5. Conduct systematic studies of particle size effects on void nucleation and examine the competition between void nucleation and brittle cracking at particles (a key unresolved issue in the ductile to brittle transition).

ACKNOWLEDGEMENT

This paper was written under the auspices of the DARPA Materials Research Council, Contract #MDA903-82-C-0428 with The University of Michigan.

ON MECHANICAL CONNECTIONS BETWEEN STRENGTH AND TOUGHNESS

B. Budiansky, A. G. Evans, & J. W. Hutchinson

Yield strength and fracture toughness are uneasy companions: enhancing the one has often been observed to degrade the other. Hope endures that with increased understanding of the microstructural processes involved in plastic deformation and fracture, materials can be designed that are both very strong and very tough. This note discusses some continuum mechanical relations among yield strength, fracture toughness and tearing strength that may provide a useful background to this problem.

We shall, for simplicity, assume ideal plasticity, with the understanding that strain hardening could be taken into account crudely through the use of an effective yield stress chosen to reflect microstructure influences on hardening rates. The macroscopic parameters to be considered are then:

a	crack length
σ_y	tensile yield stress
$\epsilon_y = \sigma_y/E$	tensile yield strain
J	Rice's J integral
J_{Ic}	critical value of J for mode-I crack growth initiation
δ_{Ic}	critical crack-tip opening at $J = J_{Ic}$
$T_0 = \frac{E}{\sigma_y^2} \left(\frac{dJ}{da} \right)_0$	Paris tearing modulus at initiation

The well-known relation (e.g. Hutchinson 1979)

$$J_{IC} = \sigma_y \delta_{IC} / \alpha \quad (1)$$

with $\alpha \approx .65$ holds in plane strain. The recent studies by Rice and his associates (e.g. Rice 1982) provide the asymptotic mode-I relation

$$\delta(r) = (\beta \epsilon_y) r \log \frac{\frac{\zeta J}{E \epsilon_y^2} \exp\left(\frac{\alpha E}{\beta \sigma_y^2} \frac{dJ}{da}\right)}{r} \quad (2)$$

for the crack-opening displacement (COD) near the tip of a plane-strain growing crack. Here $\beta \sim 5.5$ and $\zeta \sim .55$. If (following Rice) we postulate that growth will continue for a critical $\delta = \delta_c$ at $r = \delta_c / \lambda$, we get the differential equation

$$\frac{\lambda}{\beta \epsilon_y} = \log\left(\frac{\zeta \lambda}{E \epsilon_y^2} \frac{J}{\delta_c}\right) + \left(\frac{\alpha E}{\beta \sigma_y^2} \frac{dJ}{da}\right) \quad (3)$$

for $J(a)$ during crack growth. The tearing modulus at initiation ($J = J_{IC}$), with the use of (1), is therefore

$$T_0 = \frac{\lambda}{\alpha \epsilon_y} - \frac{\beta}{\alpha} \log\left(\frac{\zeta \lambda}{E \epsilon_y} \frac{\delta_{IC}}{\delta_c}\right) \quad (4)$$

Eg(3) integrates to relations like that shown in Fig. 1. For $a \rightarrow \infty$, $\frac{dJ}{da} \rightarrow 0$, and J approaches the steady state value J_{SS} . From (3) and (4), it follows that J_{SS} , J_{IC} , and T_0 are related by

$$J_{SS}/J_{IC} = \exp\left(\frac{\alpha T_0}{\beta}\right) \quad (5)$$

Thus, moderately large values of T_0 can lead to very large values of J_{SS} , as shown by the dotted curve in Fig. 2.

We now wish to speculate on the effects of microstructure on J_{IC} and T_0 (and hence J_{SS}) through its influence on ϵ_y and the critical parameters δ_{IC} , δ_C , and λ . Let us suppose that both crack initiation and crack growth are associated primarily with the nucleation, growth, and coalescence of voids at inclusions; and that yield strength is primarily dependent on grain size, and on the dislocation-blocking effects of precipitates and dispersoids. Appropriate microstructural parameters are therefore:

ρ_g	grain size
ρ_i	inclusion size
ρ_p	precipitate (or dispersoid) size
c_i	inclusion concentration
c_p	precipitate concentration

Guided by dimensional considerations, we now suggest that the parameters δ_{IC} , δ_C and λ in Eqs. (1) and (4) for J_{IC} and T_0 obey relations of the forms

$$\frac{\delta_{IC}}{\rho_i} = f(c_i, \epsilon_y) \quad (6)$$

$$\frac{\delta_C}{\rho_i} = g(c_i, \epsilon_y) \quad (7)$$

$$\lambda = h(c_i, \epsilon_y) \quad (8)$$

On the other hand, let us say that

$$\epsilon_y = q(c_p, \rho_p/b, \rho_g/w, w/v) \quad (9)$$

when b is the Burgers' vector, w is a characteristic slip-band width, and v is slip-band spacing.

We now suggest that the functions f , g and h in Eqs. (6-8) often depend weakly, if at all, on ϵ_y . The reason is that void coalescence, as well as the instability or strain localization process that may drive coalescence to its final stage is a strain-controlled phenomenon. (There may be important exceptions, which we discuss later.) With this presumption we are led to the following conclusions:

- a) Microstructural reduction of grain size, with no change in the inclusion size or concentration, lead to increased yield strength (larger ϵ_y), leave δ_{IC} , δ_C , and λ relatively unchanged, and hence produce larger values of J_{IC} , smaller values of tearing modulus T_0 , and hence possibly much smaller values of J_{SS} .
- b) Changes in precipitate size or population that increase ϵ_y have the same implications: increased J_{IC} , decreased T_0 .
- c) Increases in inclusion size (but not concentration) increase δ_{IC} and δ_C (leaving their ratio unchanged) and do not affect either λ or ϵ_y . Hence δ_{IC} goes up, but T_0 is not affected.

One of these conclusions that might be somewhat at variance with experience is that in (b) which predicts higher δ_{IC} when tailoring of precipitates is used to increase ϵ_y . To rationalize this, we return to the possibility mentioned earlier that δ_{IC} might vary with ϵ_y . The discussion by Hutchinson, Budiansky and Evans (1982) in this volume shows that if inclusion interfaces are strong enough, void nucleation and coalescence could be simultaneous. For material in this supercritical domain, increasing ϵ_y could reduce the intensity of the strain

field needed for nucleation, coalescence and crack growth. Accordingly, δ_{IC} (and δ_c) may, in this range, be sharply decreasing functions of ϵ_y . Accordingly $J_{IC} = \sigma_y \delta_{IC} / \alpha$ could conceivably decrease even when σ_y goes up.

Another possibility to be considered is that measurement of J_{IC} could be blurred by the presence of a high tearing modulus. Thus, in Fig. 1 (schematic) $\dot{J}_{SS} < J_{SS}$, $\dot{J}_{IC} > J_{IC}$, but based on practical offset values of $(a-a_0)$, it could easily be concluded that $J_{IC} > \dot{J}_{IC}$.

It may be noted that Eqs. (6) and (1), taken together, are consistent with the relation

$$K_{IC} = \{2\sigma_y E (\frac{\pi}{6})^{1/3} (2\rho_i)\}^{1/2} c_i^{-1/6} \quad (10)$$

proposed by Hahn and Rosenfield (1975). Thus, with

$$J_{IC} = \frac{(K_{IC})^2 (1-\nu^2)}{E} \text{ the Hahn-Rosenfield proposal gives}$$

$$f = 4\alpha \left[\frac{\pi}{6c_i} \right]^{1/3} (1-\nu^2) \quad (11)$$

as the function in (6); note the independence of ϵ_y .

The magnitudes of the changes that might be induced microstructurally in T_0 are shown in Fig. 2. Here we show T_0 vs. ϵ_y as given by Eq. (4) for various values of λ , and the arbitrary assumption $\delta_{IC} = \delta_c$. (No real rationale for this choice is offered, but note that the term in (4) containing δ_{IC}/δ_c is generally negligible.) A plausible estimate for λ can be made on the basis of an observed value of T_0 for a given ϵ_y .

Changes in T_0 due to change in ϵ_y can then be estimated by staying with the appropriate λ value. Thus, if $T_0 = 40$ for $\epsilon_y = .53 \times 10^{-3}$, then $\lambda \sim .025$. Then doubling ϵ_y to 1.16×10^{-3} would bring T_0 down to 12. The nominal value of J_{IC} would double, but J_{SS} would drop to 7% of its previous value.

ACKNOWLEDGEMENT

This paper was written under the auspices of the DARPA Materials Research Council, Contract #MDA903-82-C-0423 with The University of Michigan.

REFERENCES

- | | |
|---|---|
| Hahn, G.T. & Rosenfield, A.R. 1975 | Met. Trans. A, <u>6A</u> , pp. 653-658. |
| Hutchinson, J.W. 1979 | <u>Nonlinear Fracture Mechanics</u>
Technical University of Denmark
(Course notes) |
| Hutchinson, J.W., Budiansky, B., Evans, A.G. 1982 | Ductility Variations with Volume Fraction and Strength of Inclusions, this volume. |
| Rice, J.R. 1982 | Elastic-Plastic Crack Growth, in Mechanics of Solids, ed. H.G. Hopkins and M.J. Sewall, Pergamon Press. |

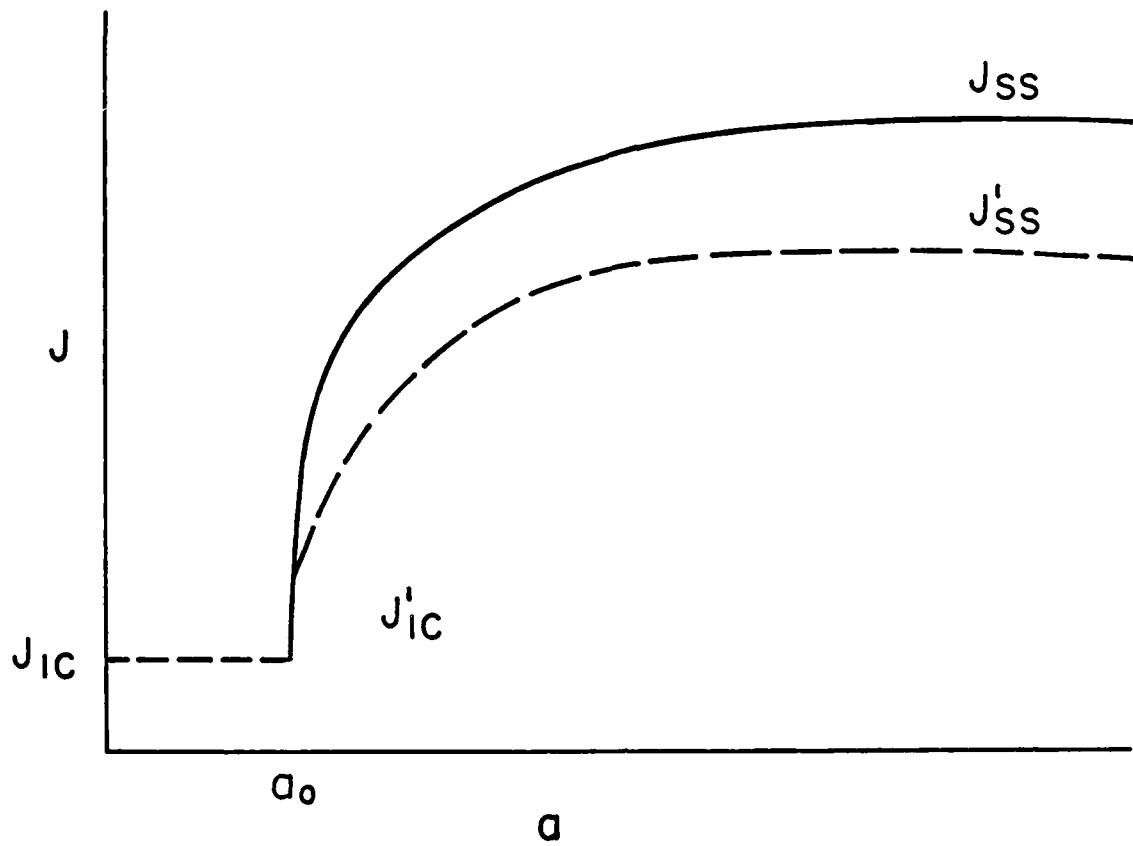


Figure 1. J vs a during crack growth.

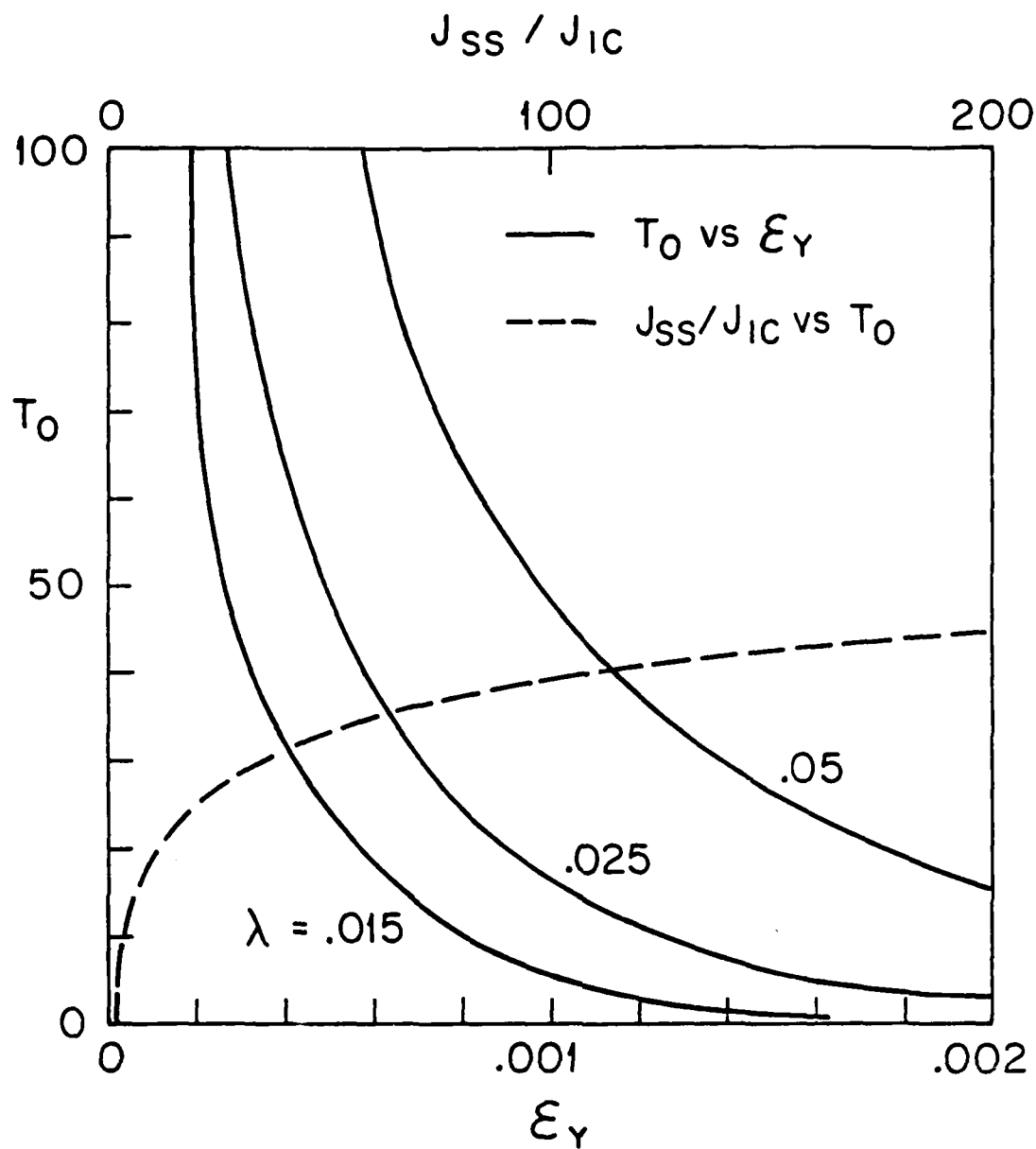


Figure 2. Tearing modulus T_0 vs ϵ_y ; J_{SS}/J_{IC} vs T_0 .

DUCTILITY VARIATIONS WITH VOLUME FRACTION
AND STRENGTH OF INCLUSIONS

J. W. Hutchinson, B. Budiansky & A. G. Evans

Once nucleated, a field of voids undergoes relatively homogeneous growth until deformation becomes unstable with essentially all subsequent straining being localized in a single sheet of voids. In high strength, low strain hardening metals, the localization tends to be a shearing process, while in lower strength, high hardening metals, the preferred process involves necking-down between voids on a plane perpendicular to the maximum principal stress direction. High levels of stress triaxiality promote the latter mode over the shearing mode. The onset of either of these localization modes brings about an abrupt termination of homogeneous straining and marks the end of ductility. Microscopic observations indicate that only a relatively small amount of void growth usually occurs during the stage of homogeneous straining. High strength, low strain hardening materials generally display the least amount of void growth prior to localization. If the inclusions are sufficiently strong in these materials, it appears that void nucleation can trigger the localization process and thereby essentially eliminate the stage of homogeneous void growth.

In what follows, a discussion will be given of the effect on ductility of varying two micro-structural variables; inclusion strength and volume fraction. Emphasis will be placed

on whether localization is preceded by a period of homogeneous void growth or whether it is precipitated by void nucleation. For simplicity, it will be assumed that voids are nucleated at the inclusions over a narrow strain range centered about the strain ϵ_N , and, for definiteness, we will be concerned with ductility ϵ_f in a uniaxial tension test so that the effect of stress state is not explicitly at issue.

For a given material (with a given yield strength, hardening capacity, etc.), the curve in Fig. 1 gives the hypothetical relation between the localization strain, or ductility ϵ_f^0 and the inclusion volume fraction f , assuming voids are nucleated at all inclusions at zero strain ($\epsilon_N=0$). A delay in the onset of nucleation (i.e., an increase in ϵ_N) will increase the strain to localization, but we now argue that this increase can be expected to be small as long as $\epsilon_N < \epsilon_f^0$. That is, we will argue that, as long as $\epsilon_N < \epsilon_f^0$, then it is approximately true that

$$\epsilon_f = \epsilon_f^0 \quad (1)$$

The argument hinges on the hypothesis that the void growth process is not expected to be strongly history dependent. It is expected that at a given strain, a void will have almost the same volume once it is completely nucleated as it would have had if it had been nucleated at zero strain. This hypothesis is rigorously correct for a linearly or nonlinearly elastic solid. Although it cannot be strictly correct for a plastically de-

forming solid due to the inherent path-dependence of plastic straining, we suspect it may correct to a first approximation. Calculations will have to be performed to directly confirm (or disprove) this conjecture. Indirect qualitative evidence for this hypothesis is that voids are almost always observed to be popped open. One would expect to see crack-like void/shapes just following nucleation if void growth was strongly history dependent.

Adopting the idealization implied by (1), we next note, using the same reasoning, that nucleation will trigger localization when $\epsilon_N > \epsilon_f^0$, so that then $\epsilon_f^0 = \epsilon_N$. Thus ϵ_f is either ϵ_f^0 or ϵ_N , depending on whether localization is growth-controlled ($\epsilon_N < \epsilon_f^0$), or nucleation-controlled ($\epsilon_N > \epsilon_f^0$); so

$$\epsilon_f = \max(\epsilon_f^0, \epsilon_N) \quad (2)$$

as depicted in Fig. 2. In the region of nucleation-controlled localization, a drop in f has little effect on ductility, while an increase in ϵ_N has little influence on ductility in the growth-controlled region.

The transition between regimes corresponds to the point (f^*, ϵ_N) on the curve of ϵ_f^0 vs. f . Given a material with a void volume fraction f and a nucleation strain ϵ_N , it follows that the material lies in the nucleation-controlled or growth-controlled regime depending on whether the point (f, ϵ_N) lies above or below, respectively, the curve of ϵ_f^0 vs. f , as shown in Fig. 3. An extreme example of such a transition has been

found by Kazinczy and Backofen (1961) and Chin, et.al. (1964) in connection with a ductile-ductile transition temperature in high purity aluminum. At temperatures below the transition, voids were nucleated and subsequent localization determined ductility. Above the transition temperature, no voids could be nucleated ($\epsilon_N = \infty$), so that essentially unlimited ductility was obtained.

The processes of nucleation, growth and localization have been purposely idealized in the above discussion to bring out the existence of the regimes of growth-controlled localization and nucleation-controlled localization as sharply as possible. The transition between these regimes will be blurred by several factors including: (1) any spread in the strain range for nucleation about ϵ_N , and (2) the tendency of the history dependence of void growth to delay localization beyond ϵ_f^0 in the growth-controlled regime when ϵ_N is nearly ϵ_f^0 . Even accounting for these complications, it should be clear that the commonly proposed addition rule for ductility, given by:

$$\epsilon_f = \epsilon_N + \epsilon_f^0 \quad (3)$$

is not likely to have general validity.

ACKNOWLEDGEMENT

This paper was written under the auspices of the DARPA Materials Research Council, Contract #MDA903-32-C-0428 with The University of Michigan.

REFERENCES

- (1) G.Y. Chin, W.F. Hosford and W.A. Backofen, Trans. Met. Soc. A.I.M.E., 1964, 53, 55.
- (2) F. de Kazinczy and W.A. Backofen, Trans. Amer. Soc. Metals, 1961, 53, 55.

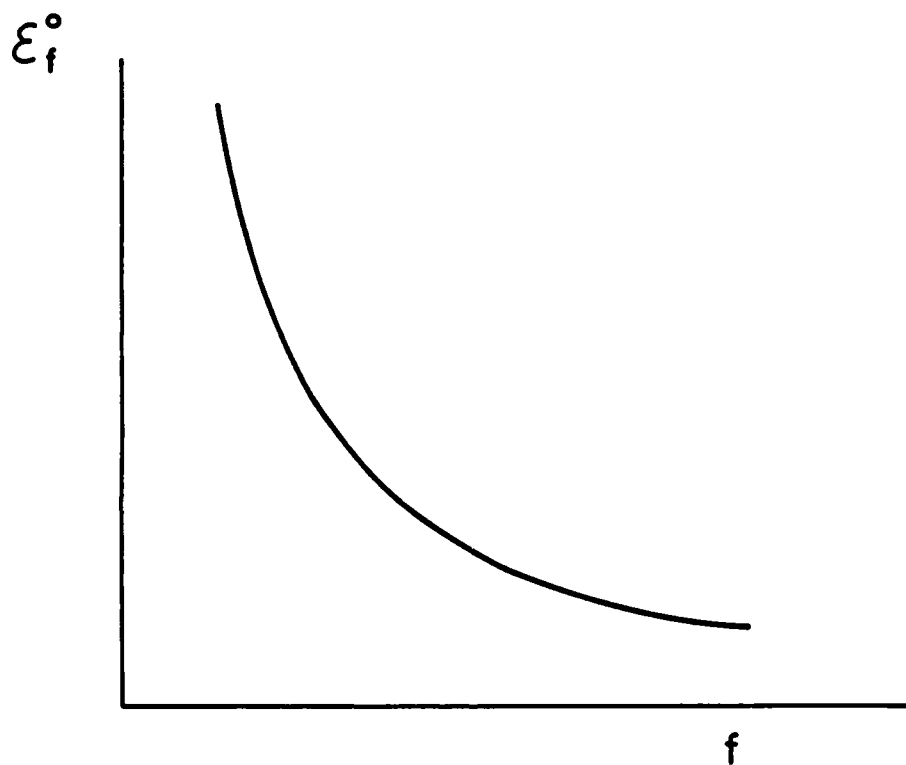


Figure 1. Ductility as a function of volume fraction of void nucleating inclusions, assuming voids nucleate at zero strain.

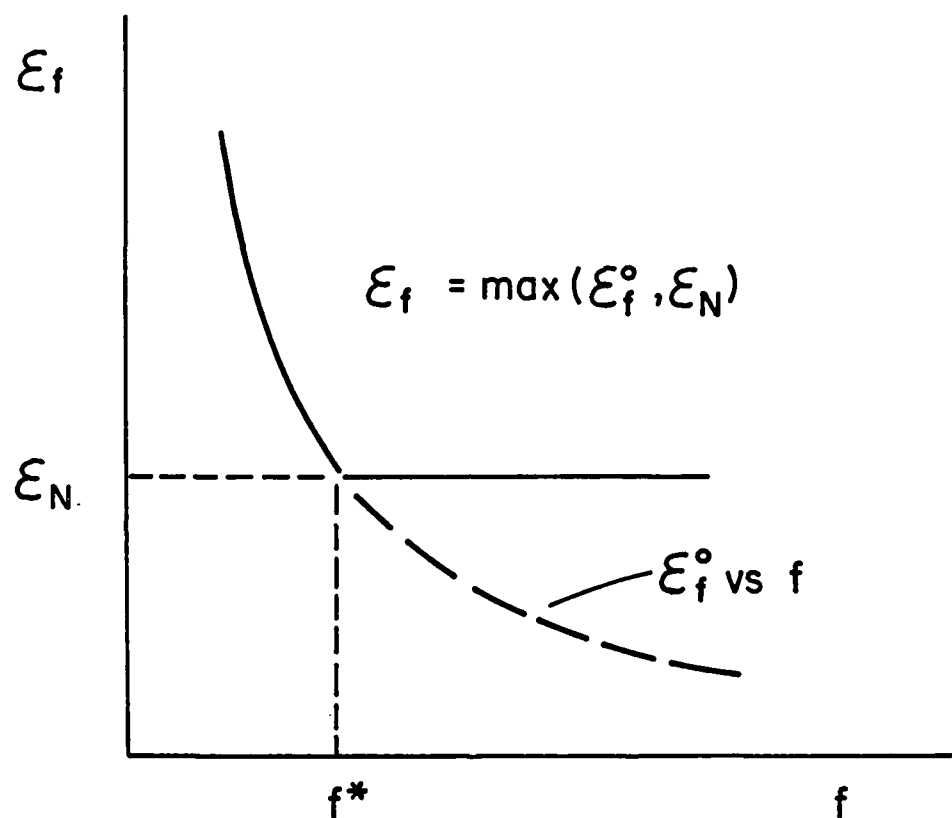


Figure 2. Ductility as a function of volume fraction of void nucleating inclusions, assuming voids nucleate at strain ϵ_N .

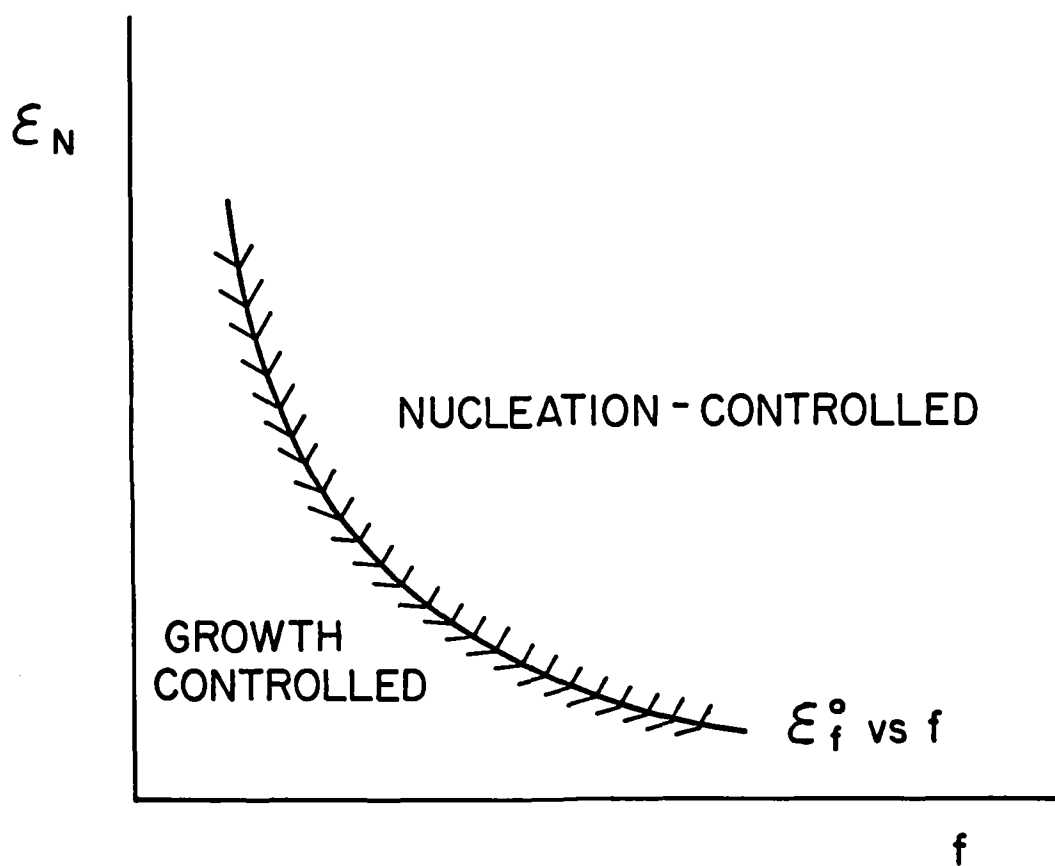


Figure 3. Regimes of nucleation-controlled and growth-controlled localization.

CRYSTAL SLIP FACTORS IN BRITTLE FRACTURE INITIATION

J. P. Hirth

INTRODUCTION

There is some evidence¹ for the Ritchie, et al, model² of brittle fracture wherein cracked carbides exist at grain boundaries a few grain diameters ahead of a precrack and spread, causing failure, when the stress intensity (or stress in a smooth bar) reaches a critical value in the vicinity of the carbide. A necessary condition for such a fracture is that the particles be cracked. More generally, a decohered particle or a cracked grain boundary could also act as a nucleus for a spreading cleavage crack. In the limit that cracking occurs in the plastic microstrain regime, the events leading to particle cracking must occur in the crystal slip regime of behavior. For larger plastic strains, a crystal slip view must merge into a continuum view of the crack initiation process.

Here, we present an approximate hierarchy of cases going from the crystal slip to the continuum level. The resulting relations are discussed in terms of predicted microstructural events. Some attention is given to the possibility of propagating a crack into the matrix.

Various microstructural lengths enter the problem and these are depicted in Fig. 1. Plastic shear in Fig. 1 is envisioned as occurring in either sharp dislocation pileups on a single slip plane or as a blunted pileup (slip band).

STRESS INTENSITY FACTORS

The stress at the tip of a pileup is given in dislocation theory³ by

$$\sigma_i = \sigma N \quad (1)$$

where the number of dislocations is

$$N = \frac{\sigma \pi (1-\nu)}{\mu} \left(\frac{d}{b} \right) \quad (2)$$

Here σ is the applied stress resolved on the slip plane, μ is the shear modulus, ν is Poisson's ratio, b is the magnitude of the Burgers vector, and d is the pileup length. We consider the more effective pileup emanating from sources near the centers of grains or nearly midway between particles so d is related to microstructural parameters as in Fig. 1.

A particle can crack or decohere, or a grain boundary can separate, when the intensified stress σ_i becomes greater than a critical stress σ^* . For a completely brittle crack, σ^* would be a material parameter related to the surface energy of the critical sized crack a^* . For the case where there is local plasticity, σ^* can depend on the local flow stress in the vicinity of the crack nucleus. Thus, the critical condition is

$$\sigma_i > \sigma^* \quad (3)$$

For the sharp pileup, the combination of Eqs. (1) and (2) gives the relation for σ_i in Eq. (4) in Table 1. The conditions on the relation are twofold. First, N in Eq. (2)

must exceed unity for the concept of a pileup to be physically meaningful, which translates roughly to $(b/d) < (\sigma/\mu)$ as shown in Table 1. Second, if pileup-pileup interactions are to be negligible, $(d/8) < L$. This can be envisioned in terms of the superdislocation analogy of the pileup, the stress field of a pileup relating to that of a superdislocation of Burgers vector magnitude Nb at a position $d/8$ from the tip of a pileup. Closer to the tip, of course, the pileup field becomes that $\sim 1/\sqrt{r}$, with r the distance from the tip, corresponding to the mechanics equivalent mode II crack analogy of the pileup. However, the superdislocation analogy shows that pileup-pileup interactions occur only when $(d/8) \gtrsim L$.

As the pileup blunts (slip band widens) via double cross slip events, the intensified stress at the pileup tip relaxes. Essentially, the pileup can become a blunted pileup if dislocation dipoles are superposed on the sharp pileup. The field of the dipole is cancelled over a distance w . For this case the field can be found by smearing the pileup over the width w and integrating the smeared distribution. The result is that the stress concentration at the pileup tip is reduced by a factor b/w as shown in Eq. (5) in Table 1. This pileup is equivalent to the reduction of the stress intensity $\sigma_I(r) = K_{II}/\sqrt{r}$ ahead of the crack in a continuum calculation for a mode II crack. For the atomically sharp crack the singularity terminates at $r \sim b$ where nonlinear atomic-bond effects become important. With the crack tip smeared, the singularity is

removed and $\sigma_i(r) = K_{II}/\sqrt{w}$ at the crack tip. The stress is roughly constant for $r < w$, and at about $r \sim w$ changes over to the form $\sigma_i = K_{II}/\sqrt{r}$ characteristic of the sharp crack. If the concentrated stress is to nucleate a crack, the spacing of the critical-sized crack nucleus a^* relative to w is important. If $a^* \gg w$, the energy release $G \sim K_{II}^2/E$ balancing the energy required to create the crack (surface energy and local deformation) is dominated by the K_{II} field corresponding to Eq. (4). If $w > a^*$, the field is the weaker elastic field corresponding to eq. (5).

When the spacing between intense pileup becomes small, unusual effects occur which have not been appreciated in the pileup literature, although they are known in the continuum mechanics - stress intensity factor literature³. When $d/8 \gtrsim L$, a stack of a large number of edge dislocation pileups interact in such a way that the intensified stress is increased by a factor $3d/L$. For a screw dislocation pileup, the situation differs. The screw dislocation analogs of Eqs. (4) and (5) have the same form of dependence of σ , d , b and w . However, when $d/8 \gtrsim L$ and screw pileups interact, the intensified stress is decreased by a factor L/d . These results are, of course, two dimensional, but they may roughly apply even for equiaxed grains near the point on the grain boundary where the pileups become pure edge or pure screw. What is needed for a more accurate treatment of the equiaxed grain case is a solution for the case of a set of circular pileups (or mode II-III circular

cracks) stacked in a cylindrical array. The two-dimensional edge dislocation enhancement of $3d/L$ is certainly an overestimate for the circular pileup case.

For a blunted pileup intersecting a particle when $D < w$ only a fraction w/D of the pileup is blocked by the particle. Thus for Eq. (5) or the blunted version of Eq. (6) or (7), the intensified stress would be reduced by an additional factor of D/w as noted in Eq. (8). Finally if w/d or $w/L > \sigma/\mu$, no meaningful pileups exist and instead the dislocations resemble a Taylor array which can be effectively smeared into a continuous distribution, giving a simple elastic-ideal plastic solution and no stress concentration, Eq. (9).

RELATION TO MACROSCOPIC PROPERTIES

Insofar as a cracked carbide or grain boundary is a necessary condition for brittle fracture, and since a critical sized nucleus for such a crack forms under the assistance of the stress concentration σ_i , the above results should provide at least qualitative guidelines for trends of fracture resistance as a function of microstructure. Another relevant relation to pileups is the strain produced by operation of a pileup, given for the edge dislocation case by

$$\begin{aligned}\epsilon &= \frac{\pi(1-\nu)\sigma}{4\mu} & L > d \\ \epsilon &= \frac{\pi(1-\nu)\sigma}{4\mu} \left(\frac{d}{L}\right) & L < d\end{aligned}\tag{10}$$

With the criteria that small σ_i or large ϵ are favorable fracture resistance parameters, the microstructural effects are as follows.

Grain Size: A small grain size d always favors a small σ_i as shown in Table 1. Indeed, Eqs. (4) or (5) lead to Hall-Petch type behavior of the fracture stress $\sigma \propto d^{-1/2}$. If $d > L$, however, a decrease in d reduces the strain which a given stress produces. This effectively increases the work hardening rate, which would decrease the tendency for plastic instability, and hence which could be a favorable effect for small enough d values. This latter effect alone would be inconsistent with experimental observation.

Strain Localization: In the microstrain or low strain limit, plastic instability would be manifested as shear on a limited number of slip planes, or large L . This would increase the strain at a given stress, Eq. (10), which would be helpful. For screw pileups, a decrease in L would also be beneficial through a decrease in σ_i . However, for edge dislocation pileups, a decrease in L would increase σ_i and hence be a detrimental effect if the two-dimensional result applies.

Stacking Fault Energy and Cross-Slip: For materials with low stacking fault energy, the tendency for cross-slip is reduced and pileups should be sharp. A high stacking fault energy should lead to cross-slip, broadening of the pileup to w , and hence a beneficial effect. In low-symmetry crystals the limitation of slip systems tends to prevent cross-slip, a

detrimental effect. In bcc metals at low temperatures the dislocation core structure promotes slip on {112} planes and suppressed cross-slip, again a detrimental effect.

Interstitial Pinning; Other Weak Obstacles: As shown in Fig. 2, σ_i can always be reduced if nearby dislocations move or nearby sources are activated by the intensified stress ahead of the pileup tip. Thus any factor which decreases the likelihood of source operation or which decreases the mobility of dislocations should be detrimental to fracture resistance. Dislocation pinning, which would accomplish the above detrimental effect, is provided, in roughly decreasing order of pinning strength, by interstitial (C,N) dislocation atmospheres in bcc metals, precipitates, prior deformation (work hardening), and solid solution effects.

Particle Size: Particles provide the indirect effects of restricting grain size or dislocation cell size, an effect which increases with decreasing D for a given volume fraction of dispersoid, because of the attendant decrease in particle spacing. For small enough D , of the order of tens of nanometers, boundaries can bypass the particles by thermal fluctuation, and the effect is lost. Aside from the indirect effects, small D is directly beneficial if Eq. (2) applies. Finally, if $D < a^*$, a crack cannot stably form in the particle, so small D would be helpful in this regard also.

Impurity Effects: Adsorption of impurities to grain boundaries or dispersoid interfaces leads to their adsorption

on the surfaces of cracks formed at these locations, particularly if decohesion is the cracking mode of the particle. In the very brittle limit, this effect becomes important in promoting cracking by reducing σ^* .

Dispersoid Properties: Dispersoids which are themselves hard and brittle, such as MnS inclusions in steels, also promote cracking by reducing σ^* .

The above trends are mostly consistent with experimental observations. They predict that fracture resistance should be promoted by a decrease in grain size (with a limit), increased stacking fault energy, large number of available slip systems, decreased interstitial content in bcc metals, decreased diffuse hardening (by precipitates, for example), decreased particle spacing, and decreased content of hard inclusions. Fine slip spacing is favorable in the limit of Eq. (9), but reduced slip spacing can be unfavorable according to Eq. (6). Thus, the predictions are ambivalent with regard to slip spacing.

Some Aspects of Crack Propagation: Once a microcrack has formed in a particle or a grain boundary, it must propagate into the matrix to produce transgranular cleavage. At the grain size level, added energy must be supplied to create cleavage steps or tear ridges as the cleavage plane changes orientation upon crossing a grain boundary. At a finer scale, a microcrack in, say, a particle must propagate into the matrix locally rather than blunting. The statistics of the probabil-

ity of this occurrence as a function of particle size distribution is considered in the next paper (Evans and Hutchinson). There are some other factors at the microstructural level that we now consider briefly for the case of quenched and tempered steel as an example.

The orientation relationship between austenite and ferrite is $(211)_\alpha // (001)_{cm}$; $[001]_\alpha // [100]_{cm}$, $[111]_\alpha // [010]_{cm}$.⁴ Thus, the primary cleavage plane of $(001)_{cm}$ is inclined at 35° or 66° to the primary $\{100\}_\alpha$ cleavage planes of ferrite. The secondary cleavage plane of $(010)_{cm}$ is inclined at 54° to the $\{100\}_\alpha$ planes. Thus, a carbide particle within a grain is not favorably oriented for propagation of a crack into ferrite. Neither are such particles favorably oriented for propagation from ferrite into carbide, a factor that could be important in crack growth. At a grain boundary, the carbides are oriented with respect to one grain to reduce surface energy. However, they are randomly oriented with respect to the second grain. Thus, some fraction of grain boundary carbides are likely to be oriented for cleavage crack propagation and grain boundary carbides can be more detrimental, but on a statistical distribution basis. If recrystallization or grain growth is imposed subsequent to carbide precipitation as in "process-annealing", the orientation relation would be lost for many of the carbides, and bulk carbides could become favorably oriented for cleavage propagation. Thus, in the brittle fracture regime one might be cautious about attributing changes in behavior to

grain size changes alone if the changes were accomplished in the above manner.

Carbides have larger volumes per iron atom than the matrix and smaller thermal expansion coefficients. Thus residual stresses in the particles from precipitation and cooling should be compressive in nature and would tend to reduce the brittle fracture tendency.

If a crack nucleus starts to grow in a particle or grain boundary, it will gain inertia. This dynamic effect would tend to promote crack propagation into the matrix, but calculations are needed to determine the magnitude of this effect. If a particle decoheres, this effect should be diminished because of the nonplanar trajectory of the growing crack nucleus.

ACKNOWLEDGEMENT

This paper was written under the auspices of the DARPA Materials Research Council, Contract #MDA903-82-C-0428 with The University of Michigan.

REFERENCES

1. R. O. Ritchie, W. L. Server and R. A. Wullaert, Met. Trans. A, 10A, 1557 (1979).
2. R. O. Ritchie, J. F. Knott and J. R. Rice, J. Mech. Phys. Solids 21, 395 (1973).
3. H. Tada, P. Paris, and G. Irwin, The Stress Analysis of Cracks Handbook, Del Research Corp., Hellertown, PA, 1973.
4. W. C. Leslie, "The Physical Metallurgy of Steels", McGraw-Hill, New York, 1981, p. 100.

TABLE 1. STRESS CONCENTRATIONS σ_i AT PILEUP TIP

	Conditions
a. Sharp Pileup	
$\sigma_i = \frac{\sigma^2 \pi (1-\nu)}{\mu} \frac{d}{b}$	(4) $\frac{b}{d} < \frac{\sigma}{\mu}, \frac{d}{\delta} < L$
b. Blunt Pileup (slip band)	
$\sigma_i = \frac{\sigma^2 \pi (1-\nu)}{\mu} \frac{d}{w}$	(5) $\frac{w}{d} < \frac{\sigma}{\mu}, \frac{d}{\delta} < L$
c. Interacting Pileups	
Edge: $\sigma_i = \frac{\sigma^2 \pi (1-\nu)}{\mu} \frac{3d^2}{L}$ (b or w)	(6) $\frac{b \text{ or } w}{d} < \frac{\sigma}{\mu}, \frac{d}{\delta} > L$
Screw: $\sigma_i = \frac{L}{w} \frac{\sigma^2 \pi}{\mu}$	(7) $\frac{b \text{ or } w}{d} < \frac{\sigma}{\mu}, \frac{d}{\delta} > L$
d. Blunt Pileup width greater than particle diameter for particle barrier case.	
$\sigma_i = \frac{D}{w} \times \sigma_i \text{ of (5) or (6)}$	(8) as above plus $D < w$
e. Pileups smear into an effective dislocation continuum.	
$\sigma_i = \sigma$	(9) $\frac{w}{d} \text{ or } \frac{w}{L} > \frac{\sigma}{\mu}$

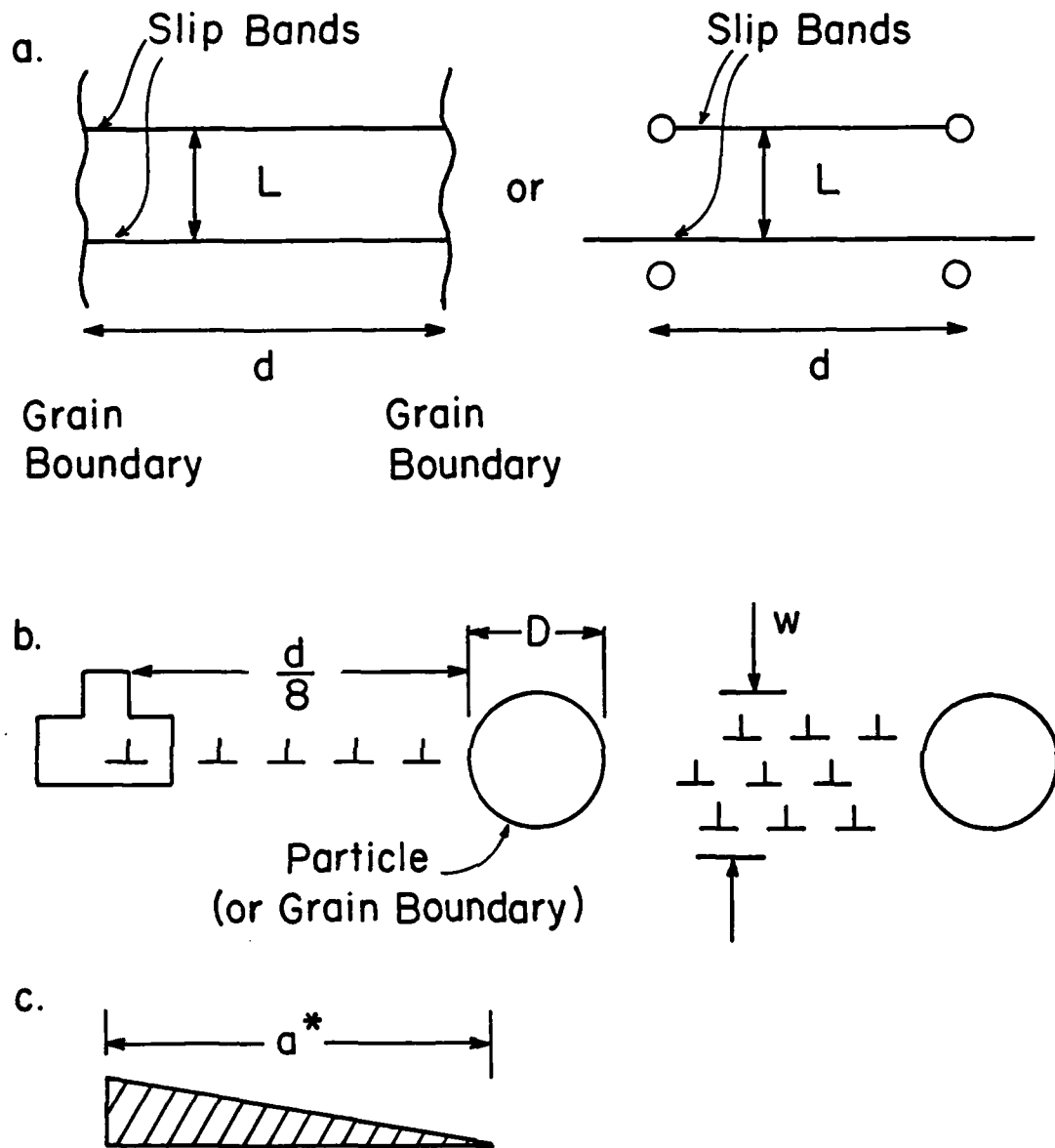


Figure 1. Various microstructural dimensions: in (a) d is grain diameter or particle spacing, L is slip band spacing. In (b) the particle diameter is D , a sharp pileup of dislocations has no width, but a blunted pileup has a width w . In (c), a^* is the vertical sized crack nucleus. In (b) the superdisposition equivalent of the crack is shown at a distance $d/8$ from the crack tip.

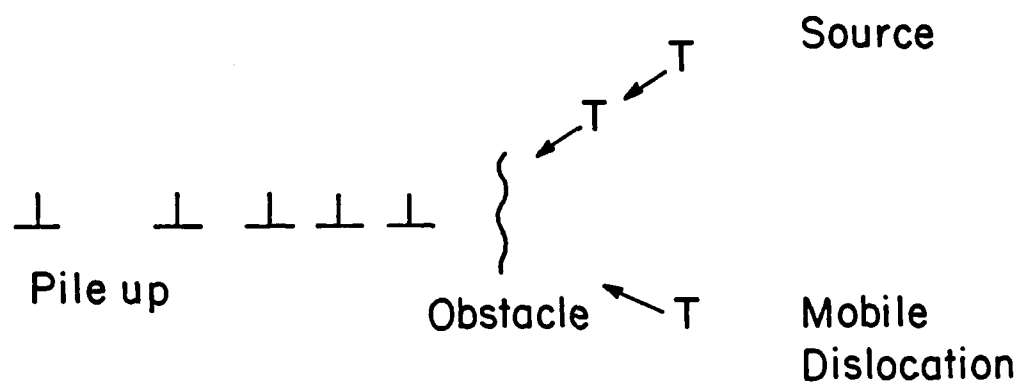


Figure 2. Reduction in σ_i by source activation or other dislocation motion in the vicinity of the pileup.

BRITTLE FRACTURE AND THE DUCTILE TO BRITTLE TRANSITION IN MILD STEEL

A. G. Evans, J. W. Hutchinson and B. Budiansky

The brittle fracture of mild steel at low temperatures has been rationalized as a phenomenon dictated by the brittle extension of cracked carbides into the ferrite matrix, within the elastic/plastic stress field of a major crack (Ritchie, et al, Curry and Knott). A weakest link statistical analysis of this process has been conducted (Evans and Hutchinson) and reveals the following features.

A maximum probability of carbide activation occurs at a critical distance, X_c , ahead of the crack,

$$X_c \sim \left(\frac{\sigma_0}{S}\right)^{N+1} \left(\frac{K_{IC}}{\sigma_0}\right)^2 \quad (1)$$

where σ_0 is the yield strength, S the average strength of the cracked carbides, K_{IC} is the fracture toughness and N is the hardening exponent ($N > 1$). The critical distance is thus related to the size distribution of grain boundary carbides (which determines S) and the stress - strain curve of the material. There is no explicit dependence of X_c on the prior austenite grain size. Hence, in contrast to prior suppositions (Ritchie, et. al) a characteristic distance based on the grain size is not involved in the brittle fracture of mild steel - at least when a cracked carbide activation mechanism obtains.

The statistical analysis (based on the growth of cracked carbides) can also be used to predict trends in toughness with material properties. This analysis requires that, to ensure major crack advance, cleavage cracking initiates at sites along the crack front with a spacing proportional to the grain size. Then,

$$K_{IC} \sim \frac{S^{(N-2)/2} (E\gamma_p)^{3/4}}{\sigma_0^{(N-1)/2} (df)^{1/4}} \quad (2)$$

where E is Young's modulus, γ_p is the energy needed to propagate the cleavage crack from the carbide into the ferrite, d is the grain size and f is the volume concentration of carbides. The term $E\gamma_p$ arises because the carbide size r has been related to strength by, $S \propto \sqrt{E\gamma_p/r}$. Observed trends in toughness with grain size obtained by Curry and Knott (Fig. 1) and with temperature* conform rather well with the statistical result. Trends with carbide size and volume concentration, obtained by Rawal and Gurland, are correctly ordered but not quantitatively predicted by Eq. (2).

The ductile to brittle transition in the statistical model can be considered to result from two effects. Firstly, the critical distance X_C reduces as temperature increases and

*The dependence of K_{IC} on temperature is contained in σ_0 and has precisely the same form as the Ritchie, et. al. result, which demonstrates good predictability of temperature effects.

eventually becomes smaller than the distance ahead of the crack, X_0 , at which the normal stress exhibits a maximum. At this point, the failure probability (at given K_I) must decrease rapidly with further increase in temperature (because the stress at the maximum failure probability site then decreases as temperature increases). Secondly, the cleavage resistance of the ferrite, γ_p , must increase as slip becomes more homogeneous at elevated temperature (Hirth); an ensuing transition to large γ_p (resulting in void formation rather than brittle crack extension at the carbides) provides a large increase in K_{IC} (Eq. 2).

It is not evident at this juncture that a statistical model based on a cracked carbide distribution constitutes a complete description of brittle fracture and the ductile to brittle transition. Various stages of cleavage crack stability (R-curve effects) may be involved. Firstly, it is noted that the K_{IC} for small cleavage cracks must increase from the cleavage value ($\sim 2 \text{ MPa } \sqrt{\text{m}}$) to the macrocrack value ($\sim 30 \text{ MPa } \sqrt{\text{m}}$) as the crack - initiated from the carbide particle - extends outward (Fig. 2). The rate of increase in K_{IC} dictates initial stability; cleavage crack stability for crack sizes between d (the grain size) and $\sim 100 d$ can be conjectured for reasonable R-curve choices. Consequently, for relatively large $X_c (> 3d)$, stable cleavage cracking in advance of the major crack may obtain. Furthermore, macroscopic R-curve behavior may apply to carbide induced cleavage cracks that coalesce with the major

crack. This behavior is a natural consequence of the extension of the crack tip into the plastic zone; a non-zero tearing modulus obtains for initial crack growth in small scale yielding even in the presence of a brittle crack, c.f. transformation effects (Budiansky, et al). Hence, the crack may in some instance be required to extend by several grain diameters, after cleavage crack coalescence, prior to unstable growth. A grain size effect on toughness may thus ensue.

The potential R-curve effects described above are clearly amenable to experimental study, by examining crack tip zones prior to unstable growth. Acoustic microscopy would be an ideal instrument for such studies because of its ability to detect small brittle cracks. The outcome of stable cleavage fracture studies would provide a complete basis for predicting fracture behavior in the brittle range.

ACKNOWLEDGEMENT

This paper was written under the auspices of the DARPA Materials Research Council, Contract #MDA903-82-C-0428 with The University of Michigan.

REFERENCES

- R. O. Ritchie, J. F. Knott and J. R. Rice, J. Mech. Phys. Solids 21, (1973) 395.
- D. A. Curry and J. F. Knott, Metal Science, Jan 1976, p. 1.
- J. P. Rawal and J. Gurland, Met. Trans. 8A (1977) 691.
- B. Budiansky, J. W. Hutchinson and J. C. Lambropoulos, Intl. J. Solids and Structures, in press.

CONSIDERATIONS ON THE SUPERCOMPUTER CHIP

D.K. Ferry, T.C. McGill, R.S. Bauer, H. Ehrenreich,
G.H. Vineyard, P.A. Wolff, and M.S. Wrighton

It is generally acknowledged that computers 10^3 times as fast as today's fastest "supercomputer" will be required to process image-based data expected in the decades ahead. Computer scientists and systems architects have directed these designs toward the area of large-scale multi-processor networks, in which speed is gained through massive parallel arrays of relatively slow processors¹. Indeed, the clock speeds envisioned in individual processing elements in nearly all proposed supercomputers (including the Japanese fifth-generation, NASA's massively-parallel-processor, and the Denelcor HEP) are lower than either the Iliac IV or current supercomputers such as the Cray I and Cyber 205. In fact, VHSIC goals of 100 MHz (and $0.5\mu\text{m}$ technology) exceed the speeds of all of the above machines. On the other hand, clock speeds and data rates are currently not set by the available switching speeds of LSI devices, but by the requirements of off-chip communication².

The advent of VLSI generally facilitates a cost-effective design of the future supercomputers. Two reasons for this are immediately obvious. First, VLSI allows much greater functionality on a chip, and therefore secondly, VLSI reduces the number of off-chip communications, which leads to a higher "functional throughput" for the processor. In short, however, the aim of supercomputers is to maximize brute speed and to

facilitate large scale numerical calculation. In both, it is necessary to maximize parallelism and incorporate VLSI.

While clock speeds have generally been held to cycle times of the order of 10MHz in most supercomputer projects to date¹, higher speeds are easily possible. For example, cycle time in the Cray I is 12.5 nsec, and this machine by-and-large does not utilize LSI. Designs of new supercomputers are suggesting clock speeds up to 150 MHz. At the same time, we are seeing VLSI dimensions approach the submicron regime. Moreover, there are requirements for brute speed in many applications such as front-end processors and analog-to-digital convertors. It becomes fruitful to ask, therefore, whether there are limits on these various quantities; limits that are such that we can no longer continue to blindly make things smaller and faster. In the following, we attempt to show that the limitations established by our current understanding of technological and material factors are considerable.

To date, speeds in multi-chip systems or multi-processors have had to be held down due to inter-chip communications that requires driving relatively long transmission lines between chips. Even with microprocessors, this remains the case in supercomputers, where word lengths of 64 bits are used. For example, the Motorola 68000 is a 16 bit I/O machine (32 bits are used internally) and would compose only one bit-slice portion of a multi-chip processing element were it used in a supercomputer. This is changing, however. The new HP microprocessor is a full

32 bit machine on a single chip, yet is only a nominal $1.0\mu\text{m}$ technology. When full VHSIC capabilities are achieved, one can readily conceive of 64 bit machines on a single chip with nominal minimal dimensions of $0.5\mu\text{m}$ or less.

We can therefore conceive of a 64 bit, single chip microprocessor with on-board memory. This latter requirement is crucial if speeds are to be increased. It is necessary to have not only the quick access local register stack, but also the intermediate cache memory on-chip. Thus, only large block data moves are made at slower off-chip time limitations. In future sub-micron technology, such a chip will probably remain at today's 1cm^2 area dimension, yet will be powerful enough to serve as the processing element itself.

The requirements of electromagnetic propagation across the chip suggest that delay times as large as 100 psec can be encountered, so that clock speeds of the order of 3 GHz are the upper limit that can be used on this size chip. This then becomes a primary limitation on future VLSI. At this point, we have to ask whether we can expect to achieve this speed by extrapolating current devices. In doing so, one can utilize results obtained in ring-oscillator circuits. However, one must be aware that ring-oscillators are analog devices with very little inter-stage load capacitance. On the other hand, delay times in logic circuits are limited by inter-stage nodal capacitance³. Consequently, ring-oscillator results must be 4-5 times faster than that expected in logic circuits; i.e., delay times

of 20-25 psec are required for the above microprocessor. The status of current laboratory (experimental) technology follows:

Bell Telephone Laboratories⁴ has pushed Si MOSFET technology well into the submicron region. Measurements on ring-oscillators, in which devices had effective gate lengths $L_g=0.3\mu\text{m}$, indicated that delays of 30 psec were achievable. However, scaling arguments of Chatterjee⁵ and analyses by Ferry³ indicate that this may be the limit on speed in Si, and clock rates of 3GHz are at or beyond the capabilities of Si (1-2 GHz should be achievable however).

Hughes Research Laboratories (HRL)⁶ has achieved delay times of 34 psec in ring oscillators of GaAs depletion-mode MESFET logic. Scaling laws are expected to hold here, and GaAs logic should meet the required speed with $L_g = 0.25-0.4\mu\text{m}$.

HRL⁷ has also achieved delay times of 120 psec in InP MOSFET ring oscillators. While these results are new and there are little data on the limitations to scaling in these devices, it is expected that this technology can meet the required speed with $L_g=0.5\mu\text{m}$.

Thomson-CSF (France)⁸ has achieved 15 psec delay times in ring oscillators fabricated by modulation-doping in GaAs/GaAlAs MBE technology for $L_g=1.0\mu\text{m}$. Clearly this technology appears to be capable of the required speed.

We caution however that only Si has been demonstrated in VLSI. Considerable materials development is required before the other technologies are ready, although these technologies offer

both speed and lower power advantages. The payoff however is large. Whereas, currently proposed supercomputers seek 10BIPs, the super-microprocessor based system should achieve in excess of 1000 BIPs.

These considerations lead to the following conclusions concerning supercomputers. First, the demands of very high functional speed ($>1000\text{BIPs}$) requires the largest possible degree of parallelism, both in the system and within each chip. Secondly, however, limitations such as the vaunted "Amdahl's law" and the need for very-high speed front-end processing require that the highest possible speed be achieved within a single processing element. What is required therefore is a supermicroprocessor chip that is 1 cm^2 in size and is at the $0.25\text{-}0.5\mu\text{m}$ gate length technology. We emphasize that the speeds envisioned here appear to be beyond the extendable limits of Si VLSI. As a result DARPA must have a program in emerging materials technology to support this growth. There are a number of key areas that should be addressed in such a program; some of these are:

- * An investment in intermediate GaAs technology for high speed, low power integrated circuits to start the application of their technology to LSI. Pilot-plant production of such devices should begin as soon as possible.
- * A longer range program to develop supplementary and very high speed, low power devices and technologies (e.g. HEMT, InP MOS, and heteroepitaxial devices).

- * A clear role for materials science to support these technology programs and to explore possible future directions. This program should also address key questions in the areas of contacts and interconnections, passivation/activation, contacts, and heteroepitaxy.

ACKNOWLEDGEMENT

This paper was written under the auspices of the DARPA Materials Research Council, Contract #MDA903-82-C-0428 with The University of Michigan.

REFERENCES

1. For general reviews, the reader is referred to:
 - a. R. D. Levine, Sci. Am., January 1982.
 - b. E. K. Yasaki, Datamatism 28(1), 110(1982).
 - c. D. H. Schaefer and J. R. Fischer, Spectrum 19(3), 32(1982).
 - d. R. Bernhard, Spectrum 19(7), 26(1982).
2. R. Keyes, Proc. IEEE 63, 740(1975).
3. D. K. Ferry, Adv. Electron. 58, 311(1982).
4. D. L. Fraser, Jr., H. J. Boll, R. J. Bayruns, N. C. Wittwer, and E. N. Fuls, in ESSCIRC Dig. Tech. Paper, 1981, p. 201.
5. P. K. Chatterjee, W. R. Hunter, T.C. Holloway, and Y. T. Lin, IEEE Electron Dev. Letters EDL-1, 220(1980).
6. P. T. Greiling, F. S. Ozdemir, C. F. Krumm, B. L. Sun, and R. F. Lohr, Jr., in IEEE Electron Dev. Mtg. Tech. Dig., 1979, p.670.
7. M. Clark and C. L. Anderson, private communication.
8. N. T. Linh and D. Delagebeaudeuf, in Proc. of the Workshop on the Physics of Submicron Structures, to be published.

VERY SMALL AND HIGH SPEED SEMICONDUCTOR DEVICES

T. C. McGill, D. K. Ferry, H. Ehrenreich & R. S. Bauer

INTRODUCTION

The continued development of new epitaxial growth techniques and high resolution lithography has led to the development of several semiconductor devices which have one or more submicron dimensions. As device dimensions are reduced, it becomes possible to pack more devices on a chip, to achieve higher integration levels, and to operate the devices at a higher speed, whether for logic or for microwave applications.

In a previous section, for example, the feasibility and requirements on device speed were discussed in regard to a supercomputer-on-a-chip, the super-microprocessor. It was found, in that discussion, that one generally needs lateral dimensions well below a micron and speeds of 3GHz were expected. To achieve these goals will require a considerable step forward in understanding of the devices and materials, as well as in fabrication technology. This remains true whether the devices are used for the entire microprocessor or just for the high speed front-end processors, such as analog-to-digital conversions and signal processing.

On the other hand, it is also possible to utilize the submicron-dimensioned devices to move to higher frequencies in applications as microwave sources. In most cases, devices operating above 20 GHz are limited by transit-time effects. To

achieve the development of phased-array radars in the 100-300 GHz region requires the development of sources well beyond current capabilities.

In view of these considerations, the MRC hosted a three-day meeting in which the general status of materials, devices, and modeling was discussed. The program and list of attendees are attached. It was the goal to utilize this meeting as a base upon which to build further considerations on the areas of very small and high speed devices. To this end, we present in the following a synopsis of the various presentations and discussions that occurred and then present general observations and recommendations about the field.

MEETING HIGHLIGHTS

Analysis of High Speed Devices

The first day of the meeting included a technical discussion of the methods for analyzing very small ($<0.5\mu\text{m}$) and very high speed ($<2\text{ps}$) devices. Device modeling plays a very important role in this field, in that it provides a method of evaluating the performance of a given device structure without going through the rather expensive (and time consuming) effort of fabricating the device. Even after a device has been fabricated, it is relatively difficult to determine all that is occurring in the physical device, unless modeling is utilized. Hence, the device simulation programs also provide us with methods of understanding the measurements on a physically realized device.

The session began with a discussion by Professor D.K. Ferry (Colorado State University) of some of the difficulties in treating the transport in the very small and very fast devices. The general problem is that for small devices, the standard transport models that have been used for analysis begin to break down in this regime. For example, in GaAs, the velocity is not simply related to the applied electric field since the carriers do not have the opportunity to establish a steady-state in the time that is required to transit the device. This leads to new phenomena, such as velocity overshoot involving the transport in the channel. Ferry and co-workers have developed a suitable approach to this problem, which has been used to analyze the performance of various proposed device technologies. They conclude that there are substantial advantages to using technologies based on the III-V materials as far as speed and power possibilities. These include both metal-electrode-semiconductor-field-effect transistors (MESFET) and metal-oxide-semiconductor-field-effect transistors (MOSFET). Using these standard device configurations, frequencies as high as 20GHz could be realized in logic circuitry. These calculations include the effects of realistic values for the nodal capacitances and are not simply ring-oscillator results. The devices fabricated using III-V semiconductors can be substantially faster (about a factor of 3 to 10) than those currently made with Si MOSFET technology. In order to reach these higher performances, the devices must be operated in the so-called "velocity-overshoot" regime.

Professor Ferry also discussed the behavior of systems composed of interacting devices. For example, there is considerable discussion on the use of highly parallel systems based on arrays of microprocessors, which are generically equivalent to arrays of devices. Yet, very little attention has been paid to the questions of stability or instability of such systems. Physically these systems look very much like the discrete version of partial differential equations that can produce unstable solutions. These interactions, particularly in device arrays, may make possible new systems such as associative memories or whole new classes of devices and circuits.

H. L. Grubin (Scientific Associates, Inc.) gave a presentation on his simulations of the transport in various device structures. His studies include the effect of inhomogeneities in the doping profile. From his studies, he concludes that to attain three terminal devices that can perform at frequencies greater than 100GHz, it will be necessary to achieve strict control of the distribution of the carriers that are injected into the gated region of the device and may require materials with substantially different transport properties from those currently under study.

K. K. Thornber (Bell Laboratories) discussed some processes that may limit the performance of high speed devices. The major conclusion of his talk was that we must pay attention to the spreading of carriers in the packet of charge that is transiting the gate region of devices, as the presence of

velocity dispersion introduces additional broadening of the charge packet. Some of the basic results of his theory have been verified at Bell Laboratories. To illustrate the importance of this phenomenon, he gave an example of a Si MOSFET with an oxide thickness of 20nm, a gate voltage of 1.0V, and a tangential electric field of 40kV/cm. This leads to a minimum time interval of 12ps for the transfer of a 1 μ m wavepacket (a time very close to the minimum time that has been observed in Si MOSFETs). He also stressed the importance of using transport coefficients that are appropriate to this high frequency regime. Diffusion, as well as the velocity, of the carriers for very small and fast devices could be substantially different from the values used in current devices.

P. A. Blakey (University of Michigan) presented a perspective on high-speed, three-terminal devices achieved from the modeling of two-terminal devices (i.e., microwave diodes). He stressed the importance of obtaining self-consistent studies of new device configurations. In particular, he indicated that the contact and control mechanisms are crucial to the operation of microwave devices. The planar-doped-barrier transistor (PDBT), the permeable-base transistor (PBT), and other so-called "ballistic" transistors are all thought to be space-charge limited. From his calculations, he concludes that microwave diodes may operate up to 400GHz, but three-terminal transistors could well be limited to 60 GHz.

Proposed Devices:

On the second day, a discussion on specific proposals for a variety of devices and the results that have been obtained so far was held. The discussion started with Professor H. Kroemer (University of California, Santa Barbara). He described a number of ideas for the use of heterojunctions to improve the performance of devices. In particular, he described the modulation doped high-electron-mobility transistor (HEMT), which makes use of a GaAs-GaAlAs heterojunction to produce an undoped channel in which the electrons have a very high mobility. Based upon results reported by groups working in Japan and France, this device currently holds the record (15 psec at 300K) for speed in a ring-oscillator configuration. He also indicated that heterojunctions may have a very important impact on the trade-off between bipolar and field-effect transistors. The heterojunction technology makes possible some very novel new device configurations for bipolar transistors, such as dense, integratable emitter-coupled logic (the technology currently used in the Cray I). The recent advances in preparation of thin layers by molecular beam epitaxy (MBE) and chemical vapor deposition (CVD) make it possible to envision the manufacturing of large numbers of heterojunction devices that could have very substantial performance advantages over the currently used homojunction technologies. Here, the primary gain is achieved by using wider band-gap materials for emitters and possibly for collectors as well.

M. Heilblum (IBM) discussed the current status of the IBM work on the ballistic hot electron transfer amplifiers (BHETA). Following up on a suggestion originally made by C.A. Mead, he is attempting to revive the use of metal-insulator-metal-insulator-metal (MOMOM) transistors. In this device, the control of the charge is obtained by tunneling through thin insulating films between two metals. Heilblum has proposed a number of new versions of this device based on the currently available technologies of MBE, and is assembling a system to fabricate these devices. Theoretical projections suggest that these devices could operate at frequencies extending into the infrared.

Professor L. Eastman (Cornell) reported on some of his recent results on obtaining ballistic transport in small devices. Again, these devices are extensions of the Mead suggestion to semiconductors. The major idea in this approach is that under certain situations, where the carriers are not allowed to become too hot, the carriers can behave as if they are moving in a ballistic fashion, and hence, attain average velocities that are thought to be as high as 5×10^7 cm/sec. These speeds translate into a response time of less than a picosecond for $0.1 \mu\text{m}$. He has explored a number of structures in an attempt to exploit this phenomenon. These structures include the planar-doped-barrier transistor (PDBT) and the vertical-ballistic-electron transistor (VBET). Eastman's group has made measurements on some of these structures at very low frequency and conclude that

the characteristics of the devices are consistent with what one would expect for ballistic transport.

The permeable-base transistor (PBT) was described by W. Lindley (Lincoln Laboratories). This device is basically a solid-state analog of a triode vacuum tube with the transport occurring through GaAs with the control being carried out by a grid of W electrodes embedded in the GaAs. His projections indicate that this device could operate at frequencies as high as 500GHz. However, performance has been limited to the 100GHz range so far. The primary problem seems to be the preparation of GaAs with the proper properties in the region between the gate electrodes that form the "grid".

Professor D. S. Pan (University of California, Los Angeles) gave a presentation on one of his new ideas for overcoming some of the limitations that currently exist on microwave diodes. Pan proposed a superlattice-like structure consisting of layers of Ge interspersed with layers of GaAs. This structure could be used as distributed microwave source that would result in a device that could yield power at very high frequencies and that could not be obtained in other ways. The principal message was that the new technologies that are becoming available make it possible for us to consider entirely new concepts for devices through the use of microstructural fabrication.

Materials:

Most of the devices discussed here push the current materials technology to its limit. Hence, we had two talks to identify some of the major materials issues. The first was by P. Petroff (Bell Laboratories). He indicated that interfaces and the methods of growth were essential to the fabrication of these devices. Defects, strain, and clustering of constituent atoms could affect the performance of the devices. Not all conceivable heterostructures can be fabricated, since the growth may be subject to various types of instabilities that will lead to highly inhomogeneous materials. He appealed for measurements to formulate surface phase diagrams which could be used to discuss the growth mechanisms.

G. Woodall (IBM) presented some insights about the requirements on materials and processing for attaining a successful high-speed device technology. In the long run, we must have a technology that will allow us to treat large areas with high yields. He highlighted several critical areas in the field of materials preparation. These included: substrates; ion implantation; Schottky barriers; ohmic contacts; MBE defects, impurities, and doping control; and passivation. While substantial progress has been made on a number of these fronts in the last few years, few are solved at the levels required for inclusion in a device technology.

HIGHLIGHTS OF THE DISCUSSION

At the conclusion of each day's presentations, a round table discussion was held. The first day's discussion centered on the questions associated with device modeling. It was emphasized that many of the parameters that are important in device modeling are not very well known. In particular, we do not know the values of some of the scattering matrix elements and features of the band structure that govern the transport. Hence, the models are somewhat qualitative. We also do not know the boundary conditions (contacts) for the injection of charge into the gate or channel regions. The importance of examining the limits due to charge spreading was also re-emphasized. It was further emphasized that device modeling can act as a guide in the development of high speed devices.

The discussion at the end of the second day centered on the heterojunction devices proposed during the day. In particular, the issue of the determining factors for the band structure transition in going from one semiconductor to another (the so-called band offsets) was discussed. These properties play an important role in determining the performance of various heterostructure devices. Other critical interfacial properties include the role of defects, electromigration, and the stability of the interface. The importance of using a fully self-consistent analysis of the proposed high speed devices was emphasized, as the high-frequency behavior of these devices could well be limited by space-charge limitations. It seemed to be

concluded that the proposed high-speed devices that are based on ballistic transport could only result in low power devices. The precise details of the shapes of the depletion regions and transport in these areas, was identified as a problem in some of the high speed devices and should be looked into.

The round table discussion on the third day returned to the question of heterojunction devices and further materials considerations. Control over the injection of charge by using heterostructures looks very promising, although there are problems associated with the growth of the heterostructures and this was identified as an important area for future study. The promise of using distributed sources to obtain microwave power was discussed and it was concluded that some serious thought should be given to this possibility. There remains a question as to the manufacturability of any of these advanced technologies, and, it was concluded that we may have quite a way to go in this area. Work is still needed in the area of substrates and materials control as well. Yet, given the very limited experience with production of even GaAs devices, it is difficult to assess the overall limitations that may be imposed by the materials and processing.

PERSPECTIVES

In this section, we want to draw together ideas and conclusions that were obtained as they relate to very small or very high speed devices. Foremost are material considerations, since

the argument, as always, is whether an alternative to Si exists and, if so, which material best supplements the capabilities of Si. In the logic area, this is perhaps easier as it is clear that we cannot continue to scale Si indefinitely. Rather, as was pointed out earlier, it is reasonable to assume that Si will be limited to the 1-2GHz range. Several of the III-V materials, notably GaAs and InP, offer the advantages of higher speed at the same dimensional scale as Si, if overshoot effects can be effectively utilized. GaAs MESFET technology is very promising, and a sizable investment in this area has already been made. InP is especially promising as a follow-on technology to GaAs, as it is an MOS technology that is circuitry compatible to current Si architectures.

There is a temptation to pursue InGaAs, lattice-matched to InP, as a promising material. Caution should be exercised here, as little is known of the upper conduction band structure. Uncertainties in the band structure, which strongly affect the v-E curve at high fields, were not included in the early Monte Carlo results, so that its attractiveness may be limited to its higher low-field mobility. Moreover, the ternaries and quaternaries are substantially more prone to clustering and inhomogeneous growth peculiarities. It is essential that an understanding of the properties of this material be sorted-out prior to any major commitment.

Microwave Sources:

Devices such as the GaAs permeable-base transistor (PBT) hold considerable promise for very high frequency sources. Even though the modeling programs suggest that the devices are space-charge limited, this is not a real drawback. Indeed, it supports the contention that these are solid-state analogs to the vacuum triode, and the results obtained to date (20GHz f_T and projection of oscillations to 100GHz) are not incompatible with results predicted by a high-frequency triode model (when modified for collisions). In smaller structures, use as a source to several hundred GHz should be achievable. It is apparent, however, that obtaining high overshoot (or "ballistic") velocities is critical, so that Si devices are not likely to exceed a few tens of GHz.

The hot electron transistors, such as planar-doped-barrier transistor or the metal-oxide-metal-oxide-metal structure, are not as well developed. However, space charge could affect their performance and should be considered. Good, self-consistent field calculations, using realistic transport equations, need to be carried out for these devices.

Modeling:

It is clear that good modeling approaches which feature full two-dimensional self-consistent field approaches and include accurate transport equations are now feasible. The importance of accurate transport equations is illustrated by the charge spreading arguments. The presence of charge spreading

has been known in velocity dispersive media for some time, and while the presence of non-Gaussian charge packets and long-time tails has been recognized in Monte Carlo calculations for semiconductor devices, the significance of these factors in modern semiconductor devices has not been fully appreciated. The simple, intuitive arguments presented by Thornber clearly indicate that this effect can be very significant in small devices. It also seriously brings into question time-of-flight measurements used to infer the diffusion constant by charge packet spreading.

The interaction of devices assumes considerably more importance as the dimensions shrink into the submicron regime. It is important that modeling not be constrained to a single device working in isolation. The feedback mechanisms of inter-device interactions must be understood. Indeed, cooperative effects within arrays of devices may hold promise for new device phenomena.

Heterostructures:

The use of molecular-beam epitaxy and metal organic CVD to grow artificial structures composed of multiple thin layers is one of the truly exciting frontier areas in solid-state electronics. Clearly, the importance of heterojunction structures is well recognized, but the possibilities of engineering artificial structures with unusual energy dispersion characteristics should not be overlooked. Yet, we are approaching this area with little fundamental knowledge. Such crucial information as two-dimensional phase diagrams, kinetic coefficients, clustering

tendencies, or interfacial understanding, either electronic or chemical, are vast voids of understanding.

RECOMMENDATIONS

It remains clear that many materials questions, problems, and opportunities remain. In future applications for high-speed processing and for microwave sources, much work must still be done. Based upon the presentations and summaries above, it is our feelings that DARPA should adopt a stance that maintains a major program in this area. The discussions indicate that out of this field will evolve a device technology which could have major military implications in the 1990's and beyond. The development of systems utilizing any one of the major opportunities mentioned in the introduction would justify the entire program.

There are a number of key areas that should be addressed in such a program. Some of these are:

- The design of new devices and the exploration of new device concepts that could have major impact in any one of these fields.
- The investigation of important material properties that are key to the production of these devices. Such a program should include the investigation of the mechanism for growth of heterostructures, as well as, the properties of the heterostructures such as band offsets, interfacial structure, thermal properties, defects, and band structure parameters.

- The investigation of the limits on high speed device operation. This would include the role of charge spreading and various transport mechanisms.
- The actual operation of devices at high frequencies to assess their performance without the need of extrapolating low frequency characteristics to high frequency.
- The continuation of efforts in device modeling that include realistic treatments of transport, self-consistency, and boundary and environment effects.

ACKNOWLEDGEMENT

This paper was written under the auspices of the DARPA Materials Research Council, Contract #MDA903-82-C-0428 with The University of Michigan.

VERY SMALL & VERY HIGH SPEED DEVICES

JULY 12, 1982

NAME

Dee-Son Pan	Univ. of CA., Los Angeles
Peter Blakey	University of Michigan
Sven Roosild	DARPA/DSO
J. Woodall	IBM
P. Kroemer	Univ. of CA., Santa Barbara
Bob Bauer	Xerox
Lester Eastman	Cornell University
Dave Ferry	Colorado State University
Larry Cooper	ONR
Hal Grubin	Science Research Associates
Harry H. Wieder	Univ. of CA., San Diego
George Vineyard	BNL/MRC
P.A. Wolff	MIT
Mark S. Wrighton	MIT/MRC
Elliott Levinthal	DARPA
H. August Macleod	University of Arizona
Henry Ehrenreich	Harvard/MRC
Bill Lindley	MIT Lincoln Lab
Ed Hucke	University of Michigan
William B. Bridges	Caltech
Karvel Thornber	Bell Labs
John Hirth	Ohio State University
E.C. Van Reuth	DARPA
Richard Reynolds	DARPA
M.J. Sinnott	University of Michigan
Tom McGill	Caltech

MATERIALS RESEARCH COUNCIL MEETING
ON
VERY SMALL AND VERY HIGH SPEED DEVICES

JULY 12-14, 1982

Monday, July 12, 1982

I. INTRODUCTORY SESSION

<u>SPEAKER</u>	<u>TITLE</u>
R. A. Reynolds (DARPA)	DARPA's Program Needs in this area
S. Roosild (DARPA)	Very High Frequency Device Program
L. Cooper (ONR)	USER Program

II. BASIC CONSIDERATIONS

D. K. Ferry (CSU)	Fundamentals of and Limitations on High Speed Devices
H. L. Grubin (SRA)	Device Simulations
K. K. Thornber (BL)	Charge Spreading as a Fundamental Limit on High Speed Devices
P. Blakey (U.Mich.)	mm-Wave Devices
	Round Table Discussion

Tuesday, July 13, 1982

III. NOVEL DEVICES & STRUCTURES

H. Kroemer (UCSB)	Novel Heterojunction Devices
M. Heiblum (IBM)	Novel High Speed Devices
L. Eastman (Cornell)	Recent Results on High Speed Devices
W. Lindley or A. Murphy (Lincoln Labs)	The Permeable Base Transistor
	Round Table Discussion

VERY SMALL & VERY HIGH SPEED DEVICES (CONTINUED)

Wednesday, July 14, 1982

III. NOVEL DEVICES & STRUCTURES - CONTINUED

<u>SPEAKER</u>	<u>TITLE</u>
D. S. Pan (UCLA)	Novel Structures as Sources

IV. MATERIALS

P. Petroff (BL)	Structural Inhomogeneities in III-V Alloys
G. Woodall (IBM)	Materials Preparation
	Round Table Discussion
	Summary & End of Meeting

DIAGNOSTICS FOR VLSI SEMICONDUCTOR DEVICES

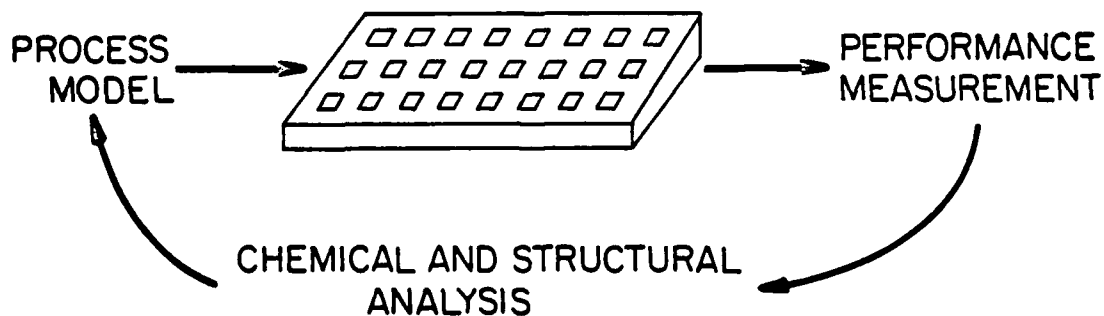
R. S. Bauer and T. C. McGill

INTRODUCTION

As integrated circuit technology continues to evolve, the overriding factor controlling the devices and processing is the extreme tolerances required to achieve effective operation of millions of electronic material regions. The Materials Research Council considered the limitations of current analytic tools in providing the necessary window on impurity concentrations, doping profiles, lateral dimensional tolerances, and non-destructive chemical speciation. To provide an overview of the vastness of the problems in microanalysis, we will take a simplified view of the VLSI development process and present examples in current GaAs and Si technologies.

A key feature required for understanding and controlling of integrated circuit (IC) processing is the microanalysis of device features which influence circuit performance. IC development can be decomposed into the following steps:

FABRICATION



This diagram illustrates the crucial role that analysis and understanding provide for what the process models actually produce. In a systems sense, without the positive feedback provided by microanalysis, the VLSI technology process can become unstable.

To understand why microanalysis can be so fundamental to VLSI development, we must distinguish among the various regions affecting electrical behavior. It is clear that as dimensions of devices are reduced, we must be able to measure and analyze material regions whose lateral size becomes much less than $1\mu\text{m}$. Current GaAs permeable base transistors (PBT) contain channels 1600\AA wide and of $0.25\mu\text{m}$ Si MOSFET's channel length have been studied in the laboratory. One important question to explore is how we will determine chemical and structural characteristics over these sorts of lateral dimensions.

There is the separate question of our ability to detect impurities and imperfections at very low concentrations in bulk substrate material or introduced unintentionally during processing. As devices become very small, the sensitivity of individual VLSI elements to fluctuations drastically affect yields and operation of circuits requiring extreme uniformity (e.g., A/D converters). In the case of Si integrated circuits, transition metal impurities are known to "poison" a process line. There is new evidence that Cu and Fe at average densities in the 10^{11} - 10^{12} cm^{-3} range can kill device lifetimes. It becomes an enormous problem to determine when degradation is caused by such ex-

trinsic centers. Luminescence and deep level transient spectroscopy (DLTS) are capable of detecting foreign levels in the band gap, but chemical identification depends on prior studies using standards containing known impurities. Chemical analysis procedures, such as secondary ion mass spectroscopy (SIMS) provide, at best, a detection level down to 10^{14} - 10^{15} cm⁻³ with a dedicated spectrometer. Perhaps most revealing, the process and device models do not incorporate these deep traps or account for impurity-impurity interactions which may lead to density fluctuations. This makes it impossible to use the computer simulations in a reverse analysis mode to track down the origin of reduced carrier lifetime.

In bulk material, similar fluctuations in small concentrations of deep levels can destroy performance. GaAs MESFET's work on the principle that the metal electrode can turn off conduction in a doped semiconductor layer by applying a voltage relative to the semi-insulating GaAs substrate. The high resistivity of the substrate material is produced by a deep level designated as EL2. The origin of EL2 is not known. If it is a native defect, such as an anti-site location in the lattice or complexed with a vacancy, then direct analysis will be very difficult. Its stability during processing and the role of background impurities can lead to fluctuations at the active layer/-substrate interface which prevent device turnoff when a potential is applied to the metal electrode. Again in this case, the

concentrations of such species as $\sim 10^{14} \text{ cm}^{-3}$ Mn in bulk GaAs, push the detection limits of our analytical tools.

To explore the application and limitations of current analytical concepts to problems such as these, a meeting was held for Materials Research Council members. On July 15, twenty scientists and engineers met to consider the state-of-the-art and identify critical needs for development of diagnostic tools. A copy of the agenda and list of attendees is appended. We conclude that new analytical concepts and combinations of highly sophisticated tools are required for controlling VLSI electronic technology.

MEETING HIGHLIGHTS

The MRC meeting on this topic was organized by Professor T. C. McGill of Caltech and Dr. R. A. Reynolds of DARPA. Six talks were presented encompassing a range of issues in VLSI analysis. This section will highlight on a topical basis, the major points discussed during the meeting.

DARPA Requirements - R. A. Reynolds (DARPA):

In considering the problems of analysis, a view of DARPA's near-term "future" requirements are embodied in the permeable base transistor (PBT). As being developed at Lincoln Labs, this device derives its properties from a buried W grid in a uniformly doped n-GaAs layer. The channel controlling electrical activity is about 10^{-10} cm^2 in area. To characterize the high speed electron transport, one should resolve the impurity

concentrating with a 10-50Å depth resolution. This translates into an analytic volume of only 10-50 ata-cc's (i.e., $1-5 \times 10^{-17}$ cm³). Consider then a region of the material containing only a total of 500-2500 atoms. Even if our analytic technique could detect a single impurity atom in such a small region, we would be characterizing concentrations of 2×10^{16} cm⁻³ in the GaAs. Reynolds pointed out that a minimum detection of, at least 10^{15} cm⁻³ or 20 ppb are required to analyze the fields and concomitant high frequency switching of a PBT currently doped at 10^{16} cm⁻³. This order-of-magnitude discrepancy in ultimate capability versus analytic need translates directly into similar Si shortfalls for VLSI circuits.

Process Modeling - T. Thurgate (INTEL):

The current state of Si IC technology development begins with a one-dimensional process model (SUPREM) developed at Stanford under DARPA support. When coupled with a one-dimensional device model (SEDAN), the procedure for inventing new processes involves circuit fabrication and performance measurements which critically depends on the detailed experimental microanalysis used for the empirical modeling upon which the SUPREM program is based. From Thurgate's presentation, it was learned that in the simulation of MOS processes for 1-2µm devices, years transpired between process step initiation to implementation in the product line. It also was clear that months of running split lots of Si wafers are saved by using such models. However, if an unusual failure occurs or a new

technology is desired, but is not included in the existing programs, a purely empirical approach is often taken.

In the discussion, it became clear that the reliance on process models will increase for both design and failure analysis as device requirements become more stringent. In turn, this was seen as possibly limiting innovation. The knowledge embodied in the extensively tested SUPREM program serves as the effective catalogue of processing steps available to the engineer. Further, the process line itself must be controlled within the parameters used to develop the models. Within these limitations, pushing VLSI technology to dimensions in the $0.5\mu\text{m}$ range does not present unmet demands on current models.

Non-Destructive Imaging - P. Petroff (Bell Labs):

The use of electron probes for microscopy and associated analysis offers one of the broadest spectrum of capabilities of any technique. In a wide ranging presentation, Petroff summarized some of the elegant work that has been done, both on the atomic level and at the micron level of resolution. One particularly important example of transmission electron micrograph results was the observation of bulk and interface dislocations in III-V LPE material. A substantial clustering of defects around dislocations was shown to be enhanced by device operation (in that case $\text{GaAs-Ga}_x\text{Al}_{1-x}\text{As}$ laser diodes).

The ability to image a small portion of a sample and then conduct chemical analysis on a specified portion is a rather unique advantage of probes that produce charged particles.

While ion probes can be used in such a mode, electron stimulated imaging produces both direct secondary electron "pictures" and diffraction images of extraordinary detail. It is difficult to directly understand chemical contrast results from the interference of primary and scattered electron TEM beams. In order to properly interpret such "photographs", computer simulations of the proposed structure on a $\sim 10\text{\AA}$ scale must be carried out. The ability to then use the electron loss spectroscopy (ELS), auger electron spectra (AES), or energy dispersed x-rays (EDX) for chemical analysis provides a powerful analytic approach to device materials problems.

Most of the techniques which are used for chemical analysis require destruction of the sample during testing. If the speciation can be obtained by a coordination of different techniques, then non-destructive probes offer some novel capabilities. Deep level transient spectroscopy (DLTS) and luminescence measurements provide routine detection of impurities and defects down to the $\sim 10^{13}\text{cm}^{-3}$ level. These can be combined with a scanning TEM to produce a map having a few microns lateral spatial resolution (for cathodoluminescence and scanning DLTS). The truly powerful results using these techniques have come when levels were first identified in other experiments, such as optical studies, employing standards containing higher concentrations of the suspected center. With this background information, DLTS provides the capacity to localize the impurity/defect level in the band gap, to determine its depth from the free surface/-

electrical interface, and to quantify its concentration in a non-destructive manner.

Detection Limits for Impurities - H.W. Schmitt (Atom Sciences):

Throughout the development of VLSI devices, there has been a continuing discussion of the need for characterizing and controlling the starting substrate material. This concern is present for Si, as well as the III-V materials. In Si IC's, for example, yields are profoundly affected by changes in the background oxygen concentration in the substrate material because of significant defect and impurity gettering during processing. It then was very intriguing to hear about the one part per trillion (1ppt) routine detection level claimed for resonance ionization spectroscopy (RIS).

The basis for this new analytic technique is the selectivity relative to "background" atoms obtained by laser pumping at resonant ionization levels of the desired element. With the exception of He and Ne, all atoms of the periodic table can be excited with a unique set of one and/or two photon transition energies. Schmitt claimed that with a "shopping list" of possible species, only five minutes was required to determine if an element was present at concentrations of $5 \times 10^{10} \text{ cm}^{-3}$ (i.e., 1 ppt).

The volume analyzed and time for a complete characterization are limited by the initiation process and set-up time for changing laser dyes. In the configuration discussed, a pulsed Ar^+ ion beam is used to create a vapor of 10^{10} atoms per pulse

in synchronism with the 30Hz repetition rate of the analyzing laser. The volume consumed for analysis of each element was said to typically be only about 7% of a monolayer of atoms over a 2mm diameter spot. This must be multiplied by the number of elements to be analyzed and the apparent inefficiency in laser excitation of only a portion of the atom vapor "cloud". The first promise for this technique (over something like SIMS) is in bulk analysis where the laser selectivity provides a detectivity advantage without concern for spatial resolution.

Dopant Profiles - C. Evans (C. Evans & Associates):

Charles Evans provided a comprehensive review of many materials characterization tools. Emphasis was on direct chemical analysis where lateral and depth resolution were prime considerations in determining detection limits. This proved to be a very provocative way to approach analysis of devices. For example, it was pointed out that for characterization of features in the $1\mu\text{m}$ range, a $10\mu\text{m}$ probe is as "useless" as a 1cm , broad area technique. X-ray photoelectron spectroscopy (XPS) is one such case because of $100\mu\text{m}$ to 1mm minimums for the area of the x-ray illuminated spot.

Only a few techniques currently allow chemical analysis on the submicron scale. Energy and wavelength dispersive x-ray spectrometers and an SEM or TEM are presently limited to $1\mu\text{m}$ lateral and in-depth resolutions. As Petroff also pointed out, electron energy loss spectroscopy (EELS) coupled with a TEM could yield elemental analysis with resolutions comparable to

the probe size of 3-30Å. State-of-the-art scanning auger microscopes (SAM) have 500-1000Å lateral resolution, with depth sensitivities in the 50Å range when sputter profiling is employed.

Many of these techniques require dedicated instruments. SIMS is a good example of a probe which has been commercialized as both a stand-alone tool and as an add-on attachment. In the former, the sputtering is optimized to a 0.3-0.6µm spot (with 50-200 Å depth resolution). As an accessory, 100µm Ar⁺ ion beams are typical and detection limits can be five orders of magnitude less than O₂ or Cs excitation.

When one attempts to characterize dopant levels over submicron dimensions, the analysis volume becomes so small that detection limits may prohibit obtaining chemical analysis. Evans showed that in a hypothetically optimized system, the minimum practical doping concentration that could be detected with a 200Å probe depth in a 0.1µm device was $3 \times 10^{17} \text{ cm}^{-3}$.

Laterally Resolved Chemical Analysis - R.L. Seigler & W. Parker (Hughes):

Considerable chemical analysis is presently accomplished by ion beam sputtering through the sample of interest. Secondary ions (SIMS), secondary electrons (ion microprobe), or electrons from a separate electron probing beam (ELS, AES) are then analyzed to yield chemical information. The spatial resolution for these techniques is usually governed by the characteristics of the ion source. Considerable advances could be expected from new primary ion beam sources.

Seigler and co-workers at Hughes have been working for a number of years to develop liquid metal ion sources for selective semiconductor doping. Parker reported on the application of these finely focussed ion beams for microprobe analysis. The sources can achieve 1 Amp per cm^2 current density independent of probe diameter in a 10-100Å spot. These characteristics were calculated for both a liquid metal (Ga^+) or a gaseous field ionization (proton) source.

A number of applications were discussed. With such a source, AES or SIMS profiling can be accomplished on the cleaved edge of a wafer. Depth resolution would no longer be degraded by sputter damage in going through thousands of Å of overlayer before the region of interest is uncovered for analysis. For thin doping layers of only a few hundred Å, the ion mixing and knock-on processes can obscure the information of interest.

The major application of these techniques is presently for high resolution ion microprobe imaging. In collaboration with Professor R. Levi-Setti at the University of Chicago, defect structures on a micron scale could be identified by comparison of ion images and secondary electron images.

PERSPECTIVES

In this section, we present ideas on future concepts which evolved as a result of our meeting and discussion. Our foremost conclusion is that analysis of what goes on in the material is no longer an option but is key to the advancement of VLSI technology. Improved control of an "uncharacterized"

process will not work as concentration and dimensional tolerances become more stringent. Examples of current problems in Si VLSI and GaAs MESFET technologies were presented in the introduction. Here we note general limitations that will be imposed if we simply rely on incremental advances of currently available tools. Their spatial resolution and detection limits are summarized in Table I at the end of this chapter.

The present view of how VLSI will be accomplished, takes the premise that scaling present models and technologies will achieve lateral feature sizes in the 1000Å-5000Å range. Even tightened control (through automation) of uncertain processes will not succeed in producing economical yields. A review of the numbers for a MOSFET channel is instructive. For even half micron gates, alignment tolerances for metalizations must be within a few hundred Å of the oxidized Si boundary. The SiO₂ gate insulation will only be ~100Å thick, requiring a compositional and strain uniformity on the scale of a few atomic layers. In fact, at the ~0.1µm gate limits being explored in some laboratories, a defect or impurity concentration of 1ppm (i.e., part per million) represents a single atomic imperfection.

The amount of material intentionally added to the semiconductor for control of device electrical activity will also be on an atomic scale. For the 1000Å gate transistor considered above, a moderate doping of 10^{17} cm^{-3} is achieved by incorporating only 10 foreign atoms below the dielectric region. It

TABLE I
SUMMARY OF LIMITATIONS FOR SOME CURRENT DIAGNOSTIC TECHNIQUES

TECHNIQUE	PARTICLE		SPATIAL RESOLUTION		DETECTION
	PROBE	ANALYSIS	DEPTH	LATERAL	
Transmission Electron Microscope (TEM)	e^-	e^- photons	$\sim 1000\text{\AA}$, image $\sim 1\mu\text{m}$, analysis	$\sim 3\text{\AA}$, image $\sim 1\mu\text{m}$, analysis	$\sim 5 \times 10^{18}$ (with wavelength Dispersive Spectrometer)
Deep Level Transient Spectroscopy (DLTS)	(voltage)	(capacitance current)			$\sim 10^{13}$
Luminescence	photons, e^-	photons	$\sim 1-5\mu\text{m}$	$\sim 1-5\mu\text{m}$	
Secondary Ion Mass Spectrometry (SIMS)	Cs, O ₂ ions	ions	50-200 \AA	0.3-0.6 μm	$10^{14}-10^{15}$
Resonance Ionization Spectroscopy (RIS)	photons (laser)	ions	25-200 \AA	1mm	$\sim 5 \times 10^{10}$
Rutherford Backscattering Spectroscopy (RBS)	He ⁺ ions	He ⁺ ions	25-200 \AA	1mm	5×10^{18} -5×10^{20}
X-ray Photoelectron Spectroscopy (XPS)	photons	e^-	3-25 \AA (50-200 \AA , profile)	1mm	$\sim 5 \times 10^{19}$
Auger Electron Spectroscopy (AES)	e^-	e^-	5-30 \AA (50-200 \AA , profile)	500-1000 \AA	$\sim 5 \times 10^{19}$

follows that fluctuations in low concentrations of unknown impurities ($\sim 10^{14} \text{ cm}^{-3}$) can cause substantial variations in monolithic device performance. Defects in the interface regions can serve as centers for agglomeration of impurities or electron traps which can kill channel conduction. In general then, the small dimensions of VLSI lead to an enhanced sensitivity of circuit performance to structural and chemical fluctuations on an atomic level.

The result of these considerations is that analysis of the origins of device behavior will become a requirement for achieving "standard" VLSI. The requirements on the diagnostic tools will, in turn, be much more stringent than are available today. We will require techniques which can detect fluctuations of atomic concentrations at the few parts per trillion level. This must include a chemical identification of the impurity, as well as the knowledge that unwanted species are present. With greatly reduced volumes controlling electrical behavior, the total amount of material available in the device regions places severe constraints on analytic tools. When doping profiles need to be analyzed to moderate $5 \times 10^{14} \text{ cm}^{-3}$ levels, the total "sample" may contain less than the 10^8 atoms necessary to include a single dopant. Such constraints will place renewed emphasis on non-destructive, in situ techniques.

RECOMMENDATIONS

The thrust for new analytic concepts during the coming decade should be to improve detection of a few particles resid-

ing in a submicron volume. New tools and combinations of techniques offer the most promise.

Detectivity:

The resonant ionization spectroscopy (RIS) provides extremely fine chemical specificity. The interesting feature of this technique is that it can be combined with other dedicated instruments. For example, a pulsed dye laser could be added to a dedicated SIMS to achieve orders of magnitude reduction in unwanted background ion yield. Note that the total signal is not improved by this method, but the specificity of the measurement to the desired element is enhanced. Considerable experimental work, by more than a single group is required to exploit this relatively simple idea. As suggested below, this enhanced ability to detect elements could be exploited on a fine dimensional scale, if advances in initiation sources (e.g., sputtering) are applied to this measurement.

We should emphasize that most of the methods discussed here are destructive in order to obtain chemical identification. DLTS and luminescence measurements provide some of the most sensitive methods for probing small concentrations. In fact, for some centers, such as anti-site defects, they are probably the only techniques which can monitor the presence of important levels. These methods should be pursued much more vigorously for such outstanding questions like the origin and device effect of the EL2 level in GaAs and the pinning centers at Schottky barrier interfaces.

Lateral Resolution:

There have been considerable advances in our ability to study materials on an atomic depth scale. For example, synchrotron radiation has provided non-destructive surface sensitivity of $\sim 5\text{\AA}$ for VLSI interface growth and metallurgy. However, there are only a few methods for achieving fine lateral resolution. Electron microscopy provides spatial information by the fineness of the probing source. However to a large extent, this technique is limited by sample preparation difficulties.

The application of finely focussed profiling sources to otherwise large area analysis techniques deserves increased emphasis. The $1\text{A}/\text{cm}^2$ Ga ion beam source being developed at Hughes provides a 100\AA or smaller spot size for sputtering. The application of this source for SIMS is under investigation. This may be of limited value because standard O_2 and Cs ion beams of $\sim 0.5\text{ }\mu\text{m}$ dimension already provide orders of magnitude enhanced positive and negative ion yields for analysis. However, combined with a laser RIS capability, a single atom detection capability could be exploited over 100\AA cubic volume. Considerable payoff in improved analytical tools could come from longer lived liquid metal ion sources and the availability of a variety of primary ion species.

Again, the notion of combining advantageous features of a number of techniques should be tried. The Nd:YAG laser microprobe offers the promise of a new ablative method for producing a vapor from a sample volume on the order of $1\text{ }\mu\text{m}$ in diameter by

1000Å deep. The present mass analysis is done with conventional SIMS-type analyzers. This same laser initiation technique could be applied to the resonant ionization spectroscopy (RIS) to obtain impurity concentrations in the 10^{14}cm^{-3} range within the minimum possible analytic volume.

Correlated Analysis:

When one considers the affects of fluctuations in numbers of atoms over dimensions of 1000Å and below, it can be concluded that advances in VLSI technology will remain a research issue for the next decade. The input to process modeling provided by materials and device analysis will become increasingly vital to design advances. This observation is borne out by such case histories as the attempt to create semi-insulating GaAs substrates for MESFET technology by intentional doping with Cr. This ultimately was found to be an unfruitful approach, as was found using SIMS measurements. Advances in the materials growth art (viz., LEC pullers) have provided a new avenue for achieving suitable substrate conductivity.

The future mode of analytical research should involve an intimate coupling of materials growth and device processing with the characterization tools. The chemical and structural probing of device changes can best be studied in situ. When impurity or defect fluctuations occur at the 10^{12}cm^{-3} level and degrade circuit performance and device yield, the best method of tracking down the origin of the problem will be by preparing the device in a controlled way and passing it through an inert environment

such as an ultra-high vacuum interlock to an analytic system. These types of PROCESSING-INTERLOCK-ANALYSIS systems are being constructed in a few industrial labs. Most are aimed at understanding and controlling the new device capabilities offered by molecular beam epitaxial (MBE) growth of III-V's. This should become the standard for analysis of Si processing as well.

One must recognize that analytical instruments alone cost in the \$500K range--be it SIMS, SAM, STEM or ESCA. The controlled preparation/processing systems alone cost in the \$300K range--be they MBE or multi-purpose, UHV metal deposition systems. The investment in support and instrumentation to provide such an integrated analytical approach is therefore around \$1M start-up per institution, and \$150-200K operating expenses per year. The level of sophistication of diagnostic tools now demands such expenditures. We believe such a coordinated thrust will be necessary to provide the analytic feedback to process modeling if we are to leapfrog the present VLSI technology to the 0.1 μ m level.

ACKNOWLEDGEMENT

This paper was written under the auspices of the DARPA Materials Research Council, Contract #MDA903-82-C-0428 with The University of Michigan.

ANALYTICAL CONCEPTS FOR VLSI

Thursday, July 15, 1982

Materials Research Council Meeting
Scripps Elementary School
2225 Torrey Pines Road

Introductory Remarks

R. A. Reynolds (DARPA)

Successes and Failures of Process Modeling for VLSI

T. Thurgate (Intel)

Electron Probe Techniques for the Characterization of
VLSI Devices

P. Petroff (BL)

Resonance Ionization Spectroscopy

H. Schmitt (Atom Sciences)

SIMS and Other Techniques for Identification of Atomic
Species in Semiconductor Devices

C. Evans (Evans & Associates)

High Resolution Ion Beams

R. L. Seigler and W. Parker (Hughes Research Labs)

Round Table Discussion

ANALYTICAL CONCEPTS FOR VLSI

July 15, 1982

ATTENDEES

Tim Thurgate	Intel
Bob Bauer	Xerox
T. C. McGill	Caltech
Sven Roosild	DARPA
Charles Evans	Evans & Associates
Mark Wrighton	MIT
Jerry Woodall	IBM
Peirre Petroff	Bell Labs
Bill Lindley	MIT Lincoln Lab
Henry Ehrenreich	Harvard
Paul Raccah	U. of Ill. Chicago
Hal Schmitt	Atom Sciences, Inc.
Jim Parks	Aton Sciences, Inc.
Jack Furdyna	Purdue U.
P. A. Wolff	MIT
Dick Reynolds	DARPA
S. S. Lau	Univ. of Cal, San Diego
A. Yariv	Caltech
R. L. Seigler	Hughes
W. Parker	Hughes

DEVICE SCALING LIMITATIONS ON VLSI DIAGNOSTICS

R. S. Bauer

As devices become smaller and electronic material regions contain less atoms, it is clear that the analysis of small concentrations and chemical fluctuations becomes more difficult. One can calculate the limits of detection from consideration of

- (1) lateral feature size
- (2) depth resolution for useful diagnosis
- (3) efficiency of particle excitation and collection
- (4) transmission of the spectrometer

Now consider standard design rules for device structures. In the case of Si MOSFET technology, very simple relations are used for device scaling.¹ For a device density increase of α^2 , the channel length and width will each be reduced by α . The gate oxide and conduction regions will be reduced in depth by α as well. One then predicts a scaling of the material volume available to the diagnostic tool by α^{-3} . The detectivity however is helped by another feature of the scaling rules. To properly control conductivity, and thereby maintain acceptable fluctuations in threshold voltage for device operation, the doping density in the Si is increased by α . The net analytic signal will then scale as $1/\alpha^2$ as circuit integration increases.

We can then calculate the concentration limits that can be detected by the measurement of a single atom or ion within the device feature of interest. We will consider the size range from current advanced pilot manufacturing to the smallest

research laboratory device objectives. Then for (1) above, we take features ranging from $1\mu\text{m}$ down to 1000\AA . The depth of useful diagnosis, (2), is a maximum of 1000\AA for $1\mu\text{m}$ channel technology. For present diagnostic systems, the combination of (3) and (4) is typically 1% detection of available particles. One then obtains the lowest curve (---) shown in Fig. 1. This line gives the lower limit for the concentration of chemical species or fluctuations in the density of elements that would be observed by single particle detection.

This is the standard type of computation that is normally presented when there are discussions of device materials characterization limits.²

The actual device designs present further restrictions on diagnostic possibilities. If we consider the functional requirements for devices, as much as an order of magnitude less detection will be theoretically possible. We will take two cases to show how device design makes the situation worse than has previously been discussed.

Returning to the Si MOSFET example, a couple of aspects suggest a greater than α^{-2} scaling. First, as the electronic material regions become smaller, the interface between the layers becomes more important.³ Analysis of the abruptness of transition regions and of the location of impurity and dopant levels requires finer depth definition. In addition there are regions where intentional dopant profiling is not the requirement but impurity concentration fluctuations are of interest.⁴

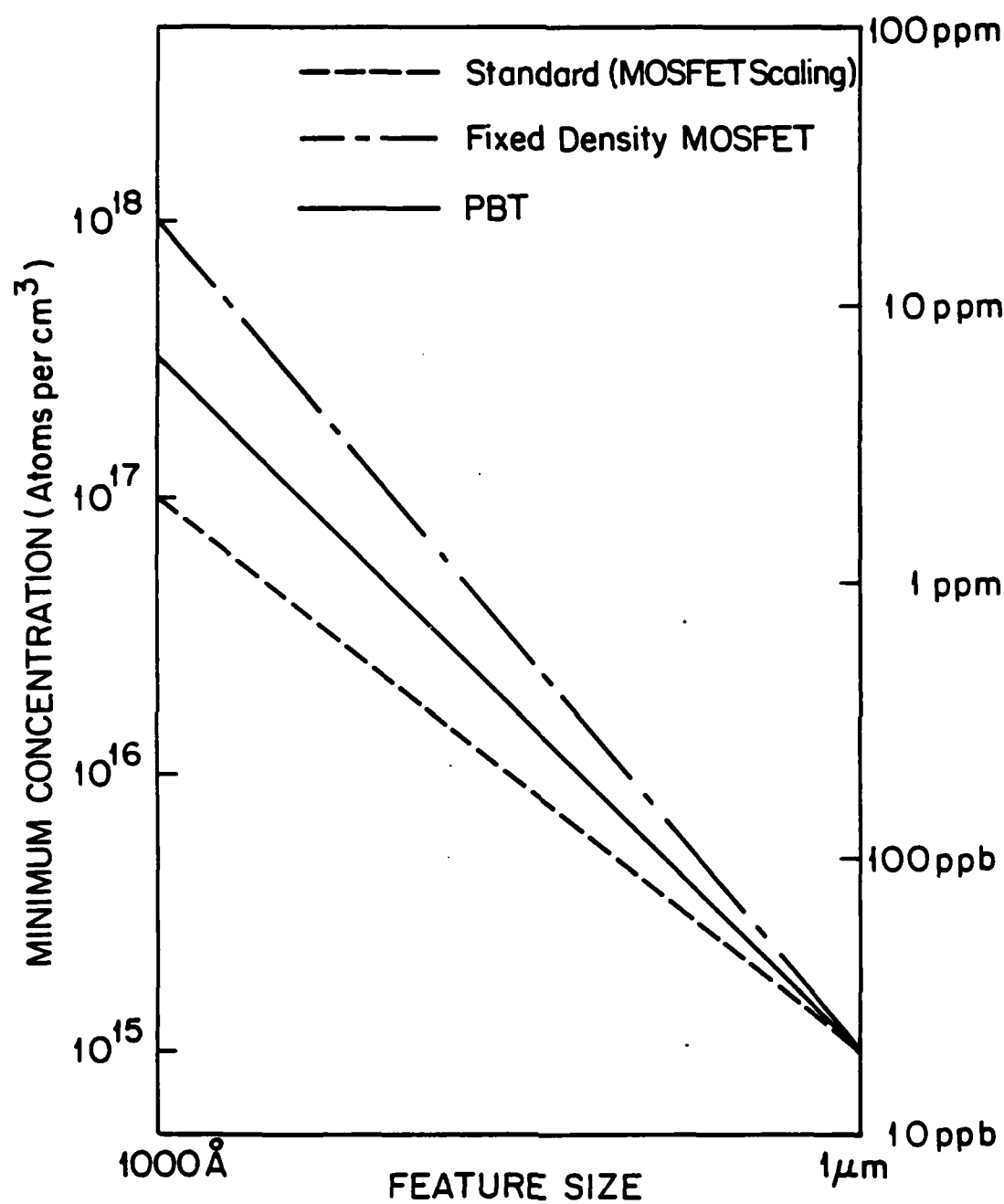


Figure 1. VLSI device scaling limits on single particle detection.

These extrinsic atoms will not be scaled in average concentration as device dimensions are reduced. Both of these considerations independently show that scaling of MOSFET's will more likely cause a $1/\alpha^3$ reduction in analytic signal. The upper line (-----) in Fig. 1 gives this minimum detection limit. Note that at $0.1\mu\text{m}$ feature size, only 10^{18}cm^{-3} concentrations could be measured.

The actual limits for most device diagnoses will probably lie between these two predictions. Take for example the GaAs permeable base transistor (PBT). In that device, a scaling consideration is the impedance of the final structure.⁵ To couple the high frequency power out of the transistor, there must be a match to the external circuit impedance. This presents a different scaling constraint on the device. In the MOSFET case, the channel length was scaled the same as the channel width (i.e., each by $1/\alpha$). For the PBT, reducing the source-drain dimension by $1/\alpha$ would lead to a $1/\sqrt{\alpha}$ reduction in channel length to maintain a constant device impedance.⁵ The net analysis volume will then scale as $\alpha^{-5/2}$. This is shown by the solid line (____) in Fig. 1.

Once again, the same message comes through. In all scaling approximations, the device design causes additional constraints to the useful application of diagnostic tools. For example, we found that it may not be possible to see atoms at levels of interest in $0.1\mu\text{m}$ structures. With peak doping densities of $1-5 \times 10^{17}\text{cm}^{-3}$, these new device considerations may mean

the difference between present spectrometers being useful in VLSI analysis and their not being able to diagnose important fluctuations of electrically active species.

ACKNOWLEDGEMENT

This paper was written under the auspices of the DARPA Materials Research Council, Contract #MDA903-82-C-0428 with The University of Michigan.

REFERENCES

1. R. H. Dennard, F. H. Gaensslen, H-N Yu, V. L. Rideout, E. Bassous, A. R. LeBlance, "Design of Ion-Implanted MOSFET's with Very Small Physical Dimensions," IEEE J. Solid-State Circuits, SC-9, 256 (1974).
2. see for example C. A. Evans Jr. and I. D. Ward, "Overview of Ion and Electron Beam Techniques for the Analysis of Electronic Materials," Proceedings of the Microelectronics Measurement Technology Seminar, O. D. Trapp, ed. (Benwill Publishing Co, N.Y., (1980) p.10.
3. R. H. Dennard, "Technology Challenges for Ultrasmall Silicon MOSFET's," J. Vac. Sci. Technol. 19, 537 (1981).
4. R. W. Keyes, "Physical Limits in Digital Electronics," Proc. IEEE, 63, 740 (1975).
5. D. K. Ferry, private communication (1982).

SCHOTTKY BARRIER INFRARED CHARGE COUPLED DEVICE ARRAYS

T. C. McGill and D. K. Ferry

INTRODUCTION

Infrared imagers are a key component of many military systems that are either in production or are planned. In the last decade, the complexity and applications of imagers has grown very substantially. We are now entering a time when many military systems will require large arrays of detectors that will provide imaging information for direct display and processing. For some systems, performance will be the major goal, but for others, price and ease of production will be a major consideration.

Currently there are two DARPA supported programs to produce these imaging arrays. These are the HgCdTe arrays and the silicide-silicon Schottky barrier detector arrays. The MRC was asked to look at the technical areas that could result in a substantial improvement in the performance of the latter arrays.

We purposefully avoided the difficult system question of determining which detector array is "better" since this decision will require detailed considerations of the mission and wavelength range that is required.

To inform the MRC of some of the problems in these systems, a one day meeting was held on July 19. The program for this meeting and the list of attendees is attached.

MEETING HIGHLIGHTS

The meeting began with an introduction by Dr. F. Shepherd (RADC). He first described the generic array.^{1,2} The individual detectors in the array consist of a silicide-silicon Schottky barrier. The band diagram and mechanism for conversion of the infrared photons into electrical current are illustrated in Fig. 1. The infrared photons pass through the transparent Si substrate and are absorbed by electron-hole production in the silicide. The holes are then injected into the p-type silicon substrate. The charge generated by this mechanism is collected by a charge coupled device and the data is clocked out to produce an image. For purposes of discussion here, the main considerations are the barrier height which governs the injection of holes into the semiconductor and the thermally produced current which gives a competing signal (the dark current).

The mechanism for converting the infrared photons into current involves first the absorption of the infrared photon by the electrons in the silicide. This produces holes that have energies that range all the way from slightly below the Fermi level E_f of the silicide to $E_f - h\nu$. Only those holes whose final state energy is below the barrier energy level can be collected by the silicon. This leads to a factor in the quantum efficiency that goes as

$$h\nu - \phi$$

In addition, the electron must also have an energy in the direction of the barrier that is large enough to overcome the

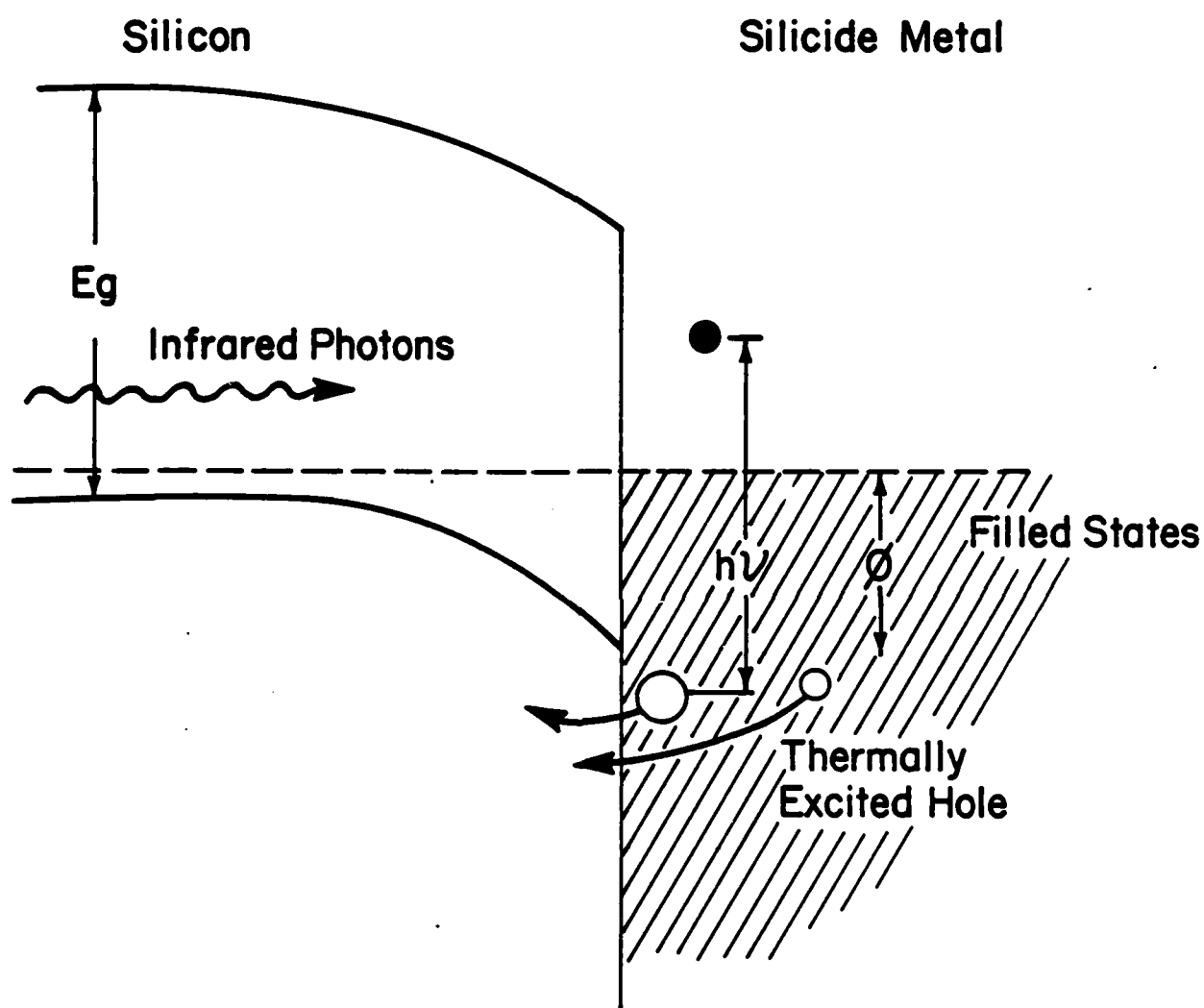


Figure 1. Schematic illustration of Schottky barrier infrared detector. The illustration is for p-type Si. The current is carried by holes.

barrier. This leads to another factor of $h\nu - \phi$ which results in the total quantum efficiency going as

$$\Gamma \approx \begin{cases} C_1(h\nu - \phi)^2/h\nu & h\nu > \phi \\ 0 & h\nu < \phi \end{cases}$$

This expression for the quantum efficiency turns on rather slowly for representative values of c_1 . Hence, one must have $h\nu$ substantially higher than ϕ to obtain reasonable values of quantum efficiency.

The dark current density J of the reversed biased Schottky barrier is given by a modified Richardson law.

$$J = A^{**}T^2e^{-\phi/kT},$$

where A^{**} is the effective Richardson constant, ϕ is the barrier height, and kT is the thermal energy at a temperature T . This dark current competes with the photoinduced current. Hence, one would like to keep it as small as possible. However, it depends exponentially on the same barrier that limits the turn on of the quantum efficiency.

Shepherd pointed out a number of advantages and disadvantages of the Schottky barrier imager. The principal advantages are associated with the fact that the devices make use of the very well developed Si technology. These include low cost, outstanding uniformity and potential for near term scale up. The primary disadvantages for current arrays that he listed are: limited spectral range (1.1 to 4.7 μm), low operating tempera-

tures ($<95\text{K}$), limited active area, and low quantum efficiency. The wavelength response could be extended by using IrSi.

Dr. W. Kosonocky (RCA)² presented some of the results that they have obtained with the platinum and palladium silicide infrared arrays. They have succeeded in fabricating 32×63 element arrays with thin PtSi and Pd_2Si active layers. The performance of these structures operating at 80K is quite impressive. They have achieved very good thermal images in the $3\text{--}5\mu\text{m}$ range. He stressed that in the design of these detectors the metal film had been made very thin ($<100\text{\AA}$) and the metal layer had been backed up by optical thin films that resulted in most of the IR radiation being absorbed in the silicide. The thin silicide layer made it possible for carriers reflected from the back interface to return to the silicide-silicon interface and hence, perhaps contribute to the current. Further, Kosonocky indicated that, in the case of the PtSi detectors, they had found that the performance of the detectors could be improved by changing the method of processing the devices.

Dr. N. Foss (Honeywell) reported that very similar results to those of Kosonocky. He noted that the finite area covered by the detector arrays led to spatial aliasing. He also reported that the detector response could be extended to $6.0\mu\text{m}$ using IrSi. Dr. M. Cantella (RCA) discussed some of their efforts to model the focal plane arrays and discussed the systems applications. He also showed impressive results obtained with these imagers.

We then turned to the major problem that the MRC could address with respect to improving these detector systems. Dr. D. L. Smith (Honeywell) reviewed some of the systematics of the barrier heights of silicides and indicated our current very limited understanding of the structure of the silicide-silicon interface and the value of the barrier height ϕ . The primary conclusion that could be drawn from this discussion is that we do not understand enough about this interface problem to see exactly how to improve the performance of these devices.

Professor S. Lyon (Princeton) gave us the benefit of some of his thinking on improving the performance of these detectors systems. He suggested that one should attempt to increase the quantum efficiency since this would allow better performance at a given temperature and allow operation at higher temperatures for the same performance level. He suggested two ways of increasing quantum efficiency. One was to reduce the number of carriers that are photo-excited but do not have sufficient energy to make it over the barrier. He hoped to do this by replacing the metal by a heavily doped semiconductor which would have the required barrier properties for blocking the unexcited charge. The second approach which was to be combined with the first was to increase the optical fields in the absorbing layers by incorporating small metal particles in the layers that would have resonances that could focus the fields.

Professor S. S. Lau (University of California, San Diego) presented a brief discussion on what is known about the

formation of silicides.³ He also brought up the possibility of an electron type silicide-silicon barrier. This barrier was ErSi_2 which has a barrier energy of 0.39eV.⁴

ROUND TABLE DISCUSSION

During the meeting, a number of questions were identified as subjects for the round table discussion. They included: Are presently available device parameters adequate for some systems applications? How much improvement can be achieved by an accurate understanding of the Schottky barrier physics? What are the advantages of the 3-5 μm versus the 8-14 μm bands? What is the nature of the silicide-Si interfaces that are currently being produced? How uniform are they with respect to dark current and quantum efficiency?

The discussion focused primarily on the first question. The general consensus of those present at the meeting was that the Schottky barrier detectors currently being made were useful in some applications. The disadvantages of lower operating temperature, lower quantum efficiency, and perhaps more restricted wavelength range of operation were discussed. Systems considerations, such as the available cooling capacity and the requirements for device performance, could not be defined carefully enough to decide this issue clearly.

The desirability of improving quantum efficiency was discussed. It was concluded that this improvement, along with the improvements in the wavelength sensitivity of the Schottky barriers and the reduction in dark current are the major places

where a real contribution to improved performance could be made.

RECOMMENDATIONS

Overall, the performance of the silicide-silicon infrared charge coupled device arrays was impressive. The technology could lead in the near term to uniform, cheap infrared imaging arrays in the 3-5 μ m range. For this reason, we would recommend:

- A study of systems requirements aimed at comparing these arrays with others that may be available or could become available in the near term. The study should include an estimate of the total systems cost, including refrigeration requirements.
- If the answer to the study is that the current arrays can satisfy systems requirements, a manufacturing methods study for this technology is recommended.
- The materials science and device physics of these detector arrays should be pursued in a research program. It is possible that structures could be formed that have substantially improved performance over those already being made. Such a program should not only study the currently used silicide-silicon systems but investigate the possibilities for others as well. The fact that little is known of the materials properties of the silicides complicates any search for better performance and clearly shows the need for this research program.

This technology is sufficiently promising that it may become the technology of choice for some applications of infrared detector arrays.

ACKNOWLEDGEMENT

This paper was written under the auspices of the DARPA Materials Research Council, Contract #MDA903-82-C-0428 with The University of Michigan.

REFERENCES

1. F. D. Shephard and A. C. Yang, "Silicon Schottky Retinas for Infrared Imaging", 1973, Int. Electron Devices Meeting, Tech. Digest, pp. 310-313.
2. W. F. Kosonocky, "Schottky-Barrier Infrared CCD Image Sensors", Proceedings of Infrared Information Symposium, May, 1982.
3. M. A. Nicolet and S.S. Lau, "Formation and Characterization of Transition Metal Silicides", Electronics: Microstructure Science, edited by N. Einspruch (Academic Press), Supplement A.
4. K. N. Tu, R. D. Thompson and B. Y. Tsuur, Appl. Phys. Lett. 38, 627 (1981).

SCHOTTKY BARRIER INFRARED CHARGE COUPLED DEVICE ARRAYS

Materials Research Council Meeting
Scripps Elementary School
2225 Torrey Pines Road

Monday, July 19, 1982

Introductory Remarks
S. Roosild (ARPA)

Schottky Barrier CCD Focal Plane
W. Kosonocky (RCA)

Schottky Barrier IR CCD Systems
N. Foss (Honeywell)

Engineering of IR Systems
F. Shepherd (RADC)

Systems Applications for IR Arrays
M. Cantella (RCA)

Trends in Silicide Barrier Heights
D. Smith (Honeywell)

Novel Approaches for Improving Quantum Efficiency
S. Lyon (Princeton)

Silicide Formation
S. Lau (UCSD)

Round Table Discussion

SCHOTTKY BARRIER IR-CCD ARRAYS

Attendees

Sven Roosild	DARPA	202-694-5800
George Vineyard	BNL	516-282-3335
Bill Spicer	Stanford	415-497-4643
Freeman Shepherd	RABC	617-861-2224
Wolfgang Elser	NVIEOL	703-664-1431
Michael Cantella	RCA, AS	617-272-4000, X3303
Walter Kosonocky	RCA Lab	
S.S. Lau	U. of Cal. San Diego	714-452-3097
Norman A. Foss	Honeywell	612-378-4142
Darryl Smith	Honeywell	612-378-5580
Steve Lyon	Princeton	609-452-4635
David Ferry	Colo. State Univ.	303-491-6600
Tom McGill	Caltech	213-356-4849
John Lambe	J.P.L.	213-354-8238
Henry Ehrenreich	Harvard	617-495-3213
Juri Valge	C.S. Draper Lab	617-258-2576
Mark Wrigton	M.I.T.	617-253-1597
John Tower	RCA, ATL	609-338-3883
Barbara Korenjak	RCA Labs	609-734-2896
E.E. Huccke	U. of M./MRC	

POSSIBLE IMPROVEMENTS IN SCHOTTKY BARRIER INFRARED
CHARGE COUPLED DEVICE ARRAYS

T. C. McGill

INTRODUCTION

Silicide-silicon Schottky barriers are the detector elements in Schottky barrier charge coupled device arrays. The performance of the detector is governed by the quantum efficiency as a function of wavelength and the dark current. For optimum performance, we want the dark current to be less than the current induced by the black body radiation and signal. Hence, improvement in detector performance requires a reduction in dark current or increase in quantum efficiency or both.

Quantum Efficiency:

The standard treatment of the photo-excitation of carriers over a barrier follows that due to Fowler.¹ When this treatment is applied to a single free electron model of the metal, it yields an expression for the quantum efficiency Q at frequency ω ,

$$Q = \frac{\alpha \lambda}{8E_F \hbar \omega} (\hbar \omega - \phi)^2 \quad (1)$$

where α is the absorption constant for the metal, λ is the mean free path for electron in the metal, E_F is the Fermi energy of the metal, and ϕ is the barrier height. The constants are lumped together in a constant C_1

$$C_1 = \frac{\alpha \lambda}{8E_F} \text{ and } Q = \frac{C_1 (\hbar \omega - \phi)^2}{\hbar \omega} \quad (2)$$

In deriving this expression, it is assumed that the thickness of the metal is much greater than the electron mean free path. The transmission through the barrier region is assumed to be one. In this expression, one power of $\hbar\omega - \phi$ is produced by the fact that only a fraction of the carriers excited have energy sufficient to make it over the barrier. A second power of $\hbar\omega - \phi$ is produced by the requirement on the carrier that it have an energy perpendicular to the barrier that is greater than the barrier energy to make it over the barrier.

Evaluation of constant in Eq. (1) yields a small value for Q .

If we take

$$\alpha\lambda = 1,$$

$$E_F \approx 5\text{eV},$$

then

$$C_1 = 0.025 \text{ eV}^{-1}.$$

The quantum efficiency for this value of C_1 and $\phi=0.208\text{eV}$ (the barrier energy for platinum silicide) is plotted in Fig.1.

This small value of the constant C_1 and the resulting quantum efficiency is the result of losing carriers excited by the photons through a number of mechanisms. First, one excites some carrier with energy less than the barrier height. Second, some of the carriers are excited sufficiently far the metal that they undergo collision and do not make it to the barrier with sufficient energy to be collected. Finally, we lose all the carriers that are headed in the wrong direction.

Attempts to increase the quantum efficiency have concentrated on doing away with of the loss mechanisms and decreasing the value of the barrier energy. Thin film layers ($d \leq 100\text{\AA}$) have been fabricated with an optical reflector at the back. These structures have the advantage that most of the photons are absorbed within an electron mean free path of the interface and hence, have the opportunity to make it over the barrier. Carriers which are headed in the wrong direction can scatter off the back wall of the silicide and return to make another attempt at the barrier.² In these structures, the quantum efficiency is found to still go as

$$Q = C_1(\hbar\omega - \phi)^2 / \hbar\omega \quad (3)$$

but C_1 is found to be much larger. For PtSi_3 ,

$$C_1 \approx 0.54 \text{eV}^{-1}.$$

This value is much larger than the thick film theoretical value in Eq. (1), and gives a much larger quantum efficiency which is shown in Fig. 1.

It should be noted, however, that the behavior of the quantum efficiency is still substantially less than the values that would be obtained if all the carriers, with energy greater than the barrier height, were collected and all the photons absorbed. For this case, the quantum efficiency is given by

$$Q = (\hbar\omega - \phi) / \hbar\omega \quad (4)$$

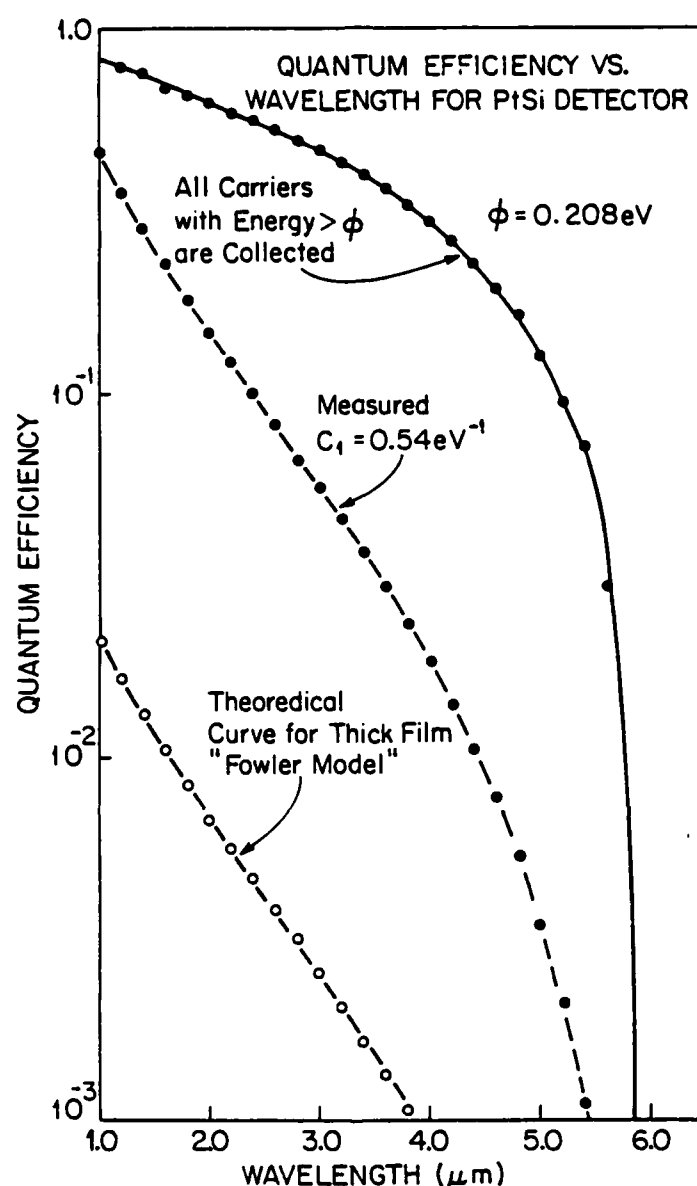


Figure 1. The quantum efficiency versus wavelength of the incident infrared photon. The barrier energy (ϕ) is assumed to 0.208eV, giving a cutoff of 5.96 μ m. The lowest curve () is $Q_1 = c_1(\hbar\omega - \phi)^2 / \hbar\omega$ for the value of c_1 estimated from the thick film theoretical formula (i.e., $c_1 = 0.025\text{eV}^{-1}$). The second lowest curve () is $Q_1 = c_1(\hbar\omega - \phi)^2 / \hbar\omega$ for the value of c_1 obtained experimentally in a thin film sample. The upper curve () in the quantum efficiency, if we assume that all the photons are absorbed and all the carriers which have sufficient energy to make it over the barriers are collected.

This expression for Q is also plotted in Fig. 1. From this figure, we see that the "ideal" quantum efficiency is substantially larger than that obtained experimentally. This discrepancy suggests that even with the current thin film silicide, we are only collecting a small fraction of the carriers which are photo-excited.

The improvement in performance due to such an improvement in quantum efficiency is shown in Fig. 2. In this figure, the noise equivalent delta temperature ($NE\Delta T$) is plotted. This quantity is the value of ΔT that produces a signal to noise ratio of one. For the purpose of this calculation, we have assumed that the noise is entirely shot noise from the background and dark current. At low temperatures, $NE\Delta T$ is independent of detector temperature since the dark current is small compared to the current due to the background photon flux. At high temperatures, the dark current dominates. The major result of this calculation is that, if the "ideal" quantum efficiency could be obtained, then the temperature at which the detector could be operated for $NE\Delta T$ equal to 0.05K could be increased from 80K to 110K. This increase in operating temperature could make this detector system useful in a large number of applications.

The chances of obtaining such an increase in quantum efficiency are difficult to assess. Historically, most quantum efficiencies from Schottky barriers show behaviors like

$$Q \sim (\hbar\omega - \phi)^\alpha$$

where α is typically 2 or greater. However, it might be

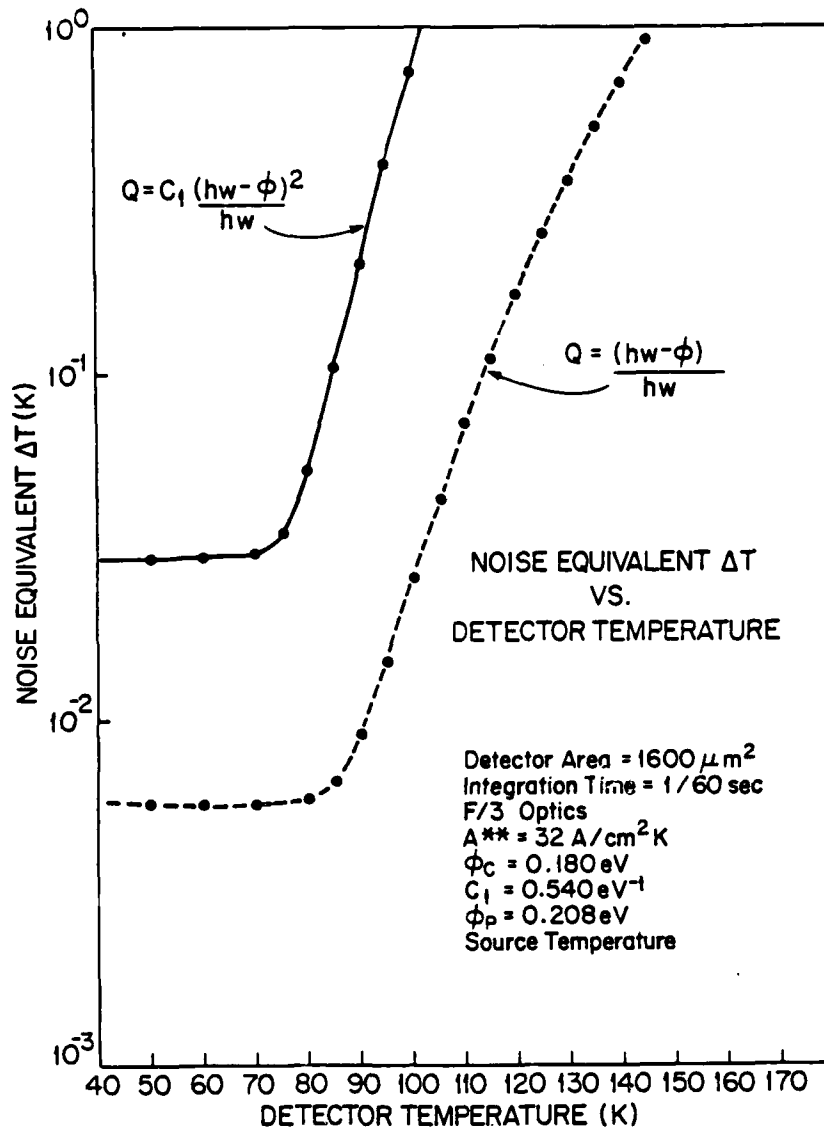


Figure 2. The noise equivalent ΔT versus the detector temperature. The upper curve () is for the experimental quantum efficiency. The lower curve () is for the "ideal" quantum efficiency, in which all the carriers with sufficient energy to make it over the barrier are collected and all the photons are absorbed. The calculations assume that shot noise from the background and dark current limit the performance of the detector.

possible to change the processing in such a way to break down the conservation of parallel K across the interface sufficiently to remove one power of $\hbar\omega - \phi$ from Eq. (2), and hence, give a variation like Eq. (4). However, we do not know that such processing would yield a coefficient out in front that would give large quantum efficiencies.

In summary, the major result of this section is the observation that in spite of the improvement in quantum efficiency that have been obtained, the current devices are far from the quantum efficiency that would be obtained if all the carriers with energy sufficiently large to make over the barriers were collected.

Dark Current:

The dark current density fits fairly well to the standard Richardson expression

$$J_D = A^{**}T^2 e^{-\phi/kT} \quad (5)$$

where A^{**} is the effective Richardson constant, ϕ is the barrier height. There are two parameters in Eq. (5) that can be varied, A^{**} and ϕ . The value of A^{**} for a well-formed Schottky barrier in p-type Si⁵ with all the corrections is about 32 A/cm²K². However, Kosonocky³ has reported values of A^{**} which are as low as 5 A/cm²K². This low value suggests a non-uniform interface with hot spots which have a lower barrier energy than the rest of the interface. This effect would decrease the active area, and hence, yield smaller values of A^{**} . These devices also show

a smaller value of ϕ in the dark current, and hence, do not lead to substantial decreases in the dark current.³

One might also attempt to increase the barrier height. If one does this, then the quantum efficiency would go down, since the barrier height governs how many carriers make it over the barrier.

The excited barriers for photo-response ϕ_p are not in general equal to the barrier that governs the dark current ϕ_c . The two processes are different. In the thermionic emission, the distribution of carriers incident on the barrier goes as $e^{-E/kT}$, where E is the energy of the carriers. In the photo-response process, the distribution of carriers incident on the barrier is approximately uniform in energy. The transmission of the carrier across the barrier region is the same in the two processes. Hence, in the thermionic process, any region of low barrier is strongly weighted while in the photo-response process, the weighting on low barrier regions is much weaker. This phenomenon results in $\phi_p > \phi_c$, the wrong direction for improved performance of the device. Hence, it is unlikely that the dark current can be suppressed at the same time that the quantum efficiency is kept high.

General Comments:

Much of our understanding of the phenomenon associated with Schottky barriers is based on very simple models which are inappropriate to real silicide-silicon interfaces. For example, the band structure effects in the silicide are not included.

(In fact, the band structures for the silicide are not known.) We assume that the parallel component of the carrier wave vector is conserved in crossing the interface. Yet since the silicide and silicon are not even approximately lattice matched, the parallel component of wave vector is not a meaningful quantity in going across the barrier. The modifications in the carrier wave functions due to the confinement in a thin film have not been included. The transport and transmissions in the silicide and the reflection at the interfaces is treated in a very simple manner. The precise nature of the interface region which is assumed to be very abrupt is not really known. This rather sad state of our knowledge forces attempts to increase the quantum efficiency and reduce the dark current to be largely empirical.

ACKNOWLEDGEMENT

This paper was written under the auspices of the DARPA Materials Research Council, Contract #MDA903-82-C-0428 with The University of Michigan.

REFERENCES

1. W. B. Fowler, Physical Review 38, 45 (1931).
2. V. E. Vickers, Applied Optics, 10, 2190 (1971).
3. W. F. Kosonocky, "Schottky-Barrier Infrared CCD Image Sensors", Proceedings of Infrared Information Symposium, May 1982.
4. S. M. Sze, Physics of Semiconductor Devices, 2nd Ed., (John Wiley and Sons, 1981), p.255-263.
5. J. M. Andrews and M. P. Lepselter, Solid-State Electronics, 13, 1011 (1970).

MAGNETIC SEMICONDUCTORS

Report of Meeting held on July 16, 1982

H. Ehrenreich

The materials of interest here are substitutional alloys based on HgTe, CdTe, and CdSe. The substitution in question involves the cation. If the substituted atom is magnetic, as in the case of Mn, [e.g. (Hg, Mn)Te], the semiconductor will exhibit interesting magnetic properties in addition to the variation of the band gap with composition which renders the material optically tunable in the infrared. If the substituted atom is non-magnetic, as in the case of (Hg, Cd)Te, only the effects associated with IR detector applications remain.

Furthermore, one must distinguish the "small" gap materials based on HgTe, with "large" gap materials based on CdSe, which are of importance respectively in the IR and visible. In the latter case alloying with Mn permits matching to powerful lasers and the concomittant exploitation of the magnetic properties such as huge Faraday rotations, spin-flip in FIR lasers, etc.

The IR detector capabilities of (Hg, Cd)Te are presently being exploited. The magnetic properties associated with both small and large band gap 2-6 alloys are under investigation. While they are very exciting from a scientific standpoint, the question of their ultimate usefulness remains open, although prospects appear promising.

The preceeding discussion supplies the setting for the questions posed by R. A. Reynolds (DARPA) at the outset of the symposium: (1) Is (Hg, Mn)Te likely to emerge as a better IR sensor material than (Hg, Cd)Te? (2) Do Mn substituted 2-6 compounds form a class of materials with properties that are sufficiently unique as to motivate intensive research on these materials because of technological applications?

The general issues discussed at the meeting concerned: (1) The crystal perfection achievable in (Hg, Cd)Te and the effects of imperfections, including alloying effects, on electronic and optical properties; (2) Small gap magnetic semiconductors that might be utilizable as IR detectors in comparison to (Hg, Cd)Te; (3) Large gap magnetic semiconductors, such as (Cd, Mn)Se that are transparent to parts of the visible spectrum.

Two of the principal conclusions are worth stating at the outset. (There are several others, which are stated in the discussion below.)

(1) The chemical binding of both the magnetic and non-magnetic substituted 2-6 alloys of interest is sufficiently ionic that stoichiometry problems of the sort encountered in oxides are likely to be important.¹ Whether this problem is genuinely inimical to device performance is not clear. However, in this respect Mn substituted HgTe compounds are not likely to be better than Cd substituted materials except in one respect: to achieve a band gap of a given magnitude it is necessary to

incorporate only half as much Mn as Cd in HgTe. The crystal perfection is thus likely to be better.

(2) While none of the technological applications of the wide band gap magnetic semiconductors have yet been reduced to practice, some optical devices appear sufficiently promising that a super-critical basic research effort should be maintained. Since ONR is already supporting some of this effort, funding by DARPA should be complementary rather than duplicative.

A list of speakers and their topics, as well as are containing the participants at the meeting is appended to this report. It should be noted that P. L. Anderson (TI) did not make a formal presentation. His remarks, based largely on his published work², were entirely informal.

J. K. Furdyna³ presented an overview dealing with the electrical, optical, and magnetic properties of (Hg, Mn)Te. Much of this material is contained in Ref. 2. He stressed that Mn is the only element in the 3d row that enters both HgTe and HgSe in appreciable concentrations. Presumably this is due to the spherical, half-filled d shell of Mn and the fact that the bonding in these materials has a predominantly ionic character. The other transition metals have crystal and ligand field splittings that make the tetrahedral coordination, characteristic of a substitutional site in a zinc-blende structure, unfavorable. Indeed, if the d electrons corresponding to a spherical shell of d electrons plays little role in bonding, then Mn should be exchangeable for Cd, Hg, and Zn, which is the case. Mn^{++} is known to have a strong tetrahedral site preference.

Furdyna and Wolff both emphasized that (CdMn)Te contains a number of magnetic phases: paramagnetic, antiferromagnetic, and spin glass. The last of these is of considerable current interest to physicists.

(CdMn)Te is of particular interest since it can be made at compositions for which it is transparent. Both the narrow and wide gap alloys possess large controllable g values arising from both Landau diamagnetism and Mn paramagnetism. The observed Faraday rotations are huge. In (CdMn)Te, whose band gap can be changed from 1.6 eV to the visible by changes in composition, a range which includes the HeNe laser wavelength for 20% Mn, the wavelength of oscillations of the transmitted signal is 5nm. (The sample is placed between polarizers and the wavelength is altered). The fact that the gap can be adjusted, as a function of composition x , to powerful laser wavelengths and can be further adjusted by the application of magnetic fields is potentially important for optical communication. Furthermore, materials like (CdMn)Se can be fabricated to have high optical quality.

(HgMn)Te is known to exhibit a large negative magnetoresistance: At He temperatures the resistance decreases by 2 orders of magnitude upon application of a field of 50 kG.

It may be that Mn clusters exist in these materials and that vacancies exist in moderate to large concentrations.

P. L. Anderson (TI) made several important observations: Dislocations can exist in large densities of 10^5 to 10^8 cm^{-3} . The composition may not be uniform throughout the material

($x=\pm 0.035$). However, the best material appears to be close to the homogeneity specifications set by IR detector requirements. Raccah pointed out that his optical homogeneity analyses indicated that material prepared by TI was among the very best. (The details of manufacturing processes, of course, were not discussed.)

In regard to crystal perfection, it was noted that the Te lattice is nearly perfect, that cation vacancies are probable, Te vacancies possible, and that Te interstitials are highly unlikely. The Hg in Hg-based salts is very mobile, in contrast to Cd in Cd based salts. By and large most impurity effects can be described by substitution for group 2 and 6 constituents and valency differences. The phase diagram suggests that (Hg Cd)Te exists only in the presence of appreciable ($\sim 10^{19} \text{cm}^{-3}$) concentrations of type 2 vacancies.

The fact that post-annealing is effective at lower temperatures implies that cation vacancies are compensated by impurity donor concentrations. The accompanying contribution by Ehrenreich and Hirth suggests that some of these arise from jogs at dislocations.

The preceding considerations led to the question as to whether there had in fact been an appreciable improvement in the quality of (HgCd)Te material during the past few years. (There Bridgman, Epitaxial, and other methods for preparing this material.)

P. Raccah has used electroreflectance, a differential

optical measurements technique, to study questions of crystal perfection with extraordinary care. Since he has examined a larger number of samples coming from different sources, his commentary was extremely useful in corroborating some of the statements concerning sample quality. He has also used electroreflectance to study details of the electronic structure that are of particular interest to theorists. He obtains the principal gaps E_0 and E_1 as a function of composition, the widths of the peaks (connected with alloy broadening and/or crystal imperfections), and the variation of these gaps with composition. The last phenomenon is termed "bowing" since this variation can usually be represented as a quadratic function of x . The term in x^2 reflects the effects of alloying directly.

The observed widths of 0.1eV were thought by Raccah to be largely artifacts of crystal preparation. However, Ehrenreich⁴ pointed out that based on his alloy electronic structure calculations, these widths were at least qualitatively consistent with theoretical expectations based on alloying effects alone. While no detailed comparisons have not been made, the bowing observed by Raccah appears to be quite consistent with the theoretical results.

Raccah also discussed experiments which showed that after cleavage and annealing crystals became n-type. This behavior was associated with cleavage damage. This effect is explained in the accompanying note of Ehrenreich and Hirth.

P. A. Wolff's presentation stressed the properties of wide gap semiconductors. The principal subjects under discus-

sion were (1) the unique properties of semimagnetics, (2) bound magnetic polarons and their conjectural use as high density memories, and (3) tunable sources for visible, near IR, and FIR radiation. These points are discussed in an accompanying paper by Wolff.⁵ While there are materials preparation problems with the 2-6 alloys discussed here, which may continue to be present, it appears likely that these materials even in their present state will be useful and reliable IR detectors. Furthermore, a whole host of new applications for the magnetic semiconductors may lie just beyond the horizon. At present, its too early to be sure. There appears to have been substantial, evolutionary progress in the fabrication and understanding of these materials. R&D activities directed both at deeper scientific understanding and technical applications should continue to be funded.

ACKNOWLEDGEMENT

This paper was written under the auspices of the DARPA Materials Research Council, Contract #MDA903-82-C-0428 with The University of Michigan.

REFERENCES

1. See accompanying paper by H. Ehrenreich and J. P. Hirth in these Proceedings.
2. P. L. Anderson, H. F. Schaaake, and J. H. Tregilges, J. Vac. Sci. Tech. 21, 125(1982).
3. J. K. Furdyna, J. Vac. Sci. Tech. 21, 220(1982).
4. K. C. Hass, H. Ehrenreich, and B. Velicky, (Submitted to Phys. Rev.).
5. P. A. Wolff, Accompanying paper in these Proceedings.

Magnetic Semiconductors

July 16, 1982

DARPA Materials Research Council Meeting

INTRODUCTION: R. A. Reynolds & P. A. Wolff

Overview: J. K. Furdyna (Purdue)

Precipitation and Phase Stability: P. L. Anderson (TI)

Optical Properties: P. Raccah (U.Ill.-Chicago Circle)

Speculations about Wide Gap Magnetic Semiconductors:
P. A. Wolff (MIT):

Discussion: Physical Properties Relevant to IR
Detectors

Meeting Summary

Informal presentations were also made by H. Ehrenreich (Harvard)
and G. B. Wright (ONR).

Attendees
MAGNETIC SEMICONDUCTORS
July 16, 1982

Sven Roosild	DARPA
Phil Anderson	Texas Inst., Dallas
Dick Reynolds	ARPA
P. A. Wolff	MIT
George Vineyard	BNL
Mark Wrigton	MIT
T. C. McGill	Caltech.
J. K. Furdyna	Purdue
M. J. Sinnott	Michigan
H. Augus Macleod	University of Arizona
R. S. Bauer	Xerox
Paul M. Raccach	U. of Ill.
George B. Wright	ONR
Amnon Yariv	Caltech
John Hirth	OSU
Henry Ehrenreich	Harvard

DISLOCATIONS, JOGS, AND VACANCIES IN (HgCd)Te

H. Ehrenreich and J. P. Hirth

(HgCd)Te at relatively low vacancy concentrations is known to form as a p-type material with $\sim 10^{19} \text{ cm}^{-3}$ excess Te.¹ A post-annealing process in a Hg rich atmosphere renders the material weakly n-type. This behavior has been associated² with the formation of Hg vacancies and Te clusters when the material is formed. The latter are partially dissolved during the post-anneal.

We shall argue that edge dislocations containing jogs can form an important vacancy source, through the incorporation of the group 2 element in the jog. Furthermore, the resulting complex involving the dislocation is a donor, whose presence may be responsible at least in part for the transformation to the n-type form.

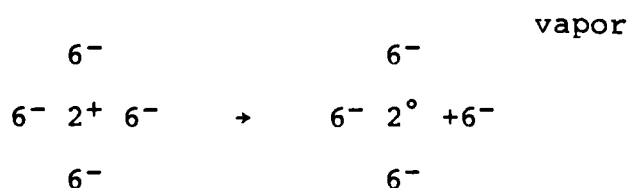
The argument assumes that the crystal is appropriately viewed as an ionic rather than as a covalent material. This view, in fact, may have relevance to many of the 2-6 compounds. Its applicability to oxides has long been realized. Its relevance to materials like (HgCd)Te suggests that problems concerning stoichiometry, characteristic of the oxides, may also be of importance here. The commonly held view that, given enough care, (HgCd)Te can be fabricated with nearly perfect stoichiometry as can, for example, GaAs, may thus be simply incorrect. An ionic view of the constituents suggests that the anions (to

be denoted 6^{-Q}) are much larger than the cations (2^{+Q}). The extreme ionic view would suggest $Q=2$. For (HgCd)Te the value $Q=1$ is more nearly appropriate.

The ionic view is also consistent with the assumption that the valence band (at least its upper portion) has predominantly 6^{-Q} character, and that the conduction band is largely 2^{+Q} . We shall assume this here.

(HgCd)Te is known to contain large edge dislocation densities (10^5 - 10^8 cm $^{-2}$)³. Entropic considerations suggest that during crystal growth the free energy is lowered if the dislocations have jogs, as shown in Fig. 1. A donor is formed upon absorption of a bulk type 2 ion at a jog.

Another source of type 2 vacancies is connected with the solid-vapor equilibrium at crystal formation temperatures. This may be visualized by use of the following schematic diagram, drawn assuming $Q=1$:



or the reaction $2^{+}6^{-} \rightarrow 2^{\circ}6^{-} + \text{hole in acceptor state}$. This also shows that 2^{+} vacancies will form acceptor states.

The jog shown in Fig. 1 is neutral, having a 2^{+Q} and 6^{-Q} ion respectively at its edges. However, jogs would preferentially occur at the smaller 2 sites where the strain energy due to the dislocation is smaller. Because it is possible to remove

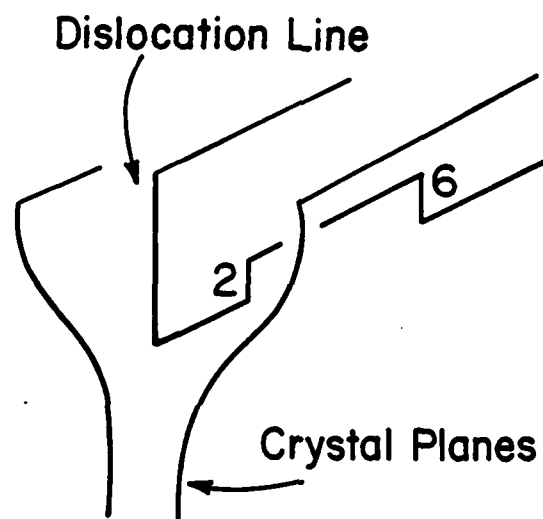


Figure 1. A neutral edge dislocation with a dislocation line having two jogs, having respectively a 2^{+Q} and 6^{-Q} at the corner.

a substitutional 2 ion and place it at the jog corner occupied by the 6 ions without substantial strain energy penalty, a process which increases the number of jogs and therefore the entropy of the solid during its formation, it seems plausible to assume that this is what happens.

The transfer process in detail is the following for the case $Q=1$. A charge $-Q$ is transferred from one of the neighboring 6^{-Q} ions to the 2^{+Q} atom, rendering it neutral. The neutral atom is removed leaving behind an M-center, in alkali halide parlance. An M center corresponds to an acceptor. The 2° atom is now placed on the 6-ion jog corner. The resulting center is a donor. This process thus results in a donor-acceptor pair, which, however, need not be spatially correlated since both constituents will be seen to be neutral.

A rough estimate of the donor binding energy can be obtained by thinking of the jog not in terms of the sharply demarcated regions shown in Fig. 1, but rather as a more diffuse localized region having a density deficit, or equivalently as a region having a somewhat larger interatomic spacing $r=r_0 + \delta r$. Here r_0 is the lattice constant characteristic of the pure crystal.

An electron situated on a jog corner cation will experience a slightly altered Madelung potential $V(r)$ due to the local dilatation:

$$V(r) \approx -(\alpha'e^2/\epsilon r) (\delta r/r_0)$$

Here α' and ϵ are respectively the Madelung constant and dielec-

tric constant appropriate to this region. For the present rough estimate we shall assume $\alpha' \approx 2$, $\epsilon \approx 10$, and $\delta r/r_0 \approx 0.1$. We obtain $V(r) \approx -0.2$ eV.

We associate this value of $V(r)$ with the donor binding energy. This interpretation rests on the fact that in the present view an extra electron situated in a stationary position on a cation in the perfect crystal is regarded as being located at the bottom of the conduction band. This electron experiences a positive (repulsive) Madelung potential since it sits in an environment having negative effective charge. The local dilatation reduces the potential, thereby lowering the energy of the electron by $V(r)$.

The cation vacancy acceptor level has been estimated by calculations based on an idealized non-ionic model of Swarts, Daw, and McGill⁴. For the Cd concentration of interest this level is found to coincide with the valence band edge within 0.1 eV. (While the calculated level, strictly speaking, overlaps the valence band, uncertainties in the model are consistent with a picture in which the acceptor level lies within the band gap close to the band edge.)

The band diagram, resulting from the present considerations including the position of donors and acceptors has the form shown in Fig. 2. Experimental results⁵ indicate the band gap to be $E_g \approx 0.1$ eV for $x \approx 0.2$. The donor level therefore is degenerate with the valence band and lies below the acceptor level, which nearly coincides with the valence band edge. At

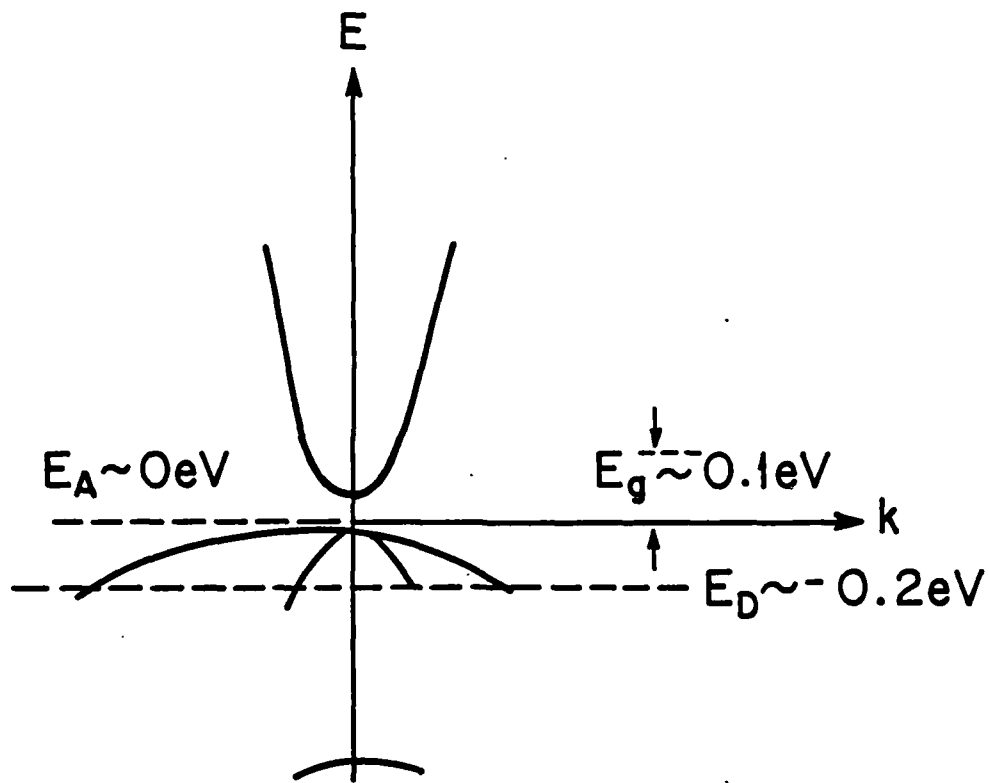


Figure 2. Energy band structure near the band edge of $(\text{Hg}_{1-x}\text{Cd}_x)\text{Te}$ for $x \approx 0.20$ sharing the energetic position E_D of the "jog corner" donors arising from dislocations and the acceptor levels E_A associated with vacancies, according to Swarts et al⁴.

moderate temperatures, therefore, the donor level is filled. The acceptor level causes the sample to be p-type, consistent with experiment.

At the meeting, Raccah discussed experiments wherein after cleavage and annealing, crystals were n-type and associated the n-type behavior with cleavage damage. After the damaged layer was etched away, the crystal reverted to p-type behavior. The present hypothesis would be consistent with Raccah's results if the donors introduced by the cleavage were dislocation jogs. It is well known for ionic crystals that athermal cation vacancies and associated cation jogs are produced during deformation by dislocation intersections.

The acceptor levels are present in roughly the same concentration as that corresponding to the precipitated Te atoms. Their large concentrations ($\sim 10^{19} \text{cm}^{-3}$) suppresses thermal excitations to the conduction band. Because of their high mobility, electrons would dominate the electrical transport properties if they were present in even moderately low concentrations. The post-anneal in the presence of a Hg rich atmosphere eliminates many of the cation vacancies and diminishes the concentration of Te precipitates. The jog corner donor sites that have been postulated in this note may or may not remain. The dislocations should not anneal out at the low annealing temperatures involved at $\sim 250^\circ\text{C}$. The excess cation jogs will remain if the energy of formation of a jog-cation vacancy pair is less than the formation energy of a cation vacancy-hole-neutral vapor atom product.

In any case, the acceptor concentration is reduced sufficiently to permit the observed conversion to n-type behavior.

The present picture of acceptors in (Hg, Cd)Te is attractive because of its simplicity. According to it acceptors are solely associated with cation vacancies, and not with dislocations or Te-interstitials⁽⁶⁾. We emphasize that the present view that dislocations give rise to donors is based on an ionic rather than a covalent view of the material. In purely covalent materials like Ge and Si, edge dislocations are well known to act as acceptors.

As already pointed out, the ionic view of these materials suggests that stoichiometry problems may be endemic to the entire class of materials including (HgMn)Te, (HgMn)Se, etc. If so, the magnetic semiconductors are unlikely to be better as infrared detector materials than their non-magnetic counterparts.

ACKNOWLEDGEMENT

The authors are grateful to P. L. Anderson and P. Raccah for discussions that stimulated this work.

This paper was written under the auspices of the DARPA Materials Research Council, Contract #MDA903-82-C-0428 with The University of Michigan.

REFERENCES

The list below is minimal. A more complete and contemporary set may be found in the Proceedings of the Minneapolis Conference on HCT in J. Vac. Sci. Technol., 21(1), May/June 1982.

1. R. T. Delves, Brit. J. Appl. Phys. 16, 343 (1965).
2. P. L. Anderson, H. F. Schaake, and J. H. Tregilgas, J. Vac. Sci. Technol. 21, 125 (1982).
3. P. L. Anderson, (Private Communication).
4. C. A. Swarts, M. S. Daw, and T. C. McGill, J. Vac. Sci. Technol. 21, 198 (1982).
5. See for example J. K. Furdyna, J. Vac. Sci. Technol. 21, 220(1982).
6. A. J. Strauss and R. F. Brebrick, J. Phys. Chem. Solids 31, 2293(1970).

SPECULATIONS CONCERNING APPLICATIONS OF SEMIMAGNETIC SEMICONDUCTORS

P. A. Wolff

INTRODUCTION

Semimagnetic semiconductors are alloys made by replacing a fraction of the cations in II-VI compounds by transition metals. $(\text{Cd}_{1-x}\text{Mn}_x)\text{Te}$ and $(\text{Hg}_{1-x}\text{Mn}_x)\text{Te}$ are typical examples. These materials are novel because they combine the important features of conventional semiconductors with those of magnetic solids. In contrast to other magnetic semiconductors, they have reasonable transport properties and simple, well-defined band structures (usually similar to those of the binary, host compounds). They also exhibit a variety of magnetic phases (paramagnetic, spin glass, anti-ferromagnetic) as a function of composition. Finally, there is a large exchange interaction between conduction electron (or hole) spins and those of the paramagnetic ions. That interaction gives rise to several remarkable effects such as giant g -values, large Faraday rotations, and bound magnetic polarons (BMP).

Semimagnetics have been studied intensively¹. Their properties are now fairly well understood. That work suggests several applications for them. None has yet been tested. Thus, the ideas outlined below are still speculative.

INFRARED DETECTORS

$(\text{Hg}_{1-x}\text{Cd}_x)\text{Te}$ is currently the material of choice² for infrared detectors. Its electronic properties are well-suited to such applications, and the gap can easily be adjusted to the wavelengths of primary interest. The close lattice match between HgTe and CdTe ($\Delta a/a \approx 0.3\%$) facilitates epitaxy on CdTe substrates. In addition, $(\text{Hg},\text{Cd})\text{Te}$ forms a native oxide with superior properties³.

Despite these advantages, $(\text{Hg},\text{Cd})\text{Te}$ is not without problems. It is difficult⁴ (if not impossible) to prepare in homogeneous, bulk single crystals. There is evidence⁵ that processed $(\text{Hg},\text{Cd})\text{Te}$ contains micro-inclusions (≈ 1000 Å in size) of Te or Te-rich material. Considerable care in surface treatment is required to prevent the out-diffusion of mercury from $(\text{Hg},\text{Cd})\text{Te}$.

$(\text{Hg}_{1-x}\text{Mn}_x)\text{Te}$ has band structure and electronic properties similar to those of $(\text{Hg}_{1-x}\text{Cd}_x)\text{Te}$, and should perform similarly as an IR detector. However, its band gap tunes twice as rapidly with x-value than that of $(\text{Hg},\text{Cd})\text{Te}$. For example, in $(\text{Hg}_{1-x}\text{Mn}_x)\text{Te}$, $E_G = 0.12$ (the CO_2 laser energy) at $x = 0.12$, whereas an x-value of 0.23 is required to achieve that condition in $(\text{Hg}_{1-x}\text{Cd}_x)\text{Te}$. Intuitively, one suspects that a lower concentration of the third component would facilitate crystal growth. There are, in fact, indications that homogeneous crystals of $(\text{Hg},\text{Mn})\text{Te}$ are easier to grow⁷ than those of corresponding gap, in $(\text{Hg},\text{Cd})\text{Te}$. It is pertinent, therefore, to consider

(Hg,Mn)Te's potential as an IR detector material. Though this alloy is not inherently superior to (Hg,Cd)Te in its electronic properties, it is conceivable that it has advantages in terms of materials preparation and device fabrication. The following points emerge from this consideration:

1. Bulk Crystals

Growth of homogeneous, bulk crystals of given band gap (say $E_G = 0.12$ eV) may be easier⁷ in the (Hg,Mn)Te system than in the (Hg,Cd)Te system. Further work, to confirm this statement, would be useful. It is not clear whether or not the problem of constitutional supercooling, which complicates the growth of bulk (Hg,Cd)Te crystals, also affects epitaxial growth of this material.

2. Epitaxy

(Hg,Mn)Te is less favorable for epitaxy than (Hg,Cd)Te. (Hg,Cd)Te is nearly lattice-matched to CdTe (within 0.3%). On the other hand, the mismatch for the (Hg_{0.88}Mn_{0.12})Te/CdTe system is about 0.6% - probably too large for successful epitaxy. More complicated substrates, such as Cd(Se,Te) or (Cd,Mn)Te, will be needed.

3. Defects, Surfaces, etc.

As-grown (Hg,Mn)Te crystals are heavily p-type, due to Hg vacancies. Annealing in Hg vapor reduces the vacancy concentration and may convert the material to n-type. n-type samples, with moderate carrier concentrations ($n \approx 10^{16}/\text{cc}$), have

also been made via In-doping. In these respects, $(\text{Hg}_{1-x}\text{Mn}_x)\text{Te}$ appears similar to $(\text{Hg}_{1-x}\text{Cd}_x)\text{Te}$.

Little is known about the surface of $(\text{Hg},\text{Mn})\text{Te}$ crystals, or the oxides which grow there. Favorable surface chemistry is a prerequisite for device applications.

TUNABLE SOURCES

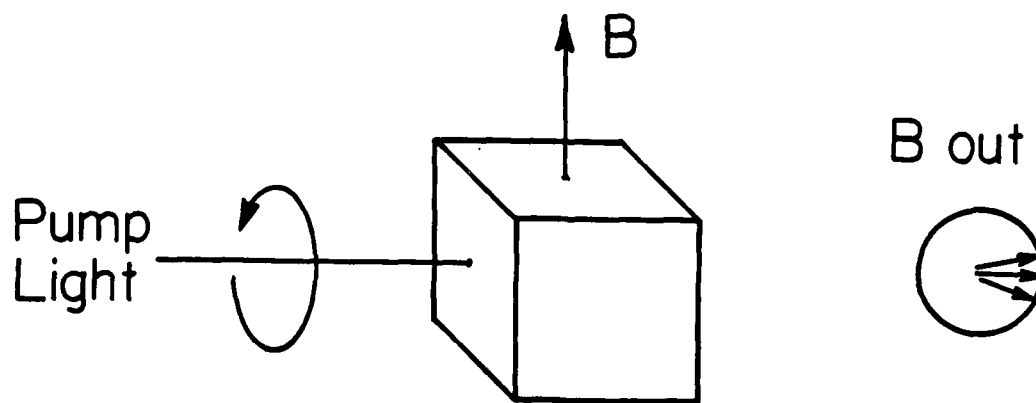
At low temperatures the g-values of electrons in $(\text{Cd},\text{Mn})\text{S}$, $(\text{Cd},\text{Mn})\text{Se}$, and $(\text{Cd},\text{Mn})\text{Te}$ are larger than 100. As a consequence, the spin-flip energy can be tuned, with modest magnetic fields, over ranges exceeding 100 cm^{-1} . This tunability is evident in spin-flip Raman scattering experiments⁸. Moreover, recent work has shown that, with pump laser energies near the band gap, the spin-flip cross section is huge⁹. Heiman has taken advantage of this fact to demonstrate⁹ stimulated spin-flip Raman scattering in $(\text{Cd},\text{Mn})\text{Se}$. The source can be tuned by over 100 cm^{-1} with fields below 20 kG. There seems no reason, in principle, why stimulated spin-flip Raman scattering cannot be achieved in other $(\text{Cd},\text{Mn})\text{Se}$ samples, as well as in $(\text{Cd},\text{Mn})\text{S}$. Such devices would provide magnetically tunable sources covering a considerable portion of the visible spectrum.

A more interesting potential application of the spin flip process is in the generation of tunable, far infrared radiation (at the spin resonance frequency). Dobrowolska et.al.¹⁰ have recently demonstrated that the spin flip process in $(\text{Cd},\text{Mn})\text{Se}$ has a sizable electric dipole matrix element. Thus, whenever electron spins are coherently excited in $(\text{Cd},\text{Mn})\text{Se}$, one

anticipates copious FIR emission at the spin resonance frequency. Spin flip laser action naturally produces such spin coherence; Heiman¹¹ estimates tunable, FIR outputs in the 100 watt range under such circumstances. This scheme is similar, in principle, to one already demonstrated¹² (though with far lower power) in InSb.

Two other techniques might also be used to create spin inversion or spin superradiance in (Cd,Mn)Se. Optical pumping of wurtzite-type semiconductors can be used to produce 100% spin-polarized electrons in the conduction band. With appropriate circular polarization, this method generates an inverted conduction electron spin population. The lower (spin down) laser level is depleted by recombination, thus permitting dipole-allowed, spin flip lasing to proceed.

Finally, a superradiant spin population can be generated in (Cd,Mn)Se by optically pumping with picosecond pulses in the geometry illustrated below:



Pulses, whose length (τ) satisfies the condition $\omega_S \tau < \pi$, are required to maintain superradiance - otherwise the whole fan of spin angles is populated, and the system has no net moment.¹³ FIR is emitted in a short, intense bursts at frequency ω_S .

MEMORIES

The bound magnetic polaron (BMP) is one of the most interesting new features observed in semimagnetic semiconductors. These complexes are the analogues, in semimagnetics, of conventional donors and acceptors. They have been studied in both n-type⁸ [(Cd,Mn)S, (Cd,Mn)Se] and p-type¹⁴ [(Cd,Mn)Te] materials. The donor-like BMP, for example, consists of an electron bound to a positive charge. Through its exchange interaction, the electron polarizes the Mn^{++} spins within its orbit, giving rise to a large ferromagnetic spin cloud. In (Cd_{0.95}Mn_{0.05})Se, for instance, the donor radius is $\sim 40\text{\AA}$; the orbit contains 400 Mn^{++} spins and, at low temperatures, has a net moment of 10-20 μ_B . In thermal equilibrium these moments are randomly oriented. However, given a pinning mechanism, one can imagine aligning each of them in a prescribed direction - and thus using each BMP to store a few bits of information. For $x < 0.17$ (the percolation limit) semimagnetics are paramagnetic and one does not anticipate pinning. On the other hand, for larger x-values, the Mn^{++} ions form a spin glass. In this range the tangled spin glass network could well provide the viscous forces to impede rotation of BMP moments, and thus permit information storage.

These ideas are visionary at present, since pinning mechanisms for BMP have not yet been identified, nor do we have techniques for addressing them or reading information stored in them. Nevertheless, the concept is sufficiently intriguing (raising the possibility of a memory storing $\approx 10^{16}$ bits/cc.) to suggest further research - of considerable inherent interest - on the subject. The most immediate problem is to determine relaxation rates and relaxation mechanisms for BMP, in both the paramagnetic and spin glass phases. Though the statistical mechanics of BMP is now fairly well understood¹⁵, there has been little work on their dynamics. This question might be addressed via nonlinear optical techniques, taking advantage of the large spin flip cross section. Such methods have already been used¹⁶ to determine spin relaxation rates (T_1 and T_2) in n-InSb. Alternatively, if the magnetization of BMP can be detected, frequency dependent magnetization measurements could be used to determine relaxation times for BMP moments. At low temperatures these times are expected to be in the millisecond range, since T_1 , for a single Mn^{++} ion, is of order 10^{-4} sec.

At this stage, it is hard to imagine a technique for aligning a single BMP. However, the Raman interaction might be used to align those BMP lying within the focus [order $(1\mu)^3$] of a laser beam. Petrou et al.¹⁷ have recently observed intense Raman scattering due to Mn^{++} ion paramagnetic transitions in (Cd,Mn)Se. The existence of such an interaction implies that Mn^{++} ions, subjected to a circular polarized optical field,

will experience an alignment force equivalent to a magnetic field in the propagation direction. The strength of this "effective" field is determined by the Raman cross section, which has not yet been measured (though is known to be large). Nevertheless, theoretical estimates, based on the model of Ref. 17, indicate that effective fields in the 10 kG can be achieved with current laser powers. Such fields, if applied for periods exceeding the relaxation time of BMP, are more than adequate to align the moments of these complexes.

ACKNOWLEDGEMENT

This paper was written under the auspices of the DARPA Materials Research Council, Contract #MDA903-82-C-0428 with The University of Michigan.

BIBLIOGRAPHY

1. R. R. Galazka and J. Kossut, Proc. Intl. School Narrow Gap Semiconductors, Nimes, France, p. 245; J. A. Gaj, Proc. 15th Intl. Conf. Physics of Semiconductors, Kyoto, J. Phys. Japan 49(1980), Suppl. A, p. 797.
2. See Panel Discussion on Technology, Proc. Conf. on Physics of Narrow Gap Semiconductors, Linz, 1981 (Springer-Verlag, Berlin, 1982) p. 280.
3. See H. Freir, *ibid*, and Refs. therein.
4. Nonlinear optic experiments indicate considerable inhomogeneity in (Hg,Cd)Te crystals. This work is discussed by Paul W. Kruse and John F. Ready, Nonlinear Optical Effects in $\text{Hg}_{1-x}\text{Cd}_x\text{Te}$, Semiconductors and Semimetals, Vol. 16 (Academic Press, New York 1981), pp. 230-235. Their conclusions are confirmed by unpublished measurements of Muehlner, Kash, Khan, Wolff, and Wood.
5. P. L. Anderson, H. F. Schaaake, and J. H. Tregilgas, J. Vac. Sci. Technol. 21, 125(1982).
6. J. K. Furdyna, J. Vac. Sci. Technol. 21, 220(1982).
7. R. T. Delves, Brit. J. Appl. Phys. 16, 343(1965).
8. M. Nawrocki, R. Planel, G. Fishman, and R. Galazka, Proc. 15th Intl. Conf. Phys. of Semiconductors, Kyoto, 1980, J. Phys. Soc. Japan 49(1980), Suppl. A, p. 823.
9. D. Heiman (to be published).
10. M. Dobrowolska, A. Witkowski, J. Furdyna, T. Ichiguchi, and H. D. Drew, Bull. APS 27, No. 3, Abstract Kell; also M. Dobrowolska, J. Furdyna, T. Ichiguchi, H. D. Drew, and P. A. Wolff (to be published).
11. D. Heiman (private communication).
12. Van Tran Nguyen and T. J. Bridges, Phys. Rev. Letters 29, 359(1972); Terrence L. Brown and P. A. Wolff, *ibid* 29, 362(1972).
13. This technique for generating superradiant spin populations is discussed in the 1982-85 FBNML proposal to NSF, p. 68.

14. A. Golnik, J. A. Gaj, M. Nawrocki, R. Planel, and C. Benoit a la Guillaume, Proc. 15th Intl. Conf. Physics of Semiconductors, Kyoto, 1980, J. Phys. Soc. Japan 49(1980) Suppl. A, p. 819.
15. T. Dietl and J. Spalek, Phys. Rev. Letters 48, 355(1982); D. Heiman, P. A. Wolff, and J. Warnock, paper to be presented at 16th Intl. Conf. Physics of Semiconductors, Montpellier, France, September 1982.
16. V. T. Nguyen, E. G. Brukhardt, and P. A. Wolff, Optics Comms. 16, 145(1976).
17. A. Petrou, D. L. Peterson, S. Venugopalan, R. R. Galazka, A. K. Ramdas and S. Rodriguez, Phys. Rev. Letters (in press).

THE SEMICONDUCTOR SPACE-CHARGE TRIODE

D. K. Ferry and T. C. McGill

With the advent of molecular-beam epitaxy, it has become possible to conceive, and to fabricate, some truly clever and innovative semiconductor device structures. One of these is the permeable-base transistor (PBT), in which a tungsten grid is embedded within a GaAs active region. In concept, the device is really analogous to a vacuum triode whose small dimensions offer promise for a microwave source in the 100-500 GHz region.

The PBT, however, is usually analyzed by a field-effect transistor (FET) model in which the tungsten grids are assumed to be buried Schottky-barrier gate electrodes.¹ For this model, the dominant transport length is the thickness of the grid structure (which corresponds to the gate length in the FET), and this length is typically of the order of $L = 200\text{\AA}$, with effects scaling as $1/L$. There are considerable questions about such a model, however, not the least of which is that L is small compared to the Debye length. Carried to the extreme of low doping, the channel is always "cut off". Yet, this is the classic triode case, in which current control by the gate is exercised not by channel-width modulation, but by modulation of space-charge in the emitter-gate region.

The analysis can not be truly that of a vacuum diode, however, because collisions occur within the semiconductor and these affect the device dynamics. Nevertheless, evaluation of

the high-frequency triode equations, modified for the presence of collisions, yield results surprisingly close to those obtained experimentally. This suggests that the analogy is a good one and that predictions of a very-high frequency source are valid. In the following, the modified space-charge equations are presented and a discussion of the high frequency limits is given. The approach closely follows the format presented by Spangenberg², although this latter author treats the traditional collision-free case.

SPACE-CHARGE CURRENTS IN A DIODE

The basic equations for a space-charge limited (SCL) diode are obtained by consideration of Poisson's equation

$$\nabla \cdot \mathbf{E} = \rho / \epsilon, \quad (1)$$

and the equation-of-motion for the carriers

$$m \frac{dv}{dt} = eE - \frac{mv}{\tau} \quad . \quad (2)$$

In a semiconductor, (2) is not strictly correct at high electric fields because of the presence of energy relaxation and a variation of τ with mean carrier energy. As a parametric equation, however, with τ being a fitted parameter, (2) has a degree of usefulness (not the least of which is that the following equations are tractable). As long as the precise details of the transient behavior are not crucial, (2) provides a useful method of approach and τ is fitted to more precise calculations.³

The general form of the current involves a combination of drift and displacement currents (diffusive forces are included via the total potential), or

$$J = \rho v + \epsilon \frac{\partial E}{\partial t} = \epsilon \frac{\partial E}{\partial t} \frac{\partial x}{\partial t} + \epsilon \frac{\partial E}{\partial t} = \epsilon \frac{dE}{dt} , \quad (3)$$

and

$$J_0 t = \epsilon E = \frac{\epsilon m}{e} \left(\frac{dv}{dt} + \frac{v}{\tau} \right) . \quad (4)$$

Using the integrating factor $\exp(t/\tau)$, we may now solve for the velocity

$$v = \frac{e J_0 \tau^2}{m \epsilon} \{ r - (1 - e^{-r}) \} , \quad (5)$$

and for the position

$$x = \frac{e J_0 \tau^3}{m \epsilon} \left(\frac{r^2}{2} \right) - v \tau , \quad (6)$$

where $r = t/\tau$ scales the time variation of the problem. From (5) and (6), we can now compute the average velocity through the space-charge region as

$$\langle v \rangle = \frac{d}{T} = (v_t/2) f(R) , \quad (7)$$

where

$$v_t = \lim_{t \rightarrow T} v(t) \quad (8)$$

$R = T/\tau$, T is the transit time, and

$$f(R) = \{ 1 - (1 - e^{-R})/R \}^{-1} - 2/R . \quad (9)$$

Generally, in space-charge problems one still needs to solve for the potential in terms of J_0 in order to eliminate this latter quantity from the above equations. However, in semiconductors, the high-field transport properties usually conspire to limit v_t , and hence to determine T from (7). We follow this procedure here.

HIGH-FREQUENCY LIMIT

It is of interest to determine the upper frequency limit of the semiconductor triode as an amplifier. This generally reduces to specifying f_T , the cut-off frequency of the device. In actual fact, however, such a specification depends upon the circuit in which the device is operated. A more common reference point is the frequency at which the output efficiency has dropped to a given percentage of the low-frequency value. This can be done fairly easily through the use of a few simplifying assumptions, first put forward by Gavin⁴ and followed here. The arguments are based upon considerations of the efficiency of the device as a class C oscillator. The drain current pulse is assumed to be a steady value that flows for one-quarter of a period, i.e., $i_d = I_d$ for $-\pi/4 < \omega t < \pi/4$, and zero otherwise. The corresponding drain voltage becomes

$$V_a(t) = V_{a0} - V_{a1} \cos(\omega t) \quad , \quad (10)$$

and the power loss is

$$W_{pl} = \frac{1}{2\pi} \int_{-\pi/4}^{\pi/4} I_d (V_{a0} - V_{a1} \cos\theta) d\theta \quad , \quad (11)$$

where $\theta = \omega t$. Thus,

$$W_{p1} = \frac{I_d}{4} \left[V_{a0} - \frac{2\sqrt{2}}{\pi} V_{a1} \right] . \quad (12)$$

The efficiency begins to drop off when electron transit-time effects cause the drain current pulse to lag the a.c. drain voltage by an angle $\theta_t = \omega T$, where T is the transit-time. The power loss under these conditions increases, and is given by

$$\begin{aligned} W_{p2} &= \frac{1}{2\pi} \int_{-\pi/4+\theta_t}^{\pi/4+\theta_t} I_d (V_{a0} - V_{a1} \cos \theta) d\theta \\ &= \frac{I_d}{4} \left[V_{a0} - \frac{2\sqrt{2}}{\pi} V_{a1} \cos \theta_t \right] . \end{aligned} \quad (13)$$

The efficiencies for the two cases are given by

$$\eta_1 = 1 - (W_{p1}/W_0) , \quad \eta_2 = 1 - (W_{p2}/W_0)$$

where $W_0 = I_d V_{a0}/4$ is the input power. The difference in efficiency is thus

$$\begin{aligned} \Delta \eta &= \eta_1 - \eta_2 = \frac{2\sqrt{2}}{\pi} (V_{a1}/V_{a0}) [1 - \cos(\omega T)] \\ &\approx \frac{\sqrt{2}}{\pi} (V_{a1}/V_{a0}) \omega^2 T^2 . \end{aligned} \quad (14)$$

The result (14) is significant in that all microwave devices, both vacuum-tube and semiconductor devices, eventually exhibit this $1/f^2$ behavior in the high-frequency limit, which reinforces confidence in the present approach.

To compute the relevant transit-time, one now needs to compute appropriate electrode potentials. The normal case in vacuum triodes⁴ is to set $V_{g,max} = V_{a,min} = V_{a0}/10$, so that the transit-time is determined by acceleration in the emitter-gate space-charge region and free-flight in the gate-collector region. This is not possible in the thick semiconductor layers used here for the gate-drain (drain and collector are used interchangeably for this device as are emitter and source) region. Here we assume $V_{g,max} = V_{a0}/10$, but take the field in the gate-drain region to be sufficiently high to maintain velocity saturation in this collision dominated regime. Thus, while T_{eg} is given by (7)-(9), T_{gd} must be found from v_t , at the gate, decaying to the bulk v_{sat} . In this region

$$v(t) = v_t e^{-t/\tau} + v_{sat}(1 - e^{-t/\tau}) \quad , \quad (15)$$

and an appropriate average velocity is

$$\langle v \rangle_{gd} = v_{sat} + (v_t - v_{sat})(1 - e^{-R})/R \quad . \quad (16)$$

Thus, with $\langle v \rangle_{eg}$ given by (7), the total transit-time is

$$T = \frac{d_{sg}}{\langle v \rangle_{eg}} + \frac{d_{gd}}{\langle v \rangle_{gd}} \quad . \quad (17)$$

For a 50% drop in efficiency, we take $\Delta\eta = \eta_1/2$, or

$$\Delta\eta = \frac{\sqrt{2}}{\pi} (V_{a1}/V_{a0}) = \frac{2\sqrt{2}}{\pi} (V_{a1}/V_{a0}) [1 - \cos(\omega t)]$$

or

$$f_T = (2\pi T)^{-1} (\pi/3) \quad . \quad (18)$$

In Table I, we present the values calculated for a current PBT technology, as well as for a proposed future device. The experimental f_T measured on this device is also given for reference.

Table I. GaAs PBT Amplifier

d_{sg}^*	0.3 μm	0.1 μm
d_{gd}^*	1.0 μm	0.1 μm
V_{a0}	2 V	1 V
v_t	3×10^7 c/s	5×10^7 cm/s
τ	2.1×10^{-13} s	1.8×10^{-13} s
t_{sg}	2.2×10^{-12} s	5.1×10^{-13} s
t_{gd}	6.45×10^{-12} s	2.5×10^{-13} s
T	8.65×10^{-12} s	7.6×10^{-13} s
f_T	19.3 GHz	210 GHz
$f_T(\text{exp})$	19.6 GHz	-

*W. T. Lindley, private communication. d_{gd} has been shortened to account for depletion effects.

UPPER OSCILLATION FREQUENCY

Also of interest is the maximum frequency at which oscillation can be achieved. Again, it depends upon the circuit, but with proper design (at least in vacuum tubes), it is the transit-time which dominates the behavior. As the frequency is raised, the gain falls off until the gate bias becomes zero. The carriers will then flow between the electrodes. The assumptions remain that of the previous section, but V_a is assumed to rise to the total V_{a0} . Thus, the potential of the gate plane (as opposed to the electrodes) is V_a/μ , where μ is the amplification factor of the analogous tube. Thus, we have a reduced gate voltage and much greater field (nearly constant) in the gate-drain region. The transit time in the source-gate region is given by

$$t_{sg} = \frac{2 d_{sg}}{v_t(V_a/\mu)f(R)} \quad , \quad (19)$$

while t_{gd} still is found from (15). An estimate of μ may be taken from the experimental results as ≈ 10 for a typical device. Thus, we may readily calculate the results, recognizing that the oscillator ceases to oscillate when the transit-time is some fraction k of a cycle, or

$$f_{\max} = \frac{k}{T_{cp}} \quad . \quad (20)$$

For structures such as the PBT, the value of k should be about that of a "light-house" triode, or 0.75. These results are shown in Table II.

Table II. GaAs PBT Oscillator

T	$8.65 \times 10^{-12} \text{s}$	$7.6 \times 10^{-13} \text{s}$
f_{max}	87 GHz	990 GHz
$f_{\text{max}}(\text{exp})$	100 GHz	-

DISCUSSION

The analysis presented here treats the PBT as an equivalent triode with semiconductor rather than vacuum as the inter-electrode material. The agreement is highly suggestive, leading to the speculation that space-charge injection at the forward-biased n^+-n source junction is important. Control of this space-charge by the gate electrodes, rather than channel pinch-off, is the dominant control mechanism. If this is correct, then the critical parameter to achieve high frequencies is not the gate structure itself, but rather the thickness of the GaAs layers in the source-gate and gate-drain regions. Indeed, very high frequencies should be achievable in GaAs, due to the overshoot velocity, if the various values of d can be pared to a total of $0.2 \text{ }\mu\text{m}$.

ACKNOWLEDGEMENT

This paper was written under the auspices of the DARPA Materials Research Council, Contract #MDA903-82-C-0428 with The University of Michigan.

REFERENCES

1. C. O. Bozler and G. D. Alley, IEEE Trans. Electron Dev. ED-27, 1128 (1980).
2. K. R. Spangenberg, Vacuum Tubes (McGraw-Hill, New York, 1928).
3. H. L. Grubin, D. K. Ferry, G. J. Iafrate, and J. R. Barker, in VLSI Electronics: Microstructure Science, N. Einspruch, Ed., Vol. 3 (Academic Press, New York, 1982).
4. M. R. Gavin, Wireless Engr. 16, 287 (1939).

OPPORTUNITIES FOR RESEARCH IN CONDUCTING POLYMERS AND MONOLAYER TECHNIQUES

M.S. Wrighton

INTRODUCTION

Research activity in the area of conducting polymers and Langmuir-Blodgett films has stimulated interest in a variety of application areas that might be of interest to the Defense Advanced Research Projects Agency (DARPA). Accordingly, a workshop was held at the July, 1982 meeting of the Materials Research Council (MRC) on these subjects. The program is given as Appendix A and the list of participants is Appendix B. The objectives of the workshop were to (1) summarize applications of interest to DARPA, (2) survey the status of the field, and (3) identify research opportunities for DARPA, especially those that are of generic importance that will lead to a knowledge base of sufficient depth and breadth to allow the charting of a path to technologically practical applications. This report emphasizes the connection of molecule-based materials to electronic devices.

LANGMUIR-BLODGETT FILMS

The monolayer materials considered here are monolayers formed by so-called Langmuir-Blodgett techniques that were summarized in the 1981 MRC report¹. The films formed by the Langmuir-Blodgett technique² have the following general properties³: (1) the films can be very thin monolayers, perhaps

10-20Å, or can be built to thicknesses of hundreds of angstroms using multilayer synthesis techniques; (2) monolayers can be thermodynamically stable, but are mechanically fragile; multilayers are also regarded as fragile, perhaps more so than monolayers; (3) the structure of monolayers may be dynamic; and (4) the molecules making up a monolayer or multilayer assembly are oriented. A variety of physical measurements can, in principle, be made to establish the structure of monolayer and multilayer assemblies. Fig. 1 is a representation of the synthetic procedure for a multilayer assembly that can be formed on a solid substrate and for which strong evidence exists for structure and composition.^{2,3}

For the past 50 years or so Langmuir-Blodgett films have been the object of fundamental study by chemists, physicists, and biologists.²⁻⁵ However, only in the last dozen years have so-called active molecules been incorporated into monolayer and multilayer assemblies.⁶⁻⁹ While not all potential applications for monolayers and multilayers hinge on the incorporation of active functional groups, much of the current interest does stem from the more difficult to synthesize molecules having interesting optical and chemical properties. Further, many practical applications could stem from the ordering of active molecules in the assembly, justifying the enthusiasm associated with proof of structure for assemblies like that represented in Fig. 1.

Some of the more interesting experiments in recent years that illustrate the utility of functionalized molecules in

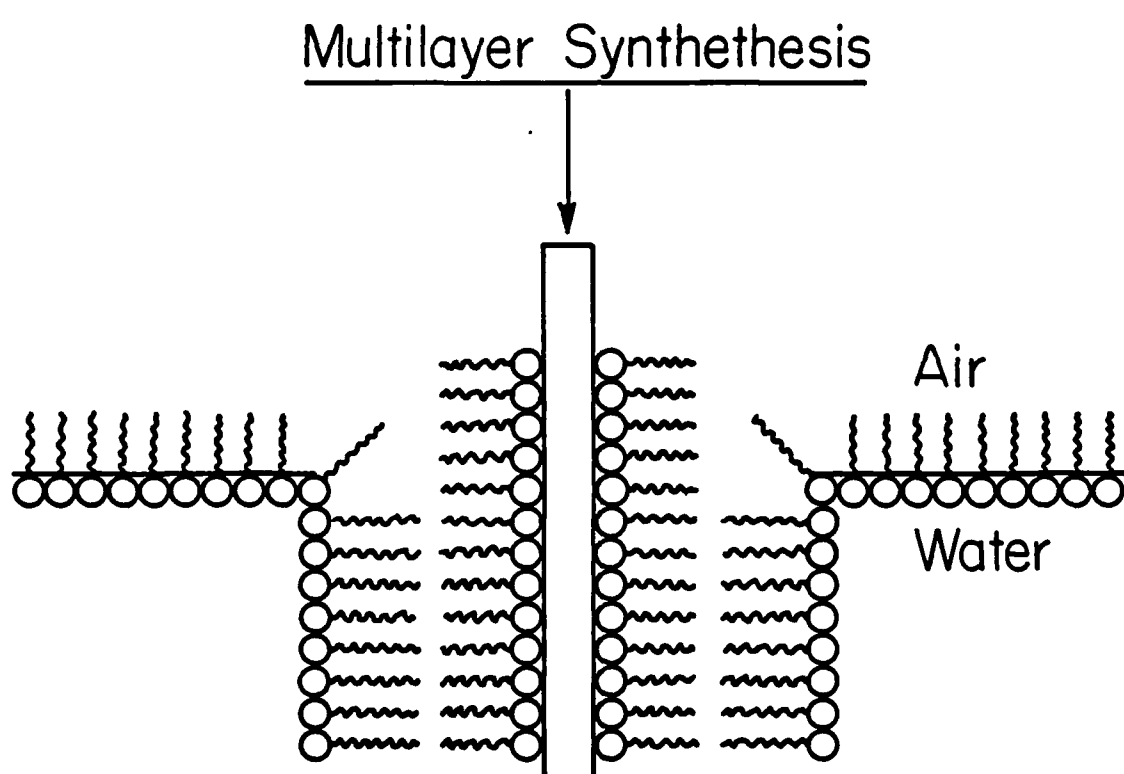


Figure 1. Representation of multilayer film synthesis by the Langmuir-Blodgett technique.

Langmuir-Blodgett films are summarized in the following paragraphs.

1. Distance Dependence of Energy Transfer.^{7,8} Consider the multilayer assembly represented by Fig. 2 where a light absorbing donor molecule is separated by a spacer or set of spacer molecules from an energy transfer quencher molecule. Study of the quenching of the fluorescence of the donor as a function of spacer thickness has given information concerning the distance dependence of energy transfer efficiency.

2. Funnelling Optical Excitation.^{7,8,10} Another set of energy migration experiments has shown that optical energy can be "concentrated" in a manner analogous to that in natural photosynthesis where there are a few active centers among a large number of light-absorbing chlorophyll molecules. For illustration, Figure 3 represents the sort of multilayer assembly used to show that light energy absorbed by one molecule present in a ~300-fold excess compared to an acceptor results in efficient luminescence from the dilute species.

3. Excited State Electron Transfer.⁷⁻⁹ Experiments using multilayer assemblies like that represented in Fig. 2, where the light absorber is an excited state electron transfer reagent and the quencher is a redox reagent, have been carried out to determine factors influencing electron transfer rates. As in the energy transfer experiments, the architecture of the assembly and durability on the timescale of the experiments are essential to interpretation of the results.

Electron and Energy Transfer

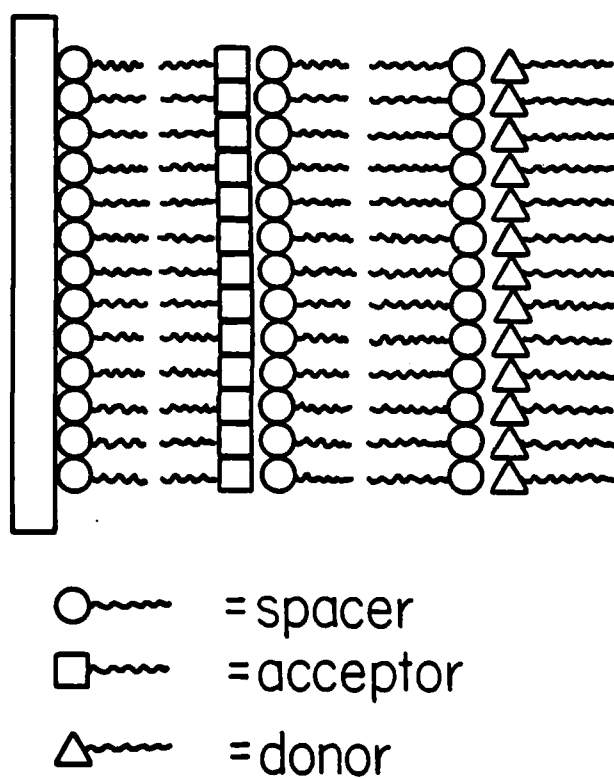
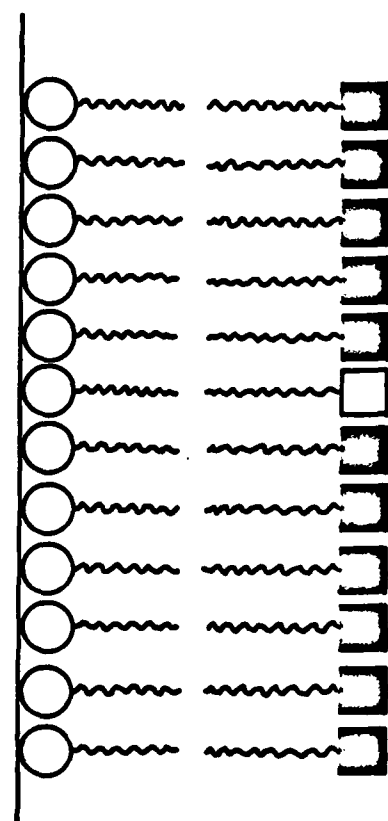


Figure 2. Multilayer assembly for excited state electron transfer and energy transfer studies.



- ~~~~ fatty acid, e.g. stearic acid
- ~~~~ light absorber
- ~~~~ energy acceptor by
energy transfer from the
the light absorber

Figure 3. Representation of multilayer assembly used to study optical funnelling.

4. Polymerizable Films.¹¹⁻¹⁴ Multilayers of e⁻-beam polymerizable ω -tricosenic acid, $\text{CH}_2\text{CH}(\text{CH}_2)_{20}\text{COOH}$, can be deposited onto solid substrates. As negative resist, a 450Å thick layer assembly was shown to give a resolution of ~600Å using e⁻-beam polymerization.¹³ UV and X-ray sensitive films from diacetylene carboxylic acids, $\text{CH}_3(\text{CH}_2)_n\text{-C}\equiv\text{C-C}\equiv\text{C-(CH}_2)_m\text{COOH}$, can also be polymerized.^{11,14}

5. Electroluminescence.¹⁵ Thin films (~500Å) formed from derivatives of anthracene sandwiched between two electrodes exhibit blue electroluminescence. A key in this experimentation was the prior demonstration that relatively short aliphatic chain derivatives of anthracene could be used to form monolayers and multilayers. This allows the functional groups, anthracene, to be close to each other to insure good conduction through the film.

6. Photoelectrochemistry. Excited state electron transfer from a monolayer of a derivative of $\text{Rn}(2,2'\text{-bipyridine})^{2+}$ on an optically transparent SnO_2 electrode¹⁶ illustrates one of the many photochemical experiments⁶⁻⁸ carried out with visible-light responsive monolayer systems. The "sensitized" photocurrent for the SnO_2 suggests the possibility that visible light can be used to oxidize H_2O .

The research mentioned above and other experimentation testifies to the scientific vitality associated with the study of Langmuir-Blodgett films. A lengthy list of potential practical applications has emerged including:

- * Display Devices
- * MIS Devices
- * Interfaces with Biological Systems
- * Solar Energy Converters
- * Optical Waveguides
- * Planar Lasers
- * Resists for Microlithography
- * Capacitors
- * Non Linear Optical Devices
- * Chemical Sensors
- * Imaging Devices
- * Lubricants
- * Corrosion Suppressors
- * Heat Exchange Surfaces
- * Ambient Temperature Infrared Detectors
- * Suppressors of H₂O Evaporation
- * Adhesives

However, it is evident that Langmuir-Blodgett films have not achieved widespread use in any applications and most of the potential applications would be regarded as long term (>10 years), high-risk possibilities. At present there are no commercial applications of Langmuir-Blodgett films. Further, U.S. expertise, even in basic science of monolayer techniques, is low compared to Western Europe.

RECOMMENDATIONS REGARDING LANGMUIR-BLODGETT FILMS

A DARPA program in thin, molecule-based films is recommended. The Langmuir-Blodgett technique comprises but one path to the synthesis of such films and could be especially useful to establish proof-of-concept in applications. The program should focus on the physical and chemical properties unique to thin, molecule-based films including especially the possibility of oriented functional groups, chemical reactivity, tailorability, and substrate interactions. Research in this field should be undertaken with the knowledge that it is an interdisciplinary problem area where chemists will play a critical role, since molecules having new properties are required. Research teams should be of at least critical size, diverse in expertise, and supported by an array of analytical characterization tools such as microscopy, surface spectroscopies, and instrumentation to evaluate practical aspects. The critical manpower size for a research team would seem to be in the range of three to five. The research in thin, molecule-based films would seem to be well-suited to universities with facilities for interdisciplinary experimental programs.

It should be emphasized that the recommended program involves an area that is still at the research laboratory stage, but the rationale for the recommendation to have a DARPA program rests in the conviction that there will be practical applications of consequence for thin, molecule-based films. Two additional considerations, albeit of secondary importance to DARPA,

are that (1) in the U.S., basic science of monomolecular and multilayer films for electronic materials has not been actively pursued, while foreign efforts have been substantial, especially in Great Britain, West Germany, France, and Japan, and (2) thin film techniques, and perhaps Langmuir-Blodgett techniques especially, may offer unique insight into physical and chemical properties such as tunnelling, unidirectional electrons transfer, energy transfer, synthesis of oriented polymers, and biological membranes.

Since the recommendations for a DARPA program rests on the conviction that unique, practical applications will exist, it is appropriate to indicate some promising areas. One is the area of MIS devices. Insulating Langmuir-Blodgett films have been deposited onto InP and low interface state density has been claimed.¹⁷ A drift-free InP FET has also been claimed and the barrier height for n-InP has been improved from ~ 0.4 to ~ 0.9 eV by sandwiching a Langmuir-Blodgett film between the InP and the metal.¹⁸ A second area of promise is the resist materials for microlithography where good resolution has been demonstrated¹³; clearly molecule-based systems for resists will be useful, since organic materials are presently used for this purpose. A third promising area concerns chemical detection and biological interfacing devices where both will depend on the connection of electronic systems to chemical or biological systems at the molecular level. Fourth, preliminary results for integrated optics are encouraging; waveguides,¹⁹ second harmonic generators, and

electrooptic effects generally could stem from work with diacetylenes.¹⁴

Research issues that require resolution still remain before there is a clear path to a technology employing thin, molecule-based films. These include the structure and integrity of the film. For example, will a Langmuir-Blodgett insulating film of a MISFET survive subsequent processing steps and what is the long-term life? While the Langmuir-Blodgett films may have integrity and orientation with respect to the substrate onto which they are grown, what about the structure after deposition of a contact? What is the role of impurities in film growth and what growth conditions are required to achieve reproducibility? If the Langmuir-Blodgett technique emerges as unique, what can be done to automate the technique and improve throughput? These questions should be among those addressed in components of a DARPA program in the area of thin, molecule-based films.

CONDUCTING POLYMERS

Conducting polymers, specifically electronic conducting polymers, have been actively studied in recent years.²⁰ Perhaps the best known of these materials are $(\text{SN})_x$ ²¹ and polyacetylene,²² but there are a number of organic polymers that have high conductivity. Table I shows some of the polymer systems studied in this connection. It should also be noted that considerable effort has been directed toward the conducting properties of molecular crystals.²³ Generally, conducting organic materials require doping with species such as I_2 , AsF_5 , or Na.

There is considerable concern regarding stability to air and heat in such systems. Nonetheless, a material such as polyacetylene can be fabricated in a large sheet that resembles a metallic foil in appearance and yet is very lightweight. Organic polymer has a density of $\sim 1 \text{ g/cm}^3$ whereas Cu has a density of 8.92 g/cm^3 . It is also evident that there are many existing applications for polymers including the use of photoconductor materials in copying machines as an identifiable practical use of a polymer in an active electronic device. Piezoelectric polymer materials also have commercial significance. Future applications for conducting polymers may include their use as an active element in high energy density batteries, as shielding material, as a component in printing inks, as antistatic coatings, as photovoltaic cells, and as key elements in electromechanical devices.

RECOMMENDATIONS REGARDING CONDUCTING POLYMERS

Conducting materials formed from the polymerization of molecules, e.g. polyacetylene from acetylene, comprises a field of potential long-range interest to DARPA. A few university groups and industrial laboratories have programs in this area. Basic research advances hinge, in large measure, on synthetic chemistry. The experimental results obtained so far do not justify a major DARPA effort at this time. Difficulties associated with known conducting polymers such as the need for dopants and heat and air instability can possibly be overcome through the design and synthesis of new polymers. Present conductivi-

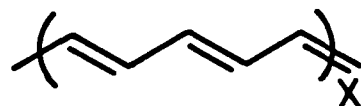
ties for the polymers in Table I are $\sim 10^3$ lower than copper, but doped graphite can exceed copper in conductivity.²⁰ It should be noted that polymers filled with a conducting materials such as graphite will offer many of the same properties as a conducting polymer formed from monomer units. Research of conducting polymer materials should be supported at a low level for several reasons: (1) to undergird the effort on thin, molecule-based films; (2) to maintain awareness in the field; and (3) seed, new innovative research programs of high quality. Conducting polymers would offer unique features such as the ability to span a wide range of conductivities through structural modifier atoms and doping type and level, advantages associated with polymer processing, and molecular specific properties that could be exploited in a variety of ways.

ACKNOWLEDGEMENT

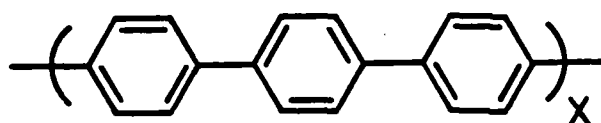
This paper was written under the auspices of the DARPA Materials Research Council, Contract #MDA903-82-C-0428 with The University of Michigan.

Table I. Some Electronically Conducting Polymers

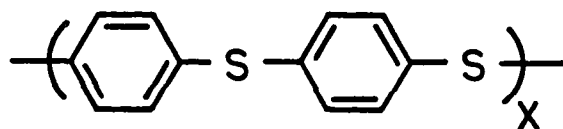
1. Polyacetylene



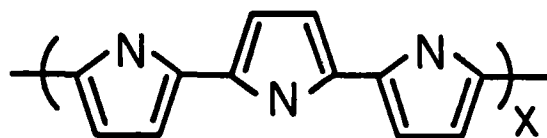
2. Poly-p-phenylene



3. Poly-p phenylenesulfide



4. Polypyrrole



REFERENCES

1. M. S. Wrighton, "Use of Monomolecular Layer Techniques in Microlithography," Preliminary Reports, Memoranda and Technical Notes of the Materials Research Council Summer Conference, Vol. II, La Jolla, California, July, 1981, pp. 145-159.
2. (a) K. B. Blodgett, J. Am. Chem. Soc., 1935, 57, 1007; (b) K. B. Blodgett, I. Langmuir, Phys.Rev., 1937, 51, 964; (c) H. Kuhn, D. Mobius, H. Bucher, in Physical Methods of Chemistry, vol. I, Part IIIB, A. Weissberger, B. W. Rositor, eds., Wiley, New York, 1972.
3. G. L. Gaines, Jr., Insoluble Monolayers at Liquid-Gas Interfaces, Interscience, New York, 1966.
4. G. L. Gaines, Jr., in Surface Chemistry and Colloids, vol.7. M. Kerker, ed., Butterworths, London, Chapter 1.
5. V. K. Srivastava, Phys. Thin Films, 1973, 7, 311.
6. (a) P. S. Vincett, G. G. Roberts, Thin Solid Films, 1980, 68, 135. (b) G. G. Roberts, P. S. Vincett, W. A. Barlow, Phys. Technol., 1981, 12, 69.
7. H. Kuhn, D. Mobius, Angew. Chem. Int. Ed. Engl., 1971, 10, 620.
8. (a) H. Kuhn, J. Photochem., 1979, 10, 111 Pure Appl. Chem., 1979, 51, 341 and 1981, 53, 2105; (b) D. G. Whitten, Angew. Chem., 1979, 91, 472.
9. D. Mobius, Accs. Chem. Res., 1981, 14, 63.
10. M. Vandevyver, A. Ruaudel-Teixier, Thin Solid Films, 1980, 68, 129.
11. B. Tieke, G. Lieser, G. Wegner, J. Polym. Sci., Polym. Chem. Ed., 1979, 17, 1631.
12. A. Cemel, T. Fort, Jr., J. B. Lando, J. Polym. Sci., Part A1, 1972, 10, 2061.
13. A. Barraud, C. Rosilio, A. Ruaudel-Teixier, Solid State Technol., 1979, 22(8), 120.
14. A. F. Garito, MRC Meeting, La Jolla, July, 1982.

15. (a) P. S. Vincett, W. A. Barlow, F. T. Boyle, J. A. Finney, G. G. Roberts, *Thin Solid Films*, 1979, 60, 265; (b) G. G. Roberts, M. McGinnity, *Solid State Commun.*, 1979, 32, 683.
16. R. Memming, F. Schroppel, *Chem. Phys. Lett.*, 1979, 62, 207.
17. (a) G. G. Roberts, K. P. Pande, W. A. Barlow, *IEEEJ. Solid-State Electron Devices*, 1978, 2, 169; and *Electron. Lett.*, 1977, 13, 581. (b) R. W. Sykes, G. G. Roberts, T. Fok, D. T. Clark, *IEE Proc. Part I*, 1980, 127, 137; (c) G. G. Roberts, in *Insulating Films on Semiconductors*, Proceeding of the Second International conference, INFOS 81, Erlangen, Fed. Rep. of Germany, M. Schulz, G. Pensl, eds., Springer-Verlag, Berlin, 1981, p. 56.
18. C. M. Stickley, S. D. Grant, *Report of Visits to Britain and France Regarding Langmuir-Blodgett Films*, BDM/W-82-382-TR, July 8, 1982 [Private Communications.]
19. (a) C. W. Pitt, L. M. Walpita, *Electrocomp. Sci. and Tech.*, 1977, 3, 191; (b) E. Colombini, G. L. Yip, *Trans. IECE Jap.*, 1978, E61, 54.
20. (a) R. H. Baughman, J. L. Bredas, R. R. Chance, R. L. Elsenbaumer, L. W. Schacklette, *Chem. Rev.*, 1982, 82, 209; (b) G. B. Street, T. C. Clarke, *IBM J. Res. Develop.*, 1981, 25, 51.
21. (a) V. V. Walatka, Jr., M. M. Labes, J. H. Perlstein, *Phys. Rev. Lett.*, 1973, 31, 1139; (b) G. B. Street, R. L. Greene, *IBM J. Res. Develop.*, 1977, 21, 99.
22. A. G. MacDiarmid, A. J. Heeger, *Synthetic Metals*, 1980, 1, 101.
23. A. F. Garito, A. J. Heeger, *Accs. Chem. Res.*, 1974, 7, 232.

Appendix A

DARPA/MRC MEETING CONDUCTING POLYMERS AND MONOLAYER TECHNIQUES

July 21-22, 1982

Scripps Elementary School
2225 Torrey Pines Road

Wednesday, July 21, 1982

Introduction: M. Wrighton, R. Reynolds/DARPA, K. Wynne/ONR

"Overview of Unique Polymer Properties"

A. F. Garito, University of Pennsylvania

"Rational Synthesis of Conducting Polymers"

T. J. Marks, Northwestern University

"Langmuir-Blodgett and Related Methods of Thin Film
Formation: Overview and Recent Applications"

G. L. Gaines, Jr., General Electric R&D Center,
Schenectady, New York

"Future Applications of Langmuir-Blodgett Films"

A. Ruaudel-Teixier, Centre d'Etudes Nucleaires de Saclay

"The Use of Multilayers and PCSR in Order to Produce
Submicron Resolution Polymer Resists, Optical Waveguides,
and Photoactive Polymer Resists"

S. E. Rickert, Case Western Reserve University

"Microlithography for VLSI"

H. Sachdev, IBM, Poughkeepsie

Summary of Significant Research and Technological
Opportunities - All Participants

Thursday, July 22, 1982

Round table discussion - All Participants

Appendix B

PARTICIPANTS

<u>Name</u>	<u>Affiliation</u>
M. S. Wrighton	M.I.T./MRC
A. F. Garito	U. of Penn.
K. J. Wynne	ONR
S. E. Rickert	Case Western Reserve University
L. E. Cross	Penn State/MRC
Angus Macleod	U. of Arizona
Schuyler Grant	BDM Corp.
Annie Ruauadel	Commissariat Energie Atomique France
Henry Ehrenreich	Harvard/MRC
Harbans Sachdev	IBM
Krishna Sachdev	IBM
Elliott Levinthal	DARPA
Gordon Kim	Stanford U.
T. C. McGill	Caltech/MRC
D. K. Ferry	Colo. State Univ.
George Vineyard	Brookhaven/MRC
Harry V. Winsor	AFOSR/NE
J. L. Margrave	Rice Univ.
E. E. Hucke	U of Michigan
M. J. Sinnott	U of Michigan
E. J. Friebele	DARPA
R. R. Neurgamkar	Rockwell
C. M. Stickley	BDM
Dick Reynolds	DARPA
Tobin Marks	Northwestern
George Gaines	GE

DARPA PERSPECTIVE ON POLYMER OPPORTUNITIES

R. E. Green

Historically, the Materials Sciences Division of DARPA has supported research efforts on a number of projects concerned with polymeric materials and composites. Currently, research is being supported in conducting polymers, the carbon-carbon turbine engine, and metal matrix composites. Partially as a result of DARPA's earlier pioneering efforts, polymer based composites are playing an ever increasing role in military structures. The example of military aircraft is particularly illustrative, where the F-4 had no composites based on structural weight, while the F-15 has 2%, the F-18 10%, and the AV-8B 26% composites on the same basis. Moreover, the design of newer revolutionary aircraft, such as the forward swept-wing, is only possible because of the use of graphite epoxy materials and processing to attain the necessary greater wing stiffness without greater weight. Conventional wings are not stiff enough to withstand the high dynamic pressures of high-speed flight encountered in the forward swept-wing design. The price of greater stiffness using conventional metallic materials is normally greater weight, which reduces both maneuverability and high-speed capabilities. The high strength, high stiffness, light weight, non-energy intensive polymeric matrix composite materials are extremely attractive for this and other similar military applications.

The LearFan 2100 is the first all-composite aircraft to be developed. More and more composite materials are being used

in helicopters and engineers from a number of major aircraft manufacturing firms believe that an 85% composite helicopter is feasible. Not only will this helicopter offer an expected 22% weight savings, but it will possess improved resistance to projectile damage and a smaller radar cross-section than if it were made from metallic materials. Compared with the total absence of composites in the B-707 the newer B-747, and B-767 consist of approximately 30% composite structures.

Composite materials also offer many advantages for space applications, particularly those made from carbon-carbon. These composites possess outstanding mechanical and thermal properties and show evidence of being the most laser damage resistant of all structural materials.

For these and other related reasons it was deemed desirable to hold a two day session on "Polymer Opportunities" during the Materials Research Council meeting and to invite experts in the various aspects of polymers and polymer based composites to bring the Council members up-to-date on the present status of developments in this field and to suggest areas where new innovative research would lead to marked advances in the production and application of these materials.

ACKNOWLEDGEMENT

This paper was written under the auspices of the DARPA Materials Research Council, Contract #MDA903-82-C-0428 with The University of Michigan.

OPPORTUNITIES IN POLYMERS

J. L. Margrave

INTRODUCTION

A two day workshop on opportunities in polymers explored opportunities for DoD to exploit fully the potential of polymeric materials. Keynoted by Professor P. J. Flory, Nobel Laureate in Chemistry from Stanford University, the meeting addressed topics ranging from polymer synthesis to engineering.

Growth in the use of polymers has been so great that the physical volume has exceeded that of steel. Applications in the private and military sectors include transportation, building materials and electronics and packaging. The use of polymers in transportation has been growing rapidly as evidenced by the Lear fan jet which is made almost entirely from polymer matrix composites. By the turn of the century it is anticipated that composites will become the dominant materials in aircraft. For military applications where performance is at a premium even a higher use percentage can be expected. Polymers are replacing other materials because of high specific properties, energy efficiency, corrosion resistance and ease of fabrication. A recent survey of the National Research Council on research opportunities in synthetic polymers identified accelerated tests for long term performance, mechanisms of degradation, theory underlying failure phenomena, polymers in demanding environments, extraordinary strength and multi-phase systems. All these areas

have potential impact for DoD applications of polymeric materials. The following summary of speakers' comments at the workshop provide further insight into opportunities for DoD in polymer science and engineering. The summaries are followed by conclusions that outline a DARPA program in polymeric materials and engineering.

SUMMARY OF SPEAKERS' COMMENTS

Professor P. J. Flory of Stanford University spoke of the high potential of polymers in applications demanding high specific stiffness and strength. Attainable values are in excess of 10X those of metals and the potential for even greater tensile properties is large. In Flory's view there is insufficient activity in the design of materials that approach theoretical limits. These properties are controlled by the chemical and physical structure of macromolecules and Flory presented his recent work in which semi-empirical methods are used to calculate the minimum energy structure of polymers using, as examples, polyisobutylene and polycarbonate. The calculations yield potential energy surfaces which can be used to determine the theoretical tensile modulus. It was pointed out that calculated tensile modulus values would serve as measures against which to assess the effectiveness of processing conditions in achieving maximum properties.

Professor D. A. Tirrell of Carnegie Mellon University presented an overview of methods of polymer synthesis, including recent advances in new methods targeted towards specific

polymers. In particular, the technique of free radical ring opening polymerization was presented as a way of synthesizing polymers with rings in the backbone. Such polymers have greater rigidity and hence the potential for high specific tensile properties. The preparation of α,ω difunctional polymers using the Inifer technique was discussed. In this technique there is chain transfer involving exchange of the active center from one chain to another. The method has utility in producing terminal function groups used to prepare block and network polymers. Photoinitiation of ionic polymerization was presented as a method of lowering the energy of monomer ring opening as in the case of epoxies.

Professor F. Karasz of the University of Massachusetts presented an overview of well-known polymer blends. These materials result from physical mixtures of two or more polymers, although in most cases only two components are used. The resultant mixture, or blend, falls into two categories, compatible, in which the individual polymers mix at the molecular level, and incompatible, in which phase separation occurs resulting in a variety of interesting microstructures. Polymer blends are becoming an important class of engineering plastics since mechanical properties can often be enhanced and processibility can be improved. Despite the extremely large number of possible combinations of known polymers only very few form compatible blends as a result of the low energy of mixing. Furthermore, for a

given blend system there are regions of compatibility depending on composition and temperatures.

Professor K. L. DeVries of the University of Utah gave an overview of mechanical properties of polymers and the molecular basis of the limits in performance properties. Using a polystyrene cup as an example he demonstrated the relationship between molecular orientation and failure modes. The cup was observed to fail by tangentially running cracks as a result of preferential molecular orientation in that direction produced during processing. This would suggest that by processing to lessen molecular orientation performance could be improved. According to DeVries, this is but one example of how knowledge of molecular structure and its relationships to performance properties can be used to improve performance. Professor DeVries then discussed the role of chain scission and free radicals in mechanical durability of polymers. Experiments were described in which electron spin resonance spectroscopy was utilized to correlate free radical production with the state of mechanical strain and stress. Chain scission was presented in the framework of the kinetic theory of bond rupture as the primary molecular event leading to mechanical degradation. An outstanding question to be addressed according to DeVries is the relationship between the number of free radicals produced by mechanically activated chain scission and the total resultant number of chain scissions.

Dr. R. K. Eby of the National Bureau of Standards presented an overview of polymer failure. Citing the rapid growth of polymers in critical defense related applications he pointed out the need for accelerated testing, lifetime prediction techniques, and nondestructive evaluation methods to insure optimal performance. Examples were given of premature failure as a result of dielectric breakdown, chemical attack, loss of protective additives, excessive wear, brittle fracture and environmental stress cracking. The approach to improved polymer durability is to better understand the interrelationships between molecular structure and failure mechanisms. Short term testing to predict long term performance often suffers from inaccurate models of failure under the in-service conditions. A DoD procurement specification for a helicopter rotor seal was given as an example of an improper accelerated test methods with the result that the part failed in a time much shorter than that predicted by the test method. A possible nondestructive test method for mechanical durability based on a spectroscopic technique utilizing the improved sensitivity of Fourier transform infrared was discussed. Related work at the NBS was presented in which the question of free radicals and chain scissions raised by Professor DeVries in his talk was addressed. Dr. Eby concluded with an example of the importance of the degree of cure in the mechanical performance of polymer based composite materials. In this work, also carried out at NBS, it was shown that the compatibility of composites with various liquids is strongly

dependent on the degree of cure. Spectroscopic, dielectric and ultrasonic methods were presented as ways of monitoring the completeness of cure. In summary, Eby pointed out that improved predictive techniques represent an urgent need and that they offer the potential for increased performance, life, and reliability of polymers in DoD applications.

The last three presentations concerned polymer engineering. Professor S. Becker of MIT illustrated the importance of macrostructures in failure of objects made from polymer fibers. Professor K. L. Reifsnider of Virginia Polytechnic Institute discussed engineering aspects of fiber reinforced polymer-based composites. The importance of a complete mechanical properties characterization of composites was stressed. Failure of composites was viewed as a three part process involving the polymer matrix, the matrix reinforcement interface and the fiber reinforcement. In Professor Reifsnider's view failure of a polymer composite ultimately involves failure of the fiber reinforcement. Professor E. G. Henneke, also of Virginia Polytechnic, presented an overview of NDE methods as applied to polymer composites. These included scattering techniques such as optical inspection and x-ray methods, ultrasonic techniques, acoustic emission and thermography. In the last mentioned method the test specimen is subjected to small amplitude vibrations and a temperature profile of the specimen is recorded using an IR camera. Correlations are observed between the thermogram and other techniques.

CONCLUSIONS

Workshop participants defined four major categories of polymer research opportunities. A summary of these categories with examples for each are given in the table following. There are two approaches that provide opportunity for pay-off.

One is a program which focuses on a particular class of polymer but which extends across all four of the categories in the table. While individual participants emphasized the need for research in a particular category, it should be recognized that successful application of a new polymer will require ability to 1) characterize it, 2) process it into end products, and 3) evaluate and predict useful life under the service conditions. A successful program should involve an iterative process where processing limitations can guide modifications in synthesis and improved characterization leads to better failure analysis. The class of polymers which appear to be most promising for major materials innovation are "rigid-rod" polymers which by virtue of a high degree of orientation of the molecular covalent bonds possess extremely high specific strength in the covalently bonded direction. One such commercial polymer, "Kevlar", has already made a major impact as a high strength material. Improved materials of this type (stronger, cheaper, processible in bulk objects, more durable) hold promise as a major new frontier in materials research.

The second recommended approach is to concentrate on the critical problem of developing methods for characterizing and

POLYMER OPPORTUNITIES

I. SYNTHESIS

- Rigid-rod Polymers
- Coupling Agents
- New kinds of Matrix-polymers
- Precursors to Boron, Carbon & Silicon-based Polymers

II. DESIGN & MATERIALS CONSIDERATIONS

- Lifetime Prediction Tests
- Multi-components Materials
- Intractable Materials (Thermoset)

III. PROCESSING

- Geometry of Fiber Arrangements
- Evaluation of Matrix-cure Process
- Bulk "Rigid-rod" Polymers
- Novel Molding Techniques
- Joining (Adhesive Binding)
- Coatings
- Radical Innovations in Fabrication
(3-D, Large Scale)
- Solution Processing
- Co-cured Processes

IV. SERVICE USE

- Multimode Loading
- Degradation Mechanisms
(Hostile Environments)
- Failure Criteria
- NDE & Lifetime Prediction
- Mechanical Properties
 - Analytical Techniques for Predicting Modulus
- Testing & Evaluating - Dynamic Loading
- Materials Design & Optimization
(Flywheel)

predicting accurately the service life of polymers used in DoD applications. Such a project could greatly reduce the incidence of unexpected failures and would make it possible to take greater advantage of the increased performance potential which polymers offer through their greater specific strength, corrosion resistance, etc. It should address problems concerned with a variety of polymers found in a broad range of DoD interests. It would be a good first project since it would bring DARPA managers into contact with a broad range of problem areas for which improved polymers are needed. Thus, it would serve to identify key areas and opportunities for subsequent projects.

ACKNOWLEDGEMENT

This paper was written under the auspices of the DARPA Materials Research Council, Contract #MDA903-82-C-0428 with The University of Michigan.

MRC WORKSHOP ON POLYMER OPPORTUNITIES

July 22-23, 1982
Scripps Elementary School
La Jolla, California

SESSION I - July 22

Chairman: J. Margrave

"DARPA Perspective on Polymer Opportunities"
R. E. Green, DARPA

"Conformation of Polymers"
P. F. Flory, Stanford University

Discussion

"Polymer Synthesis"
D. A. Tirrell, Carnegie Mellon University

Discussion

SESSION II - July 22

Chairman: R. Baughman

"Polymer Blends"
F. E. Karasz, University of Massachusetts

Discussion

"Mechanical Properties"
K. L. DeVries, University of Utah

Discussion

SESSION III - July 23

Chairman: P. Lindenmeyer

"Failure of Polymers"

R.K. Eby, National Bureau of Standards

Discussion

"Fibers"

S. Backer, Massachusetts Institute of Technology

Discussion

"Engineering Aspects of Composites"

K.L. Reifsnider, Virginia Polytechnic Institute

Discussion

"Nondestructive Evaluation of Composites"

E.G. Henneke, Virginia Polytechnic Institute

Discussion

SESSION IV - July 23

Chairman: R. Green

General Discussion: The intent of this general discussion is to summarize the present status of the subjects covered and to identify future scientific and technological goals.

SOLID STATE PROPERTIES OF POLYMER BLENDS

F. E. Karasz

INTRODUCTION

The most generally used and accepted criterion for polymer-polymer miscibility (compatibility) continues to be the appearance of a single glass transition temperature (combined with the disappearance of the T_g 's of the constituents). Nevertheless, there are binary systems in which this criterion is inapplicable (e.g., in which the T_g 's of the proposed constituents are too close, or in which the T_g 's are masked by partial crystallinity in either or both constituents, etc.). In addition, this single T_g criterion suffers from at least two more fundamental drawbacks. Firstly, it does not in itself, provide any information about the microscopic, i.e., monomer level, structure of the mixture, and secondly it is a criterion which of necessity reflects conditions some tens of degrees above the glass transition temperature interval, i.e., there is an inevitable nonequilibrium intrusion into a problem which is already complicated in many respects. The T_g criterion thus cannot normally yield information about equilibrium states below the T_g ; this is especially troublesome if there are upper critical solution phenomena in this temperature regime.¹

Partly because of these limitations, complementary means for studying miscibility or near-miscibility are being increasingly used. For example, scattering methods (light, x-ray or

neutron, at angles appropriate to the dimensional levels to be studied) can yield substantial information about chain conformation and homogeneity in certain cases. Scattering techniques have the advantage that, in principle, they can be used under conditions of thermodynamic equilibrium, i.e., far above T_g , though the interpretations are seldom without potential ambiguities. The study of dielectric relaxations also can yield substantial additional information in favorable cases, as will be discussed below. Finally, we draw attention to the quite useful technique of solution calorimetry which can provide not only quantitative thermodynamic data concerning heats of mixing but can also reveal, uniquely, information about equilibrium states below the T_g of a binary polymer system. This is accomplished, in essence, by taking advantage of the fact that a solvent will depress the T_g of the polymeric blend far below the experimental measuring temperature regime.

PHASE BEHAVIOR

The system Poly(2,6-dimethyl phenylene oxide) (PPO) and polystyrene has served as a useful prototype for totally compatible amorphous systems. By employing copolymers of styrene and either 2-or 4-chlorostyrene, it is possible to obtain systems which display phase separation in an experimentally observable temperature range. Figure 1 indicates the phase behavior of PPO with styrene-co-2-chlorostyrene copolymers of the indicated composition in 50/50 weight % mixtures. The boundary separating one and two phase regimes is the approximate locus of a series

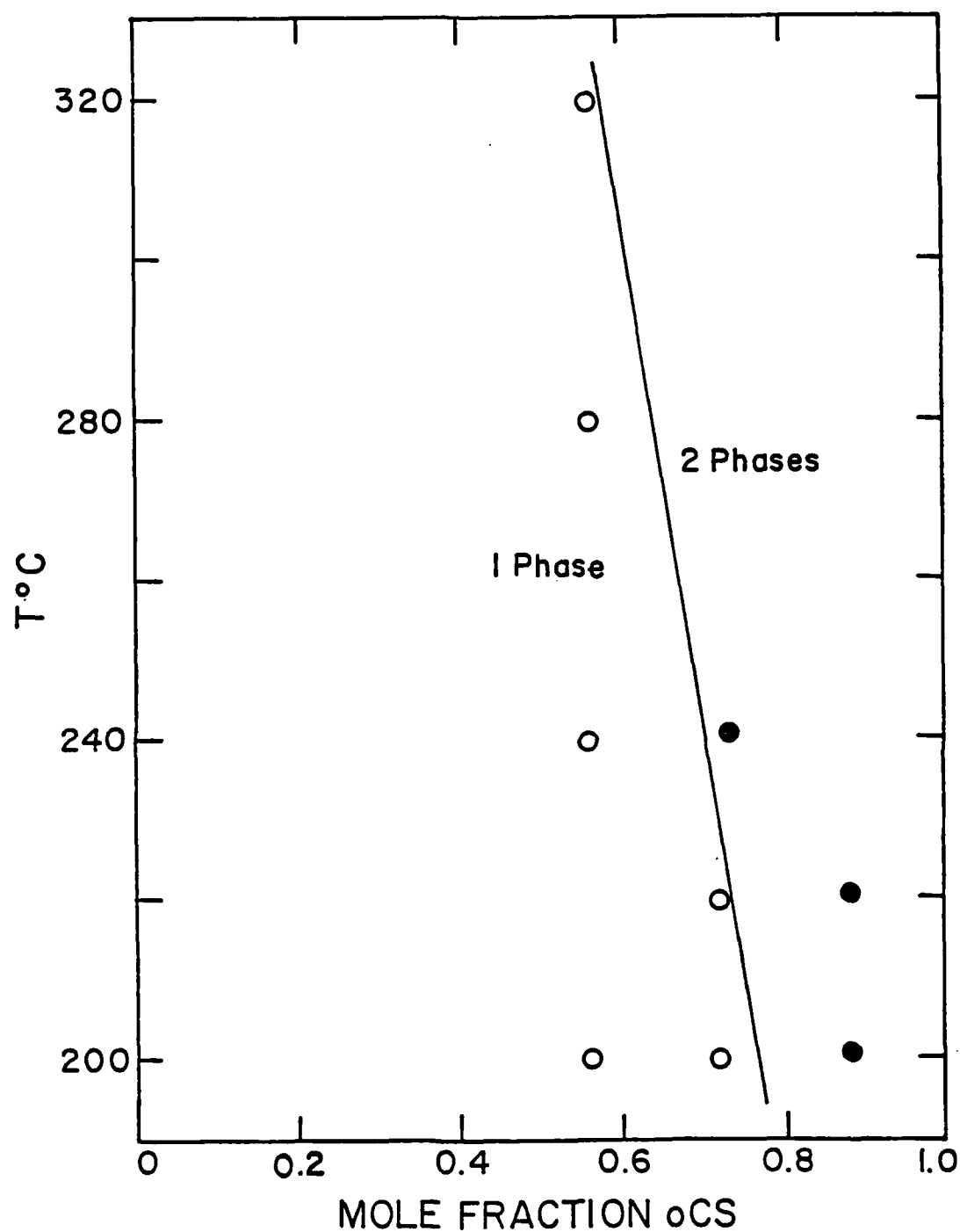


Figure 1. Phase behavior for 50/50 weight percent mixtures of PPO and PS/PoCS copolymers of indicated composition as a function of annealing temperature.

of lower critical solution temperatures for these copolymers and PPO. It may be observed that this data thus confirms qualitatively that indeed PPO and PS are "very" compatible, since the LCST, if it exists, would appear to be some hundreds of degrees above the experimental range, while conversely there is an indication that pure poly(4-chlorostyrene), normally considered immiscible with PPO, would yield a single phase system in the vicinity of 100°C if equilibrium could be attained. The phase behavior for other halogen-containing styrene copolymers with PPO has been observed with qualitatively similar results. Copolymers of 2-and 4-chlorostyrene display more subtle behavior; although both the pure polymers are incompatible with PPO, it was found that there is a miscibility "window" for copolymers containing approximately 25 to 60 mole % of 4-chlorostyrene. This "window" narrows with increasing temperature; above 290°C no copolymer in this series is compatible with PPO.²

DIELECTRIC MEASUREMENTS: POLYSTYRENE/POLY-2-CHLOROSTYRENE

The system polystyrene (PS)/poly-2-chlorostyrene (PoCS) is compatible in the region of the T_g (from 100 to 130°C, according to composition) and remains so up to decomposition temperatures, around 300°C. However, by varying the molecular weight of the PS, for example, while holding constant that of the PoCS component, it is possible to produce systems which phase separate in accessible temperature regimes above T_g, indicative therefore, of a lower critical solution temperature phenomenon. This effect was found to be quite sensitive to the

PS molecular weight. A change from $M_w = 1 \times 10^4$ to 3.7×10^4 produced, respectively, systems which resisted separation up to 320°C or in which two phase behavior was observed at 150°C . The PS/PoSC system is useful for a dielectric study because, in good approximation, relaxation in the former component may be neglected; the relatively large dipole moment in the PoCS however, provides a convenient molecular probe of the conformational states in the system. Further it is readily possible to compare the physically blended system with the random copolymer of the same composition. It develops that in terms of T_g , the blended and copolymeric systems behave identically (yet the latter of course, phase separate) while in the dielectric behavior it is possible to distinguish subtle differences in the two systems.

Dielectric measurements yield the effective dipole moment per repeat unit μ_e . This parameter can be obtained from measurements of the limiting high and low frequency dielectric constants, ϵ_u and ϵ_R , respectively, for the system from

$$\epsilon_R - \epsilon_u = \frac{3\epsilon_R}{2\epsilon_R + \epsilon_u} \cdot \frac{4\pi}{3kT} \cdot \left(\frac{\epsilon_u + 2}{3}\right)^2 N g \mu_o^2$$

where N represents the dipolar density, and μ_o is the dipole moment of the isolated repeat unit.

In polymer systems effects are usually discussed in terms of the Kirkwood-Frolich correlation parameter g , defined by:

$$g = \mu_e^2 / \mu_o^2$$

In bulk systems, the parameter g , in effect, reflects primarily conformation restrictions imposed on the system by main chain covalent connectivity.

In the copolymer g is a substantial function of composition, as is seen in Fig. 2. The general increase in g with increasing styrene content can be ascribed to a shielding of dipolar correlations in the chlorostyrene unit dipoles as the latter become diluted by the inert styrenic units, and can be accounted for in a dyad correlation model or, more completely, in a rotational isomeric calculation. This fact indicates a predominantly short range contribution. In the PS/POCS blends, in contrast, g is independent of composition (provided that phase separation is not permitted, see below). This implies that the conformational state of the dielectrically active PoCS chain is unaffected by diluting PS chains. The effective dipole moment for the system, of course, decreases linearly on such dilution. It appears that PS is a very poor solvent for PoCS, as indeed has been implied from the calorimetric data. PS and PoCS are "barely" compatible.³

The differences between the copolymers and the blends are brought out if one examines the half-widths of the respective α -relaxation peaks, Fig. 3. In the copolymers the latter is essentially independent of composition (about 2.1 decades); in the blends the half-widths are quite dependent. In the 50/50 composition blend the half-width is typically broader by one decade or more for the higher molecular weight systems. This

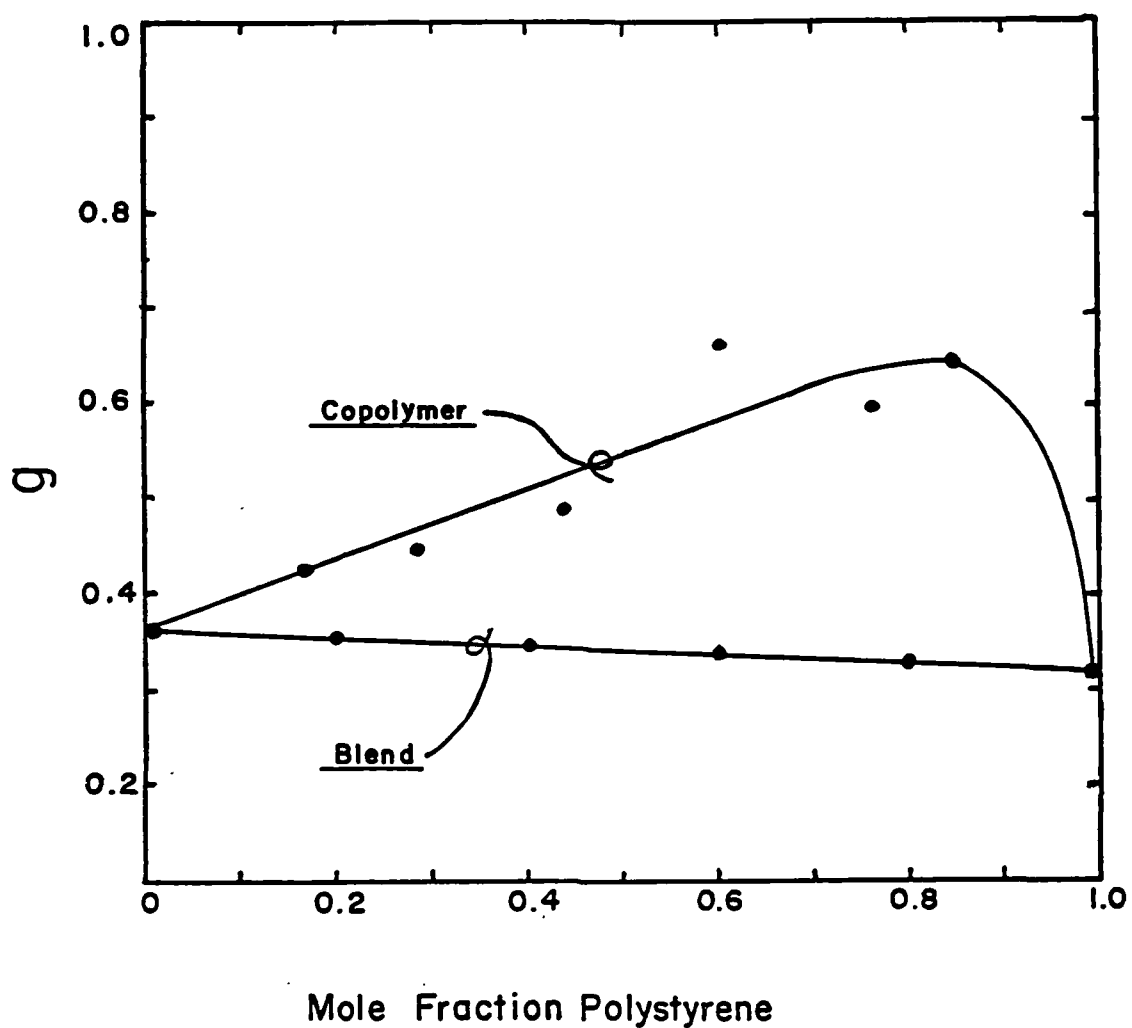


Figure 2. Dipole-dipole correlation parameter g for indicated compositions of PS/PoCS blends and random copolymers.

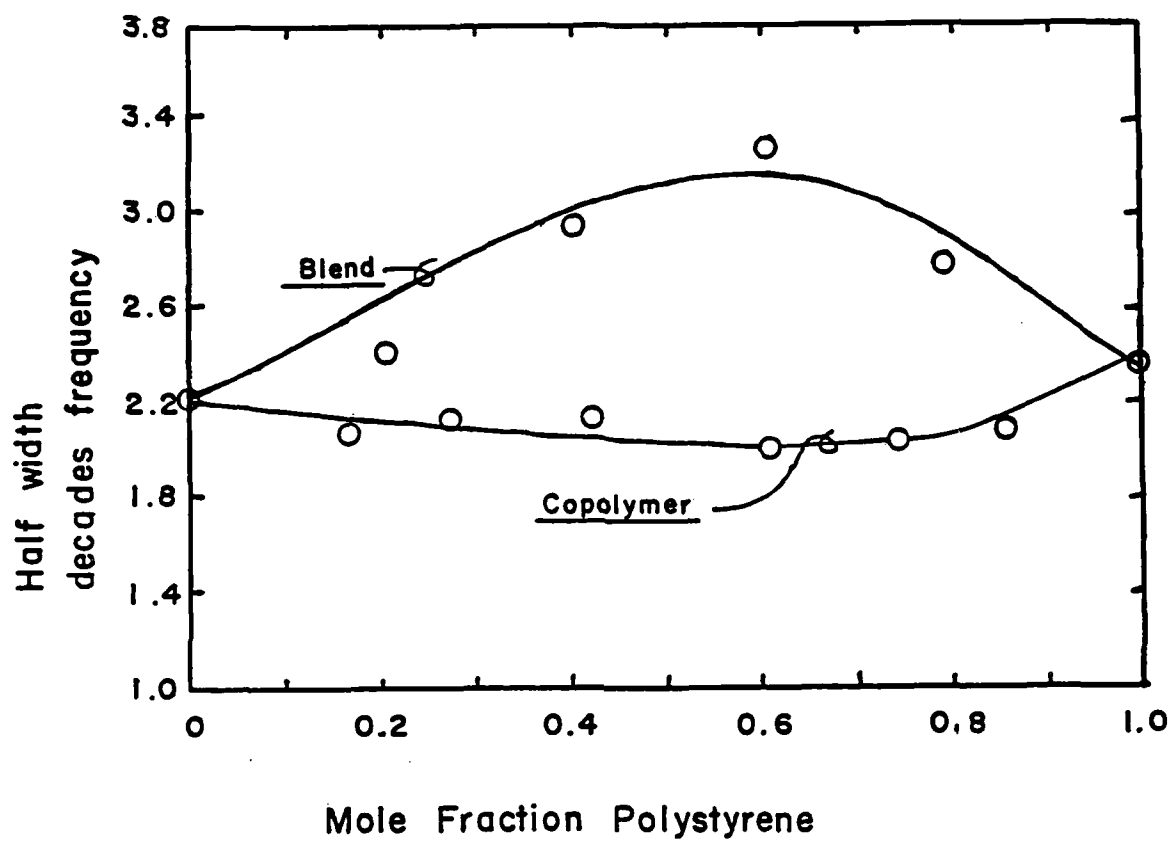


Figure 3. Half width at half height of α -loss (T_g) maximum in indicated compositions of PS/PoCS blends and random copolymers.

could be accounted for by a distribution of molecular environments, however, the behavior of the g parameter discussed above implies a constancy in dipolar correlations.

The dielectric loss curves reflect phase separation, as is implied from the above discussion. Thus one may observe (Fig. 4), a narrowing of the relaxation above the LCST in a typical system, 40/60 PS/POCS. The final normalized loss peak for the phase separated system is close to that for the unblended POCS. This implies a decrease in local heterogeneity in the separated phases.

It is seen that dielectric relaxation studies can yield considerable information concerning the local structure which appears to be absent in conventional calorimetric studies of T_g . Although the latter are invaluable for providing an overall assessment of compatibility or incompatibility, interpretation of fine structures in the phenomenon must be treated with caution.

SOLUTION ENTHALPY MEASUREMENTS

Because of experimental limitations the free energy of mixing, ΔG_m , is not directly measurable in polymer-polymer mixtures. Indirect access to this quantity (or, in fact, to the corresponding enthalpy ΔH_m) is however available from heat of solution measurements, in which the latter quantity is measured separately for the constituents and blend; ΔH_m is of course obtained from the weighted difference. This method is also subject to experimental problems arising from the fact that the measurements are normally performed at temperatures at which

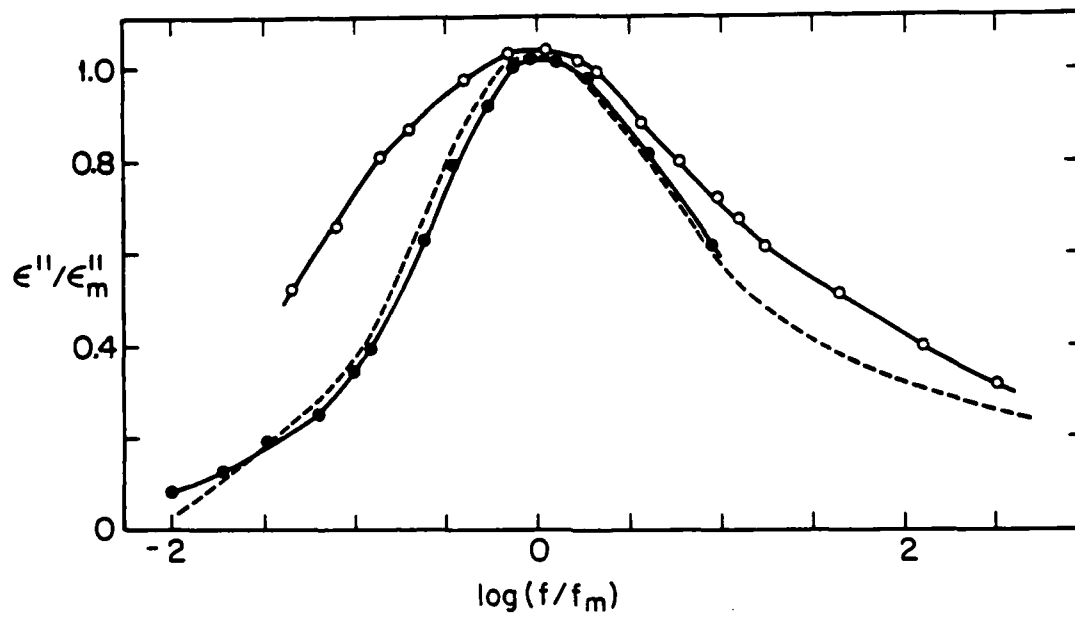


Figure 4. Normalized frequency dependencies of the α -loss peak for a 40/60 weight percent PS/PoCS blend above (•), and below (o) the LCST. The dashed line represents the loss peak for pure PoCS, 151-165°C.

samples are below their respective T_g 's; not only is this state subject to a certain enthalpic ambiguity arising from the precise sample thermal history, but in practice a major fraction of the measured partial molar enthalpy ΔH_s represents the change in state from glass to super-cooled ΔH_s liquid. The desired parameter is the heat of infinite dilution of the latter state in the chosen solvent. This problem could be overcome, though for these systems only in principle, by performing the solution enthalpy measurements close to, or preferably above, the T_g of the samples.

In spite of these problems, ΔH_m studies have provided valuable quantitative data for model compatible systems. Moreover, advantage can be taken of the fact that the ΔH_s can be obtained at temperatures below T_g to obtain information about equilibrium states in this temperature regime unobtainable by other means. Thus we have observed positive ΔH_m in systems known to be relatively incompatible. This can come about only because the equilibrium state at the dissolution temperature for the polymer-polymer blend was one of substantial phase separation. The blended samples, however, having been prepared at temperatures within the one phase regime in the phase diagram, retained their homogeneity as they were cooled below their respective T_g 's. These concepts are again illustrated in the PS/PoCS system. Figure 5 shows the heat of mixing for this blend in which the PS has a molecular weight of 20,000. Such a system is known to undergo phase separation above a LCST at

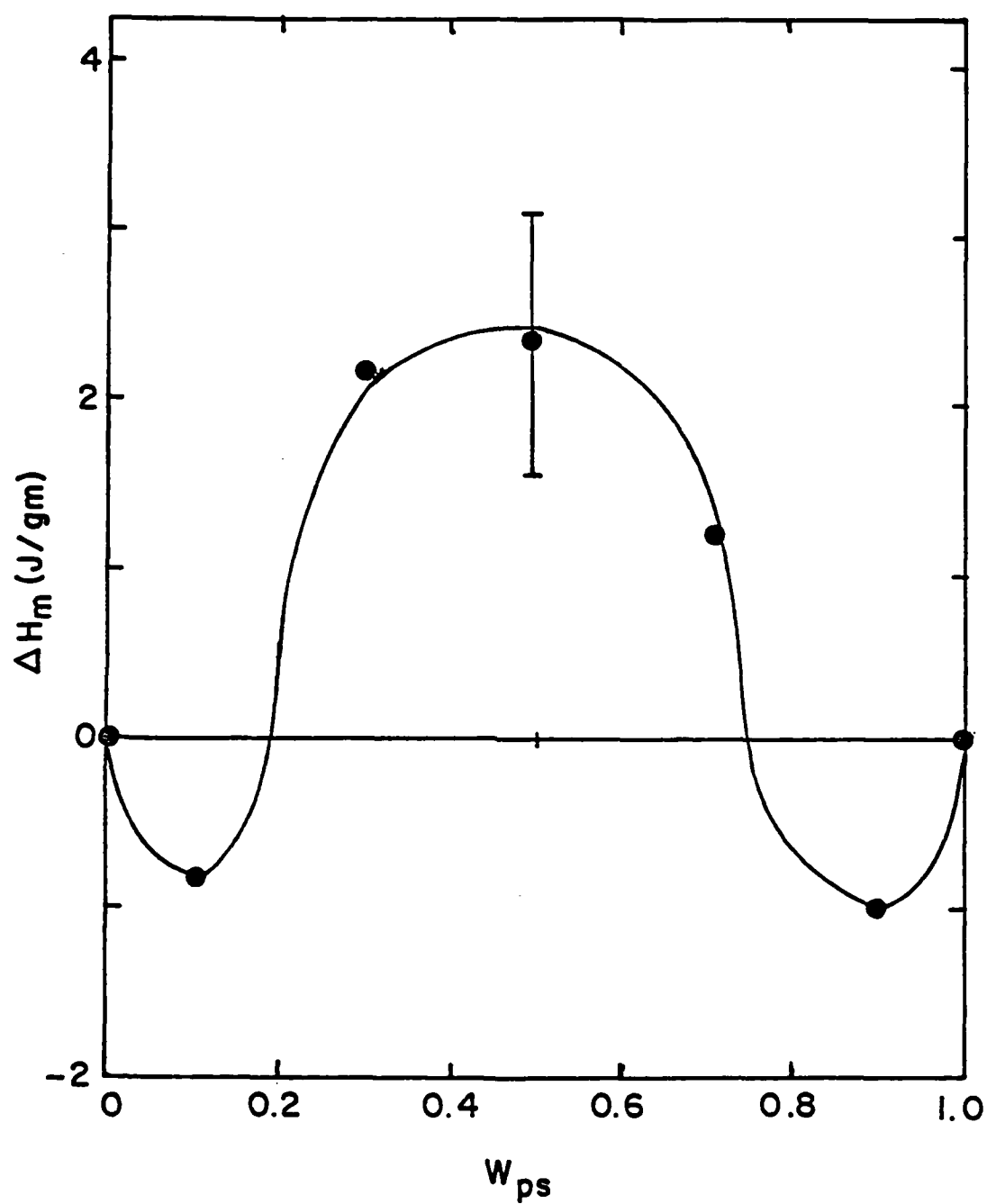


Figure 5. Heats of mixing for PS/PoCS blends as a function of blend composition.

around 200°C; samples prepared between the latter temperature and the T_g (~120°C) are however compatible. Nevertheless, such blends display positive ΔH_m 's for most compositions when ΔH_m is obtained from dissolution measurements carried out at 35°C.

ACKNOWLEDGEMENT

This paper was written under the auspices of the DARPA Materials Research Council, Contract #MDA903-82-C-0428 with The University of Michigan.

REFERENCES

1. W. J. MacKnight, F. E. Karasz and J. R. Fried in Polymer Blends (D. R. Paul and S. Newman, eds.), Academic Press, New York, 1978.
2. P. S. Alexandrovich, F. E. Karasz and W. J. MacKnight, *Polymer*, 18, 1022 (1977).
3. P. S. Alexandrovich, F. E. Karasz and W. J. MacKnight, *J. Macromol. Sci.-Phys.* B17, 501 (1980).
4. F. E. Karasz and W. J. MacKnight, *Pure and Appl. Chem.* 52, 409 (1980).

MECHANICAL PROPERTIES OF POLYMERS

L. K. DeVries

INTRODUCTION

Molecular behavior of materials is a complex phenomenon that has only recently begun to be understood in terms of the basic mechanisms responsible. Such studies are currently the subject of considerable research interest. Even in materials, such as metals, that are usually crystalline with long range order, properties generally prove to be sensitive to structure. Ultimate properties are almost always related to the defect structure for the materials. An analysis of structure-property relationships in polymers is particularly complex since properties are not only functions of the polymers chemical nature but highly dependent (more so than most other common materials) on intricacies of physical structure. For example, polymers that are chemically similar but whose physical structures differ can have tensile moduli varying from 10^7 to 10^{11} dynes/cm² (10^2 to 10^7 psi). It is well established that at the lower end of this scale (e.g., in elastomers) the resistance to deformation is due to entropic forces (1-2) while at the other extreme (extended chain configurations) it is hypothesized that the very high modulus in the chain direction is due to the polymer chain's inherent stiffness. While less dramatic, morphology can also have a pronounced effect on strength. Depending on the intricacies of structure, chemically similar polymers can have practical tensile strengths over the range: 1) 10^7 to 10^8 N/m² (1.5 to 20

ksi) for rubbers; 2) 2×10^7 to 2×10^8 N/m² (3 to 30 ksi) for glassy sy and semi-crystalline plastics; 3) 2×10^8 to 10^9 N/m² (30 to 150 ksi) for highly oriented fibers and films in the direction of orientation; and 4) as much as 4×10^9 N/m² (600 Ksi) for extended chain fibers. In the latter two cases the strength and stiffness are highly anisotropic.

Analysis of the properties of polymers is further complicated by several other factors. For example, time plays a more significant role in the properties of polymers than in most other materials. Not only are polymers generally viscoelastic but they also often exhibit chemical and physical aging. Viscoelasticity, as the name implies, indicates the material exhibits a combination of viscous and elastic properties. Chemical and physical aging are the titles given to designate the changes in chemical and physical structure that occur with the polymer's age. These time effects all manifest themselves in the polymer's response to mechanical stress.

Polymers are often used in conjunction with other materials such as composites. The most familiar types are the fiber filled composites such as fiberglass and carbon, boron, or Kevlar filled advanced composites. Granular filled composites such as clay used as an extenderd in some plastics or the ground quartz added to dental plastics to increase their wear resistance also represent an important class of materials. In these cases the presence of a second phase as well as the interface

between polymer and filler increases the complexity of the analysis of their response to mechanical loads.

Polymers are also commonly used as adhesives. The study of these important systems is complicated by the interface(s) and the constraints put on the adhesive by the adherend(s).

One might approach the study of mechanical properties (e.g., fracture) from two distinctly different views; a macroscopic approach or an atomic (or molecular) viewpoint. In the first which has become very popular in engineering design the material is viewed as a continuum (with perhaps mathematically introduced flaws) and some type of functional relationship is developed between response (e.g., failure) and the stresses and/or strains in the material. This approach allows the prediction of response such as creep, failure, etc. for specific loadings and sometimes provides the engineer with a satisfactory design tool. However, materials are basically not continua and hence a thorough understanding of their properties must include an understanding of occurrences on an atomic or molecular scale. In the molecular viewpoint, an attempt is made to establish a relationship between the applied loads and the forces resulting in the extension, slippage, rearrangement or rupture of molecular or atomic bonds. The accumulation of these events then leads to the macroscopic response or properties. Through an understanding of molecular responses it should be possible to obtain improved insights into expected behavior under actual service conditions, to make possible simplifying assumptions in design

and analysis, to make quantitatively meaningful extrapolations, and to plan better characterization experiments. This type of information should also be helpful by providing insight into how morphology and structure might be modified to enhance materials properties, e.g., by processing techniques.

This presentation will make the very ambitious attempt of outlining various aspects of both of these viewpoints. By necessity these outlines will be cursory at best but will hopefully provide some insight into methodology, structure-property relationships, etc. The author would like to emphasize one other point, while because of his personal familiarity and experience many of the examples will be taken from work at the University of Utah. It should be made clear that significant studies in these areas are being conducted at many academic, governmental and industrial laboratories.

EXPERIMENTAL OBSERVATIONS OF MOLECULAR PHENOMENA ASSOCIATED WITH FRACTURE

There has been no dearth of theories or molecular models to explain fracture in polymers. Many of these have been able to claim some agreement with macroscopic behavior. For a little more than a decade, however, experiments have been available that could be directly related to atomic occurrences during deformation and fracture.

Electron Spin Resonance

To date the most extensively used method for this purpose has been electron spin resonance (ESR) spectroscopy. In

polymeric materials, one might expect the formation of two free radicals (unpaired electrons), upon homolytic scission of covalent backbone bonds. If formed in sufficient quantity these free radicals should be amenable to detection by ESR. The method was first suggested and used by Zhurkov¹ and his colleagues in Leningrad, Russia. Since then ESR-fracture studies have been reported in the United States^{2,3}, in Germany^{4,5}, in England⁶, and Japan⁷.

The first and most extensive studies have been on oriented polymer fibers and films, most notably nylon. Such studies have provided some interesting insights into fracture behavior. For example, on the basis of these studies it appears that in at least some materials: (a) fracture can be described in terms of stress aided thermally activated processes^{1,8}, and some ESR behavior can be related to specific proposed polymer morphology⁹. (b) The key to obtaining good agreement between experimental ESR observations of the extent of bond rupture (free radical production) and fracture models based on absolute reaction rate theory is taking account of the variation in local stress on the loading carrying chains in oriented polymers. (c) Experimental evidence suggests that the strength of this class of polymer can be significantly affected by processes that alter the stress distribution among these chains¹⁰.

For example, Fig. 1 shows the strength of oriented nylon fibers as a function of a "standard derivation" of the load distribution among the load carrying chains. From this it would

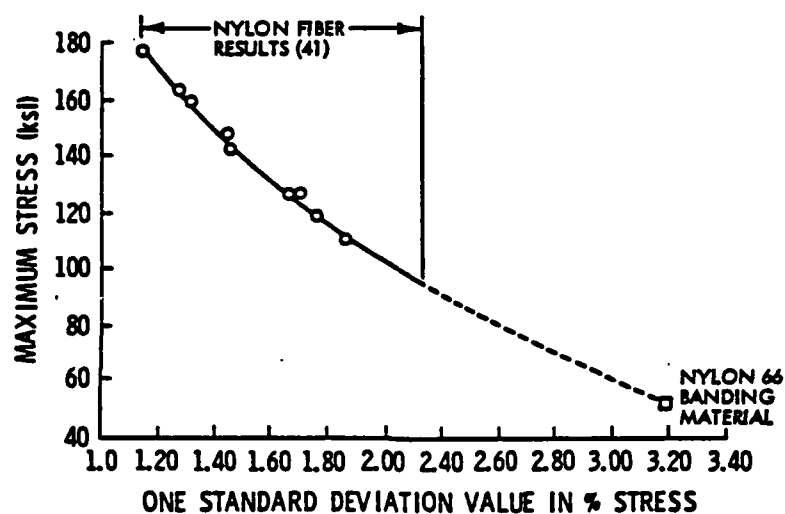


Figure 1. Effect of width of apparent stress distribution on ultimate strength of oriented nylon.

appear that the key to obtaining high strength in fibers is not only to increase the number of the tie chains but to distribute the load as uniformly as possible among these tie chains.

ESR has also been used to study fracture mechanisms in rubber, it has proven to be a very sensitive and informative means of monitoring bond rupture in unsaturated rubbers, under combined stress and exposure to ozone¹¹. By comparing the ESR results, rate of macroscopic crack growth, stress relaxation (or creep rate) and using rubber elasticity it is possible to arrive at some interesting deductions, on the manner in which ozone cracks develop and proceed through a material. It has also been demonstrated that the ESR results, can be correlated with a "molecular level" Griffith-type energy balance. That is, cracks propagate, i.e., bonds rupture only if (and at rates dependent on) sufficient strain energy present. Excellent numerical correlation, between the "energy released" from the stress field and the number of free radicals detected by ESR was observed for relaxation, creep and cyclic loading tests.

Cryogenic and space applications (in the binder of some solid propellants and in low-temperature seals, for example) require that rubber withstand very low temperatures, where it normally becomes brittle and cracks can propagate easily through the material. Andrews, Reed and coworkers¹² have demonstrated that prestraining the rubber before cooling can drastically modify its fracture behavior. In their studies and subsequent studies by Brown, DeVries, and William¹³ a variety of rubbers

ranging from natural rubber to silicone were prestrained (100% at room temperature) before reducing the temperature to -50°C (or below). When further stressed at these low temperatures, the rubbers did not fracture in a brittle manner but exhibited a yield point followed by significant plastic deformation before failure accompanied by the production of a great many free radicals. In a nutshell they had become "tough" in the engineering sense.

Infrared Spectroscopy

A major disadvantage to the use of ESR in studying polymeric fracture is the fact that most polymeric fibers are inherently unstable entities. The unpaired electron associated with the free radical has an affinity for other unpaired electrons, as a consequence, free radicals can combine with other free radicals or certain impurities. In this way the free radicals are annihilated. The spectrometer "sees" only the net number of radicals present. Radicals produced by fracture in nylon and ozone in rubber are fairly stable with a half life of approximately an hour at room temperature. Radicals in many other polymers are very unstable at room temperature with half life of a second or less. To help alleviate the problem studies have been made at cryogenic temperatures at which most free radicals are quite stable and some workers^{14,15} have added various free radical stabilizers to polymers with some success. Nevertheless this problem has limited the use of ESR to selected polymers and comparatively short term tests. Additional tools to study other

polymers and longer term tests, e.g., creep, fatigue, etc., would therefore be very useful. Infrared spectroscopy may prove to be just such a tool.

When chain scission occurs in polymers, new end groups can result that may be amenable to detection by infrared spectroscopy (IR). IR spectroscopy is not a new tool for polymeric end group analysis but to our knowledge it has only recently been used to study mechanical degradation during fracture. This interesting technique was first pioneered at the Institute of Materials Research, in Leningrad, USSR. Zhurkov, Novak and Vettegran have recently reported studies where the formation of CH_3 and $\text{C}=\text{C}$ bonds during deformation of selected polymers¹⁶ was monitored by IR. In these studies, two specimens; one unstrained and the other fractured, were interposed in the balanced light beams of a double beam spectrometer. In this mode the spectrometer records the difference in absorption of the undeformed and the fractured specimen. In principle, this should subtract out the end groups originally present in the material and indicate only those resulting from fracture. They report strong absorption bands at 910, 965, 1379 and 1735 cm^{-1} . These are attributed respectively to $(\text{RCH}-\text{CH}_2)$, $(\text{RCH}-\text{CHR}^1)$, $\text{R}-\text{CH}_3$ and (RCHO) groups.

IR has a significant inherent advantage over ESR, in that, end groups once formed should be comparatively stable. This should allow the investigation of materials that cannot be studied by ESR, as well as facilitate investigations of long

term creep, fatigue, aging and similar behavior where the time required would allow too much radical decay. The intriguing prospects of this method have lead to the initiation of related studies at Case Western Reserve University, the University of Utah and the National Bureau of Standards. For example, Fig. 2 shows a comparison between the IR spectra of undeformed and fractured polyethylene recorded with the NBS FTIR spectrometer.

IR spectroscopy has also been used to investigate bond stretching in polymers¹⁷⁻¹⁹. It has been demonstrated that stresses on polymeric bonds results in a slight but measurable shift in its IR absorption frequency. This has made it possible to gain insight into how load is distributed among polymeric chains and might help determine how processing might affect this load distribution.

Other Methods

The extent of bond rupture detected by ESR and IR would suggest that significant changes in molecular weight should occur during fracture. Preliminary studies at the University of Utah, by B. Crist of Northwestern University²⁰, and by D. K. Roylance of M.I.T.²¹ demonstrate that this is indeed the case. In these studies the observed changes in molecular weight (a few percent) appear to correspond approximately to what would be expected from the ESR results. Figure 3 shows the change in molecular weight with strain for nylon. This curve in essential features is identical to free radical concentration versus strain obtained by ESR.

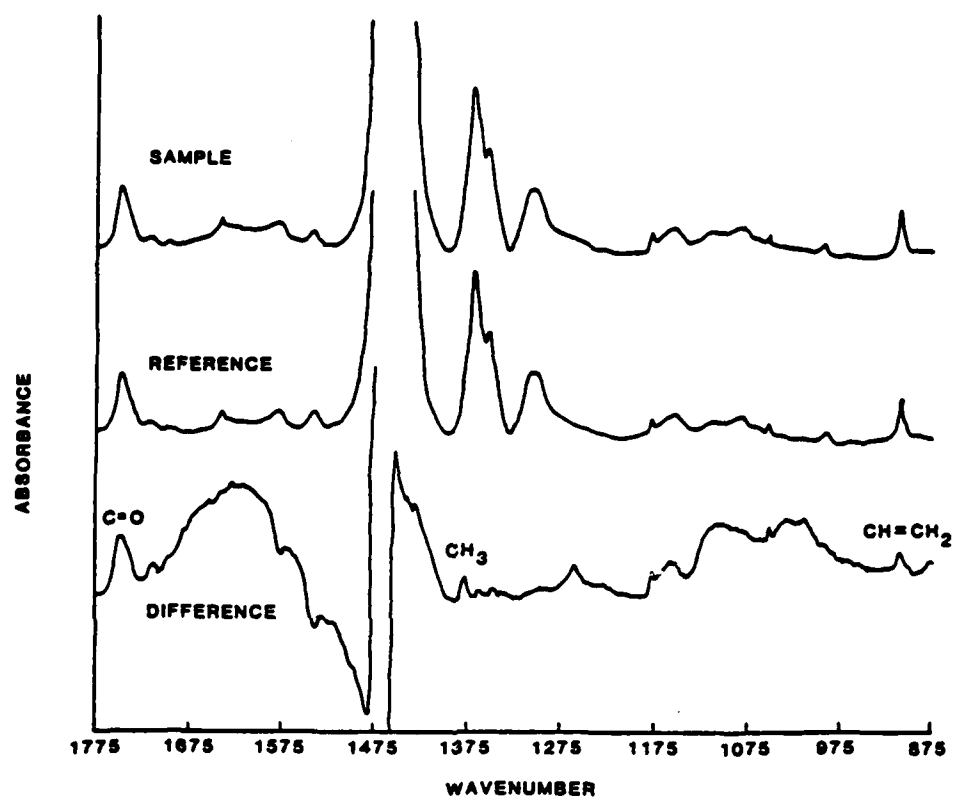


Figure 2. FTIR spectra for polyethylene fibers fractured in tension.

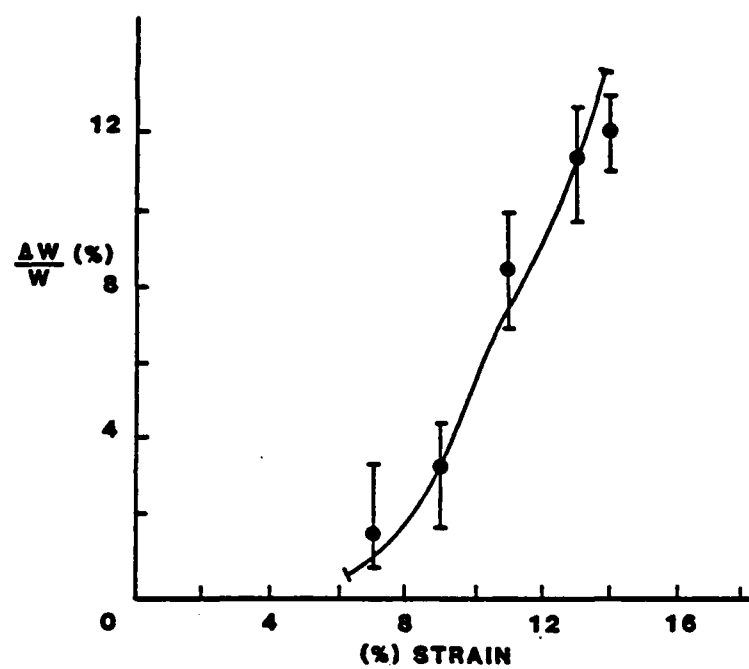


Figure 3. Change in molecular weight for Nylon 6 fibers pulled to various strains.

Stress Environmental Degradation on Polymers

An important property of polymers is their ability to withstand environmental attack. Polymers are in fact often used specifically for their corrosion resistance. Polymers themselves are, however, vulnerable to some types of chemical attack. Some rubbers in particular are known to be susceptible to cracking due to the combined effects of stress and ozone^{11,22}. More recently²³ it has been demonstrated that stress and certain environmental agents (e.g., O₃, SO₂, NO_x) have a synergistic effect on some plastics in that their combined effect is greater than one would anticipate from the sum of their two individual effects. For example, the degradation in strength of nylon fibers exposed to NO_x at various sustained strains is shown in Fig. 4.

Molecular Models of Dynamic Viscoelastic Responses of Polymers

To this point our attention has been directed primarily to ultimate or failure properties. Significant research is also being done in other areas. R. H. Boyd and his associates²⁴, for example, have developed the first apriori model to explain in terms of fundamental molecular processes a relaxation process in a polymer. In this study molecular mechanics are being applied to modeling of relaxation processes in bulk polymers, especially crystalline polymers. Energy functions and computer algorithms have been developed that simulate rather well the energetics of these systems. A successful model for the α -relaxation in PE was developed and is the first detailed molecular model for a

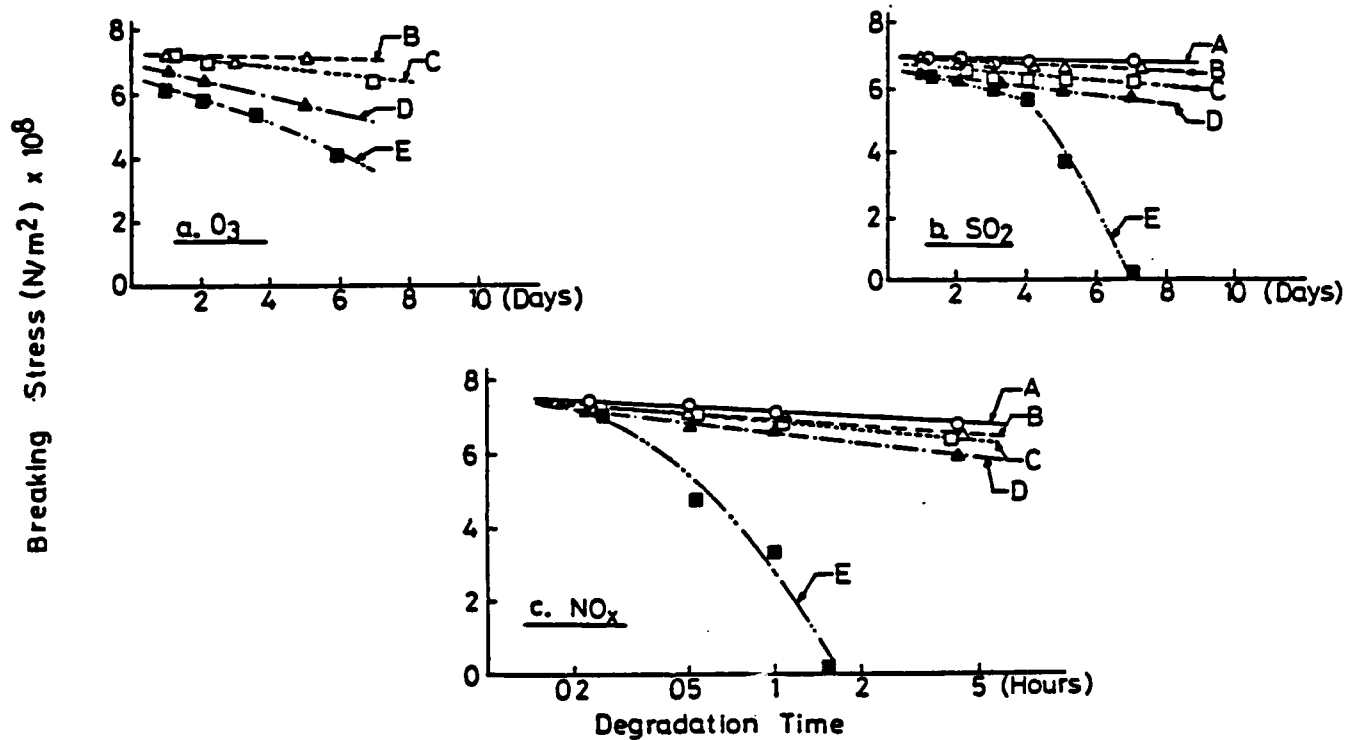


Figure 4. Degradation in strength as a function of time for Nylon 6 fibers in various environments, (a) O₃, (b) SO₂ (concentration ~5% by volume), (c) NO₂ (concentration 2.58% by volume). A is no load B, C, D and E are at strains corresponding to 60, 70, 80, and 90% of ultimate load, respectively.

specific relaxation process in a polymer. Figure 5 shows that the agreement between the theoretically predicted behavior and experimental observation is really quite good especially considering the paucity of adjustable parameters in the model.

Processing Dependence of Physical, Mechanical and Electrical Properties

Paul Phillips and his associates have been exploring the effect of processing on polymer properties. The physical, mechanical and electrical properties of crystalline polymers depend significantly on the mode of processing. Important variables commonly encountered are the pressure and temperature histories as well as melt orientation prior to crystallization. Various research projects currently investigate the synergistic effects of these variables. Fundamental research into the effects of pressure on the kinetics of crystallization, the melting process and the glass transition has recently resulted in the first complete phase diagram for a polymer which incorporates both equilibrium transition temperatures and crystallization kinetics (see Fig. 6). At elevated pressure new phases with special morphologies can be produced resulting in major changes in mechanical properties. These effects are also being studied. The effect of pre-stress or pre-strain is difficult to investigate in a quantitative fashion due to relaxation effects and so these investigators are currently studying lightly cross linked polymers so that the pre-deformation process can be relatively well specified. The ultimate aim of the study of cross linked polymers is to investigate the effect of morphology on

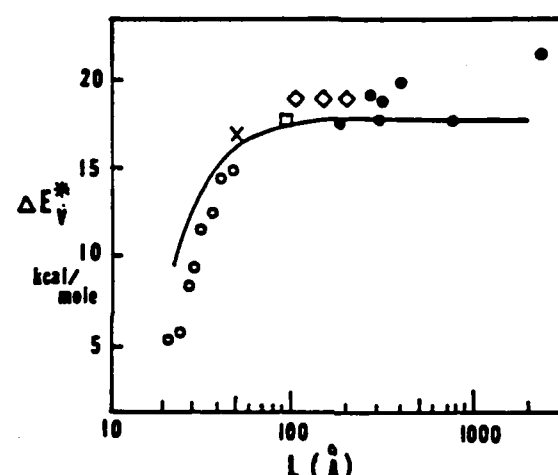


Figure 5. Comparison of calculated and experimental constant volume activation energies for dielectric loss process versus chain length (paraffins) and crystal thickness (polyethylenes). Points represent experimental data for different paraffins. Curve is from R. H. Boyd, J. Poly. Sci. 16, 1227 (1978).

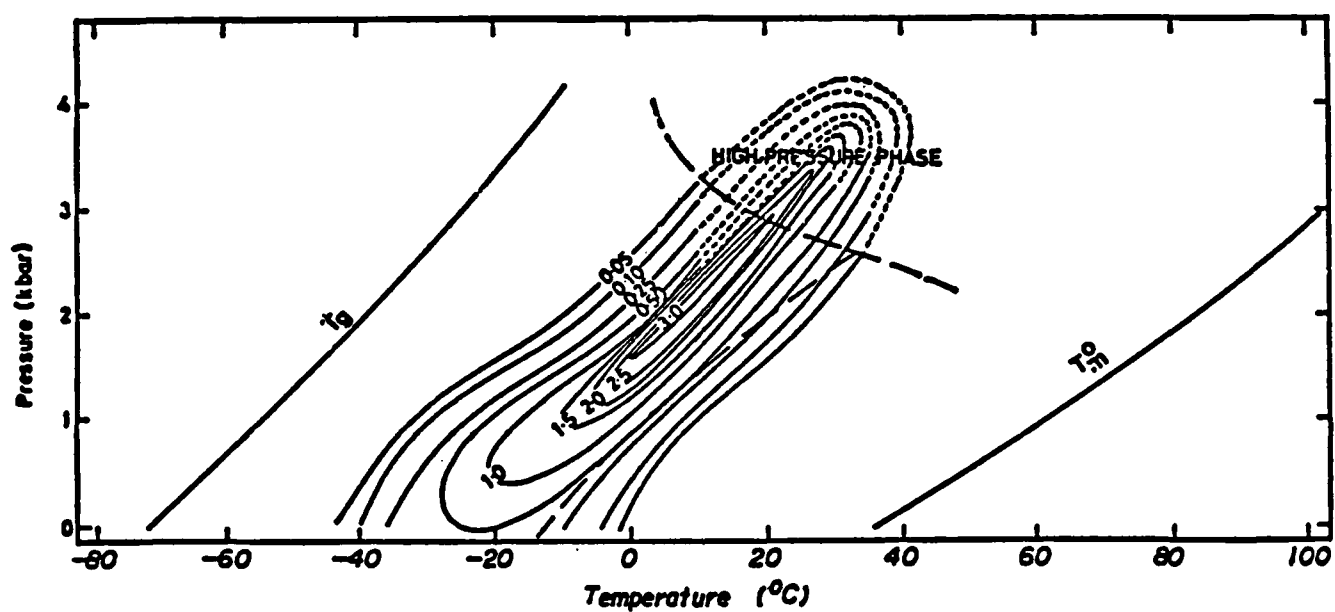


Figure 6. Phase diagram for polyethylene. Unpublished results of Paul Phillips.

electric breakdown in insulation. Another area of study involves the ability of oriented polyethylene to orient absorbed small aromatic molecules. Studies completed so far suggest very strongly that these molecules are so tightly bonded to the polymer crystals that they are immobilized until the melting point is approached.

Adhesive Failure

In almost all designs component parts must be connected. Mechanical connections (bolts, pins, rivets, etc.) have the inherent disadvantage of introducing stress risers such as holes. This has stimulated considerable interest in the use of adhesives most of which are polymers. There are critical questions here as well. For example, by what tests can the quality of an adhesive be best determined and what do the results of this test mean in terms of the strength of a practical joint. Testing is important in all aspects of material science and engineering but in no area is it more important than for adhesives. A large number of tests have been proposed and a number of these standardized by such societies or agencies as ASTM and various federal government groups. Most of these, however, might be classified as "average stress tests" in which the force is divided by some contact area. One might reasonably argue that failure is a local phenomena dependent more on the peak stresses than the average stress. More recently it has been proposed that the use of the concepts of fracture mechanics might alleviate this problem²⁵. An important question is what molecular factors in

the adhesive contribute to the magnitude of the adhesive fracture energy.

ACKNOWLEDGEMENTS

Major portions of the author's research have been supported by the National Science Foundation Polymer Program DMR-79-2590.

This paper was written under the auspices of the DARPA Materials Research Council, Contract #MDA903-82-C-0428 with The University of Michigan.

REFERENCES

1. S. N. Zhurkos and E. E. Tomashevskii, Proceedings of the Conference on the Physical Basis of Yield and Fracture, p. 200, London: Oxford University Press, 1966.
2. K. L. DeVries, D. K. Roylance and M. L. Williams, J. Polymer Sci. A-1: 8, 237 (1970).
3. A. Peterlin, J. Materials Sci. 6, 490 (1971).
4. J. Becht, K. L. DeVries and H. Kausch, Eur. Polymer J. 7, 105 (1971).
5. H. Kausch, Int. J. Fracture Mechanics 6, 301 (1970).
6. R. Notarjan and P. E. Reed, J. Polymer Sci. A-2 10, 585 (1972).
7. T. Nagamura and M. Takayanogi, J. Polymer Sci. 13, 567 (1975).
8. K. L. DeVries, B. A. Lloyd and M. L. Williams, J. Appl. Phys. 42, 4644 (1971).
9. A. Peterlin, Textile Res. J. 42, 20 (1972).
10. J. B. Park, Ph.D. Dissertation, University of Utah 1971.
11. K. L. DeVries, E. R. Simonson and M. L. Williams. J. Macro. Sci. B-4. 671 (1970).
12. W. T. Mean and P. E. Reed, Polymer Eng. Sci. 14, 22 (1974).
13. R. D. Brown, K. L. DeVries and M. L. Williams, Polymer Network: Structural and Mechanical Properties, New York: Plenum Publishing Corp., pp. 409-430, 1971.
14. M. K. Davis, Electron Parmagnetic Resonance Studies of Molecular Fracture in Oriented Polymers, Ph.D. Thesis, Texas A&M University, 1970.
15. T. C. Chiang and J. P. Sibilea, J. Polymer Sci. 10, 2249 (1972).
16. S. N. Zhurkov, V. E. Korsukov Fiz. Tverd. Tela 15, 2071 (1973).
17. S. N. Zhurkov, et.al., Fracture, p. 545. London: Chapman and Hall, 1969.

18. D. K. Roylance and K. L. DeVries, *Polymer Lett.* 9, 443, (1971).
19. R. Wool, Ph.D. Thesis, University of Utah 1974.
20. Personal communication with B. Crist, Northwestern University.
21. Personal communication with D. K. Roylance, Massachusetts Institute of Technology.
22. M. Braden, A. N. Gent, *J. Appl. Polymer Sci.* 3, 100 (1960).
23. K. L. DeVries and M. Igarashi, Chapter 2 in *Polymer Characterization by ESR and NMR*, Ed. A. E. Woodward and F. A. Bovey, ACS, Washington, D.C. (1980).
24. M. Mansfield and R. H. Boyd, *J. Polymer Sci.* 16, 1227 (1978).
25. G. P. Anderson, J. B. Bennett and K. L. DeVries, *Analysis and Testing of Adhesives*, Acad. Press (1979).

DURABILITY OF POLYMERS

R. K. Eby

In the seven decades since Baekland introduced the first commercially successful plastic produced entirely by the reaction of small molecules, synthetic polymers have come to fill an overwhelming number of needs, many generated by the very availability of these extraordinary new materials.¹ The increase in production and use has been spectacular. The average annual growth rate of about 10 percent sustained over the past two decades is three to four times that of other materials. The production of synthetic polymers in the United States reached an all-time high of 23 million metric tons in 1979, corresponding to a volume of material exceeding that of steel. This production formed the basis for about \$90 billion of value added by manufacture (a measure of the relative economic importance of manufacturing among industries) and for the employment of 3.4 million people. Polymers represent a large, rapidly expanding, and important class of materials of importance to both the economy and national security.

The commodity polymers now being produced in such large volumes reflect the science of an earlier period.¹ Polymers also have a critical high-technology aspect that does not show in tonnage figures but will become increasingly important in the future. In many applications they have unusual leverage in that small quantities may be capable of yielding large returns. For example, weight reduction in airplanes and automobiles through

replacement of metal components by polymers provides improvements in operating efficiency that can translate into enormous savings in fuel. Resistance of polymers to specific forms of corrosion can drastically reduce replacement costs of components that are subject to a variety of hostile environments, and can lessen national dependence on critical materials such as chromium and manganese. Milligram quantities of advanced polymers consumed in the production of each electronic microcircuit are indispensable in that industry.

The growth of polymers has three components: substitution for other materials, new products based on the unique properties, and growth in the use of all materials. The first makes a major contribution. Synthetic polymers are used to make motorcycle drive sprockets, 55 gallon shipping containers, load-bearing components of aircraft, pumps for corrosive and abrasive fluids, large and small pipes, ropes, guy wires, helmets, windows, structures, and sea vessels. The list of such applications is very long and in each application, a polymer has replaced another material.

However, the rapidity of the growth and substitution has led to the design and evaluation of the new polymer products often being done on the basis of criteria and tests developed for polymers in other applications or even for other materials.

Some short-term tests designed to accelerate the degradation processes have been used. Frequently these are not adequate for more than ranking the performance of the polymers under a single

set of conditions that might not be producing the same effects as the service conditions. As a result, polymers often fail prematurely and unexpectedly. Polyester-polyurethane copolymers had to be replaced in military aircraft, nylon ropes have broken and killed people on ships, nylon timing gears have failed as have power cables, electrical bus bar supports, and equipment components. A long list of premature failures has resulted from an extensive number of mechanisms and imperfections. This is an especially important problem for national security applications which often involve premium performance obtained by innovative uses of polymers in adverse environments. If the advantages of polymers are to be fully exploited through innovative use, meaningful lifetime prediction and nondestructive characterization methods must be developed. This need has been widely recognized. For example, a recent National Research Council report lists research opportunities in polymer science in the General Conclusions. One-half of these deal with accelerated tests for long term behavior, failure and degradation of polymers.

Development of useful accelerated test methods for lifetime prediction involves three major steps. (1) Identification of the macroscopic or perceived mode of failure. (2) Identification of the underlying microscopic or molecular mechanism. (3) Relating the microscopic events to the process of failure. The latter is sometimes difficult since the factors affecting service life can be numerous and difficult to quantify. Nevertheless, both it and the second step are essential since the

extrapolation of accelerated test results to long times at the service conditions requires the use of a correct model for the extrapolation.

An example can be given with the hydrolitic aging of polyester urethane elastomers. These materials are used in a variety of military applications ranging from bearing seals to the potting of electronic components. For some applications, an accelerated lifetime prediction test was based on changes in the tensile modulus with aging time. Molecular scissions occur during aging and these scissions can be related to the decrease in modulus. Thus, if both the relation between rate of scission and aging conditions and the relation between scissions and tensile modulus are adequately known, the service life can be predicted satisfactorily. This test method is adequate for a number of elastomers. In the case of the polyester-polyurethanes, however, the test failed to predict the service life with sufficient accuracy. As a result, components failed unexpectedly and had to be replaced at considerable expense. The cause of this failure was identified as being the fact that in these polymers chain scission gives the urethane segments sufficient mobility to crystallize.² Crystallization increases the tensile modulus and counteracts the decrease ordinarily associated with scission. Thus the model usually used for extrapolation was incorrect. If one, however, takes note of the molecular degradation process which is the acid-catalyzed hydrolysis of the ester group, a successful model for extrapolation can be developed.³

Since each chain scission produces one acid group, the acid content and reciprocal molecular weight change by equivalent amounts with degradation. The process can be treated as pseudo first-order and a test method can be based on the measurement of acid content. This method meets all three requirements given in the previous paragraph and produces satisfactory results.

In summary it should be emphasized that the need for improved predictive tests is urgent if the full potential of polymers increased performance, service life, and service reliability is to be obtained.

ACKNOWLEDGEMENT

This paper was written under the auspices of the DARPA Materials Research Council, Contract #MDA903-82-C-0428 with The University of Michigan.

REFERENCES

1. Polymer Science and Engineering: Challenges, Needs and Opportunities, Report of the Ad Hoc Panel on Polymer Science and Engineering, National Research Council (1981).
2. Daniel W. Brown, Robert E. Lowry and Leslie E. Smith, ACS Symposium Series, No. 95, Durability of Macromolecular Materials, R. K. Eby, Editor, 145 (1979).
3. Daniel W. Brown, Robert E. Lowry and Leslie E. Smith, Macromolecules 13, 248 (1980).

ENGINEERING ASPECTS OF COMPOSITE MATERIALS

K. L. Reifsnider

The title of this discussion is especially pertinent to the basic thesis of this discussion. It is precisely the "Engineering Aspects of Composite Materials" which have been the driving force for the vigorous interest and activity in the field, and which lead us to conclude that composite materials will play a critical and central role in the development of engineering components and structures for civilian and military purposes. They have already begun to do so, especially in air frames where composite material use is quickly becoming the rule, rather than the exception with attendant increases in performance and efficiency which could not be obtained in any other known way.

The engineering aspects of composite materials can be grouped under three categories, namely strength, stiffness and life. Composite materials have several unique properties and behavioral characteristics under each of these categories. One general point of importance is that the stiffness, strength and life of high-performance composite materials is very great, especially on a unit weight basis. In fact, it is generally assumed that composite materials have greater combined capability for strength stiffness and life than any other type of engineering material known at this time. Hence, these materials are especially important for engineering tasks which require the

greatest extremes of properties and performance. But perhaps the general characteristic of composite materials that is of greatest consequence for engineering purposes of all types is the capability for these materials, themselves, to be "engineered", i.e., composite materials can be "designed" and "constructed" with a specific special engineering function in mind. In the opinion of this writer, this characteristic is the most important basic reason for the current and projected growth of the engineering use of composite materials.

The use of "modern" composite materials is, by engineering standards, a relatively recent phenomenon. It is hardly necessary to remind the reader that our familiarity with the properties and behavior of composite materials is generally less than with more conventional materials. Moreover, our present philosophies, design schemes (especially optimization methods) and conceptual anticipations of future possibilities are peculiar to the properties and behavior of homogeneous materials, and are not generally transferable in a simple way to composite material use. Indeed, since composite materials are so various and different from one another, it is difficult even to establish "generic" characteristics that can be used to form the basis of rational engineering representations with any practical generality.

Engineering and scientific personnel, and the agencies which support their work, are faced with at least two critical and particularly pressing challenges at this point in the per-

spective of this writer. In the "short term", it is essential to improve our capability to characterize, understand, represent and anticipate the nature and behavior of common types of composite materials pertinent to engineering purposes. Better methods and development of current methods for nondestructive evaluation of composite materials are needed, for example, to support this learning process. Representations of behavior based on mechanistic behavior (rather than purely phenomenological approaches) must be developed if anticipation (and creative design) is to be possible.

The second challenge perceived, is the need to develop rigorous methods of exploiting the capability of composite materials to be engineered for specific performance. The need here is substantially influenced by the relatively poor communication between materials and mechanics technical communities. This challenge includes a great need for attention to communication and especially interdisciplinary activity, not only research, but also educational programs.

Perhaps, in closing, it is useful to narrow our view for a few moments. Let us glance at a few current issues which in the context of the writer's prejudices, present good opportunities for progress. One of these has to do with the "rigorization" of nondestructive characterization methods, especially the development of methods based on the same principles of mechanics and physics which control the behavior of the materials to be characterized. The easiest contrast that comes to mind for

demonstration of this point is the comparison of classical NDE and NDT techniques which concentrate on locating and providing strictly geometrical information about internal "defects" and flaws (discontinuities in general), with an NDE method like the measurement of (tensor) stiffness values and their changes which can be related to the nature of internal damage and, most importantly, directly related to the consequent mechanical response of the material (or component) by direct substitution of stiffness information into the constitutive equations in the discipline of mechanics. The development of such techniques relates to another opportunity, having to do with "long-term behavior".

Composite materials change their properties and behavior during the application of load histories over periods of time common to engineering applications in ways that are greatly different from that of metals and other homogeneous materials in many respects? Comprehensive theory-sensitive investigations of this behavior are badly needed, especially for the purpose of developing models which can be used to anticipate the durability, life and safety of engineering structures at any point in their service history. No issue has greater importance to the feasibility of building critical structures using composite materials. Unfortunately, part of the field is supported by only the most primitive primordial philosophy. Recent work has, however, suggested that mechanistic models can be developed which may, eventually, provide a rational approach to residual property and behavior prediction.

Any brief summary such as this one must ultimately fail to address all of the important points and issues at hand. The complexity of composite materials and related endeavors virtually assures this failing. Yet, this complexity, and the attendant flexibility and "designability" of composite materials represents an unparalleled opportunity for engineering exploitation. Given the wide recognition of the present and expected capabilities of composite materials and the world wide activity in the field, this writer believes that the major question of consequence to our effort in this country is "will we be leaders, followers, participants, or nonparticipants in this exploitation?"

ACKNOWLEDGEMENT

This paper was written under the auspices of the DARPA Materials Research Council, Contract #MDA903-82-C-0428 with The University of Michigan.

NONDESTRUCTIVE EVALUATION OF COMPOSITES

E. G. Henneke

INTRODUCTION

Nondestructive inspection and evaluation of advanced filamentary composite materials is an area fraught with many interesting and complex problems. Indeed, more problems exist in applying NDE methods to composites than to homogeneous materials. For both types of material, we are faced with the same difficulties in understanding the mechanics of the phenomena associated with the nondestructive test (NDT) method, the mechanics of the interaction of these phenomena with the material under investigation, and the proper interpretation of the data gathered by the test. For homogeneous materials, the present state of knowledge dictates that the NDT method should be able to detect, locate, size and orient any cracks present in the material. Then, using the relatively well-developed theory of fracture mechanics, we should be able to predict the expected serviceability of the material. For composite materials, we cannot state presently exactly for what type of damage we should look, since we do not know what causes the final catastrophic failure. We can state with some degree of certainty that final failure is not caused by propagation of a single crack in a self-similar fashion.

The damage which develops in composite laminates as a result of various load histories consists of matrix cracking, fiber-matrix debonding, delaminations and fiber breaks. The

final failure occurs when the integrated damage state develops to some critical level. Presently, efforts are under way to determine, if possible, the critical integrated damage state which precedes final failure. We presently know that the developing damage depends upon such things as the material properties, laminate stacking sequences, laminate geometry (presence of holes, free edges, etc.), environment, and load history. Since all of these parameters can be, and are, varied during the manufacture or service life of any laminate, it is mandatory for us to develop knowledge of the critical damage state and of nondestructive evaluation procedures to detect such incipient critical damage states.

REVIEW OF NDT METHODS PRESENTLY IN USE

There are a variety of NDT techniques which are available for the study of materials, Fig. 1. These techniques may be classified for our purposes as being specific or general. Specific techniques are those which are capable, under certain conditions, of providing detailed information about the specific modes of damage which are present in the laminate. General techniques are those which do not provide such specific data but, rather, describe field information on the total damage state present. Research in both types of NDT methods is warranted since, as already stated, it appears that the final critical damage state is a complex agglomeration of several damage modes. Field, or general, information is in general easier to obtain. If we are able to develop the appropriate knowledge,

NONDESTRUCTIVE TEST METHODS

Specific Techniques

- Microscopy
- Radiograph (X-ray, neutron)
- Surface Replication

General Techniques

- Optical Interferometry
- Ultrasonic (C-scan, attenuation, velocity)
- Acoustic Emission
- Stress Wave Factor
- Stiffness
- Thermography
- Vibration (resonance, damping)

Figure 1.

so that we can interpret this data, general NDT methods would be the preferred approach. The major reason for this is that specific techniques develop so much damage information that the experimentalist is inundated with data. Interpretation is more difficult simply because there is more data to interpret. However, study of the specific techniques is also required so that we can develop the desired knowledge on damage-mechanical property correlation in the laboratory.

Surface replication and X-ray stereography are examples of specific NDT methods which are capable of identifying to some degree the precise nature and mode of damage which develops in composite laminates during loading. Surface replication has the advantages of being simply applied, providing a permanent record, and being relatively easy to interpret. To apply the technique, a strip of cellulose acetate tape is placed on the laminate edge, melted with acetone, and allowed to dry on the surface. When the tape is removed and observed under magnification, matrix cracks and delaminations are easily recorded and identified. A large number of destructive tests have been performed to verify that the edge-observed damage is closely representative of that which exists through the width of laboratory coupon specimens. Figure 2 presents an example of a replica obtained on a graphite epoxy laminate.

X-ray stereography, usually performed with an opaque enhancer such as zinc iodide or tetrabromoethane (TBE) is also a specific technique which is capable of providing detailed infor-

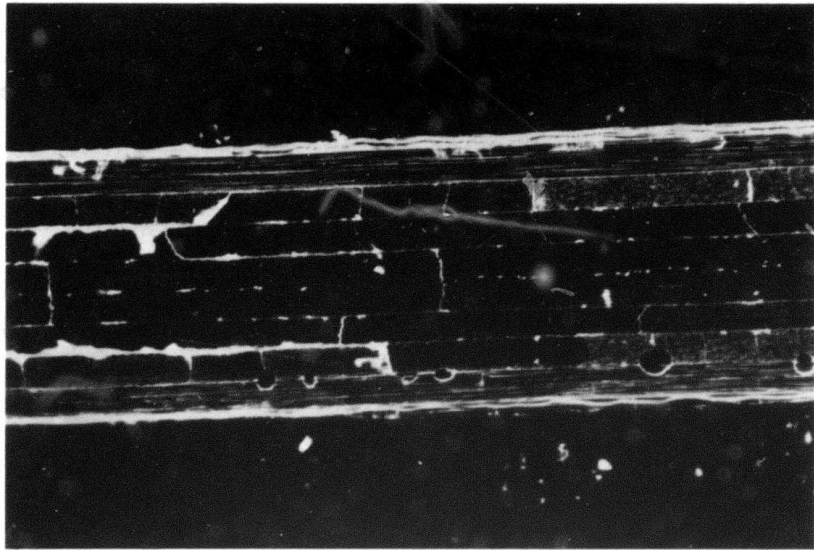


Figure 2. Replica of edge of $[0, \pm 45, 90]_S$ graphite epoxy specimen showing transverse cracks in off-axis plies.

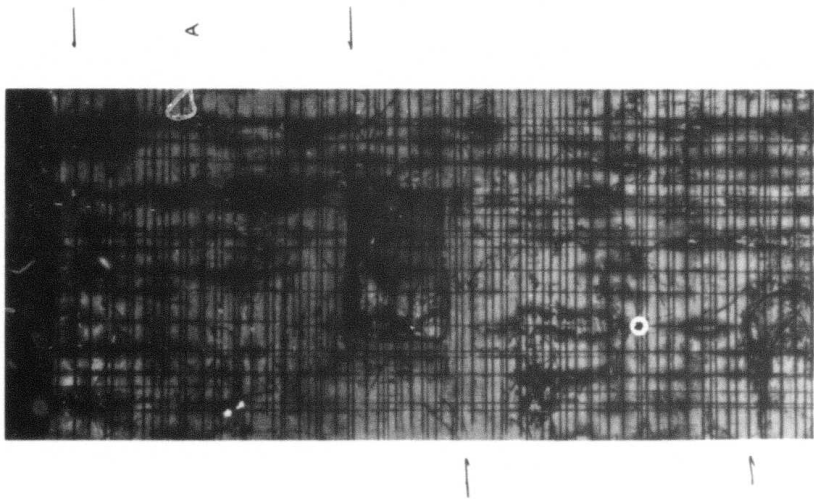


Figure 3. Replica of edge of $[0, \pm 45, 90]_S$ graphite epoxy specimen showing transverse cracks in off-axis plies.

mation on matrix cracking, delamination, and perhaps even fiber-matrix debonding. Figure 3 is an example of an X-ray radiograph. To perform stereography, two such radiographs are made such that one is tilted at approximately 15° with respect to the incident beam of X-rays and relative to the other. When viewed binocularly, one is able to perceive the three-dimensional pattern of damage and thereby identify not only the presence of certain modes of damage, but also the precise location of the damage through the depth of the material.

Both of these specific NDT methods have limitations which restrict their potential utility for examination of in-service engineering components. Replication, for example, requires the presence of a free edge. X-ray stereography, in addition to having the usual disadvantages associated with making X-ray radiographs, also is limited to the study of relatively thin laminates, of the order of 8-12 laminae thick. For thicker laminates, so much damage is present that the observer simply becomes unable to mentally assimilate and interpret all the data presented to him. For these reasons, it appears that the general techniques which provide field information on the damage state are potentially more useful for development for service inspection. However, the specific techniques are invaluable for laboratory use in providing knowledge about micro-mechanical damage processes.

The general NDT techniques which have been applied to composites include ultrasonic attenuation or velocity measure-

ments, ultrasonic C-scan, acoustic emission, stiffness measurement, vibrothermography, and stress wave factor. Generally, one must use more than one of these methods in order to provide complementary information on the integrated damage state. These techniques are all capable of monitoring some change in material characteristics resulting from developing damage. Typically the change measured is an integrated effect of the entire damage state present. As an example, Fig. 4 shows ultrasonic C-scans of damage developing in the vicinity of a notch which was machined into the center lamina prior to laminate manufacture. If one were to apply a specific technique to the same specimen, he would find that the damage consists of both longitudinal and transverse matrix cracking and small regions of delaminations. The C-scan obviously presents simply an agglomerate view of this damage. As a second example, Fig. 5 presents the change in ultrasonic attenuation and strain versus load in a graphite epoxy laminate. At the knee in the load-strain curve, the attenuation begins to rise rapidly. The replication method shows that at this load point, there is a saturated spacing of transverse cracks in the weakest plies and as the load continues to increase above this point, the cracks begin to open up. The passage of the ultrasonic wave is progressively influenced by the increasing width of these cracks. Hence, again, this is a technique which is influenced by the aggregate damage state but which does not serve to identify the individual cracks. As a final example, the stress wave factor technique, as developed by



Figure 4. Ultrasonic C-scans showing damage development with fatigue cycles in $[0,90]_S$ graphite epoxy laminate.

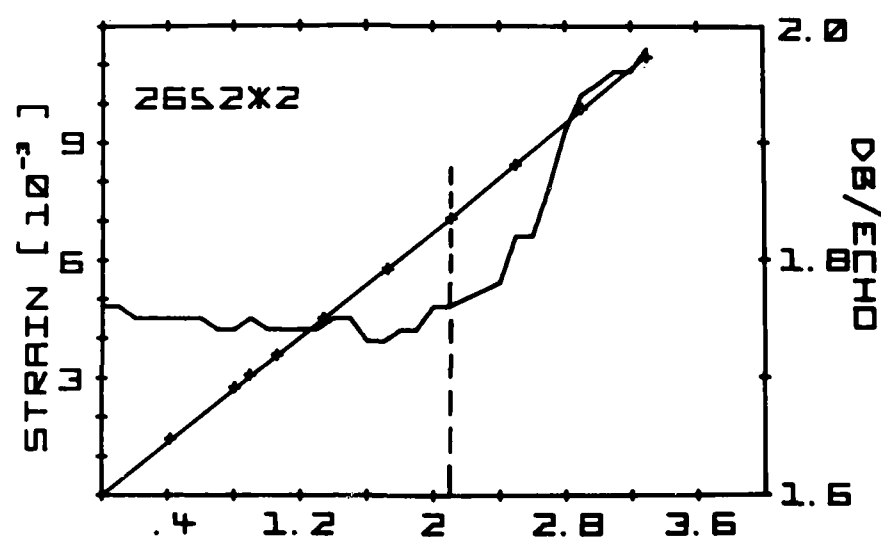


Figure 5. Ultrasonic attenuation and strain versus load in $[0,\pm 45,90]_S$ graphite epoxy laminate.

Vary and co-workers, provides a measurement parameter which again is affected by some volume of material. Interestingly, the parameter experimentally correlates very well with the final failure site, Fig. 6. Other examples could be cited for some of the other techniques. But the point to be made here is that these NDT methods provide some measure of the integrated damage state which, if appropriate research and development are pursued, should be capable of providing quantitative data to aid in the evaluation of material quality and prediction of expected serviceability.

In summary, the present state of the nondestructive evaluation of composite laminates is hampered by the lack of our knowledge on what constitutes a final, critical damage state. Until a failure theory comparable to that of fracture mechanics exists, a nondestructive evaluation procedure will be incomplete. On the other hand, we presently have available a number of nondestructive test methods capable of yielding various information about the material state. Indeed, knowledge of the critical damage state will most likely be attained only through the application of NDT methods. In any case, the potential for NDE of composites has been verified but much additional work remains if this potential is to be realized.

AREAS FOR FUTURE RESEARCH

As discussed in the previous section, nondestructive testing methods have added immeasurably to our knowledge of the complex damage states which develop in composite materials as a

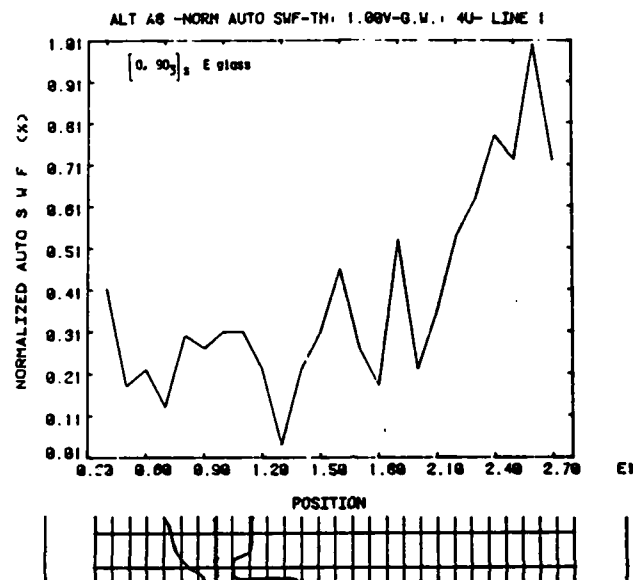


Figure 6. Variation of stress wave factor with position in E-glass epoxy laminate. Schematic diagram below graph shows location of failure in quasi-static tension test.

result of mechanical loads. Even so, the state of knowledge which deals with the application and interpretation of NDT methods to composite materials is woefully meager. Much of the work which appears in the literature dealing with NDT of composites discusses the application of NDT methods which were originally developed for homogeneous materials. Furthermore, the NDT methods are applied in an attempt to find flaws (usually meaning cracks, delaminations, or regions containing voids) without any firm understanding as to what, if any, effect such flaws, even if they exist, might have upon the mechanical properties of the materials. Many NDT applications have dealt with the inspection of composite materials having simulated or manufactured flaws. While such work indeed verifies or negates the potential application of NDT methods for finding those particular types of flaws in composites, it does nothing for verifying whether such flaws arise as a natural consequence of manufacture or loading and, if so, what effects such flaws might have upon mechanical or other properties. The smaller number of papers in the literature which deal with the study of damage development by NDT suffer from a lack of cohesiveness that a single, well-guided program would give. The major point to be made from all of this is that nondestructive testing and evaluation of composite materials has reached a stage where a major program, well-organized and structured, involving several different research groups, is required. Some thoughts about what might be covered by such an effort are presented in the following paragraphs.

First, in order to develop good, qualitative and quantitative, nondestructive evaluation techniques for composite materials, work needs to continue on the study of damage development during various loading histories. We need to know and understand the mechanics of damage development as it leads to and presages final failure. Final failure may be either catastrophic separation of the material or a degradation in stiffness or other mechanical property which is essential for its design use. The mechanics of final failure of composite materials is presently not completely known. It is evident from past work that catastrophic failure does not occur as a result of the growth of a single crack in a self-similar fashion. For the establishment of quantitative NDE to composite materials, we must first know what the precritical damage state is so that the evaluation of the nondestructive inspection data can proceed properly. To summarize in a more specific fashion, the first objective of a major research effort in NDE of composites would be to identify critical damage states and to develop analytical mechanics models which predict material behavior when the damage state is known.

Secondly, research efforts must be undertaken which study the mechanics of the NDT methods themselves. For example, for ultrasonic techniques, we must study the analytical and experimental properties of wave propagation in composite laminates. For thermography techniques, we must learn the causes of heat development. For stiffness measurement, we must study

the mechanics of laminae interaction and the resulting loss in load carrying ability when the weaker plies develop matrix cracks. Additional specific examples might be given, but again we can summarize and state that the second objective of a major research effort would emphasize the development of a quantitative analytical understanding of the mechanics of the phenomena associated with NDT methods.

Thirdly, research efforts should be coordinated to study the mechanics of the interaction of the NDT phenomena with the developing damage in the laminate. Only by thorough and complete understanding of this interaction will we be able to develop evaluation procedures which have some hope of being able to quantitatively predict such things as expected remaining lifetimes of in-service composite structures. To perform such work, it will be necessary to have an interdisciplinary effort between NDT specialists, mechanical testing specialists, and mechanics analysts. Only by performing all aspects of the work together can we hope to make headway in this very complex problem.

The present state of our knowledge of NDT of composite materials has reached a point where a major research effort, if well-coordinated, can make enormous progress. Specific areas in which major breakthroughs may be made quickly, if given support, are ultrasonic (attenuation, velocity, and C-scan), acoustic emission, thermography, stiffness, X-ray radiography and tomography, and stress wave factor. This conclusion is based upon

careful review of the literature¹ and work performed in the laboratory of the Materials Response Group at Virginia Tech.

ACKNOWLEDGEMENT

This paper was written under the auspices of the DARPA Materials Research Council, Contract #MDA903-82-C-0428 with The University of Michigan.

REFERENCE

1. E. G. Henneke, II and John C. Duke, Jr., "A Review of the State-of-the-Art of Nondestructive Evaluation of Advanced Composite Materials," Final Report, Union Carbide Corporation, Oak Ridge National Laboratory, PO No. 19X13673V, September 1979.

NONDESTRUCTIVE EVALUATION OF POLYMERS

G. S. Kino

ABSTRACT

Suggestions are made for a basic research program on non-destructive evaluation of composites. At the present time NDE of composites is at a relatively immature and elementary level.

We suggest that there should be development of scattering theory and experimental methods for assessing typical types of damage in composites. We also suggest that new techniques including measurement of acoustic velocity, thermography, photo-acoustics and X-ray tomography be developed. These would be useful for evaluation of early damage, curing problems and moisture degradation. In each case quantitative theories connecting the mechanical behavior and life prediction with the NDE measurement method need to be developed.

NON-DESTRUCTIVE EVALUATION OF POLYMERS

G. S. Kino

INTRODUCTION

Composites are becoming more and more widely used in aircraft and other military vehicles because of their high strength to weight ratios, ease of manufacture and cost effectiveness.

It is apparent from the discussions at the conference on Polymer Opportunities that these materials will be still more widely used in the future but that better predictions and testing of their reliability in service and better testing techniques in the factory are needed. The NDE techniques required are similar to those employed on metals. But the special and mechanical properties of composites must be taken into account in the design of specialized apparatus for testing them. Consequently, a high quality basic research program on NDE of composites is needed. Virtually no theory relating mechanical properties of composites and damage in composites to the measurement methods employed now exists. The measurement methods and technology that has been used is crude and empirical in nature. Therefore, we suggest that:

- (1) Scattering theory and associated experimental techniques be developed to assess typical types of damage in composites.

- (2) New techniques including measurement of the variations of acoustic velocity, thermographic and photoacoustic methods

and acoustic emission methods be developed to evaluate adhesion of bonds, curing, and the early onset of damage in composites.

(3) X-ray tomographic techniques for assessment of damage and poor curing of composites should be examined.

(4) The connection between such measurements and the effect of moisture degradation and chemical damage should be examined.

We discuss these suggestions in more detail below. Many of the ideas discussed are based, in part, on a paper on "Non-Destructive Evaluation of Polymers" by E. G. Henneke delivered at the Conference. It is apparent from his talk that there is a great deal of originality in his work, but with the use of a better technology many of the techniques described could be considerably improved.

X-RAY TECHNIQUES

Composites should lend themselves well to the use of X-ray tomography. This technique which is now widely employed in medical practice yields an image of a slice through the sample with a 2D 1 mm definition of regions with as little as 1% change in density. Thus it should be very effective in showing up delaminated regions, lack of curing and other problems in composites.

The basic idea is to use a single X-ray source with multiple detectors. The part to be examined is placed between the source and the detectors and rotated in steps through 360°. By using a computer to interpret the recorded data a very high quality image of a slice through the part is obtained. The

problem, as it is in medical practice, is the high cost of the machine. Such a sophisticated system would only be effective if well utilized.

ACOUSTIC ATTENUATION MEASUREMENTS

Henneke described fairly effective methods of measuring damage in graphite polyamid strips 1/16" thick. Working with a 5 MHz 1/2" diameter transducer and a quartz buffer rod he observes that attenuation tends to increase in regions where the failure load is low. The attenuation increases more rapidly with frequency when the acoustic beam passes through damaged regions. These effects are just what would be expected if delamination and cracks occurred in the damaged regions.

The following changes should be made:

- (1) Replace the transducers with efficient medical-type transducers which are intended to work into a low impedance medium like a composite. There is a very large mismatch in impedance between a quartz buffer rod (15×10^6 Rayls) and the composite (probably 3×10^6 Rayls). Medical transducers are required to operate into body tissue (1.5×10^6 Rayls). Better still, well matched transducers should be designed for this application.

- (2) Use focused transducers in a C scan mode to obtain better definition.

- (3) With thin samples, work with efficient well matched transducers operating at as high a frequency as possible so as to obtain better definition and more differentiation in attenuation between damaged and undamaged regions. In the example

given this would probably involve using medical-type 7.5 or 10 MHz focused transducers.

(4) For thicker samples try working in a reflection mode. In a composite, however, because of the multiple internal reflections present, it will probably be better to work in transmission.

(5) Develop a simple theory to predict attenuation variation with frequency for different types and sizes of damaged regions.

ACOUSTIC VELOCITY MEASUREMENTS

R. K. Eby of NBS, in a talk on "Failure of Polymers" demonstrated that both acoustic velocity and attenuation vary rapidly with the curing of the material. Attenuation peaks at the point where the material is changing from the liquid to the solid state while there is a monotonic increase of acoustic velocity by a factor of approximately 1.5 as the material changes from the liquid to the solid state.

We might therefore expect that it would be worthwhile to use scanned acoustic beam methods to measure velocity as well as attenuation.

The use of focused acoustic beams would give much better differentiation of regions of interest than has been obtained heretofore. Uncured regions or badly cured regions which could lead to delamination or to cracking might well be easy to observe in measurements of the kind.

Damaged regions would certainly show up in this type of measurement, but could probably be identified more easily from attenuation measurements. Better theoretical insight into the behavior of acoustic waves in bonds could and should be obtained by referring to the large body of literature on acoustic measurements of chemical relaxation effects.

There was some discussion of the application of acoustic emission measurement methods to composites. It is apparent that when a sample is placed under a cyclic load, delaminated and damaged regions should emit acoustic waves.

A major advantage that may occur with composites is that high frequency acoustic waves are rapidly attenuated in these materials. Therefore by using transducers operating at frequencies greater than 5 MHz, and scanning along the sample, or using an array of such transducers it may be relatively easy to localize the source of acoustic emission and hence the damaged region, as the sample is cyclically loaded.

THERMOGRAPHY

Henneke described in his talk a thermographic measurement technique in which a thin composite sample was excited at a frequency of the order of 18 kHz and its temperature observed with an infrared imaging system. Damaged regions showed up sometimes to have a higher temperature. But because of standing waves at 18 kHz, this did not always occur. If, however, the frequency was varied the damaged region would always show up at

some frequency to have an increase in temperature over that of the surrounding material.

It is apparent that this technique could be improved by one of several techniques. These are:

(1) Use of an FM chirp source varying from say 15-30 kHz repetitively and carry out infrared measurements as before.

This should eliminate resonance problems;

(2) We recognize that this technique is, in fact, another application of a technique closely related to photoacoustics. Thus, we might consider a scanned measurement in which a relatively high frequency focused acoustic beam (1-2 MHz) is used to heat the sample by propagating through it. By measuring the temperature with an infrared detector placed on the other side of the sample, which is scanned in unison with the heating source, regions of increased attenuation, i.e., damaged regions would show up very clearly as hot spots.

(3) For thicker samples with possible internal damage a second scanned probing acoustic transducer could be used to measure changes in velocity or attenuation. These should be most severe in heated regions because the rate of change in acoustic velocity or attenuation of plastic with temperature is very rapid, as compared to metals.

In this connection there may also be the possibility of using such a focused heating beam to cure regions placed under pressure, which had been poorly cured in the first place.

The examples given badly need examining theoretically. Obviously some calculations of the heat diffusion in composites and of the effect of temperature on acoustic attenuation and velocity is needed.

THE CONNECTION WITH MOISTURE DEGRADATION

It is apparent that composites are subject to degradation due to moisture or contact with various types of liquids. One would expect there to be fairly rapid changes in attenuation under these conditions. Some work has already been carried out at the Science Center of North American Rockwell on this subject. Further investigations of this kind would obviously be of great importance.

ACKNOWLEDGEMENT

This paper was written under the auspices of the DARPA Materials Research Council, Contract #MDA903-82-C-0428 with The University of Michigan.

MATERIALS WITH CONTROLLED DAMPING PROPERTIES

P. H. Lindenmeyer

The purpose of this paper is to suggest a novel approach to the production of materials in which the vibrational and damping characteristic may be controlled and tailored to a particular application without changing their composition and consequently their other physical and chemical properties. The approach is based upon nonequilibrium irreversible thermodynamics and therefore is applicable in principle to any material. Our approach was inspired by the theory of dissipative structures¹ for which I. Prigogine was awarded the 1977 Nobel prize, however, we have deviated significantly from this theory toward the use of an experimental rather than a theoretical basis (see attached extended abstract).

The damping properties of a material are usually considered as materials constants in much the same manner as the elastic constants or moduli. In fact the damping of a material is generally expressed in terms of the "imaginary moduli" - so named because of the convenience of using complex numbers as a means of expressing the solution to the equation for the vibration of a damped forced oscillator which in the simplest case is

$$m\ddot{x} + 2mk\dot{x} + m\omega_0^2 x = F(t) \quad (1)$$

where x , \dot{x} , and \ddot{x} are the displacement, velocity and acceleration, m the mass, $F(t)$ the forcing function and k and ω_0 the damping and elastic constants.

In more general terms the displacement must be expressed as a second order tensor, ϵ and the damping and elastic constants as matrices appropriate to fourth order tensors so that

$$M\ddot{\epsilon} + R\dot{\epsilon} + S\epsilon = F(t) \quad (2)$$

Even this generalization represents a considerable simplification since we are to assume that the components of the matrices M , R and S are constants and have the symmetry properties attributed to them in linear elasticity theory. We are interested in materials for which the linear approximations of Eqs. (1) and (2) are not sufficiently accurate to express their behavior. With such nonlinear materials M , R and S matrices may have antisymmetric components as well as being functions of the amplitude of the displacement. Specifically the antisymmetric components of S give rise to circulatory motion and those of R to gyroscopic motion.² Under these conditions damping is no longer uniquely determined by the coefficient of velocity and one can encounter damping and vibrational phenomena that are not even suggested by the linear approximations.

Now where can one find or make such nonlinear materials?

Prigogine has shown that when a thermodynamic system is constrained to be sufficiently far from equilibrium by the exchange of energy and/or matter with its environment, it can become unstable and undergo a discontinuous change into what he has termed a "dissipative structure." Although his proposed criteria for this instability have received much criticism in

the literature^{2,3,4} no one questions the existence of such instabilities or dissipative structures. A dissipative structure is formed whenever the interaction between the flow of energy (i.e., power) and the motion of matter become sufficiently non-linear so that the uncompensated dissipation of energy can be reduced by the formation of an inhomogeneous rather than a homogeneous structure.

We have been investigating the theory of such dissipative structures for the past five years every since we first realized⁵ that is such instabilities occur during a physical or chemical process which involved solidification, the dissipative structure would be frozen into the solid and would remain even after the environmental forces which caused it to form were removed. In particular all polymer solidification involves such processes and all polymer morphology can be considered as frozen or time degenerate dissipative structure⁵.

One of the important results of this investigation has been the realization that the flow of energy can result from dynamic fluctuations as well as from continuous gradients. Consequently, one has the possibility of increasing the rate of energy flow (power) without effecting the average thermodynamic parameters of the system. It thus becomes possible to carry out solidification processes or chemical synthesis that result in solids while simultaneously varying the amount of dynamic fluctuations in thermodynamic or pseudo thermodynamic forces. This results in a wide variety of frozen or time degerate dissipative

structures having properties that can vary drastically from the from the equilibrium properties of these same composition.

Note: The concept of carrying out solidification or chemical synthesis under the influence of fluctuating thermodynamic or pseudo thermodynamic forces at their resonance frequency is presently the subject of patent action and should be considered as proprietary information.

Thus although there is only one true equilibrium structure for a given composition at a given uniform temperature and pressure, there surely exist an indefinite number of so called dissipative structures whose physical and chemical properties differ significantly from those of the equilibrium structure.

We therefore suggest that if it is desired to modify the damping and vibrational properties of a given material, this can be accomplished by carrying out its solidification or synthesis under the influence of dynamic fluctuations with controlled frequency and amplitude.

A recent review of the use of vitreous enamels as vibrational damping materials⁶ at high temperatures summarizes what they feel to be the desirable characteristics of such materials. Since the maximum damping of such materials occurs in the region above the glass transition, they suggest that suitable materials should be selected in a way to avoid as much as possible glasses that tend to (1) devitrify, (2) phase separate, (3) volatilize or react, or (4) flow under gravity or centrifugal force.

We suggest that the avoidance of phase separation is an unnecessary criterion since under the proper circumstances a phase separation into two or more phases, one of which partially

devitrifies could very well result in a very superior damping material. The devitrified phase would be expected to add considerable stability to the system reducing the possibility of volatilization, reaction or flow.

On the other hand if this phase separation occurs as a consequence of the formation of dissipative structure, the characteristic size(s) of the two (or more) phases would be determined by frequency of the dynamic fluctuations causing the dissipative structure to form. Since one criterion for the formation of a dissipative structure is a maximum in the uncompensated dissipation of energy, it should be possible to tailor the structure, at least to some degree, to the temperature and frequency desired.

ACKNOWLEDGEMENT

This paper was written under the auspices of the DARPA Materials Research Council, Contract #MDA903-82-C-0428 with The University of Michigan.

REFERENCES

1. P. Glansdorff and I. Prigogine, "Thermodynamic Theory of Structure, Stability and Fluctuations," Wiley-Interscience, New York (1971).
2. B. H. Lavenda, "Thermodynamics of Irreversible Processes," Halsted-Wiley, New York (1978).
3. J. Keizer and R. F. Fox, Proc. Nat. Acad. Sci. USE 71, 192 (1974).
4. R. Landauer, Phys. Rev., A12, 636 (1975).
5. P. H. Lindenmeyer, Polymer J. 11, 677 (1979). Polymer Eng. Sci. 17, 1965 (1979).
6. B. Kumar and G. A. Graves, Ceramic Bull. 61, 480 (1982).

A NOVEL APPROACH TO AN EXPERIMENTALLY BASED NONEQUILIBRIUM THERMODYNAMICS

by Paul H. Lindenmeyer

May 1982

EXTENDED ABSTRACT

A rigorous equilibrium thermodynamics permits one to use the thermodynamic properties obtained from static measurements made on the surfaces of two systems at equilibrium to calculate the thermodynamic properties of the combined system once it has again attained equilibrium. In practice, one of these systems, called the environment, is assumed to be very large so that its properties do not change by a measurable amount. In an exactly analogous manner, our approach makes dynamic measurements on systems that are not necessarily at equilibrium and permits calculations of the combined system as a function of time.

This approach is based upon controlled dynamic fluctuation and measurement techniques that have only become feasible with recently developed microprocessor and data reduction technology. It becomes equal to the usual linear nonequilibrium thermodynamics as the amplitude of these dynamic fluctuations is reduced and to equilibrium thermodynamics when the amplitude becomes zero.

We first recognized that, from an experimental point of view, the difference between equilibrium and nonequilibrium is arbitrarily dependant upon the measurement precision and the time and distance scales adopted by the observer. Consequently, these time and distance scales can be used to operationally define the state of the system. In combination with the amplitude of the imposed dynamic fluctuations, they can be used to actually control the time evolution of the system and to some extent effect its final state.

Instead of making the usual Gibbs assumption and obtaining a generalized Gibbs-Duhem relationship, we take the total Legendre transform of energy with respect to all the extensive properties of the system. This has the effect of reformulating the second law of thermodynamics so that the burden of accounting for the time evolution of the system is shifted from the concept of entropy, which can only be rigorously defined for an isolated system at or near equilibrium, to the concept of an excess energy that is applicable to open or closed systems.

Thus, we suggest that "It is the minimization of the change in excess energy within the system of interest — not the increase in entropy of the universe — that represents the practical embodiment of the second law." By defining the change in excess energy as the uncompensated dissipation of energy, we can equate the second law to the variational principle of minimum dissipation of energy. This principle can, in turn, be shown to be the Eulerian time derivative of Hamilton's principle of varying action.

The difficulty in applying the principle of minimum dissipation of energy to a system that can exchange energy or matter with its environment, comes in applying the necessary constraint that at a stationary state there must be a balance of power between every point in the system and between the system and its environment. If the nature of the environment is such that this constraint can be expressed as a kinematic relationship between the variables rather than between their differentials (i.e. if the constraint is holonomic rather than non-holonomic), the excess energy evolves to a stationary state by the usual linear nonequilibrium thermodynamics, where Onsager's reciprocal relations apply and the dissipative forces can be derived from a potential. In the more general or non-holonomic case, the Euler-Lagrange equations do not have unique solutions, the excess energy functional may not become stationary but may continue to evolve with time. It is with this most general case where our approach becomes most unique.

Instead of trying to devise vector or local potentials or some other means that will yield an analytic solution to the Euler-Lagrange equations, we take advantage of the fact that the time and distance scales of the observer as well as his measurement precision, may be combined to determine the state of the system from an operational point of view. By defining the extremizing function of the excess energy functional as the difference between the intensive variables averaged over an experimentally determined volume at a given time and the same variables averaged over an experimentally determined interval of time at a given position within the system, we obtain a function that is both differentiable and experimentally measurable.

This experimentally measurable extremizing function is central to our approach. Using this function and its Eulerian time derivative, we can approximate the variation of the excess energy functional in a manner exactly analogous to the way one can experimentally approximate the derivative of an ordinary measurable function. The procedure involves driving one or more of the intensive environmental variables in a sinusoidal fashion and measuring the response of the systems extensive properties.

The applications of this experimentally based nonequilibrium thermodynamics can be grouped into three categories. In the first category are those applications where one wishes simply to measure the overall kinetic and thermodynamic properties of a complex system in contact with a nonuniform environment which prevents it from reaching a true equilibrium. These applications involve increasing the amplitude of the dynamic fluctuations only to the point where one can just measure the onset of irreversibility.

A second category of applications occurs when a system is in contact with a uniform environment but has not yet reached equilibrium because of internal kinetic inhibitions. By increasing the dynamic fluctuations of the environment to the point where one obtains the onset of asymmetry, it becomes possible to accelerate the approach to equilibrium without changing the average thermodynamic properties of that equilibrium state.

However, the most exciting applications of the thermodynamics occur when these dynamic fluctuations are used to drive a nonequilibrium system further and further from equilibrium until the point of instability is reached. We do not attempt to resolve the controversy that exists in the literature concerning the criteria for such instabilities — we suggest instead that they can be experimentally measured by varying the dynamic power (i.e. the frequency and amplitude of the environmental fluctuations) until a discontinuity in the systems response is measured. When this happens, the system undergoes a spontaneous and discontinuous change into what Prigogine has called a "dissipative structure". Such structures are formed whenever the interaction between the flow of energy (i.e. power) and the motion of matter becomes sufficiently nonlinear so that the dissipation of energy can be decreased by some kind of rotational flow. If the system is undergoing a physical transformation or a chemical synthesis that results in the formation of a solid, these dissipative structures may be expected to persist for long periods of time even after the environmental conditions that caused them to form have been removed. Thus, although there is only one true equilibrium structure, of a given composition when exposed to a uniform environment of temperature and pressure, there may exist an indefinite number of solid dissipative structures that are operationally at equilibrium within the measurement precision of the observer.

We believe our approach provides an experimentally based formalism that can (1) explain a large number of known facts, (2) be used to measure the overall kinetic and thermodynamic properties of complex systems, (3) accelerate the approach to equilibrium or predict the time required to do so, and (4) suggest quite unique methods of controlling solid state structures by the application of dynamic fluctuations.

ACOUSTIC MICROSCOPY

R. Mehrabian

Successful application of acoustic microscopy to materials characterization has two requirements. The first is a sophisticated microscope facility, covering at least the range 50 MHz - 1 GHz, in both transmission and reflection with a choice of lens apertures. Digital image store, with several planes, and facilities for arithmetic and image processing are desirable. For quantitative work, it must be possible to scan along the lens axis and to analyse the resulting information.

The second requirement is an imaginative and systematic understanding of the interaction of ultrasound with materials features of interest. In reflection this includes imaging theory where there are elastic discontinuities across the surface of the specimen, as well as the effect on the reflected signal of bulk attenuation. In transmission it includes all the mechanisms that can affect the wave; both purely mechanical effects such as damping and scattering, and also electrical and magnetic effects.

Future Research

Application of newly developed ultrasonic generation, detection and analysis techniques employing state of the art laser and optical technologies for basic characterization and real-time monitoring of solid state reactions occurring in rapidly solidified microstructures. The thrust should be toward characterization (NDC) of microcrystalline alloys. By means of

NDC, both preparation processes and structural stability upon thermomechanical treatment, of microcrystalline alloys should be investigated. Emphasis should be placed on alloys of potentially practical application, e.g., iron-aluminum, and titanium-base alloys in which particular chemical additions and metallurgical processes may enhance their mechanical and physical properties. The NDE techniques should be applied in a complementary fashion to the conventional destructive techniques, e.g., optical and electron micrography, electrical and magnetic techniques, and determination of mechanical properties.

Further Areas for R&D in the Field of Instrumentation

Optimization of ultrasonic NDC by means of laser generation and detection for contactless applications when the sample material is subjected to hostile environment, e.g., high temperatures and pressures, liquid state, etc.

Exploratory investigation of the capabilities of eddy current conductivity measurements for process monitoring and control of preparation and characterization of microcrystalline structures obtained through rapid solidification technology.

ACKNOWLEDGEMENT

This paper was written under the auspices of the DARPA Materials Research Council, Contract #MDA903-82-C-0428 with The University of Michigan.

QUANTITATIVE APPLICATIONS OF ACOUSTIC MICROSCOPY
TO MICROSTRUCTURAL EVALUATION

G. S. Kino

ABSTRACT

Acoustic microscope images of surface structure of metals are already clearly delineating individual crystallites and grain boundaries. It is suggested that the acoustic microscope can be modified to provide quantitative evaluation of a number of microstructural properties of metals which it has not been possible to determine before. This would provide much of the basic information required for use in theories relating fracture toughness, yield and hardness and macroscopic acoustic measurements, to the microstructural properties of a metal.

In its unmodified form the microscope could yield direct information on the nature of the fracture phenomenon which occurs ahead of the crack tip in steel. It is suspected that carbide inclusions some distance from the crack tip may be cracked (the cracks being of the order of micrometer long) and lead to the growth of the main crack. Acoustic microscope observations of a stressed cracked sample could provide the information needed to check the theories now being developed on this subject (Evans, Hutchinson, Budiansky, Hirth).

By modifying the transducer electrode structure of the acoustic microscope appropriately, it would be possible to measure the Rayleigh wave velocity and attenuation in any

direction along the surface of an individual crystallite. At a later stage it should also be possible to measure the velocity of leaky longitudinal waves propagating parallel to the surface. This should make it possible to directly measure the anisotropic elastic properties of individual crystallites, and attenuation and velocity change due to the presence of precipitates. Again this type of experimental information would be the only way of obtaining a detailed check being developed on theories the effect of microstructural variations in steel on acoustic wave propagation (Kino, Evans).

A scaled up version of the microscope operated at frequencies of 10-20 MHz would provide similar information on the variation of macroscopic properties of metal related to texture and residual stress.

QUANTITATIVE APPLICATIONS OF ACOUSTIC MICROSCOPY TO MICROSTRUCTURAL EVALUATION

G. S. Kino

INTRODUCTION

It is apparent that macroscopic acoustic measurements of attenuation and velocity in metals give results which depend qualitatively and quantitatively on the internal microstructure of the material, as do macroscopic mechanical properties, such as Young's modulus, yield strength, hardness, and fracture toughness. However, our understanding of the connection between the results of acoustic measurements and macroscopic or microscopic mechanical properties of a material is not adequate at the present time. Even our qualitative understanding of the physics of the problem is poor.

One reason for the difficulty is that for many industrial materials, like steel, for instance, we do not have sufficient knowledge of the microscopic properties of the individual pearlite and martensite crystallites. In the same way the effect of dislocations and of precipitates in polycrystalline aluminum on acoustic velocity and attenuation or other measurable acoustic properties has not been studied in any detail.

Therefore, to further our understanding it is important first to study the acoustic properties of polycrystalline materials at the microscopic level. Measurement techniques based on the principle of the acoustic microscope are well suited to this application. Quate and Briggs have shown that the scanning

acoustic microscope (SAM) produces good images of surface structure, crystallites and grain boundaries at the surface of a metal. The device gives only very limited quantitative information on the acoustic properties of an individual crystallite¹.

I suggest that in addition to applying the device in its present form to image surface structure a modified acoustic microscope could and should be developed for the purpose of measuring the elastic properties of individual crystallites, crystalline anisotropy, the effect of precipitates on elastic properties, and the relation between macroscopic texture and residual stress effects and the microscopic properties of individual crystallites.

We first describe the microscope structure envisaged, then give a description of some of the measurements that could be carried out.

THE MODIFIED ACOUSTIC MICROSCOPE

An acoustic microscope, with a lens structure illustrated in Fig. 1a, uses a lens to focus a parallel acoustic beam emitted from a ZnO transducer. The beam is emitted into a liquid medium (usually water) and is focused to a small spot on the substrate being examined. The reflected beam passes through the lens and is received by the same transducer. The size of the focused spot is typically of the order of one acoustic wavelength in water, e.g., 15 μm at 100 MHz, 1.5 μm at 1 GHz, and 5000Å at 3 GHz.

When the focal point is located a distance h below the substrate a Rayleigh wave can be excited by the rays incident at an angle θ_R to the normal, where $\sin \theta_R = V_w/V_R$, V_w is the acoustic wave velocity in water, and V_R the Rayleigh wave velocity on the substrate. The wave travels a distance $\lambda = 2h \tan \theta_R$ along the substrate is reradiated to the lens and received at the transducer. A second set of rays normally incident on the substrate is also reflected back to the transducer and interfere with the rays which travel along the Rayleigh path. When the lens is moved up and down, the two sets of rays yield signals at the receiving transducer which alternately are in or out of phase. A measurement of the spacing between the maxima or minima of these interference patterns make it possible to obtain an estimate of the average acoustic velocity of the Rayleigh wave.

We suggest that the microscope structure and operating procedures can be modified in several ways to provide more quantitative information:

1. Short tone bursts can be used to excite the microscope. Two time separated tone bursts will be received corresponding to the Rayleigh wave and normally reflected pulses. The phase difference of the reflected tone bursts can then be measured extremely accurately by well established methods to determine the Rayleigh wave velocity with high precision (as much as one part in 10^5). The disadvantage of this technique is that it is most suitable for use at frequencies below 100 MHz where the definition may be relatively poor;

2. The signals from the normally reflected waves and Rayleigh waves can be spatially separated by dividing up the transducer electrode into 5 parts, as illustrated in Fig. 1b.

Suppose first the electrodes A and C and electrodes B and D are connected together and the two sets of electrodes are connected across a balanced transformer as shown in Fig. 2a. Because of the balanced configuration there will be no excitation of signals on the center electrode and vice versa. The center electrode can be used to provide information on the distance of the lens from the substrate and as has been shown already by Liang et al.¹ the phase of the return echo from the normal ray can be compared with a reference signal and used in a negative feedback circuit to keep the spacing of the lens from the substrate constant. The total signal detected on the transformer will consist of the sum of two Rayleigh waves propagating in the x and y directions respectively. Thus a measurement of the phase of this signal provides a measure of the average Rayleigh wave velocity corresponding to the isotropic part of the elastic constant.

By using the configuration of Fig. 2b, and finding the difference in phase of the signals passing in the x and y directions the velocity difference of the corresponding Rayleigh waves can be determined. Furthermore, by rotating the lens the directions for maximum and minimum Rayleigh wave velocity the slowness curve for the phase velocity can be found. In addition

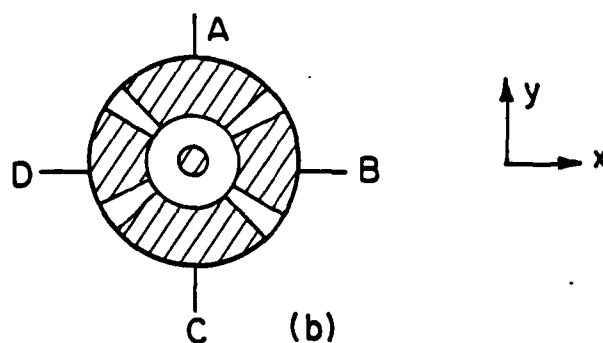
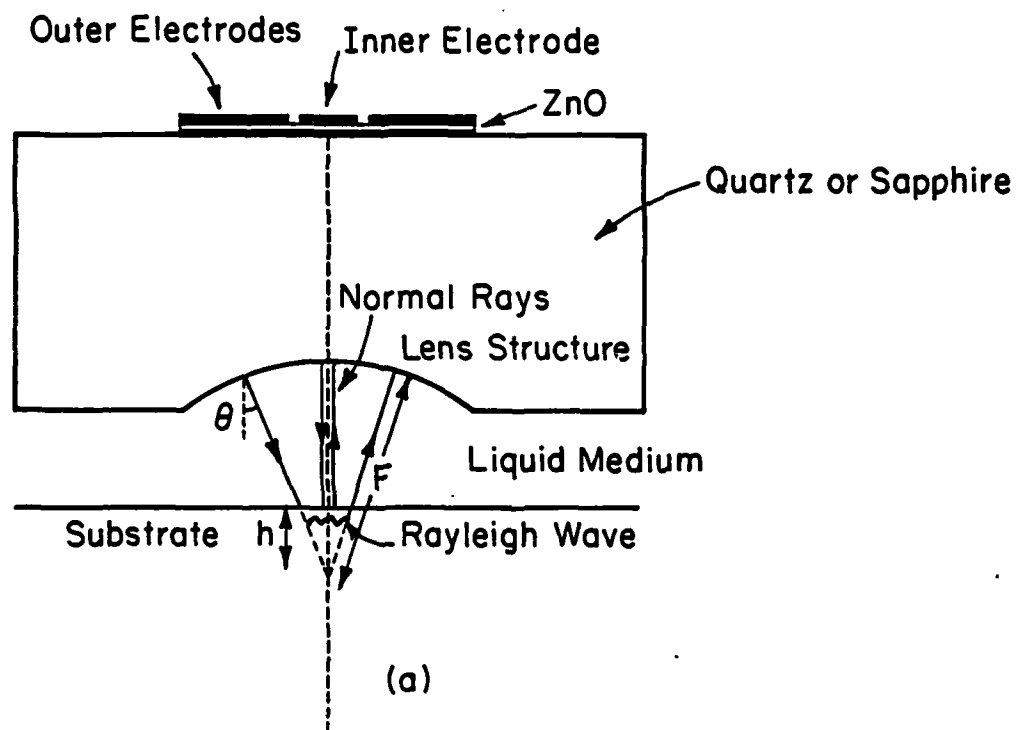


Figure 1. Modified Acoustic Microscope Structure.

- a. The basic acoustic microscope structure showing ray paths.
- b. Modified electrodes for measurement of Rayleigh velocity and anisotropy.

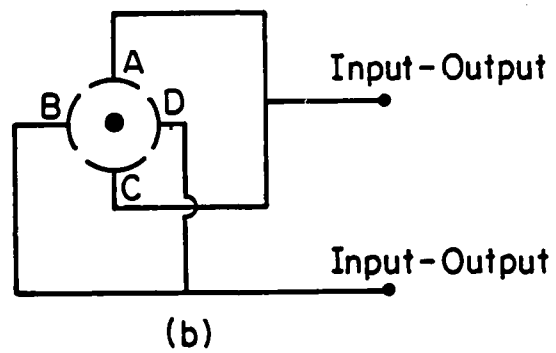
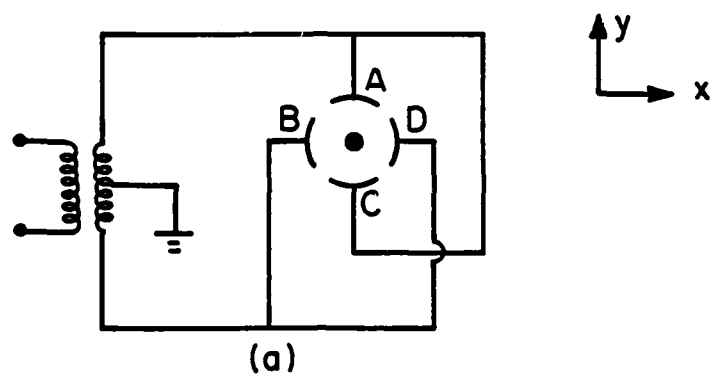


Figure 2. Two circuit configurations for quantitative measurements with the surface acoustic microscope.

the variation of attenuation of Rayleigh waves with angle can be determined.

By using a smaller diameter set of transducer electrodes which cannot excite Rayleigh waves, there is also the possibility of exciting leaky longitudinal waves and measuring the velocity and attenuation of the longitudinal skimming waves as a function of angle. As the Rayleigh wave velocity is very close to the quasi shear wave velocity in a crystal, these two sets of measurements carried out on the surfaces of individual crystallites should with some computation and extension of the required theory make it possible to determine the effective elastic constants of the crystallites which are present. We note that measurements of this type have already been made by Ash et al. with Rayleigh waves on large single crystals.^{3,4}

It is apparent that for complete interpretation of these measurements an inversion theory must be developed. Some of the work required has been carried out by Ash and his coworkers^{3,4}. Further iterative techniques needed to fit the measured values of velocity as a function of angle to a set as "best fit" elastic constants could certainly be developed. As we usually know the crystal type being observed, it should be possible by measuring the symmetry of the measured slowness curves to determine those crystallites which have their faces normal to one of the axes of symmetry of the crystal and carry out the measurements on such crystallites.

Measurements of the Effects of Particles and Inclusions

It has been suggested by Evans, Hirth, Hutchinson and Budiansky that cracks in steel can grow due to the effect of small carbide particles of the order of 1 μm diameter. If these particles are themselves cracked and are located a few microns from the tip of the crack, the stress fields associated with them can cause crack growth.

The use of the acoustic microscope in its normal imaging mode is an obvious way to check their theory. A flat sample would have to be prepared by chemical-mechanical polishing and a high frequency 3 GHz microscope employed; the definition of this microscope would be $\sim 4000\text{--}5000\text{\AA}$. Thus one might hope to observe the particles and even scattering of Rayleigh waves from the cracks directly. By applying an acoustic microscope modified in the manner described to this problem there is a good possibility of measuring the amplitude of the waves reflected from the particle as a function of direction of excitation relative to the particle and the crack within it. We would expect, furthermore, that the Rayleigh wave velocity would be affected by the large stresses near the crack tip and these velocity changes could be measured. Hence with some development of the measurement techniques it may be possible to obtain a great deal of information about the nature of the growth of cracks in steels. Earlier work at low frequencies has already shown that relatively small cracks can be observed from the standing Rayleigh wave pattern associated with them.

It is apparent that the same techniques can be used relatively easily to check on the effects of larger pearlite inclusions in steels. The use of the modified microscope should make it possible to measure the elastic properties of such pearlite regions. In addition it should be possible to measure the growth of cracks as they approach such regions.

In all cases we would envisage using a three point bending jig in conjunction with the microscope to make it possible to apply stress to open up cracks during the measurement. It would be convenient in this situation to make use of the positioning system with negative feedback already described, to maintain a constant distance between the lens and the sample surface.

MACROSCOPIC MEASUREMENTS WITH MICROSCOPE METHODS

We have, so far, concentrated on the design of modified acoustic microscope structure for highly precise measurements of microstructure. The same design can and should be scaled for use at lower frequencies in the 5-10 MHz range where the focal spot diameter would be of the order of 150-300 μm and Rayleigh wave velocity measurements could be carried out over regions of the order of 5 mm diameter. In this case the device would lend itself extremely well to measurements of texture variation and even near surface stresses.

By using broad band transducers it should be possible to carry out surface wave measurements over a wide range of frequencies where the Rayleigh wave penetration depth may vary

from 50 to 500 μm . In this case if the material properties such as hardness vary with depth, the Rayleigh wave velocity will vary with frequency. By using an inversion calculation on the measurements, with computer techniques now commonly available, it should be possible to determine how the elastic properties of the material vary with depth. Typically, simplifying assumptions such as the assumption of a constant Poisson's ratio are very helpful in simplifying this process.

As an example it has been shown that in some steels the longitudinal wave velocity varies linearly with hardness in a Jominy bar quench test. It is therefore conceivable to use the low frequency microscope lens system to measure case hardness variation with depth as well as texture variations and other macroscopic properties of interest.

CONCLUSION

The acoustic microscope is a powerful tool for measurement of microstructural and bulk properties of metals. With some changes in the design and structure it should be possible to modify the device to carry out measurements for the first time of the elastic properties of anisotropic single crystallites, stress variations near cracks, scattering of acoustic waves from small particles. Properties of the bulk material could also be measured with a scaled up version of the microscope.

The development of such techniques gives the promise of providing information, available with no other measurement

method, on microstructural properties of materials and will provide an important tool to check theories now being developed.

ACKNOWLEDGEMENT

This paper was written under the auspices of the DARPA Materials Research Council, Contract #MDA903-82-C-0428 with The University of Michigan.

REFERENCES

1. G. A. D. Briggs, "Acoustic Microscopy for Materials Studies," DARPA Conference on Microstructure Evaluation, MRC, July 1982.
2. C. F. Quate, "Scanning Acoustic Microscopy," in Scanned Image Microscopy, E. A. Ash, Ed., Academic Press, 1980.
3. E. A. Ash, Proc. Ultrasonic Symposium, IEEE, 1978.

ACOUSTIC ATTENUATION AND VELOCITY MEASUREMENT AS A PROBE FOR MEASUREMENT OF MICROSTRUCTURE & RESIDUAL STRESS IN METALS

G. S. Kino

INTRODUCTION

We shall attempt to deal here with the various types of externally excited acoustic probes which can be used to measure microstructural properties. The acoustic methods employed may be divided into two types: (1) those used for examining the surface or near-surface properties; and (2) those used for examining the bulk properties.

Class (1) includes the acoustic microscope, photo-acoustic methods and, at the present time, the use of surface acoustic waves in the frequency range from 1 MHz to 4 GHz. It also includes the use of various kinds of acousto-optic non-contacting probe techniques, the noncontacting EMAT probe, etc. As the wavelength involved can be as low as 4000\AA , and the definitions may well improve still further, the scanning acoustic microscope technique and associated surface probing methods are capable of examining single crystallites. The use of lower frequency surface acoustic waves, on the other hand, can yield information on macroscopic surface quantities.

The Class (2) techniques are, at the present time, mainly based on the measurement of velocity and attenuation of shear or longitudinal wave acoustic beams and to a far lesser extent, scattering of acoustic beams from the microstructure. Because the attenuation or scattering may be quite large in typical

metals, the frequencies employed are typically in the 2-100 MHz range, and the corresponding acoustic wavelengths vary from 30 micrometers to several millimeters, with most of the work based on measurements at the lower frequency, longer wavelength end of the range.

THE CAPABILITIES OF THE VARIOUS TECHNIQUES

We will now discuss the capabilities for evaluating microstructure of the various types of techniques, both at the present time and the possibilities for the future.

The Acoustic Microscope

Present capabilities: The device shows excellent reflection images of surface structure. Cracks, dislocations and individual crystallites are easily observed. Spots where the adhesion of thin films is poor, can be observed. This makes it very important as an analytical tool for semiconductor devices and for VLSI. Another example of use in this field is that of observation of the adhesion and exposure of photoresist.

Acoustic microscopes are becoming commercially available (Leitz, Olympus). They are easy to use but slower (approximately 1 minute) to form an image than an optical microscope. The test definition obtainable ($\sim 5000\text{\AA}$) is over a field of view approximately $1\text{mm} \times 1\text{mm}$. As with any new device of this kind, not all features of the images are well understood, and some experience is needed to obtain images in the most easily interpretable form.

A great deal of information is available in an image, but as yet, the full quantitative capabilities of the device have not been used. In the reflection mode, the contrast is mainly due to phase interference between a Rayleigh wave passing along the surface and a wave reflected from the surface essentially at normal incidence. By moving the focus in and out, measurements of the acoustic surface wave velocity, and hence, a quantity related to the elastic properties of the surface can be obtained. The properties of multiple layers of different films, such as metal on SiO_2 on Si, a thin paint film, and so on, can be determined to some extent. Recently, by the use of short 50 MHz tone bursts and accurate phase measurements, such velocity measurements have been made to an accuracy of at least 1 part in 10^4 , but with a definition of only 1mm, as yet.

Transmission microscopy has been used on thin samples less than 2mm thick. But it has not yielded very good results in microstructural measurements.

Possibilities for the future: An acoustic microscope has been operated at liquid helium temperatures, with a definition of 900Å. The best room temperature definition will probably be improved to 3000Å.

With some effort, new lenses could be made to measure the anisotropic elastic properties of crystals and grain interfaces at the surface. Again, there is the possibility that these techniques could be developed to measure near surface stresses around a crystal grain. As further experience is

gained by metallurgists with the acoustic microscope, we would expect to develop information on signatures associated with different types of defects. The device should prove to be very useful for obtaining information on surface damage due to machining processes.

The same methods could, and should be, scaled to operation at much lower frequencies. This should provide information on macroscopic quantities near the surface. By working over a broad frequency band, it should be possible to measure depth profiles of near surface variations of mechanical properties. Measurement of case hardness profiles is an important application. Here the Rayleigh wave velocity variation with frequency is determined. As the acoustic velocity varies with the hardness and the Rayleigh wave penetration depth varies with frequency, hardness profiles can be measured with this technique.

Transmission microscopy will have limited usefulness because of the speckle problem due to scattering from many grains, and, at the present time, poor control over focusing inside a solid. Reflection imaging from internal defects and microscopic structure could be developed. The development of short pulse systems will be needed along with considerable development of special purpose lenses and a better theoretical understanding of the problems involved. But, all work of this kind, where at very good definition in the micrometer range is required will be limited to relatively thin samples (<1 mm), because of the high attenuation associated with very high frequency acoustic waves.

Photoacoustic Microscopy

This technique makes use of a focused modulated heat source, usually a laser beam or electron beam, to periodically vary the temperature of a spot on the surface of the substrate being examined. The variation in temperature, in turn, causes thermal expansion and contraction of the material in the neighborhood of the heated spot which can excite an acoustic wave. The temperature reached depends on the heat capacity and conductivity near the region being radiated by a laser spot. The size of the heated region is determined by the thermal diffusion length. With modulation at frequencies below 10 KHz, the thermal diffusion length is in the fractional millimeter range in metals. At very high frequencies, the thermal diffusion length may be less than 1 micrometer.

These thermal effects can be detected by a variety of methods. Some examples are:

(1) An air cell above the sample. The air is heated, causing a pressure wave, which is detected by a microphone.

(2) The mirage effect. The heated air above the sample has its refractive index changed due to the temperature gradient. This will deflect a probing laser beam passed parallel to the sample surface. Vertical deflections are associated with the temperature gradients normal to the surface and horizontal deflections with the temperature gradients parallel to the surface.

(3) An infrared detector for measuring the surface temperature.

There are many examples of method (1) in the literature. Method (2) seems to be the most sensitive of these three (1 millidegree) while less vibration sensitive and independent of surface roughness and surface emissivity. But it requires the use of very long (~1 meter) carefully aligned laser beam. As temperature is measured directly, the output signal level depends on the thermal conductivity of the material;

(4) An acoustic transducer placed on the opposite side of the sample will detect the acoustic waves excited at the laser beam modulation frequency by the modulation of the thermal expansion;

(5) A probing laser beam reflected from the sample surface can be used to detect the acoustic or thermal wave excited by the heat modulation.

Present capabilities: Most of the emphasis has been placed on using method (1) and (4). The technique basically measures changes in heat absorption thermal conductivity and heat capacity with emphasis, to a lesser extent, on the elastic properties of the material. Several examples of good images of closed and open surface cracks, and to a limited extent, of inclusions in metals and ceramics have been given in the literature.

It would appear to be possible to measure elasticity or possibly residual stress with this technique. An example, given

by Lukkuula is that of a metal coin lapped flat. The original pattern on its face shows up clearly in a photoacoustic image.

By using electron beam excitation from an SEM, Rosenzwaig has obtained clear high definition images of highly doped regions in semiconductors. This is due to the change in thermal conductivity in these regions. Quate has used an argon laser beam modulated at 800 MHz to excite the surface through an optical microscope and employed his acoustic microscope as the detector. This has produced clear images of surface structure in metals, of adhesion of films, and of the effect of laser annealing of metal films, i.e., the difference between an amorphous and crystalline layer.

Possibilities for the future: The theory of photoacoustic microscopy needs to be developed further, to determine the connection between microstructural properties and images formed. Clearly we can observe gross effects of heat conduction. But can we observe changes on thermal conduction across a grain boundary. There are possibilities of using the phase modulation of a probing acoustic beam by temperature variation as a probe to measure residual stress (Salama); here the rate of change of acoustic velocity with temperature varies with stress. If we can use a modulated acoustic beam to heat the interior of a metal, there are possibilities of using these methods to measure internal friction.

Clearly photoacoustic microscopy has provided excellent information on near-surface structures. With further develop-

ment, it should provide information on surface change, variation in near-surface microstructural properties, hardness, etc. But, it is not yet clear whether developments of these techniques have potential for internal measurement of materials.

Velocity Measurements

Present status: Changes in the velocity, as a function of frequency or position, can be detected to 1 part in 10^6 in flat laboratory samples. As stress changes the acoustic velocity, good measurements of inhomogeneous applied stress fields can be made. To a limited extent, residual stress measurements have been obtained using these techniques, both with contacting and noncontacting (EMAT) probes. Surface waves and focused beam have been employed to measure near surface stresses and highly unhomogeneous internal stress fields. The change in acoustic velocity has also been associated empirically with hardness and texture. In certain steels, the velocity variation varies linearly with Rockwell hardness. But the velocity changes drastically with composition. So this empirical relation is useful only in a limited sense. The shear wave velocity depends on the direction of polarization with respect to the rolling direction or texture. Thus, shear wave measurements do provide an easy empirical technique for measurement of texture. There is some variation of velocity with grain size.

Bulk Wave Measurements of Attenuation, Velocity & Scattering

These techniques make use of a probing acoustic beam typically a few millimeters in diameter to determine acoustic

velocity attenuation, and to a limited extent, backscattering from microstructure. Shear wave and longitudinal wave probes have been employed. By the nature of the method, macroscopic average of microstructural material properties are taken. Thus, measurements of macroscopic quantities related to the mechanical properties of materials are taken, although by observing the angular variation of attenuation, velocity and backscattering, some information on microstructural properties can be obtained.

It should be emphasized that there is a great deal of empirical information on material properties available from these techniques which is not always easy to explain with fundamental theory based on the physics of the problem. We will discuss several examples of such results. The wave velocity varies with frequency in a way which depends on the grain size and texture.

On the other hand, the dispersion of surface waves is affected by the variation of material parameters near the surface due to the fact that the penetration of these waves is approximately one wavelength. Some limited measurements of hardness variation and hydrogen embrittlement have been made on a semi-empirical basis using this property.

Future status: For stress measurements, particularly residual stress measurements, better calibration techniques need to be worked out. Progress has been made in sorting out texture effects from stress effects. Further progress is possible and

must be made to obtain unequivocal measurements of residual stress.

The understanding of the relation between microstructural properties and macroscopic mechanical properties is still weak. Therefore, it is not surprising that the connection between acoustic velocity measurements and microstructural properties is even more weakly understood.

Obviously the theory of acoustic propagation in such media needs to be developed further, as is discussed below. But it is apparent that it is unlikely that the theory will ever cover all the myriad of possible effects that can occur.

Therefore, considerable reliance must be placed on empirical methods. We can and should develop a better theory of the effects of texture on the phase velocity, but the effect of hardness, yield point and so on, on the acoustic velocity may always have to be based on empirical data. But, if with the cooperation of metallurgists, suitable samples can be provided in which only one microstructural parameter, such as grain size or texture is varied at a time, then it may be possible to put the empirical methods on a more systematic basis.

It will be necessary to develop techniques to measure velocity dispersion over a frequency range of several octaves. This again will tend to put the results in a more systematic format.

Attenuation Measurements

Present status: The theory of acoustic scattering from the grains has received considerable attention over the years. Frequencies for which the acoustic wavelength λ is such that $\lambda \gg D$, the average grain size the attenuation per unit length is of the Rayleigh type and is proportional to $f^4 \bar{D}^3 \mu^2$, where $\mu = c_{11} - c_{12} - 2c_{44}$. At higher frequencies, the attenuation is said to be stochastic and vary as $\mu^2 \bar{D} f^2$.

In practice, the Lifshitz and Parkomovski theory predicts the measured attenuation in the low frequency regime quite accurately, but does not do as well at higher frequencies. Reasonable predictions of grain size in materials like aluminum and copper can be made from acoustic attenuation measurements.

The results are far cruder for mixed phase materials like the carbon steels. Empirical techniques based on impedance mismatch ideas predict a minimum loss at approximately 0.4% carbon content, which seems to match with experiment.

Recent surface wave measurements show some peaks in attenuation of aluminum associated with peaks in hardness.

Work by Alex Vary indicates some empirical relations exist in certain materials between the frequency dependence of attenuation and yield strength. But, there is no good physical justification for these results.

Future progress: Just as with velocity measurements, the theory needs to be developed further for simple grain scattering attenuation and for multiple phase effects. Then

checks need to be made to determine if other effects, such as grain boundary losses, anelasticity due to heat loss from grain to grain, losses due to presence of dislocations and so on, are important. So far, very little systematic study has been made on practical materials to check out the relative importance of these effects and how they might be used to determine microstructure and mechanical properties.

Once more, a great deal of reliance will need to be placed on empirical test methods. But at the very least, we would expect that the development of the theory should make it possible to predict the grain size distribution, and texture from measurement of attenuation and velocity.

Scattering Measurements

Present status: Very little has been done on scattering from microstructure. There is some work by Geobbel's in Germany. But to obtain useful results, a great deal of spatial averaging must be used.

The basic idea is that by employing short pulses and looking at the frequency spectrum of backscattered radiation, information can be obtained about the variation of properties with depth, grain size and so on.

Future possibilities: By making use of the techniques developed for speckle holography and for scattering from rough surfaces, further useful developments can be expected.

ACKNOWLEDGEMENT

This paper was written under the auspices of the DARPA Materials Research Council, Contract #MDA903-82-C-0428 with The University of Michigan.

THE EFFECTS OF DISLOCATIONS ON ACOUSTIC ATTENUATION IN METALS

G. S. Kino

It has normally been assumed that grain scattering in metals is the dominant cause of acoustic wave attenuation. The effect of dislocations on attenuation is normally regarded as too small compared to grain scattering to be of interest. Such dislocations have only been measured unequivocally in single crystal materials.

A reexamination of these assumptions, based on the Granato Lucke Theory of dislocation damping has been made. We predict that for dislocation densities of $10^6/\text{cm}^2$, and loop lengths of $1\mu\text{m}$, the attenuation of shear waves or Rayleigh waves varies as the square of the frequency approaching a maximum value, virtually independent of the loop length, of the order of 3 db/cm at frequencies in the 20-30 MHz range. This attenuation should vary approximately inversely with the temperature and as the square of the frequency, while grain scattering attenuation should be independent of temperature, and vary as the fourth power of the frequency for small grain materials ($D \ll \lambda$, where D is the grain diameter and λ the acoustic wavelength). At frequencies in this range grain scattering attenuation in fine grain materials, is of the order of 0.1 to 0.3 db/cm. We suggest that a direct measurement of plasticity in metals, such as fine grain steels could be made by measuring attenuation as a function of stress when the material is stressed into the yield

range. Our predictions seem to be confirmed by experiments carried out with Rayleigh waves propagating on steel sheets at a frequency of 20 MHz by Droney and Klinmar.¹ These authors measured a change in attenuation under yield conditions of the order of 0.1 dB/cm.

We further suggest that application of techniques closely related to photoacoustic methods may provide a very powerful method of measuring effects due to dislocations. By using either a surface acoustic wave heating source modulated at a frequency of the order of 100 Hz, due to the dislocation interactions, the temperature of a steel sheet may be modulated by a few degrees. Therefore, the amplitude and the phase of a second probing Rayleigh wave beam will suffer a weak modulation which could easily be detected with a lock-in amplifier. Thus, because grain scattering radiates power into the bulk of the material, and causes very little temperature rise, we may be able to separate out the effect of dislocations by the use of photoacoustic methods.

Furthermore, as the acoustic velocity variation with temperature does depend on the stress present, it may be possible to separate out the effects of residual stress from the effects of plastic yield by making separate measurements of the rate of change of Rayleigh wave velocity with temperature when the sample is heated by a modulated laser beam.

The temperature modulation itself is measurable by the techniques suggested by Murphy at the conference on Microstruc-

ture Characterization.² Therefore, this technique too could be used as a method of measuring the acoustic absorption due to dislocation interactions.

ACKNOWLEDGEMENT

This paper was written under the auspices of the DARPA Materials Research Council, Contract #MDA903-82-C-0428 with The University of Michigan.

REFERENCES

1. B. E. Droney and R. Klinman, "Ultrasonic Techniques for Determining Mechanical Properties of Steels," Proc. Topical Conference on Applications of Physics in the Steel Industry, Lehigh University, Bethlehem, PA, October 1981.
2. J. C. Murphy and L. Hamdt, "Photothermal Imaging Applied to Microstructural Analysis," DARPA MRC Conference on Microstructural Evaluation, July 1982.

MEASUREMENT OF ATTENUATION DUE TO DISLOCATIONS

G. S. Kino

The effect of dislocations on propagating acoustic waves in polycrystalline metals is usually ignored because it is normally assumed that grain scattering is the dominant effect. We find it interesting to reconsider this phenomenon anew, for if it can be measured it would provide useful information on residual stress states and the state of plastic strain of material which has been stressed beyond the yield point.

Recent measurements by Droney and Klinman¹ on low carbon sheet steel samples, using 20 MHz surface waves propagating between two fixed wedge transducers 2 inches apart does seem to show some evidence of this effect.

In Fig. 1 we show their stress-strain curve for this material, yield occurs at a stress of 40 ksi. In Figs. 2 and 3 we show their result for the variation of attenuation and transit time between fixed transducers with stress. It will be observed that there is a change in attenuation of as much as 0.3 db/inch and a relative change in transit time of as much as 1.5 parts in 10^3 . The results obtained here have rather large fluctuations but do seem to indicate that there may be a real effect present.

We try and estimate in this paper how large these effects should be. We find that on the basis of relatively crude assumptions based on the work of Granato and Lucke^{2,3}, we

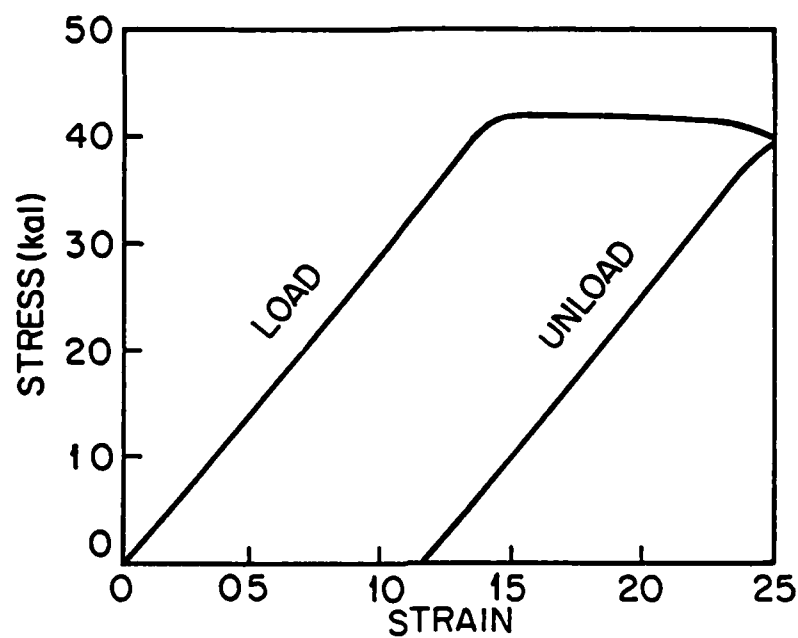


Figure 1. Stress-strain curve for sheet steel tensile sample (after Droney¹).

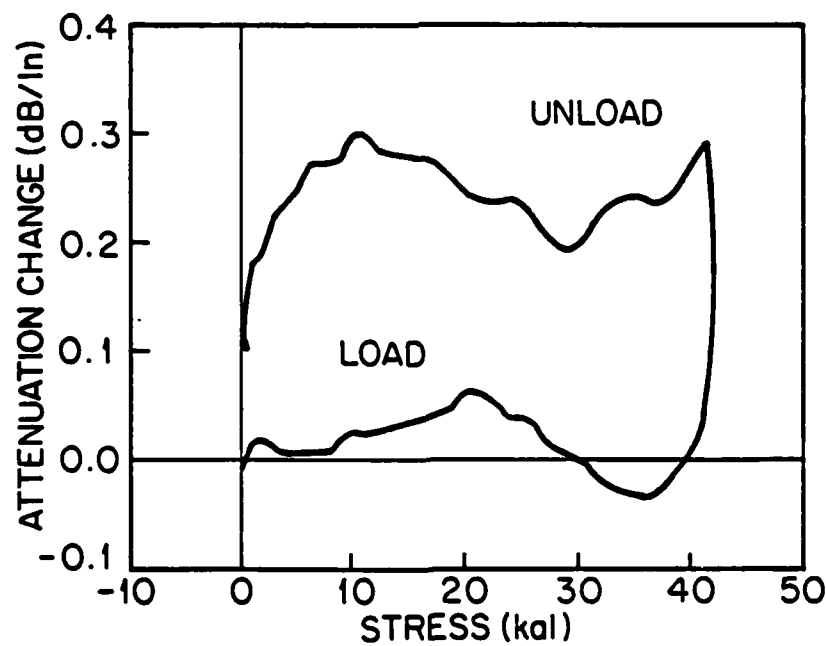


Figure 2. Attenuation change during tensile test (after Droney¹).

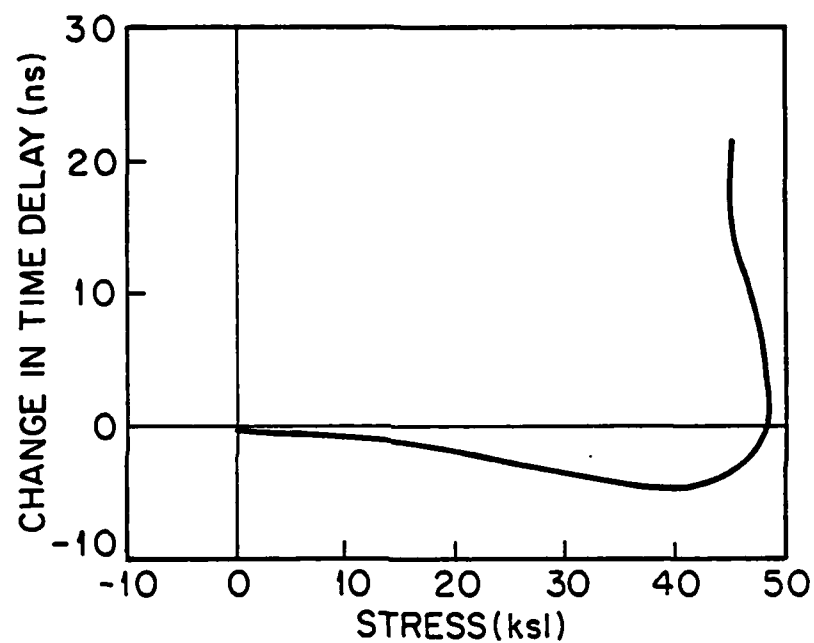


Figure 3. Example of propagation time for surface wave transducers held at a fixed distance (2") apart. Tensile test on sheet steel sample covered loading to plastic region, then hold (after Droney¹).

might expect attenuation and velocity changes comparable to the values observed. But we have had to guess at the dislocation density. Fortunately, however, in the range of frequencies used the attenuation is virtually independent of the dislocation loop lengths providing they are less than 1 or 2 μ r length.

The results obtained certainly indicate that the effect is a marginally measurable one at best. However, small changes in attenuations of laser light passing through a gas when there are small amounts of other constituents present are very commonly measured by photoacoustic methods. We therefore suggest the development of a photoacoustic type of technique for this purpose.

Suppose a Rayleigh wave acoustic beam is modulated at a frequency of the order of 100 Hz; the acoustic wave will heat the surface region of the material when power is lost from it by interaction with dislocations. The temperature of the surface will therefore be modulated at a 100 Hz rate. We suggest the use of a second probing beam whose phase delay will be modulated by the small fluctuations in temperature of the material due to this heating effect. As there is very little heat dissipated near the surface by grain scattering which scatters power into the bulk, this method of probing may provide a very sensitive way to detect the small amount of attenuation due to dislocation damping.

Calculation of Attenuation and Velocity Change Due to the Presence of Dislocations

Trueell and Elbaum give the following formula for the attenuation α of a shear wave due to the presence of dislocations:

$$\alpha = \left[8.68 \times 10^{-6} \frac{4Gb^2}{\pi^4 C} \Lambda L^2 \omega_m \right] \frac{(\omega/\omega_m)^2}{1 + (\omega/\omega_m)^2} \frac{db}{\mu\text{sec}} \quad (1)$$

This formula should still be approximately true for Rayleigh waves which contain most of their energy in shear wave components.

The frequency where the damping attains half its maximum value is

$$\omega_m = \pi^2 C / L^2 B \quad (2)$$

where $A = \pi \rho b^2$, ρ is the density of the material, b is the Burgers vector of the dislocation loop, $c = 2Gb^2/\pi(1-\nu)$, G is the shear wave elastic constant, ν Poisson's ratio, L the loop length, and Λ is the dislocation density. The parameter B is associated with damping of the loop motion and has been calculated by Leibfreid³ to be

$$B = 3kT \frac{z}{10V_t a^2} \quad (3)$$

where a is the lattice spacing V_t the transverse wave velocity, z the number of atoms in the elementary cell, k is Boltzmann's constant.

At low frequencies where $\omega \ll \omega_m$ we note that

$$\alpha = 8.68 \times 10^{-10} \frac{2(1-\nu)}{\pi^3} \frac{B}{\pi^2 C} \Lambda L^4 \omega^2 \frac{db}{\mu\text{sec}} \quad (4)$$

and attenuation varies as the square of the frequency. In the range of interest to us the relative change in velocity due to the presence of dislocations

$$\frac{\Delta V}{V} = - \frac{2(1-\nu)}{\pi^3} \Lambda L^2 \quad (5)$$

while if $\omega \gg \omega_m$ the attenuation is

$$\alpha_m = 8.68 \times 10^{-6} \frac{4Gb^2\Lambda}{B} \frac{db}{\mu\text{sec}} \quad (6)$$

and is independent of loop length when $\omega \gg \omega_m$. We note that $\Delta V/V$ is still given by Eq. (5) for a dislocation loop length of 1 μm dislocation density $\Lambda = 10^{10}/\text{m}^2$, and Poisson's ratio of $\nu = .35$

$$\frac{\Delta V}{V} = -4 \times 10^{-4} \quad (7)$$

So the velocity change due to the presence of dislocations is small although it may be measurable.

We consider the case of aluminum or steel. For aluminum with $V = 3 \times 10^3 \text{ m/sec}$, $p = 2.7 \times 10^3 \text{ kg/m}^3$, $b = 2 \times 10^{-10} \text{ m}$, $a = 3 \times 10^{-10} \text{ m}$, $L = 1 \mu\text{m}$, $z = 12$, $\Lambda = 10^{10}/\text{m}^2$, then $A = 2.16 \times 10^{-19}$, $B = 5.52 \times 10^{-5}$, $G = 2.43 \times 10^{10}$, $C = 9.52 \times 10^{-10}$, $\omega_m = 1.7 \times 10^8$ or $f_m = 2.7 \times 10^7$, the resonant frequency of the loop is $\omega_0 = \pi(C/A)^{1/2}/L$ or $\omega_0 = 2.1 \times 10^{11} \text{ sec}^{-1}$.

Since $\omega_m \ll \omega_0$ the motion of the dislocation loop is very heavily damped and resonance of the loop cannot be observed.

It will be observed that when a Rayleigh wave interacts with dislocations in a polycrystalline f.c.c. metal such as iron or aluminum, the shear component of stress may be at virtually any angle to the dislocation line. Hence, we must multiply our estimate of $\Delta V/V$ by α by $\langle \cos^2 \theta \rangle$ where θ is the angle between the direction of particle motion in the metal and the string. The average value of $\langle \cos^2 \theta \rangle$ is $1/3$. So on this basis the maximum value of attenuation in aluminum or steel due to the presence of 10^6 dislocations/cm² is 2 db/ μ sec or 5 db/inch.

Such an attenuation would be low compared to that due to grain scattering in aluminum at 20 MHz. However, in fine grain steels the attenuation of Rayleigh waves at 20 MHz could be expected to be 1 db/inch or less (which is not the same as the heating effect).

If we now compare this estimate to the results obtained by Droney and Klinman we find that the attenuation estimated here is about 6 times larger than their maximum experimental value, while their maximum experimental change in relative velocity between transducers a fixed distance (2 inches) apart is approximately 1.3×10^{-3} a figure considerably larger than our theoretical estimate which would be nearer to 1×10^{-4} when the spread in alignment angles is taken into account. But we might expect larger changes in acoustic velocity due to the change in the thickness of the metal sheet.

Photo Acoustic Techniques

We now assume that the dislocation attenuation is larger than thermoelastic attenuation. Furthermore we assume that grain scattering attenuation is virtually independent of temperature and causes very little heat dissipation from Rayleigh waves because the scattered energy is not dissipated at the point of scattering.

There is therefore the possibility that we can use a photoacoustic effect to measure the relatively small amount of attenuation due to the presence of dislocations.

We suggest two possible techniques, heating with a modulated light source and heating with a modulated acoustic surface wave beam, modulated at frequencies of the order of 100 Hz. Such a heat source has a diffusion length of

$$d = \sqrt{\frac{2\kappa}{pC}} \nu \quad (8)$$

where κ is the thermal conductivity, p the mass density, C the heat capacity per unit volume of the material and ν the radian frequency of the modulation. For aluminum the diffusion length at 100 Hz is of the order of 0.5 mm.

Now by using modulated Rayleigh wave beam with a center frequency of the order of 30 MHz the heat loss due to the dislocation interactions will cause the near surface temperature to fluctuate. This temperature fluctuation can be detected directly by deflection of a laser beam passed over the surface of the material, as described by Murphy. Alternatively it could

be detected by using a second surface wave beam passing at right angles through the same region as a probe. As the temperature of this region is varied the phase of the probing beam changes and the resulting phase modulation can be detecting with great sensitivity using the FM modulation scheme described by Liang⁸. The magnitude of this phase modulation will depend directly on the magnitude of the dislocation loss.

If instead a modulated laser beam is used to heat the metal surface there will now be some change of Rayleigh wave amplitude due to the fact that the Rayleigh wave attenuation caused by dislocation damping varies with temperature. However, the same technique would affect the phase of a probing Rayleigh wave beam in a way which would be virtually independent of dislocation damping. On the other hand this phase modulation would now depend on the applied stress as described by Salama because the rate of change of acoustic wave velocity with temperature varies with stress.

Hence it may be possible to examine the effects of stress and dislocation damping in the same material by using these two closely related probing methods.

DISCUSSION

We conclude that it is worthwhile to examine new techniques for measurement of dislocation damping in polycrystalline materials. The evidence for the effects seen by Droney et al. is weak, in part because of the crudeness of their measurement

method.¹ We therefore suggest the use of photoacoustic types of techniques to increase the sensitivity of the measurement.

We have suggested here that a technique based on the absorption of a modulated acoustic beam caused by the original damping of the coin changes the thermal conductivity and hence changes the temperature of the surface in accordance with the plastic strain of the region of interest. If this is indeed so, then we might expect the laser beam irradiation technique might be more useful than or at least as useful as the acoustic beam absorption method for showing up the presence of dislocations and plastic strain.

In our calculations we have assumed, for simplicity, that the acoustic interactions with dislocations is probably the best approach to use. However, we also suggest that techniques based on the use of a modulated laser beam may provide important information.

It is not completely clear, however, whether laser beam excitation or surface acoustic wave excitation of temperature fluctuations is likely to interact most strongly with dislocations. As an example which might indicate laser beam excitation as being the best technique to use, it is interesting to consider the experiments of Lukkuula⁶. He polished the surface of a coin flat, so its original imprint could not be detected. He then irradiated the coin with a focused chopped laser beam, which modulated the surface temperature at a frequency of a few hundred Hertz. He detected the temperature fluctuation by

standard photoacoustic methods. Then by scanning the laser beam over the surface of the sample he was able to produce a reasonable image of the original imprint on the coin. He gave no explanation for this effect. We might hypothesize that the presence of dislocations causes the thermal conductivity to change and hence changes the temperature modulation of the substrate. So the image obtained reproduces the plastic strain of the polished surface of the coin.

In the analysis we have carried out, we have assumed for simplicity that the loop length is $L \sim 1 \mu\text{m}$ and the loop density Λ is $10^{10}/\text{m}^2$. In practice we might expect the density to vary with the degree of plastic strain ϵ_p as

$$\Lambda = \Lambda_0 + C\sqrt{\epsilon_p} \quad (9)$$

with $\Lambda_0 \sim 10^{10}/\text{m}^2$. According to Hirth, Λ could increase to $10^{16}/\text{m}^2$ at $\epsilon_p \sim .2$ to $.5$. But in this case the maximum dislocation length would only be $L = 1/(\Lambda)^{1/2}$. So as Λ increases and ω_m becomes very large. If the frequency is kept constant, Eq. (4) show that the attenuation would eventually decrease as $1/\Lambda$. Thus it may be wise to operate at fairly high frequencies perhaps even using acoustic microscope methods to measure dislocation densities several orders of magnitude higher than $10^{10}/\text{m}^2$.

It is apparent that if the measurements do show dislocation effects a considerable development in the theory of dislocation damping will be required.

ACKNOWLEDGEMENT

This paper was written under the auspices of the DARPA Materials Research Council, Contract #MDA903-82-C-0428 with The University of Michigan.

REFERENCES

1. B. E. Droney and R. Klinman, "Ultrasonic Techniques for Determining Mechanical Properties of Steels," Proc. Conference on Applications of Physics in the Steel Industry, Lehigh University, Bethlehem, PA (1981).
2. A. Granato and K. Lucke, "Theory of Mechanical Damping Due to Dislocations," J. Appl. Phys. 24, 338 (1953).
3. R. Truett, C. Elbaum and B. B. Chick, Ultrasonic Methods in Solid State Physics, Academic Press, (1969).
4. G. Busse and A. Rosenzwaig, Appl. Phys. Lett. 36, 815 (1980).
5. L. C. Aamdt and J. C. Murphy, J. Appl. Phys. 52, 4903 (1981).
6. M. Lukkuula, S. G. Askerov, Electronics Letters 16, 84 (1980).
7. J. Hirth, Private Communication.
8. K. Liang, S. D. Bennett, B. D. Khuri Yalent and G. S. Kino, "High Resolution Measurement of Surface Velocity Perturbation at 50 MHz," Proc. DARPA AFML Review of Progress in Quantitative NDE, La Jolla, August 1982.

ACOUSTIC ATTENUATION AND VELOCITY CHANGE IN TWO PHASE MATERIALS

G. S. Kino and A. G. Evans

The acoustic attenuation and velocity are known to depend sensitively on microstructure in multiphase alloys. However, little fundamental understanding of the observed trend has emerged. Preliminary attempts have thus been made to examine effects of microstructure on acoustic properties, as an eventual basis for relating acoustic measurements to mechanical properties. Emphasis has been placed on microstructural trends in steels.

The acoustic attenuation depends primarily on grain size, grain shape and the elastic anisotropy of the grains (small effects of dislocation also obtained at low frequencies). The elastic anisotropy of the grains can be appreciably influenced by the presence of second phases. Hence, second phases affect both attenuation and mechanical properties. The association between attenuation and hardness are illustrated for various heat treatment processes applied to steels.

The elastic anisotropy of cubic ferrite grains is characterized by the parameter,

$$\Delta C = C_{11} - C_{12} - 2C_{44} \quad (1)$$

For ferrite grains the anisotropy is -1.3346. A similar anisotropy can be expected for martensite. The presence of pearlite grains is shown to increase the anisotropy (vis-a-vis ferrite or martensite) by modifying the symmetry to hexagonal. The

modified anisotropy is calculated by regarding the pearlite as orthorhombic (carbide) plates in a ferrite matrix. Conversely, carbide spheres (spheroidite or tempered martensite) are shown to exhibit a reduced cubic anisotropy, $\Delta C = 0.9845$. These predictions are consistent with attenuation measurements which demonstrate that (for constant grain size) the attenuation in pearlite/ferrite exceeds that in martensite which, in turn, exceeds the attenuation of tempered martensite.

The effects of carbon content on the attenuation of a pearlitic steel can also be rationalized by noting that the attenuation has the form,

$$\alpha = \alpha_p f^2 + (1-f^2) \alpha_f + 2f(1-f)\alpha_{fp} \quad (2)$$

Where f is the volume concentration of pearlite, α_p is the attenuation of pearlite, α_f the attenuation of ferrite and α_{fp} the attenuation attributed to the ferrite/pearlite interfaces. For reasonable choice of α_{fp} , the attenuation exhibited exhibits a maximum at ~5.5% C, in accord with experimental observations.

These preliminary results are encouraging, in that trends in attenuation with microstructure occur in a manner consistent with changes in the elastic anisotropy of the grains. However, it is clearly premature to determine whether attenuation relates uniquely to mechanical properties. Experimental studies are required. A cautionary note concerns the inability of acoustic scattering to determine precipitate size (only precipitate shape, volume concentration and coherency influence

scattering, (Evans and Williams); precipitate size and spacing exert a major influence on mechanical properties.

ACKNOWLEDGEMENT

This paper was written under the auspices of the DARPA Materials Research Council, Contract #MDA903-82-C-0428 with The University of Michigan.

EFFECTS OF PRECIPITATES ON ACOUSTIC ATTENUATION

A. G. Evans and J. C. Williams

Precipitates can exert two possible influences on the attenuation of ultrasonic waves, by virtue of their effects on grain scattering and internal friction. The former is associated with the influence of the precipitates on the acoustic impedance ($\sqrt{\text{modulus} \times \text{density}}$) anisotropy of the grains. For incoherent precipitates, the elastic modulus is dictated by the volume concentration and shape of the precipitates, independent of the precipitate size. Hence, when coarsening is not accomplished by significant shape changes, attenuation by grain scattering should be insensitive to precipitate size and hence, a poor indicator of mechanical properties (which are strongly size dependent). Conversely, substantial shape changes (such as spheroidization) should result in detectable changes in grain scattering.

Coherent precipitates are likely to modify elastic properties to an extent contingent upon the magnitude and sign of the coherency strains. Large coherency strains can induce significant elastic non-linearity and modify the effective elastic constants. The transition from coherency to incoherency could thus result in a change in the grain scattering amplitude. The trend would depend upon the sign of the hydrostatic component of the coherency strain (tensile or compressive).

Internal friction effects associated with precipitation can be either amplitude dependent or amplitude independent in nature. The type and extent of this damping depend on the density and loop length of mobile dislocations associated with the precipitates. These should be divided into two types. There are interfacial dislocations which are present in the precipitate/matrix interface (and which accomodate the misfit between the precipitate and the adjacent matrix) and geometrically necessary dislocations which are stored in the matrix to accomodate the strain gradient present after plastic deformation (if the precipitates do not deform). Of these, the interfacial dislocations are rigidly confined to the interface and thus, cannot bow out or move to any significant extent. The density of geometrically necessary dislocations scales with the microscopic strain and the average distance between these dislocations decrease with strain. The loop length of these dislocations should also bear a relationship to the precipitate size. For a reasonable loop length ($<1\mu$) around precipitates, the first amplitude independent internal friction peak occurs in the GHz range. The long wavelength internal friction solution should thus obtain,

$$\alpha = 4 \times 10^{-2} L^4 \rho \omega^2 / c_t^2 b \ln^2(L/b)$$

where ρ is the density and L the loop length of the mobile dislocations, ω is the frequency, b the Burgers vector, and c_t the wavelength. Inserting a reasonable upper bound for the mobile

dislocation density ($\sim 10^{10} \text{m}^{-2}$) reveals that significant attenuation (several dB/cm) in the MHz range (~ 10 MHz) only develops when the loop length $> 1 \mu\text{m}$. This loop length is outside the usual range of precipitate size at peak hardness. Significant contributions to attenuation from precipitate related internal friction are thus deemed unlikely.

ACKNOWLEDGEMENT

This paper was written under the auspices of the DARPA Materials Research Council, Contract #MDA903-32-C-0428 with The University of Michigan.

PROSPECTS FOR ACOUSTIC EMISSION DETERMINATION
OF MICROSTRUCTURE AND THE CONTROL OF METALS PROCESSING

Hayden Wadley

The intensity of acoustic emission from deformation, fracture and phase transitions is very dependent upon microstructure. Using existing instrumentation it should now be possible to search for correlations between properties of acoustic emission and critical metallurgical variables such as grain size, precipitate type and distribution, inclusion content, etc., and to explore the feasibility of using such relations for inprocess control of microstructure.

Welding is a very promising ongoing application of AE inprocess monitoring. Its major weakness is an inability to assess the significance of the detected sources. The new measurement methods at NBS have opened the way to measure the source properties of martensitic phase transformations and fracture. These properties should now be measured for:

- a) Model predictive systems
- b) Industrially relevant systems

This may then open the possibility for "online" defect assessment during processing.

COMMENTS ON THE WORKSHOP
ON NONDESTRUCTIVE MICROSTRUCTURE CHARACTERIZATION

G. H. Vineyard

The workshop on Nondestructive Microstructure Characterization (July 6 and 7) stimulated some blue sky thinking which is outlined here. It is not claimed that these ideas have been proved workable, nor that any of them has been tried out before. The very crowded schedule of this session of the MRC has prevented me from following through on the ideas and so they are set down in raw form as a possible basis for further work.

1. H. Wadley discussed acoustic emission from dynamic defects (cracks, etc.). Normally a single transducer on the surface of the specimen is employed to detect this emission and problems always occur with low signals in the presence of general noise. Two or more detectors could be applied simultaneously to the sample and correlations in the outputs of the detectors could be examined to improve the signal to noise ratio. For example, suppose two detectors at different locations are employed. Let the voltage output of the detectors be $v_1(t)$ and $v_2(t)$, respectively. The normal observation is of $v_1^2(t)$, and blips at more or less random times are expected. One could also observe $v_2^2(t)$, and $v_1(t)v_2(t+\tau)$, where τ is an arbitrary time delay introduced by the detector circuitry. Now a signal will consist of a blip at time t in v_1^2 , at, say $t+\tau$ in v_2^2 and also at t and $t+\tau$ in the cross product. $\langle v_1(t)v_2(t+\tau) \rangle$ will contain less noise than $\langle v_1^2(t) \rangle$ or $\langle v_2^2(t) \rangle$ because of the relative

independence of the noise signals from different detectors at displaced time. Identification of τ also gives information on the position of the source of the signal. Cross correlation in the signals from three detectors narrows the possible locations to a line and from four narrows it to a point (or a small number of points). There will actually be further cross correlations with waves of different polarization and with echoes which have been ignored in this discussion, and which will have to be sorted out.

2. Wadley's talk also provoked the thought that, in the case of insulators there might be observable electromagnetic emission in addition to acoustic emission from dynamic defects. If abruptly opening crack separates electric charge some EM emission must occur (peel a strip of scotch tape from its reel in a dark room and you can see the effect). Rudimentary examination indicates that in the most obvious models (charge moving with the material) electromagnetic energy radiated will be smaller than acoustic energy radiated by several orders of magnitude, but the models employed may not be adequate. I believe there is need for theoretical treatment of the problem in more depth, and possibly for some experiments. The charge separated in the opening of a crack will tend to recombine in small discharges of some kind. These will be rapid compared with the speeds of movement of gross material, and that would make the EM radiation much larger than allowed for in the model I have treated. Also in the special case of ferroelectric substances

the effects might be enhanced, although these are not common materials of concern for NDE. Comparison with work done years ago on radiation from charged dislocations in alkali halides might also be fruitful.

3. J. C. Murphy discussed photothermal imaging for materials characterization. Here the interruption of heat flow from a sudden temperature pulse by small cracks, grain boundaries, etc., in and near the surface was seen and used as an indicator of such para-surface discontinuities. I would point out that microwave radiation falling on a metal surface induces electric currents parallel to the surface in a shallow layer determined by the "skin depth", δ . (For example, for copper at 3 cm wavelength $\delta = 7 \times 10^{-5}$ cm; δ varies inversely as the square root of the frequency of the radiation and directly as the square root of the resistivity of the material.) Discontinuities that impede heat currents will also impede electric currents and this pile up of charge will produce scattered EM radiation at a distance as well as local electric and magnetic fields around the discontinuities, both of which, in principal, are observable. This suggestion has some of the features of the old magnaflux crack detection system, although the scale of structures would be much finer. In that system cracks were made visible by painting a magnetic powder on the surface.

A second thought growing out of this one is that the heating of the surface by microwaves can be considerable, and discontinuities on the scale of the skin depth will make the

heating non-uniform. This should be readily observable with infrared viewers now available. One could construct an infrared microscope to allow very fine structures to be seen. The heating would instead be caused by acoustic waves, even low frequency flexing of a part. Defects, grain boundaries, etc., would be expected to produce local concentrations of heat through local acoustic dissipation.

4. Another physical effect which has not been utilized, to my knowledge, to reveal surface characteristics in the "patch effect", that is the variation of the work function of a metallic surface with crystalline orientation and varying chemical constitution of the surface. It would seem that low energy electron microscopy would be the easiest way to observe this. The effect can produce electric potentials near the surface which vary by a volt or so over distances of a grain diameter.

ACKNOWLEDGEMENT

This paper was written under the auspices of the DARPA Materials Research Council, Contract #MDA903-82-C-0428 with The University of Michigan.

NONLINEAR OPTICAL MATERIALS FOR LASER PROTECTION

A. Macleod, L. E. Cross, A. Yariv and C. M. Stickley

INTRODUCTION

Approximately 40 experts drawn from industry, universities, and the services met with several members of the Materials Research Council in a Workshop to discuss techniques and materials which could be used to protect optical systems against damage or blinding by laser radiation. A listing of the participants is given in Appendix A and the topics presented in reviewing the nature of the laser threat and some current responses appear in Appendix B.

The primary goal of the workshop was to identify and define approaches to the diverse problems which DARPA should pursue which are associated with protecting high gain optical systems operating in the wavelength range from 0.4 to 14 μm against damage or saturation by irradiation from in-band laser frequencies.

Approximately half of the proceedings were classified as secret and classified aspects of the meeting will not be discussed here. In terms of classification, generic approaches to laser hardening are unclassified; specific approaches in a general area are classified as confidential and specific approaches for specific systems are classified as secret. Public release of any information on the topic is prohibited. We therefore refrain from discussing possible solutions to the problem in any but the most general terms.

It is now clear that laser irradiation poses a real threat for virtually all optical systems including the human eye. This threat is extremely complex because of its great variability and its exceptionally rapid development. There is no standard threat in terms of wavelength, pulse length, repetition frequency or power density all of which may vary from event to event or even during the same event. Combinations of threats may exist together.

If we define the hardening requirement as:

Threat capability/Susceptibility level

then current calculations for hardening requirements show variations of 5 to 10 orders of magnitude.

The characteristics and requirements of the optical system in question are as important as the characteristics of the threat in determining the level and nature of the protection which is required. Of greatest importance is whether or not the optical system must continue to operate during and in spite of the laser irradiation or whether it has simply to be protected from damage. And then there is the classification of a threat to the system as either "in-band" or "out-of-band". In-band irradiation is one with wavelengths within the operating spectral band of the optical system. Such irradiation can, and may often be intended to jam the operation of the system even if it fails to destroy it. The irradiation must be reduced to safe levels or eliminated with as little impairment to the operation of the optical system as possible, and only rarely is it sufficient

simply to block incident light from the system during the threat. Out-of-band irradiation, however, does not coincide with an operating spectral region of the optical system and can be eliminated by ensuring that the transmittance of the optical system to that particular wavelength is sufficiently low. In what follows we shall be concerned principally with in-band radiation.

A complication which frequently exists is that protection systems must be fitted to already existing optical systems. This implies that there are constraints on the shape, size and configuration of the hardening devices and that the losses introduced by their insertion into the system must be minimized.

CURRENT CONCEPTS FOR PROTECTING OPTICAL SYSTEMS

Present and proposed device structures may be divided into two broad general categories, i.e., techniques which seek to use spectral filtering of the whole field of view and techniques which attempt spatial filtering of all wavelengths from specific spatial locations in the focal plane.

Spectral Filters

Fixed frequency filters

A promising type of fixed rejection filter is the rugate filter, which is an interference filter in which there is a cyclic variation of refractive index, rather than discrete layers, giving a characteristic displaying narrow reflectance bands.

Practical realization of the theoretical filter concepts are being attempted both for visible and IR systems using films in the SiO_xN_y , Si-Ge, and AlAs-GaAs systems.

With the developing agility of laser systems it is probable that fixed frequency filters will offer only a first generation of protection, however, the technology involved in this phase may also be of major use in helping to extend the utility and dynamic range of other possible protection mechanisms.

Active tuneable filters

Tuned Fabry-Perot systems have been demonstrated for visible light, agility being provided by piezoelectric tuning of the plate separation, or by electro-optic tuning of the index medium in the cavity.

The piezoelectric system offers a large stable operation, but is very slow, being intrinsically limited by the mechanical resonances of the device. The electro-optical system is much faster (probably 1 μsec or less) but is presently of very limited operation due to the high half-wave voltage in available electro-optic crystals.

A much more sophisticated EO analogue of the Harris acousto-optic filter was also discussed. This multilayer structure in AgGaS_2 provides the possibility for agile pass band shaping, etc.

One working piezoelectrically tuned active filter was in fact demonstrated at the meeting.

Spatial Filters

Optical Switches

Laser-induced plasmas reflect strongly and may be used as reflecting switches. Total internal reflection between a linear and a nonlinear medium may be induced or cancelled by the refractive index changes accompanying high power incident light. A liquid film between two surfaces at oblique incidence may be made to vaporize and cause total internal reflection when power levels are high. A particularly promising type of material is one which exhibits a phase change in the solid. Vanadium dioxide is such a material with a phase change from semiconducting to metallic in the infrared as its temperature rises through 62°C. This material can be built into a thin-film system exhibiting high transmittance for powers below the switch point and high reflectance for powers above. Although the transition is triggered thermally, fast switch times can be achieved. The main delay consists of the time to pump the necessary latent heat associated with the change into the material. Much work has been done to explore sputter deposition techniques for large area films. A major shortcoming of the present films is the very limited dynamic range between transmitting and reflecting conditions. Attempts are being made to extend this range by optical matching techniques and by cascading film switches.

Other phase change systems which are being explored for optical switches include $\text{Ti}_2\text{SeAs}_2\text{Te}_3$ glass, CVD SmS, SmSe and

SmTe metal: TCNQ systems and ferroelectric:paraelectric switching in BaTiO₃ films.

Optical Limiters

Optical limiters normally rely for their operation on some nonlinear behavior of an optical material. The most straightforward arrangement involves self-focusing of a beam which upsets the operation of a train of lenses focusing the output of the system on a detector of small aperture. This limits the energy actually falling on the detector. Such a device must be used at a focal plane of the optical system and since a fraction of the rejected energy reaches the plane of the detector although outside the aperture, it is difficult to image more than one picture element at a time.

Limiting by laser-induced self focusing has been demonstrated in CS₂ for $\lambda = 1.06 \mu\text{m}$ using 40 ps pulses at power levels ~25 KWatt peak. The limiting point in the power curve can be controlled by dilution with ethanol, and modified power levels are also available in the strong Kerr effect liquids like nitrobenzene. Laser-induced self-focusing has been observed at much longer pulse lengths also.

Longitudinal inhomogeneous travelling waves produced by oblique incidence of a homogeneous wave at an interface between a linear and a nonlinear medium show a self-limiting of transmitted power, the level at which the limiting action occurs falling with increasing angle of incidence. Self-limiting can also be achieved by nonlinear nonresonant absorption (caused by pair excitation processes).

Saturation at molecular vibration levels, self limiting in stimulated Brillouin and Raman scattering both in bulk and fiber systems are other possibilities.

NOVEL IDEAS

A number of novel ideas were discussed at the meeting, including variants of the above, the possibility of throw-away elements for protection which would simply fail at a particular radiation level, the use of photorefractive materials in the form of optical fibers and the use of fibers in general which could take advantage of the advances in producing single crystal fibers at Stanford. The incorporation of a low concentration of molecules having vibrational resonances at the wavelength of interest into an isolating matrix so that a saturation occurs, enhanced by geometrical resonances, could make a device possible which switches from absorbing to transmitting at a particular power level. A Raman-scattering cell using liquid nitrogen was proposed in which complete conversion could be obtained between exciting and scattered light before the cell saturated. For higher power levels the scattered light would then remain constant. For fixed wavelength threats, the use of material with appropriate absorption lines was suggested and some evidence presented indicating that searches for suitable materials might not be too difficult. Then there is the possible use of conducting smokes for field enhancement leading to breakdown at appropriate power levels in power limiting cells.

Metallic meshes of various types are used as filter elements in the far infrared, usually beyond 50 μm . A particularly interesting idea proposed at the meeting was the use of these meshes, either alone or in conjunction with phase-transition materials², as saturable switches in the shorter wavelength regions. Cruciform meshes with phase-transition materials bridging the gaps appear qualitatively to have promise, although metallic properties are rather less suitable in the middle infrared and may cause difficulties.

DISCUSSION

It is clear that a universal solution to laser hardening does not exist, and in fact by the very nature of the problem, cannot exist. On the other hand it is possible to do research which will be useful in a generic sense. For example, a focal-plane switch which changes from transmitting to reflecting in those areas where either the intensity or the incident power exceeds prescribed limits would be very useful. Such a switch, or any device developed to do this job, should have broad absorption bands to make it useful against wavelength-agile lasers. Laser development is extremely rapid and successful providing the attacker with a major advantage in that he can choose the nature of the threat. This implies the necessity for a continuing evolution of threat-defeating devices to counter the ever increasing threats. Ideally these devices should be of a thin film form for easy insertion into systems, and possess broad absorption bands. A second approach should include non-thin film

devices, e.g., fibers, or the use of bulk media to defocus or deflect the beam.

An important point which emerged from the meeting is that the field is certainly not limited in terms of concepts but that there is a serious lack of suitable materials. Many speakers pointed to the fact that information on the properties of materials, especially their non-linear ones, is frequently either lacking completely or ambiguous and incomplete. Workers must often rely on measurements made abroad, particularly in iron-curtain countries. There is an accompanying lack of materials preparation facilities which makes it difficult to obtain high quality samples of materials once they have been identified. Several factors contribute to this situation. Work in the preparation and measurement of materials requires a long-term commitment and a dedication. Results are often slow in coming and frequently lack the spectacular quality of data associated with the development of a new device concept. Measurement equipment and facilities are expensive and support for such facilities is not generally available. It is significant that the meeting was told that the best lithium niobate being grown at the present time is in the Peoples' Republic of China. Japan is far ahead of us in the growing of ferroelectrics. It is clear that a positive effort to encourage materials research in the United States is required.

The design of responses to laser threats tends to flow from the knowledge of material properties rather than the

reverse. Thus the continuing evolution of hardening systems that we see as necessary, can only be continuously successful if it is matched by a corresponding effort in materials. Greatest progress tends to be made when materials and device people work together and ways to encourage this type of cooperation should be found.

RECOMMENDATIONS

Phase transition materials in thin-film form offer a most promising approach for the construction of focal-plane limiters. Unfortunately a good thermally switchable material for use in the visible spectral region is not presently known. It is suggested that a strong effort be made to identify materials that would be useful in this wavelength region and to produce them in suitable thin-film form.

Current research efforts in laser protection are strongly focused upon bulk and thin film optical materials. It is recommended that consideration be given to the possible development of optical fiber filters and limiters. Possible options could include: single-mode optical fibers with composition or dimensional modulation for high efficiency rugate filters; photo-refractive fibers which could act as self tuning agile rugate filters; and fibers with core materials exhibiting a negative index change under increased power levels which could provide power limiting through loss of the guide function.

Metal mesh filters are a well established technology for microwave and millimeter wave frequencies. Using modern

lithography techniques, dimensions appropriate for longer wavelength infrared operation are certainly possible. If such filters can be made to operate efficiently they will offer a powerful method to enhance and control field and power levels in current and future optical switches. Work to explore and extend the frequency range for such mesh filters should be supported.

ACKNOWLEDGEMENT

This paper was written under the auspices of the DARPA Materials Research Council, Contract #MDA903-82-C-0428 with The University of Michigan.

REFERENCES

1. G. H. Vineyard, A Proposed Breakdown Switch for Laser Protection. Proc. DARPA Materials Research Council, Summer 1982.
2. D. Eden, Advanced Technology Center, Vought Corporation.

APPENDIX A.

NON-LINEAR OPTICS

July 22-23-24

E. J. Friebele	DARPA/MSO	202-694-1346
A. Yariv	MRC/Caltech	213-356-4821
M. Stickley	MRC/BDM	703-827-2559
A. L. Gentile	Hughes Res. Labs	213-456-6411
J. F. Lotspeich	" " "	" "
Rich Potember	Johns Hopkins APL	301-792-7800
J. Len Gibbs	Army Missile Lab.	205-876-2055
J. C. Fraser	DARPA/STO	202-694-1569
C. M. Wiggins	BDM/ALBO	505-848-5523
W. R. Woody	AFWAL/MLPJ	513-255-6671
C. M. Phillippi	"	513-255-2334
N. Ogle	Lockheed	415-493-4411
A. Title	"	" "
John Tracy	Rockwell Science Center	805-498-4545
Jar-Mo Chen	Martin Marietta Labs	301-247-0700
M. J. Soileau	N. Texas State U.	817-788-2626
S. C. Seitel	U.S. Naval WPNS CTR	714-939-3049
J. A. Detrio	U of Dayton	513-229-3527
R. R. Neurgaonkar	Rockwell/MRDC	805-498-4545
Narayan P. Murarka	IIT Research Institute	312-567-4543
G. H. Vineyard	BNL/MRC	516-282-3335
L. E. Cross	MRC/PSU	814-865-1181
J. M. O'Hare	U of Dayton	513-229-2331
M. Sparks	Scientific Research Center	213-271-5270
Harry V. Winsor	AFOSR/NE	202-767-4931
Robert L. Byer	Stanford	415-497-0226
Dayton D. Eden	Vought Corp.	214-266-5112
Wm. R. Graver	Riverside Research Inst.	703-522-2310
William W. Durand	Honeywell, Inc.	612-378-4785
Darryl L. Smith	" "	612-378-5580
Ed Cullender	Army NVEOL	703-664-5780
Howard Lowdermilk	LLNL	415-422-5498
A. J. Sievers	Cornell U	607-256-6422
B. Bendow	MRC/BDM Corp.	505-848-5567
H. A. Macleod	U of Ariz	602-626-3025
N. A. Diakides	US Army NVEOL	703-664-5847
S. Grant	BDM	203-827-7565
C. L. Tang	Cornell	607-256-8920
A. F. Garito	U of Penn.	215-898-5810
B. O. Seraphin	U of Ariz.	602-626-2263

APPENDIX B.

NONLINEAR OPTICAL MATERIALS FOR LASER PROTECTION
July 21-23, 1982

Organizers: E. J. Friebele, M. Stickley, and B. Seraphin

July 21, 1982

I. Problem Definition and Program Overview (SECRET)

Welcome and Opening Remarks - E. J. Friebele, DARPA

Tactical Threat Definition (NOFORN) - W. Woody, AFWAL

Strategic Threat and DARPA Programs - W. R. Graver,
Riverside Research (NOFORN)

Army Requirements (NOFORN) - N. Diakides, & E. Callender,
NV & EOL

AF Concepts and Materials Needs - C. Phillipe, AFWAL

Navy Requirements and Programs - E. J. Friebele, NRL

Hardening Requirements Analysis - C. Wiggins, BDM

Thin Film Requirements and Countermeasure Requirements -
D. Eden, Vought

July 22, 1982

II. Existing and Promising Materials and Concepts I (SECRET)

Tunable Rejection Filter Concepts - A. Title, Lockheed

Nonlinear Optical Materials and Laser Hardening Concepts -
M. O'Hare, U. Dayton

Narrowband Rugate and Wavelength Agile Filters - N. Muraka,
IITRI

Tunable Narrow Band Filters - J. Tracy, Rockwell

Optical Self-Action in Prevention of Laser Damage -
M. J. Soileau, N. Texas State U; S. Seitel, NWC

Nonlinear Materials for Laser Countermeasures - W. W.
Durand and D. L. Smith - Honeywell

Vanadium Dioxide Switches - W. Case, Vought

Discussion

SCRIPPS ELEMENTARY SCHOOL

July 22, 1982

III. Existing and Promising Materials and Concepts II
(UNCLASSIFIED)

Electronically Agile IR Filters Research - J. Lotspeich
and A. Gentile, Hughes

Optical Phase Transitions in Organic Semiconductors -
R. Potember, Johns Hopkins APL

Chalcogenide Materials - B. Seraphin, U. Arizona

Chalcogenide Switch - J. Chen, Martin Marietta

Nonlinear Optical Polymers - A. Garito, U. Pennsylvania

July 23, 1982

IV. Physical Phenomena Opportunities and Limitations; New and
Promising Materials and Concepts (UNCLASSIFIED)

Problem Overview and Materials Requirement Summary -
W. Woody, AFWAL

Short Presentations and Round Table Discussion -
B. Seraphin, U. Arizona

R. Byer, Stanford

J. Detrio, UDRI

D. Eden, Vought

H. Lowdermilk, LLNL

A. MacLeod, U. Ariz.

R. Hellwarth, USC

D. Mills, UC-Irvine

A. Sievers, Cornell

M. Sparks, SRC

A. Yariv, Cal Tech

C. Tang, Cornell

H. Winsor, AFOSR/NE

Discussion, Continued.

A PROPOSED BREAKDOWN SWITCH FOR LASER PROTECTION

G. H. Vineyard

A class of laser protection devices is based on the avalanche breakdown in a gas or other medium induced by the electric field of the incident radiation (a radiant power density of 1 MW/cm^2 means an r.f. electric field amplitude of about 30,000 volts/cm). Breakdown produces a conducting plasma which can reflect a large fraction of the incident power, and recovery can be relatively fast when the power is turned off. The TR box in a radar set operates on the same principle in the microwave realm.

For many systems of interest, the breakdown threshold for a switch of this kind may be unacceptably high, even when the switch is placed at a focal point of an optical system. There are means of reducing the breakdown threshold, however, and in the following, a scheme for doing this is proposed. To the best of my knowledge this approach has not been discussed before. It appears that it would work in the wavelength range longer than 2 or 3 microns (whether it could be taken to shorter wavelengths is not clear) and it would offer broad-band protection from a few microns up.

Consider a medium in which we wish to induce avalanche breakdown by an electromagnetic wave. Disposition of small particles of metallic or high dielectric constant material in the medium will concentrate the field at the particles and re-

duce the breakdown threshold by some amount. If the particles have sharp points the reduction should be still greater. The localization of the regions of enhanced field may tend to prevent the large scale breakdown desired. A more systematic and more powerful field enhancement can be achieved by the concept presented below.

So-called metallic mesh filters for the infrared have been known for quite a few years¹. One form of filter consists of a periodic lattice of small squares of metal deposited on an insulating substrate (see Fig. 1). Let the lattice spacing of the squares be g , the width of the gaps be b , and assume that the squares are thin compared with the wavelength, λ , of the radiation. Also assume, for the moment, that the metal is perfectly conducting. Then this array will be transparent, at normal incidence, for $\lambda > fg$, when f is a factor less than, but of the order of magnitude of unity (For oblique incidence high transmission requires $\lambda > 2g$). Also, by symmetry, the transmissivity of the array is the same in all polarizations. There is a concentration of electric field in the gaps between the squares. If E_0 is the incident field (now considered parallel to a square edge), the field in the gap will be

$$E \approx \frac{g}{b} E_0$$

(To demonstrate this formula consider the squares replaced by long parallel strips of spacing g (center to center) and \rightarrow sepa-

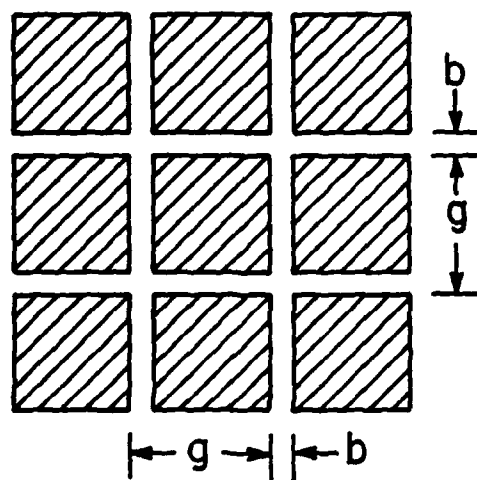


Figure 1.

ration b , with axes perpendicular to E . Assume that $\lambda \gg g$. There is now an equivalent electrostatic problem in which the above expression for E becomes exact. Cutting channels transverse to the strips and reducing λ perturbs the problem only modestly, hence the above result).

Taking $E = \frac{g}{b} E_0$ it is apparent that large enhancements of the field will occur in all the transverse gaps. The dielectric medium adjacent to the array will now break down at a power density lower by a factor $(\frac{b}{g})^2$ than the breakdown power in the absence of the array. There appears to be no reason why b/g could not be as small as $1/10$, and quite possibly it could be made much smaller yet. Thus a large reduction in the power threshold for breakdown could be obtained. Upon breakdown, the array would become almost perfectly reflecting.

There is an implausibility in the assertion that, without breakdown the array is nearly transparent even though $b/g \ll 1$. The resolution of the paradox can be seen by applying Huygen's principal to calculate the field beyond the array in terms of the field at the array. The fields in the gaps are contributing in phase to the far field, and the amplitude on the average is the same with and without the array. Therefore the far field is the same. The array would be transparent for any positive gap width until the width became comparable with the thickness of the squares (that is, the dimension perpendicular to the plane of the array.)

The array of squares has been presented because the principles of operation are most easily understood in this example, but many other shapes could be considered and squares probably do not give the optimal pattern. Diamonds, crosses, squares with rough edges, etc., should all be considered. In particular, crosses (see Fig. 2) would have some advantages.

The discussion up until now has assumed that the mesh is made of perfect conductor. For real metals the conductivity and related optical properties will be less than ideal. The noble metals (Cu, Ag, and Au) all have reflectivities above 95% in the band $1\mu < \lambda < 12\mu$, and for Cu and Ag the reflectivity is above 98%. The skin depth (for power) for each of these metals is about $.03\mu$ at $\lambda = 1\mu$, going down to $.02\mu$ at $\lambda = 10\mu$. Above 10μ the metallic character is even better. Without going into an involved analysis, it is plausible that the very high reflectivity for a surface and the very low skin depth means that a real array would function substantially as outlined above. Experimental evidence is available in the literature¹ for wavelengths above 50μ .

The breakdown medium could be a gas, a dielectric liquid, or even a solid. Surface breakdown on the solid substrate when interfaced with a vacuum would also occur at a field strength which would probably be strongly dependent on the exact nature of the surface.

Many questions remain to be answered: How quickly can the breakdown occur? (Because of the small distances involved

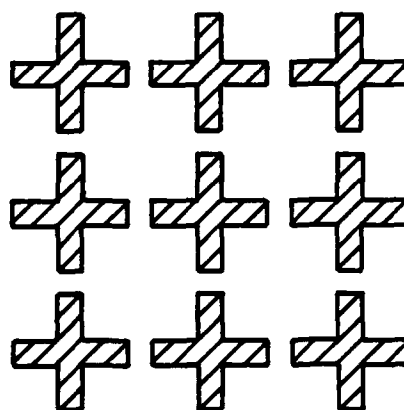


Figure 2.

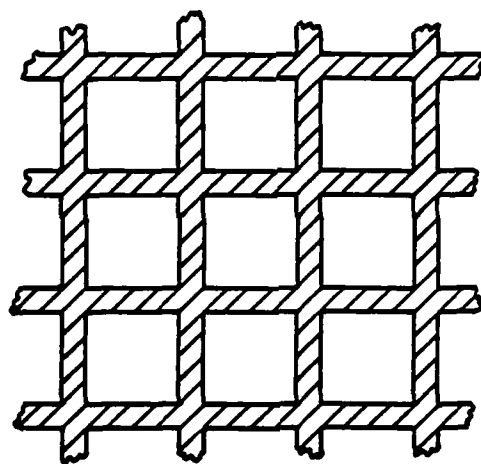
it should be fast). How quickly will the discharge be quenched when the exciting field is turned off? Can the device recover without damage, or how many times can it function before being damaged? How can it best be fabricated and how small can b and g be made in practice? Are there ways to enhance the breakdown (surface treatments; provision of further asperities; biasing fields; preionization of the medium, etc.). Finally, what would the insertion loss actually be, and how complete is the reflection after breakdown of the array?

A companion device can also be mentioned. A mesh of the form of Fig. 3 is nearly perfectly reflecting for $\lambda > g$, becoming perfectly reflecting for all $\lambda \gg g$. This so-called inductive mesh carries a current in the legs parallel to E . Inserting sections of material in each leg which can limit the current would cause the reflectivity to become small at currents above the limiting level. In the extreme form, thinner sections in each leg would be vaporized at a threshold power, after which the reflectivity would be very small. This then is a fuse. It suffers from the drawback of not being reusable, of course.

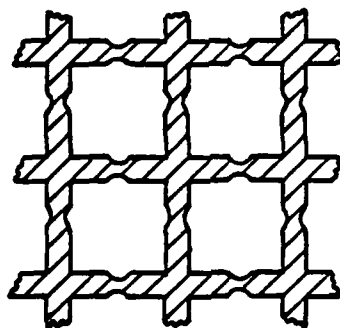
It appears to the writer that the concepts of protective devices outlined here warrant further examination.

ACKNOWLEDGEMENT

This paper was written under the auspices of the DARPA Materials Research Council, Contract #MDA903-82-C-0428 with The University of Michigan.



Inductive Mesh (Reflecting)



Fuse Based on Inductive Mesh

Figure 3.

REFERENCES

1. R. Ulrich, "Interference Filters for the Far Infrared." Applied Optics 7, 1087 (1968).

K. D. Moller and W. G. Rothschild, Far-Infrared Spectroscopy. Wiley-Interscience, New York (1971).
Sec. 3.B.

Driscoll and Vaughn, Handbook of Optics, Secs. 8.104-8.107.

THE FUNDAMENTAL LIMITS
ON THE SPECTRAL PURITY OF LASER FIELDS

A. Yariv

ABSTRACT

The quantum mechanical limits to the spectral purity of the laser output are considered using a simple model.

I. The Phase Noise

An ideal monochromatic radiation field can be written as

$$\epsilon(t) = \text{Re} [E_0 e^{i(\omega_0 t + \theta)}] \quad (1)$$

where ω_0 the radian frequency and E_0 the field amplitude are constant. A real field including that of lasers undergoes random phase and amplitude fluctuations which can be represented by writing

$$\epsilon(t) = \text{Re} [E(t) e^{i[\omega_0 t + \theta(t)]}] \quad (2)$$

where $E(t)$ and $\theta(t)$ vary only "slightly" during one optical period.

There are many reasons in a practical laser for the random fluctuation in amplitude and phase. Most of these can be reduced in theory, to inconsequence by various improvements such as ultra stabilization of the laser cavity length and the near elimination of microphonic and temperature variations. There remains however a basic source of noise which is quantum mechanical in origin. This is due to spontaneous emission which con-

tinually causes new power to be added to the laser oscillation field. This new power, not being coherent in phase with the old power, causes phase as well as amplitude fluctuations. These are responsible, ultimately, for the deviation of the evolution of the laser field from that of an ideal monochromatic field, i.e., for the quantum mechanical noise.

Let us consider the effect of one spontaneous emission event on the electromagnetic field of a single oscillating laser mode. A field such as Eq. (1) can be represented by a phasor of length E_0 rotating with an angular (radian) rate ω_0 . In a frame rotating at ω_0 we would see a constant vector E_0 . Since $E_0^2 \propto \bar{n}$, the average number of quanta in the mode, we shall represent the laser field phasor before a spontaneous emission event by a phasor of length $\sqrt{\bar{n}}$ as in Fig. 1. The spontaneous emission adds one photon to the field and this is represented according to our convention, by an incremental vector of unity length. Since this field increment is not correlated in phase with the original field the angle ϕ is a random variable (i.e. it is distributed uniformly between zero and 2π). The resulting change $\Delta\theta$ of the field phase can be approximated for $\bar{n} \gg 1$ by

$$\Delta\theta_{\text{one emission}} = \frac{1}{\sqrt{\bar{n}}} \cos \phi \quad (3)$$

Next consider the effect of N spontaneous emissions on the phase of the laser field. The problem is one of random walk since ϕ may assume with equal probability any value between 0 and 2π .

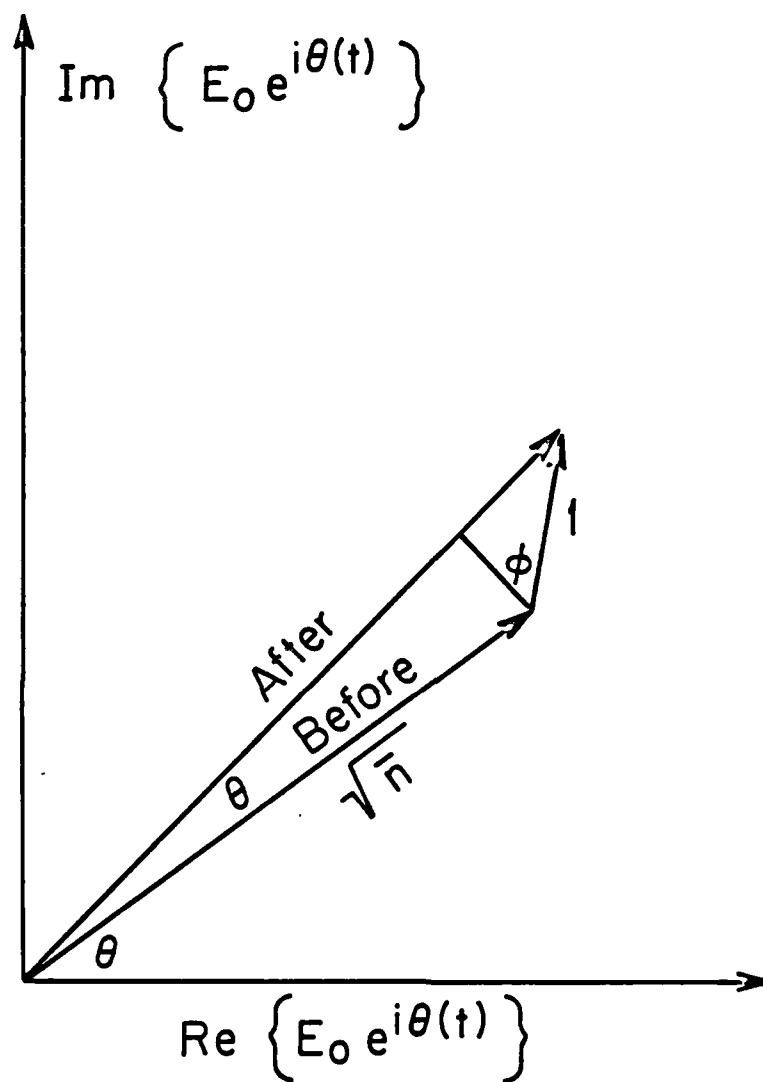


Figure 1. A phasor diagram showing the laser field complex amplitude before and after the spontaneous emission of a photon into the laser mode. The field phase changes by $\Delta\theta$.

We can then write

$$\langle [\Delta\theta(N)]^2 \rangle = \langle (\Delta\theta_{\text{one emission}})^2 \rangle N \quad (4)$$

and from (3)

$$\langle [\Delta\theta(N)]^2 \rangle = \frac{1}{n} \langle \cos^2 \phi \rangle N$$

where $\langle \rangle$ denotes an ensemble average, taken over a very large number of individual emission events.

Expression (4) is a statement of the fact that in a random walk problem the mean squared distance traversed after N steps is the square of the size of one step times N . The mean ensemble deviation $\langle \Delta\theta(N) \rangle$ after N spontaneous emissions is of course zero. Any one experiment, however, will yield a non-zero result. The mean squared deviation is thus non zero and is a measure of the phase fluctuation. To obtain the (rms) phase deviation in a time t we need to calculate the average number of spontaneous emission events $N(t)$ into a single laser mode in a time t .

The total number of spontaneous transitions per second into all modes is N_2/t_{spont} where N_2 is the total number of atoms in the upper laser level 2 and t_{spont} is the spontaneous lifetime of an atom in Eq. 2. The total number of transitions per second into one mode is thus

$$\frac{N_{\text{spont}}}{\text{sec-mode}} = \frac{N_2}{t_{\text{spont}} p} \quad (5)$$

where

$$p = \frac{8\pi\nu_0^2 \Delta\nu V n^3}{c^3} \quad (6)$$

is the number of modes interacting with the laser transition i.e., partaking in the spontaneous emission. V is the mode volume, $\Delta\nu$ the linewidth of the atomic transition responsible for the laser gain. We can rewrite (5) as

$$\frac{N_{\text{spont}}}{\text{sec-mode}} = \left(\frac{N_2}{\Delta N_t} \right) \frac{(\Delta N_t)}{t_{\text{spont}} p} \quad (7)$$

where ΔN_t is the population inversion $(N_2 - N_1 \frac{g_2}{g_1})$ at threshold. Next we use the result

$$\Delta N_t = \frac{p t_{\text{spont}}}{t_c}$$

where t_c is the photon lifetime in the resonator and obtain

$$\frac{N_{\text{spont}}}{\text{sec-mode}} = \frac{\mu}{t_c}, \quad \mu \equiv \frac{N_2}{\Delta N_t} \quad (8)$$

The number of spontaneous transitions into a single mode in a time t is thus

$$N(t) = \frac{\mu t}{t_c} \quad (9)$$

We recall here that in an ideal four-level laser $N_1=0$ and $\Delta N_t = N_2$, i.e., $\mu = 1$. In a three-level laser, on the other hand, μ can be appreciably larger than unity. In a ruby laser at room temperature, for example, $\mu \approx 50$. This reflects the fact that for a given gain the total excited population N_2 of a three-level laser must exceed that of a four-level laser by the factor μ since gain is proportional to $N_2 - N_1 \frac{g_2}{g_1}$. Equation (8) is also equivalent to stating that above threshold there are always μ spontaneously emitted photons present in a laser mode.

Using Eq. (9) in (4) we obtain for the root mean square phase deviation after t seconds

$$\Delta\theta(t) \equiv <[\Delta\theta(t)]^2>^{1/2} = \sqrt{\frac{1}{2\bar{n}} \left(\frac{\mu t}{t_c}\right)} \quad (10)$$

The maximum time t available for such an experiment is the integration time T of our measuring apparatus so that

$$\Delta\theta(T) = \sqrt{\frac{1}{2\bar{n}} \left(\frac{\mu T}{t_c}\right)}$$

The rms frequency excursion caused by $\Delta\theta$ is

$$(\Delta\omega)_{\text{RMS}} = \frac{\Delta\theta(T)}{T} = \sqrt{\frac{\mu}{2\bar{n} t_c T}} \quad (11)$$

We can cast the last result in a more familiar form by using the relations

$$P_e = \frac{\bar{n}\hbar\omega_0}{t_c}, \quad B = \frac{1}{2T}$$

Here P_e the power emitted by the atoms (i.e., the sum of the useful power output plus any power lost by scattering and absorption) B is the bandwidth in Hz of the phase measuring apparatus. The result is

$$(\Delta\omega)_{\text{RMS}} = \sqrt{\frac{\mu\hbar\omega_0}{P_e t_c^2}} B \quad (12)$$

From the experimental point of view $\Delta\omega$ is the root mean square deviation of the reading of an instrument whose output is

the frequency $\omega(t) \equiv d\theta/dt$ of the laser field. We will leave it as an exercise to design an experiment that measures $\Delta\omega$.

Ring laser gyroscopes sense rotation by comparing the oscillation frequencies of two counter propagating modes in a rotating ring resonator. Their sensitivity, i.e., the smallest rotation rate which they can sense is thus limited by any uncertainty $\Delta\omega$ in the laser frequency. Experiments have indeed demonstrated a rotation measuring sensitivity approaching the quantum limit as given by Eq. (12).

A more rigorous analysis based on a Van der Pol model of a laser oscillator yields for the spectral density function of $\Delta\omega(t)$

$$W_{\Delta\omega}(\Omega) \cong \frac{\hbar\omega_0\mu}{2\pi t_c^2 P_e} \frac{g(\Omega + \omega_0)}{g(\omega_0)} \quad (13)$$

where $g(\omega)$ is the normalized laser gain profile. We also used the relation $r = (2t_c)^{-1}$.

If the detection system which measures $\Delta\omega$ has a bandwidth B (i.e., it integrates only to $T=(2B)^{-1}$ seconds), then the mean square frequency fluctuations that it will measure will be

$$\langle(\Delta\omega)^2\rangle = \int_0^{2\pi B} W_{\Delta\omega}(\Omega) d\Omega \approx 2\pi W_{\Delta\omega}(0) B \quad (14)$$

where in the last approximation we assumed that $2\pi B < \Delta\omega_{\text{gain}}$, i.e. B small compared to the width of the atomic transition responsible for the gain (in semiconductor lasers for example $\Delta\omega_{\text{gain}} \approx 2 \times 10^{13}$ while $B < 10^9$ so this condition is amply fulfilled).

Using the expression $W_{\Delta\omega}(0) = \frac{\hbar\omega_0\mu}{2\pi t_c^2 P_e}$ we have

$$\langle (\Delta\omega)^2 \rangle = \frac{\hbar\omega_0\mu B}{t_c^2 P_e}$$

or

$$(\Delta\omega)_{\text{RMS}} \equiv \langle (\Delta\omega)^2 \rangle^{1/2} = \sqrt{\frac{\hbar\omega_0\mu B}{t_c^2 P_e}} \quad (15)$$

which is the same as Eq. (12).

II. The Field Spectrum

Next we address the case where one measures directly the spectrum of the optical field

$$\epsilon(t) = \text{Re} \{ E(t) e^{i[\omega_0 t + \theta(t)]} \} \quad (16)$$

using, say, a scanning Fabry-Perot etalon. If the etalon has a sufficiently high spectral resolution, the measurement should yield the spectral density function $W_\epsilon(\omega)$ of the laser field. We will, consequently, proceed to obtain an expression for this quantity. We make use of the Wiener-Kintchine theorem according to which $W_\epsilon(\omega)$ is the Fourier. Integral transform of the field autocorrelation function $C_\epsilon(\tau)$

$$W_\epsilon(\omega) = \frac{1}{2\pi} \int_{-\infty}^{\infty} C_\epsilon(\tau) e^{-i\omega\tau} d\tau \quad (17)$$

$$C_\epsilon(\tau) \equiv \langle \epsilon(t) \epsilon(t+\tau) \rangle \quad (18)$$

where the symbol $\langle \rangle$ represents, as above, an ensemble average.

Using

$$\varepsilon(t) = \text{Re}\{E(t) e^{i[\omega_0 t + \theta(t)]}\} \quad (19)$$

we obtain

$$C_\varepsilon(\tau) = \frac{1}{4} \{E(t) e^{i[\omega_0 t + \theta(t)]} + E^*(t) e^{-i[\omega_0 t + \theta(t)]}\} \\ \times \{[E(t+\tau) e^{i[\omega_0(t+\tau) + \theta(t+\tau)]}] + E^*(t+\tau) e^{-i[\omega_0(t+\tau) + \theta(t+\tau)]}\} \quad (20)$$

Now, for example,

$$\langle E(t) E(t+\tau) e^{i[2\omega_0 t + \theta(t) + \theta(t+\tau)]} \rangle = 0$$

Since it corresponds to averaging a signal oscillating at twice the optical frequency over many periods. So if we keep only the slowly varying terms in $C_\varepsilon(\tau)$ we obtain

$$C_\varepsilon(\tau) = \frac{1}{4} \langle E(t) E^*(t+\tau) e^{i[-\omega_0 \tau + \theta(t) - \theta(t+\tau)]} \\ + E^*(t) E(t+\tau) e^{i[\omega_0 \tau - \theta(t) + \theta(t+\tau)]} \rangle \quad (21) \\ = (I(\tau) + I^*(\tau))$$

$$I(\tau) \equiv \langle E^*(t) E(t+\tau) e^{i[\Delta\theta(t, \tau) - \omega_0 \tau]} \rangle \\ \Delta\theta(t, \tau) \equiv \theta(t+\tau) - \theta(t) \quad (22)$$

The main contributions to the laser noise are due to fluctuations of the phase $\theta(t)$ and not the amplitude $E(t)$ since the amplitude fluctuations are kept negligibly small by gain saturation. Taking advantage of this fact we write $\langle E^*(t) E(t+\tau) \rangle = \langle E^2 \rangle \approx \text{constant}$ so that

$$\begin{aligned}
I(\tau) &= \langle E^2 \rangle e^{-i\omega_0 \tau} \langle e^{i\Delta\theta(t, \tau)} \rangle \\
&= \langle E^2 \rangle e^{-i\omega_0 \tau} \langle 1 + i\Delta\theta - \frac{\Delta\theta^2}{2} - i \frac{\Delta\theta^3}{3!} + \frac{\Delta\theta^4}{4!} + \dots \rangle
\end{aligned} \tag{23}$$

Using $\langle \Delta\theta^n \rangle = 0$ for n odd and assuming $\langle \Delta\theta^2(t, \tau) \rangle \ll 1$ we obtain

$$\langle e^{i\Delta\theta(t, \tau)} \rangle \approx 1 - \frac{\langle \Delta\theta^2(t, \tau) \rangle}{2} \tag{24}$$

Using our result (Eq. 10) $\langle \Delta\theta^2(t, \tau) \rangle = \frac{1}{2\bar{n}} \left(\frac{\mu\tau}{t_c} \right)$ in (24) yields

$$\langle e^{i\Delta\theta(t, \tau)} \rangle = e^{-\frac{\mu\tau}{4\bar{n}t_c}} \tag{25}$$

and from (20) and (23)

$$C_E(\tau) = \frac{1}{4} \langle E^2 \rangle e^{-\frac{\mu\tau}{4\bar{n}t_c}} (e^{i\omega_0 \tau} + e^{-i\omega_0 \tau}) \tag{26}$$

The spectral density function of the laser field $W_E(\omega)$ the quantity observed by a spectral analysis of the field, is given according to Eqs. (17) and (26) by

$$W_E(\omega) = \frac{\langle E^2 \rangle}{8\pi} \int_{-\infty}^{\infty} e^{-\frac{\mu\tau}{4\bar{n}t_c}} e^{-i\omega\tau} (e^{i\omega_0 \tau} + e^{-i\omega_0 \tau}) d\tau \tag{27}$$

$$\begin{aligned}
&= \frac{\langle E^2 \rangle}{8\pi} \frac{\left(\frac{1}{4\bar{n}t_c} \right)}{\left(\frac{\mu}{4\bar{n}t_c} \right)^2 + (\omega - \omega_0)^2} + \frac{\left(\frac{1}{4\bar{n}t_c} \right)}{\left(\frac{\mu}{4\bar{n}t_c} \right)^2 + (\omega + \omega_0)^2}
\end{aligned} \tag{28}$$

It is customary to define the spectral density function such that the "power" of the field in a given frequency interval is obtained by integrating $W_E(\omega)$ only over positive frequencies.

The total signal power is conserved by keeping only the first term on the right side of Eq. (28) and multiplying by two, so that

$$W_E(\omega) = \frac{\langle E^2 \rangle}{4\pi} \left[\frac{\frac{1}{4\bar{n}t_C}}{\left(\frac{\mu}{4\bar{n}t_C}\right)^2 + (\omega - \omega_0)^2} \right] \quad (29)$$

which corresponds to a Lorentzian shaped function centered on the nominal laser frequency ω_0 with a full width at half maximum of

$$(\Delta\omega)_{\text{laser}} = \frac{\mu}{2\bar{n}t_C} \quad (30)$$

Recalling that the total power emitted by the electrons is $P_e = \bar{n}\hbar\omega_0/t_C$ and defining the passive resonator line-width $\Delta\nu_{1/2} = (2\pi t_C)^{-1}$, we can rewrite (30) as

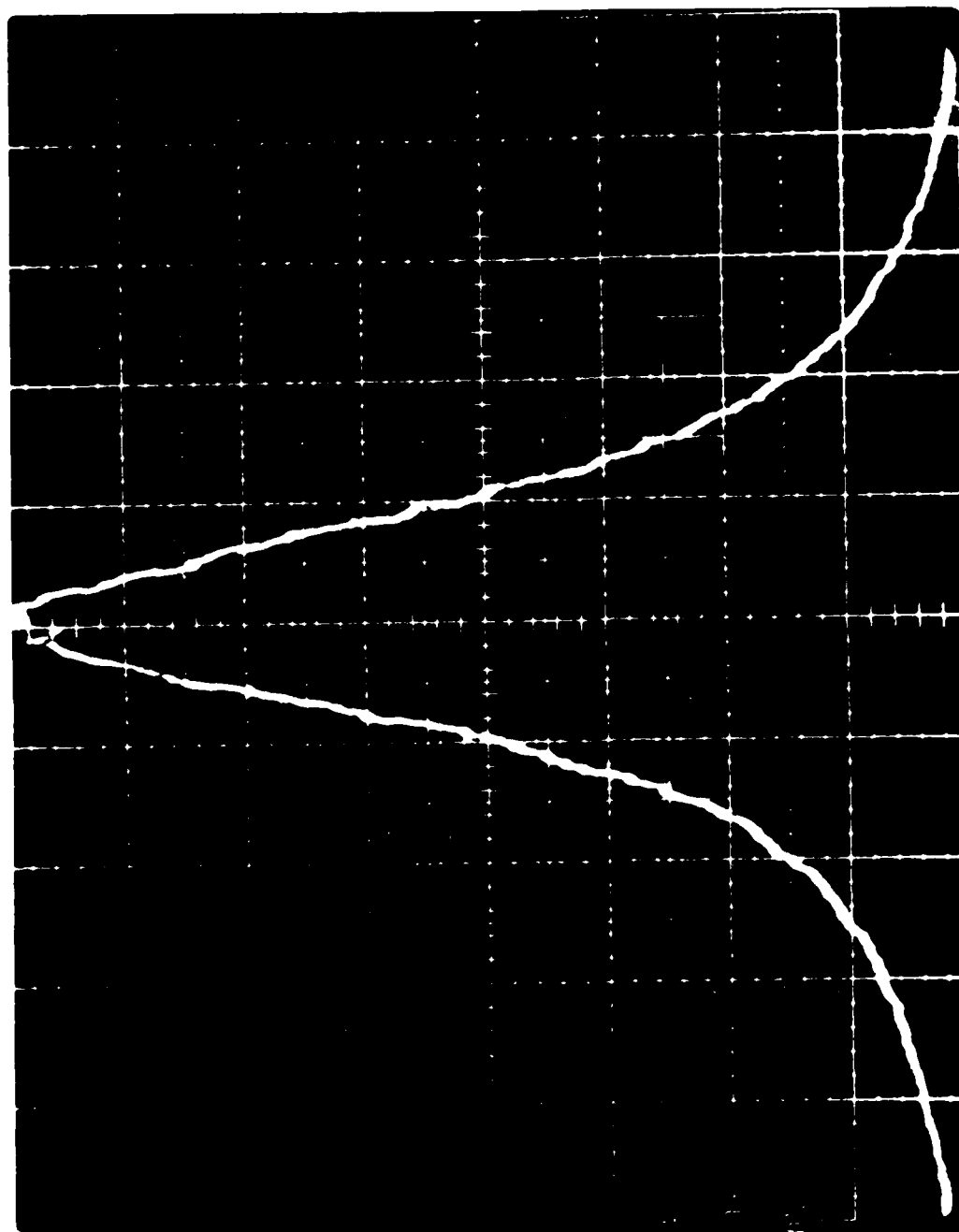
$$(\Delta\nu)_{\text{laser}} = \frac{(\Delta\omega)_{\text{laser}}}{2\pi} = \frac{2\pi\hbar\nu_0(\Delta\nu_{1/2})^2\mu}{P_e} \quad (31)$$

which is a convenient form, since the quantities appearing in it are obtainable by straightforward measurements or calculations.

An experimentally measured laser field spectrum $W_E(\omega)$ is shown in Fig. 2.

III. Comparison to Experiment

To obtain an order of magnitude estimate of the linewidth $(\Delta\nu)_{\text{laser}}$ predicted by Eq. (31), we will calculate it in the case of two largely different types of CW lasers: (1) a He-Ne laser; and (2) a semiconductor GaAs laser.



— 40MHZ

Figure 2. The observed Lorentzian lineshape of the laser field spectrum.

(1) He-Ne laser

$$\nu = 4.741 \times 10^{14} \text{ Hz } (\lambda = 6328 \text{ \AA})$$

$$l(\text{distance between reflectors}) = 100 \text{ cm}$$

$$\text{Loss} = (1-R) = 1\% \text{ per pass}$$

From these numbers we get

$$(\Delta\nu_{1/2}) = \frac{1}{2\pi t_c} = \frac{(1-R)c}{2\pi n l} \approx 5 \times 10^5$$

$$(\text{i.e., } t_c = 3.2 \times 10^{-7} \text{ s})$$

and from Eq. (31), assuming $\mu = 1$ (i.e., $N_1 \ll N_2$)

$$(\Delta\nu)_{\text{laser}} \approx 2 \times 10^{-3} \text{ Hz}$$

at a power level $P_e = 1 \text{ mw}$.

The predicted linewidth is thus so small as to be completely overwhelmed in almost all experimental situations by extraneous causes, such as vibrations and temperature fluctuations.

(2) Semiconductor laser

We use as a typical example, the case of a GaAs laser with the following pertinent characteristics

$$P_e = 3 \text{ mw}$$

$$\nu = 3.529 \times 10^{14} \text{ } (\lambda_0 = 0.85 \mu\text{m})$$

$$\Delta\nu_{1/2} = \frac{(1-R)c}{2\pi n l}$$

$$R(\text{reflectivity}) = 30\%$$

$$l = 300 \mu\text{m}$$

$$n = 3.5$$

$$\mu = 3 \text{ (at } T=300\text{K)}$$

This results in $\Delta\nu_{1/2} \sim 3 \times 10^{10}$

$$(i.e. t_c = \frac{1}{2\pi\Delta\nu_{1/2}} = 5 \times 10^{-12} s)$$

and

$$(\Delta\nu)_{laser} = 1.49 \times 10^6 \text{ Hz}$$

The experimental curve of Fig. 3 shows the predicted (Eq. 31) P_e^{-1} dependence of $(\Delta\nu)_{laser}$ but the measured values of the linewidth are larger by a factor of ~ 70 than those predicted by the analysis. This discrepancy has been considered by Henry¹, and by Vahala and Yariv². It was shown that the analysis leading to Eq. (31) ignores the modulation of the index of refraction of the laser medium which due to fluctuations of the electron density caused by spontaneous emission. When this effect is included the result is to multiply Eq. (31) by the factor

$$1 + \left(\frac{\Delta n'}{\Delta n''} \right)^2$$

where $\Delta n'$ and $\Delta n''$ are, respectively, are the changes in the real and imaginary parts of the index of refraction "seen" by the laser field due to some change in the electron density. The factor $1 + \left(\frac{\Delta n'}{\Delta n''} \right)^2$ can be calculated from measured parameters of the laser. Its value is ~ 70 in typical cases, enough to reconcile the observed data of Fig. 3 and the prediction of Eq. (31).

The big difference, over 9 orders of magnitude, between the limiting linewidth of conventional, say gas, lasers and semiconductor lasers is due mostly to the very short photon lifetime t_c in semiconductor laser resonators. At a given power

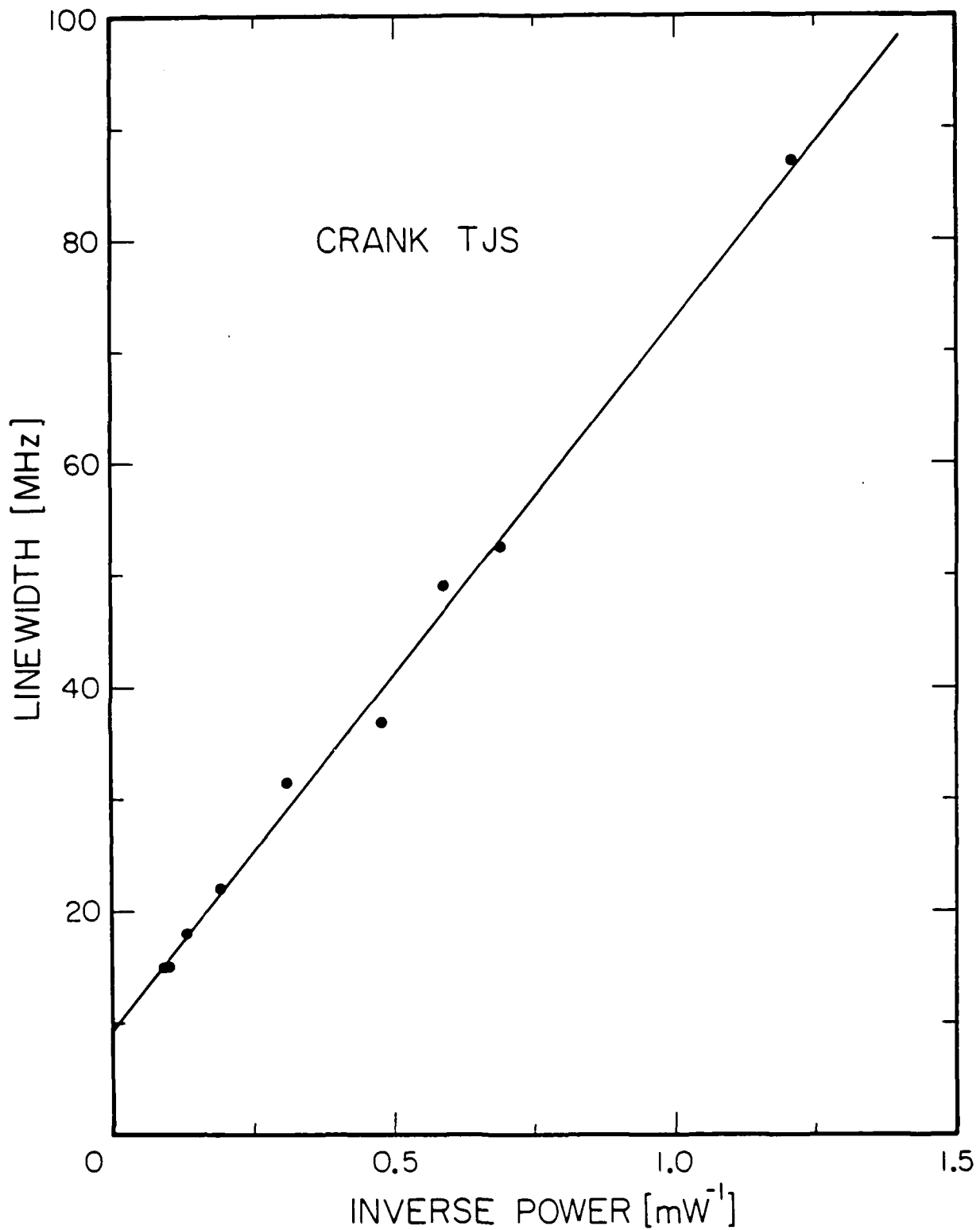


Figure 3. The experimentally observed laser field linewidth as a function of the power output in the case of a semiconductor GaAs laser.

output we have from Eq. (31) $(\Delta\nu)_{\text{laser}} \propto (\Delta\nu_{1/2})^2 \propto t_c^{-2}$. In the above examples, we obtained $t_c \approx 3 \times 10^{-8}$ s in the case of the He-Ne laser, and $t_c \approx 5 \times 10^{-12}$ s in the semiconductor laser. Since $t_c \sim \frac{\lambda n}{c(1-R)}$, the main hope of increasing t_c in a semiconductor laser, thus lowering the linewidth $(\Delta\nu)_{\text{laser}}$, is to increase λ by placing the laser in an external resonator (which requires antireflection coating on one of the laser facets) and by using high reflectance mirrors $R \sim 1$. Semiconductor laser linewidths in the KHz regime should be possible.

ACKNOWLEDGEMENT

This paper was written under the auspices of the DARPA Materials Research Council, Contract #MDA903-82-C-0428 with The University of Michigan.

PHOTOREFRACTIVE MATERIALS AND OPTICAL PROCESSING

A. Yariv, M. Stickley, E. Cross, & A. Macleod

INTRODUCTION

There is an increasing realization in DoD that optical processing (OP) techniques could play an important role in a variety of situations which require the processing of large amounts of data in short times.

A two-day meeting was held on July 19-20 to consider the problem of optical processing. An agenda of the meeting is enclosed herein. It brought together most of the active participants in this field including specialists in devices, crystal growth, system applications and nonlinear optics. The meeting was effective in identifying the most promising approaches and the critical problem areas where remedial attention is needed.

BACKGROUND MATERIAL

Optical Processing lacks the inherent agility and decision making flexibility which is inherent in electronic computers. There exist, however, many tasks to which it is naturally suited. Special operations which electronic computers perform serially are carried out by OP's in parallel--essentially instantaneously. One obvious example is the function of Fourier transformation of an image.

Intelligent use of optical processors in conjunction with electronic computers could in some cases greatly reduce the data handling capacity required of the latter, a capacity

estimated at 10^{10} - 10^{11} equivalent digital multiplications per second in the near future.

Some of the functions which can be performed with OP techniques include:

1. Optical Image Correlation and Convolution
2. Image Enhancement
3. Image Subtraction and Differentiation
4. Vector Matrix Multiplication
5. Distortion Correction in Optical Propagation
6. Dynamic Distortion Correction in Laser Resonators
7. Radar Pulse Processing including Spectral Excision and Spread Spectrum Techniques
8. Underwater Acoustic Communication
9. Processing of Seismic Data
10. Three Function Multiplication and Manipulation in Real or Fourier Space

The key building blocks for OP can be divided roughly into two categories:

A. Spatial Light Modulators (SLM)

These are the devices which convert an incoherent image to an equivalent spatial modulation on a coherent laser beam. This is done usually by converting the incoherent intensity pattern to an equivalent electric field pattern in a photosensitive medium which is also electrooptic (EO). The field then causes, via the EO effect, a spatial pattern of birefringence which is then used to (spatially) modulate an incident laser beam thereby

transferring the original incoherent image onto the coherent (laser) beam.

In certain projected designs of SLM's the image information can be impressed on the SLM electronically rather than by an incident incoherent image field.

B. Optical Processor (OP)

These are the devices which perform the nonlinear optical processing operations including the ones listed above. In most cases they require that the fields incident on the processor originate in spatial light modulators. They consist most often of large ($\sim 1 \text{ cm}^3$) photorefractive crystals which are capable of multiplying in real time three input optical fields.

An archetypal example, sketched in the figure, shows how an optical processor can be made to correlate an incident image $f(x)$ with an electronically stored image $g(x)$.

An electronically stored input field $g(x)$ is impressed via SLM 1 on the optical beam 1. An incoherent image $f(x)$ is converted by SLM 2 into a coherent beam 2. A lens $L1$ renders the Fourier transforms F and G of $f(x)$ and $g(x)$, respectively, in the focal plane inside the nonlinear crystal. A third plane, wave 3 of the same frequency as that of 1 and 2, is incident on the crystal from the right. The nonlinear crystal multiplies the Fourier transform fields F and G and that of the beam 3 to yield a field AGF^* which travels to the left. This field is Fourier transformed by $L1$ to yield an optical field proportional to the correlation g^*f in plane U .

The figure demonstrates the key buildup blocks which are needed eventually, in a practical optical processor.

These are:

1. Optically addressed SLM
2. Electronically addressed SLM
3. Nonlinear optical crystals for field multiplication
4. Detector arrays with attendant readout electronics

Some specialized applications can and will be performed before all the building blocks listed above become available. We believe, however, that the magnitude of the challenge, the number of technical problems which need to be solved and the sophisticated overall monitoring required are such that DARPA's involvement in launching a coordinated optical processing development effort is essential.

In what follows we will consider, one at a time, the main components listed above which are needed for the implementation of an OP. We will discuss briefly their present state of development, and proceed to make specific recommendations.

OPTICALLY ADDRESSED SPATIAL LIGHT MODULATORS

During the meeting, we heard descriptions of a number of operating devices including one based on microchannel electron multiplication due to C. Warde of M.I.T. (an early version of which was constructed by Hamamatsu of Japan), one Russian device, the PRIZ, based on the use of the photorefractive crystal BSO, and a US device, the PROM. Three other devices were proposed: a membrane-microchannel electron multiplier, a hybrid

device using silicon phototransistors and PLZT electrooptic plates, and a transverse E-field SLM concept.

One conclusion to emerge from the meeting is that the Russian work and their fundamental understanding of the utilization of the electrooptic effect in SLM's is ahead of ours (there are two or three sizeable groups pursuing this work in the USSR). Beyond the PROM, which has excellent promise if the electrooptic material BSO can be brought under control and improved, the nearest to a practical operating device in the US is that of C. Warde of M.I.T.

RECOMMENDATION

DARPA should support a two-thrust effort in this area: One to further develop SLM's with emphasis on devices whose feasibility has been demonstrated. It should also support a strong effort in photorefractive material growth and characterization with emphasis on properties important in SLM's. The crystal BSO used in the Russian PROM-like and PRIZ devices, and in a PROM device seems to be a leading candidate for SLM applications.

ELECTRONICALLY ADDRESSED SPATIAL LIGHT MODULATORS

These are SLM's where the input spatial information which is to be impressed as spatial modulation on a laser beam is fed into the SLM electronically--most likely by a two dimensional array of CCD devices or transistors. A difficulty with this approach is that if it is to be serially addressed and have

a 1 KHz frame rate, then the CCD's or transistors will have to operate at a 1 GHz data rate.

The only effort currently in progress and described at the MRC on electronically addressed SLM's is still in a very early stage. This effort is underway at Lincoln Laboratories, and was described by R. Kingston. A second approach was proposed by TRW; it might also be optically addressed.

RECOMMENDATION

One approach in this area should be supported. The need to integrate a very large number of ($\sim 10^6$) of electronic switching elements with an equal number of electrooptically controlled pixels make for an extremely difficult problem. It should only be undertaken by an organization which can muster all of the requisite technologies and theoretical understanding, preferably under one roof, or at least under a number of closely operating and interacting roofs.

NONLINEAR OPTICAL CRYSTALS

These are the crystals which, as illustrated in the figure, perform the nonlinear optical field image processing. The physical phenomenon which has proven most efficacious for this purpose is the photorefractive effect--i.e., the change in the index-of-refraction properties of the crystal due to incident light. The effect is present only in electrooptic (non-centrosymmetric) crystals and is due to either impurities or defects or both. The crystals with the best performance to date

are BSO and, especially, barium titanate (BaTiO_3) and strontium barium niobate (SBN), which are ferroelectric. In the last two mentioned crystals, the effect is very large compared to BSO but appreciably slower.

The amazing fact to emerge from the meeting is that in none of the above materials is the origin of the impurities responsible for the photorefractive effect known or understood. It is not even known which impurities are present in the crystals. All the experiments to date were performed on a "take what you get" basis.

RECOMMENDATION

Support a strong research and development effort in each of the three materials which have been used to date (BSO, SBN, BaTiO_3) since there is insufficient knowledge to favor any one of them at the moment. These research efforts should also allow for an examination of promising new coefficients. In each case the research should start with the growth of "base line" materials, i.e., materials which possess sufficient purity and perfection so that the effect of subsequent intentional doping and growth conditions on the photorefractive effect can be determined. It is mandatory that each such material growth will be undertaken by a team which includes the crystal growers, the experts on material analysis and characterization and the non-linear optical experts--all working in close coordination. The work should be carried out, preferably, in one organization or if absolutely necessary in two organizations working closely

together but where one organization has clear responsibility for the project.

DETECTOR ARRAYS AND READOUT ELECTRONICS

This is an important area which is pursued on its own by the imaging community. It is likely that the spectral regions of interest and performance characteristics for imaging and for SLM will not coincide so that some effort in this direction, especially to assess the applicability of available devices or present development efforts to SLM application, will be needed.

SUMMARY

Optical processing shows considerable promise in alleviating the present and future data handling requirements of many applications. There is, at present, no coherent program which will insure that all the critical issues are addressed in parallel so that none will slow down the progress of the field.

The single most important problem is the primitive state of control, characterization, and understanding of photorefractive materials which are the key element in both the spatial light modulators and the optical processors. Specific recommendation for addressing this problem are made above. The emphasis in the recommended research efforts is on coordination between crystal growth, characterization and the application efforts. In addition, development efforts in a small number of device configurations for spatial light modulation should be undertaken.

Conclusions and Recommendations

- I. Conclusion: Optical signal processor (OSP) have great promise for complementing digital devices and enabling achievement of exceptionally high multiplication rates for specific DoD applications involving vector matrix multiplication array correlation, etc., but major efforts are needed in wide band gap, oxide-type materials and in specific optical processing structures (devices) in order to realize this potential.

Four wave mixing promises to enable optical systems to be developed for real time holography, image processing and distortion correction but advancement in the same specific oxide-like crystals are needed as for optical signal processing.

Recommendation: DARPA should initiate a major effort in materials and devices for optical signal processing and for four-wave mixing applications.

- II. Conclusion: Materials improvements will occur most rapidly and economically if crystal growth, characterization in the desired application, and other characterization is all done iteratively under one roof with people dedicated to these tasks.

Recommendation: Future efforts in oxide-type materials growth, use, and other characterization should be done at one facility. Where this is not possible, structure the

program so that the lead facility does at least two of the above functions.

- III. Conclusion: Serious efforts to improve materials will not be fruitful until the material has been "cleaned-up" to a baseline level containing one part in 10^5 - 10^6 impurities.

Recommendation: Programs should be structured so the "baseline" quantity materials are produced before other types of characterization are done.

- IV. Conclusion: Several reasonably mature materials are of interest (BSO, BaTiO_3 , SBN, and related family members) and it is not possible a priori to select one over the other.

Recommendation: Support efforts on all three types of materials. One research institution could serve as the lead organization for more than one material thus reducing costs.

- V. Conclusion: Present materials characterization techniques are sufficiently sensitive and reproducible if research personnel are used who are dedicated to the job.

Recommendation: Beyond trying techniques (e.g., SIMS, etc,) developed for semiconductor technology, no special materials characterization techniques need development.

- VI. Conclusion: The OSP applications community needs SLMs for use as rapidly as possible. The oxide-type materials will be most important for PROM/PRIZ-type devices. Other near

term SLM devices should be developed through organizations which will make them for sale to others.

Recommendations: Support a major effort on the micro-channel SLM as being the best, nearest term non-PROM/PRIZ SLM which will come close to meeting the desired specifications of 10^6 pixels, 30 db dynamic range, 1KHz frame rate, one second or longer storage time, and less than 3% non-uniformity.

ACKNOWLEDGEMENT

This paper was written under the auspices of the DARPA Materials Research Council, Contract #MDA903-82-C-0428 with The University of Michigan.

NAVY LASER HARDENED ELECTROOPTIC COMPONENTS AND SENSORS

DETERMINED SUSCEPTIBILITY LEVELS AND DEVELOP HARDENING

APPROACHES FOR SENSORS AND COMPONENTS

1) FLIR'S - DETECTORS, COMPONENTS (WINDOWS, FILTERS),

OPTICAL TRAIN ELEMENTS

2) ELECTRONICS - LOWEST LEVEL SUSCEPTIBILITY

3) OPTICAL SWITCHES - CHALCOGENIDE

4) ION IMPLANTATION TECHNIQUES

NAVY HARDENING APPROACHES

INTRINSIC HARDENING

- * DEMONSTRATED HARDENED ELECTONICS FOR MISSILE SEEKER & FLIR
- * THERMALLY HARDENED HgCdTe DETECTOR DEVELOPED
- * SATURATION OF ABSORPTION IN DETECTOR MATERIAL AT HIGH INTENSITIES: SELF-LIMITING DETECTOR

EXTRINSIC HARDENING

- * OPTICAL SWITCH: CHALCOGENIDE $\text{Ti}_2\text{SeAs}_2\text{Te}_3$
- * LASER REJECTION FILTER
SINGLE LINE VS. FREQUENCY AGILE THREAT
BROAD BAND - TOO MUCH INSERTION LOSS

IR OPTICAL SWITCH APPROACH

REQUIREMENTS

- * LOW INSERTION LOSS - ABSORPTION, SCATTERING, MTF, ETC.
- * LOW SWITCHING THRESHOLD - TUNED TO SYSTEM
- * HIGH DYNAMIC RANGE
- * OPERATION IN RELEVANT SPECTRAL BANDS

CANDIDATES

- * OPTICALLY ACTIVATED SWITCH, E.G. VO_2 , CHALCOGENIDE

THRESHOLDS CLOSE TO COMPONENT DAMAGE
SECONDARY FOCAL PLANE MAY BE REQUIRED

- * ELECTRICALLY ACTIVATED SWITCH

POTENTIAL OPERATION AT LOW LEVELS NOT YET
SUCCESSFULLY DEMONSTRATED

MEETING ON
PHOTOREFRACTIVE MATERIALS AND SPATIAL LIGHT MODULATORS
FOR OPTICAL PROCESSING

July 19-20, 1982

Organizers: M. Stickley and A. Yariv

July 19, 1982

I. DEFENSE APPLICATIONS AND TECHNOLOGY NEEDS

Overview of DoD Applications and Technology Needs, and
Special Navy Needs - J. Lee, NRL.

Special Army Applications and Technology Needs -N. Berg, &
J. Pellegrino, HDL.

Special AF Applications and Technology Needs - J. Neff,
AFOSR, J. Ludman, RADC.

II. PHOTOREFRACTIVE MATERIALS AND APPLICATIONS

Overview of Photorefractive Materials and Figures of Merit
-M. Klein and R. Pastor, Hughes.

Crystal Growth of Barium Titanate - A. Linz, MIT.

Real Time Holography, Image Processing, and Distortion
Correction Using Four Wave Mixing in Photorefractive
Crystals -A. Yariv, Cal Tech.

Comparison of Soviet PRIZ and US PROM Devices -D. Casasent,
CMU.

Tungsten Bronze and Perovskite Structural Families for
Image Processing Applications - R. Neurgaonkar, Rockwell.

BSO and Thin Film EO Materials - A. Tanguay, USC.

MEETING ON
PHOTOREFRACTIVE MATERIALS AND SPATIAL LIGHT MODULATORS
FOR OPTICAL PROCESSING
(continued)

July 20, 1982

III. ADVANCED SLM CONCEPTS

The Microchannel Spatial Light Modulator -C. Warde, MIT.

The Microchannel Plate Membrane Light Modulator -A. Fisher
and J. Lee, NRL.

A Silicon/PLZT SLM - S. Lee, UCSD.

A Transverse E-Field SLM Concept - S. Yao, TRW.

Recommendations to BMD/ATC on Optical Processing
P. Hammerling, La Jolla Inst.

A High Speed Electrically Addressed SLM -R. Kingston, LL.

V. DISCUSSION

CARBON/CARBON TURBINE ENGINES

E. E. Hucke

The advantages gained by employing strong, light carbon-carbon (C/C) composites in turbine engines which operate at inlet temperature of 3500°F have been demonstrated in a DARPA feasibility study. In general, greater fuel efficiency can be translated into longer range and the superior materials properties can be exploited in reduced engine size and greater specific thrust. The magnitudes of the gains are such as to justify an ambitious program to extend the temperature to the 3500°F range, especially in light of the recent encouraging engineering applications with highly stressed C/C parts in the 2500-2900°F range.

The actual construction of such an engine requires major advances in C/C turbine hardware design, properties evaluation, component reliability, and in coating technology. A two day meeting was held to identify the major problems and suggest possible solutions. A program and list of attendees is attached.

The major problems can be separated into mechanical and chemical categories. The first is mainly concerned with methods by which the exceptional uni-directional properties of current C/C materials can be utilized in structures requiring three dimensional loading. The second results from the need to provide fool-proof oxidation resistance for the C/C, since the usual

combustion atmospheres will oxidize the structure in times too short to consider for even limited engine duty.

Recommendations for C/C Engines

1. Establish a materials program for further improving the C/C properties emphasizing co-pyrolysis techniques with emphasis on strength vs. toughness.
2. Design and construction of controlled temperature and more closely simulated chemical environment for evaluation of coated test specimens.
3. Mechanical property evaluation after exposure to test conditions instead of relying solely on weight loss.
4. Phase stability studies in coating systems of interest as outlined in the Rapp-St. Pierre study.
5. Fixing firm time and material temperature goals for screening.
6. Re-examine the reducing topping cycle concept in order to eliminate coatings that must operate above 2500-2900°F.
7. Begin a short study to predict the strength and toughness properties of 1μ and $.1\mu$ grain size isotropic graphite.
8. Solicit ideas to produce $.1\mu$ and 1μ graphite in test quantities.

ACKNOWLEDGEMENT

This paper was written under the auspices of the DARPA Materials Research Council, Contract #MDA903-82-C-0428 with The University of Michigan.

CARBON-CARBON TURBINE ENGINE MEETING

July 14-15, 1982

DARPA Materials Research Council Meeting

July 14

Status Carbon/Carbon Technology for Expendable
Turbine Engines - B. A. Forcht, Vought Corporation

Assessment of Analytical Methods for Structural
Analysis of Carbon/Carbon GTE Components -
J. Schutzler, PDA

Carbon/Carbon Substrate Architecture of Design
Candidates for In-flow Radial Turbine Wheel -
J. Schutzler, PDA

Feasibility of Weaving an In-flow Radial Turbine
Carbon/Carbon Composite Wheel - FMI

Physical and Mechanical Property Data Generation -
Stu Starrett, Southern Research Institute

July 15

Generic Silicon Carbide Conversion Coatings for
Carbon/Carbon Substrates - R. E. Yeager, Vought
Corporation

Sputtered Deposited Metal Oxide Coatings for
Providing 3500°F Oxidation Protection to
Carbon/Carbon Composites - Ed Courtwright, Battelle,
N.W.

Electron Beam and Laser Deposited Metal Oxide Coating
Systems - Ernest Demaray, Airco Temescal

Discussion and Recommendations

CARBON/CARBON TURBINE ENGINE MEETING

July 14-15, 1982

Brennan Forcht (214) 266-4796
Manager, Carbon/Carbon Research
Vought Corporation
P.O. Box 226144
Dallas, TX 75266

R. E. Yeager (214) 266-4796
Vought Corporation
P.O. Box 226144
Dallas, TX 75266

R. Ernest Demaray (415) 841-5720
Airco Temescal X-380
2850 7th Street
Berkeley, CA 94710

J. Schutzler (714) 556-2800
PDA, Engineering
1560 Brookhollow Drive
Santa Anna, CA 92705

E. Courtwright (509) 373-2603
Battelle Northwest Laboratories
231-E Bldg.
Richland, Washington 99352

S. Starrett (205) 323-6592
Southern Research Institute
P.O. Box 3307-A
Birmingham, AL 35255

Ronald Kerans (513) 255-4769
AFWL/MMLM 255-4739
Wright Patterson AFB
Ohio 45433

Jim Crawford (207) 282-5911
Fiber Materials Incorporated
Biddeford Industrial Park
Biddeford, Maine 04005

COMMENTS ON CARBON/CARBON COMPOSITES DEVELOPMENT

J. C. Williams

The properties of Carbon/Carbon composite materials appear to offer tremendous potential for high temperature applications. However, before they can be used reliably in highly stressed components additional confidence needs to be developed in the reproducibility of the properties of the base material. Also, the behavior of the coatings requires considerably more study. To this end, several areas for basic research are suggested below. These areas are intended to improve and broaden the fundamental understanding of these materials and should be viewed as complementary in nature with respect to the ongoing development work which was described during the two day session.

1. Materials Characterization

It appears that a more extensive post-mortem analysis of test specimens would ensure that the materials in duplicate test specimens are indeed similar in structural characteristics. Such an analysis should provide a rational basis for minimizing the scatter in the data. Inasmuch as the structure of C/C composites is more complex than most metallic alloys, there appears to be a broader range of structural possibilities which can result from what is ostensibly a fixed process. Such variations in structure should lead to a corresponding variation in properties. Thus a more comprehensive model which relates structure

and properties would be helpful in analyzing and rationalizing variations in properties. Such a model would also help in identifying optimum structures with respect to particular properties and applications.

2. Coating Studies

The successful use of C/C composites at elevated temperatures, e.g., 3000°F, depends largely on the performance of the coatings used to prevent catastrophic oxidation. In this regard several aspects of coating performance appear to require improved fundamental understanding and thus warrant further study.

First, the nature of the reaction between the coating and the C/C substrate is not well understood. The effect of Zr additions to SiC seem to produce significant changes in coating performance but these are not well-characterized. To provide an improved insight into this it is suggested that both surface chemistry and local chemistry variations through the coating thickness would provide some very useful information regarding the effects on and role of Zr and other additions on coating structure and integrity. To do this scanning auger microscopy (SAM) and scanning transmission electron microscopy (STEM) could be employed. Both of these techniques provide complementary information with higher spatial resolution than is achievable via microprobe or conventional auger spectroscopy. Second, the substrate wetting by the glassy phase(s) in coatings is usually assumed but the details of this wetting process are generally not

well characterized. Accordingly, studies of glassy phase/substrate contact angle as a function of temperature and glassy phase composition would shed considerable light on the wettability of the substrate. This in turn would yield useful information for the design and selection of self-healing coatings or components of coatings.

In summary, the continued development of C/C composites may be more rapid and may possibly proceed more smoothly if there is greater emphasis placed on parallel supporting technology studies. Improvement of the basic understanding of the nature of these materials and the associated coating systems will permit them to be adapted to new applications in a more optimal way. In turn, this can lead to a reduction in the amount of trial and error which has naturally accompanied some of the early developmental activities and applications studies.

ACKNOWLEDGEMENT

This paper was written under the auspices of the DARPA Materials Research Council, Contract #MDA903-82-C-0428 with The University of Michigan.

CARBON-CARBON ENGINE

A. Macleod

Progress on the demonstration project is impressive, has demanded considerable engineering skill and ability and may eventually succeed. This will leave us with a demonstration of the feasibility of carbon-carbon material for an engine at 3500°F.

We now need to expand this work beyond feasibility demonstration. A base of scientific data for the materials is now necessary, especially with respect of the coatings. A number of areas need more detailed investigation. There are significant changes in the microstructure of the demonstration coatings during high temperature exposure. What do these changes represent? What is the character and composition of the apparently melted zones? What about the cracks? Can we construct a model for the coating, particularly in terms of its resistance to oxygen penetration? Even the simplest, crudest model would be useful and would permit us to plug in measured results.

Any thin-film system is subject to an enormous number of parameters, especially process parameters, and it is only when we can vary these parameters in a systematic way and measure coating properties, gradually placing points in the multidimensional space that represents the behavior and properties of the coating, that we can begin to make progress.

Once we reach the stage of making predictions which are realized, then we can say we have some control over the coating. I believe we now need a project or series of projects to address these fundamental aspects.

ACKNOWLEDGEMENT

This paper was written under the auspices of the DARPA Materials Research Council, Contract #MDA903-82-C-0428 with The University of Michigan.

Once we reach the stage of making predictions which are realized, then we can say we have some control over the coating. I believe we now need a project or series of projects to address these fundamental aspects.

ACKNOWLEDGEMENT

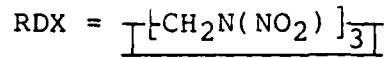
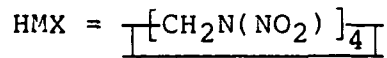
This paper was written under the auspices of the DARPA Materials Research Council, Contract #MDA903-82-C-0428 with The University of Michigan.

ENERGETIC MATERIALS

J.L MARGRAVE

The science and technology of energetic materials (propellants, explosives, etc.) were discussed by Drs. Ray Maguire and Milton Finger of the Lawrence Livermore Laboratory. Characteristics of monomolecular systems (fuel + oxidizer in the same molecule) were compared for TATB, TNT, RDX, HMX, and HNB*. Since the successful preparation of HNB, there has been interest in synthesis of related molecules as shown in Fig. 1. Most of these combine strained rings/multiple bonds with per-nitro substitution and high density. Efforts to extend the RDX and HMX systems are also in progress with Navy support, as shown in Fig. 2. The molecule decanitrobiphenyl is of interest as are some other high-density nitro-substituted aromatics, as shown in Fig. 3. The ultimate explosive would have a density >3 gr/cc, a detonation temperature >4000K, a reaction zone <1 μ and produce only low molecular weight products.

*HNB = HEXANITROBENZENE



TATB= TRIAMINOTRINITROBENZENE

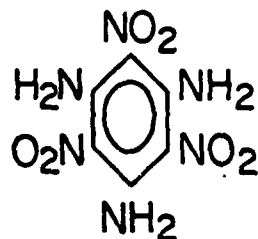
TNT = TRINITROTOLUENE

AP = AMMONIUM PERCHLORATE

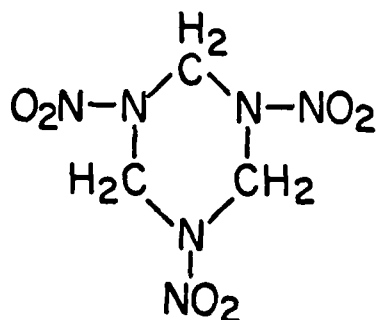
LP = LITHIUM PERCHLORATE

TNM = TETRANITROMETHANE

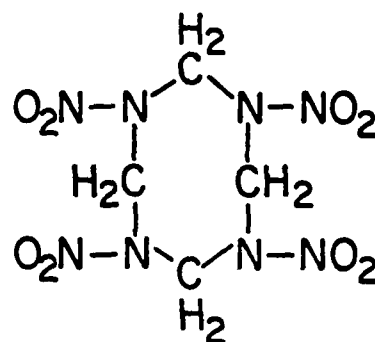
(a) TATB



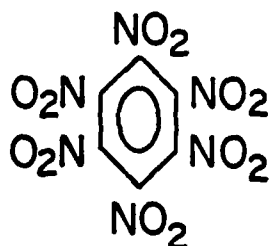
(b) ROX



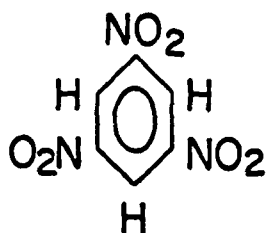
(c) HMX



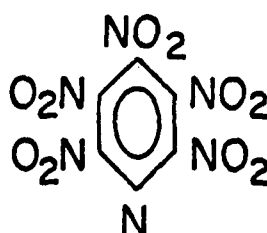
(d) HNB



(e) TNB



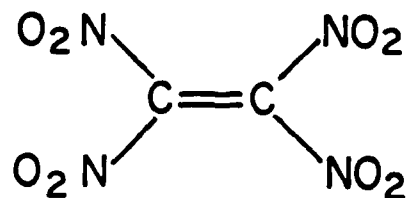
(f) PNP



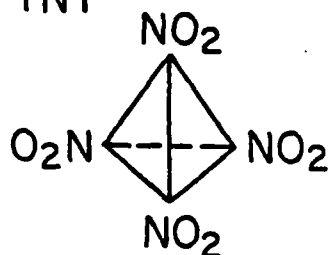
(g) DNA



(h) TNE



(i) TNT



(j)

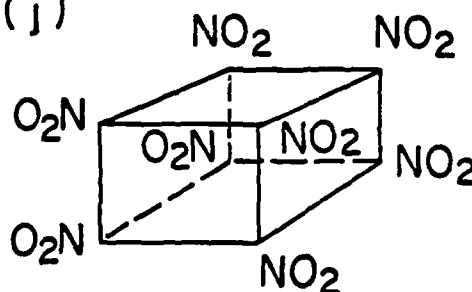
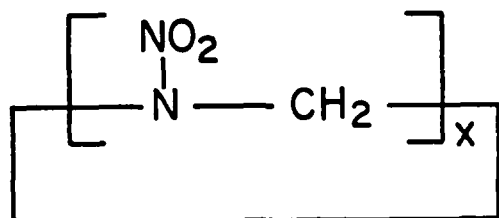
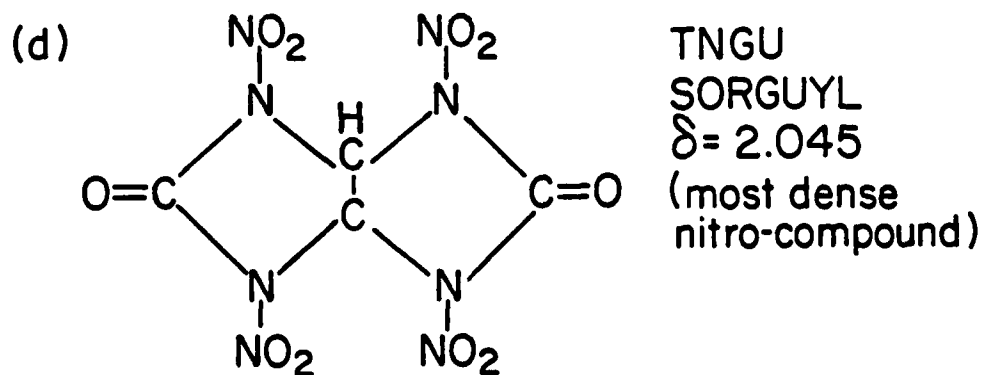
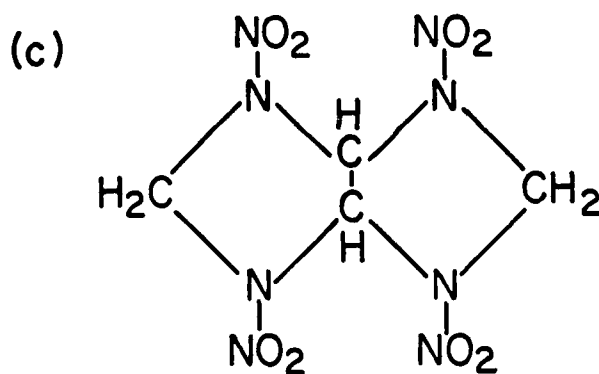
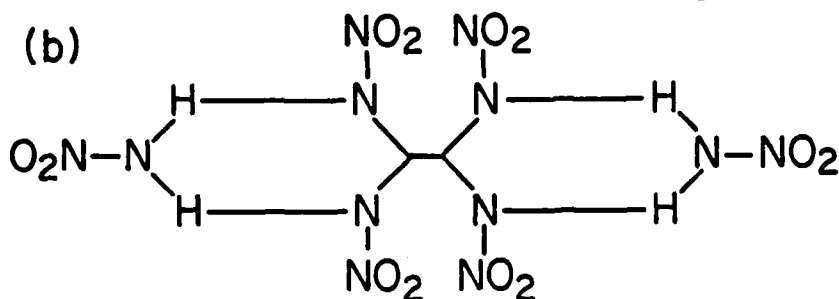


Figure 1. Some High-energy polynitro-molecules.

(a) RDX and HMX Homologs



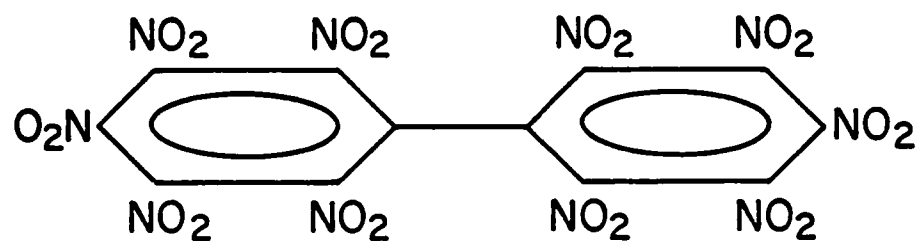
X = 3, RDX
 = 4, HMX
 = 5
 = 6 } New Materials
 = 7



TNGU
 SORGUYL
 $\delta = 2.045$
 (most dense
 nitro-compound)

Figure 2. High-energy syntheses with Navy support.

(a) Decanitro Biphenyl



(b)

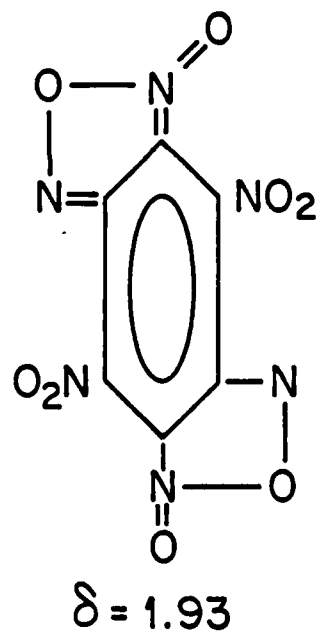
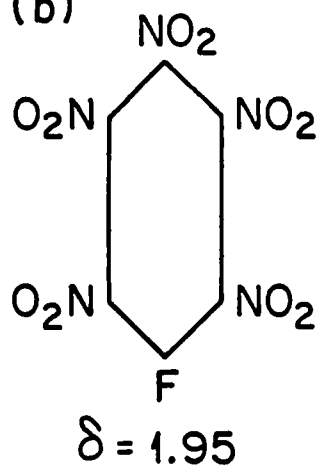


Figure 3. High-density nitro-substituted aromatics.

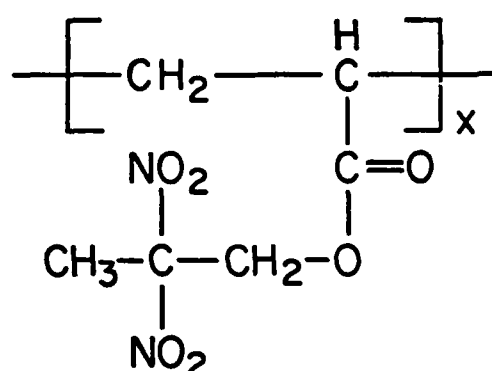
Plasticizers for holding energetic molecules in shapes need to have high densities, appreciable solubility for the system involved, as well as thermal and chemical stability and resistance to low-velocity detonations. Various currently used plasticizer systems are shown in Fig. 4.

Composite explosives contain fuel and oxidizer as separate phases. Table I lists some typical constituents of useful composite systems. In some cases (NH_4NO_3 , NH_4ClO_4 , TNT, HMX), the molecule contains both ingredients and is a self-explosive. With insensitive compounds like TATB, one may need triggers like HMX or Al. Table 2 presents comparisons of densities, heats of reaction, gaseous moles produced and average molecular weights of products for selected composite explosives.

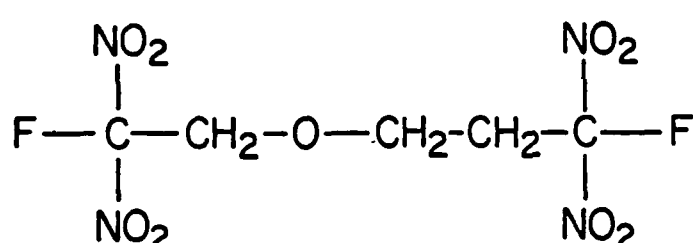
Particularly useful composites are 20% HMX, plus ZrH_2/AP (Compn. B) and 40% HMX plus ZrH_2/AP (OCTOL). Quite high on the energy production scale for composites are graphite or diamond/lithium perchlorate mixtures. Professor E. Hucke has proposed an infusion of liquid LP into foamed carbon shapes to give a composite of selected geometry and pore-size distribution.

One of the important uses for composite explosives is in shaped charges where one optimizes applications by controlling energy release rates and detonation wave velocities and achieves a precise time-geometry controlled process with smooth acceleration via gas evolution. For additional control/supplemental energy, one can use electrical heating, radiant imaging, etc. Some ideas for composite explosive systems are listed in

- (a) Nitrocellulose
 (b) Polydinitropropyl Acrylate



- (c) FEFO



- (d) Poly-Bamo

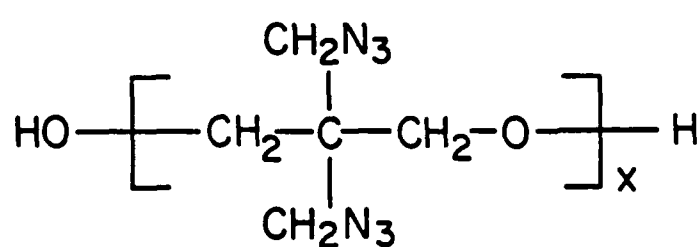


Figure 4. Plasticizers in current use.

TABLE 1

USEFUL COMPOSITE SYSTEMS

OXIDIZERS	FUELS
NH_4NO_3	TNT
NH_4ClO_4	HMX
LiClO_4	HYDROCARBON OILS
NaClO_4	ORGANIC POLYMERS
NaNO_3	METALS - Al, Mg, etc.
$\text{C}(\text{NO}_2)_4$	METAL HYDRIDES - ZrH_2
	GRAPHITE

TABLE 2

PERFORMANCE CRITERIA FOR SOME COMPOSITE SYSTEMS

	<u>OXIDIZERS</u>					
	LiClO_4		$\text{Al}(\text{NO}_2)_3$ $\text{Al}(\text{ClO}_4)_3$		NH_4ClO_4	
<u>FUELS</u> $\text{C}_{\text{diamond}}$	2.57	3.82	2.50	3.98		
	59	44	50	47		
Al	2.53	7.00	2.49	7.81		
	14	42	5	124		
ZrH_2	3.11	4.41	3.47	5.66	2.62	3.56
	31	28	28	54	52	25

gr/cc	Q
moles/gram	M

Q = heat of reaction

M = molecular weight of gaseous products

Table 3. Additional synthetic methods for producing composite explosives by use of metal atom co-condensation methods have been suggested by Margrave (Table 4).

In summary, there is clearly an important and continuing need for research/development on monomolecular and on composite high-energy materials. New high-energy molecules, more efficient syntheses and imaginative concepts for composite systems are of highest priority.

ACKNOWLEDGEMENT

This paper was written under the auspices of the DARPA Materials Research Council, Contract #MDA903-82-C-0428 with The University of Michigan.

TABLE 3

SUGGESTED NEW COMPOSITE SYSTEMS

<u>Solid Fuels</u>	<u>Solid Oxidizers</u>
C(foam)	NF_4ClO_4
Al(foam)	NF_4BF_4
	$\text{LiO}_3, \text{LiO}_2$
AlH_3	
MgH_2	$\text{CF} \cdot \text{ClF}_3$
LiH	$\text{CF} \cdot \text{ClF}_5$
	$\text{CF} \cdot \text{PF}_5$

TABLE 4

FORMATION OF COMPOSITE SYSTEMS BY CO-CONDENSATION METHODS*

<u>Fuels</u>		<u>Oxidizers</u>	
$\text{Ca} + \text{NH}_3 \rightarrow \text{Ca}(\text{NH}_3)_6$		$\text{CF}, (\text{CF}_2)_x, \text{C}_2\text{F}_6, \text{ etc.}$	
$\text{Li} + \text{NH}_3 \rightarrow \text{Li}(\text{NH}_3)$		NF_2, NF_3 $\text{ClF}, \text{ClF}_3, \text{ClF}_5$	
$\text{Al} + \text{CH}_4 \rightarrow \text{HAlCH}_3$		$\text{LiO}_2, \text{KO}_2$	
M-atoms	Al	**	LiO_3
	Mg		NO_2, NO
	Li	(and Mx	
	C	clusters)	NOF, HOF
	B		NO_3F COF_2

*Use a paraffinic wax to isolate fuel from oxidizers and from air/humidity.

**When matrix-isolated, metal atoms have approximate thermodynamic potentials of gaseous species.

A HIGH ENERGY SHAPED MICROCOMPOSITE EXPLOSIVE SYSTEM

E. E. Hucke

Recent work in tailored energy release explosive systems has centered on composites of energy rich materials. These systems are particularly attractive for metal moving applications where short time energy release is necessary.

Thermochemical considerations show that carbon with tetra-nitro-methane (CN_4O_8) and carbon with lithium perchlorate (LiClO_4) are the highest energy content materials known, although there may be some problems in initiating their reactions.

It is proposed that a shaped low density controlled microporous body of glassy carbon be infiltrated with liquid lithium perchlorate (m.p. $\sim 240^\circ\text{C}$) or tetra-nitro-methane (m.p. $\sim 17^\circ\text{C}$). In this highly dispersed microstructure initiation should be facilitated while simultaneously aiding the resistance to degradation from moisture degradation. In addition the angstrom sized void remaining within the disordered glassy carbon structure should aid in providing a rapid temperature rise during an initiating shock wave.

Stoichiometric calculations have been made which show that the required glassy carbon skeleton density falls within a range that can be made by known techniques used for making controlled porosity materials for high temperature in situ carbide reactions. This use would be a direct application of self propagating high temperature synthesis (SHS).

SOME COMMENTS ON THE RELATIONSHIP
BETWEEN FRACTURE MODES IN STRESS CORROSION CRACKING

J. C. Williams

Titanium alloys which have only a limited susceptibility to sustained load cracking (SLC) typically exhibit three distinct types of fracture. These are cleavage, fluting, and dimples (also called hole growth or microvoid coalescence). The relationship between, and occurrence of, these three distinct fracture mechanisms seems worthy of comment. The fracture mode which gives rise to sustained load cracking is the cleavage type fracture. This fracture mode has been thoroughly studied and is well-documented. However, for the purposes of this discussion, it can be characterized as a separation along or near the basal plane in a manner which is probably controlled by some critical value of the normal stress component acting on the basal plane. In alloys which contain relatively large regions of constant orientation of the hexagonal α -phase, the formation of flutes is often seen in conjunction with cleavage during SLC. These flutes also have been studied in substantial detail and have been described elsewhere in a number of published accounts. However, it is worth commenting here that the flutes seem to form by sliding off of mode II fracture along the prism planes. Thus, the plane of fracture which corresponds to the flute is always roughly 90° to the plane of cleavage during SLC. Finally, regions which do not fail either by cleavage or formation of flutes exhibit the normal dimple type of fracture.

The relationship between these fracture modes and the significance of their occurrence relative to susceptibility to SLC has been the source of confusion in several publications. The confusion originated when Sanderson and Scully suggested that the flutes were evidence for the formation of hydrides. Aitchison and Cox later showed that flutes could be formed in the absence of any environmentally assisted fracture, and therefore, if their occurrence bore any relationship to the occurrence of environmentally assisted fracture, this relationship was coincidental. Further, Chesnutt and Williams have showed that flutes could also occur in conjunction with the extension of a sharp fatigue crack and, therefore, the occurrence of flutes appear now to be more related to the sharpness to the crack than to environmentally assisted fracture per se. Thus, it now appears that the frequent occurrence of flutes in conjunction with SLC is due to the localized mode II fracture which permits the interconnection of sharp cleavage cracks which are formed due to environmental influence. The absence of or very limited extent of flutes in fast fracture regions is also worthy of comment. Since both flute formation and hole growth are competitive ductile fracture modes, the relative absence of flutes suggests that once the crack blunts by plastic flow, the stress and strain state at the crack tip tends to favor hole growth formation rather than flute formation¹. This suggestion is consistent with the frequent observation of flutes in presence of a sharp crack (either cleavage or fatigue) and the relatively

infrequent observation of them in the case of a more ductile or blunt crack.

In summary, the occurrence of flutes in and of themselves, does not constitute evidence of environmentally assisted fracture. However, since flutes tend to depend on the existence of a sharp crack in order to form, then the presence of flutes usually does indicate that sharp cracks have been present in the vicinity of the fracture regions which exhibit flutes. If the circumstances under which the flutes have formed preclude the presence of a sharp fatigue crack, then the presence of flutes is consistent with and suggestive of the occurrence of sharp, environmentally assisted cleavage cracks.

ACKNOWLEDGEMENT

This paper was written under the auspices of the DARPA Materials Research Council, Contract #MDA903-82-C-0428 with The University of Michigan.

¹An alternate point of view in the blunt, plastic crack extension mode, there are no sharp cracks to be connected by localized mode II cracking.

STRESS INTENSITY FACTORS OF DELAMINATED SURFACE COATINGS

J. W. Hutchinson, B. Budiansky & A. G. Evans

Thin coatings on a substrate are often under compression. If for some reason, the bond between the coating and the substrate fails over a small area, the compression may be sufficient to cause the coating to buckle away from the substrate and form a blister as depicted in Fig. 1. As buckling takes place, high stresses develop where the coating attaches to the substrate. Further enlargement of the blister will occur if the interface crack advances. Crack advance, in turn, will depend on the magnitude of the stress intensity factor at the crack edge. This stress intensity factor will now be estimated for several configurations.

Consider the circular blister in Fig. 1. Suppose an biaxial compressive stress σ_0 exists in the coating prior to buckling, i.e., σ_0 is the unrelieved compressive stress. We will calculate the difference between the elastic strain energy, δV , stored in the unbuckled and buckled configurations and then use the fact that the energy release rate for crack advance (per unit length of crack edge) is

$$G = \frac{1}{2\pi a} \frac{d \delta V}{da} \quad (1)$$

As long as the blister radius a is large compared to its thickness t , the blister can be modeled as a clamped circular

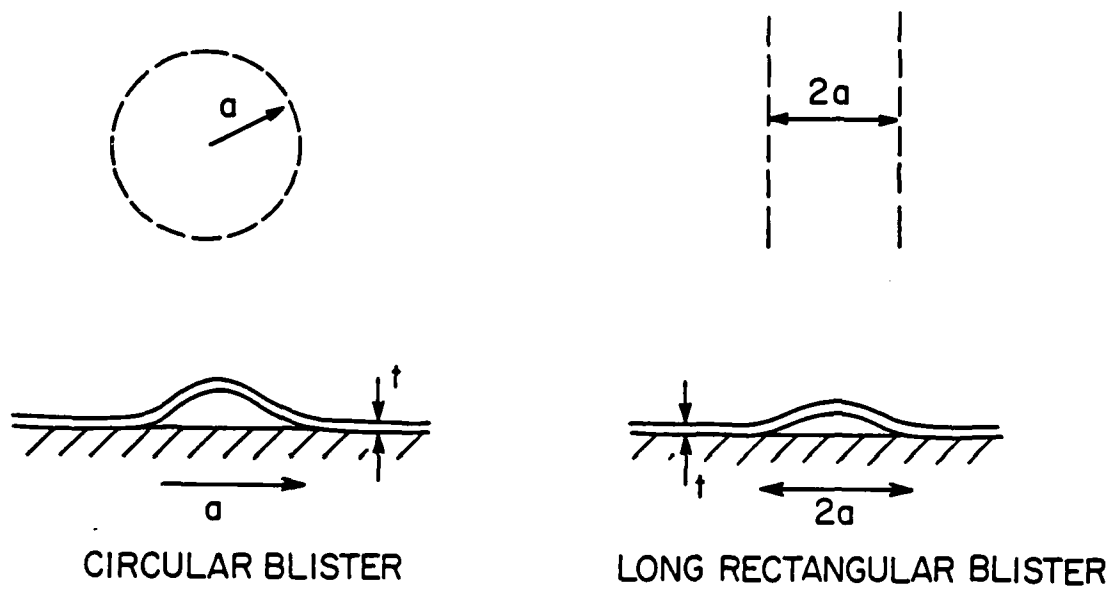


Figure 1. Geometry of buckled blisters.

plate of radius a . If the biaxial stress σ_0 in the unbuckled blister is released by cutting it out of the surface, its edge would expand outward by $(1-\nu)\sigma_0 a/E$, where ν is Poisson's ratio and E is Young's modulus. To fit the plate back in place, the edge must obviously be pushed inward by this same amount, i.e.,

$$\Delta = (1-\nu)\sigma_0 a/E \quad (2)$$

Now, a clamped circular plate compressed radially will buckle at an edge stress of

$$\sigma_c = \frac{kE}{12(1-\nu^2)} \left(\frac{t}{a}\right)^2 \quad (3)$$

where $k=14.68$. The associated inward radial displacement is

$$\Delta_c = \frac{k}{12(1+\nu)} \frac{t^2}{a} \quad (4)$$

If Δ given by (2) is less than Δ_c (i.e., if $\sigma_0 < \sigma_c$), the coating will not buckle away from the substrate. However, if $\sigma_0 > \sigma_c$, buckling will occur. The strain energy stored in the buckled blister can be evaluated using the post-buckling load-deflection of the plate which is shown in Fig. 2. The slope of the load-deflection curve of the buckled plate remains fairly constant for substantial buckling deflections. The ratio α of the normalized post-buckling to pre-buckling stiffness will have to be worked out; but based on other plate problems, it is expected to be between $1/4$ and $1/2$. The strain energy difference between the unbuckled and buckled plates, δV , is the area difference between the two load-deflection curves shown in Fig. 3, which can be expressed as

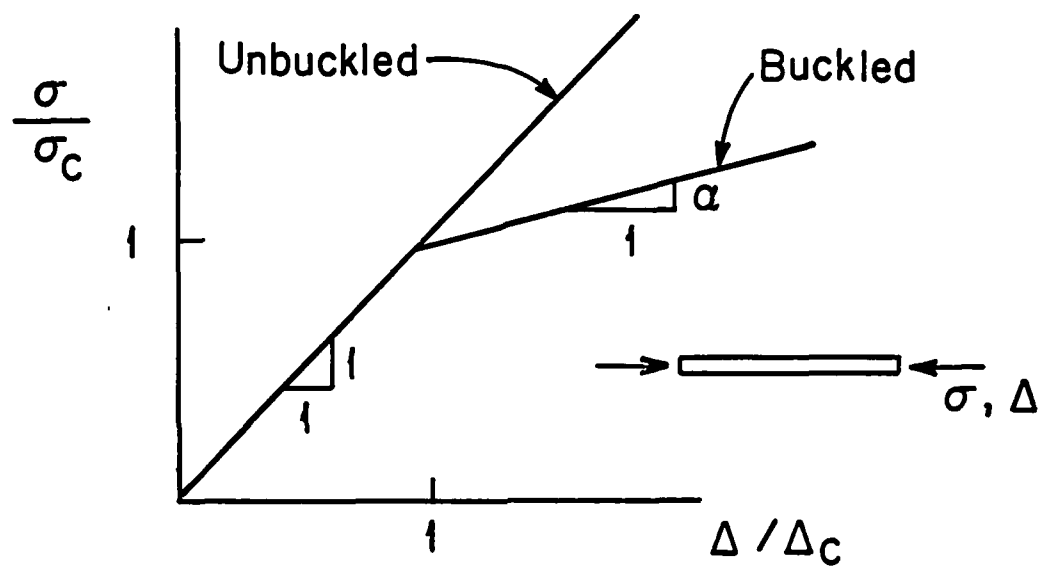


Figure 2. Normalized load-deflection curves of buckled and unbuckled clamped plate.

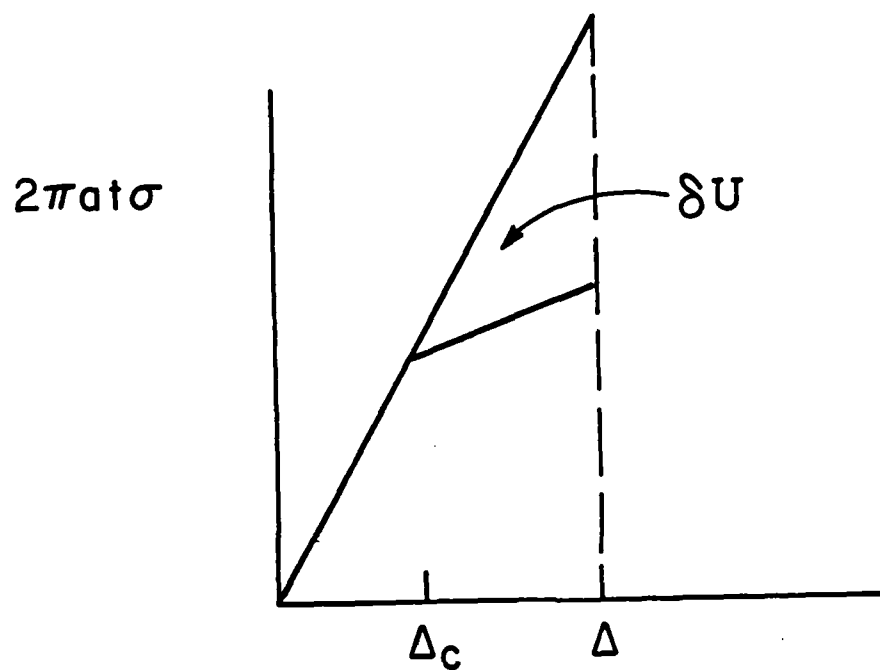


Figure 3. Strain energy difference δV between buckled and unbuckled plates.

$$\delta V = \frac{\pi(1-\nu)(1-\alpha)ta^2}{E} (\sigma_0 - \sigma_c)^2 \quad (5)$$

The stiffness of the substrate is essentially infinite compared to the coating and thus, the substrate experiences little change in strain energy. Therefore, (5) is taken as the total energy difference of the coating-substrate system.

By (1) and (3),

$$G = \frac{(1-\nu)(1-\alpha)t}{E} (\sigma_0^2 - \sigma_c^2) \quad (6)$$

Assuming the near-tip field is predominantly Mode I, the stress intensity factor K is give by $[GE/(1-\nu^2)]^{1/2}$ so that

$$\frac{K}{\sigma_0 \sqrt{t}} = \left[\frac{1-\alpha}{1+\nu} \right]^{1/2} \left[1 - \left(\frac{\sigma_c}{\sigma_0} \right)^2 \right]^{1/2} \quad (7)$$

As α increases, K increases monotonically to the limiting value

$$K = \sigma_0 \sqrt{t} \left[\frac{1-\alpha}{1-\nu} \right]^{1/2} \quad (8)$$

The corresponding result for the long rectangular blister shown in Fig. 1 is

$$\frac{K}{\sigma_0 \sqrt{t}} = \left[\frac{1}{2(1-\nu^2)} \right]^{1/2} \left[\left(1 - \frac{\sigma_c}{\sigma_0} \right) \left(1 + 3 \frac{\sigma_c}{\sigma_0} \right) \right]^{1/2} \quad (9)$$

where now σ_0 is the uniaxial compressive prestress in the coating and σ_c is its critical value for buckling:

$$\sigma_c = \frac{\pi^2 E}{12(1-\nu^2)} \left(\frac{t}{a} \right)^2 \quad (10)$$

In this case, the buckling behavior of the blister is similar to that of a wide column, and the normalized post-buckling slope α

is essentially zero. The stress intensity factor in (9) has a maximum, where $\sigma_0 = 3\sigma_c$ corresponding to

$$K = \frac{2}{\sqrt{3}} \left[\frac{1}{2(1-\nu^2)} \right]^{1/2} \sigma_0 \sqrt{t} \quad (11)$$

As a becomes large, K falls to a value which is $\sqrt{3}/2$ times (11).

ACKNOWLEDGEMENT

This paper was written under the auspices of the DARPA Materials Research Council, Contract #MDA903-82-C-0428 with The University of Michigan.

ON SIZE EFFECTS IN VOID NUCLEATION

A. G. Evans, J. W. Hutchinson and B. Budiansky

Experimental studies of void nucleation at inclusions do not provide general implications concerning effects of inclusion size. The most comprehensive studies (Argon et al) indicate that inclusion size is unimportant at small volume concentrations ($\sim < 0.01$) of Cu/Cr inclusions in Cu and TiC inclusions in a maraging steel. In this range, void nucleation occurs at an interface stress, $\sigma_i \sim 10^{-2}E$. A size effect appears to develop at larger volume concentrations of inclusions (~ 0.1); at least for Fe_3C inclusions in a spheroidized 1045 steel. Specifically, a preference for void formation at large, closely spaced inclusions was noted.

Several mechanisms of void nucleation at inclusions have been suggested. Equiaxed particles generally nucleate voids by firstly creating a separation at the interface. Inclusion cracking can also precede void formation, especially at elongated particles. The stresses needed to create the separation (or crack) are generally dictated by the plastic strain in the matrix.* A size dependence of void formation involving brittle fracture of the inclusions may then, of course, be qualitatively interpreted in terms of statistical distribution of flaws; but the presence of significant flaw distributions within inclusions of the appropriate size ($< 10 \mu m$) is debatable.

*Certain inclusions are subject to planar slip (e.g., manganese sulfide); size effects in such instances are directly explicable in terms of conventional dislocation pile-up concepts, (Cox and Low).

More generally, void nucleation will be dictated by the amplitude and scale of the tensile stresses that develop at the inclusion interface.

The stresses σ_i that develop at the interface of isolated spherical inclusions exhibit a maximum along the axis of principal applied tension (Fig.1a), can be approximated by (Argon, et al)

$$\sigma_i = Y(\gamma_p) + \sigma_T \quad (1)$$

where Y is the flow stress, γ_p is the plastic strain and σ_T is the hydrostatic component of the applied tensile stress. The interface stress can be magnified between closely spaced inclusions. An upper bound stress can be obtained from the plastic strain that develops by prohibiting flow into the matrix between the inclusions (Fig.1b),

$$\epsilon_p = (\gamma_p/2)(1-2\ell/\lambda)^{-1} \quad (2)$$

where γ_p is the shear strain, ℓ is the inclusion radius and λ the inclusion spacing. Plastic strain concentrations of this magnitude are most likely in the presence of appreciable tri-axiality. The concentrated plastic strain results in peak interface stresses

$$\sigma_i \approx \frac{Y(\gamma_p)}{(1-2\ell/\lambda)^n} + \sigma_T \quad (3)$$

where n is the work hardening coefficient.

The interface stress thus exhibits important dependences on the plastic strain, the work hardening coefficient, the triaxility and the local volume concentration of particles (as manifest in ℓ/λ). Invoking a void nucleation criterion based on a critical value of the interface stress thus anticipates coupled effects of plastic strain, triaxility and local inclusion volume concentration. Size effects are not directly involved. A size effect could emerge if the distribution in ℓ/λ exhibits an absolute dependence on inclusion size (Fig.2). Such size trends (undoubtedly dependent upon the inclusion coarsening mechanism) have not been studied. cursory inspection of typical particles (Fig.3) does not reveal a systematic influence of size upon ℓ/λ (i.e., there are as many closely spaced small inclusions -large ℓ/λ -as closely spaced large particles). Careful studies of particle spacing trends are central to the interpretation of nucleation size effects predicated on a critical nucleation stress.

Analogy with size effects in the separation of brittle inclusions from brittle matrices suggests that a critical interface stress may be an inadequate criterion for void nucleation. A local stress intensification, at facets or interface defects that scale in size with the inclusion radius*, may be more pertinent. Then an effective critical stress intensity factor,

*Faceting results in singularities at face corners. The scale of the stress field (at the interface) thus depends on the facet length and hence, the inclusion size. A suitable product of the scale and amplitude of the stress determines the stress intensity factor.

$K_C^{eff} \approx \sigma_i \sqrt{l/2}$, dictates interface separation, as expressed by the critical radius,

$$l_C \approx 2(K_C^{eff})^2 Y(1-2l/\lambda)^{-n} + \sigma_T \quad (4)$$

The separation of interfaces characteristically occurs for K_C^{eff} in the range 0.5-2 MPa \sqrt{m} . First order estimates of the critical size may be deduced from equation (4).

A second size effect exists when the inclusions are very small; viz, a minimum size below which void formation is prohibited. This minimum size is based on the requirement that the strain energy be of sufficient magnitude to provide the energy of the separated surfaces (Argon, et al). Formation of the void surfaces requires release of a proportion of the strain energy accumulation around the elastic inclusion. A prerequisite for void nucleation is thus;

$$(4/3)\pi\alpha l^3 (\sigma_i^2/2E) > 4\pi\beta l^2 \chi_f \quad (5)$$

where χ_f is the fracture energy associated with void formation ($\chi_s - \chi_i$ is a lower limit), α is that fraction of the total available strain energy (around the particle) released during void formation and β is the fraction of inclusion surface that separates. The predicted critical size is sensitively dependent upon the values of α and β . The detailed analysis needed to compute these quantities has not been performed and hence, literature estimates must be regarded as approximate.

ACKNOWLEDGEMENT

This paper was written under the auspices of the DARPA Materials Research Council, Contract #MDA903-82-C-0428 with The University of Michigan.

REFERENCES

1. A. S. Argon and J. Im, Met. Trans., 6A, (1975) 839.
2. T. B. Cox and J. Low, Met. Trans., 5, (1974) 1457.

SOME COMMENTS ON THE DIRECTIONALITY
OF HOT ROLLED TITANIUM PLATE

J. C. Williams

Because of the hexagonal symmetry of the α -phase, preferred orientation or texture of this phase can lead to anisotropic mechanical behavior. The conventional wisdom has been that β rolled products tend to have a minimum amount of texture and, therefore, a minimum amount of anisotropy or directionality of properties. While this is generally true, two factors tend to be overlooked in this somewhat sweeping statement. First, the β -phase which in turn can lead to preferred orientation of the α transformation product. Second, most β worked plate is actually finished by working down through the transus and, therefore, some directionality can result from this processing related factor.

As a general rule, the processing of Ti alloy plate high in the α/β phase field tends to promote a basal transverse texture. That is, a texture is developed in which a higher than random density of basal poles are oriented parallel to the long transverse direction of the plate. This type of texture tends to lead to higher yield strength in the transverse direction and lower fracture toughness in TL orientation compact tension specimens. In addition, and sometimes most pronounced of all, the K_{ISCC} in TL specimens can be considerably lower than that observed in LT specimens. Taken in combination, these factors raise the following question, "What is an appropriate strategy

for testing hot worked mill product in order to assure that a stress corrosion susceptible condition or orientation of a particular product is not overlooked?" In response, it is suggested that the tensile properties always be measured in both the L and T directions and that the stress corrosion testing be consistently done with the loading axis coincident with the higher yield strength direction. In those alloys in which there is no significant directionality to strength, it can be reasonably assumed that little or no preferred orientation and, therefore, no anisotropy in K_{ISCC} will be observed. It is important, however, to formalize and follow such a strategy in order to prevent overlooking unacceptably low property values. Such a strategy does permit realistic screening of substantial numbers of alloy compositions and conditions in the context of an alloy development program without having to incur the expense of performing costly fracture-related property measurements in both directions of the plate. Thus, while directionality of hot-rolled plate does exist, it can be dealt with using the above strategy without severe escalation in cost. The only penalty is that the properties which are obtained, tend to be conservative in nature.

ACKNOWLEDGEMENT

This paper was written under the auspices of the DARPA Materials Research Council, Contract #MDA903-82-C-0428 with The University of Michigan.

SYNCHROTRON RADIATION

J. W. Wagner

Because synchrotron radiation has only become available in the past few years, its application to problems in materials science is relatively new. The construction of the National Synchrotron Light Source at Brookhaven National Laboratory and facilities like the NBS/NRL hard radiation beam lines, will provide an east coast source to complement Stanford. With these facilities, users unfamiliar with the technology of synchrotron radiation focusing and monochromatization, can utilize this method. Progress should occur quite rapidly.

Specific areas of immediate interest include in situ EXAFS studies of corrosion passivation kinetics on stainless steel and real time x-ray topographic observation of recrystallization in aluminum alloys. Future work utilizing primarily the tunability of synchrotron radiation wavelength include:

1. Determination of partial radial distributions or diffraction patterns for multicomponent metallic glass and complex crystal structures.
2. Oxidations mechanisms under environmental conditions using EXAFS.

Other work primarily utilizing the high photon flux of the synchrotron to decrease data acquisition time includes:

3. Crack tip plastic zone propogation.
4. In-situ metallic glass crystallization.

5. In-situ grain boundary migration kinetics.
6. Observation of deformation anisotropy and slip band formation during indentation hardness testing.
7. Deformation studies on polycrystalline metals.
8. In-situ dynamic observations of precipitation and ordering phenomena.

ACKNOWLEDGEMENT

This paper was written under the auspices of the DARPA Materials Research Council, Contract #MDA903-82-C-0428 with The University of Michigan.

COMMENTS ON "DOPING A PLASTIC SCINTILLATOR"
by Dr. B. D. Geelhood, Naval Ocean Systems Center

M. Wrighton and T. C. McGill

The proposal seems to be a very simple one. The chemistry is feasible and through the use of a technique from the solar concentrator field one might be able to cut down on the cost of covering the area with photon detection.

Doping of Plastics

Numerous boron containing organic molecules exist. Some of these could in principle be co-polymerized with styrene. Some experts in this area include: F. Hawthorne (University of California Los Angeles); R. Grimes (University of Virginia); and S. Shore (Ohio State University). These are all in the Department of Chemistry at their respective institutions.

Doped Glass

Another possibility is to use ^{10}B enriched optical quality glass doped with luminescent metal ion, possibly Eu. In that case the boron would be used to convert the neutron into an α -particle which would excite the metal ion. The transparent glass would allow the transmission of the resulting luminescence signal to the photo-detector.

A source of expertise on the glass is Corning Glass.

Collecting the Scintillation

One of the major difficulties with the proposed detector is to come up with a mechanism for collecting and detecting the

scintillation. a method which has been successfully applied to solar cells is the so called "dye concentrator." (In fact thin concentrator masks have been invented to collect scintillations.) The layout of such a concentrator is shown in the attached figure.

Information of the solar concentrator can be obtained from Owens-Illinois; GTE Laboratories, Inc; Professor A. Zervail, California Institute of Technology; and Sandia Laboratories.

ACKNOWLEDGEMENT

This paper was written under the auspices of the DARPA Materials Research Council, Contract #MDA903-82-C-0428 with The University of Michigan.

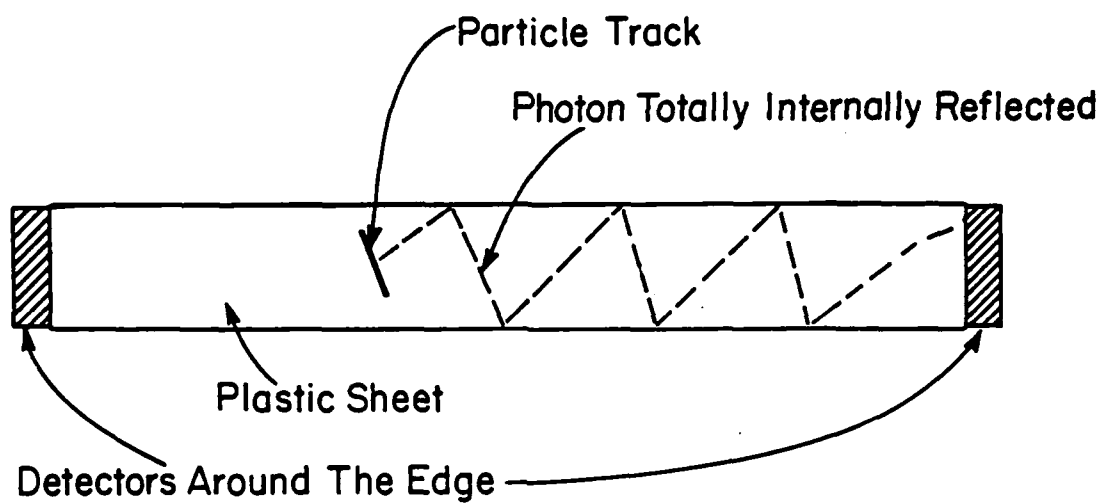


Figure 1. Plastic concentrator. This is basically a waveguide that guides the light to the detector.

KINETICS AND ENERGETICS OF SUBLIMATION OF C_n AND/OR M_xC_y SPECIES FROM GRAPHITE AND FROM METAL CARBIDES

J. L. Margrave

In spite of many Knudsen-Effusion, Langmuir free sublimation weight-loss, and mass-spectrometric studies of the sublimation of C_n -gaseous species from various graphite samples and from refractory carbides (WC, TaC, HfC, TiC, etc.), there is still ambiguity regarding the vapor phase composition. Thus, Zavitsanos¹ cites data from laser sublimation experiments on graphite with mass spectrometric monitoring which give C_3/C_1 ratios differing by a factor of 20 from equilibrium calculations². In a different pulsed ruby laser experiment, Berkowitz and Chupka³ reported a C_3/C_1 ratio only a factor of two different from equilibrium. Such discordant results (Table I) make all to speculations about the energy/gram of carbon sublimed, totally unreliable, depending on whether the predominant vapor species is C_1 (Zavitsanos) or C_3 (equilibrium), and allow values ranging from almost 60 kJ/gr for C_1 to only 20 kJ/gr. for C_3 as the vapor species.

Since over extended time periods one assumes equilibrium will be reached, it is important to know the time scale which applies and the extent of non-equilibrium sublimation which will be characteristic of laser-heated graphite and/or metal carbide systems. Recently, Smalley et al⁵ have carried out resonant, two-photon ionization studies of mass-selected metal-cluster

Table I

Relative Concentrations of C_n -species in Laser Sublimation and in Equilibrium Experiments.

Ratio	Zavitsanos ¹	Berkowitz & Chupka ³	Drowart et al ⁴	Equilibrium Janaf ²
C_2/C_1	0.58	0.85	3.00	2.22
C_2/C_3	1.51	0.31	0.62	0.47
C_2/C_4	8.60	14.7	9.97	8.39
C_2/C_5	6.20	3.97	6.28	5.65
C_2/C_6	25.00	76.00	----	----
C_2/C_7	24.00	28.30	----	----

species from a pulsed Nd.YAG laser vaporization source. Dimers and higher cluster species for Cu, Ag, Ni, Fe, Cr, Mo and W have been detected⁶. A similar study of $C_2, C_3 \dots C_n$ species should help provide definitive information about laser-pulse sublimation of graphite. One would like to know if the $C_1/C_2/C_3 \dots /C_n$ ratios are the same for various irradiation wave lengths and for pulsed or CW irradiation. Furthermore, are non-equilibrium numbers of binary species likely to be formed in pulsed or CW irradiation of refractory carbides -- Si_xC_y , Ti_xC_y , Mo_xC_y , W_xC_y , etc?

Another approach to the characterization of such species is matrix-isolation IR, visible-UV and Raman spectrometry.⁷ The high-temperature molecule Si_2C has recently been characterized by the matrix-IR technique.

ACKNOWLEDGEMENT

This paper was written under the auspices of the DARPA Materials Research Council, Contract #MDA903-82-C-0428 with The University of Michigan.

REFERENCES

1. (a) P. D. Zavitsanos, Carbon 6, 731 (1968).
(b) P. D. Zavitsanos and G. A. Carlson, J. Chem. Phys. 59, 2966 (1973).
2. JANAF Tables of Thermochemical Data, U.S. Govt. Publication, PB-168370, D. R. Stull, Editor, 1965.
3. J. Berkowitz and W. Chupka, J. Chem. Phys. 40, 2735 (1964).
4. J. Drowart, R. Burns, G. Demaria & M. Inghram, J. Chem. Phys. 31, 1131 (1959).
5. R. E. Smalley, D. Michaldopoulos, M. Geusic, S. Hansen and D. Powers, J. Phys. Chem., in press, 1982.
6. D. Powers, S. Hansen, R. Smalley et al, J. Phys. Chem., in press, 1982.
7. J. L. Margrave, R. Hauge, M. J. Berry, work in progress, 1982.
8. Z. K. Ismail, L. Fredin, R. Hauge and J. Margrave, submitted for publication, 1982.

INFRARED MATRIX ISOLATION SPECTRUM OF THE Si_2C MOLECULE

Z. Ismail, R. H. Hauge, L. Fredin, J. L. Margrave

ABSTRACT

It is difficult to prevent contamination of high-purity silicon with low-levels of carbon, probably because of the existence of stable gaseous molecules like SiC , Si_2C and SiC_2 . The infrared spectra of Si_2^{12}C and Si_2^{13}C isolated in solid argon at 15 K have been recorded in the 400-4,000 cm^{-1} region. Two absorptions at 1188.9 and 658.2 cm^{-1} that exhibit carbon-13 shifts of 35.2 and 14.9 cm^{-1} , respectively, have been detected. Based on the measured IR data, we conclude that the molecule has C_{2v} symmetry with value 110-115° for the SiCSi bond angle.

INTRODUCTION

The production of ultra high-purity silicon is of great industrial significance but one of the most difficult elements to eliminate as an impurity is carbon. This is because of the existence of stable high-temperature species like SiC , Si_2C and SiC_2 . The SiC_2 electronic spectrum has been seen in radiation from stars by several groups¹⁻⁴ and was first produced in the laboratory by Kleman⁵. Weltner⁶ studied both the absorption and emission spectra of the silicon dicarbide molecule. His matrix isolation spectra agreed with the previous gaseous observations of McKellar⁴ and Kleman⁵, but with the addition of three distinct weak bands. He also observed a series of bands at 4893 Å weak band previously observed in the gas phase^{4,5}. He

tentatively assigned this series of bands to the symmetrical Si_2C molecule with IR absorptions at 1205 and 1187 cm^{-1} in neon and argon matrices, respectively. The high resolution study of this absorption spectrum by Verma and Nagaraj⁷ using the flash discharge technique indicated that the 4906 Å band belongs to the molecule SiC_2 and not to Si_2C . Recently, Gilra⁸ studied the spectrum of C_3 in a King furnace in the 2500-6500 Å and 600-3300 cm^{-1} regions. After the addition of silicon, he observed the blue continuum earlier reported⁵ and determined its wavelength dependence. SiC_2 vibration-rotation bands were seen at 1740 cm^{-1} . Strong unidentified features at 1100-1200 cm^{-1} were also detected.

Recent mass spectrometric studies on the vaporization thermodynamics and kinetics of hexagonal silicon carbide⁹ indicated that equilibrium vapor pressures of Si, SiC_2 and Si_2C are 10-15 times higher than those reported by Drowart, et al.¹⁰

Based upon the above mentioned studies and further evidence presented in this paper, we were able to identify an IR absorption at 1188.9 cm^{-1} consistently occurring in our Si/ H_2O , Si/HF and Si/ H_2 studies^{11,12,13} as being due to disilicon carbide, Si_2C . This molecule was present as an impurity in the system as a result of silicon reacting with the high density graphite crucible. Because of its possible astrophysical importance and its presence in the vapors over the SiC, Si-SiC and C-SiC systems at high temperatures^{9,10}, the infrared study of matrix isolated Si_2^{12}C and Si_2^{13}C was undertaken.

Experimental

Vapors of Si_2^{12}C were obtained by heating elemental silicon in a high density graphite cell in the temperature range 1450-1700°C. The temperature of the cell was measured with an optical pyrometer. Vapors of Si_2^{13}C were produced by heating a mixture of elemental Si and graphite enriched in ^{13}C (90%) in the same cell under the same conditions. Gaseous disilicon carbide in excess argon was then deposited on a polished copper surface for a period of one hour. The mirror was then rotated 180° and IR reflection spectra of matrix isolated Si_2^{12}C and Se_2^{13}C were recorded on a Beckman-IR 9 spectrophotometer. Frequencies of IR absorption peaks were measured with an accuracy of $\pm 0.5 \text{ cm}^{-1}$. The rates of deposition of Si and Si_2C combined and argon were determined with a quartz crystal microbalance.

Pure silicon (99+%) was purchased from MCB. Graphite enriched in carbon-13 (90%) was supplied by Monsanto Research Corporation. Matheson argon (99.99%) was further purified by passing it through hot titanium (900°C) prior to deposition. An Air Product Displex closed cycle helium refrigerator has been used in all matrix experiments.

Spectra of trapped pure silicon showed the presence of bands due to monosilane (SiH_4) and silylene (SiH_2) which are the result of reactions of silicon atoms with molecular hydrogen on the matrix surface¹³. The hydrogen impurity probable results from cracking of the organic pump oil. Passing liquid nitrogen rather than water through the copper heat shield surrounding the

furnace considerably reduced the amount of SiH_4 and SiH_2 present in the matrix.

Detailed descriptions of the matrix isolation apparatus have been given earlier by Ismail¹⁴ and Kauffman¹⁵.

Results

During our recent studies on reactions of silicon atoms with H_2O ¹¹, HF ¹² and H_2 ¹³, there was a strong unidentified band that appeared at 1188.9 cm^{-1} in argon matrices. The intensity of this band did not depend on the concentration of H_2O or HF or H_2 (also present as an impurity in the H_2O and HF studies) in the matrices. When silicon atoms are vaporized at different temperatures from the high density graphite crucible and co-deposited with excess argon on the copper surface for a period of one hour, spectra such as those presented in Fig. 1 (A, B and C) were obtained. When a mixture of elemental silicon and graphite powder enriched in carbon-13 (90%) is heated in the same graphite crucible, and their vapors are cocondensed with excess inert gas, spectra such as those shown in Figure 1 (A', B' and C') were produced. Besides the bands due to SiH_2 and SiH_4 , one observes a peak at 1188.9 cm^{-1} that exhibits a carbon-13 shift of 35.2 cm^{-1} . The intensity of this peak increases as a function of the furnace temperature. Based upon Weltner's⁶ and Gilra's⁸ observations as well as above results, the bands at 1188.9 cm^{-1} and 1153.7 cm^{-1} were assigned to the asymmetric stretching mode of the molecules, Si_2^{12}C and Si_2^{13}C , respectively. Figure 2 shows high resolution spectra for the two

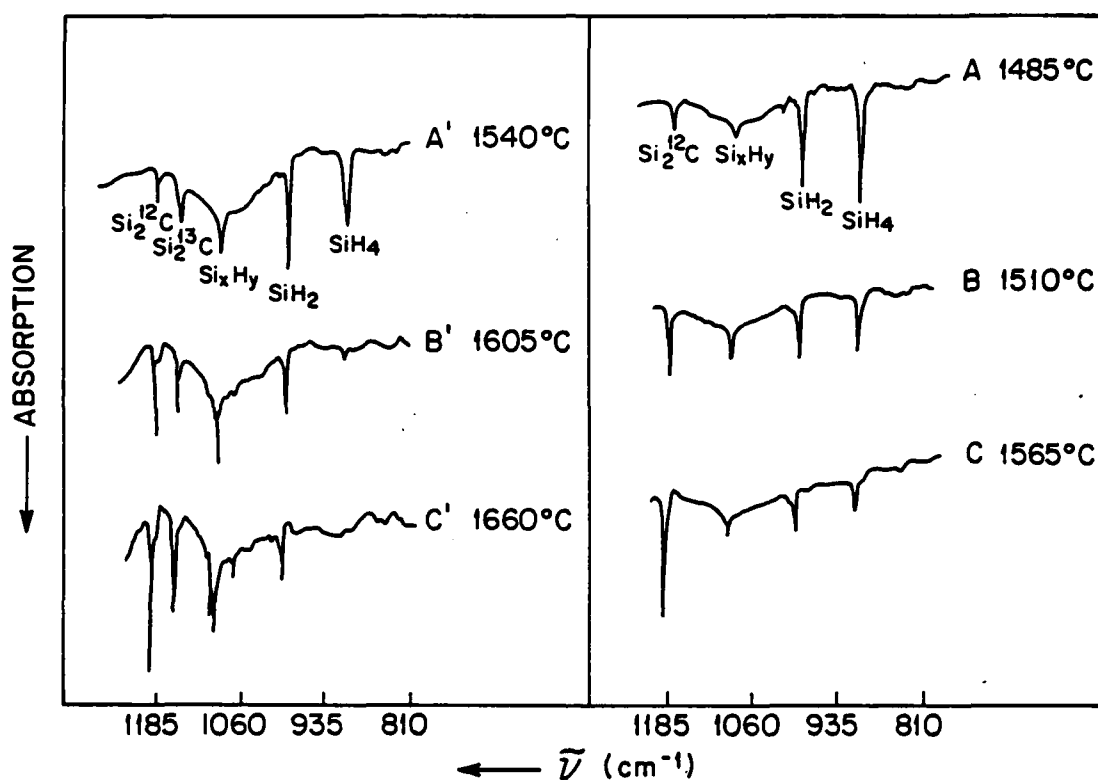


Figure 1. The asymmetric stretching region of Si_2^{12}C (A, B, C) and $\text{Si}_2^{12}\text{C}/\text{Si}_2^{13}\text{C}$ (A', B', C') in solid argon.

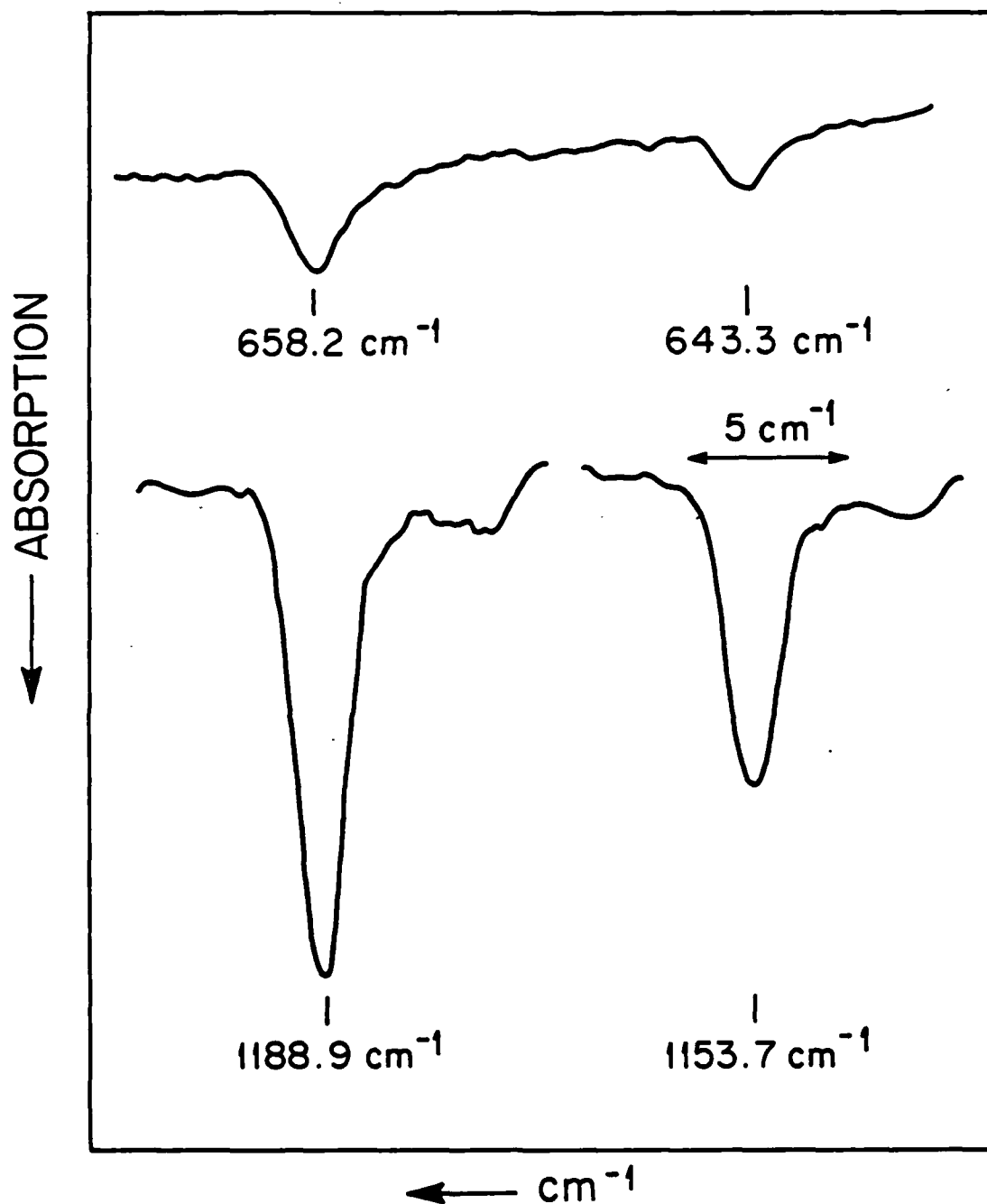


Figure 2. High resolution infrared spectra of Si₂¹²C and Si₂¹³C in solid argon.

absorption bands observed for Si_2^{12}C and Si_2^{13}C in solid argon. A weak band at 658.2 cm^{-1} was detected at a higher furnace temperature (1660°C) with a higher concentration of Si_2C as evidenced by the relative higher intensity of the 1188.9 cm^{-1} absorption peak. This new absorption at 658.2 cm^{-1} seems to grow at the same relative intensity as its counterpart at 1188.9 cm^{-1} . It shows a carbon-13 shift of 14.9 cm^{-1} .

Discussion

When silicon is vaporized with an isotopic mixture of carbon-13 and carbon-12, two new bands appear at 1153.7 cm^{-1} and 643.3 cm^{-1} , respectively, besides the two original ones observed at 1188.9 cm^{-1} and 658.2 cm^{-1} , respectively, that are due to the pure carbon-12 isotopic molecule. One can conclude from this mixed isotopic study that the molecule contains only one carbon atom. The variation of the intensity of the two absorptions exhibited by this species as a function of the furnace temperature indicates that the molecule could contain x number of silicon atoms (where $x = 1, 2, 3$). Mass spectrometric studies⁹ have shown that possible candidates that have an appreciable vapor pressure in this temperature range are Si , SiC_2 and Si_2C . Since it cannot be silicon atoms or SiC_2 , one concludes that it must be Si_2C . Another possibility is the diatomic SiC species.

The next question that arises deals with the geometry of Si_2C . Disilicon carbon may have a linear or non-linear and symmetric or asymmetric configuration. The molecules C_3 ^{16,17}

and SiC_2 ^{6,7} are known to be linear in their ground electronic states in the gas phase as well as in inert gas matrices. They both have low bending frequencies, 63 cm^{-1} for C_3 and 147 cm^{-1} for SiC_2 . By analogy to these molecules which have the same number of valence electrons as Si_2C , one would expect that disilicon carbide would be a symmetric linear molecule of D_h symmetry. For such a centrosymmetric molecule, one expects two infrared active modes that are Raman inactive: the asymmetric stretching and the bending modes. Assuming the 658.2 cm^{-1} absorption as the bending frequency, which is unlikely because of its very high value, one calculates a carbon-13 shift of 21.2 cm^{-1} compared to the measured shift of 14.9 cm^{-1} . This difference of 6.4 cm^{-1} between the observed and calculated shifts makes assignment of this frequency to the bending mode of linear Si_2C highly improbable. Further evidence against the molecule being linear is the very high anharmonicity (102.0 cm^{-1}) for the asymmetric stretching mode that would be needed to obtain agreement between the calculated and measured carbon-13 frequency shifts, $\Delta\nu_3$. Preliminary normal coordinate analyses have been carried out assuming the possible asymmetric linear configuration and the two observed frequencies, 1188.9 and 658.2 cm^{-1} , as the Si-C and Si-Si stretching modes, respectively. The results of these calculations indicate that it is impossible to get a reasonable good agreement between the calculated and the measured isotopic shift for the ν (Si-Si) mode. Another possibility is to assign this 658.2 cm^{-1} frequency to the bending mode, but

this is eliminated on the basis of the arguments given previously for the symmetric linear geometry.

If Si_2C is bent, one would expect that the symmetric structure would be thermodynamically more favorable than the asymmetric one since the SiC bond is expected to be much stronger than the SiSi bond. Assuming that Si_2C has a symmetric bent configuration, one can assign the 658.2 and 1188.9 peaks to the symmetric and asymmetric modes, respectively.

A preliminary normal coordinate analysis is being carried out for Si_2C using Schachtshneider's program¹⁸ and the measured frequencies for the asymmetric and symmetric stretching modes of Si_2^{12}C and Si_2^{13}C . A bond angle of 110° and a bond length of 1.7 Å was assumed. The Si_2C molecule is bent in an inert gas matrix and molecules like SiCO and SiN_2 are known to be nonlinear in some sites in some matrices¹⁹. SiN_2 are known to be nonlinear in some sites in some matrices¹⁹. SiN_2 in a pure N_2 matrix and SiCO in argon represent cases where almost all molecules are bent as indicated from the relative intensities of the x_2 and y_2 lines of their ESR spectra. Also, one can compare Si_2C with Cl_2O ²¹ and with S_2O ²² for which bent structures with $\angle \text{Cl-O-Cl} = 110.8^\circ$ and $\angle \text{S-S-O} = 118^\circ$ are reported.

It would also be interesting to learn more about the electronic spectrum of Si_2C and the multiplicity of its ground state. The ground state of C_3 is $1\Sigma_g$.²⁰ Weltner⁶ points out that substituting a silicon for carbon atom in C_3 would tend to lower the o_g orbital energy relative to the strongly bonding Π_u

orbital and would result in a gradual transition from singlet to triplet ground state. Although Si_2C to have a triplet ground state which may be related to its apparent nonlinearity.

ACKNOWLEDGEMENT

This paper was written under the auspices of the DARPA Materials Research Council, Contract #MDA903-82-C-0428 with The University of Michigan.

REFERENCES

1. Merrill, P. W., Publ. Astron. Soc. Pacific 38, 175 (1926).
2. Sanford, R. F., Publ. Astron. Soc. Pacific 38, 177 (1926).
3. Shane, C. D., Lich. Obs. Bull. 13, 123 (1928).
4. McKellar, A., J. Roy. Astron. Soc. Canada 41, 147 (1947).
5. Kleman, B., Astrophys. J. 123, 162 (1956).
6. Weltner, Jr., W., and McLeod, Jr., D., J. Chem. Phys. 41, 235 (1964).
7. Verma, R. D., and Nagaraj, S., Can. J. Phys. 52, 1938 (1974).
8. Gilra, D. P., Spectres. Mol. Simples Lab. Astrophys. Comm. Collog. Int. Astrophys. 21st, Universite de Liege, Liege, Je. 21-23, 1977 (Pub. 1980).
9. Behrens, R. G., and Rinehart, G. H. (Los Alamos Sci. Lab., Univ. Calif., Los Alamos, NM 87545 U.S.A.) NBS Spec. Publ. (U.S.) 561-1, 125 (1979).
10. Verhaegen, G., Stafford, F. E., and Drowart, Jr., J. Chem. Phys. 40, 1622 (1964).
11. Ismail, Z. K., Hauge, R. H., Fredin, L., Kauffman, J. W., and Margrave, J. L., J. Chem. Phys. (submitted).
12. Fredin, L., Hauge, R. H., Ismail, Z. K., and Margrave, J. L. (to be published).

13. Ismail, Z. K., Ph.D. Thesis, Rice University (1972).
14. Kauffman, J. W., Ph.D. Thesis, Rice University (1981).
16. Gausset, L., Herzberg, G., Lagerqvist, A., and Rosen, B.,
Astrophys. J. 142, 45 (1965).
17. Weltner, Jr., W., and McLeon, Jr., D. J. Chem. Phys. 45,
3096 (1966).
18. Schachtschneider, J. M., "Vibrational Analysis of
Polyatomic Molecules," Tech. Rept. Nos. 231 and 57, Shell
Development Co., Emeryville, CA (1964).
19. Lembke, R. R., Ferrante, R. I., and Weltner, Jr., W., J.
Am. Chem. Soc. 99, 416 (1977).
20. Pitzer, K. S., and Clementi, E., J. Am. Chem. Soc. 81, 4778
(1959).
- 21.
- 22.